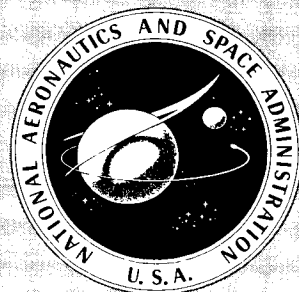


**CASE FILE  
COPY**

NASA SP-216

# **COMPRESSIBLE TURBULENT BOUNDARY LAYERS**

A symposium held at  
**LANGLEY RESEARCH CENTER**  
Hampton, Virginia  
December 10-11, 1968



**NATIONAL AERONAUTICS AND SPACE ADMINISTRATION**

# COMPRESSIBLE TURBULENT BOUNDARY LAYERS

*A symposium held at  
Langley Research Center  
Hampton, Virginia  
December 10-11, 1968*



*Scientific and Technical Information Division*  
OFFICE OF TECHNOLOGY UTILIZATION  
NATIONAL AERONAUTICS AND SPACE ADMINISTRATION  
Washington, D.C.

1969

## FOREWORD

A technical meeting on compressible turbulent boundary layers was held at the Langley Research Center on December 10 and 11, 1968. This symposium was divided into the following sessions:

### ANALYTIC APPROACHES

Chairman: Ivan E. Beckwith, NASA Langley Research Center

### TURBULENT RESULTS FROM FLIGHT AND THE EFFECT OF ABLATION

Chairman: Robert L. Trimpi, NASA Langley Research Center

### BASIC STUDIES

Chairman: Howard K. Larson, NASA Ames Research Center

### THREE DIMENSIONAL, INTERACTING, AND INLET FLOWS

Chairman: James R. Sterrett, NASA Langley Research Center

### PANEL AND GENERAL DISCUSSION

Moderator: Mitchel H. Bertram, NASA Langley Research Center

A tour of high Reynolds number hypersonic facilities was arranged by Arthur Henderson, Jr., of the NASA Langley Research Center.

This meeting was held because of increasing concern about the many uncertainties in our knowledge of compressible turbulent boundary layers and their skin friction, heating, profiles, and other characteristics at a time when we are trying to evaluate various concepts for high-speed vehicles. Consideration of fundamental problems was important; however, as much as possible, we tried to avoid an esoteric and parochial viewpoint and keep in mind engineering use. Attempts were made to resolve some apparent discrepancies which face users of research results. The symposium had papers by authorities in university, company, and government research who gave the latest analytic and experimental results. Active specialists in the field of compressible turbulent boundary layers formed the bulk of the attendees and the audience was purposely kept small enough to encourage discussion.

Mitchel H. Bertram  
General Chairman and Editor

# CONTENTS

Paper	Page
1. Opening Address: THOUGHTS ON COMPRESSIBLE TURBULENT BOUNDARY LAYERS . . . . . By John Laufer, University of Southern California	1
2. CALCULATION OF INCOMPRESSIBLE TURBULENT BOUNDARY LAYERS - A REVIEW OF THE AFOSR-IFP-STANFORD 1968 CONFERENCE . . . . . By M. V. Morkovin, Illinois Institute of Technology, and S. J. Kline, Stanford University	15
3. A METHOD OF CALCULATING COMPRESSIBLE TURBULENT BOUNDARY LAYERS . . . . . By H. James Herring and George L. Mellor, Princeton University	27
4. ANALYSIS OF SOME SIMPLIFIED MODELS OF TURBULENCE . . . . . By Robert G. Deissler, NASA Lewis Research Center	133
5. ON THE APPLICABILITY OF TRANSFORMATION THEORY TO VARIABLE PROPERTY TURBULENT BOUNDARY LAYERS WITH PRESSURE GRADIENT AND HEAT AND MASS TRANSFER . . . . . By Constantino Economos, General Applied Science Laboratories, Inc.	149
6. AN ASSESSMENT OF CERTAIN PROCEDURES FOR COMPUTING THE COMPRESSIBLE TURBULENT BOUNDARY LAYER DEVELOPMENT . . . . . By Henry McDonald, United Aircraft Research Laboratories	181
7. CALCULATION OF TURBULENT SHEAR FLOWS THROUGH CLOSURE OF THE REYNOLDS EQUATIONS BY INVARIANT MODELING . . . . . By Coleman duP. Donaldson and Harold Rosenbaum, Aeronautical Research Associates of Princeton, Inc.	231
8. HYPERSONIC TURBULENT BOUNDARY-LAYER MEASUREMENTS USING AN ELECTRON BEAM . . . . . By J. E. Wallace, Cornell Aeronautical Laboratory, Inc.	255
9. COMMENTS ON HYPERSONIC TURBULENT BOUNDARY-LAYER MEASUREMENTS USING AN ELECTRON BEAM . . . . . By William D. Harvey and Dennis M. Bushnell, NASA Langley Research Center	309
10. SUMMARY AND CORRELATION OF SKIN-FRICTION AND HEAT-TRANSFER DATA FOR A HYPERSONIC TURBULENT BOUNDARY LAYER ON SIMPLE SHAPES . . . . . By Edward J. Hopkins, Morris W. Rubesin, Mamoru Inouye, Earl R. Keener, George C. Mateer, and Thomas E. Polek, NASA Ames Research Center	319
11. COMPARISON OF PREDICTION METHODS AND STUDIES OF RELAXATION IN HYPERSONIC TURBULENT NOZZLE-WALL BOUNDARY LAYERS . . . . . By Dennis M. Bushnell, Charles B. Johnson, William D. Harvey, and William V. Feller, NASA Langley Research Center	345



12.	A COMMENT ON COMPARISON OF PREDICTION METHODS AND STUDIES OF RELAXATION IN HYPERSONIC TURBULENT BOUNDARY LAYERS . . . . .	377
	By Robert A. Jones, NASA Langley Research Center	
13.	CROSSHATCHING . . . . .	381
	By Howard K. Larson and Philip R. Nachtsheim, NASA Ames Research Center	
14.	RECENT APPLICATIONS OF THE METHOD OF INTEGRAL RELATIONS TO TURBULENT BOUNDARY LAYERS WITH HEAT TRANSFER AND PRESSURE GRADIENTS . . . . .	389
	By Jack N. Nielsen and Gary D. Kuhn, Nielsen Engineering & Research, Inc.	
15.	SOME RECENT WORK ON COMPRESSIBLE TURBULENT BOUNDARY LAYERS AND EXCRESCENCE DRAG . . . . .	411
	By K. G. Winter and L. Gaudet, Royal Aircraft Establishment, Bedford, U. K.	
16.	DOWNSTREAM EFFECTS OF BOUNDARY LAYER TRIPS IN HYPERSONIC FLOW . . . . .	437
	By E. Leon Morrisette, David R. Stone, and Aubrey M. Cary, Jr., NASA Langley Research Center	
17.	MEASUREMENTS OF TURBULENT HEAT TRANSFER ON CONES AND SWEEPED PLATES AT ANGLE OF ATTACK . . . . .	455
	By Thomas E. Polek and George G. Mateer, NASA Ames Research Center	
18.	A NOTE ON THE EFFECT OF REYNOLDS NUMBER ON THE HEATING OVER THE LEE SURFACE OF A DELTA WING AT MACH 6 . . . . .	473
	By Allen H. Whitehead, Jr., NASA Langley Research Center	
19.	BOUNDARY LAYER AND STARTING PROBLEMS ON A SHORT AXISYMMETRIC SCRAMJET INLET . . . . .	481
	By J. R. Henry, E. H. Andrews, Jr., S. Z. Pinckney, and C. R. McClinton, NASA Langley Research Center	
20.	STUDIES OF THE INTERACTION OF A TURBULENT BOUNDARY LAYER AND A SHOCK WAVE AT MACH NUMBERS BETWEEN 2 and 10 . . . . .	509
	By Earl C. Watson, William C. Rose, Shelby J. Morris, Jr., and William F. Gallo, NASA Ames Research Center	
21.	PANEL AND GENERAL DISCUSSION . . . . .	545
	Moderator - Mitchel H. Bertram, NASA Langley Research Center	

LIST OF ATTENDEES . . . . .	565
-----------------------------	-----

# THOUGHTS ON COMPRESSIBLE TURBULENT

## BOUNDARY LAYERS

By John Laufer

The RAND Corporation\* and  
University of Southern California

### SUMMARY

A qualitative discussion of compressibility effects on turbulence is given. On the basis of this, a critical examination of the calculation techniques and transformation methods used for the prediction of mean velocity and temperature distributions is made.

### I. INTRODUCTION

In recent years extensive experimental and analytical work has been performed on supersonic and hypersonic turbulent boundary layers. It is of some interest, therefore, to attempt to extract the main features of these layers from the available information and to examine the potentialities of the various methods of predicting their behavior. Unfortunately, there are at least two circumstances that make such a task extremely difficult. First, in spite of the fact that a large amount of experimental data are available, very few measurements are of a quality high enough to serve as a guide for the various calculation schemes, and even fewer are the type that could give more insight on the turbulent motion itself. It is somewhat disconcerting, for instance, that since the work of Kistler (ref. 1) in 1959 no experiments have been reported on turbulent fluctuations in a compressible flow field above Mach four. Second, the increasing capability and extensive availability of computers have opened up countless possibilities in handling the compressible-boundary-layer equations. As a consequence, the ease of access to the computer has given rise to a large number of papers that use either questionable assumptions concerning the turbulent-transport terms or extensive empiricism; both of which are difficult to assess. The present paper is not intended to be an exhaustive review of the existing literature, but rather a critical assessment of the more promising approaches to boundary-layer problems not involving real gas effects.

It is quite evident that the development of a theory for the compressible turbulent boundary layer is out of the question; even for the incompressible case no such theory exists. Consequently, most analytical studies approach the problem either semiempirically or by some mathematical means, attempting to reduce it essentially to the problem of an incompressible fluid. In general these methods may be divided into three categories:

---

\*Consultant.

(1) Parametric approach. This technique does not tackle the complete boundary-layer problem, that is, the question of the velocity and temperature distributions, but concentrates on the technologically important question of the skin friction and of the heat-transfer coefficient prediction. It introduces new parameters (such as the wall-to-freestream temperature ratio and certain Mach number functions), with the help of which it seeks a logical correlation of the experimental data. This approach will not be considered in this paper mainly because it involves only certain aspects of the general problem and because in the opinion of the writer the empiricism is based on measurements whose accuracy needs further improvement. Nevertheless, the technique -- as proposed by Spalding and Chi (ref. 2), for instance -- appears to give quite satisfactory results over a wide range of Mach number and surface temperature conditions.

(2) Direct approach. The direct approach, in which the flow parameters, such as the mean velocity and the mean temperature, are computed from the compressible boundary-layer equations after some necessary assumptions concerning the turbulent transport and correlation terms have been made. The difficulty clearly centers around these assumptions and will be discussed subsequently.

(3) Transformation method. Here a mathematical transformation is being sought that would reduce the compressible equations to their incompressible form. One may use, then, the extensive and well documented empirical information available for the incompressible case and apply it to the compressible case by means of the transformation. Obviously, such a scheme could work only if the transformation correctly reflects all of the differences exhibited by the turbulent mechanism in a compressible flow as contrasted with one in an incompressible flow.

In order to prepare a basis for a critical examination of the methods listed above, we must understand compressible shear flows far better than we do today. Nevertheless, in the following section, an attempt will be made to describe the main features of these flows in the light of our present understanding.

## SYMBOLS

$u_i, u_j; u, v$  velocity components

$x_i, x_j; x, y$  spatial coordinates

$\rho$  gas density

$h$  static enthalpy

$H$  total enthalpy

$T$  gas temperature

$p$  pressure

$\tau_{ij}$	molecular shearing stress tensor
$q_i, q_j$	heat flux
$\varphi$	dissipation function
$\delta$	boundary-layer thickness
$\mu$	viscosity
$k$	coefficient of heat conductivity
$\epsilon$	turbulent viscosity
$\Psi$	stream function
$T_0$	stagnation temperature
$T_\infty$	freestream temperature

## II. SOME SALIENT FEATURES OF A COMPRESSIBLE TURBULENT BOUNDARY LAYER

Besides the presence of vorticity fluctuations, the most obvious and characteristic feature of turbulence in a compressible medium is the presence of fluctuations in temperature and density. In addition, the pressure fluctuations, instead of being mainly the result of geometric constraints (as in the incompressible case) and of second-order importance  $[O(\overline{pu'^2})]$ , become thermodynamic variables and could, in fact, attain the same order of magnitude as the other fluctuating quantities. Clearly, this is the situation in a random sound field.

One of the first questions one has to clarify is the following: Do these various fluctuation modes interact with each other, and if so, how do they interact? The most relevant study of this question was made by Chu and Kovasznay (ref. 3), who considered a homogeneous flow field (zero gradients of the mean flow parameters) in which the amplitudes of the modes were small and comparable in magnitude. They found that interaction occurs only to second order in amplitude, the most interesting being the generation of the sound mode due to vorticity-vorticity interaction. Interestingly, the temperature (or entropy) mode does not interact with the vorticity mode to the second order. It would be a very difficult if not impossible task to extend this work to flow fields with mean gradients, like a boundary layer. At present we will have to be satisfied with some rather coarse, qualitative arguments concerning the more restrictive question of the influence of the fluctuating entropy and sound modes on the mean flow field only. Unfortunately, even to answer this simple problem one has to speculate on the effect of these modes on the vorticity mode. For this purpose we will examine the governing equations of mean motion in a spirit similar to that of Morkovin (ref. 4).

We will consider these equations in the same form as given by Favre (ref. 5), in which the quantities  $\tilde{u}_i$ ,  $\tilde{T}$ ,  $\tilde{h}$ ,  $\tilde{H}$  are mass-weighted averages indicated by the tilde sign over the symbols. The bar sign over the symbols corresponds to conventional averaging. Thus,

$$u_i = \tilde{u}_i + u'_i \quad \text{where} \quad \tilde{u}_i \equiv \frac{\overline{\rho u_i}}{\bar{\rho}}$$

therefore

$$\overline{\rho u'_i} = 0 \quad \text{and} \quad \overline{u'_i} = - \frac{\overline{\rho' u'_i}}{\bar{\rho}}$$

$$p = \bar{p} + p' \quad \text{where} \quad \overline{p'} = 0$$

Conservation of mass is given by

$$\frac{\partial \bar{\rho} \tilde{u}_j}{\partial x_j} = 0 \quad (1)$$

Conservation of mean momentum is given by

$$\frac{\partial}{\partial x_j} \bar{\rho} \tilde{u}_i \tilde{u}_j = - \frac{\partial \bar{p}}{\partial x_i} + \frac{\partial}{\partial x_j} \left( \bar{\tau}_{ij} - \overline{\rho u'_i u'_j} \right) \quad (2)$$

Conservation of mean enthalpy is given by

$$\frac{\partial}{\partial x_j} \bar{\rho} \tilde{u}_j \tilde{h} = \tilde{u}_j \frac{\partial \bar{p}}{\partial x_j} + \overline{u'_j \frac{\partial p}{\partial x_j}} + \frac{\partial}{\partial x_j} \left( \bar{q}_j - \overline{\rho h' u'_j} \right) + \bar{\varphi} \quad (3)$$

In addition it will be useful to record the following two equations:

Conservation of mean kinetic energy is given by

$$\frac{\partial}{\partial x_j} \frac{1}{2} \bar{\rho} \tilde{u}_j \tilde{u}_i \tilde{u}_i = - \tilde{u}_j \frac{\partial \bar{p}}{\partial x_j} + \overline{\rho u'_i u'_j \frac{\partial \tilde{u}_i}{\partial x_j}} + \frac{\partial}{\partial x_j} \left[ \tilde{u}_i \left( \bar{\tau}_{ij} - \overline{\rho u'_i u'_j} \right) \right] - \bar{\Phi} \quad (4)$$

Conservation of turbulent kinetic energy is given by

$$\frac{\partial}{\partial x_j} \frac{1}{2} \overline{\tilde{u}_j \rho u'_i u'_i} = -\overline{u'_j \frac{\partial p}{\partial x_j}} - \overline{\rho u'_i u'_j \frac{\partial \tilde{u}_i}{\partial x_j}} + \frac{\partial}{\partial x_j} \left[ \overline{u'_i \left( \tau_{ij} - \frac{1}{2} \rho u'_i u'_j \right)} \right] - \overline{\varphi'} \quad (5)$$

In the equations  $\overline{\tau_{ij}}$  is the mean molecular stress tensor, which in general includes the correlation between the viscosity fluctuations and the gradients of the velocity-fluctuation terms (see ref. 5). Similarly, the mean heat-flux vector contains correlation terms between the coefficient of heat-conductivity fluctuations and those of the temperature gradients. The mean dissipation function is written in two terms:

$$\overline{\varphi} = \overline{\Phi} + \overline{\varphi'} \quad (6)$$

where

$$\overline{\Phi} = \overline{\tau_{ij} \frac{\partial \tilde{u}_i}{\partial x_j}} \quad (7)$$

and

$$\overline{\varphi'} = \overline{\tau_{ij} \frac{\partial u'_i}{\partial x_j}} \quad (8)$$

In examining these equations it is immediately apparent that (without considering the enthalpy equation) they have the same form term by term as those for an incompressible flow with two exceptions: the viscous stresses and the Reynolds stresses include fluctuations in viscosity and in density, respectively. The importance of these terms, as well as of the character of the terms containing the pressure fluctuations, will be examined in some detail. For this purpose, it is convenient to discuss flows below Mach 5 separately from those above it.

#### A. Supersonic Case ( $M < 5$ )

Below Mach 5 experimental results are available concerning the fluctuating flow field which help considerably to estimate the order of magnitude of the terms under consideration. In particular the following observations, based on Kistler's work (ref. 1), can be made:

- (1) The turbulent kinetic energy distribution across the boundary layer (he actually measured  $\overline{u'^2}$  only) is qualitatively similar to that found in the

incompressible case, suggesting that the whole turbulence production mechanism also is similar in spite of the presence of temperature fluctuations.

(2) The temperature-fluctuation levels scale with an average mean temperature across the layer

$$\frac{\sqrt{\overline{T'^2}}}{\overline{T}} \approx 2 \frac{T_o - T_\infty}{T_o + T_\infty} f\left(\frac{y}{\delta}\right) \quad (9)$$

where  $f(y/\delta)$  is a function independent of the Mach number having a maximum value of about 0.1.

(3) The temperature fluctuations are essentially isobaric, so

$$\frac{T'}{\overline{T}} \approx - \frac{\rho'}{\overline{\rho}} \quad (10)$$

Incidentally, this is not a direct result of measurements, but rather is a relationship that is consistent with other observations (ref. 1). Equation (10) has the following important consequences: it implies first that in the Mach number range under consideration the energy in the sound mode is small compared to those of the vorticity and entropy modes; second, that the pressure fluctuations produced by the vorticity bearing velocity fluctuations are of higher order and can be neglected, as the velocity and temperature fluctuations cannot be.

On the basis of the above observations it is reasonable to assume that

$$\frac{\overline{\mu' \frac{\partial u'}{\partial y}}}{\overline{\mu} \frac{\partial \tilde{u}}{\partial y}} \ll 1 \quad \text{and} \quad \frac{\overline{\rho' u' v'}}{\overline{\rho} \overline{u' v'}} \ll 1 \quad (11)$$

In each case the ratios are believed to be less than 5 percent if the coefficients for viscosity to velocity gradient correlations and for density to  $u'v'$  fluctuation correlations are at most 0.3, a conservative estimate.

It is seen now that when these inequalities are introduced into the momentum, the mean, and the turbulent kinetic energy equations, the equations will not show any dependence on the temperature (or density) fluctuations in an explicit way. As for implicit dependence of the velocity field on the temperature fluctuation, it is much more difficult to draw conclusions from inspection of the equations alone. The most obvious interaction comes through the turbulent-dissipation term  $\overline{\varphi'}$  in equation (5). A dissipation rate, increased by turbulence, modifies the mean enthalpy distribution [eq. (3)] and therefore the

mean density, which in turn produces changes in the mean velocity distribution. Such a feedback mechanism is believed to be negligible in the Mach number range under consideration (ref. 4).

Barring any other less obvious dependence, one may conclude first that the temperature fluctuations produced by the vorticity modes do not back-react on the velocity field; i.e., they are passive. Second, for the case of zero pressure gradient, the momentum equation is coupled to the enthalpy equation only through the spatial variation of the mean density and viscosity. This suggests the possibility that -- as in the laminar case -- an appropriate coordinate stretching (and an assumption concerning the viscosity-density relation) would decouple the two equations. This in turn implies that the density variation has a kinematic or volumetric rather than a dynamic effect on the velocity field in a compressible turbulent medium. A similar situation might be true in the presence of mild pressure gradients when no shock waves are present in the boundary layer.

#### B. Hypersonic Case ( $M > 5$ )

Unfortunately, in the flow range above Mach 5, no detailed turbulent fluctuation measurements have been reported so far. It is therefore very difficult to talk about the fluctuations in the boundary layer and their effect on the mean velocity distribution. There are at least two circumstances, however, that will undoubtedly influence the character of the boundary layer: (1) the growing importance of the sound modes; and (2) low Reynolds number effects near the solid boundary. These will be discussed next in more detail.

(1) Nature of the pressure fluctuations. There is convincing experimental evidence that in flows in the vicinity of  $M = 5$  appreciable pressure fluctuations exist in the boundary layer. Kistler and Chen (ref. 6) reported r.m.s. pressure fluctuations of 8 to 10 percent of the mean static pressure at  $M = 5$  and  $Re_0 = 10^4$  at the wall. Under the same conditions Laufer (ref. 7) measured  $\sqrt{p'^2}/\bar{p} \approx 1$  percent just outside the boundary layer where these fluctuations are of the sound-mode type. This type of fluctuation is expected to play a more and more important role in the turbulent-energy balance with increasing Mach number.

(2) Low Reynolds number effects near the wall. As the Mach number increases, the temperature, and therefore the viscosity, near the wall increases. It is to be expected then that viscous effects diffuse farther away from the wall and dominate a larger portion of the boundary layer at higher Mach numbers. There is, in fact, some evidence (ref. 8) that the so-called two-layer model of a turbulent boundary layer with a well established "overlap" or logarithmic region might not be applicable in the hypersonic-flow regime. Unfortunately, the number of experimental observations available at present is insufficient to enable one to modify the currently accepted model.



### III. METHODS FOR PREDICTING MEAN VELOCITY AND TEMPERATURE DISTRIBUTIONS IN COMPRESSIBLE TURBULENT BOUNDARY LAYERS

As is indicated in the Introduction, there are mainly two methods available with which to study turbulent boundary layers. In this section they will be critically examined in the light of the previous discussion.

#### A. The Direct Approach

With modern computational techniques it is possible to solve simultaneous partial differential equations such as the equations of motion. However, in turbulent flows, before one may proceed with the computations, several correlation terms appear which have to be considered. For the purpose of discussion, we will consider the two-dimensional case only. After introducing the conventional boundary-layer approximations and the inequality (11), equations (1), (2), and (3) become

$$\frac{\partial \bar{\rho} \tilde{u}}{\partial x} + \frac{\partial \bar{\rho} \tilde{v}}{\partial y} = 0 \quad (12)$$

$$\bar{\rho} \tilde{u} \frac{\partial \tilde{u}}{\partial x} + \bar{\rho} \tilde{v} \frac{\partial \tilde{u}}{\partial y} = - \frac{d\bar{p}}{dx} + \frac{\partial}{\partial y} \left( \bar{\mu} \frac{\partial \tilde{u}}{\partial y} - \overline{\rho u' v'} \right) \quad (13)$$

$$\bar{\rho} \tilde{u} \frac{\partial \tilde{h}}{\partial x} + \bar{\rho} \tilde{v} \frac{\partial \tilde{h}}{\partial y} = \tilde{u} \frac{d\bar{p}}{dx} + \overline{u'} \frac{d\bar{p}}{dx} + \overline{u'_i \frac{\partial p'}{\partial x_i}} + \frac{\partial}{\partial y} \left( \bar{k} \frac{\partial \tilde{h}}{\partial y} - \overline{\rho h' v'} \right) + \bar{\mu} \left( \frac{\partial \tilde{u}}{\partial y} \right)^2 + \overline{\varphi'} \quad (14)$$

In place of equation (13), the equation expressing the total enthalpy conservation is often convenient to use. We define the mass-weighted total enthalpy as follows:

$$H = \tilde{H} + H' \quad \text{where} \quad \tilde{H} = \frac{\overline{\rho H}}{\bar{\rho}} \quad \text{and} \quad \overline{\rho H'} = 0 \quad (15)$$

thus

$$\tilde{H} = \tilde{h} + \frac{1}{2} \tilde{u}_i \tilde{u}_i + \frac{\overline{\rho u'_i u'_i}}{2 \bar{\rho}} \quad (16)$$

and

$$H' = h' + \tilde{u}_i u'_i + \frac{1}{2} u'_i u'_i - \frac{\overline{\rho u'_i u'_i}}{2 \bar{\rho}}$$

The conservation equation for total enthalpy is thus obtained by adding equations (3), (4), and (5)

$$\bar{\rho} \tilde{u}_j \frac{\partial \tilde{H}}{\partial x_j} = \frac{\partial}{\partial x_j} \left[ \bar{q}_i - \overline{\rho h' u'_j} + \tilde{u}_i (\bar{\tau}_{ij} - \overline{\rho u'_i u'_j}) + \overline{u'_i (\tau_{ij} - \frac{1}{2} \rho u'_i u'_j)} \right] \quad (17)$$

Applying now the boundary-layer approximations one arrives at the following form:

$$\begin{aligned} \bar{\rho} \tilde{u} \frac{\partial \tilde{H}}{\partial x} + \bar{\rho} \tilde{v} \frac{\partial \tilde{H}}{\partial y} = \frac{\partial}{\partial y} \left[ \bar{k} \frac{\partial \tilde{h}}{\partial y} - \overline{\rho h' v'} + \tilde{u} \left( \bar{\mu} \frac{\partial \tilde{u}}{\partial y} - \overline{\rho u' v'} \right) \right] + \frac{\partial}{\partial x_j} \overline{u'_i \tau_{ij}} + \\ + \frac{\partial}{\partial y} \frac{1}{2} \overline{\rho v' u'_i u'_i} \end{aligned} \quad (18)$$

The "direct approach" consists of the simultaneous solutions of equations (12), (13), and (18) with the appropriate boundary conditions. The main difficulty -- as in any other turbulence problem -- is the proper accounting for the correlation terms arising in these equations. Before discussing the turbulent transport terms  $\overline{\rho u' v'}$  and  $\overline{\rho h' v'}$ , the last two terms of equation (18) will be considered. In all the published works on this method these terms have been neglected. There is ample evidence (refs. 9 and 10), however, that these terms are not small, especially at the outer edge of the viscous sublayer, where they are about the magnitude of the turbulent-production term. In fact, the measurements indicate that the turbulent energy dissipation rate approximately balances the production rate across most of the boundary layer. This error clearly has to be remedied by making some appropriate assumption concerning these terms.

The problem of expressing the turbulent-transport quantities in terms of the mean velocity or enthalpy is a well known and much-discussed one even in low-speed flows. The Boussinesq formulation for the Reynolds shear stress is usually adopted. Although there are some serious objections to this formulation, there is evidence that, provided no sudden changes in pressure gradient occur, it serves as an adequate tool for mean-velocity calculations. Accordingly, we write

$$-\overline{u' v'} = \epsilon \frac{\partial \tilde{u}}{\partial y} \quad (19)$$

where the turbulent viscosity  $\epsilon$  has to be appropriately specified. In order to do that, the experimentally well-substantiated two-layer model of the boundary layer is used. In the outer region, the so-called "law of the wake" region, the suggestion of Clauser (ref. 11) for low-speed flow is adopted unchanged; i.e.,

$$\epsilon \sim \int_0^\infty (U_1 - u) dy \quad (20)$$

It is to be noted that the density does not appear explicitly in this definition. In fact, were the displacement or momentum thickness to be used for the characteristic length in the expression for  $\epsilon$ , the computation results would give unsatisfactory agreement with measurements. This is believed to be a consequence of the conclusion, given in Section II.A., that the density variation has only a kinematic effect on the turbulent exchange mechanism.

In the inner or "law of the wall" region exist several formulations for  $\epsilon$ . A good list of references is given in reference 12. It is doubtful that a "correct" formulation exists in this region. Experience indicates that the mean-velocity distribution is not very sensitive to the exact form assumed for  $\epsilon$ , provided, of course, that the formulation is consistent with the constraints imposed by the "law of the wall."

For the turbulent heat transfer, it is customary to assume that the turbulent Prandtl number is constant across the layer. This, in fact, seems to be the only practical course to take, since no reliable measurements exist, so far, especially near the wall, that would give guide lines on this subject.

The calculations using the direct approach seem to be quite promising (refs. 12 and 13). Although an incomplete energy equation is used, they show surprisingly good agreement with measured mean velocity distributions and skin-friction data in the supersonic flow regime ( $M < 5$ ). Less satisfactory agreement is obtained for the Mach number distributions and heat-transfer data. It would be most interesting to recalculate these using an improved energy equation.

### B. Transformation Method

If we accept the conclusion (in Section II) that the density variation does not couple the momentum and energy equations in a "force-like" manner but only "kinematically," one could conjecture that by an appropriate coordinate stretching, such as the Dorodnitsyn transformation, the two equations could be decoupled as is done in the laminar case. The attractive aspect of this approach is that no new assumption concerning the compressible turbulent-transport terms would have to be made. This approach was followed by several authors (refs. 14 and 15). Their work was criticized, however, mainly for two reasons: (1) they assumed without giving justification that the Reynolds stress  $\rho u'v'$  correctly transforms into its incompressible equivalent, and (2) the predicted skin-friction coefficients do not follow a Reynolds number trend shown by experiments. Later Coles (ref. 16) suggested a more general transformation and a formulation that remedied the above difficulties. For constant pressure and adiabatic flows, his method provides reliable skin-friction coefficients up to moderately high Mach numbers. Thus, the parameters in the transformation have been adjusted adequately to obtain a one-to-one correspondence between the compressible and incompressible skin friction. It is not clear, in fact it is somewhat doubtful (refs. 17 and 18), that such a correspondence in mean velocity and temperature could also be achieved throughout the boundary layer without making additional assumptions. Recently, the author looked into this question, and his results are briefly described below.

Coles' transformation is applied to the time-dependent (rather than the averaged) continuity and momentum equations with zero pressure gradient. The transformation for the stream function and coordinates is given by

$$\Psi = \sigma \psi, \quad X = \xi x, \quad \frac{\partial Y}{\partial y} = \frac{\rho}{R} \eta \quad (21)$$

where the parameters  $\sigma$ ,  $\xi$ , and  $\eta$  are functions of  $x$  alone; the coordinate  $Y$  depends on both the temporal and the spatial coordinates, and capital letters correspond to the incompressible- and lower case letters to the compressible-flow variables. After averaging the transformed equations (ref. 19), one obtains

$$\frac{\partial \bar{U}}{\partial X} + \frac{\partial \bar{V}}{\partial Y} = - \frac{\sigma}{\xi \eta} \frac{1}{\rho} \overline{\frac{\partial \rho v'}{\partial y}} + \dots \quad (22)$$

$$R \left( \bar{U} \frac{\partial \bar{U}}{\partial X} + \bar{V} \frac{\partial \bar{U}}{\partial Y} \right) = - \frac{R\sigma}{\xi \eta^2} \psi \frac{\partial \tilde{u}}{\partial y} \frac{d\sigma}{dx} + \frac{\sigma \eta}{R \xi} \frac{\partial}{\partial Y} \rho \mu \frac{\partial \bar{U}}{\partial Y} - \frac{R\sigma^2}{\xi \eta} \frac{\partial \overline{U'V'}}{\partial Y} + \dots \quad (23)$$

where higher-order terms have been neglected. It is noted that these equations reduce to the incompressible form if the following assumptions are made:

- (1)  $\sigma$ ,  $\eta$ ,  $\xi$  are constants,
- (2)  $\rho \mu = \text{constant}$ ,
- (3) the "apparent" source term in equation (22) is zero.

The first two conditions are identical to those usually imposed for the laminar problem and were also used by Mager (ref. 14). Assumption (3) is difficult to justify without some experimental information. In the outer region of the boundary layer it probably is reasonable, near the wall, less so. Perhaps a more judicious choice for the streamline transformation that would eliminate the apparent mass flow  $\overline{\rho'v'}$  across the streamline might minimize the difficulty. If this could indeed be achieved, the method would be more promising.

#### IV. CONCLUSION

It is quite apparent that in order to gain further understanding of the compressible turbulent boundary layer more basic experiments need to be performed. There are three types of measurements that would be especially useful:

- (1) An experiment in a low-speed boundary layer with heat transfer giving special emphasis to the direct measurements of  $\overline{\rho u'v'}$  and  $\overline{\rho T'v'}$  for the purpose of investigating the distribution of the turbulent Prandtl number, especially near the wall. An assessment of the importance of the turbulent-

dissipation and pressure-diffusion terms in the energy equation would also be helpful.

(2) Extension of Kistler's measurements in the range above Mach 5.

(3) More accurate measurements of mean velocity and mean temperature (or density) in the hypersonic regime.

These experiments would undoubtedly help to generate a more consistent empirical formulation of the hypersonic boundary-layer problem and would improve the present methods of mean velocity and mean temperature distributions.

#### REFERENCES

1. Kistler, Alan L.: Fluctuation Measurements in a Supersonic Turbulent Boundary Layer. *Phys. Fluids*, vol. 2, no. 3, May-June 1959, pp. 290-296.
2. Spalding, D. B.; and Chi, S. W.: The Drag of a Compressible Turbulent Boundary Layer on a Smooth Flat Plate With and Without Heat Transfer. *J. Fluid Mech.*, vol. 18, pt. 1, Jan. 1964, pp. 117-143.
3. Chu, Boa-Teh; and Kovasznay, Leslie S. G.: Non-Linear Interactions in a Viscous Heat-Conducting Compressible Gas. *J. Fluid Mech.*, vol. 3, pt. 5, Feb. 1958, pp. 494-514.
4. Morkovin, Mark V.: Effects of Compressibility on Turbulent Flows. *The Mechanics of Turbulence*. Gordon and Breach Sci. Publ., Inc., c.1964, pp. 367-380.
5. Favre, A.: Equations des Gaz Turbulents Compressibles. *J. Mecan.*, vol. 4, no. 3, Sept. 1965, pp. 361-390.
6. Kistler, A. L.; and Chen, W. S.: The Fluctuating Pressure Field in a Supersonic Turbulent Boundary Layer. *J. Fluid Mech.*, vol. 16, pt. 1, May 1963, pp. 41-64.
7. Laufer, John: Some Statistical Properties of the Pressure Field Radiated by a Turbulent Boundary Layer. *Phys. Fluids*, vol. 7, no. 8, Aug. 1964, pp. 1191-1197.
8. Bertram, Mitchel H.; and Neal, Luther, Jr.: Recent Experiments in Hypersonic Turbulent Boundary Layers. Presented at the AGARD Specialists' Meeting on Recent Developments in Boundary-Layer Research (Naples, Italy), May 10-14, 1965.
9. Laufer, John: The Structure of Turbulence in Fully Developed Pipe Flow. NACA Rep. 1174, 1954. (Supersedes NACA TN 2954.)
10. Klebanoff, P. S.: Characteristics of Turbulence in a Boundary Layer With Zero Pressure Gradient. NACA Rep. 1247, 1955. (Supersedes NACA TN 3178.)

11. Clauser, Francis H.: Turbulent Boundary Layers in Adverse Pressure Gradients. J. Aeron. Sci., vol. 21, no. 2, Feb. 1954, pp. 91-108.
12. Herring, H. James; and Mellor, George L.: A Method of Calculating Compressible Turbulent Boundary Layers. NASA CR-1144, 1968.
13. Smith, A. M. O.; and Cebeci, T.: Numerical Solution of the Turbulent-Boundary-Layer Equations. Rep. No. DAC 33735 (Contract NOW 66-0324-c), Douglas Aircraft Co., Inc., May 29, 1967.
14. Mager, Artur: Prediction of Shock-Induced Turbulent Boundary-Layer Separation. J. Aeron. Sci. (Readers' Forum), vol. 22, no. 3, Mar. 1955, pp. 201-202.
15. Burggraf, O. R.: The Compressibility Transformation and the Turbulent-Boundary-Layer Equations. J. Aerosp. Sci., vol. 29, no. 4, Apr. 1962, pp. 434-439.
16. Coles, Donald: The Turbulent Boundary Layer in a Compressible Fluid. Phys. Fluids, vol. 7, no. 9, Sept. 1964, pp. 1403-1423.
17. Crocco, L.: Transformations of the Compressible Turbulent Boundary Layer With Heat Exchange. AIAA J., vol. 1, no. 12, Dec. 1963, pp. 2723-2731.
18. Baronti, Paolo O.; and Libby, Paul A.: Velocity Profiles in Turbulent Compressible Boundary Layers. AIAA J., vol. 4, no. 2, Feb. 1966, pp. 193-202.
19. Laufer, J.: On Turbulent Shear Flows of Variable Density. AIAA Paper No. 68-41, Jan. 1968.

# CALCULATION OF INCOMPRESSIBLE TURBULENT BOUNDARY LAYERS - A REVIEW

## OF THE AFOSR-IFP-STANFORD 1968 CONFERENCE

By M. V. Morkovin and S. J. Kline

Illinois Institute of Technology and Stanford University

### SUMMARY

The primary objective of the conference reviewed was calibration of the numerous procedures for analyzing turbulent boundary layers. Summaries of the state of knowledge regarding separation, the structure of turbulence, and other related "physics" and research needs were also undertaken. Overall policy for the conference was set by the Executive Committee<sup>1</sup> with guidance from an International Advisory Board.

Conference preparation included selection and standardization of a set of base data for comparison with theory. This task was undertaken by a Committee headed by Prof. D. E. Coles. Thirty-three flows were selected and 16 of these flows made "mandatory" for workers submitting prediction papers to the conference. Ultimately, prediction of at least  $R_\theta$ ,  $H$ , and  $C_f$  for the mandatory flows were completed for 30 prediction methods, and these data are compiled in a form for ready comparison in the proceedings (refs. 1 and 2).

An evaluation committee provided a rough order of merit of reliability with which various methods predict the mandatory flows, and used this information to examine the utility and promise of various physical assumptions and mathematical frameworks.

### SORTING OUT FACTS AND THEORY IN TURBULENCE RESEARCH

Progress in prediction of turbulent shear flows has been hampered by lack of broad, reliable, standardized data. It has been typical for workers with a new theory to make comparisons with two to half a dozen flows and on this basis claim good agreement and hence a successful method. It is sobering to recognize that discrepancies of 30 percent (and in a few cases even more) existed in the published data solely owing to differences in methods by which the data had been handled by various workers. Thus not only the theories, but also the data have been rather fuzzy entities based on varying combinations of explicit and implicit assumptions. Hence, the first task of the conference was to establish a well-standardized reliable set of data. After some discussion it was decided to limit

---

<sup>1</sup>Executive Committee: D. E. Coles, M. V. Morkovin (Chairman), and G. Sovran. Advisory Board: F. H. Clauser, H. W. Emmons, H. P. Liepmann, J. C. Rotta, and I. Tani.

these data to incompressible, two-dimensional, smooth wall flows for several reasons: (1) this is a base class upon which one expects extension to other important cases such as compressible or three-dimensional flow to be grounded, (2) there are more and better data for this class than any other, and (3) the advent of the computer has led to the proliferation of methods for this class to the point where an acute problem of choice had been created for the potential user, and it seemed highly desirable to see what could be accomplished toward resolving this problem. From this attempt one should also hopefully learn a considerable amount about profitable methods for potential extension to other important cases. Fortunately, the computer also makes possible much more extensive comparisons than were typical in the era of hand computations. Even so, the magnitude of the task can be appreciated when it is realized that nearly 3000 curves are presented in the summary of output in the conference proceedings.

Ultimately, 75 workers assembled to discuss these results, needs for further research, and the status of knowledge in the underlying physics. These workers included nearly all researchers with a current prediction method, most of the individuals who have taken important data, and a major fraction of the researchers in shear flow physics. As a result, the discussions were unusually intensive, and a very large amount of significant discussion was generated, and is recorded in the proceedings. We cannot cover here all the important facets of these results, and will therefore confine ourselves primarily to a description of the points of most interest for extension to compressible flow. It should be emphasized that the results of the conference in a very real sense arise from a cooperative effort of the "boundary layer research community" since essentially all attendants contributed to the work of the conference in significant ways. However, it should be emphasized that the opinions that follow are offered as private observers and not as officers of the conference.

## THE DATA

Since the question of "What does constitute good experimental evidence for testing compressible turbulent theories?" is bound to arise at the present Symposium, it is perhaps worthwhile at the outset to quote from Coles' contribution to the Summary Session at Stanford (ref. 2). With respect to the much easier low-speed experiments, Coles commented:

"From the special vantage point provided by this<sup>2</sup> Conference, we can see that definitive mean-flow experiments are still missing in almost all areas of the boundary-layer problem. By this I mean experiments in which all of the various terms in the mean momentum equation are measured, preferably by redundant methods, and a satisfactory balance demonstrated."

In absence of such definitive experiments Coles has long called for a consistent conceptual framework within which to test the credibility of sets of turbulent experiments (refs. 3 to 5). In his detailed clarification of the uniform

---

<sup>2</sup>Reference 1, p. 434.



handling of the experimental data for the 33 turbulent layers (ref. 2), pointedly entitled "The young person's guide to the data", Coles adopts the double similarity formulations of the inner wall behavior and the outer wake behavior as the lightest analytical skeleton to bear the weight of the data. In developing the rationale of various corrections, Coles discusses many adverse factors including: three-dimensional effects; concern for tripping devices; probe size, shape and displacement; streamwise wall curvature; mean measurements in absence of corrections for turbulence effects; sensitivity of integral thicknesses to the few data points near the wall; and effects of outer intermittency. Furthermore, the 30 percent discrepancy that arises solely from inconsistent methods of handling the data contains an important warning concerning calibration of predictive theories for compressible flow in the absence of an accepted framework for standardizing the data.

Most people will agree that the accuracy and consistency of the compressible experimental information does not match that of its low-speed counterpart, dissected so clinically by Coles. It is not so long ago that Danberg (ref. 6) demonstrated that much of the earlier reported stagnation temperature data may be in error because calibration in a uniform stream may not correspond to that in a shear layer. The low Reynolds numbers of most high-speed wind-tunnel tests even raise questions concerning the fully developed state of the measured turbulent layers. In fact, most of these adverse factors are even more adverse at supersonic and hypersonic speeds. The lessons from the low-speed developments thus seem to suggest that establishment of definitive mean-flow experimental standards in the sense defined by Coles be considered as a collective "must" for the compressible turbulent community. Funding officers may appreciate that a solid expensive program now would result in large net savings in the long run as well as achieving reliable, verified theories at a much earlier time.

One suspects that it will require much more effort to bring the compressible cases to as good a basis as those now established for the incompressible cases owing to the extra degrees of freedom involved. True, dimensional arguments indicate that one still has viscous scaling near the wall, but it is variable in that it depends on Mach number and heat transfer. The scaling in the outer flow is even more controversial in regard to the effect of mean density; again we await more definitive experiments for clarification.

The sum of all this discussion suggests two things. First, without the establishment of a body of accepted standardized data, it will be difficult, if not impossible, to reach agreement on what theories, if any, are reliable predictors. There is real danger that theories for compressible flow will proliferate as the incompressible ones did in the past, and that much of this effort will be wasted because of the inability to judge the relative merits of the various procedures. The user will again be faced with an acute problem of choice, and will have even less chance of resolving it. Second, the magnitude of the task of establishing such a body of data suggests re-examination of the relative investment in experimental as opposed to theoretical effort at this time and also suggests that careful planning and cooperative efforts may be needed to reach the desired state in a reasonable time and at reasonable costs.

## PREDICTIVE PROCEDURES

Of the 30 methods compared with the 16 mandatory flows (and in many cases all 33 flows), more than half were significantly revised during the course of the preparation for the conference, and the results could be viewed in many cases as an entirely new method. Thus the effects of a large body of standardized data immediately affected the state of the art. Several methods have continued to develop after the conference as well so that today their relative standings have probably already shifted.

Despite these revisions, the conclusions of the special five man evaluation committee<sup>3</sup> contain a number of lessons for extensions to compressible flow. The most important single conclusion for this purpose, in the writers' opinion, is the following:

"Most of these methods have made use of accumulated 'know-how' and perform quite well."

Indeed, the writers believe that about a dozen of the methods predict  $R_0$ ,  $H$ , and  $C_f$  for the mandatory flows about as well as can be expected in view of the residual uncertainties in the data. This conclusion is clearly in contradiction to the widely held belief that no acceptable method existed for prediction of turbulent boundary layers. This statement emphasizes the fact that the research community as well as the users definitely did not have a clear picture of the situation prior to the AFOSR-IFP-Stanford Conference (refs. 1 and 2), and that the acute problem of choice was indeed a very real one.

The evaluation committee further recommended:

"Any method in the lower third [regarding reliable prediction of the mandatory flows] should either be improved or abandoned. Many of the well-performing methods are available from the originators so that further proliferation of methods without clearly superior features is undesirable in the opinion of the committee."

As one predictor commented after the meeting, "We have been wasting our time on this problem for some years, and it is now obvious we should stop doing so and get on with extensions to other important technical applications." As will already be obvious, the writers wholeheartedly agree, and have in fact listed some of these problems and also some matters of physics that are now missing from all the theories and need to be included in the editors' summary remarks of the AFOSR-IFP-Stanford Conference.

Also in preparation for the meeting, W. C. Reynolds of the Host Committee<sup>4</sup> prepared "a morphology of the prediction methods." Tables 1 and 2 taken from

---

<sup>3</sup>D. J. Cockrell, H. W. Emmons (Chairman), P. G. Hill, J. L. Lumley, and M. V. Morkovin.

<sup>4</sup>E. A. Hirst, S. J. Kline (Chairman), and W. C. Reynolds.

this paper show the various classes; the symbols show the first letter of the surnames of the first two authors or for single authors the first two letters of the surname; thus AD for Abbott, Diewert, Forsnes and Deboy; Al for Alber. The clarity of Reynolds' paper recommends it as an introduction to any classroom discussion of turbulent boundary layers.<sup>5</sup> It was available to the predictors 6 months in advance of the Conference and was used for standardization, for minimization of duplication, and for organization of the presentations at the Conference itself.

The evaluation committee also used this classification to study the effectiveness of various physical inputs and mathematical frameworks. Contrary to what might be expected, no preferred class or classes emerged. It would appear that success in prediction now depends more on skill in fitting and on use of sufficiently broad classes of data than on the particular framework employed. There is some suggestion that inclusion of the law of the wall (or equivalent information) is important, since all the successful methods do include this information and many less successful ones do not, but this is not explicitly clear. Moreover, it appears that the better integral procedures predict  $R_\theta$ ,  $H$ , and  $C_f$  essentially as well as the better differential (field) methods. Since the field methods generally require more initial information beyond that specified in the data for each flow, strict comparisons were difficult to make. The Evaluation Committee wished it could have had an extra week or so to assess the significant differences between the methods such as breadth of applicability, computing time and cost, ease of use, etc. Various possible approaches to evaluation of the methods are summarized by M. V. Morkovin in "On criteria of assessing prediction methods" in reference 1. Since all the methods had been set up for computer runs in the Stanford IBM 360/67 by students in order to check completeness and repeatability, it was possible to eliminate some differences regarding use of initial conditions during the week of the conference to provide the Evaluation Committee with as comparable results as possible. However, some differences are inherent and cannot be eliminated.

Regarding the viability of integral as opposed to differential schemes, the Evaluation Committee concluded:

"While the best field and integral methods are about equal in the  $10^6$ -operations era, it is anticipated that only the field methods have the potential to expand into really 3D problems (e.g., a vortex generator in a wing boundary layer) as computers reach the  $10^9$ -operations era."

The Evaluation Committee repeatedly stressed the continuing need for more and improved data for a variety of purposes including not only the extensions to compressible and three-dimensional flows, but also for such matters as the evaluation of the importance of initial conditions, the establishments of the

---

<sup>5</sup>A companion recommended survey of the physics and mathematics of turbulent boundary layers is reference 7 by P. Bradshaw.

magnitudes of effects such as wall curvature, coreolis forces, buoyancy,<sup>6</sup> etc., and the provision of data with redundant checks and complete closure of the momentum equation including three-dimensionality.

To give the reader an appreciation for the type of comparative performance dealt with, the specific results, namely  $x$ -development in the shape factor  $H$ , local skin friction  $CF$ , and local momentum Reynolds number  $R_{TH}$ , for a mild equilibrium adverse pressure gradient are shown in figure 1. This "Clauser flow no. 1" (reported in reference 8 in conjunction with the invention of the concept of equilibrium turbulent layers) decelerated slowly from 32.5 ft/sec to 21.2 ft/sec over a distance of 25 feet and yet gave many a theory substantial difficulties, especially in prediction of skin friction (second column). The corresponding comment of the editors in reference 2 reads, "There is general agreement that Clauser's two flows are slightly three-dimensional in opposite directions" illustrates the remarks of Coles regarding uncertainty in the data. The various lower-case letters in figure 1 identify variations in the given prediction method, which in some cases represent truly distinct methods.

A specific word of caution is in order about figure 1. Careful evaluation of the total performance of various methods for the 16 mandatory flows suggests that no one flow or even half a dozen flows are sufficient to establish the predictive reliability of a given method in general. It is the restriction to comparison with a relatively small number of unstandardized flows that has more than anything else frustrated earlier attempts to provide acceptable evaluations of predictive reliability. In retrospect, the writers believe that the 16 mandatory flows represent about a workable minimum for evaluation but more are desirable. With computerization of nearly all the methods, such extensive comparisons are easy, quick, and cheap provided the data are available in standardized form. The lesson for this symposium, and for future predictors is obvious.

Concerning generalizations in other directions, P. Bradshaw's "Outlook for three-dimensional procedures" (ref. 1) appeared to present a realistic, mildly optimistic program for the near future. The ad hoc Committee on Compressibility Effects reported little agreement. Probably their heart was not in the deliberations, in preparation for the better forum represented by the present Symposium.

---

<sup>6</sup>S. J. Kline and also P. Bradshaw have been collecting and are trying to collate these effects. The data show they are far from trivial. For example, Bradshaw estimates that radius of curvature of the wall as large as 300 times the boundary-layer thickness is sufficient to cause changes of a few percent; recent observations on coreolis effects show not only complete laminarization, but also turbulence production as high as four times that for the same geometry without rotation.

## PHYSICS OF THE FLOW

The conference here concerned itself primarily with two matters: (1) separation, and (2) structure of turbulent shear flows.

A summary paper by G. Sovran, "On prediction criteria for turbulent separation" explored the consensus of the turbulent community beyond the experimental information contained in reference 2. The outlook was found discouraging both experimentally and theoretically. The Evaluation Committee, furthermore, observed that the predictive methods were performing less satisfactorily even in problems without separation but with longer runs of adverse pressure gradients. It was conjectured that this result may have been partly due to experimental imbalance of the two-dimensional momentum equation even in the nominally "most two-dimensional" experiments. Nevertheless, theory in incompressible adverse pressure gradients appears less securely founded. A special ad hoc Committee was formed on "Cross-flow effects" during the Conference; its conclusions were reported at the end by J. H. Horlock and form part of the Proceedings.

In reference 7 Bradshaw states: "While it is entirely reasonable that aircraft designers should wish to predict the behaviour of turbulent boundary layers without going deeply into the physical processes which govern their development, it is by no means reasonable that those who develop calculation methods in the first place should ignore the physics of the flow or represent it by simple-minded formulae chosen for mathematical convenience rather than physical plausibility." After three days of emphasis on predictions, the Conference also focused for two half-days on the up-to-date views of the actual structure of the incompressible turbulent boundary with presentations by L. S. G. Kovasznay, S. J. Kline, J. Sternberg, I. Tani, H. K. Moffatt, and M. J. Lighthill, and vigorous discussion by W. Willmarth, R. E. Kronauer, P. Bradshaw, M. Landahl and others (ref. 1.) Much heat but more light was generated. Even the crystallization of disagreements as to probable facts and interpretations led to specific suggestions for experiments that may settle the disputes.

With respect to the present symposium, the writers believe there is no reason to suspect that the flow mechanisms which have mostly been observed for very low Mach numbers should be altered up to roughly Mach 5. However, above Mach 10 it is hard to see how the various interactions observed at low speeds can be maintained unchanged.

However, the last remark need not distress the compressible predictors unduly because the clear consensus from the AFOSR-IFP-Stanford Conference held that even the most successful low-speed prediction methods were not truly based on adequate, generally accepted physical picture of the turbulence mechanisms. The view shifted from good methods "having good physics" to "being compatible with basic physics." In the general discussion, there was unanimous agreement that all the methods remain correlative in nature. A few do draw on the modern structure information, but only to the extent of using them to suggest the forms of correlations employed in supplying equations for the excess unknowns that arise from time-averaging the Navier-Stokes equations.

At the beginning much was made of some methods providing for the "history" of the turbulent development - mathematically an extra relaxation differential equation. However, the Evaluation Committee found no evidence of clear advantage of such methods over those with the usual x-development procedures (but see ref. 7) and the ad hoc Committee on "History" reported little enlightenment from their discussions. P. Bradshaw stated that the Bradshaw-Ferriss extra lag equation really accommodates a richer variety of profiles even though it is expressed in plausible turbulence terms. In his "Outlook for improved theories," J. C. Rotta also finds the extra-equation theories inadequately physical (ref. 1). An interpretation of his message is that meaningful turbulence physics and thus true "History" will be missing until four rate equations for  $\bar{u}^2$ ,  $\bar{v}^2$ ,  $\bar{w}^2$ , and  $\bar{uv}$  are utilized in addition to the other mean equations. None of the methods represented at the AFOSR-IFP-Stanford Conference include such sophistication.

### CONCLUDING REMARKS

The AFOSR-IFP-Stanford Conference was both enlightening and sobering. It was enlightening in that many new conclusions were realized; the most important is that adequate if still imperfect methods for prediction of two-dimensional, incompressible turbulent boundary layers on smooth walls do exist. It was sobering to observe that after more than three decades of research, the data even for this base class remain imperfect in a number of ways, and that large discrepancies had existed in these data previously owing solely to lack of preparation in standard form. It was equally sobering to see how little information from modern structure work has thus far been carried into the real basis for predictive theories, and how little is known about separated flows both empirically and theoretically.

The primary lessons for extension to compressible boundary layers and other technically important cases seem clear:

(1) Based on the incompressible experience, there is good hope that given sufficiently broad, reliable and well-standardized data, and employing modern computers, adequately reliable prediction procedures can be constructed even though knowledge of the underlying physics is very incomplete.

(2) Of the several results of the incompressible experience each emphasize the importance of a sufficiently broad, reliable, and standardized set of data. This need for data raises not only the question of balance between theoretic and experimental effort at this time, but also owing to the size of the task, a question concerning the desirability of planned, cooperative efforts to achieve the necessary data rapidly and at reasonable cost.

## REFERENCES

1. Kline, S. J.; Morkovin, M. V.; Sovran, G.; and Cockrell, D. J., eds.: Computation of Turbulent Boundary Layers - 1968 AFOSR-IFP-Stanford Conference. Vol. I - Methods, Predictions, Evaluation and Flow Structure. Aug. 1968.
2. Coles, D. E.; and Hirst, E. A.; eds.: Proceedings - Computation of Turbulent Boundary Layers - 1968 AFOSR-IFP-Stanford Conference. Vol. II - Compiled Data. Aug. 1968.
3. Coles, Donald: Measurements in the Boundary Layer on a Smooth Flat Plate in Supersonic Flow. Jet Propulsion Lab., California Inst. Technol.
  - I. The Problem of the Turbulent Boundary Layer. Rep. No. 20-69 (Contract No. DA-04-495-Ord 18), June 1, 1953.
  - II. Instrumentation and Experimental Techniques at the Jet Propulsion Laboratory. Rep. No. 20-70 (Contract No. DA-04-495-Ord 18), June 1, 1953.
  - III. Measurements in a Flat-Plate Boundary Layer at the Jet Propulsion Laboratory. Rep. No. 20-71 (Contract No. DA-04-495-Ord 18), June 1, 1953.
4. Coles, D.: The Turbulent Boundary Layer in a Compressible Fluid. Rept. R-403-PR, RAND Corp., Sept. 1962.
5. Coles, D.: Measurements of Turbulent Friction on a Smooth Flat Plate in Supersonic Flow. Jour. Aero. Sci., Vol. 21, no. 7, July 1954, pp. 433-448.
6. Danberg, J. E.: The Equilibrium Temperature Probe, a Device for Measuring Temperatures in Hypersonic Boundary Layers. NOLTR 61-2, U.S. Navy, Dec. 4, 1961.
7. Bradshaw, P.: Turbulent Boundary Layers. Aeronaut. J., vol. 72, no. 689, May 1968, pp. 451-458.
8. Clauser, F.: Turbulent Boundary Layers in Adverse Pressure Gradients. J. Aeronaut. Sci., vol. 21, no. 2, Feb. 1954, pp. 91-108.

TABLE 1.- THE INTEGRAL METHODS

[Differential equations denoted by \*, algebraic equations denoted by x.  $C_1, \dots$ ,  $\alpha, \beta$  denote profile parameters, S shear integral,  $\phi_1$  mixing-length lag integral, and E entrainment rate.]

	DISSIPATION METHODS					ENTRAINMENT METHOD					MOMENT METHODS							OTHER		
	RO	AL	EN	LH <sub>1</sub>	TR	FG	ZW	HE	HR	LH <sub>2</sub>	MQ	AD	MR	MO	MC	NA	NH	FN	DT	
MOMENTUM INTEGRAL EQUATION	*	*	*	*	*	*	*	*	*	*	*	*	*	*	*	*	*	*	*	
	x	x		x			x	x	x	x				x	x		x		x	
	x						x		x			x	x	x	x		x		x	
	*						*	*	*				x	x	*				*	
outer velocity profile																				
inner velocity profile																				
shear stress profile																				
wall shear from U profiles																				
Ludwig-Tillmann Cf	x			*	x	x		x		*						x	x		x	
other Cf correlation			x							*	x									
MEAN ENERGY INTEGRAL EQUATION	*	*	*	*	*	*	*													
	x	x	x		x	x										x	x		x	
global $\rho$ correlation																				
shear stress profile																				
eddy viscosity assumption				x			x													
mixing length assumption																				
ENTRAINMENT INTEGRAL EQUATION								*	*	*										
							x	x		x										
E = f (Mean field)																				
E = F (turbulence)																				
MOMENT(S) OF MOMENTUM EQUATION												*	***		*	*	*	*	+	
												x		x		x		x	+	
												*					*			
													x		x					
empirical shear integrals																				
shear integral lag equation																				
eddy viscosity assumption																				
mixing length assumption																				
SEMI INTEGRATED MOMENTUM EQN.														*				*		
														x						
															*					
									*											
eddy viscosity assumption																				
TURBULENT ENERGY INTEGRAL EQN.									*						*					
									x											
global P-D assumption																				
local structure assumption																				
EMPIRICAL SHAPE FACTOR EQUATION																			*	
EFFECTIVE INDEPENDENT VARIABLES IN THE ORDINARY DIFFERENTIAL EQUATION SYSTEM	$\theta$	$\delta^*$	$\theta$	$C_f$	$\theta$	$\theta$	$u_\tau$	$\theta$	$u_\tau$	$C_f$	$\theta$	$C_f$	$C_1$	$\delta$	$\alpha$	$\beta$	$\theta$	$\theta$	$\theta$	
	$\delta$	$C_f$	$\delta$	$\delta$	$\delta$	$\delta$	$\delta$	$\delta$	$\delta$	$\delta$	$\delta$	$\delta$	$\delta$	$\delta$	$\delta$	$\delta$	$\delta$	$\delta$	$\delta$	
	$\pi$	$\pi$	$\pi$	$\pi$	$\pi$	$\pi$	$\pi$	$\pi$	$\pi$	$\pi$	$\pi$	$\pi$	$\pi$	$\pi$	$\pi$	$\pi$	$\pi$	$\pi$	$\pi$	

+ A general class of methods based on equilibrium flow



TABLE 2 The Differential Methods

	Mean Field Methods						Turbulent Field Methods			
	MH <sub>1</sub>	CS	NP	KA	RE		NK	BF	BB	MH <sub>2</sub>
Continuity Equation	**	**	**	**	**		**	**	**	**
Moment Equation										
Turbulent Kinetic Energy Equation								*	*	*
Eddy Viscosity Transport Equation							*			
Eddy Viscosity	x	x	x	x			x			
Mixing Length		x	x							
$-\overline{uv} = kq^2$								x		
$-\overline{uv} = kq\ell \frac{dU}{dy}$									x	x
Dissipation Length								x	x	x
Turbulent Diffusion								x	x	x
O.D.E. $\epsilon(x)$ lag eqn.					*					
Independent Variables (Effective)	U V	U V	U V	U V	U V $\epsilon(x)$		U V $\epsilon$	U V $q^2$	U V $q^2$	U V $q^2$

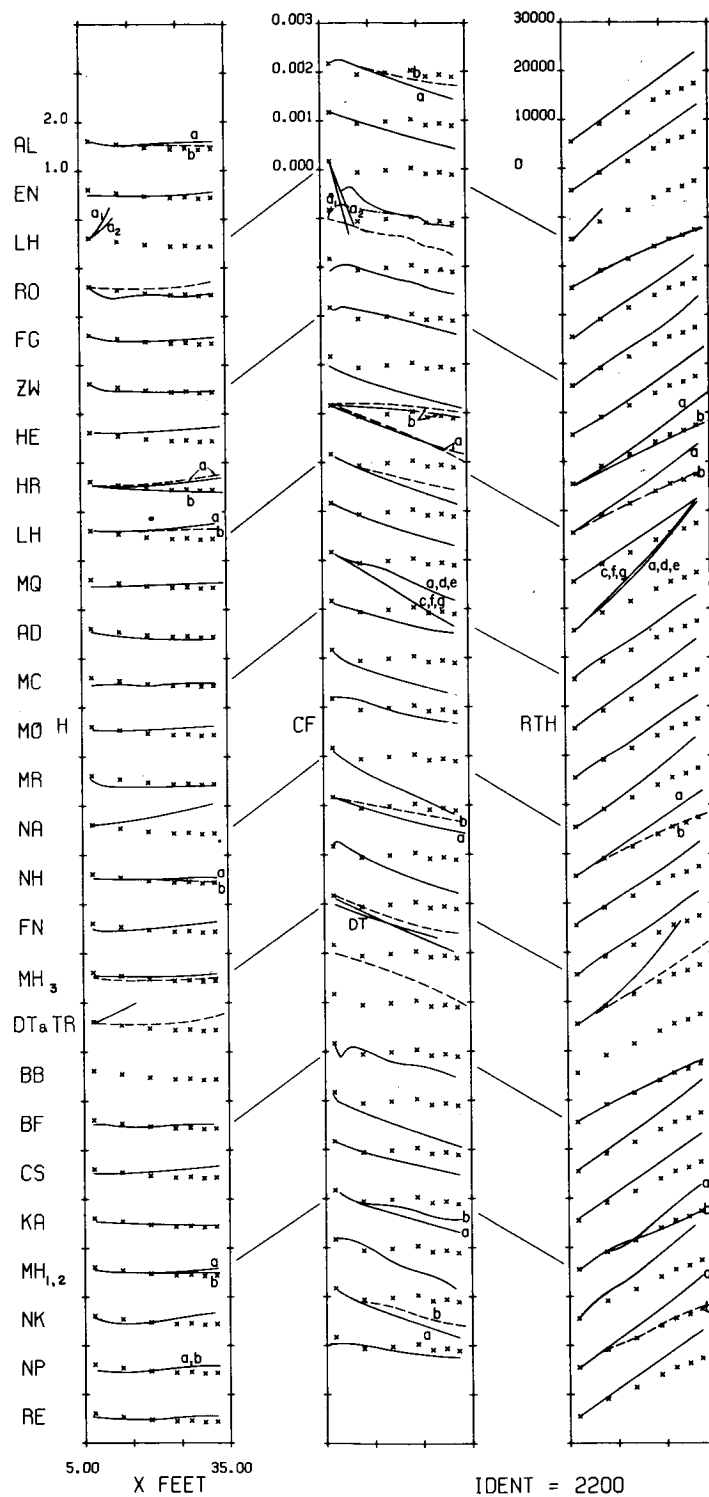


Figure 1.- Clauser flow 1.

# A METHOD OF CALCULATING COMPRESSIBLE TURBULENT BOUNDARY LAYERS\*

H. James Herring and George L. Mellor

Princeton University

## SUMMARY

The essential unknown quantity in a compressible turbulent boundary layer is shown to be the kinematic Reynolds stress, as in incompressible flow, and does not explicitly involve density fluctuations. Based on this, the incompressible turbulent viscosity proposed by Mellor is extended to include compressible flows. The same values of the three empirical constants, which were obtained solely from constant-property, constant-pressure experiments, are also used. Without making any further assumptions beyond those related to the usual time averaged boundary layer equations, this system of equations has been programmed for numerical solution. Solutions have been compared to a considerable amount of constant-pressure data in the range from subsonic flows to flows with Mach numbers around 5.0 and the comparisons are quite favorable. Much less pressure gradient data are available, but comparison was made to some axisymmetric flow data taken in a positive pressure gradient which indicated fairly good prediction of the boundary layer growth, while at the same time pointing up a systematic error in the detailed profile shape prediction in regions of finite longitudinal curvature. This effect has been identified on physical grounds but has yet to be incorporated in the turbulent viscosity model. Unfortunately high speed data taken on a flat wall in an adverse pressure gradient and with a well defined separation point do not seem to be readily available.

Heat transfer data in incompressible flows with variable pressure gradients have been checked against calculations and the comparisons are generally favorable.

---

\*Paper 3 also available as NASA CR-1144, 1968.

# TABLE OF CONTENTS

	Page
NOTATION.....	29
I. INTRODUCTION.....	34
II. ANALYSIS OF THE PROBLEM.....	35
Equations of Motion	
Effective Viscosity Hypothesis	
Heat Transfer	
III. SOLUTION OF THE EQUATIONS OF MOTION.....	45
IV. COMPARISON WITH EXPERIMENTAL DATA.....	60
Zero Pressure Gradient	
Axisymmetric Flow with a Pressure Gradient	
Heat Transfer	
V. CONCLUDING REMARKS.....	99
APPENDIX A. ORDER OF MAGNITUDE ANALYSIS FOR EQUATIONS OF MOTION.....	101
APPENDIX B. COMPARISON OF EFFECTIVE VISCOSITY HYPOTHESIS WITH ALTERNATE FORMS.....	111
APPENDIX C. EQUATIONS FOR THE RUNGE-KUTTA METHOD.....	119
APPENDIX D. ASYMPTOTIC SOLUTION FOR LARGE $\eta$ .....	122
APPENDIX E. BOUNDARY LAYER EQUATIONS OF MOTION IN AXISYMMETRIC FLOW.....	125
REFERENCES.....	129

# NOTATION

A	constant used in Equation (36) for initialization of profiles.
$A_f, A_g$	constants used in satisfying outer boundary condition.
B	exponent used in Equation (35) for external velocity distribution.
$C_i$	coefficients in pseudo-linear forms of momentum and energy equations.
$C_f$	$= \frac{\tau_w}{\frac{1}{2} \rho_e U^2}$ , coefficient of skin friction.
$C_{f,i}$	coefficient of skin friction for an incompressible flow at the same value of $R_\theta$ as $C_f$ .
D	$= (R_{LAT})_x \delta^* / R_{LAT}$
$f'$	$= (\rho_e U - \bar{\rho} \bar{u}) / \rho_e U$ .
$g'$	$= (h_e^o - \bar{h}^o) / (h_e^o - h_r)$ .
h	enthalpy
$h_r$	arbitrary reference enthalpy.
$h^o$	total enthalpy.
H	$= (h_e^o - h_r) / h_e^o$ .
k	molecular thermal conductivity.
K	Clauser constant used in the effective viscosity function (taken here to be 0.016).
$K^+$	empirical constant.
$\ell$	representative scale in x direction.

L	reference length used for $x$ in Equation (35).
M	Mach number.
$M_\infty$	Mach number used to identify data of Winter, Smith and Rotta [23] .
p	pressure
P	$= (\rho_e U)_x \delta^* / \rho_e U$ .
Pr	molecular Prandtl number defined by Equation (14).
$Pr_t$	turbulent Prandtl number defined by Equation (15).
q	heat flux.
Q	$= (\rho_e U \delta^*)_x / \rho_e U$ .
$R_{LAT}$	lateral radius of wall curvature.
$R_{LONG}$	longitudinal radius of wall curvature.
$\tilde{R}_k$	$= \delta_k^* U / \tilde{\nu}$ .
$\tilde{R}_s$	$= \delta_k^* U / \bar{\nu}_s$ .
$R_x$	$= xU / \nu_\infty$ .
$R_{\delta^*}$	$= U \delta^* / \nu_\infty$ , displacement thickness Reynolds number.
$R_\theta$	$= \theta U / \nu_\infty$ , momentum thickness Reynolds number.
$R, S$	defined by Equation (D5).
$r, s$	given by Equation (D8).
$S_t$	$= \frac{q_w}{\rho_e U (h_e - h_w)}$ , Stanton number.
t	temperature.

$u, v, w$	velocities in the directions $x$ , $y$ , and $z$ respectively.
$u_\tau$	$= \sqrt{\tau_w / \rho_e}$ , friction velocity.
$U$	velocity at the outer edge of the boundary layer.
$V$	$= U_x \delta^* / U$ .
$x, y, z$	spatial coordinates defined in Figure 1.
$y_1^+$	empirical constant.
$\alpha$	molecular diffusivity.
$\alpha_e$	$= \alpha_t + \alpha$ , effective diffusivity.
$\alpha_t$	turbulent diffusivity.
$\gamma$	$= C_p / C_v$ , ratio of specific heats.
$\delta$	approximate boundary layer thickness.
$\delta^*$	$= \int_0^\infty (\rho_e U - \bar{\rho} \bar{u}) / \rho_e U \, dy$ , displacement thickness.
$\delta_k^*$	$= \int_0^\infty (U - \bar{u}) / U \, dy$ , kinematic displacement thickness.
$\Delta$	difference between value of variable in mainstream and at wall
$\mathcal{E}$	$= \delta / \ell$ , small parameter used in order of magnitude analysis.
$\eta$	$= y / \delta^*$ .
$\eta_1$	asymptotic matching point.
$\theta$	$= \rho_e / \bar{\rho}$ , also used for $\int_0^\infty \bar{\rho} \bar{u} (1 - \bar{u}/U) / \rho_e U \, dy$ , the momentum thickness.

$\kappa$	von Karman constant in the effective viscosity function (taken here to be 0.41).
$\lambda$	$= \delta^*/R_{LAT}$
$\Lambda$	$= r/R_{LAT}$
$\mu$	molecular viscosity.
$\nu$	molecular kinematic viscosity.
$\nu_e$	$= \nu + \nu_t$ , effective kinematic viscosity.
$\nu_s$	molecular kinematic viscosity at the edge of the viscous sublayer.
$\nu_t$	turbulent kinematic viscosity.
$\nu_\infty$	molecular kinematic viscosity at the edge of the boundary layer.
$\rho$	density.
$\sigma$	constant in the effective viscosity function (taken here to be 6.9).
$\tau$	shear stress.
$T, T_h$	effective viscosity and diffusivity functions in defect form.
$\phi, \Phi$	wall and defect effective kinematic viscosity functions.
$x, X$	wall and defect layer variables for the effective kinematic viscosity function.

#### Subscripts

b	previous x station.
e	outer edge of boundary layer.



h	homogenous solution.
m	intermediate x station.
o	initial x station.
p	particular solution.
w	wall.
x	differentiation with respect to x.

### Superscripts

$(\bar{\phantom{x}})$	time average part of dependent variable.
$(\phantom{x})'$	fluctuating part of dependent variable, also used later with $f$ , $g$ and $\theta$ to denote partial derivative with respect to $\eta$ .
$(\phantom{x})^+$	non-dimensional variables defined by Equation (A1).

## I. INTRODUCTION

It is probable that a quantitative theory of the turbulent transport mechanism which, for example, gives rise to the Reynolds stress in turbulent boundary layers, will not be available in the near future. One is therefore forced to model this mechanism empirically. Most of the previous methods in the literature inject further empirical content in an attempt to side-step the analytical complexities of the time averaged equations of motion. However, with the availability of high speed computers the full equations can now be solved numerically, thus providing a predictive tool which spans a large parametric range. The parametric variables which can in principle be included in the formulation are Reynolds number, Mach number, pressure gradient, transpiration or aspiration, heat transfer and wall roughness for either planar or axisymmetric flow. Furthermore the same numerical program can be used to calculate the laminar portions of the boundary layer development. Besides serving as an effective tool for the prediction of boundary layer development, the numerical solution of the boundary layer equations is free from analytical approximation and therefore underscores the results of the turbulent transport model.

The seed of the present work was Clauser's suggestion [1,2] that the outermost part of an equilibrium boundary layer (one for which  $(U-u)/u_\tau$  represent similar profiles when  $(\delta^* dp/dx)/\tau_w$  is held constant) could be described with a constant effective viscosity. Recently Mellor [3,4] hypothesized an effective viscosity function for the entire boundary layer. This effective viscosity hypothesis successfully predicted the whole range  $(-0.5 < (\delta^* dp/dx)/\tau_w < \infty)$  of equilibrium boundary layers which represented a considerable gain since it allowed the detailed development of such layers to be calculated from a function containing only three empirical numbers. Mellor then demonstrated that the effective viscosity hypothesis gave good results for a variety of decelerating non-equilibrium flows in reference [5]. There the profiles, skin friction coefficient and boundary layer growth were all predicted well and, where it occurred, the separation point was correctly predicted. The limitations on the hypothesis are that it has a definite lower Reynolds number limit of  $R_\delta^* = 700$ , with a practical lower limit somewhat higher, and it is in error for boundary layers on walls with curvature in the streamwise direction. The latter does not represent an inadequacy in the basic approach. Experiments are still in progress to find the best way of incorporating the curvature effect into the hypothesis.

The next logical step in the development is taken here - the extension of the incompressible effective viscosity to include compressible flows with heat transfer. The restrictions on the hypothesis for incompressible flow also apply in compressible flow. Here the Reynolds number restriction must be made more specific;  $U_\delta^*/\bar{v}_s$  must be greater than 700,

where  $\delta_k^* = \int_0^\infty (U-u)/U dy$ , and  $\bar{\nu}_s$  is the kinematic viscosity at the edge of the viscous sublayer. For large Mach number  $\bar{\nu}_s$  can be substantially larger than the freestream value. The density variation in compressible flow also makes the effect of curvature even more significant. Both of these limitations will be discussed later in detail. In addition, a restriction to moderate heat transfer rate becomes necessary. This condition can probably be written

$$1 - \frac{h_e^0 / h_w}{1 + \frac{\gamma-1}{2} M_e^2} = O(1) \quad (1)$$

which if satisfied implies that only the mean density need enter into the determination of the Reynolds stress, and the previously established effective viscosity hypothesis may be adopted.

By assuming constant turbulent and molecular Prandtl numbers, the same effective viscosity function is used in the energy equation. Because the energy equation is actually solved, instead of simply assuming, for instance, constant total enthalpy across the layer, compressible boundary layers with heat transfer can be calculated.

Although the predictive scope of the calculation is much broader, this report restricts attention to a large amount of high speed adiabatic flow data with zero pressure gradient, a series of axisymmetric flow data with pressure gradients and some incompressible flow data with heat transfer.

## II. ANALYSIS OF THE PROBLEM

### Equations of Motion

Solutions of the complete, time dependent equations of motion for a compressible turbulent boundary layer are beyond the capability of available numerical methods. A number of simplifications are therefore necessary. First, using the familiar method of Reynolds averaging, the equations may be averaged in time so that the effects of the time dependent turbulent fluctuations are expressed as turbulent correlations. In a steady turbulent flow these correlations are then independent of time. Temporarily it will simplify matters to restrict the derivation to include only that region away from the wall where turbulent effects dominate and the direct effects of molecular viscosity and molecular conductivity are negligible. Using the notation shown in Figure 1, these equations may be written

$$\frac{\partial}{\partial x} (\bar{\rho} \bar{u} + \overline{\rho' u'}) + \frac{\partial}{\partial y} (\bar{\rho} \bar{v} + \overline{\rho' v'}) = 0 \quad , \quad (2a)$$

$$\frac{\partial}{\partial x} (\bar{\rho} \bar{u}^2 + \bar{\rho} \overline{u'^2} + 2\bar{u} \overline{\rho' u'}) + \frac{\partial}{\partial y} (\bar{\rho} \bar{v} \bar{u} + \bar{\rho} \overline{u' v'} + \bar{u} \overline{\rho' v'} + \bar{v} \overline{\rho' u'}) = - \frac{\partial \bar{p}}{\partial x} \quad , \quad (2b)$$

$$\frac{\partial}{\partial x} (\bar{\rho} \bar{u} \bar{v} + \bar{\rho} \overline{u' v'} + \bar{v} \overline{\rho' u'} + \bar{u} \overline{\rho' v'}) + \frac{\partial}{\partial y} (\bar{\rho} \bar{v}^2 + \bar{\rho} \overline{v'^2} + 2\bar{v} \overline{\rho' v'}) = - \frac{\partial \bar{p}}{\partial y} \quad , \quad (2c)$$

$$\begin{aligned} \frac{\partial}{\partial x} (\bar{\rho} \bar{u} \bar{h}^0 + \bar{\rho} \overline{u' h'^0} + \bar{h}^0 \overline{\rho' u'} + \bar{u} \overline{\rho' h'^0}) + \frac{\partial}{\partial y} (\bar{\rho} \bar{v} \bar{h}^0 + \bar{\rho} \overline{h'^0 v'} + \bar{v} \overline{\rho' h'^0} \\ + \bar{h}^0 \overline{\rho' v'}) = 0 \quad , \end{aligned} \quad (2d)$$

$$\bar{h}^0 = \bar{h} + \frac{1}{2} (\bar{u}^2 + \overline{u'^2} + \overline{v'^2} + \overline{w'^2}) \quad , \quad (2e)$$

$$\bar{p} = \frac{\gamma - 1}{\gamma} (\bar{\rho} \bar{h} + \overline{\rho' h'}) \quad . \quad (2f)$$

Since these turbulent correlation terms are not known a priori, it is desirable to estimate their importance to determine which are negligible. For a boundary layer this may be done with a standard order of magnitude analysis. If it is assumed that

$$\overline{\rho' v'} \approx \overline{u' v'} \left( \frac{\partial \bar{\rho}}{\partial y} / \frac{\partial \bar{u}}{\partial y} \right) \quad (3a)$$

and

$$\overline{\rho' u'} \approx \overline{\rho' v'} \quad (3b)$$

(which is consistent with equations (7) and (13) discussed below) it is shown in Appendix A that

$$\frac{\overline{\rho' v'}}{U_{\Delta} \bar{\rho}} \quad , \quad \frac{\overline{\rho' u'}}{U_{\Delta} \bar{\rho}} = O(\delta / \ell) \quad (4)$$

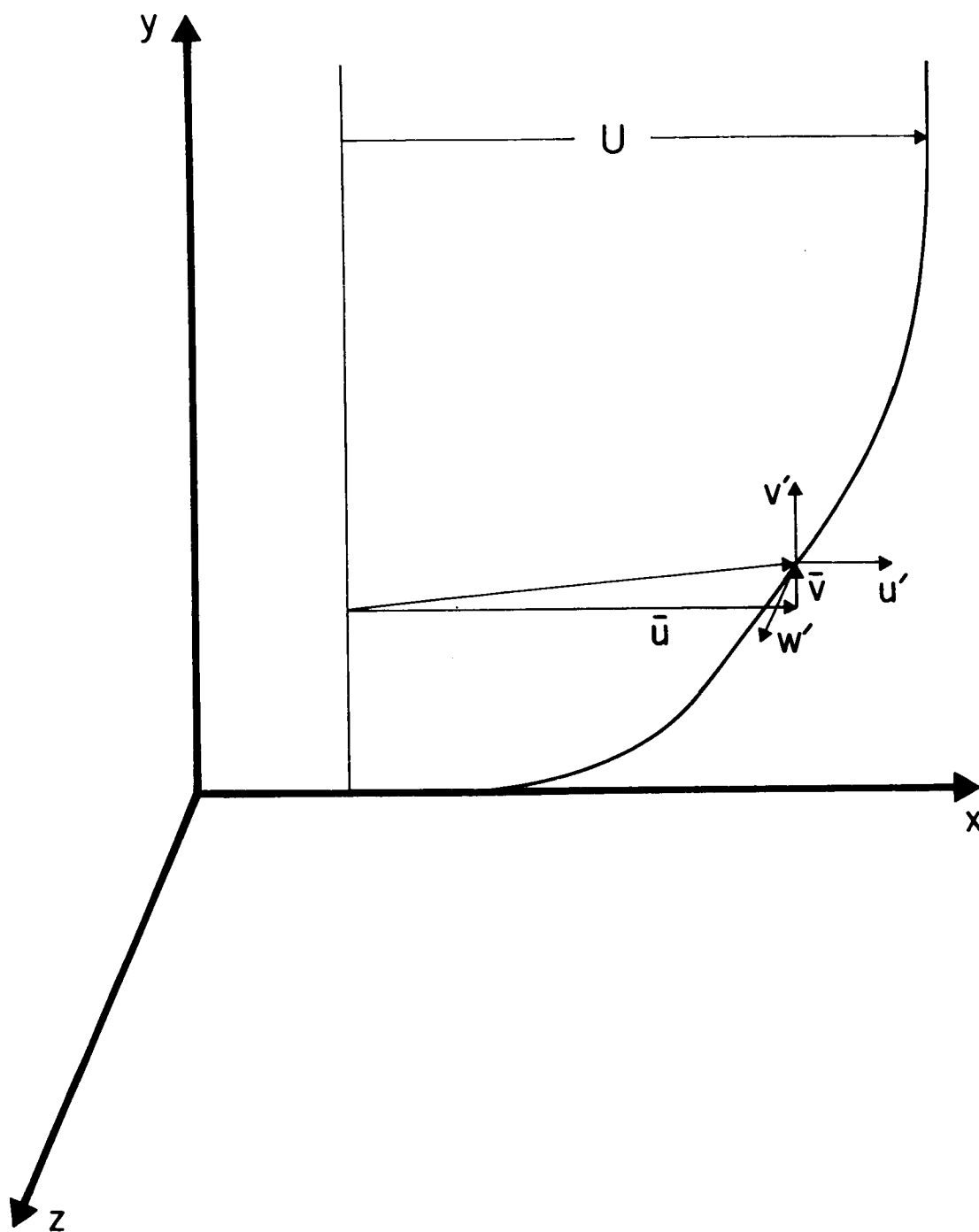


FIGURE 1. Illustration of coordinate system.

(where  $\Delta \bar{\rho}$  is the variation of  $\bar{\rho}$  across the boundary layer and  $\delta$  is the thickness of layer which is small with respect to the scale in the  $x$  direction,  $l$ ) so long as

$$\frac{\Delta \bar{\rho}}{\bar{\rho}_e} = 1 - \frac{h_e^0 / h_w}{1 + \frac{\gamma-1}{2} M_e^2} = O(1) \quad (5)$$

Presumably at some high heat transfer rate the condition will be violated. However, in flow regimes where (5) is valid, many of the correlation terms in equation (2) are shown to be negligible. The resulting equations can then be written in the form\*

$$\frac{\partial \bar{\rho} \bar{u}}{\partial x} + \frac{\partial}{\partial y} (\bar{\rho} \bar{v} + \overline{\rho' v'}) = 0 \quad , \quad (6a)$$

$$\bar{\rho} \bar{u} \frac{\partial \bar{u}}{\partial x} + (\bar{\rho} \bar{v} + \overline{\rho' v'}) \frac{\partial \bar{u}}{\partial y} = - \frac{d\bar{p}}{dx} + \frac{\partial \bar{\tau}}{\partial y} \quad , \quad (6b)$$

$$\bar{\rho} \bar{u} \frac{\partial \bar{h}^0}{\partial x} + (\bar{\rho} \bar{v} + \overline{\rho' v'}) \frac{\partial \bar{h}^0}{\partial y} = \frac{\partial}{\partial y} (\bar{q} + \bar{u} \bar{\tau}) \quad , \quad (6c)$$

$$\bar{h}^0 = \bar{h} + \frac{\bar{u}^2}{2} \quad , \quad (6d)$$

$$\bar{p}_e = \frac{\gamma-1}{\gamma} \bar{\rho} \bar{h} \quad , \quad (6e)$$

where

$$\bar{\tau} = \mu \frac{\partial \bar{u}}{\partial y} - \overline{\rho' u' v'} \quad , \quad (6f)$$

and

$$\bar{q} = k \frac{\partial \bar{h}}{\partial y} - \overline{\rho' v' h'} \quad . \quad (6g)$$

---

\*Note added after CR-1144 first appeared. This system of equations, (6a - g), was first given by Young [45], and speculation that compressibility was not directly important in determining  $\overline{u' v'}$  was provided by Morkovin [46]. Apparently, the weak condition on their applicability, implied by (5), had not been stated previously.

Molecular viscous stresses and heat flux terms have been added to the equations above to make them valid to the wall. In doing so the terms  $\overline{\mu'(\partial u'/\partial y)}$ ,  $(\kappa' \partial h'/\partial y)$  have been neglected relative to  $\overline{\mu(\partial u/\partial y)}$ ,  $\overline{\kappa(\partial h/\partial y)}$  which are themselves small everywhere but near the wall.

### Effective Viscosity Hypothesis

The influence of turbulence appears in the boundary layer equations (6a), (6b) & (6c) through the terms  $\overline{\rho'v'}$ ,  $\overline{u'v'}$  and  $\overline{v'h'}$ . However, only  $\overline{u'v'}$  and  $\overline{v'h'}$  need be considered since  $\overline{\rho'v'}$  always occurs in the combined form,  $\overline{\rho v} + \overline{\rho'v'}$ , which may be eliminated from (6b) and (6c) with the continuity equation. Therefore, in order to complete equations (6b) and (6c) the quantities  $\overline{u'v'}$  and  $\overline{v'h'}$  must be related to the mean flow variables. Since the necessary understanding of the turbulent mechanism which gives rise to these terms is not likely to be available soon, a single concise empirical assumption is the next best alternative. Following the line of argument used by Mellor [3,4,5] for incompressible flow, an empirical relation will be proposed for the terms  $\overline{u'v'}$  and  $\overline{v'h'}$  in compressible flow with heat transfer.

The empirical relation for  $\overline{u'v'}$  is couched in the form

$$\frac{\overline{\tau}}{\overline{\rho}} = \overline{v} \frac{\partial \overline{u}}{\partial y} - \overline{u'v'} = \nu_e \frac{\partial \overline{u}}{\partial y}, \quad (7)$$

where  $\nu_e$  is an effective kinematic viscosity of the type first proposed by Boussinesq. A kinematic viscosity is chosen because of the essentially kinematic nature of the velocity correlation,  $\overline{u'v'}$ . The hypothesis for the form of  $\nu_e$  rests on three assumptions which are supposed to be universally valid:

- 1) in the outer, or defect layer,  $\nu_e$  depends on only three quantities,  $\delta_k^* U$ ,  $y$  and  $\frac{\partial \overline{u}}{\partial y}$ , where  $\delta_k^* U (= \int_0^\infty (U - \overline{u}) dy)$  is the scale suggested by Clauser [2];
- 2) in the inner, or wall layer,  $\nu_e$  also depends on only three quantities,  $\overline{v}$ ,  $y$  and  $\frac{\partial \overline{u}}{\partial y}$ , where  $\overline{v}$  is the local molecular viscosity; and
- 3) in this two layer model there is a region where the layers overlap and both expressions for  $\nu_e$  apply simultaneously. It follows from the first two assumptions that in the defect layer,  $\nu_e$  must be of the form

$$\frac{\nu_e}{\delta_k^* U} = \Phi \left( \frac{\kappa^2 y^2}{\delta_k^* U} \frac{\partial \overline{u}}{\partial y} \right), \quad (8a)$$

and in the wall layer,  $\nu_e$  must be of the form

$$\frac{\nu_e}{\bar{\nu}} = \phi \left( \frac{K^2 y^2}{\bar{\nu}} \frac{\partial \bar{u}}{\partial y} \right) , \quad (8b)$$

where  $K$  is an empirical constant. Thus the hypothesis consists of two forms each individually independent of the Reynolds number, Mach number and pressure gradient. Now, as a consequence of the third assumption, it follows that the form of the effective viscosity in the overlap region must be,

$$\nu_e = \bar{\nu} \phi = \delta_k^* U \bar{\phi} . \quad (9)$$

Thus in the overlap region  $\phi$  and  $\bar{\phi}$  must be linear functions so that

$$\nu_e = K^2 y^2 \frac{\partial \bar{u}}{\partial y} . \quad (10)$$

This is a result identical to that obtained heuristically by Prandtl [6]. Here, however, it evolves as a consequence of the independence of the functional forms for the wall layer and the defect layer. Lastly, for the hypothesis to predict correctly a viscous sublayer it is clear that very close to the wall,  $\phi \rightarrow 1$ .

An alternative functional form, completely equivalent to (8) but offering some computational advantage was later offered by Mellor [5]; it may be written

$$\frac{\nu_e}{U \delta_k^*} = \phi(X) , \quad X = \frac{Ky}{U \delta_k^*} \sqrt{\frac{\bar{\tau}}{\bar{\rho}}} ; \text{ in the defect layer} \quad (11a)$$

$$\frac{\nu_e}{\bar{\nu}} = \phi(\chi) , \quad \chi = \frac{Ky}{\bar{\nu}} \sqrt{\frac{\bar{\tau}}{\bar{\rho}}} ; \text{ in the wall layer} \quad (11b)$$

Any function in the form of (8a,b) may be transformed to (11a,b) with help of the relation  $\partial \bar{u} / \partial y = (\bar{\tau} / \bar{\rho}) / \nu_e$ .



As before, in the overlap layer, we must have  $v_e = \bar{v}\phi = U\delta_k^* \phi = \kappa y(\bar{\tau}/\bar{\rho})^{1/2}$  or equivalently  $\phi = \chi$  and  $\phi = X$ . Specific functions may be determined by comparison of calculated profiles with constant pressure incompressible velocity profiles and are shown in Figure 2a,b. The specific curve fit for  $\phi(X)$  given in Figure 2b is simpler in form to that previously cited in [ 5 ] but is operationally equivalent. The value  $\kappa = .41$  is the von Karman constant and is chosen to predict correctly the experimentally observed logarithmic law of the wall (when  $\bar{\tau} \approx \tau_w$ ). The constant  $\sigma = 6.9$  is chosen to give a best fit to Laufer's data [7] in the viscous sublayer in the manner demonstrated in [ 4 ]. The outer profile  $\phi(X)$  was specified so as to conform to Clauser's suggestion that  $\phi = \text{constant} = K$  in the outer layer. Obviously this representation is not correct near the outer edge of the profile and could be replaced by another function  $\phi(X)$  which decreases for large  $y$ . However, experience indicates that this would only slightly alter the predicted profile shape.

Finally, it is clear now that relations (11a,b) are a proposal of empirical inner and outer functions for  $v_e$  even though knowledge of a differential equation for  $v_e$  is absent. Therefore a composite function can be constructed using a prescription offered by Van Dyke [8] for combining inner and outer functions (the prescription can be expressed as the sum of the inner and outer functions minus their common asymptote). Thus  $v_e$  can be written for the whole layer as

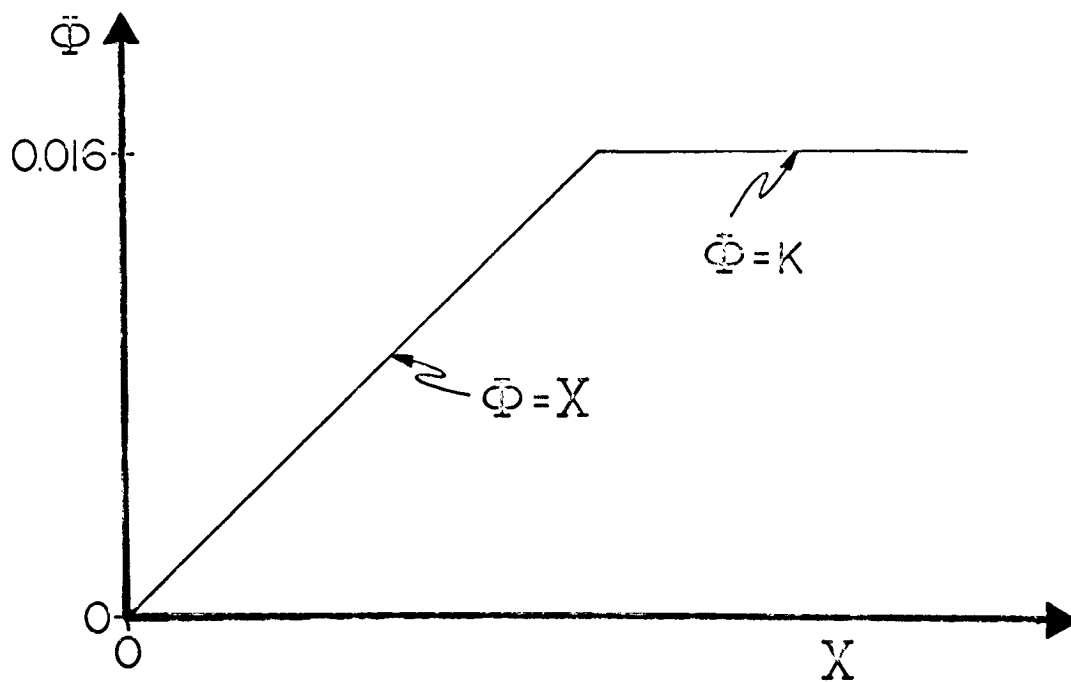
$$\frac{v_e}{v} = \phi(\chi) + \underset{\sim}{R}\phi\left(\frac{\chi}{\underset{\sim}{R}}\right) - \chi, \quad (12a)$$

or

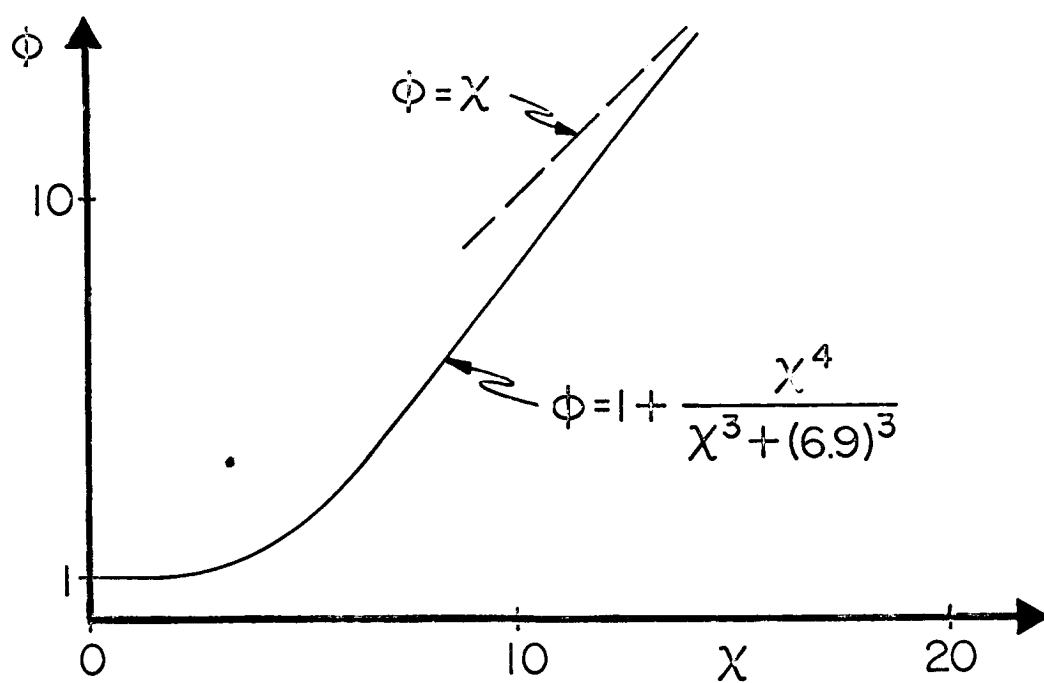
$$\frac{v_e}{\underset{\sim}{\delta}_k^* U} = \frac{1}{\underset{\sim}{R}} \phi(\underset{\sim}{R}X) + \phi(X) - X, \quad (12b)$$

where  $\underset{\sim}{R} \equiv \frac{U\delta_k^*}{v}$ . Some illustrative examples of (12a,b) in incompressible flow for several values of  $\underset{\sim}{R}$  are shown in Fig. 3. For compressible flow, the results are conceptually the same but are complicated by the molecular viscosity variation in  $\underset{\sim}{R}$  and  $\chi$ .

It is evident that (12a) or (12b) can only be valid for large Reynolds number. In fact, for  $\underset{\sim}{R}_s < 700$  the overlap layer disappears. Here the notation



a) outer layer



b) inner layer

FIGURE 2. Effective viscosity hypothesis.

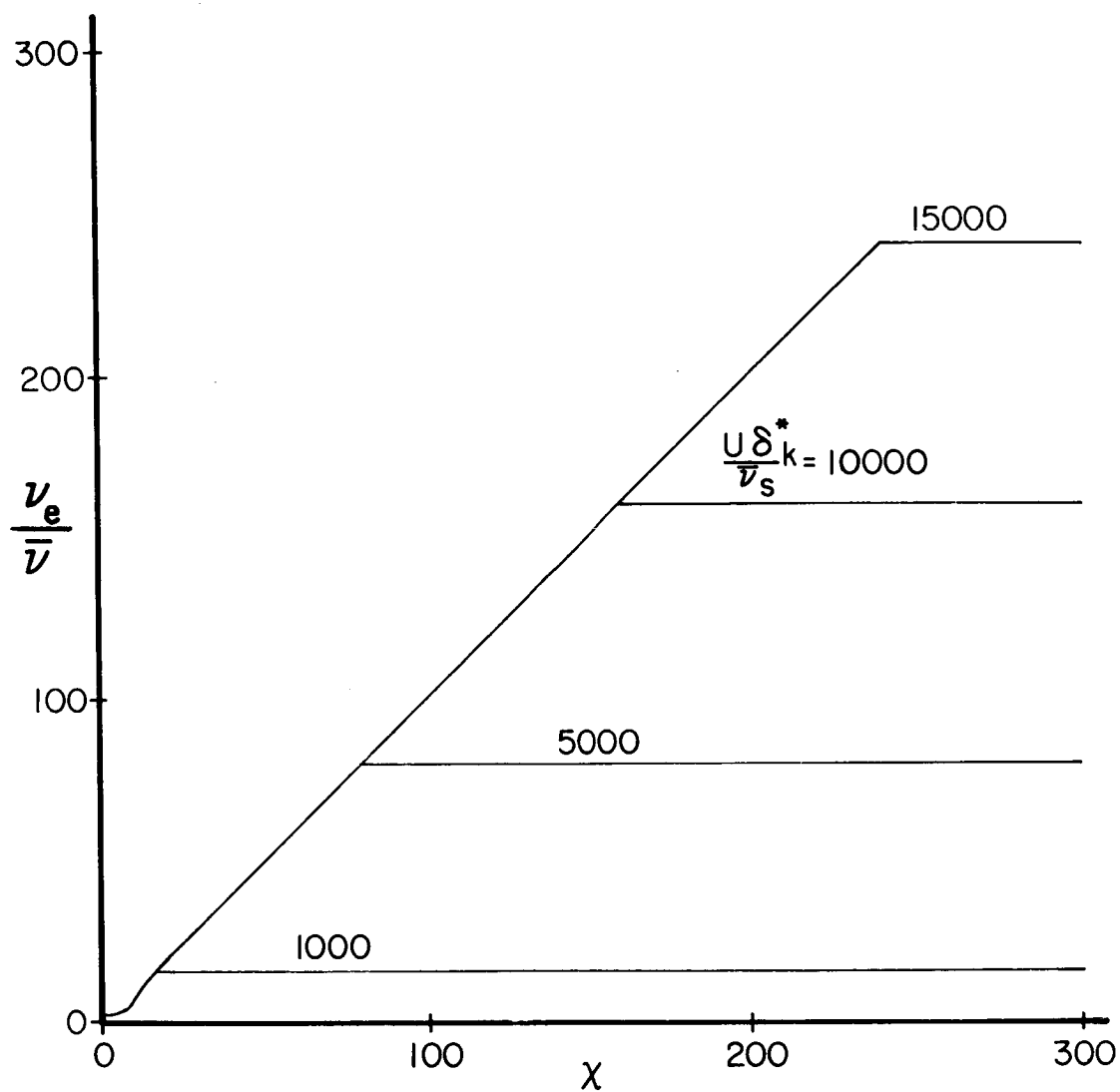


FIGURE 3. Illustration of the composite effective viscosity function for an incompressible flow.

$\tilde{R}_s$  is used to designate the value of  $\tilde{R}$  at the edge of the laminar sublayer. From experience it is apparent that, so long as  $\tilde{R}_s > 2500$ , very little error due to low Reynolds number effects is evident.

The additional complication in compressible form of the hypothesis compared to the incompressible form is that  $\bar{v}$ , as it appears in (12a) and in the definition of  $\tilde{R}$  and  $X$ , is not a constant. Therefore  $\bar{v}$  will be evaluated according to the thermodynamic property relations between  $\bar{v} = \frac{\bar{\mu}}{\bar{p}}$  and the local mean temperature and pressure. The importance of this consideration is restricted to the viscous sublayer but is nevertheless necessary to accurate predictions in the case of high Mach numbers where  $\bar{v}$  in the viscous sublayer may be much larger than  $v_\infty$ . One effect is that a large  $R_s^* (= \frac{U\delta^*}{v_\infty})$  may correspond to a much smaller  $\tilde{R}_s (= \frac{U\delta_k^*}{\bar{v}_s})$  as determined locally in the viscous sublayer. It seems that, for the data to be considered here, the difficulty is frequently encountered in high Mach number flow, and some consideration will be given to a tentative correction.

The underlying assumption that has been made both in this and most other effective viscosity hypotheses is that the Reynolds stress,  $\overline{u'v'}$ , is completely determined by the local mean flow variables. Undoubtedly this is not always the case. The history of the turbulence will probably be important in boundary layers which change rapidly over short distances. In view of this Bradshaw, Ferriss and Atwell [9] have proposed to calculate  $\overline{u'v'}$  from the equation governing turbulent energy transport using several empirical functions relating the quantities in the equation. Although it is an interesting approach, we have difficulty in understanding the conceptual basis of some of their assumptions. Furthermore, the nature of the calculation restricts prediction to regions outside of the viscous sublayer, and the numerical scheme can not be applied to laminar flows.

The other assumptions which have been made all apply to the formulation itself. First, there is the assumption of a two layer model. In this, each layer, represented by the effective viscosities (11a) and (11b), has its own scale,  $\delta_k^* U$  and  $\bar{v}$  respectively. Although there have been attempts to formulate the effective viscosity according to a one layer model, (van Driest, [10]), it has been generally acknowledged (Townsend, [11]) that two scales are necessary. The assumption of an overlap layer where both formulations apply has received strong experimental support. This fact was used by Millikan [12] to infer the velocity profile in that region.

Appendix B compares the present hypothesis with others that have appeared in the literature.

## Heat Transfer

The other quantity which must be specified is  $\overline{v'h'}$ . In order to do this, the assumption is made, following Reynolds, that the heat flux can be written as

$$\overline{q} = \overline{\rho} \alpha_e \frac{\partial \overline{h}}{\partial y}, \quad (13)$$

where  $\alpha_e$  is the effective heat diffusivity. A relation between  $\alpha_e$  and  $v_e$  can be established with the usual assumption of a turbulent Prandtl number,  $Pr_t$ . Since  $(v_e - \overline{v})$  and  $(\alpha_e - \overline{\alpha})$  are the turbulent (or eddy) viscosity and diffusivity respectively, then a turbulent Prandtl number  $Pr_t$  may be defined by analogy to a molecular Prandtl number  $Pr$ . Thus

$$Pr = \frac{\overline{v}}{\overline{\alpha}} \quad (14)$$

and

$$Pr_t = \frac{v_e - \overline{v}}{\alpha_e - \overline{\alpha}} \quad (15)$$

so that the effective diffusivity can be written as

$$\alpha_e = \frac{\overline{v}}{Pr} + \frac{1}{Pr_t} (v_e - \overline{v}) \quad (16)$$

In the most general case the turbulent Prandtl number could be a function of local variables. However, in the calculations described in Section IV, the usual assumption of constant turbulent Prandtl number was made.

### III. SOLUTION OF THE EQUATIONS OF MOTION

The steady two-dimensional flow in a boundary layer on a plane surface at moderate Mach number and heat transfer rate, from the preceding analysis, is characterized by the equations

$$\frac{\partial \bar{\rho} \bar{u}}{\partial x} + \frac{\partial}{\partial y} (\bar{\rho} \bar{v} + \overline{\rho' v'}) = 0 \quad , \quad (17a)$$

$$\bar{\rho} \bar{u} \frac{\partial \bar{u}}{\partial x} + (\bar{\rho} \bar{v} + \overline{\rho' v'}) \frac{\partial \bar{u}}{\partial y} = - \frac{d\bar{p}}{dx} + \frac{\partial \bar{\tau}}{\partial y} \quad , \quad (17b)$$

$$\bar{\rho} \bar{u} \frac{\partial \bar{h}^0}{\partial x} + (\bar{\rho} \bar{v} + \overline{\rho' v'}) \frac{\partial \bar{h}^0}{\partial y} = \frac{\partial}{\partial y} (\bar{q} + \bar{u} \bar{\tau}) \quad , \quad (17c)$$

$$\bar{p} = \frac{\gamma - 1}{\gamma} \bar{\rho} \bar{h} \quad , \quad (17d)$$

$$\bar{h}^0 = \bar{h} + \frac{\bar{u}^2}{2} \quad . \quad (17e)$$

From equations (7) and (13) the effective shear stress and heat flux are

$$\bar{\tau} = \bar{\rho} \nu_e \frac{\partial \bar{u}}{\partial y} \quad , \quad (17f)$$

and

$$\bar{q} = \bar{\rho} \alpha_e \frac{\partial \bar{h}}{\partial y} \quad . \quad (17g)$$

The effective viscosity, from equations (11) and (12), is

$$\nu_e = \bar{\nu} \phi(X, \underline{R}) + U_{\delta_k}^* [\Phi(X) - X] \quad (18a)$$

$$X = \frac{KY}{U_{\delta_k}^*} \sqrt{\frac{\tau}{\rho}} \quad (18b)$$

and

$$\underline{R} = U_{\delta_k}^* / \bar{\nu} \quad (18c)$$

and from equation (16) the effective conductivity is

$$\alpha_e = \frac{\bar{v}}{\text{Pr}} + \frac{1}{\text{Pr}_t} (v_e - \bar{v}) \quad . \quad (18d)$$

The Sutherland molecular viscosity relation,

$$\frac{\bar{v}}{v_\infty} = \left( \frac{\bar{h}}{h_e} \right)^{5/2} \frac{(h_e/c_p) + 110^\circ}{(\bar{h}/c_p) + 110^\circ} (h_e/c_p \text{ in } ^\circ\text{Kelvin}) , \quad (19)$$

is used to evaluate  $\bar{v}$  in equations (18a) and (18d). Finally the appropriate boundary conditions are

$$\bar{u}(y, x_0) = u_0(y) \quad , \quad (20a)$$

$$\bar{u}(0, x) = 0 \quad , \quad (20b)$$

$$\bar{v}(0, x) = 0 \quad , \quad (20c)$$

$$\lim_{y \rightarrow \infty} \int_0^y [\rho_e u - \bar{\rho} \bar{u}(y')] dy' = \rho_e U \delta^* \quad , \quad (20d)$$

$$\bar{h}^0(y, x_0) = \bar{h}_0^0(y) \quad , \quad (20e)$$

$$\bar{h}(0, x) = h_w(x) \quad , \quad \text{or} \quad \bar{q}(0, x) = q_w(x) \quad , \quad (20f)$$

$$\lim_{y \rightarrow \infty} \int_0^y \bar{\rho} \bar{u} [\bar{h}_e^0 - \bar{h}^0(y')] dy' \quad \text{is bounded.} \quad (20g)$$

The integral boundary conditions on  $\bar{u}$  and  $\bar{h}^0$  are more restrictive than the usual,

$$\lim_{y \rightarrow \infty} \bar{u}(y, x) = U \quad , \quad (21a)$$

and

$$\lim_{y \rightarrow \infty} \bar{h}^0(y, x) = h_e^0 \quad . \quad (21b)$$

As noted by Hartree, the conditions, (21), admit two types of solution for large  $y$

$$U(x) - \bar{u}(y, x) \quad \text{and} \quad h_e^0 - \bar{h}^0(y, x) \sim e^{-y^2} \quad , \quad (22a)$$

and

$$U(x) - \bar{u}(y, x) \quad \text{and} \quad h_e^0 - \bar{h}^0(y, x) \sim y^{-a} \quad , \quad (0 < a) \quad . \quad (22b)$$

The second of these forms predicts infinite displacement, momentum and enthalpy thicknesses and therefore is not a valid solution. The integral boundary condition specifically avoids this and allows only the form (22a) .

It is convenient to introduce the following definitions:

$$f'(\eta, x) = \frac{\rho_e U - \bar{\rho} \bar{u}}{\rho_e U} \quad (23a)$$

$$\theta(\eta, x) = \frac{\rho_e}{\bar{\rho}} \quad (23b)$$

$$g'(\eta, x) = \frac{h_e^0 - \bar{h}^0}{h_e^0 - h_r} \quad , \quad (23c)$$



$$\eta = y/\delta^* \quad . \quad (23d)$$

Although frequently it would be more useful to have  $f'$  be a function of velocity only, the stream function-like form of  $f'$  above makes incorporation of the continuity equation much simpler. An arbitrary reference enthalpy,  $h_r$ , is used and can be defined in any way which is convenient to a particular problem. For example, we could set  $h_r = 0$  or in the case of low Mach number it is often convenient to set  $h_r = h_w$  at some reference wall location. Finally, the use of the normalized variable  $\eta$  largely divorces the change in thickness of the boundary layer, represented by  $\delta_x^*$ , from the change in shape, represented by  $f'_x(\eta)$  and  $g'_x(\eta)$ . It is therefore possible to use a fixed distribution of  $\eta$  grid points in the numerical calculation rather than one in which the spacing grows with the thickness of the boundary layer.

Substitution of these parameters into equations (17b) and (17c) yields

$$\begin{aligned} \left\{ \frac{\delta_k^*}{\delta^*} \frac{\tau}{\theta} \left[ \theta(1 - f') \right] \right\}' &= \left\{ Q \theta (\eta - f) - \delta^* \theta f'_x \right\} f'' \\ &+ \left\{ (V\theta + \delta^* \theta_x) (f' - 2) + \delta^* (\theta f'_x - \theta' f_x) + Q \theta' (\eta - f) \right\} f' \\ &+ \left\{ Q \theta' \right\} f + \left\{ V(\theta - 1) + \delta^* (\theta_x - \theta f'_x + \theta' f'_x) - Q \theta' \eta \right\} \end{aligned} \quad (24a).$$

$$\begin{aligned} &\left[ \frac{\delta_k^*}{\delta^*} \frac{\tau_h}{\theta} \left\{ -g'' + \frac{\frac{\gamma-1}{2} M_e^2}{H(1 + \frac{\gamma-1}{2} M_e^2)} \left[ \frac{\tau}{\tau_h} - 1 \right] \left[ \theta^2 (1 - f')^2 \right]' \right\} \right]' \\ &= \left\{ Q(\eta - f) - \delta^* f'_x \right\} g'' - \delta^* (1 - f') g'_x \end{aligned} \quad (24b)$$

The density ratio is found from equations (17d) and (17e),

$$\theta = \frac{2 \left( 1 + \frac{\gamma-1}{2} M_e^2 \right) (1 - Hg')}{1 + \sqrt{1 + \frac{\gamma-1}{2} M_e^2 (1 - f')^2} \left( 1 + \frac{\gamma-1}{2} M_e^2 \right) (1 - Hg')} \quad (25)$$

Primes indicate differentiation with respect to  $\eta$  and,

$$Q = \frac{(\rho_e U \delta^*)_x}{\rho_e U} \quad , \quad (26a)$$

$$V = \frac{U_x \delta^*}{U} \quad , \quad (26b)$$

$$H = \frac{h_e^o - h_r}{h_e^o} \quad (26c)$$

From (12b) and (16) the effective viscosity and conductivity are

$$\tau = \frac{\nu_e}{\delta_k^* U} = \frac{1}{R} \phi(\tilde{R} X) + \phi(X) - X \quad , \quad (27a)$$

$$\tau_h = \frac{\alpha_e}{\delta_k^* U} = \frac{1}{R} \frac{1}{Pr} + \frac{1}{Pr_t} \left( \tau - \frac{1}{R} \right) \quad . \quad (27b)$$

Here, since the effective viscosity and conductivity have been expressed in terms of the defect variables throughout the layer,  $\tilde{R}$  must appear explicitly in the wall layer parts of both formulations. The boundary conditions are

$$f'(\eta, x_0) = f'_0(\eta) \quad , \quad (28a)$$

$$f(0, x) = 0 \quad , \quad (28b)$$

$$f'(0, x) = 1 \quad , \quad (28c)$$

$$\lim_{\tilde{y} \rightarrow \infty} f(\eta, x) = 1 \quad , \quad (28d)$$

$$g'(\eta, x_0) = g'_0(\eta) \quad , \quad (28e)$$

$$g'(0, x) = \frac{h_e^0 - h_w(x)}{h_e^0 - h_r} \quad \text{or} \quad g''(0, x) = - \frac{\delta^* q_w(x)}{\rho_w v_w (h_e^0 - h_r)} \quad , \quad (28f)$$

$$\lim_{\tilde{y} \rightarrow \infty} g(\eta, x) \quad \text{is bounded.} \quad (28g)$$

These partial differential equations are parabolic in the  $x$  direction and are therefore well suited to conversion to ordinary differential equations in  $\eta$  by replacement of the  $x$  derivatives with finite differences. This is done according to a scheme used successfully by Mellor [ 5 ] . The  $x$  derivatives of the functions,  $f'$  ,  $g'$  and  $\delta^*$  are written as

$$f'_x = \frac{f' - f'_b}{\Delta x} , \quad (29a)$$

$$g'_x = \frac{h' - h'_b}{\Delta x} , \quad (29b)$$

$$\delta^*_x = \frac{\delta^* - \delta^*_b}{\Delta x} , \quad (29c)$$

$$\Delta x = x - x_b , \quad (29d)$$

where  $f'_b$  ,  $g'_b$  , etc. are the known profiles and  $f'$  ,  $g'$  , etc., are the profiles to be calculated. The values of  $f'_x$  and  $g'_x$  best approximate the derivative of  $f'$  and  $g'$  at  $x_m$  , the midpoint between  $x_b$  and  $x$  . This can be used to advantage by defining the average values of the variables between  $x_b$  and  $x$  as

$$f'_m = \frac{1}{2}(f'_b + f') , \quad (30a)$$

$$g'_m = \frac{1}{2}(g'_b + g') , \quad (30b)$$

$$\delta^*_m = \frac{1}{2}(\delta^*_b + \delta^*) , \quad (30c)$$

$$M_{e_m} = \frac{1}{2}(M_{e_b} + M_e) , \text{ etc.} \quad (30d)$$

and then rewriting equations (24a), (24b) and (25) in terms of them. These equations are

$$\begin{aligned}
 & \left\{ \frac{\delta_k^*}{\delta_m^*} \frac{r_m}{\theta_m} \left[ \theta_m (1 - f'_m) \right]' \right\}' = \left\{ Q \theta_m (\eta - f_m) \right\} f''_m \\
 & + \left\{ \left( V \theta_m + \frac{\delta_m^*}{\Delta x} \theta_x \right) (f'_m - 2) + Q \theta'_m (\eta - f_m) - \frac{\delta_m^*}{\Delta x} \theta_m (1 - f'_m) \right\} f'_m \\
 & + \left\{ Q \theta'_m + \frac{\delta_m^*}{\Delta x} \left[ \theta_m (1 - f'_m) \right]' \right\} f_m \\
 & + \left\{ V (\theta_m - 1) + \frac{\delta_m^*}{\Delta x} \theta_x - Q \eta \theta'_m + \frac{\delta_m^*}{\Delta x} \left[ \theta_m (1 - f'_m) f'_b - (\theta_m (1 - f'_m))' f_b \right] \right\} \\
 & \hspace{25em} (31a)
 \end{aligned}$$

$$\begin{aligned}
 & \left[ \frac{\delta_k^*}{\delta_m^*} \frac{r_{hm}}{\theta_m} \left\{ -g''_m + \frac{\frac{\gamma-1}{2} M_{em}^2}{H \left( 1 + \frac{\gamma-1}{2} M_{em}^2 \right)} \left[ \frac{r_m}{r_{hm}} - 1 \right] \left[ \theta_m^2 (1 - f'_m)^2 \right]' \right\} \right]' \\
 & = \left\{ Q (\eta - f_m) - 2 \frac{\delta_m^*}{\Delta x} (f_m - f_b) \right\} g''_m \\
 & - \left\{ \frac{\delta_m^*}{\Delta x} (1 - f'_m) \right\} g'_m + \left\{ \frac{\delta_m^*}{\Delta x} (1 - f'_m) g'_b \right\} , \hspace{2em} (31b)
 \end{aligned}$$

$$\theta_m = \frac{2 \left(1 + \frac{\gamma-1}{2} M_{e_m}^2\right) (1 - Hg'_m)}{1 + \sqrt{1 + \frac{\gamma-1}{2} M_{e_m}^2 (1 - f'_m)^2 (1 + \frac{\gamma-1}{2} M_{e_m}^2) (1 - Hg'_m)}} \quad (31c)$$

$$\theta_x = 2 \frac{(\theta_m - \theta_b)}{\Delta x} , \quad (31d)$$

$$Q_m = \frac{\rho_e U \delta^* - (\rho_e U \delta^*)_b}{\rho_{em} U_m \Delta x} , \quad (31e)$$

$$V_m = \frac{(U - U_b) \delta^*}{U_m \Delta x} , \quad (31f)$$

$$\eta_m = \frac{y}{\delta_m^*} . \quad (31g)$$

The equations above are a set of ordinary differential equations involving only the variables  $f'_m$ ,  $g'_m$ , etc. to be calculated and the known profiles,  $f'_b$ ,  $g'_b$ , etc. Once  $f'_m$  and  $g'_m$  have been obtained, the profiles at  $x$ , the position of interest, are simply

$$f'(\eta) = 2 f'_m(\eta) - f'_b(\eta) , \quad (32a)$$

$$g'(\eta) = 2 g'_m(\eta) - g'_b(\eta) , \quad (32b)$$

$$\delta^* = 2 \delta_m^* - \delta_b^* , \text{ etc.} \quad (32c)$$

A problem is encountered when using the finite difference method described above. If, for some reason, the known profile at  $x_b$  is not accurate, this inaccuracy is passed on with small attenuation to succeeding profiles. This situation results from the fact that near the wall the profiles adjust very quickly to local conditions. Therefore instead of approaching the correct profile more slowly as the outer layer does, the layer near the wall will immediately assume the correct values for the midpoint at each step in  $x$ . If the profile at  $x_b$  is incorrect, it will be projected through the correct midpoint profile with equation (32a) to an equally incorrect profile at position  $x$ . Besides producing profiles which are incorrect near the wall, this overshoot causes oscillating skin friction and heat transfer coefficients. An alternative to the method above is the backward difference method which, although the  $x$  derivatives are less accurate, is free of this overshoot. There the equations would be solved in the form (24a) and (24b), and the  $x$  derivatives would be approximated by

$$f'_x = \frac{f' - f'_b}{\Delta x} , \quad (33a)$$

$$g'_x = \frac{g' - g'_b}{\Delta x} , \text{ etc.} \quad (33b)$$

However by combining the two difference methods, the overshoot, when it occurs, can be greatly reduced, and yet sufficient accuracy can be maintained. This is accomplished by calculating the intermediate profile somewhere between  $(x - x_b)/2$  and  $x$  according to the relation

$$f'_m = f'_b + (f' - f'_b) \left( \frac{x_m - x_b}{x - x_b} \right) , \quad (34a)$$

$$g'_m = g'_b + (g' - g'_b) \left( \frac{x_m - x_b}{x - x_b} \right) , \text{ etc.} \quad (34b)$$

In places where the boundary conditions change rapidly and overshoot is

likely,  $x_m$  can be made closer to  $x$  ; in places where overshoot is unlikely,  $x_m$  can be closer to  $(x - x_p)/2$  for accuracy. Also, using this method with  $x_m$  set close to  $x$  , poor guesses for the initial profiles  $f'_0(\eta)$  and  $g'_0(\eta)$  will still result in acceptable profiles several  $x$  positions downstream.

Another device was found to be convenient in connection with initial profiles. In many boundary layer calculations initial velocity and enthalpy profiles are not known. Even when comparing calculations with established data, as in Section IV , initial profiles are not completely specified. This is true, for instance, in the sensitive region near the wall. What is known are the conditions of pressure gradient and heat transfer under which the layer developed and the Reynolds number and displacement thickness at the  $x$  position where the calculation is to begin. The initial profiles were therefore produced by recalculating the input profile with several simplifying assumptions. It was assumed that the pressure gradient was produced by a velocity distribution of the form

$$\frac{U}{U_0} = \left( \frac{x}{L} \right)^B, \quad U(L) = U_0 \quad (35)$$

and that the growth of  $\delta^*$  was linear

$$\frac{\delta^*}{L} = A \left( \frac{x}{L} \right), \quad (36)$$

which gives the result that

$$\frac{U_x \delta^*}{U} = A B \quad \text{and} \quad Q = \frac{(\rho_e U \delta^*)_x}{\rho_e U} = A \left[ 1 + B(1 - M_e^2) \right] \quad (37)$$

are independent of  $x$  . Finally the profiles  $f'$  and  $g'$  are assumed to be unchanging with  $x$  . The momentum and energy equations then become ordinary differential equations in  $\eta$  to be solved for  $f'$  and  $g'$  . The resulting profiles were satisfactory even though the Reynolds number was not allowed to change from profile to profile and therefore the skin friction coefficient and Stanton number are not exact. Then, since there was a slight



discontinuity in values like  $C_f$  and  $\delta^*$  between the reset profile and the first profile moving forward, it was found best to allow space to calculate profiles at two or three stations before the initial station.

The solution of the ordinary differential equations (31a) and (31b) was carried out iteratively. The succession of calculations in a single iteration was as follows. The momentum equation (31a) was solved for  $f'_m$ ,  $f''_m$  and  $\delta_m^*$ . Then the parameters  $Q$  and  $V$  were recalculated based on the new  $\delta_m^*$ . The energy equation was solved next for  $h'_m$  and  $h''_m$  and then  $\theta_m$  was determined from equation (31c). Finally the effective viscosity and conductivity were calculated from (27a) and (27b) using the variables at  $x_m$ . This method proved very satisfactory. The solution of the energy equation followed the iterations of the momentum very well. Therefore it was unnecessary to have an internal iteration loop for the energy equation to assure its convergence as did Smith and Clutter [13]. Speed of convergence for the whole loop varied, but no cases required more than seven iterations, and in simple cases two iterations were sufficient.

A fourth degree Runge-Kutta method was used to solve equations (31a) and (31b). In order to use this method the  $f'$  and  $g'$  equations were written in pseudo-linear form

$$\left\{ C_6(\eta) [f'' + C_5(\eta)] \right\}' = C_3(\eta) f'' + C_2(\eta) f' + C_1(\eta) f + C_4 \quad (38)$$

where the coefficients are the quantities in brackets in equations (31a,b). These coefficients were evaluated from the solution obtained from the previous iteration. The Runge-Kutta equations for the solution of (38) are given in Appendix C.

The calculation of each equation was begun from the wall with the specification of two boundary conditions as given by (28). The outer boundary conditions on (31a) and (31b) were met with the use of an asymptotic solution for large  $\eta$  which assured the correct exponential behavior as shown in equation (22a). The derivation of the asymptotic solution is performed with the additional simplifying assumption that the turbulent Prandtl number is unity (see Appendix D). For compressible flow with heat transfer the asymptotic forms of  $f'$  and  $g'$  can be expressed in terms of  $f'$  and  $g'$  at point  $\eta_1$ , far out in the layer,

$$f'(\eta, x) = f'(\eta_1, x) \exp \frac{(\eta_1 - 1)^2 - (\eta - 1)^2}{2r(x)}, \quad (39a)$$

$$g'(\eta, x) = g'(\eta_1, x) \exp \frac{(\eta_1 - 1)^2 - (\eta - 1)^2}{2r(x)}, \quad (39b)$$

$$r(x) = \left( \frac{\rho_{e0} U_0 \delta_0^*}{\rho_e U \delta^*} \right)^2 r(x_0) + \frac{2K}{(\rho_e U \delta^*)^2} \int_{x_0}^x \frac{\delta_k^*}{\delta^*} (\rho_e U)^2 \delta^* dx \quad (40)$$

The numerical solutions were matched to the asymptotic solution by exploiting the effective linearity of equations (31a) and (31b). Both homogeneous and particular solutions were obtained for each equation. The solution of the homogeneous equation was added to the particular solution in the proportion to make the numerical solution join the analytical solution at  $\eta_1$ . In this manner the third inner boundary condition which had been guessed to perform the integration was reset to the proper value afterwards. This was done according to the equations

$$f' = f'_p + A_f f'_h, \quad (41a)$$

$$g' = g'_p + A_g g'_h, \text{ etc.} \quad (41b)$$

The constants  $A_f$  and  $A_g$  are obtained using the derivatives of equations (39a) and (39b), evaluated at the matching point  $\eta_1$ ,

$$f''(\eta_1) = - \frac{(\eta_1 - 1)}{r} f'(\eta_1), \quad (42a)$$

$$g''(\eta_1) = - \frac{(\eta_1 - 1)}{r} g'(\eta_1) \quad . \quad (42b)$$

Therefore  $A_f$  and  $A_g$  are given by

$$A_f = - \frac{f_p''(\eta_1) + \frac{(\eta_1 - 1)}{r} f_p'(\eta_1)}{f_h''(\eta_1) + \frac{(\eta_1 - 1)}{r} f_h'(\eta_1)} \quad , \quad (43a)$$

$$A_g = - \frac{g_p''(\eta_1) + \frac{(\eta_1 - 1)}{r} g_p'(\eta_1)}{g_h''(\eta_1) + \frac{(\eta_1 - 1)}{r} g_p'(\eta_1)} \quad (43b)$$

The method of calculation from an operational viewpoint is as follows. First, profiles of  $f'$  and  $g'$  are read into the program as functions of  $\eta$ . These profiles correspond to the first  $x$  position,  $x = x_1$ , say. If these profiles are complete and satisfactory as they stand, they are used unaltered. If, on the other hand, they are not the desired initial profiles, approximate initial profiles are calculated for the required initial Mach number, Reynolds number, displacement thickness, lateral wall curvature, and heat transfer rate or wall temperature. If the  $f'$  and  $g'$  profiles are to be recalculated, the input profiles are used as initial guesses.

Next the values of the mainstream Mach number and wall heat flux or temperature are read in corresponding to the discrete values of  $x$  at which profiles are to be calculated. Also read in for each  $x$  is a number between 0.5 and 1.0 which indicates the position in the interval between  $x$  values where the actual calculation of the profile is to take place. Then the profiles and parameters for each succeeding  $x$  position are calculated and reported until the last  $x$  position has been reached.

#### IV. COMPARISON WITH EXPERIMENTAL DATA

##### Zero Pressure Gradient

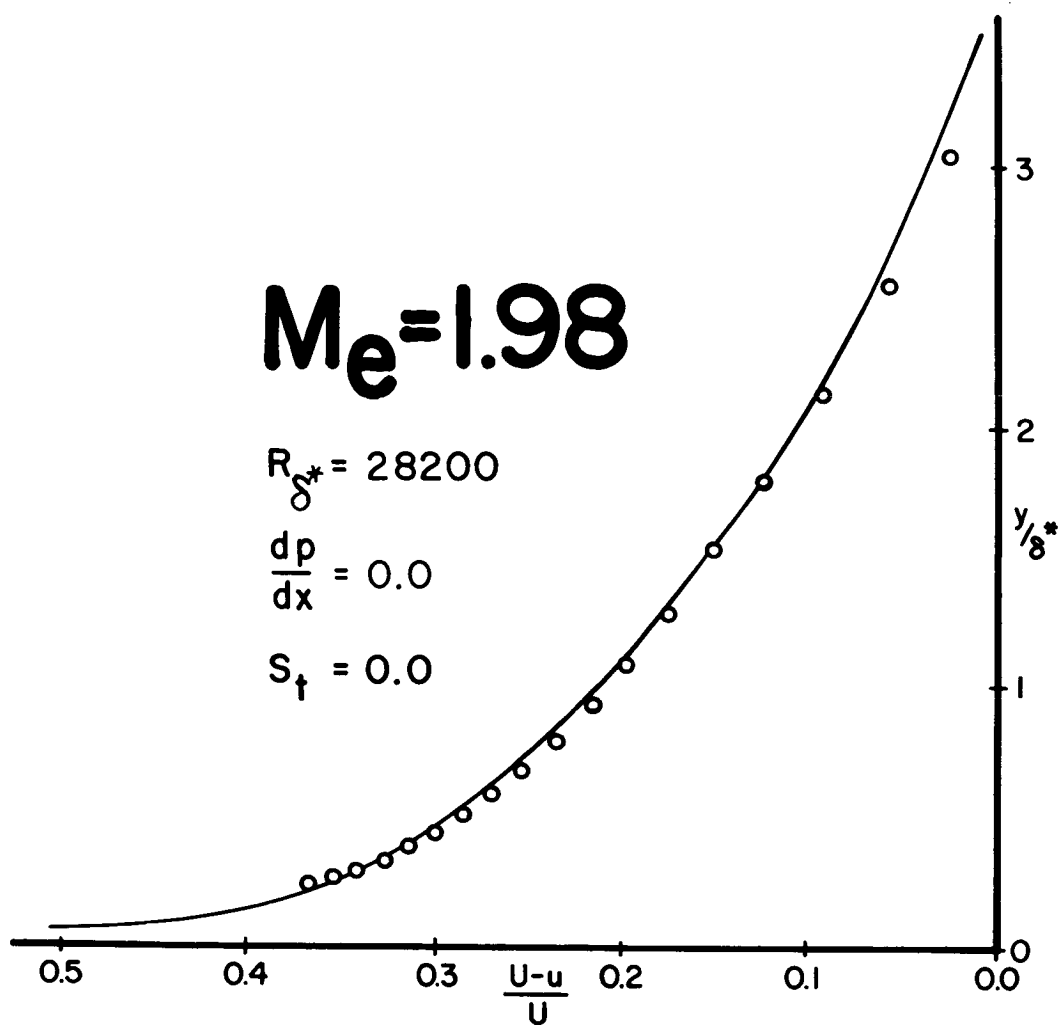
A wide variety of experimental velocity profiles measured in constant pressure adiabatic flows are available. Calculations were performed for a few of these profiles representing a range of Mach number from 2 up to 4.5. No data at lower Mach numbers are compared because there are few experiments in the transonic region. This is the result of experimental difficulties not related to the development of the boundary layer itself. Furthermore, the boundary layer in the subsonic and transonic range differs only slightly from the incompressible boundary layer.

Calculations for the flows considered were begun by generating an initial constant pressure profile internally as described in Section III. Then, starting at a Reynolds number somewhat below that of the data profile, the calculation proceeded until the data Reynolds number was reached. These profiles were calculated two ways, once with the assumption  $h^0(y) = h_e^0$  (or  $g'(\eta) = 0$ ) and once using the full energy equation with  $Pr = .78$  and  $Pr_t = 1.0$ . The results were identical within the accuracy of the graphs. Experimental profiles were chosen which had values of  $U\delta_k^*/\bar{v}_s$  above 2500, where  $\delta_k^*$  is the kinematic displacement thickness and  $\bar{v}_s$  is the local molecular viscosity at the edge of the laminar sublayer. As explained in Section II this criterion assures that the hypothesis is well within its range of validity. The calculations and experiments are compared in Figures 4 through 9.\* It is clear from the figures that the prediction of the velocity profiles and skin friction coefficients is remarkably good.

Further comparison with established results was provided by calculating the skin friction coefficient for constant pressure adiabatic flows over a range of Mach number.† The calculations were carried out as described for the profiles above. Initial profiles were generated and then allowed to develop until a high enough  $R_\theta$  had been reached. Then, for  $R_\theta$  of 2000 and 7000, the skin friction was normalized by the corresponding, incompressible skin friction. Above  $M_e \approx 1$ , in the  $R_\theta = 2000$  case, the Reynolds number  $R_s (= U\delta_k^*/\bar{v}_s)$  was below 2500; therefore that curve was not continued. Above  $R_\theta = 7000$ , there was no discernable change of the calculated values of  $C_f/C_{f_i}$  with  $R_\theta$ . The results of these calculations are compared with experimental skin friction coefficients from Kuethe [ 20 ] in Figure 10.

\*Data from references 14, 15, and 16.

†Data from references 14, 17, 18, and 19.



$$C_{f_{\text{exp.}}} = 0.00202, \quad C_{f_{\text{the.}}} = 0.00201$$

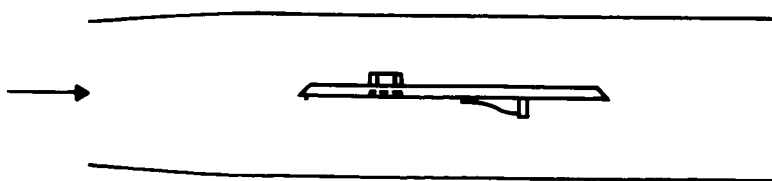
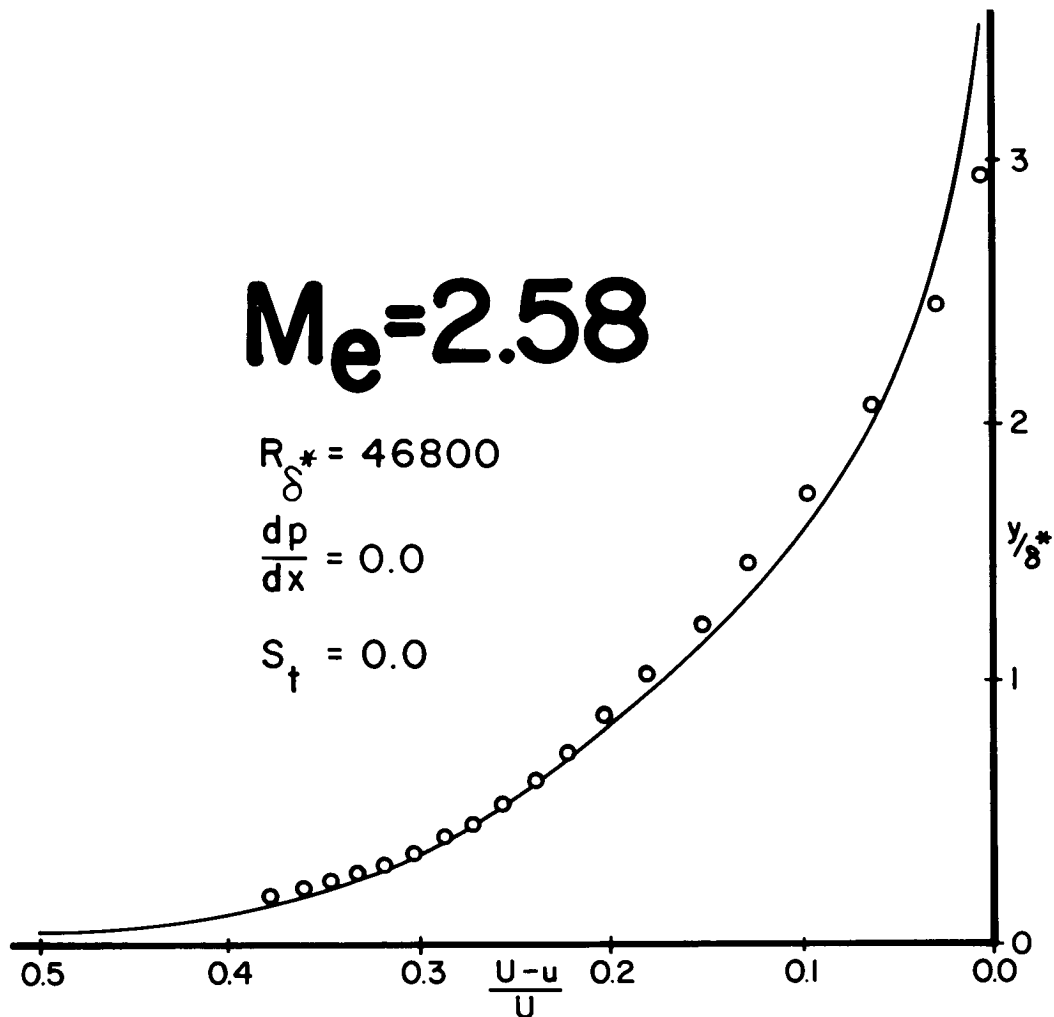


FIGURE 4. Comparison between a velocity profile measured by Coles [14] on a flat plate at  $M_e = 1.98$  and the calculated profile shown with an unbroken line. The experimental skin friction, which was measured with a floating surface element, is also compared with the calculated value.



$C_{f_{\text{exp}}} = 0.00166, \quad C_{f_{\text{the.}}} = 0.00170$

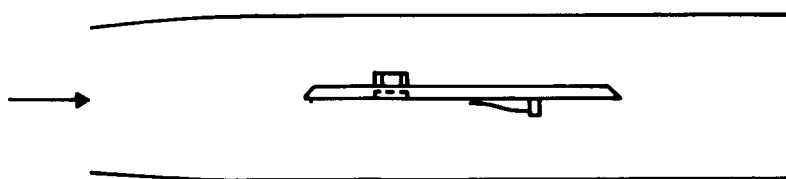
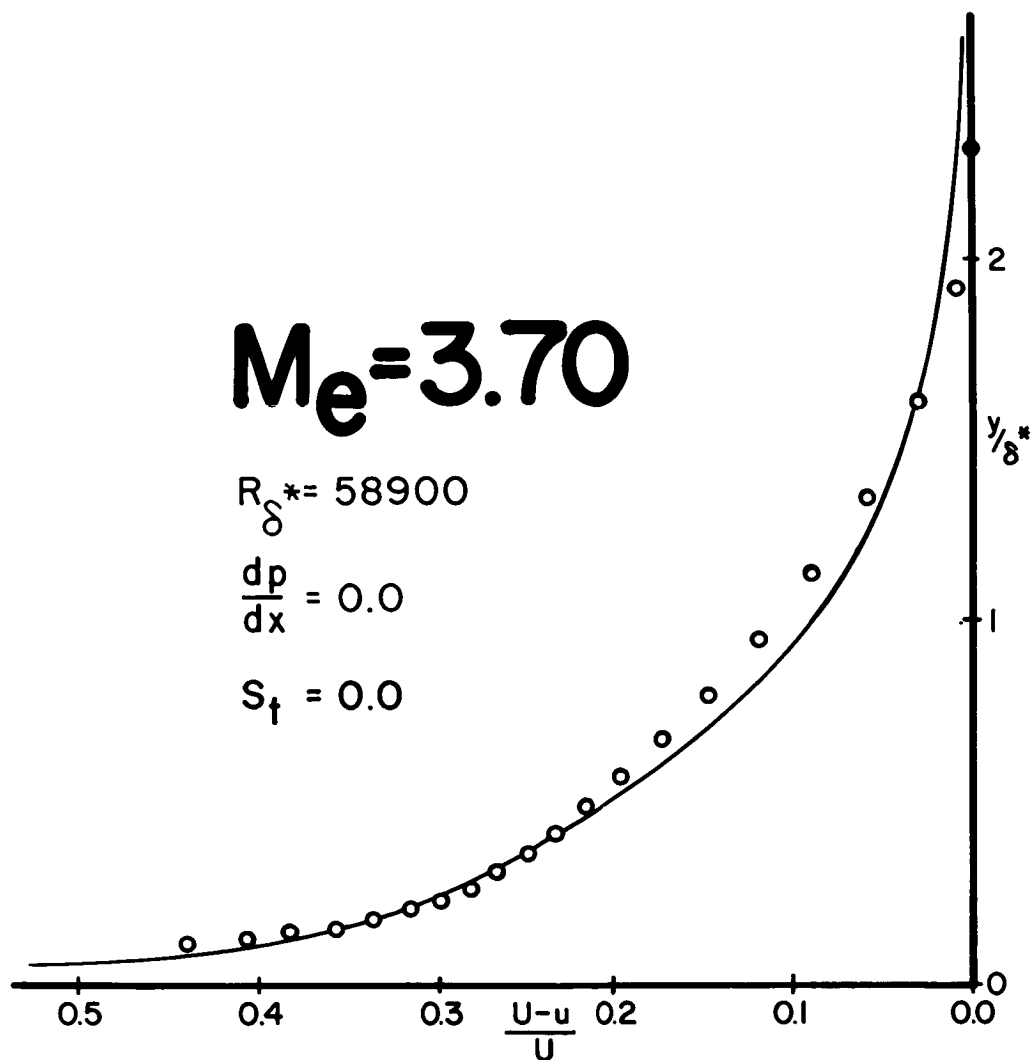


FIGURE 5. Comparison between a velocity profile measured by Coles [14] on a flat plate at  $M_e = 2.58$  and the calculated profile shown with an unbroken line. The experimental skin friction, which was measured with a floating surface element, is also compared with the calculated value.



$C_{f_{exp.}} = 0.00138, \quad C_{f_{the.}} = 0.00145$

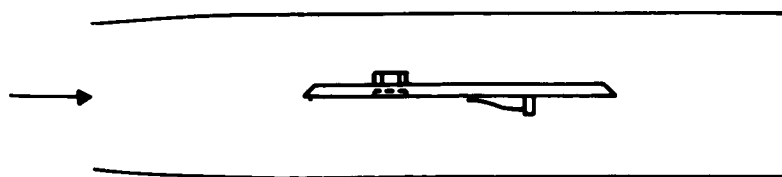
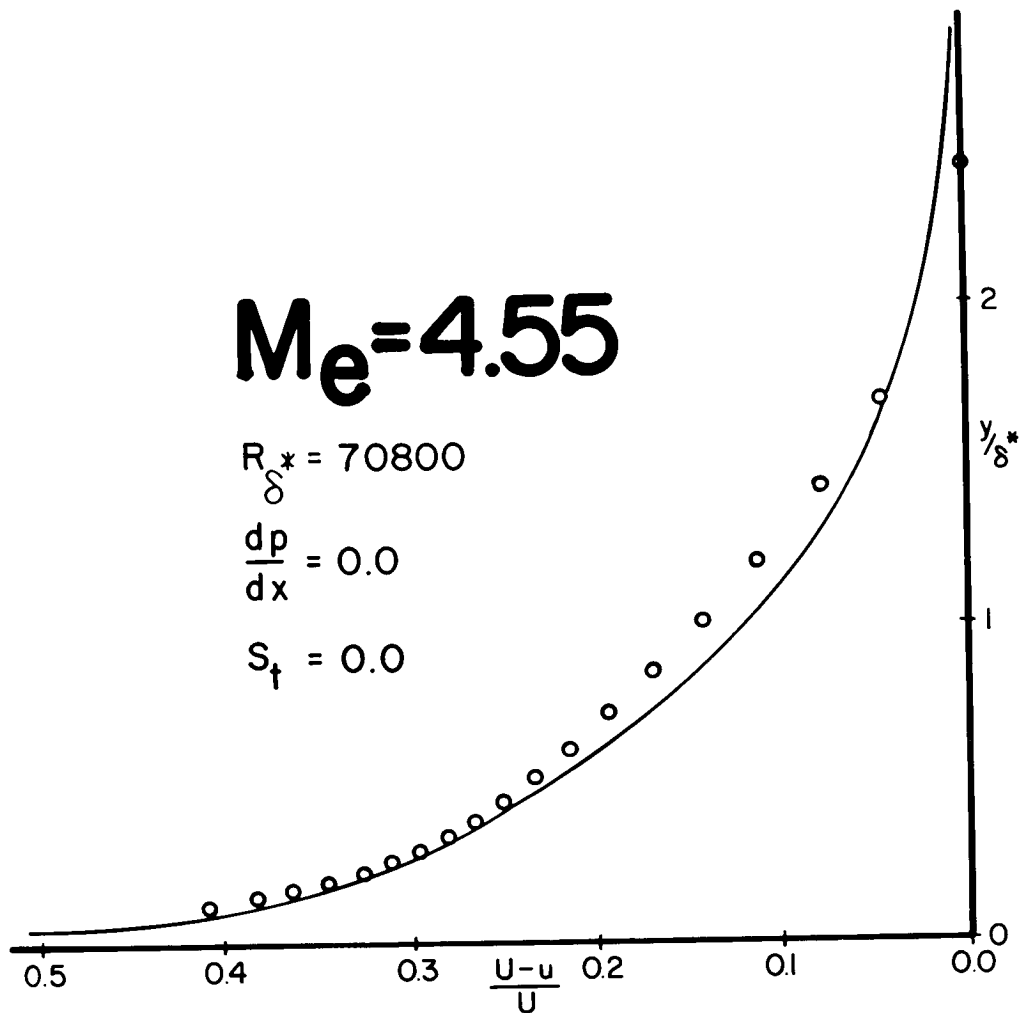


FIGURE 6. Comparison between a velocity profile measured by Coles [14] on a flat plate at  $M_e = 3.70$  and the calculated profile shown with an unbroken line. The experimental skin friction, which was measured with a floating surface element, is also compared with the calculated value.



$$C_{f_{exp.}} = 0.00122, \quad C_{f_{the.}} = 0.00126$$

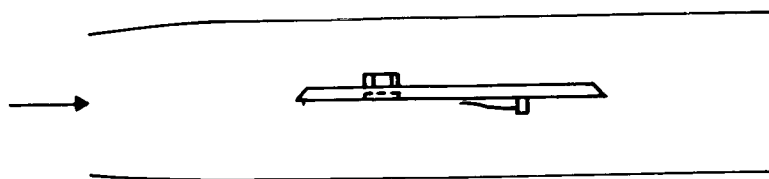


FIGURE 7. Comparison between a velocity profile measured by Coles [14] on a flat plate at  $M_e = 4.55$  and the calculated profile shown with an unbroken line. The experimental skin friction, which was measured with a floating surface element, is also compared with the calculated value.



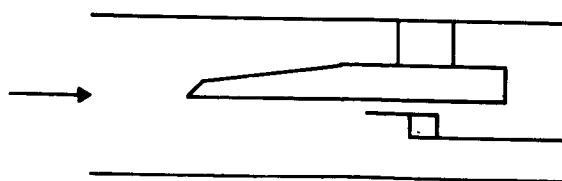
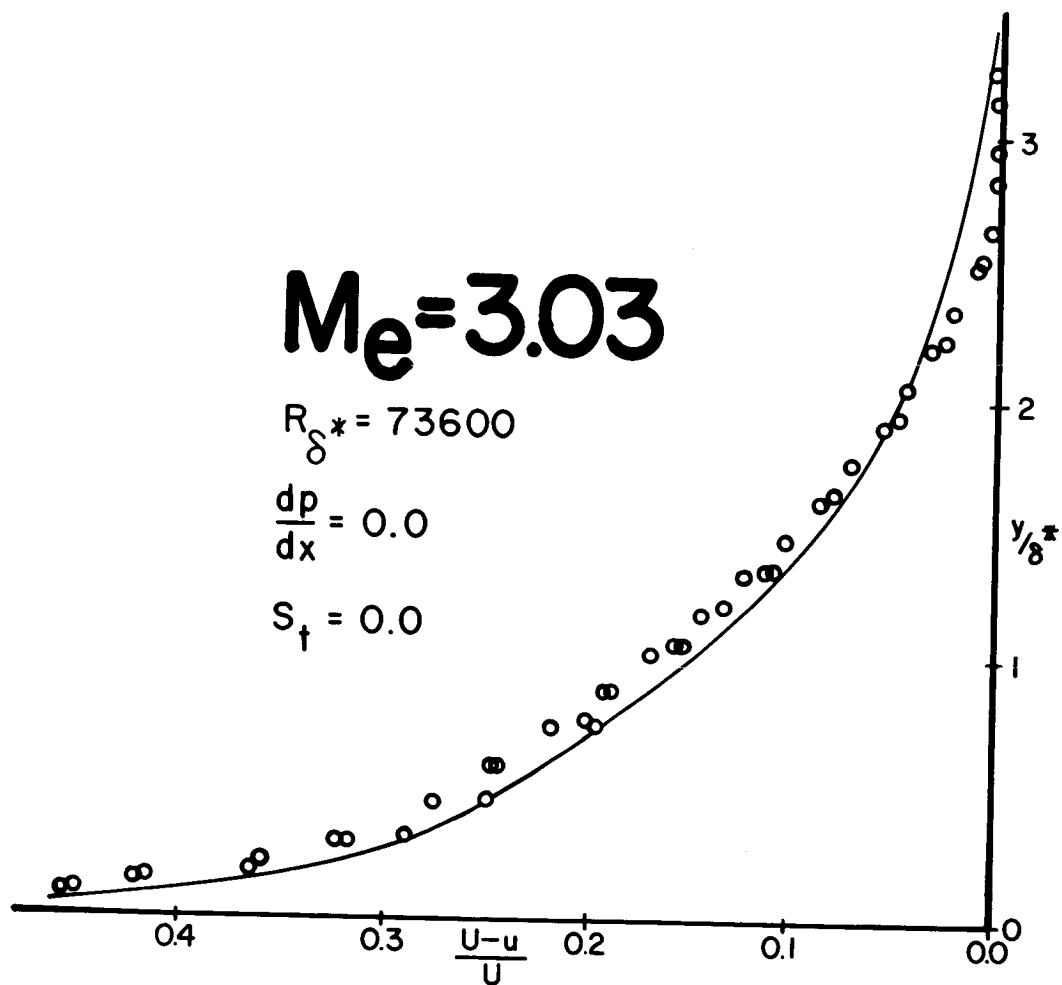
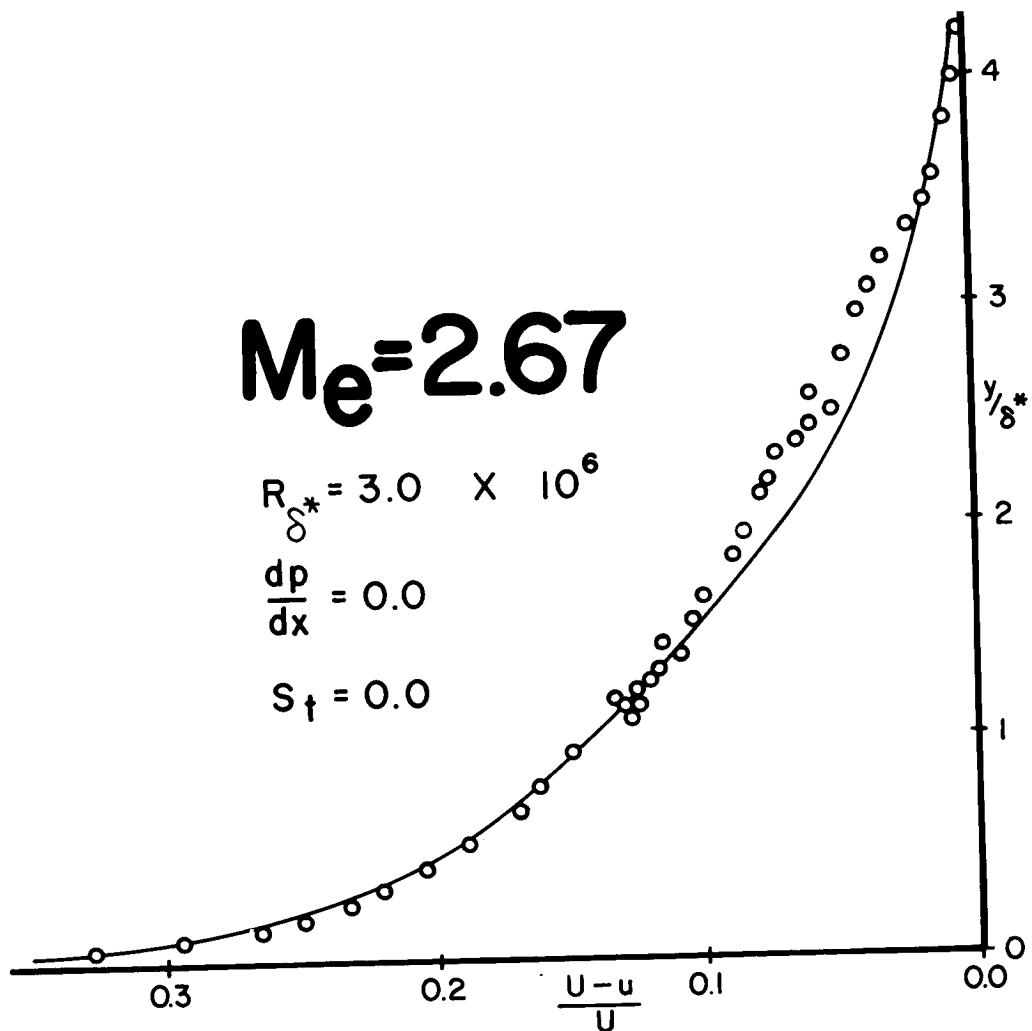


FIGURE 8. Comparison between a velocity profile measured by Nothwang [15] with a pitot tube on a flat plate at  $M_e = 3.03$  and the calculated profile shown with an unbroken line.



$$C_{f_{exp.}} = 0.000862, \quad C_{f_{the.}} = 0.000856$$

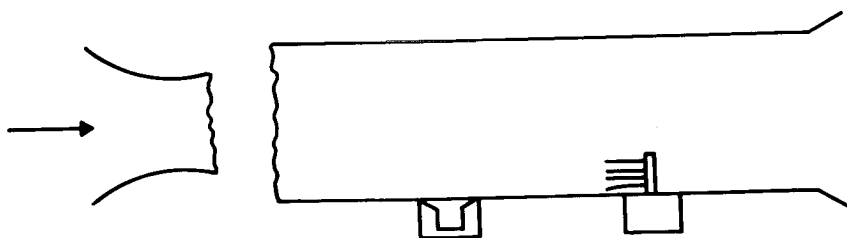


FIGURE 9. Comparison between a very high Reynolds number velocity profile measured by Moore and Harkness [16] on a tunnel wall at  $M_e = 2.67$  and the calculated profile shown with an unbroken line.

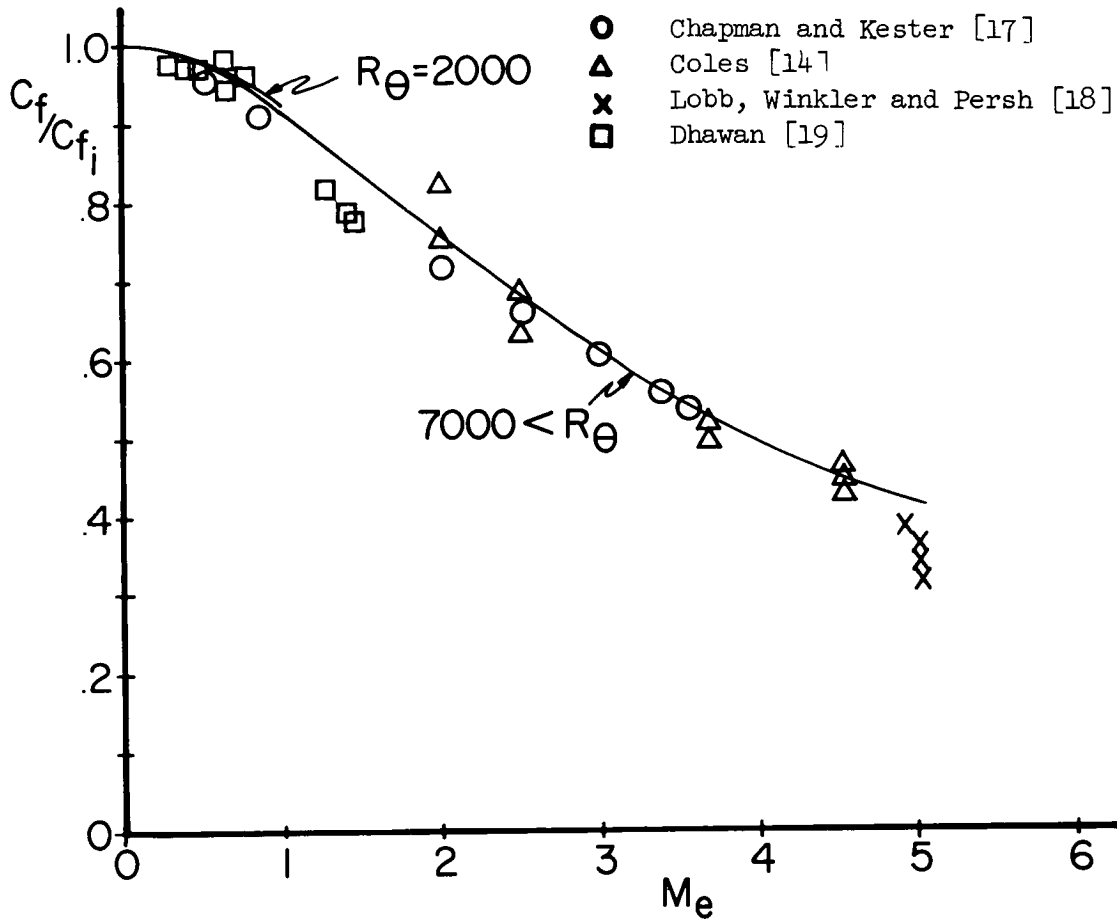


FIGURE 10. Comparison between experimental skin friction measurements obtained by a number of investigators (after Kuethe [20]) and the calculated skin friction.  $C_f/C_{f_i}$  is the ratio of compressible skin friction coefficient to incompressible skin friction coefficient at the same value of  $R_\theta = 2000$ , and one for  $R_\theta$  greater than 7000. The calculation for  $R_\theta = 2000$  does not extend beyond  $M_e = 1$  because of the Reynolds number limitation on the effective viscosity hypothesis.

Again the comparison with the data is favorable.

Having seen the degree of success achieved by the effective viscosity assumption in cases where  $\underline{R}_s$  is high enough, it is valuable to study the nature of the error incurred for small values. Some examples of this are shown in Figures 11 through 16\*. Figure 11 illustrates this especially well. Beginning with the first profile, for which the calculated value of  $\underline{R}_s$  is 1260, a progressive improvement in the theoretical prediction is evident up to the last profile for which  $\underline{R}_s$  is 2440. However, although the shape of the profile is not too good for low  $\underline{R}_s$ , the growth of  $\delta^*$  is quite accurate as is also shown in Figure 11. The calculation of this series was begun by generating a constant pressure profile internally at the appropriate Mach number. Because of the slight discontinuity in skin friction and other parameters after the generated profile, which was mentioned in Section III, this profile was calculated for approximate values of  $\delta^*$  and  $R_\delta^*$  at  $x_0$  somewhat upstream of the first profile measurement at  $x = 5.95$ . Trial calculations were made from  $x_0$  up to  $x = 5.95$  so that  $\delta^*$  and  $R_\delta^*$  matched the experimental values at  $x = 5.95$ .

The importance of considering  $\underline{R}_s (= U\delta_k^*/\bar{v}_s)$  rather than the external Reynolds number  $R_\delta^* (= U\delta^*/v_\infty)$  is brought out in Figure 12, where  $R_\delta^*$  would be sufficiently high if the Mach number were low. However, the Mach number is high, making  $\underline{R}_s$  too low and therefore the theoretical prediction is poor. Figures 13 through 16 also exhibit the same effect for a range of Mach numbers. At the beginning of each series the prediction is poor and, although it improves slightly as the layers develop and  $\underline{R}_s$  increases, the Reynolds number is still not high enough at the end of each series, especially in the higher Mach number cases. In spite of this, it is interesting to note that the growth of  $\theta$  is predicted accurately. For the calculation of the sets of profiles shown in Figures 13 through 16, as in Figure 11, both  $\delta^*$  and  $R_\delta^*$  matched the experimental values at the initial  $x$  station according to the procedure described above.

Because of the variation of  $\bar{v}$  across the layer, boundary layers with low values of  $\underline{R}_s$  occur in practice much more frequently in compressible flows than in incompressible flows. It would be useful to modify the

---

\*Data from references 18, 21, and 22.

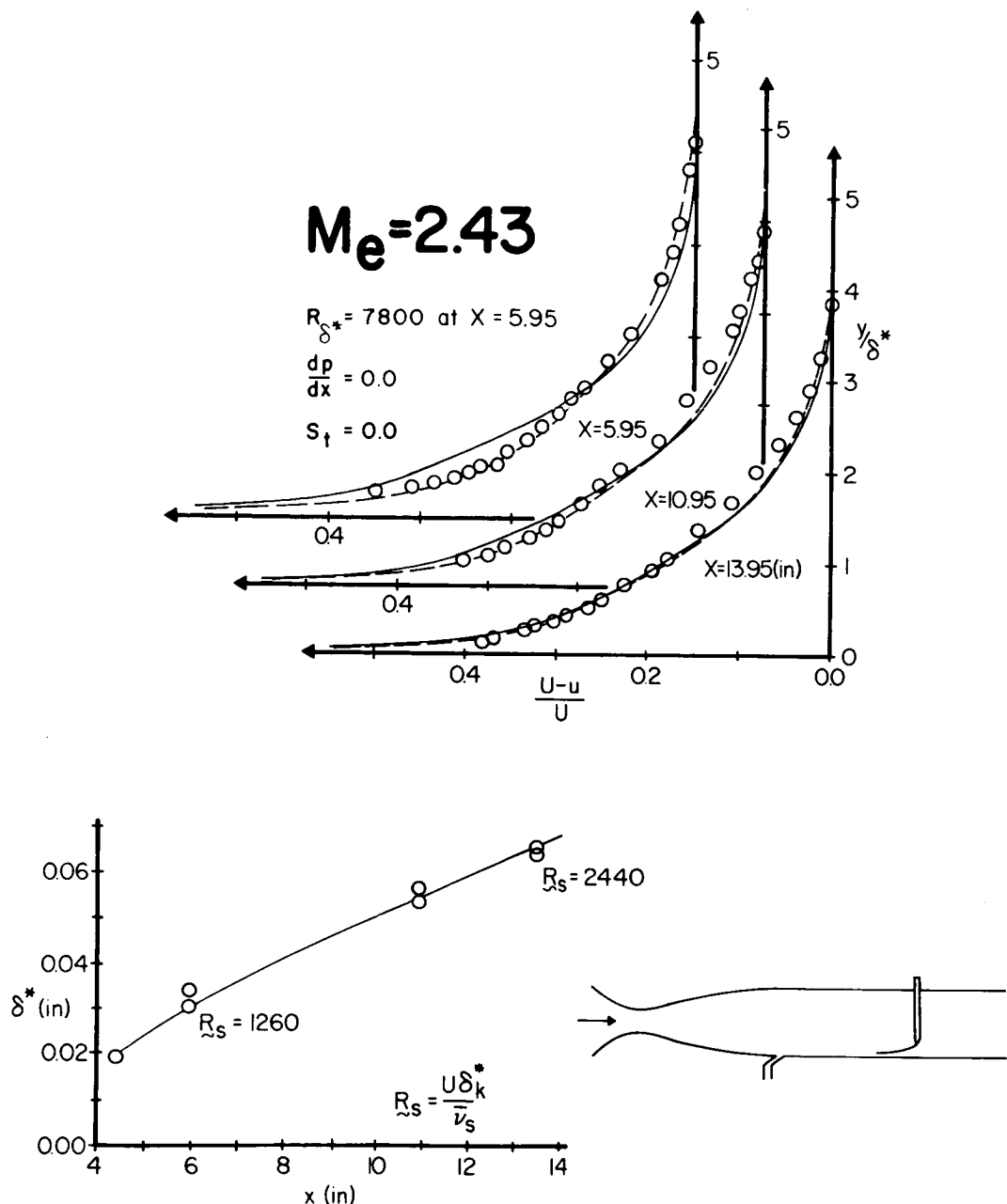


FIGURE 11. Comparison between a series of velocity profiles measured by Monaghan and Johnson [21] on the flat wall of a tunnel and the calculated profiles. Profiles calculated using  $K = 0.016$  in the effective viscosity function are shown with unbroken lines, and profiles calculated using  $K = 0.016 [1 + (1100/\tilde{R}_s)^2]$  are shown with dashed lines. The measured growth of  $\delta^*$  with  $x$  is compared with the calculated growth illustrated with an unbroken line. The calculated growth of  $\delta^*$  for both values of  $K$  are indistinguishable. The initial and final values of  $\tilde{R}_s$  are also given.

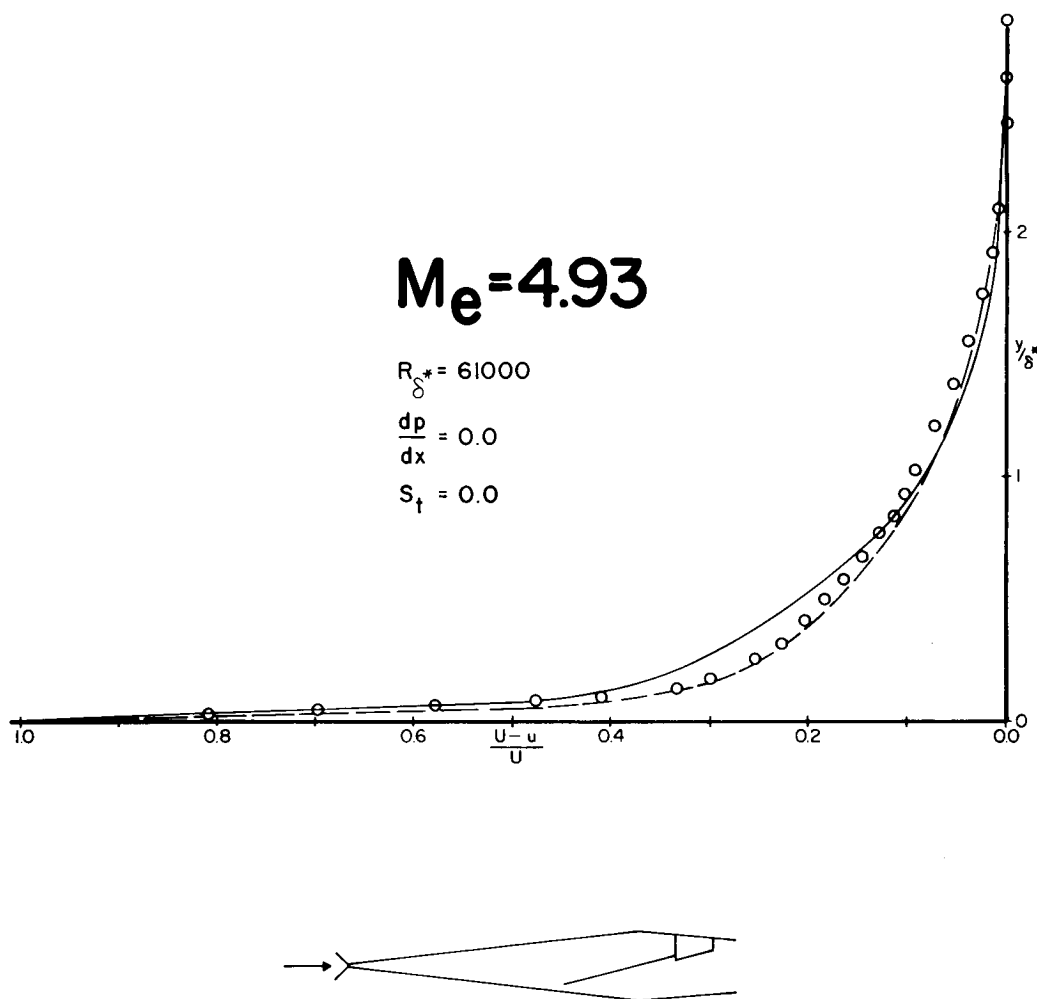


FIGURE 12. Comparison between a velocity profile measured by Lobb, Winkler and Persh [18] on a flat tunnel wall and calculated profiles. The profile calculated using  $K = 0.016$  in the effective viscosity function is shown with an unbroken line and the profile calculated using  $K = 0.016 [1 + (1100/\tilde{R}_s)^2]$  is shown with a dashed line. The value of  $\tilde{R}_s (= U\delta_k^*/\sqrt{\nu_s})$  for this profile is 1050.

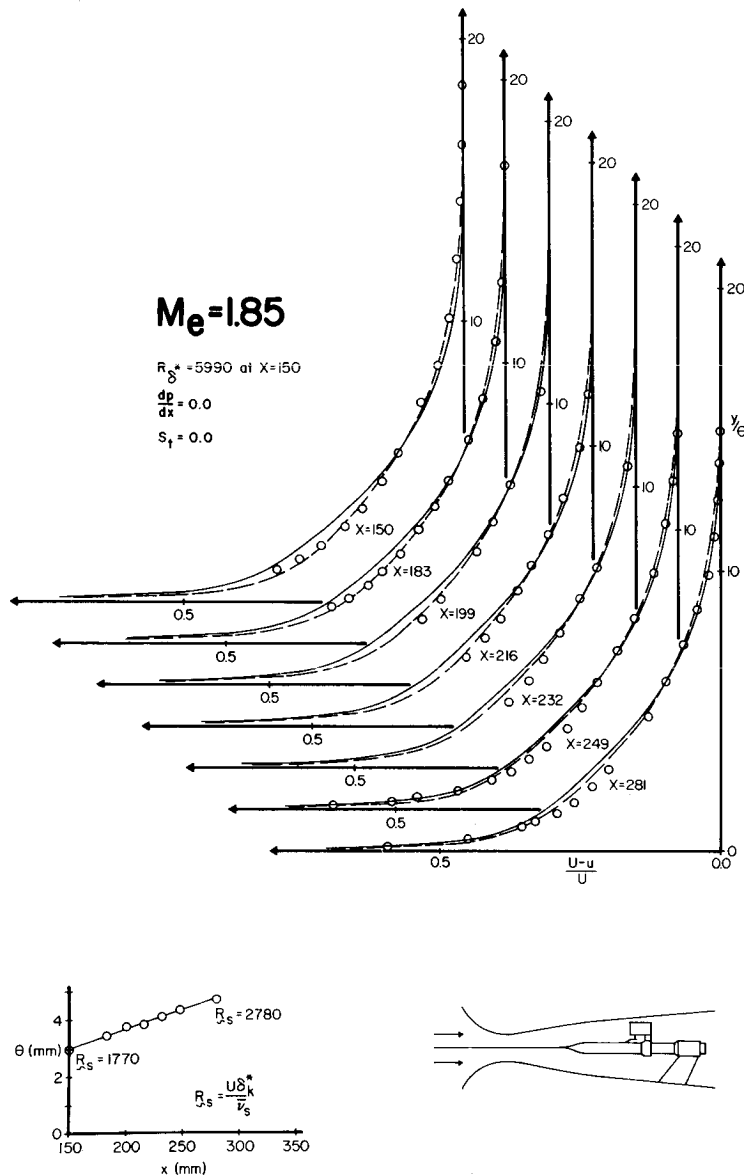


FIGURE 13. Comparison between a series of velocity profiles measured by Michel [22] on a cylindrical model whose radius was large with respect to the boundary layer thickness and the calculated profiles. Profiles calculated using  $K = 0.016$  in the effective viscosity function are shown with unbroken lines and profiles calculated using  $K = 0.016X [1 + (1100/\tilde{R}_s)^2]$  are shown with dashed lines. The measured growth of  $\theta$  with  $x$  is compared with the calculated growth illustrated with an unbroken line. The calculated growth of  $\theta$  for both values of  $K$  are indistinguishable. The initial and final values of  $\tilde{R}_s$  are also given.

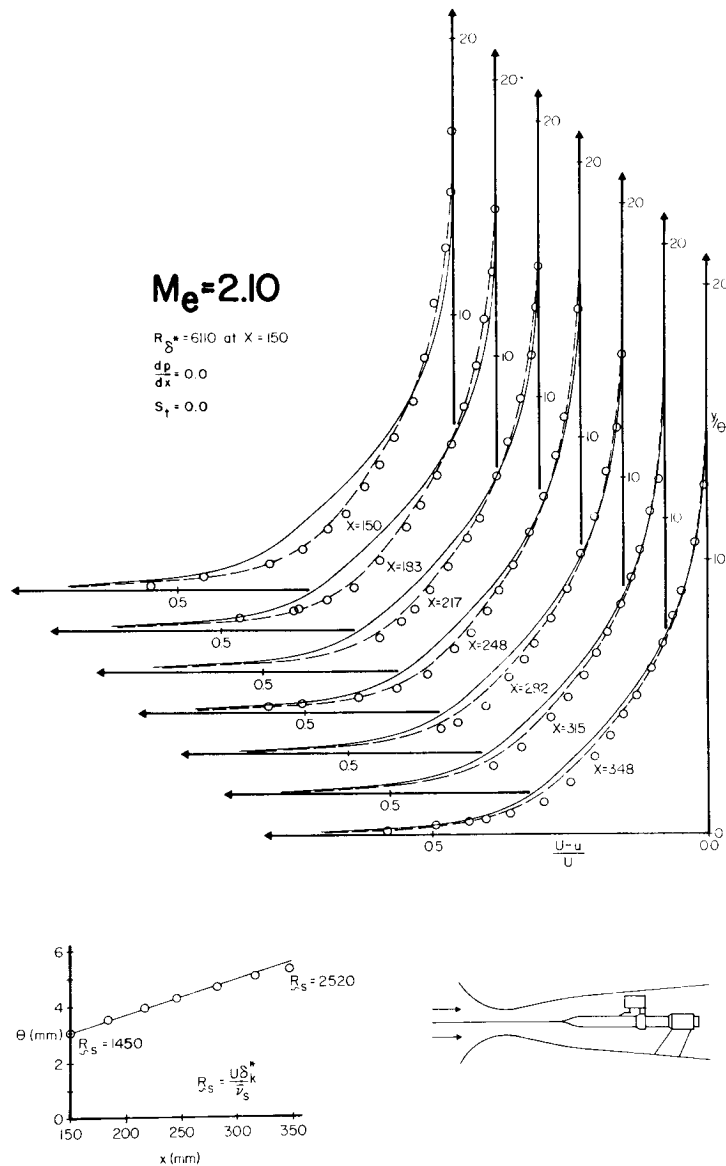


FIGURE 14. Comparison between a series of velocity profiles measured by Michel [22] on a cylindrical model whose radius was large with respect to the boundary layer thickness and the calculated profiles. Profiles calculated using  $K = 0.016$  in the effective viscosity function are shown with unbroken lines and profiles calculated using  $K = 0.016 X [1 + (1100/\tilde{R}_s)^2]$  are shown with dashed lines.

The measured growth of  $\theta$  with  $x$  is compared with the calculated growth illustrated with an unbroken line. The calculated growth of  $\theta$  for both values of  $K$  are indistinguishable. The initial and final values of  $\tilde{R}_s$  are also given.



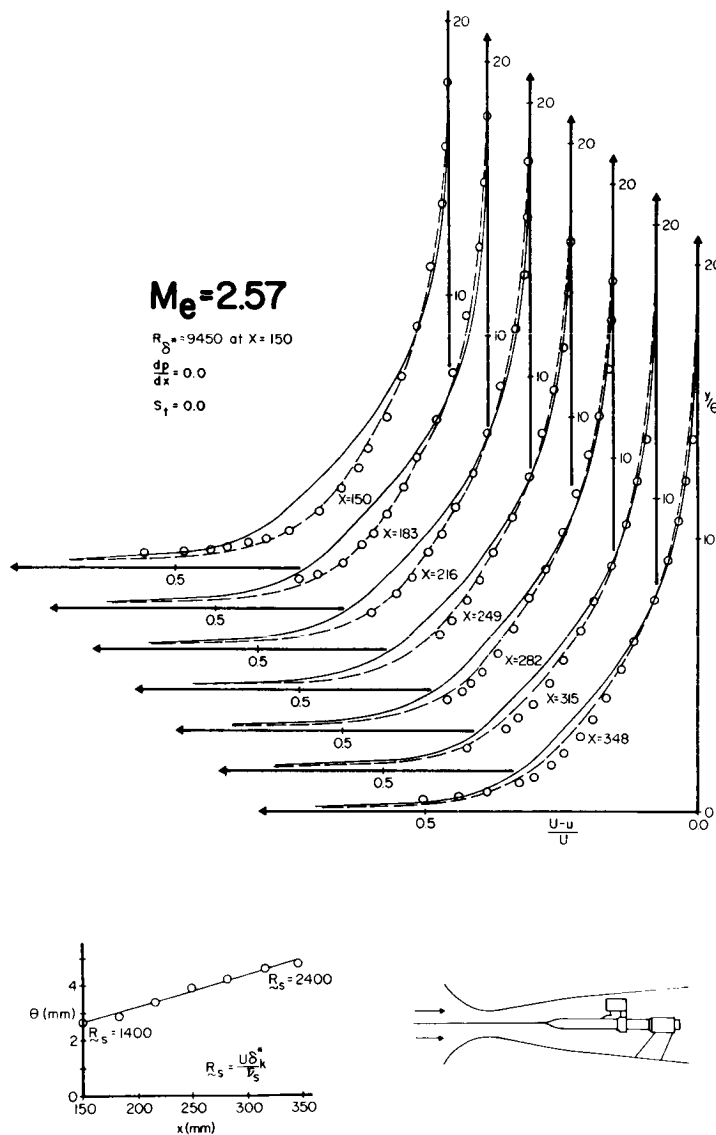


FIGURE 15. Comparison between a series of velocity profiles measured by Michel [22] on a cylindrical model whose radius was large with respect to the boundary layer thickness and the calculated profiles. Profiles calculated using  $K = 0.016$  in the effective viscosity function are shown with unbroken lines and profiles calculated using  $K = 0.016 \times [1 + (1100/\tilde{R}_s)^2]$  are shown with dashed lines.

The measured growth of  $\theta$  with  $x$  is compared with the calculated growth illustrated with an unbroken line. The calculated growth of  $\theta$  for both values of  $K$  are indistinguishable. The initial and final values of  $\tilde{R}_s$  are also given.

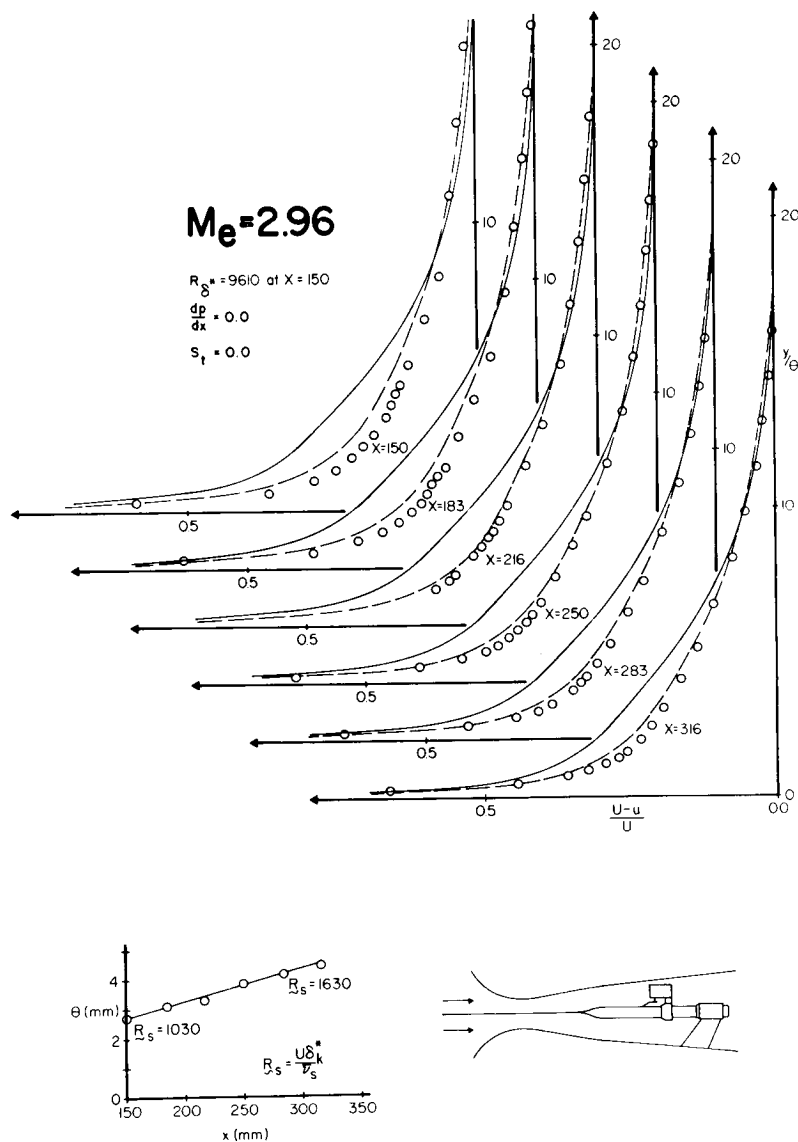


FIGURE 16.

Comparison between a series of velocity profiles measured by Michel [22] on a cylindrical model whose radius was large with respect to the boundary layer thickness and the calculated profiles. Profiles calculated using  $K = 0.016$  in the effective viscosity function are shown with unbroken lines and profiles calculated using  $K = 0.016 \times [1 + (1100/\tilde{R}_s)^2]$  are shown with dashed lines.

The measured growth of  $\theta$  with  $x$  is compared with the calculated growth illustrated with an unbroken line. The calculated growth of  $\theta$  for both values of  $K$  are indistinguishable. The initial and final values of  $\tilde{R}_s$  are also given.

behavior of the effective viscosity to account for this. Accordingly, some numerical experiments were performed with trial amendments to the effective viscosity function for low Reynolds numbers. The most successful method seemed to be to vary  $K$  according to the following rule

$$K = .016 \left[ 1 + \left( \frac{1100}{\tilde{R}} \right)^2 \right] \quad (44)$$

Then the overlap layer, which ordinarily would have disappeared as the outer region met the sublayer, is maintained. Although this procedure maintains the essential overlap layer specified in the third assumption of the hypothesis, the device used is somewhat artificial. The results of this correction are shown as dashed lines on the velocity profiles where the Reynolds numbers were too low for the usual effective viscosity. The profiles in all cases are considerably improved. Of course, this approach is merely exploratory and the principle conclusion seems to be that it works. Furthermore, it does not seem to represent a truly systematic extension of the first order hypothesis represented by equation (12).

#### Axisymmetric Flow with a Pressure Gradient

Variable pressure gradient data are also rare, due to the greatly increased difficulty of carrying out boundary layer investigations in flow with Mach waves. The pressure gradient experiments performed by Winter, Smith and Rotta [ 23 ] were chosen for comparison here. These data are complete and carefully taken, but the results include other effects besides pressure gradients since measurements were taken on a surface of revolution. The effects, which must be accounted for, include lateral and longitudinal curvature as well as freestream Mach number variation. Although the Mach number variation is not excessive, the change in lateral curvature causes strong convergence and divergence of the stream lines. Furthermore, in some places the approximation that  $\delta/R_{LAT} \ll 1$  was no longer valid and the equations of motion had to be written in axisymmetric form (see Appendix E). The approximation that the boundary layer was perpendicular to the axis of symmetry was still valid, however, since  $\delta/R_{LONG} \ll 1$ .

Boundary layer development was calculated for four series of profiles. The approximate Mach number range represented is from 0.5 to 3.3 and the approximate Reynolds number range is from  $U\delta^*/\nu_\infty = 5000$  to 45000. The lowest Mach number flow had only small changes in Mach number, whereas the Mach number variation in the other flows was more substantial. Calculations

were begun by generating profiles internally under the proper conditions of pressure gradient and lateral radius gradient for a station upstream of the first measured profile. Then trial calculations were carried out to find the Reynolds number and displacement thickness at the upstream station that would result in the experimental conditions at the first experimental profile. The final calculations were initialized with these values. The Mach number distributions in Figure 17, and the assumption of an adiabatic wall were used as boundary conditions. Calculations were performed twice, first with the assumption of constant total enthalpy, ( $g' = 0$ ) and again using the energy equation with  $Pr = 0.78$  and  $Pr_t = 1.0$ . As in the case of the constant pressure profiles the difference was small.

Figures 18 and 19 show the experimental and theoretical variation of  $\delta^*$  and  $\theta$ . In both cases the calculated values compare very well showing that the convergence and divergence has been properly accounted for. The points marked with squares were calculated using the von Karman integral momentum equation with the experimental values of  $C_f$  and  $\delta^*/\theta$ . This verifies that the symmetry of the flow was good. The results of the skin friction calculation are shown in Figure 20. Although the tendency of the calculated  $C_f$  is correct in all cases, the prediction is generally somewhat high. At present the reason for this is not known.

The profiles are shown in Figures 21 to 24. The first few profiles compare well in most cases, which shows that the method of initializing the calculation is adequate. However, near the region of the waist of the body the calculated profiles begin to diverge from the experimental profiles. Beyond the region of the waist the Mach number distribution outside the boundary layer reported by Winter, Smith and Rotta is almost constant in each case. On the other hand, the experimental profiles change very much beyond this point. Therefore, either the external Mach number variation is not indicative of the Mach number variation inside the layer, due perhaps to the presence of Mach waves, or there is an effect other than that of pressure gradient which has not been taken into account. One possibility is the effect of longitudinal curvature on the structure of the turbulence itself. Experiments such as those of Eskinazi and Yeh [24] in constant property flow have shown that the mechanism of the turbulent motion is affected by longitudinal curvature. Mellor also pointed out [5] that this was probably a significant effect in some incompressible boundary layer flows. It is proposed that faster moving fluid farther from the wall would be inhibited from mixing with fluid close to the wall by a centrifugal force acting away from the wall on a convex wall, and encouraged to mix by a centrifugal force on a concave wall. Thus in the more stable case on a convex wall, the effective viscosity would be reduced, and on a concave wall the effective viscosity would be increased. This is the defect which is apparent in the theoretical calculations. In the region before the waist, where longitudinal curvature is small, the cal-

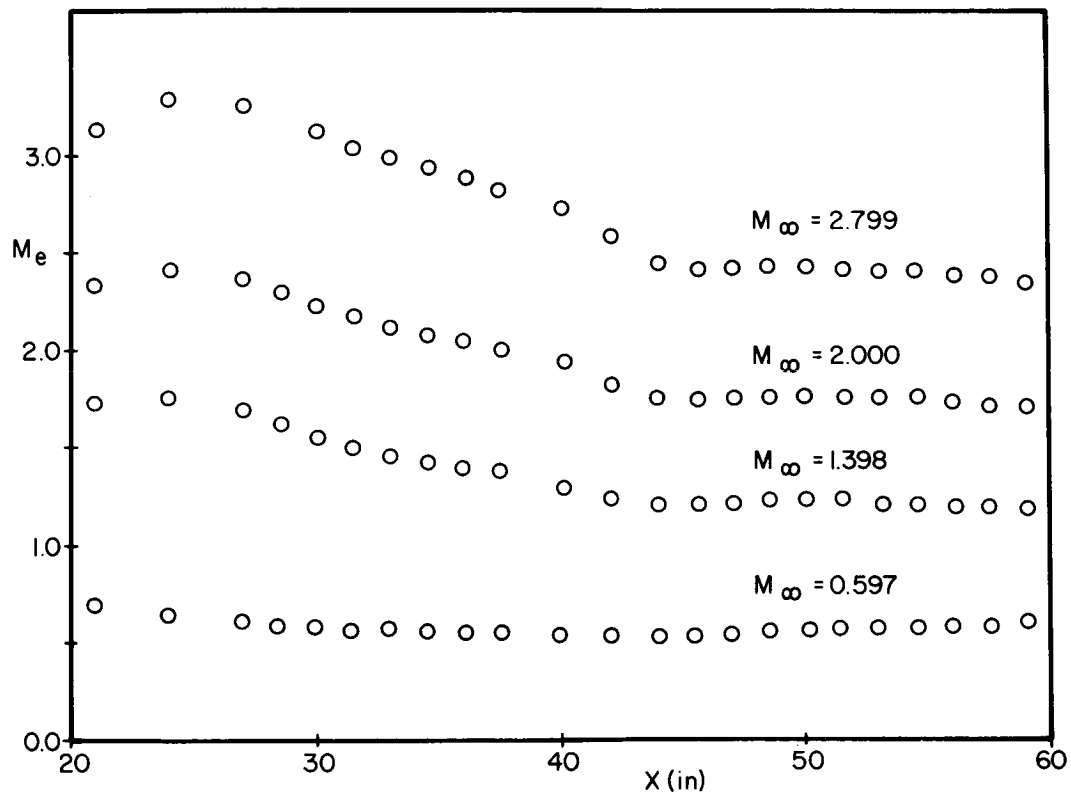


FIGURE 17. Free stream Mach number distribution measured by Winter, Smith and Rotta [23] which was used in the calculations.

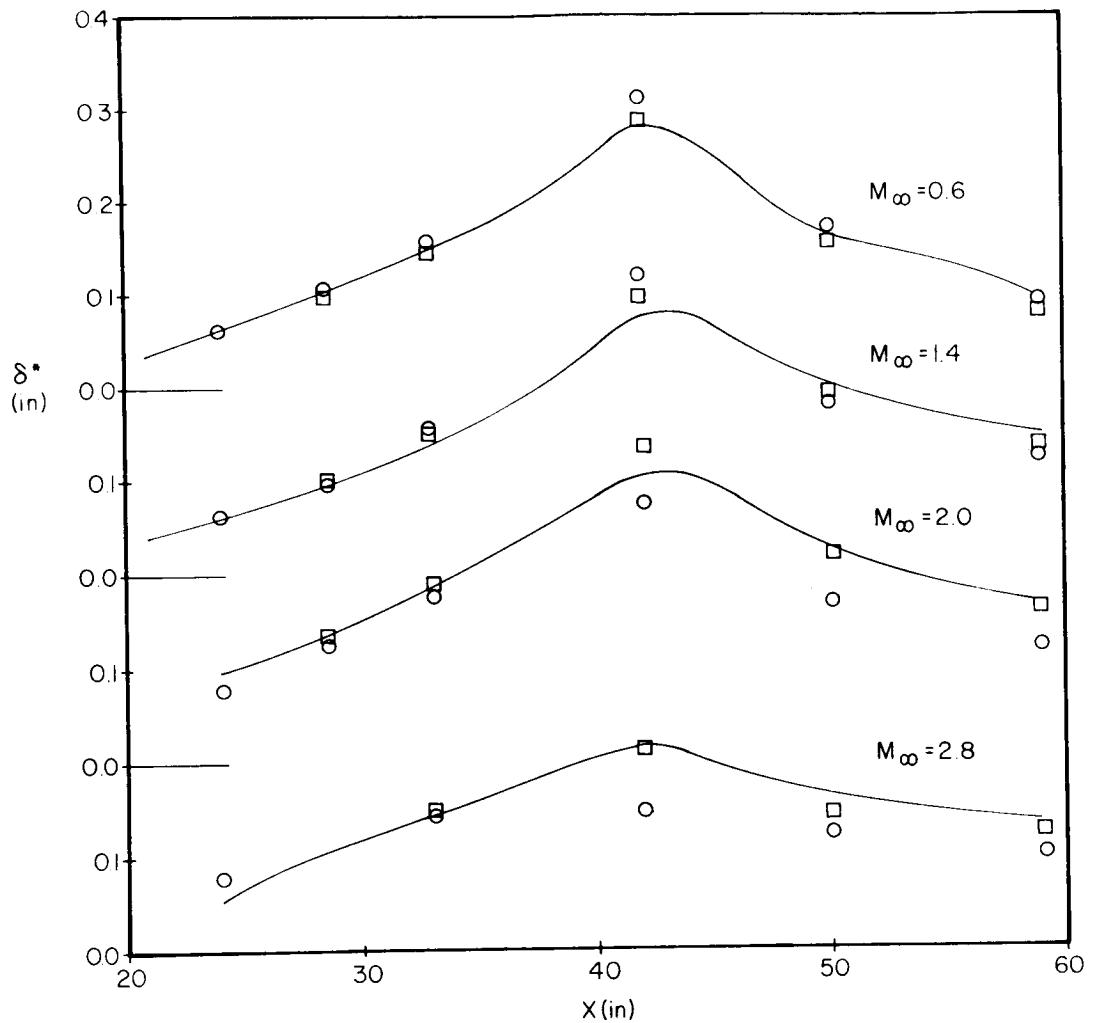


FIGURE 18. Comparison between displacement thickness variation measured by Winter, Smith and Rotta [23] and the calculated variation, shown with an unbroken line. The circles indicate the experimental values obtained directly from the profiles and the squares indicate the values calculated with the von Karman integral momentum equation beginning with the initial experimental  $\theta$  and the experimental values of  $C_f$  and  $\delta^*/\theta$ .

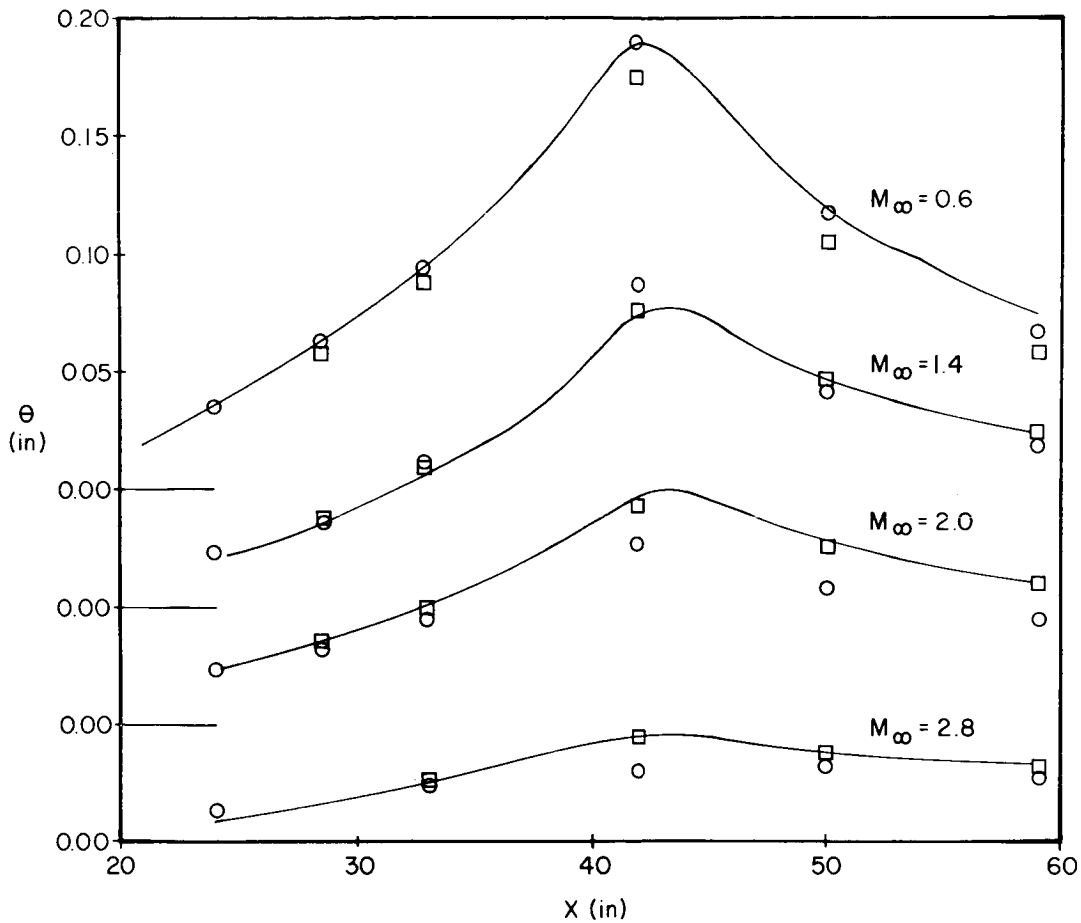


FIGURE 19. Comparison between momentum thickness variation, measured by Winter, Smith and Rotta [23] and the calculated variation, shown with an unbroken line. The circles indicate the experimental values obtained directly from the profiles, and the squares indicate the values calculated with the von Karman integral momentum equation beginning with the initial experimental  $\theta$  and the experimental values of  $C_f$  and  $\delta^*/\theta$ .

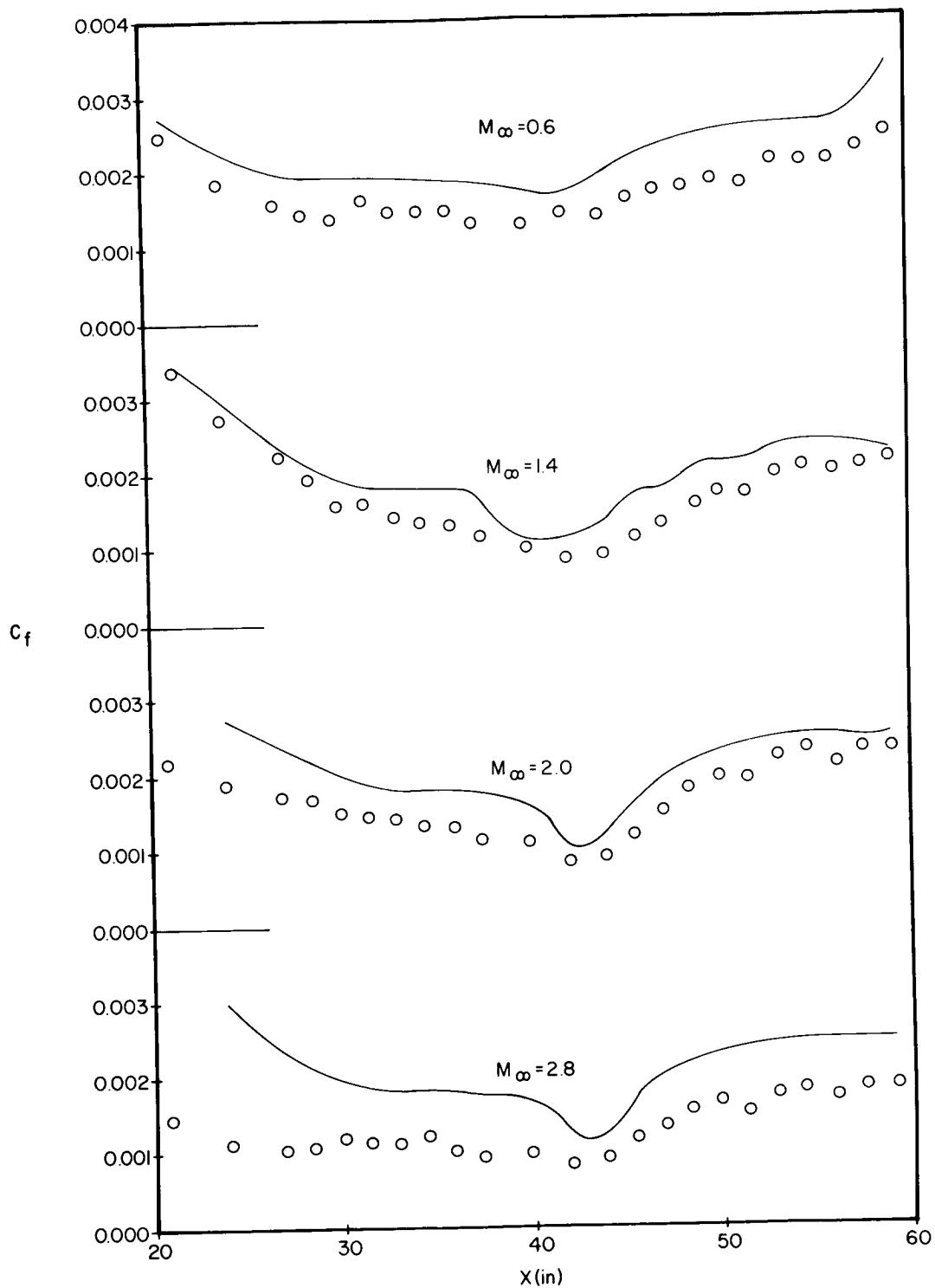


FIGURE 20. Comparison between the distribution of skin friction coefficient measured by Winter, Smith and Rotta [23] with surface pitot tubes and the calculated distribution, shown with an unbroken line.



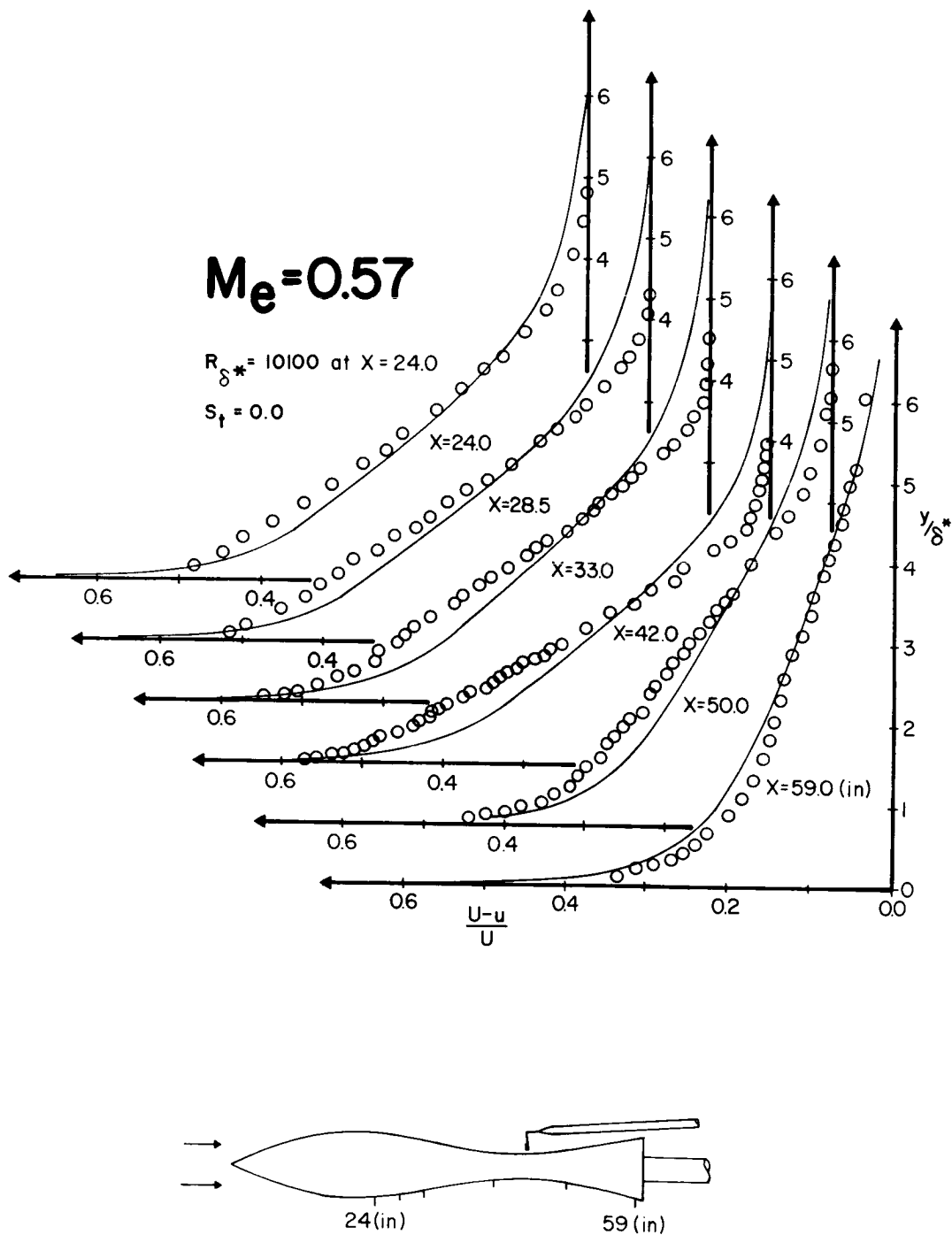


FIGURE 21. Comparison between a series of velocity profiles measured by Winter, Smith and Rotta [23] on a waisted body of revolution and the calculated profiles, shown with an unbroken line.

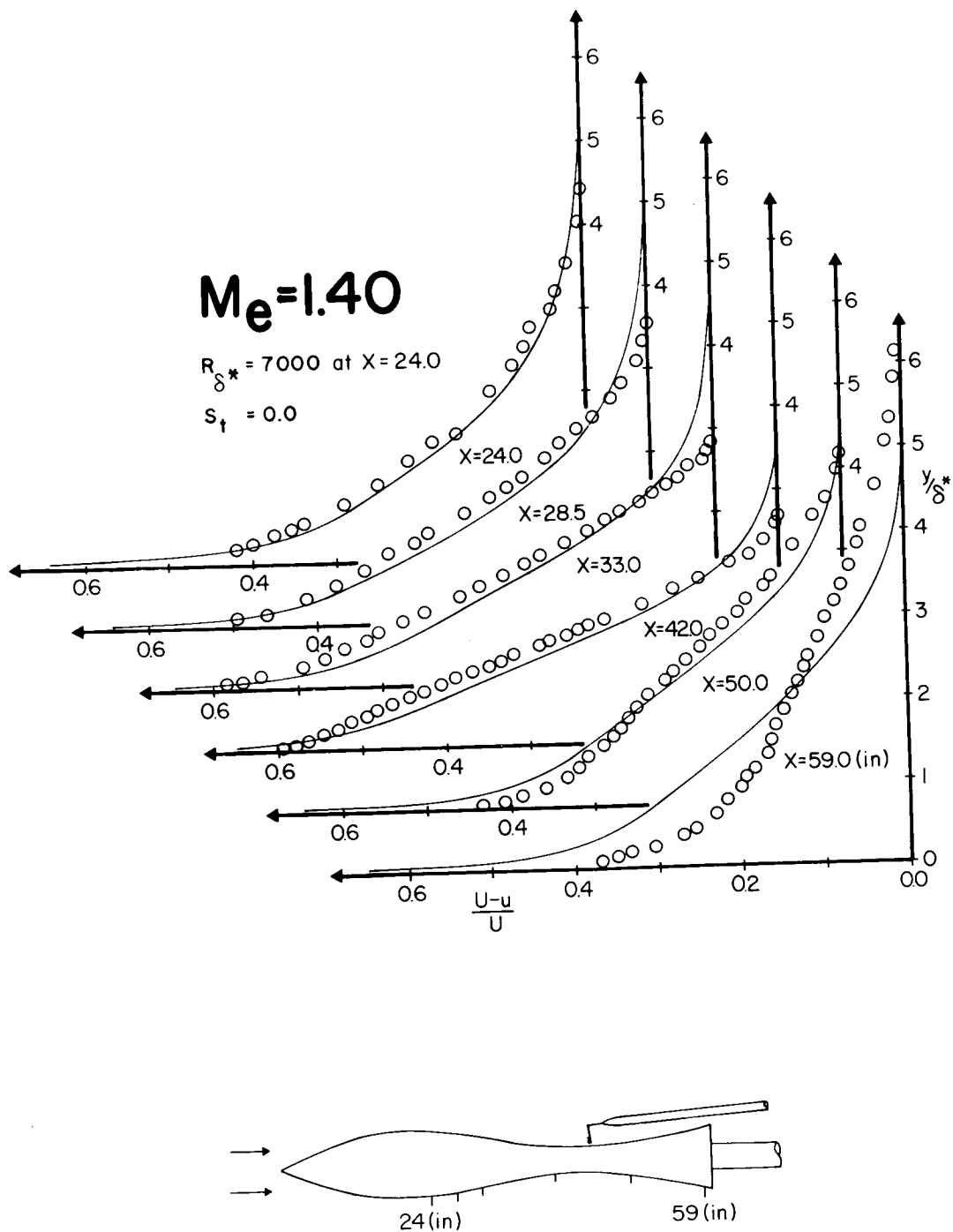


FIGURE 22. Comparison between a series of velocity profiles measured by Winter, Smith and Rotta [23] on a waisted body of revolution and the calculated profiles, shown with an unbroken line.

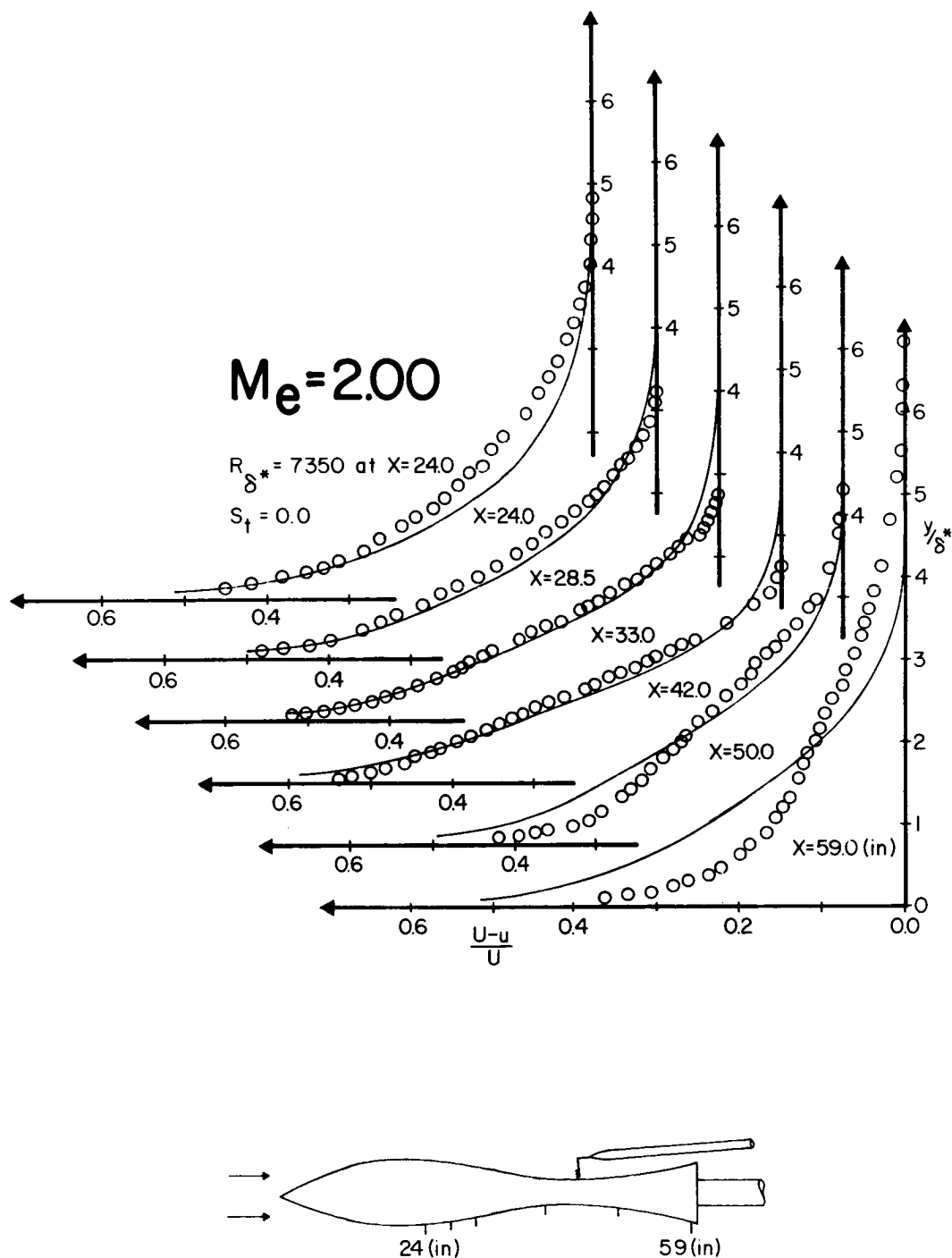


FIGURE 23. Comparison between a series of velocity profiles measured by Winter, Smith and Rotta [23] on a waisted body of revolution and the calculated profiles, shown with an unbroken line.

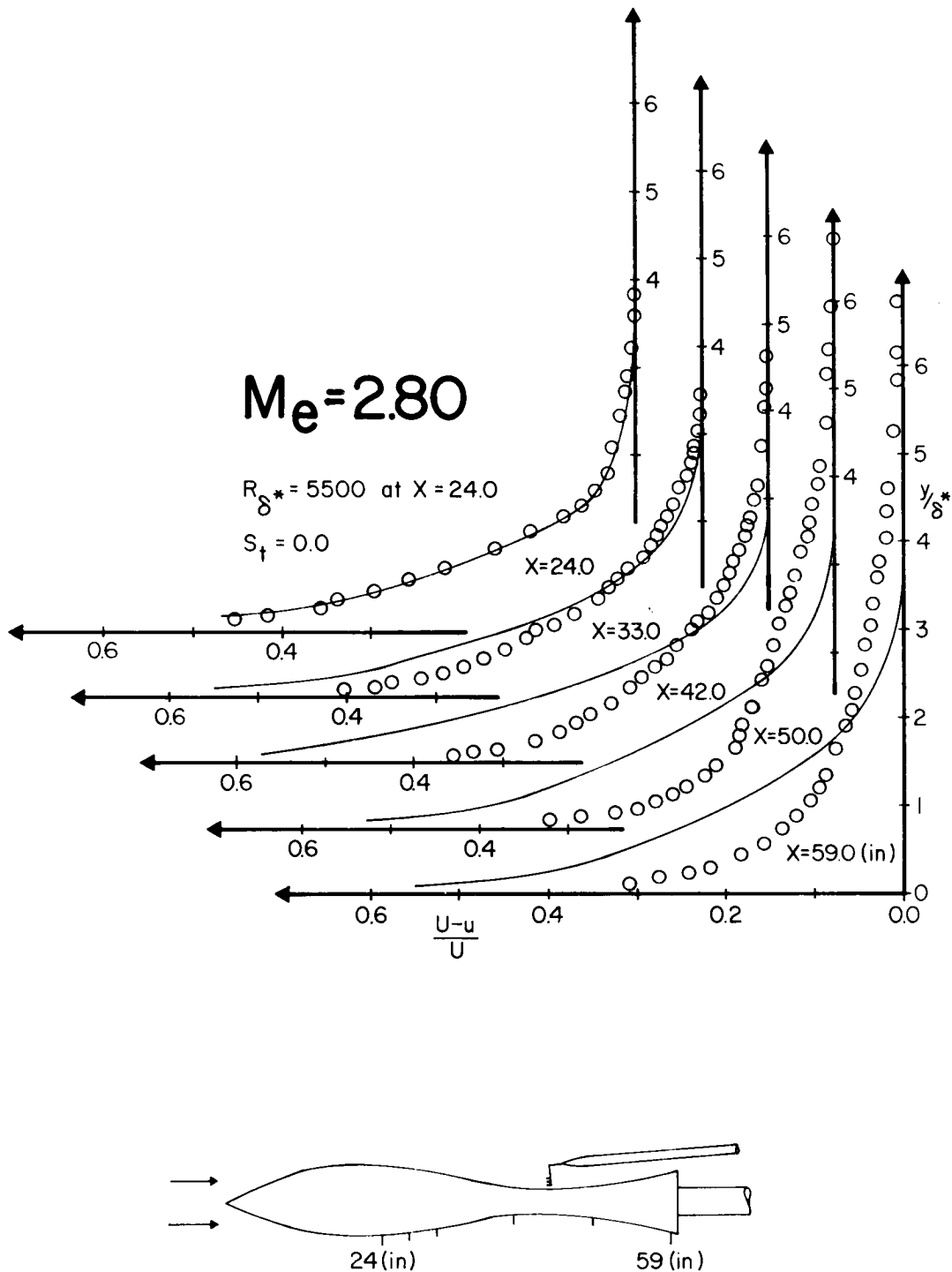


FIGURE 24. Comparison between a series of velocity profiles measured by Winter, Smith and Rotta [23] on a waisted body of revolution and the calculated profiles, shown with an unbroken line.

culations compare well. Beyond the waist, where longitudinal curvature is large, the calculated profiles are not as full as the experimental ones, indicating that the effective viscosity used in the calculations was not large enough. This effect was also apparent in calculations of data measured by McLafferty and Barber [25] on a concave surface. Here, although the experimental boundary layer did not separate, the calculated boundary layer separated after a short distance in the adverse pressure gradient. Again it is likely that this separation resulted from a lower value of effective viscosity in the calculations than in the experimental flow. Recently Rotta [26] has re-examined the Winter, Smith and Rotta [23] data. He points out that in compressible flow on an adiabatic wall the curvature effect is amplified by the density stratification. This would explain the observation that the theory predicts the profiles after the waist better for the lower Mach number cases than in the higher ones.

### Heat Transfer

Although a considerable amount of work has been done on heat transfer in turbulent boundary layers, very few temperature profiles have been measured compared to the number of velocity profiles measured. Furthermore, few heat transfer measurements have been at moderate Mach numbers. Most of the data is either from constant property or hypersonic flow. Unfortunately, the hypersonic experiments, such as Lobb, Winkler and Persh [18] and Danberg [27], were at Reynolds numbers which were too low for the hypothesis. A series of temperature profiles for an incompressible, constant density flow was calculated for comparison with some profiles measured by Reynolds, Kays and Kline [28]. Following the boundary conditions reported for the data, calculations were made at constant pressure and constant wall temperature. The profiles were calculated with  $Pr = 0.78$  and  $Pr_t = 1.0$ . A turbulent Prandtl number of one gave the best results although small variations in  $Pr_t$  had little effect. However, the data available are not sufficient to make a definitive judgment on the best value. The calculations of the series of temperature profiles are compared with the data in Figure 25. The prediction is quite good.

Another comparison is afforded by a group of Stanton number distributions measured by Moretti and Kays [29]. These again are incompressible constant density flows but they include a wide variety of longitudinal wall temperature distributions and pressure distributions. The calculations were performed with the experimental velocity and temperature boundary conditions shown in the bottom two graphs of Figures 26 to 37. The experimental Reynolds number and momentum thickness were only reported at one point in the flows. These are noted on the graphs of mainstream velocity distribution and the position of the measurement is indicated with an arrow. In order

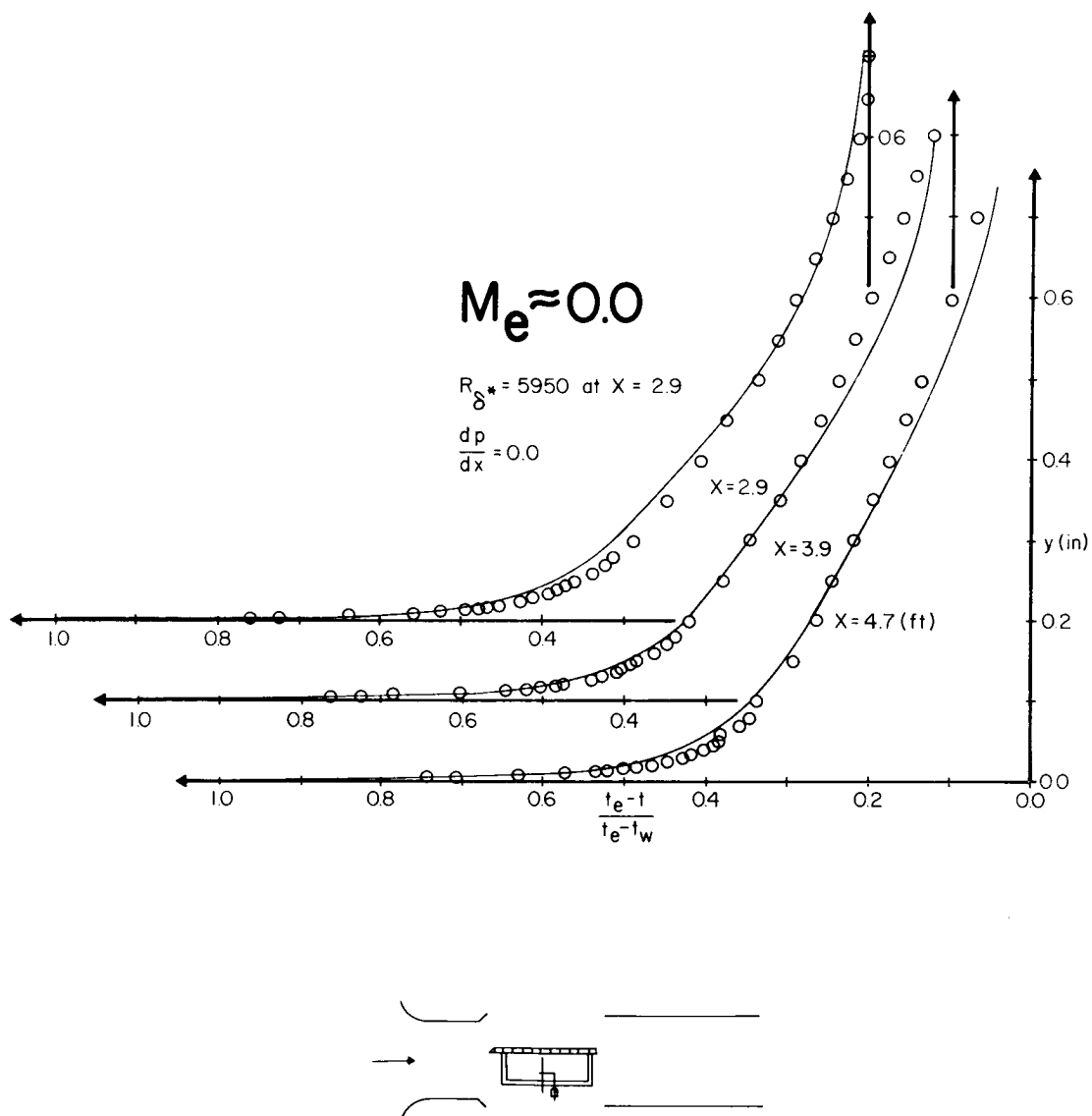


FIGURE 25. Comparison between a series of low Mach number, constant-property temperature profiles, measured by Reynolds, Kays and Kline [28] on a heated flat plate in a free jet tunnel, and the calculated temperature profiles shown with unbroken lines.

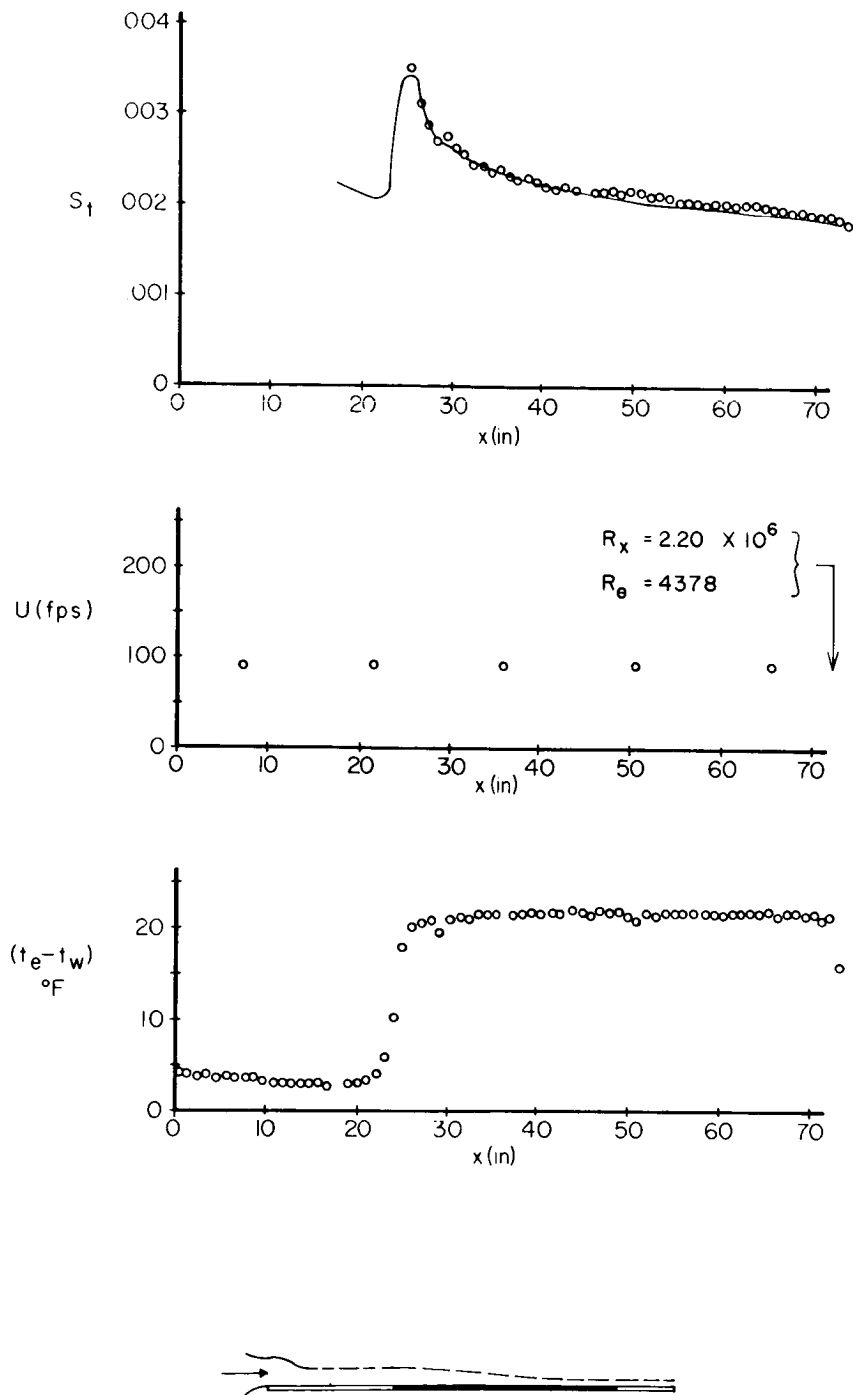


FIGURE 26. Comparison between a Stanton number distribution measured by Moretti and Kays [29] on a cooled flat plate and the calculated Stanton number distribution shown with an unbroken line. Also shown are the experimental velocity distribution and wall temperature distribution which were used for the calculations.

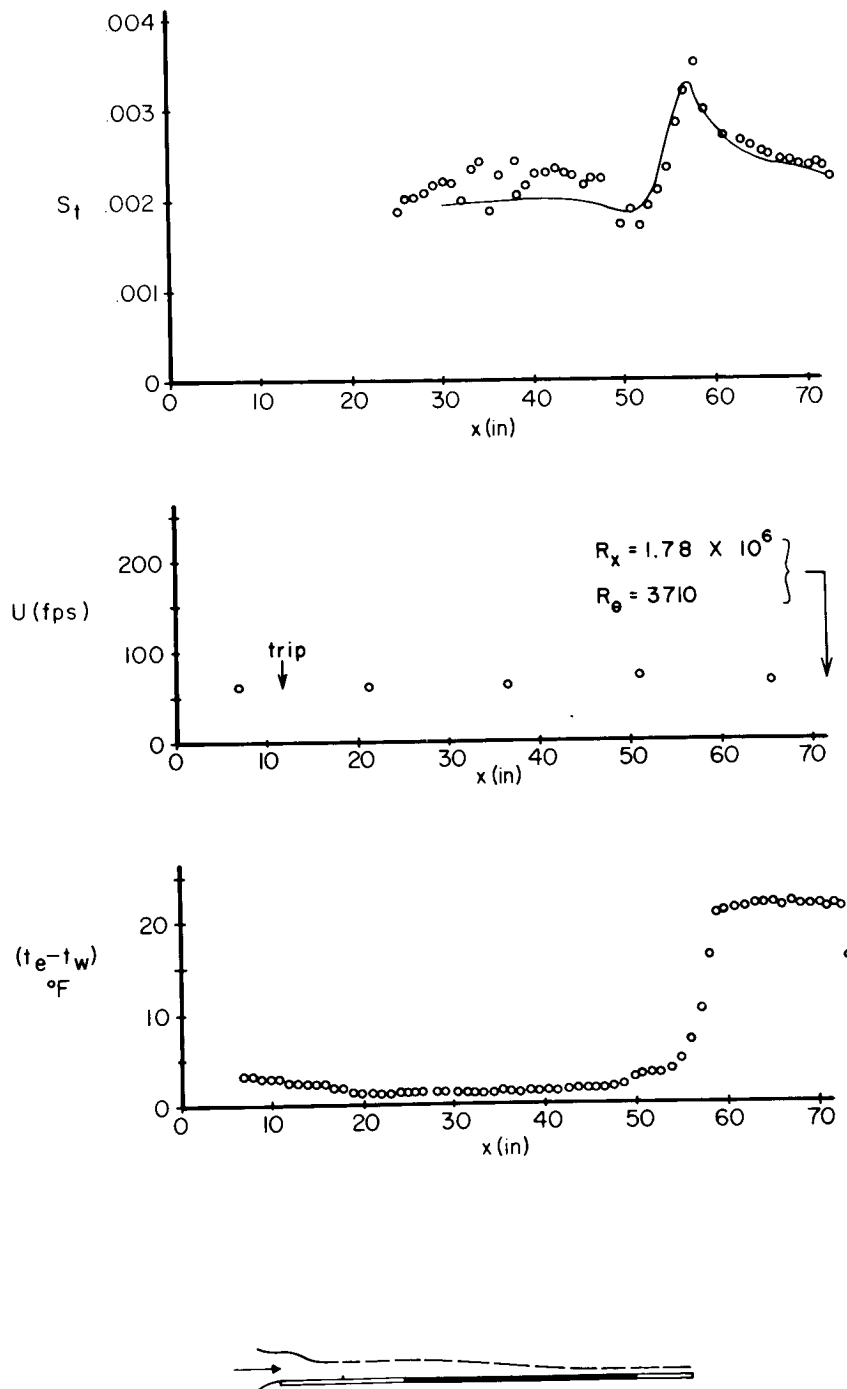


FIGURE 27. Comparison between a Stanton number distribution measured by Moretti and Kays [29] on a cooled flat plate and the calculated Stanton number distribution shown with an unbroken line. Also shown are the experimental velocity distribution and wall temperature distribution which were used for the calculations.



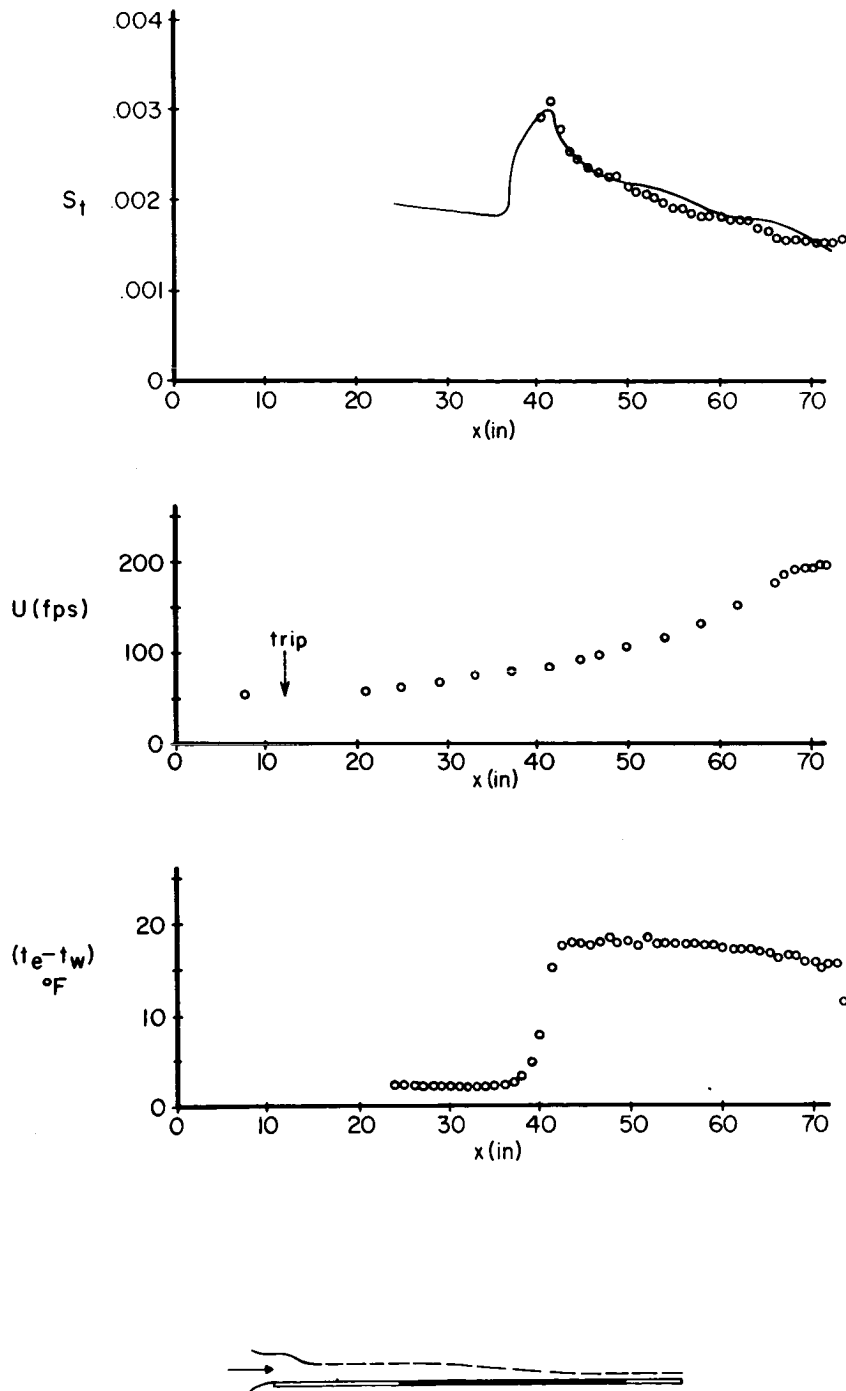


FIGURE 28. Comparison between a Stanton number distribution measured by Moretti and Kays [29] on a cooled flat plate and the calculated Stanton number distribution shown with an unbroken line. Also shown are the experimental velocity distribution and wall temperature distribution which were used for the calculations.

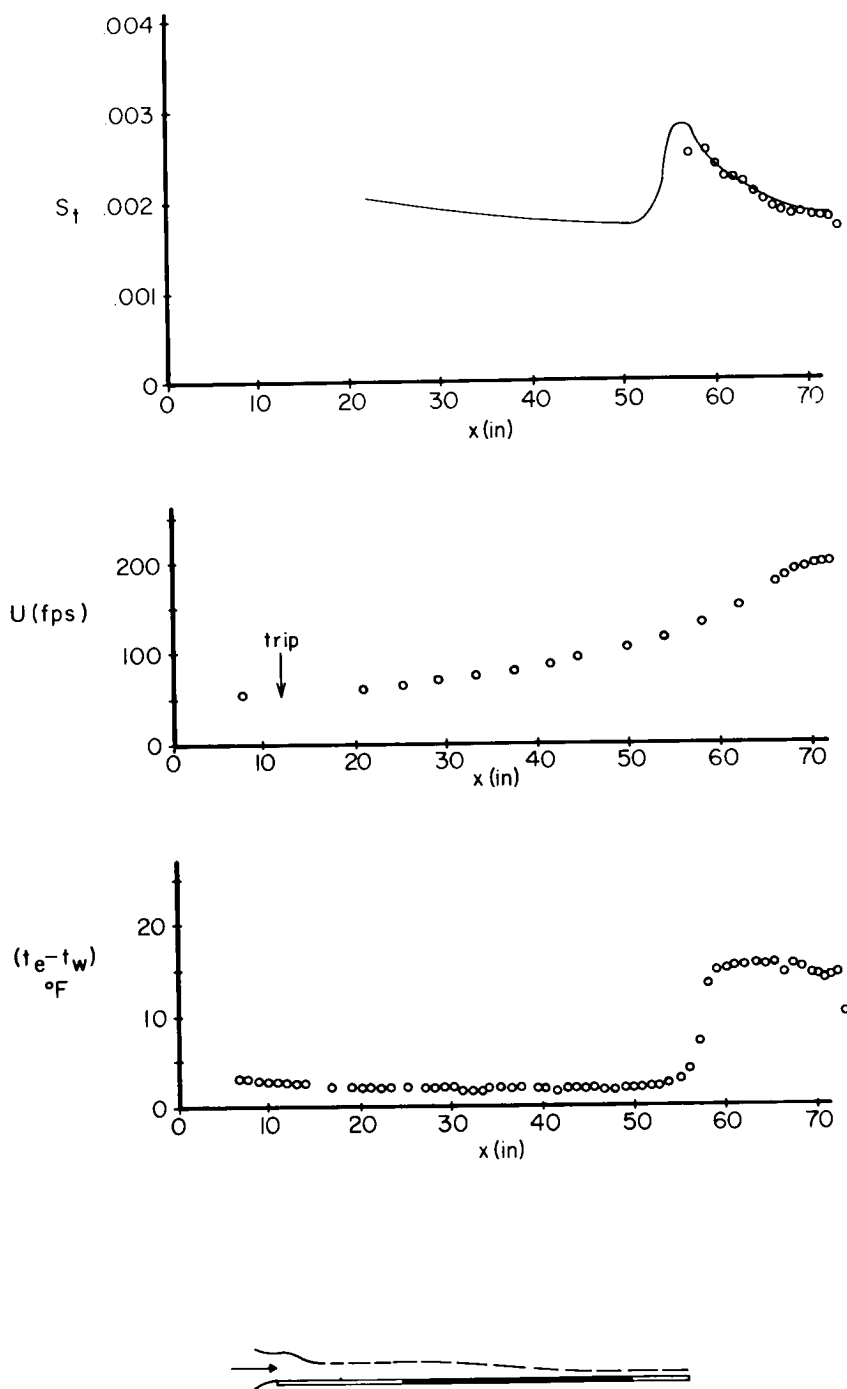


FIGURE 29. Comparison between a Stanton number distribution measured by Moretti and Kays [29] on a cooled flat plate and the calculated Stanton number distribution shown with an unbroken line. Also shown are the experimental velocity distribution and wall temperature distribution which were used for the calculations.

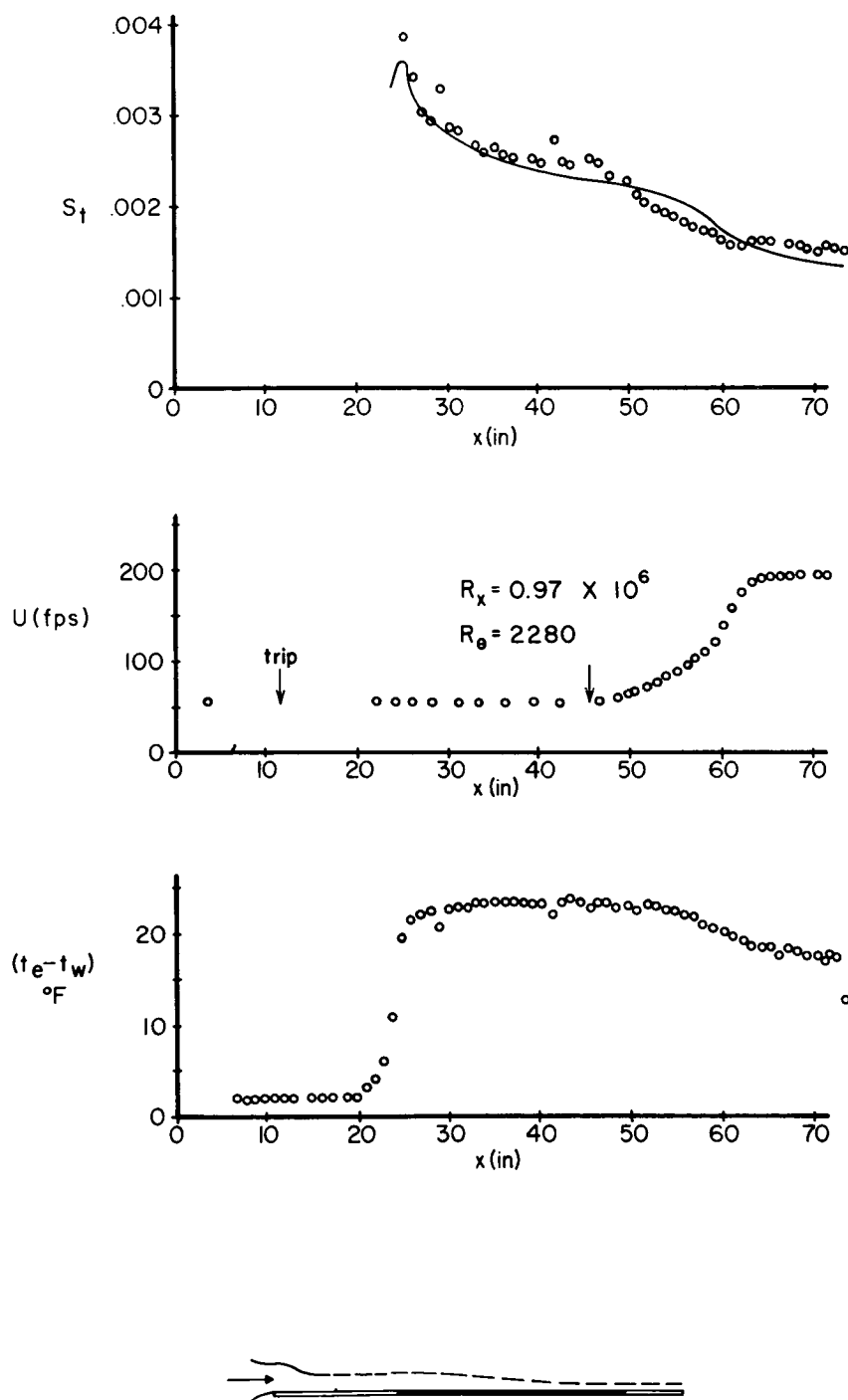


FIGURE 30.

Comparison between a Stanton number distribution measured by Moretti and Kays [29] on a cooled flat plate and the calculated Stanton number distribution shown with an unbroken line. Also shown are the experimental velocity distribution and wall temperature distribution which were used for the calculations.

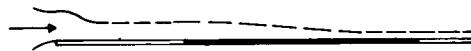
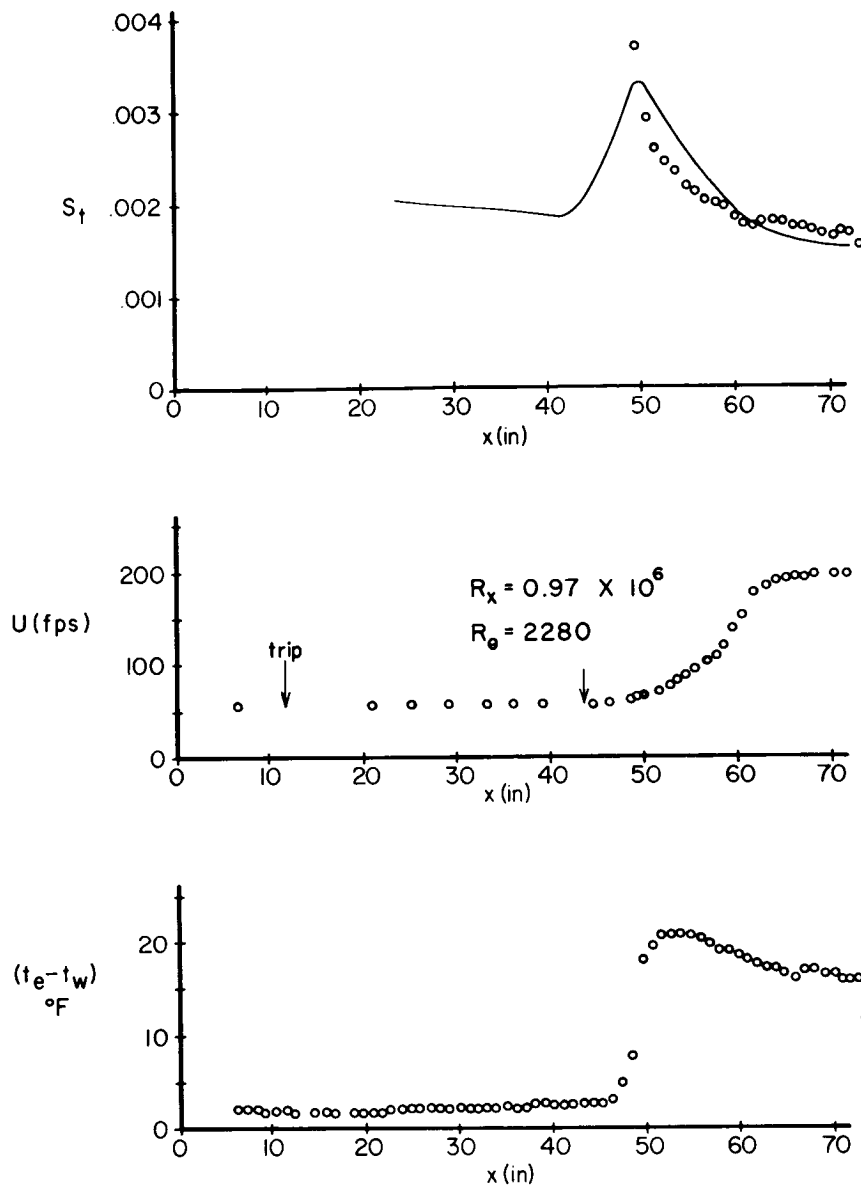


FIGURE 31. Comparison between a Stanton number distribution measured by Moretti and Kays [29] on a cooled flat plate and the calculated Stanton number distribution shown with an unbroken line. Also shown are the experimental velocity distribution and wall temperature distribution which were used for the calculations.

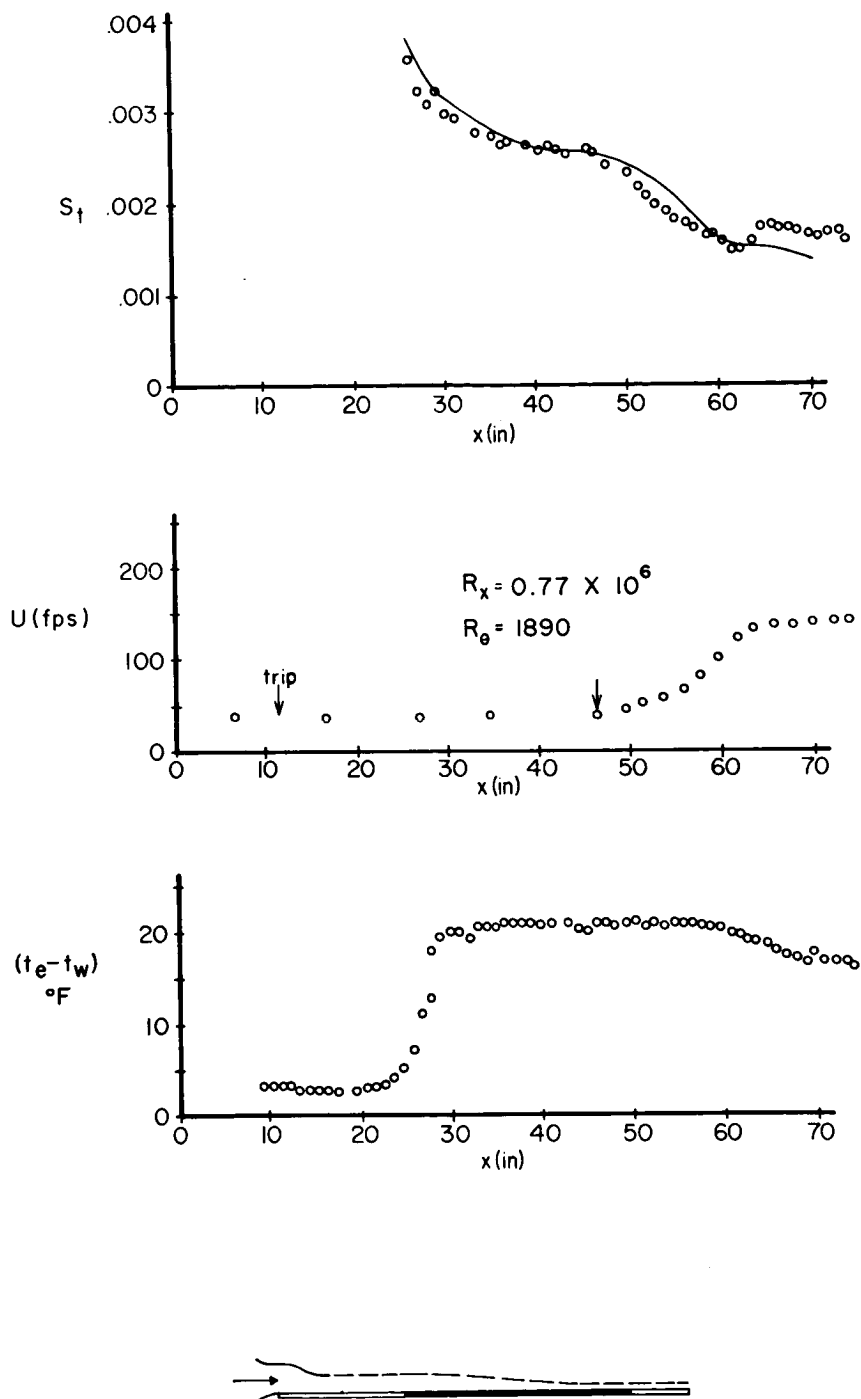


FIGURE 32. Comparison between a Stanton number distribution measured by Moretti and Kays [29] on a cooled flat plate and the calculated Stanton number distribution shown with an unbroken line. Also shown are the experimental velocity distribution and wall temperature distribution which were used for the calculations.

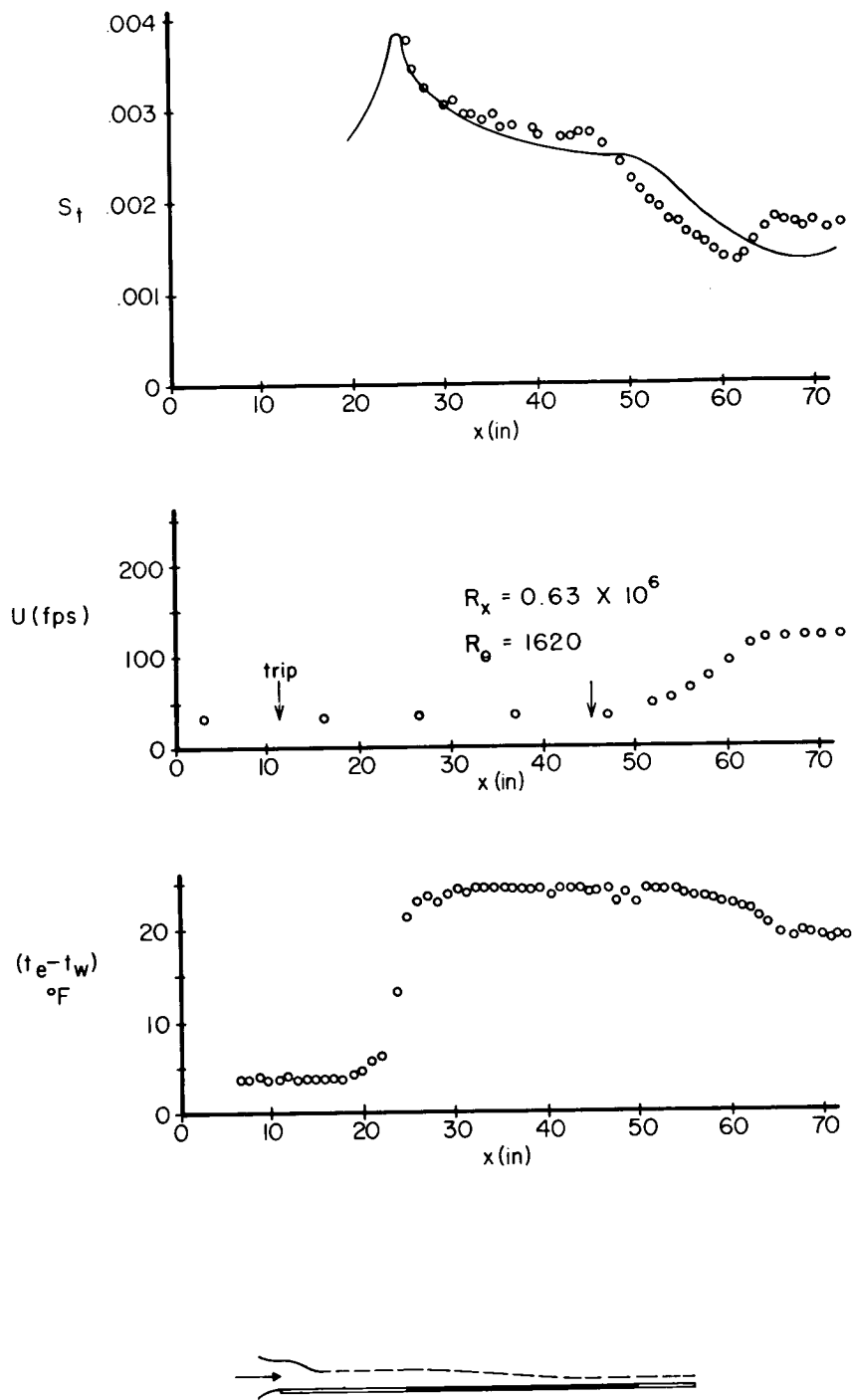


FIGURE 33. Comparison between a Stanton number distribution measured by Moretti and Kays [29] on a cooled flat plate and the calculated Stanton number distribution shown with an unbroken line. Also shown are the experimental velocity distribution and wall temperature distribution which were used for the calculations.

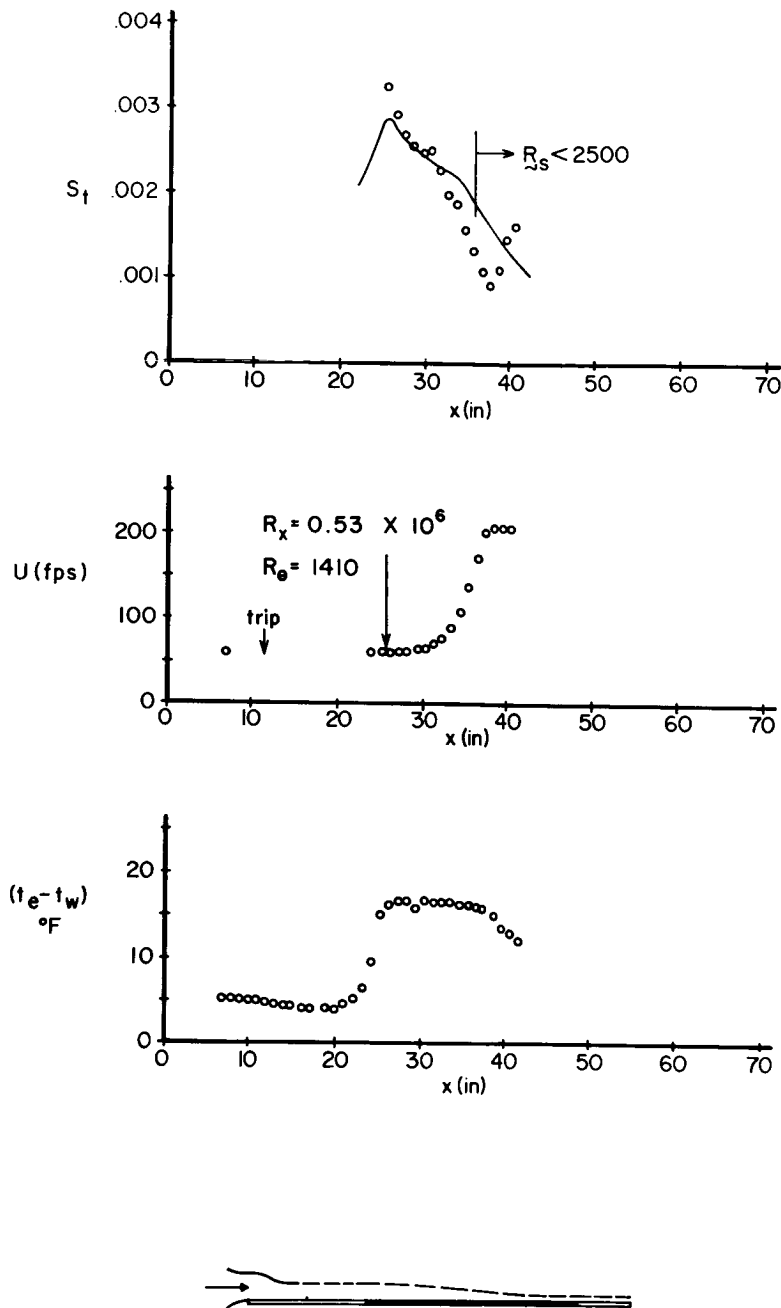


FIGURE 34.

Comparison between a Stanton number distribution measured by Moretti and Kays [29] on a cooled flat plate and the calculated Stanton number distribution shown with an unbroken line. Also shown are the experimental velocity distribution and wall temperature distribution which were used for the calculations. The  $x$  position marked with a vertical line on the Stanton number curve shows the position that  $R_s (= U\delta_k^*/\bar{v}_s)$  becomes less than 2500.

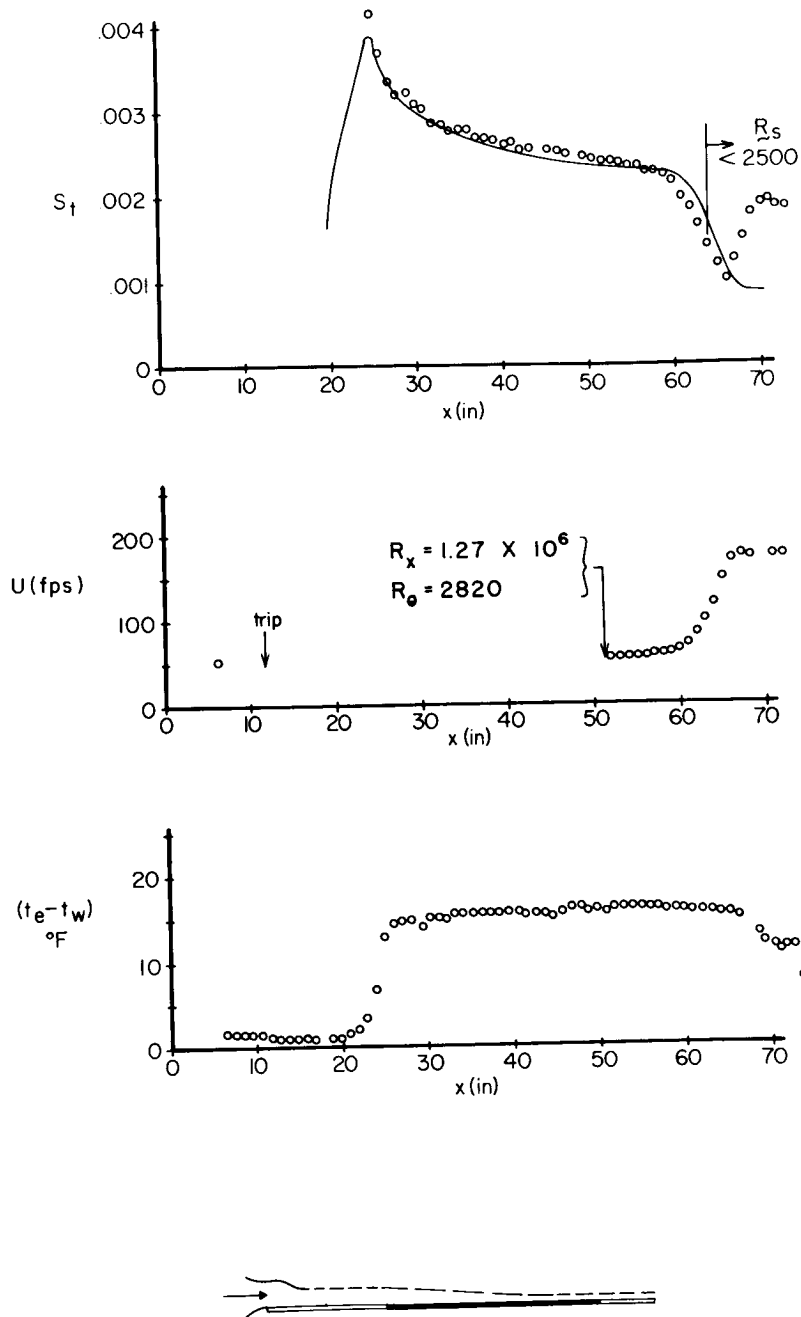


FIGURE 35. Comparison between a Stanton number distribution measured by Moretti and Kays [29] on a cooled flat plate and the calculated Stanton number distribution shown with an unbroken line. Also shown are the experimental velocity distribution and wall temperature distribution which were used for the calculations. The  $x$  position marked with a vertical line on the Stanton number curve shows the position that  $R_s (= U\delta_k^*/\bar{v}_s)$  becomes less than 2500.



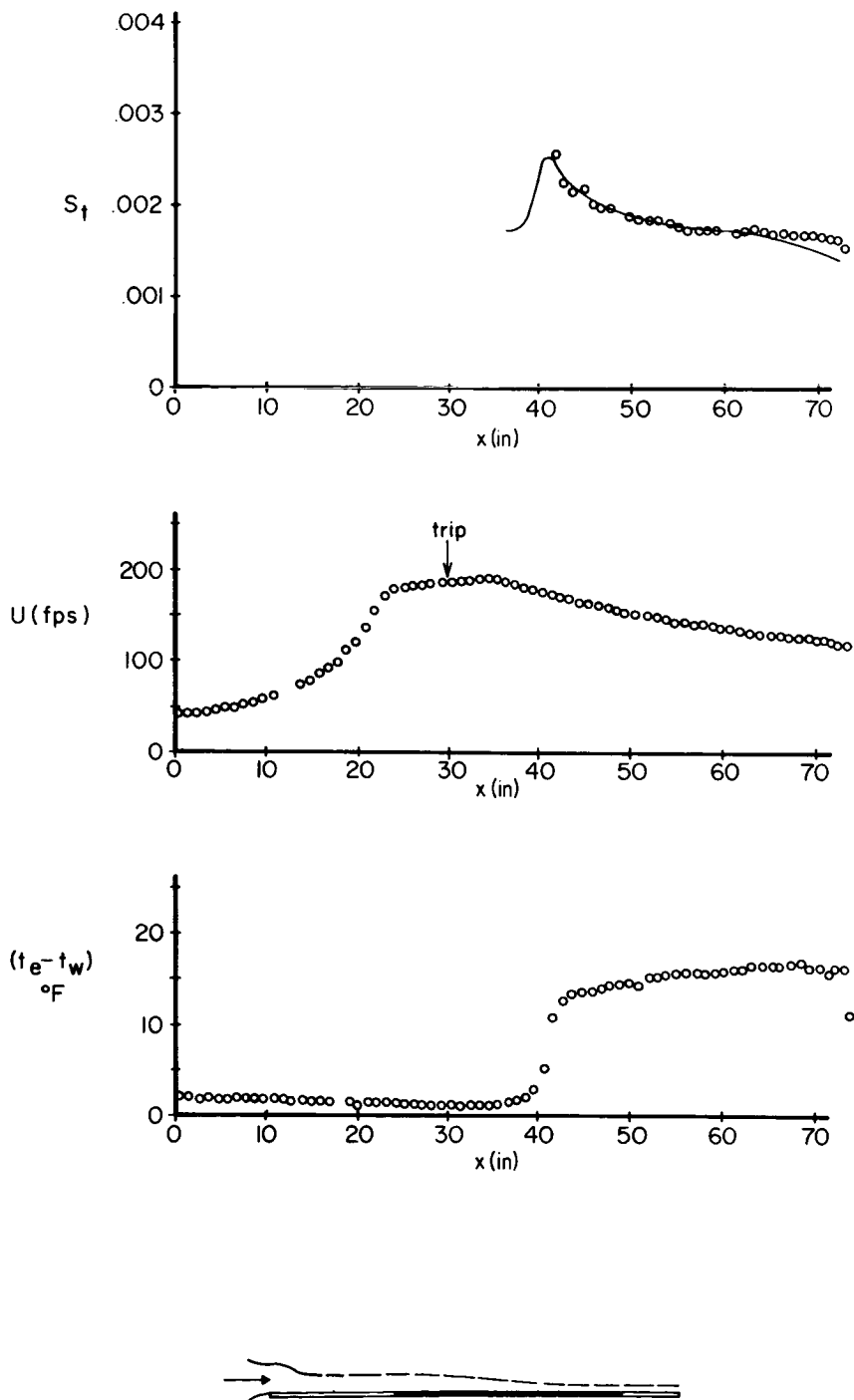


FIGURE 36. Comparison between a Stanton number distribution measured by Moretti and Kays [29] on a cooled flat plate and the calculated Stanton number distribution shown with an unbroken line. Also shown are the experimental velocity distribution and wall temperature distribution which were used for the calculations.

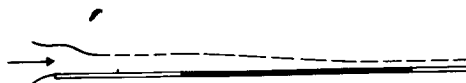
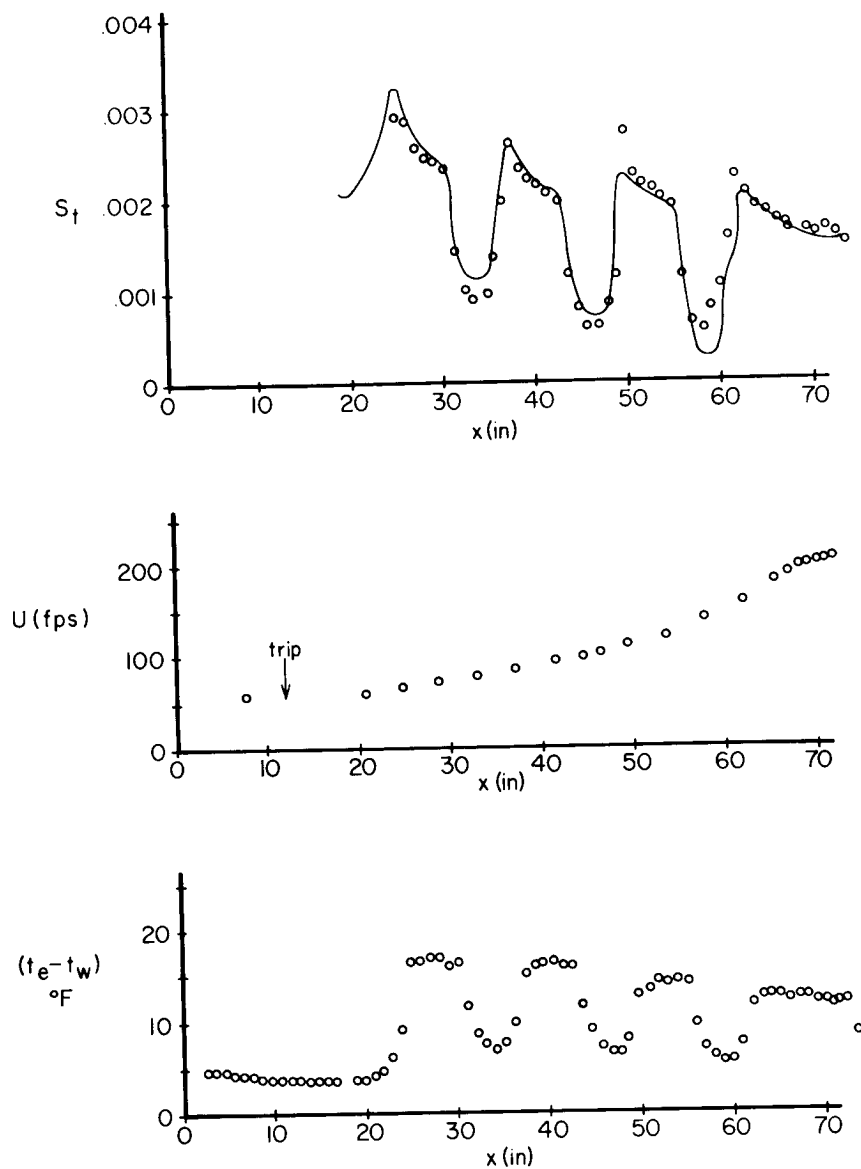


FIGURE 37. Comparison between a Stanton number distribution measured by Moretti and Kays [29] on a cooled flat plate and the calculated Stanton number distribution shown with an unbroken line. Also shown are the experimental velocity distribution and wall temperature distribution which were used for the calculations.

to match these values, preliminary calculations were made and the initial conditions reset to match the experimental momentum thickness at the reported point. Unfortunately the values of  $R_s$  for all of these flows were rather low. Although in many cases  $R_s$  stayed above 2500, the strong mainstream accelerations in other cases caused  $\delta^*$  to decrease and therefore  $R_s$  to drop below 2500. Because of this the hypothesis is in error at some of the most interesting places. Those cases in which this happens are marked with a vertical line on the Stanton number plot at the  $x$  position where it occurs.

The measured and calculated values of the Stanton number distribution are plotted together at the top of Figures 26 through 37. The rapid changes in Stanton number are predicted well in the decelerating case, Figure 36, and the cases with lower accelerating pressure gradients. Even the last case, where the temperature distribution is a series of alternate temperature steps is predicted well. The calculated Stanton numbers continue to compare well in the flows with strong pressure gradients (Figures 30 to 33) as long as  $R_s$  is above 2500. Furthermore, when  $R_s$  does go too low, the calculations still have the correct tendency for a short distance. Therefore, this is a favorable beginning for the effective diffusivity. Still more data are necessary in compressible flow at higher Reynolds numbers to test fully the validity of the effective diffusivity.

## V. CONCLUDING REMARKS

The results cited demonstrate that the effects of compressibility have been correctly incorporated into the effective viscosity hypothesis for constant Mach number flows. The effect of Mach number on the skin friction coefficient, on the profile shape, and on the growth of  $\delta^*$  are predicted quite well. It is unfortunate that more data in compressible flow with pressure gradients are not available. The only flows for which calculations were made were flows with positive pressure gradients. In these cases the results were quite good, although to complete the verification of the hypothesis data taken in flows with favorable pressure gradients and data in flows with separation are required. In the positive pressure gradient data that were examined, there were regions of almost constant pressure flow but with strong longitudinal curvature which were not predicted well. This and other circumstantial evidence seem to indicate that there is an effect of longitudinal curvature on the turbulent structure which has not as yet been included in the hypothesis. (An experimental study of wall curvature effect is in progress at Princeton University.)

Based on the limited amount of data, the results obtained using

the effective diffusivity in incompressible flow with heat transfer are also favorable. Again, it would be useful if more temperature profiles were available, especially from compressible flow, to establish further confidence in the theoretical predictions.

Princeton University  
Princeton, N.J., April 11, 1968

# APPENDIX A. ORDER OF MAGNITUDE ANALYSIS

## FOR EQUATIONS OF MOTION

An order of magnitude analysis is most conveniently performed with the equations in non-dimensional form. Accordingly, the dependent variables will be referred to their values at some point,  $r$ , in the undisturbed stream, and  $x$  and  $y$  will be referred to a representative dimension of the body,  $\ell$ , such that  $\partial u^+ / \partial x^+$  is of order unity. The new variables are

$$u^+ = \frac{u}{U_r}, \quad v^+ = \frac{v}{U_r}, \quad w^+ = \frac{w}{U_r}, \quad \rho^+ = \frac{\rho}{\rho_{e_r}}, \quad p^+ = \frac{p - p_{e_r}}{\rho_{e_r} U_r^2},$$

$$h^{o+} = \frac{h^o}{h_{e_r}^o}, \quad h^+ = \frac{h}{h_{e_r}}, \quad x^+ = \frac{x}{\ell}, \quad y^+ = \frac{y}{\ell}. \quad (A1)$$

If these variables are introduced into equations (2a) through (2f), the results are

$$\frac{\overline{\partial \rho^+ u^+}}{\partial x^+} + \frac{\overline{\partial \rho^+ u^+}}{\partial x^+} + \frac{\overline{\partial \rho^+ v^+}}{\partial y^+} + \frac{\overline{\partial \rho^+ v^+}}{\partial y^+} = 0 \quad (A2a)$$

$$(1 + \Delta \rho^+) \quad \varepsilon \Delta \rho^+ \quad \frac{(\varepsilon + \varepsilon \Delta \rho^+)}{\varepsilon} \quad \frac{\varepsilon \Delta \rho^+}{\varepsilon}$$

$$\begin{aligned}
& \overline{\rho^+} \overline{u^+} \frac{\partial \overline{u^+}}{\partial x^+} + \frac{\overline{\partial \rho^+ u^+}^2}{\partial x^+} + \frac{\overline{\rho^+ u^+} \frac{\partial \overline{u^+}}{\partial x^+}}{\varepsilon \Delta \rho^+} + \frac{\overline{\partial u^+ \rho^+ u^+}}{\partial x^+ \varepsilon \Delta \rho^+} \\
& \quad 1 \quad (\varepsilon + \varepsilon \Delta \rho^+) \quad \varepsilon \Delta \rho^+ \quad \varepsilon \Delta \rho^+ \\
& + \frac{\overline{\rho^+} \overline{v^+} \frac{\partial \overline{u^+}}{\partial y^+}}{\varepsilon \frac{1}{\varepsilon}} + \frac{\overline{\rho^+ v^+} \frac{\partial \overline{u^+}}{\partial y^+}}{\varepsilon \Delta \rho^+ \frac{1}{\varepsilon}} + \frac{\overline{\partial \rho^+ u^+ v^+}}{\partial y^+ \frac{(\varepsilon + \varepsilon \Delta \rho^+)}{\varepsilon}} + \frac{\overline{\partial v^+ \rho^+ u^+}}{\partial y^+ \frac{\varepsilon \varepsilon \Delta \rho^+}{\varepsilon}} = - \frac{\overline{\partial p^+}}{\partial x^+} \quad (A2b) \\
& \quad \varepsilon \frac{1}{\varepsilon} \quad \varepsilon \Delta \rho^+ \frac{1}{\varepsilon} \quad \frac{(\varepsilon + \varepsilon \Delta \rho^+)}{\varepsilon} \quad \frac{\varepsilon \varepsilon \Delta \rho^+}{\varepsilon} \quad 1
\end{aligned}$$

$$\begin{aligned}
& \overline{\rho^+} \overline{v^+} \frac{\partial \overline{u^+}}{\partial x^+} + \frac{\overline{\rho^+ v^+} \frac{\partial \overline{u^+}}{\partial x^+}}{\varepsilon \Delta \rho^+} + \frac{\overline{\partial \rho^+ u^+ v^+}}{\partial x^+ (\varepsilon \Delta \rho^+ + \varepsilon)} + \frac{\overline{\partial v^+ \rho^+ u^+}}{\partial x^+ \varepsilon \varepsilon \Delta \rho^+} \\
& \quad \varepsilon \quad \varepsilon \Delta \rho^+ \quad (\varepsilon \Delta \rho^+ + \varepsilon) \quad \varepsilon \varepsilon \Delta \rho^+ \\
& + \frac{\overline{\rho^+} \overline{v^+} \frac{\partial \overline{v^+}}{\partial y^+}}{\varepsilon \frac{\varepsilon}{\varepsilon}} + \frac{\overline{\rho^+ v^+} \frac{\partial \overline{v^+}}{\partial y^+}}{\varepsilon \Delta \rho^+ \frac{\varepsilon}{\varepsilon}} + \frac{\overline{\partial v^+ \rho^+ v^+}}{\partial y^+ \frac{\varepsilon \varepsilon \Delta \rho^+}{\varepsilon}} + \frac{\overline{\partial \rho^+ v^+}^2}{\partial y^+ \frac{\varepsilon + \varepsilon \Delta \rho^+}{\varepsilon}} = - \frac{\overline{\partial p^+}}{\partial y^+} \quad (A2c) \\
& \quad \varepsilon \frac{\varepsilon}{\varepsilon} \quad \varepsilon \Delta \rho^+ \frac{\varepsilon}{\varepsilon} \quad \frac{\varepsilon \varepsilon \Delta \rho^+}{\varepsilon} \quad \frac{\varepsilon + \varepsilon \Delta \rho^+}{\varepsilon} \quad \frac{(\varepsilon + \varepsilon \Delta \rho^+)}{\varepsilon}
\end{aligned}$$

$$\begin{aligned}
& \overline{\rho^+ u^+} \frac{\partial \overline{h^{o+}}}{\partial x^+} + \overline{\rho^+ u^+} \frac{\partial \overline{h^{o+}}}{\partial x^+} + \frac{\partial \overline{\rho^+ u^+ h^{o+}}}{\partial x^+} + \frac{\partial \overline{u^+ \rho^+ h^{o+}}}{\partial x^+} \\
& \overline{\Delta h^{o+}} \quad \overline{\epsilon \Delta \rho^+ \Delta h^{o+}} \quad (\overline{\epsilon \Delta h^{o+} + \epsilon \Delta h^{o+} \Delta \rho^+}) \quad (\overline{\epsilon \Delta \rho^+ \Delta h^{o+}})
\end{aligned}$$

$$\begin{aligned}
& \overline{\rho^+ v^+} \frac{\partial \overline{h^{o+}}}{\partial y^+} + \overline{\rho^+ v^+} \frac{\partial \overline{h^{o+}}}{\partial y^+} + \frac{\partial \overline{\rho^+ v^+ h^{o+}}}{\partial y^+} + \frac{\partial \overline{v^+ \rho^+ h^{o+}}}{\partial y^+} = 0 \\
& \overline{\epsilon \frac{\Delta h^{o+}}{\epsilon}} \quad \overline{\epsilon \Delta \rho^+ \frac{\Delta h^{o+}}{\epsilon}} \quad \overline{(\epsilon \Delta h^{o+} + \epsilon \Delta h^{o+} \Delta \rho^+)} \quad \overline{\frac{\Delta \rho^+ \Delta h^{o+}}{\epsilon} \epsilon} \quad (A2d)
\end{aligned}$$

$$\begin{aligned}
& \left(1 + \frac{\gamma-1}{2} M_e^2\right) \overline{h^{o+}} = \overline{h^+} + \frac{\gamma-1}{2} M_e^2 \left( \overline{u^{+2}} + \overline{u^{+'}^2} + \overline{v^{+'}^2} + \overline{w^{+'}^2} \right) \\
& \quad 1 \quad 1 \quad 1 \quad \epsilon \quad \epsilon \quad \epsilon
\end{aligned} \quad (A2e)$$

$$\begin{aligned}
& 1 + \gamma M_e^2 \overline{p^+} = \overline{\rho^+ h^+} + \overline{\rho^+ h^{+'}} \\
& \quad 1 \quad 1 \quad \overline{\epsilon \Delta \rho^+ \Delta h^+}
\end{aligned} \quad (A2f)$$

Below each term is a notation of its magnitude in accordance with the discussion which follows.

To begin with, the thickness of the boundary layer,  $\delta$ , is assumed to be considerably smaller than  $\ell$ , so that  $\partial(\ )/\partial y^+$  is of order  $1/\varepsilon$ , ( $\varepsilon = \delta/\ell \ll 1$ ). Then, on the basis of experimental evidence (Laufer [7], Kistler [30]), some assumptions are made about the turbulent correlation terms,

$$\overline{u^+ v^{+'}} = O(C_F) \quad , \quad (A3a)$$

$$\overline{u^{+2}} = O(\overline{u^+ v^{+'}}) \quad , \quad (A3b)$$

$$\overline{v^{+2}} = O(\overline{u^+ v^{+'}}) \quad , \quad (A3c)$$

$$\overline{\rho^+ u^{+'}} = O(\overline{\rho^+ v^{+'}}) \quad . \quad (A3d)$$

Now, since the change of  $y^+$  across the layer is of order  $\varepsilon$ , it is clear from (A2a) that  $\overline{v^+}$  must also be of order  $\varepsilon$ . Furthermore, if the equations are to describe a boundary layer flow, the turbulent shear stress term,  $\partial(\rho^+ \overline{u^+ v^{+'}})/\partial y^+$ , must be of the same order as the inertia terms in the  $x^+$  momentum equation. Therefore  $C_F$  must be of order  $\varepsilon$ , which is in agreement with experimental results. Finally, changes of  $\overline{\rho^+}$  and  $\overline{h^+}$  in the  $x^+$  direction are assumed to be of the same order as the changes across the layer,  $\Delta \overline{\rho^+}$  and  $\Delta \overline{h^+}$  respectively. This is in keeping with the method used for  $\overline{u^+}$ , where  $\Delta \overline{u^+}$  in the  $x^+$  direction is taken as order 1.

To make statements about terms containing  $\overline{\rho^+ u^{+'}}$  and  $\overline{\rho^+ v^{+'}}$  it is necessary to put an upper bound on  $\rho^{+'}$ . For an order of magnitude analysis it is sufficient to say that  $\rho^{+'}$  could result from several causes: a) turbulent bulk transport of fluid from regions of different density, velocity and enthalpy; b) turbulent pressure fluctuations; c) molecular viscous dissipation caused by the fluctuating velocity; and d) molecular heat transfer driven by the fluctuating enthalpy.

Except in the regions very near the wall, molecular transport is generally assumed to exert negligible effect on the mean equations of motion. The role of viscosity, or conductivity, is to establish the smallest possible scale of turbulence. But for sufficiently large Reynolds number this smallest scale is far removed from the scales of turbulence that play a role in the turbulent transport processes.



The possible effect of pressure fluctuations is not as clear. Kovasznay [31] has measured the pressure fluctuation (expressed as the mass flow fluctuation) just outside the boundary layer, which he feels to be indicative of the pressure fluctuation inside the boundary layer. He found the mass flow fluctuation to be of the order of 0.1 per cent at a Mach number of 1.75, whereas he found the velocity fluctuation in the boundary layer to be 2 to 3 per cent. Therefore, until more data are available, the assumption that the pressure fluctuations are negligible seems to be justified.

If the bulk transport is the major cause of density and enthalpy fluctuations, then the fluctuations should be correlated with the velocity fluctuations, since it is the latter which carry fluid with one density and enthalpy into regions with other average values. Furthermore, density and enthalpy should be correlated if pressure fluctuations are negligible. Both Kovasznay [31] and Kistler [30] have found a strong negative correlation between the temperature and the velocity. This should be expected since the region near the wall has a relatively lower velocity and higher temperature than the region far from the wall. Furthermore, studying a wide variety of Mach numbers and, therefore, static temperature differences across the layer, Kistler found that the distribution of static temperature fluctuations was very nearly proportional to the static temperature difference across the layer. This is also to be expected if the dominant effect is bulk transport, since more extreme fluctuations can only occur if there are wider variations of the transport property available within the layer. Although these observations are far from a proof that bulk transport is the dominant cause of density and enthalpy fluctuations, they make an assumption to that effect seem reasonable.

The conventional representation of this assumption is the Reynolds analogy. The Reynolds analogy is that the fluctuation of the transported property is proportional to the product of the gradient of the transported property and the velocity fluctuation. In the case of  $\rho^+ v^+$ , this is

$$\overline{\rho^+ v^+} \approx \overline{u^+ v^+} \frac{\overline{\frac{\partial \rho^+}{\partial y^+}}}{\overline{\frac{\partial u^+}{\partial y^+}}} \quad . \quad (A4)$$

Of course equation (A4) is consistent with equations (7) and (13), which are discussed in Section II. For an order of magnitude analysis it is adequate to approximate  $\overline{\frac{\partial \rho^+}{\partial y^+}}$  as the average density gradient across the layer,  $\Delta \rho^+ / \epsilon$ , and  $\overline{\frac{\partial u^+}{\partial y^+}}$  as the average velocity gradient,  $\Delta u^+ / \epsilon$  ( $\sim 1/\epsilon$ ). Therefore

$$\overline{u^{+'}v^{+'}} \frac{\partial \overline{\rho^{+}}}{\partial y^{+}} \bigg/ \frac{\partial \overline{u^{+}}}{\partial y^{+}} \approx \overline{u^{+'}v^{+'}} \frac{\partial \overline{\rho^{+}}}{\partial y^{+}} ,$$

or

$$\overline{\rho^{+'}v^{+'}} = O(\epsilon \Delta \rho^{+}) . \quad (A5)$$

The remaining term in the x momentum equation is the pressure gradient,  $\partial \overline{p^{+}} / \partial x^{+}$ , which must be of the same order as the inertia terms so long as the velocity in the external flow does not approach zero. However, the only term on the left hand side of the y momentum equation that is of importance is  $\partial(\overline{\rho^{+}v^{+'2}}) / \partial y^{+}$ . If the magnitude of the pressure gradient across the layer,  $\partial \overline{p^{+}} / \partial y^{+}$ , is represented by  $\Delta \overline{p^{+}} / \epsilon$ , it is clear that  $\Delta \overline{p^{+}} = O(\epsilon + \epsilon \Delta \rho^{+})$ .

By following the same approach that yielded (A5), the following relations may be shown:

$$\overline{u^{+'}h^{+'}} , \quad \overline{v^{+'}h^{+'}} = O(\epsilon \Delta h^{+}) , \quad (A6)$$

and

$$\overline{\rho^{+'}h^{+'}} = O(\epsilon \Delta \rho^{+} \Delta h^{+}) . \quad (A7)$$

For correlations involving the total enthalpy fluctuation,  $h^{o+'}$ , this quantity can be obtained by subtracting equation (A2e) from the same equation before Reynolds averaging has been performed. The result is

$$\left(1 + \frac{\gamma-1}{2} M_e^2\right) h^{o+'} = h^{+'} + \frac{(\gamma-1)}{2} M_e^2 \left[ 2\overline{u^{+}u^{+'}} + \overline{u^{+'2}} - \overline{u^{+2}} + \overline{v^{+'2}} - \overline{v^{+2}} + \overline{w^{+'2}} - \overline{w^{+2}} \right] \quad (A8)$$

Then, after multiplying (A8) by  $v^{+'}$ , for example, and Reynolds averaging, the result is

$$\overline{v^+ h^{o+}} = \frac{1}{1 + \frac{\gamma-1}{2} M_e^2} \left[ \overline{v^+ h^+} + (\gamma-1) M_e^2 \overline{u^+ u^+ v^+} \right], \quad (A9)$$

$\varepsilon_{\Delta h^+} \quad \varepsilon$

Therefore

$$\overline{v^+ h^{o+}} = O(\varepsilon_{\Delta h^{o+}}) \quad (A10a)$$

Similarly it can be shown that

$$\overline{u^+ h^{o+}} = O(\varepsilon_{\Delta h^{o+}}), \quad (A10b)$$

and

$$\overline{\rho^+ h^{o+}} = O(\varepsilon_{\Delta \rho^+} \Delta h^{o+}) \quad (A10c)$$

Having estimated the magnitudes of the terms as noted on equations (2), the significance of these terms may be assessed under various conditions. Evidently the magnitude of  $\Delta \rho^+$ ,

$$\Delta \rho^+ = 1 - \frac{h_e^o / h_w}{1 + \frac{\gamma-1}{2} M_e^2}, \quad (A11)$$

is of prime importance in the ordering of the terms. For very small Mach number and heat transfer,  $\Delta \rho^+$  is small. In this case equations (2) would simply reduce to the familiar constant property equations of motion. However, if the heat transfer is substantial or the Mach number is large,  $\Delta \rho^+$  will be of order unity. Apparently several more terms in equations (2) become important and the resulting equations can be written

$$\frac{\partial}{\partial x^+} (\overline{\rho^+} \overline{u^+}) + \frac{\partial}{\partial y^+} (\overline{\rho^+} \overline{v^+} + \overline{\rho^+ v'^+}) = 0 \quad , \quad (A12a)$$

$$\overline{\rho^+} \overline{u^+} \frac{\partial \overline{u^+}}{\partial x^+} + (\overline{\rho^+} \overline{v^+} + \overline{\rho^+ v'^+}) \frac{\partial \overline{u^+}}{\partial y^+} + \frac{\partial}{\partial y^+} (\overline{\rho^+} \overline{u^+ v'^+}) = - \frac{\partial \overline{p^+}}{\partial x^+} \quad , \quad (A12b)$$

$$\overline{\rho^+} \overline{u^+} \frac{\partial \overline{h^{o+}}}{\partial x^+} + (\overline{\rho^+} \overline{v^+} + \overline{\rho^+ v'^+}) \frac{\partial \overline{h^{o+}}}{\partial y^+} + \frac{\partial}{\partial y^+} (\overline{\rho^+} \overline{v^+ h^{o+}'}) = 0 \quad , \quad (A12c)$$

$$\left(1 + \frac{\gamma-1}{2} M_e^2\right) \overline{h^{o+}} = \overline{h^+} + \frac{\gamma-1}{2} M_e^2 \overline{u^{+2}} \quad , \quad (A12d)$$

$$1 + \gamma M_e^2 \overline{p^+} = \overline{\rho^+} \overline{h^+} \quad . \quad (A12e)$$

The  $y$  momentum equation is not included since its only contribution is to show that  $\Delta \overline{p^+} = O(\epsilon + \epsilon \Delta \overline{\rho^+})$  and therefore, the variation of  $\partial \overline{p^+} / \partial x^+$  across the layer is negligible in the  $x$  momentum equation.

It is interesting to note that the size of  $\Delta \overline{h^{o+}}$  does not serve to distinguish between the relative importance of the terms in the energy equation, but simply whether or not the equation as a whole has significance in a particular situation. In the energy equation, as in the  $x$  momentum equation, it is the magnitude of  $\Delta \overline{\rho^+}$  which selects the meaningful terms.

In equations (A12b) and (A12c) it is possible to rewrite the shear stress and heat flux terms. The turbulent shear stress may be written as

$$\tau_t^+ = - \overline{\rho^+} \overline{u^+ v'^+} \quad . \quad (A13)$$

Then with the aid of equation (A8) the third term in equation (A12c) may be

written

$$-\overline{\rho^+ v^+ h^{o+}} = -\overline{\rho^+ v^+ h^+} + \overline{u^+ (-\overline{\rho^+ u^+ v^+})} \quad . \quad (A14)$$

If the turbulent heat flux is defined as

$$\overline{q_t^+} = -\overline{\rho^+ v^+ h^+} \quad , \quad (A15)$$

equation (A14) becomes

$$-\overline{\rho^+ v^+ h^{o+}} = \overline{q_t^+} + \overline{u^+ \tau_t^+} \quad . \quad (A16)$$

When written in terms of the original variables, the boundary layer equations (2) are

$$\frac{\partial}{\partial x} (\bar{\rho} \bar{u}) + \frac{\partial}{\partial y} (\bar{\rho} \bar{v} + \overline{\rho' v'}) = 0 \quad (A17a)$$

$$\bar{\rho} \bar{u} \frac{\partial \bar{u}}{\partial x} + (\bar{\rho} \bar{v} + \overline{\rho' v'}) \frac{\partial \bar{u}}{\partial y} = -\frac{d\bar{p}}{dx} + \frac{\partial \bar{\tau}_t}{\partial y} \quad , \quad (A17b)$$

$$\bar{\rho} \bar{u} \frac{\partial \bar{h}^o}{\partial x} + (\bar{\rho} \bar{v} + \overline{\rho' v'}) \frac{\partial \bar{h}^o}{\partial y} = \frac{\partial}{\partial y} (\bar{q}_t + \bar{u} \bar{\tau}_t) \quad , \quad (A17c)$$

$$\bar{h}^o = \bar{h} + \frac{1}{2} \bar{u}^2 \quad , \quad (A17d)$$

$$p_e = \frac{\gamma-1}{\gamma} \bar{\rho} \bar{h} \quad , \quad (A17e)$$

where

$$\overline{\tau}_t = - \overline{\rho} \overline{u'v'} \quad , \quad (A17f)$$

and

$$\overline{q}_t = - \overline{\rho} \overline{v'h'} \quad . \quad (A17g)$$

## APPENDIX B. COMPARISON OF EFFECTIVE VISCOSITY HYPOTHESIS

### WITH ALTERNATE FORMS

It is interesting to compare the functional relationship for  $\nu_e$  used in other hypotheses with (8). This comparison is complicated by the fact that apparently there are no effective viscosity hypotheses in the literature (see Rotta [32], for instance) besides the present one (Mellor, [5]) that have used two scales. Some simply restrict their range of applicability to the wall layer or the defect layer. Many others, however, stipulate a wall layer relation and then assume the validity of the scaleless overlap layer formulation to the edge of the boundary layer. Since these are all essentially single layer models they will be treated as such and a comparison will be made on that basis. Furthermore most effective viscosity hypotheses were originally intended for use in incompressible flow. Many of them could be extended to include the effects of compressibility and a few have (Lin and Chen [33]). However, if they are untenable, their weaknesses are usually evident even in incompressible flow.

The first class of hypotheses in Table I is based on the assumption (references 34 and 35)

$$\nu_e = \nu_e(u_\tau, y, \bar{\nu}) \quad , \quad (B1)$$

in the wall layer. Although for small pressure gradients the results of these hypotheses may not differ greatly from the present hypothesis, they will near separation. As  $u_\tau = \sqrt{\frac{\tau_w}{\rho_e}} \rightarrow 0$  these hypotheses all yield  $\nu_e \rightarrow \bar{\nu}$

for the entire wall layer, which is clearly an unacceptable result. For the same reason, Clauser's [2] assumption for the defect layer,

$$\nu_e = \nu_e(u_\tau, y, \delta_k^* U) \quad , \quad (B2)$$

is also invalid. Besides these hypotheses\* in which  $\nu_e$  is explicitly assumed to be a function of  $u_\tau$ , most of the other hypotheses in Table I use  $u_\tau$  as

---

\*References 10 and 36.

a parameter in the condition for matching the viscous sublayer to the overlap layer. Again, near separation these conditions would cease to be meaningful. However, on the assumption that the matching conditions could be redefined, the effective viscosity functions themselves will be considered.

The next class of hypotheses are those which use a von Karman [37] similarity hypothesis for the overlap layer and which supply some other function for the viscous sublayer. When the pressure gradient is zero, the von Karman similarity hypothesis does give the correct logarithmic velocity profile in the overlap region (where  $\bar{\tau} = \tau_w$ ). It also yields the correct functional dependence,  $\bar{u} \sim \sqrt{y}$ , when  $\tau_w = 0$  at separation. However, if the constant of proportionality is adjusted to fit the zero pressure gradient case, the result for the separating flow is a factor of two too high to agree with Stratford's [38] data. Stratford's data appear to favor a variation in the overlap layer which goes as

$$\bar{u} = \frac{1}{2K} \sqrt{\frac{d\bar{p}}{dx} \frac{y}{\rho}} + \text{constant.} \quad (\text{B3})$$

This is the result predicted by the Prandtl mixing length form used in the present hypothesis. Furthermore, both of the examples of this type of hypothesis might more legitimately be called three layer models since the forms of the effective viscosity in the laminar sublayer are not the same as they are in the overlap layer. In the laminar sublayer, Bjorgum [39] assumes

$$\nu_e = \nu_e \left( \bar{u}, \frac{\partial \bar{u}}{\partial y}, \bar{v} \right), \quad (\text{B4a})$$

and Deissler [40] assumes

$$\nu_e = \nu_e(y, \bar{u}, \bar{v}) \quad , \quad (\text{B4b})$$

whereas they both use



$$\nu_e = \nu_e \left( \frac{\partial \bar{u}}{\partial y}, \frac{\partial^2 \bar{u}}{\partial y^2}, \bar{v} \right), \quad (B5)$$

in the overlap layer. It would seem that, until the need for a three layer model is evident, a two layer model represents a more concise and simple description of the data.

Table I gives two more hypotheses which do not differ greatly from the present one. The first one (Loitsianskii [41]) applies to the wall layer. Until more data are available in the laminar sublayer, a meaningful comparison with this essentially similar empirical function is not possible. The only reservation about this hypothesis is that the parameter which defines the range of the functions depends on  $u_\tau$ , as discussed above.

The last hypothesis in the table (Maise and McDonald [42]) pertains only to the defect layer. It also appears to be the only one originally proposed for compressible flow. It was presented not as an equation but in the form of a plot demonstrating the near Mach number independence of the mixing length function for constant pressure boundary layers. For this reason the equation given in the table is only an approximation. The functional relationship for  $\nu_e$  is

$$\nu_e = \nu_e \left( \delta, y, \frac{\partial \bar{u}}{\partial y} \right), \quad (B6)$$

or

$$\frac{\nu_e}{\delta^2 \frac{\partial \bar{u}}{\partial y}} = \Phi \left( \delta^2 \frac{\partial \bar{u}}{\partial y}, y, \frac{\partial \bar{u}}{\partial y} \right) \quad (B7)$$

when written in the form of an effective viscosity rather than a mixing length. The strong similarity between these apparently dissimilar hypotheses, (8a) and (B7), can be established by considering an approximate relation between  $U\delta_k^*$  and  $\delta^2 \frac{\partial \bar{u}}{\partial y}$  with the aid of Figure 38 which shows that

TABLE I: \* SUMMARY OF HYPOTHESES FOR  $\nu_e$ 

ASSUMED DIMENSIONAL ARGUMENTS	AUTHOR	SPECIFIC FUNCTIONS	RANGE
$\nu_e(u_\tau, y, \nu)$	Squire [34]	$\nu_e = \nu$	$(0 \leq y \leq y_1^+ \nu/u_\tau)$
		$\nu_e = \kappa(u_\tau y - y_1^+ \nu) + \nu$	$(y_1^+ \nu/u_\tau \leq y)$
$\nu_e(u_\tau, y, \delta_k^* U)$	Reichardt [35]	$\nu_e = \kappa[u_\tau y - y_1^+ \nu \tanh(y u_\tau / y_1^+ \nu)] + \nu$	$(0 \leq y)$
	Clauser [2]	$\nu_e = \kappa u_\tau y$ $\nu_e = \delta_k^* UK$	$(y \leq \delta_k^* \frac{U}{u_\tau} \frac{K}{\kappa})$ $(\delta_k^* \frac{U}{u_\tau} \frac{K}{\kappa} \leq y)$
$\nu_e(u_\tau, y, \frac{\partial \bar{u}}{\partial y}, \nu)$	Hama [36]	$\nu_e = (-0.1 y)^4 (u_\tau / \nu)^2  \partial \bar{u} / \partial y  + \nu$	$(0 \leq y \leq y_1^+ \nu/u_\tau)$
		$\nu_e = \kappa^2 \frac{2}{\nu}  \partial \bar{u} / \partial y  + \nu$	$(y_1^+ \nu/u_\tau \leq y)$
	van Driest [10]	$\nu_e = \kappa^2 y^2 [1 - \exp(y u_\tau / \nu A^+)]^2  \partial \bar{u} / \partial y  + \nu$	$(0 \leq y)$

\* Largely from Rotta [32].

TABLE I: (continued)

ASSUMED DIMENSIONAL ARGUMENTS	AUTHOR	SPECIFIC FUNCTIONS	RANGE
$\nu_e(\frac{\bar{u}}{\partial y}, \frac{\partial^2 \bar{u}}{\partial y^2}, \nu)$ and $\nu_e(\bar{u}, \frac{\partial \bar{u}}{\partial y}, \nu)$ or $\nu_e(\bar{u}, y, \nu)$	Bjorgum [39]	$\nu_e = \kappa^2 \bar{u}^{-2}  \partial \bar{u} / \partial y  + \nu$ $\nu_e = \kappa_2^2 ( \partial \bar{u} / \partial y )^3 / (\partial^2 \bar{u} / \partial y^2)^2 + \nu$	$(0 \leq y \leq y_1^+ \nu / u_\tau)$ $(y_1^+ \nu / u_\tau \leq y)$
	Deissler [40]	$\nu_e = n^2 \bar{u} y [1 - \exp(-n^2 \bar{u} y / \bar{v})] + \nu$ $\nu_e = \kappa^2 ( \partial \bar{u} / \partial y )^3 / (\partial^2 \bar{u} / \partial y^2)^2 + \nu$	$(0 \leq y \leq y_1^+ \nu / u_\tau)$ $(y_1^+ \nu / u_\tau \leq y)$
$\nu_e(\frac{\partial \bar{u}}{\partial y}, y, \nu)$	Loitsianskii [41]	$\nu_e = \nu$ $\nu_e = \sqrt{\kappa^4 y^4 (\partial \bar{u} / \partial y)^2 - \kappa^4 y_1^4 \nu^2 + \nu^2}$	$(0 \leq y \leq y_1^+ \nu / u_\tau)$ $(y_1^+ \nu / u_\tau \leq y)$
$\nu_e(\delta, y, \frac{\partial \bar{u}}{\partial y})$	Maïse and McDonald [42]	$\nu_e = \kappa^2 y^2  \partial \bar{u} / \partial y $ $\nu_e = \kappa^+ \delta^2  \partial \bar{u} / \partial y $	$(y \leq \delta \sqrt{\kappa^+} / \kappa)$ $(\delta \sqrt{\kappa^+} / \kappa \leq y)$

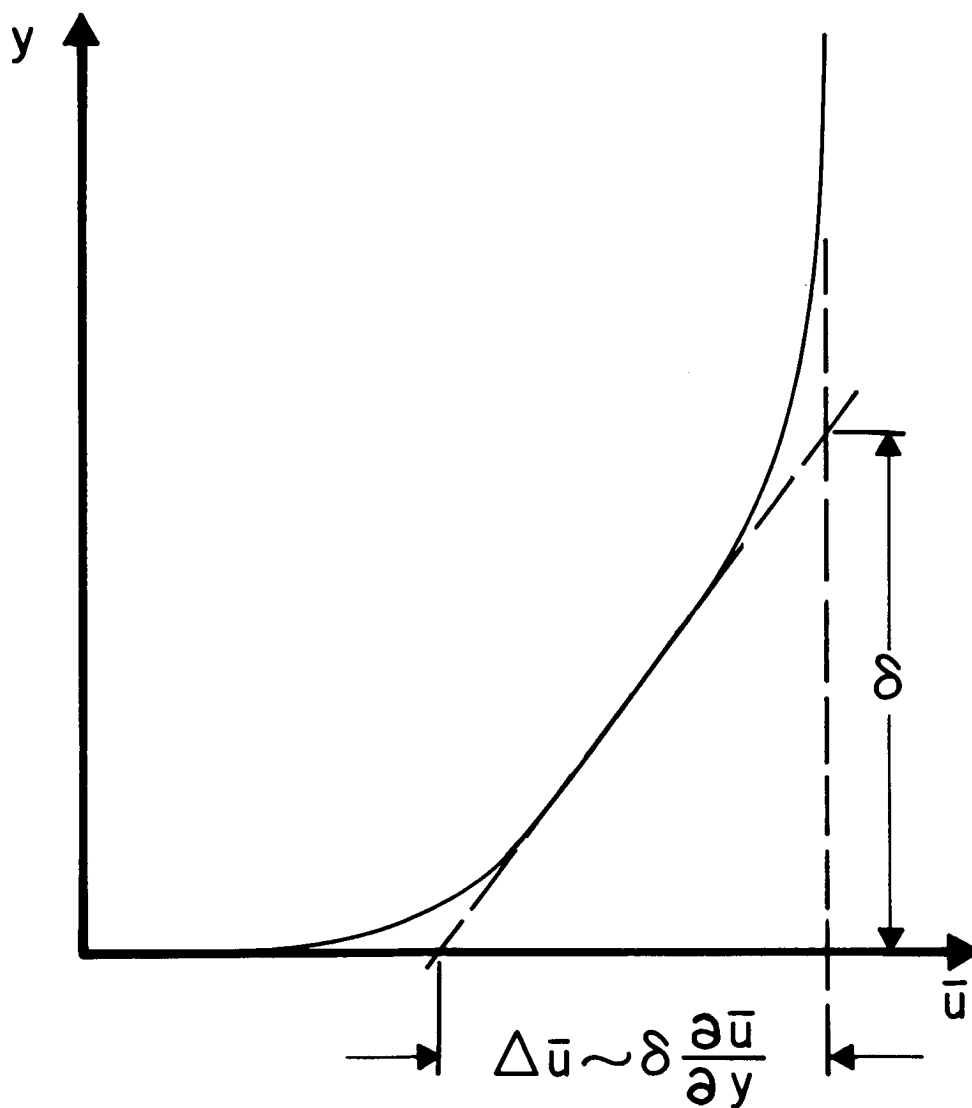


FIGURE 38. Illustration of the relationship between the effective viscosity scales  $\delta_k^* U$  and  $\delta^2 (\partial \bar{u} / \partial y)$  for the defect layer,

$$U \delta_k^* = \int_0^\infty (U - \bar{u}) dy \approx \frac{1}{2} \delta (\Delta \bar{u}) \approx \frac{1}{2} \delta^2 \left( \frac{\partial \bar{u}}{\partial y} \right)$$

$$U\delta_k^* = \int_0^\infty (U - \bar{u}) dy \approx \frac{1}{2} \delta (\Delta \bar{u}) \approx \frac{1}{2} \overline{\delta^2 \left( \frac{\partial \bar{u}}{\partial y} \right)} \quad . \quad (B8)$$

In light of equation (B8) there is probably little basis for making a choice between the two. A well defined scale such as  $\delta_k^*$  is perhaps a slight advantage over the use of the less well defined  $\delta$ . This is why (8a) was used in the present calculations.

The relationship shown in (B8) brings out the important point that  $U\delta_k^*$  is a measure of the average velocity gradient in the boundary layer. A self-consistent effective viscosity hypothesis for compressible flow could also be formulated using the average mass flow gradient,

$\rho_e U\delta^* = \int_0^\infty (\rho_e U - \bar{\rho} \bar{u}) dy$ . Several hypotheses of this type actually have been proposed for compressible turbulent wakes (Zakkay and Fox, [43]). By analogy with the argument preceeding (8), such an hypothesis might be written

$$\bar{\tau} = \mu_e \frac{\partial \bar{u}}{\partial y} \quad (B9)$$

with

$$\mu_e = \mu_e \left( \bar{\mu}, y, \frac{\partial \bar{\rho} \bar{u}}{\partial y} \right) \quad \text{for the wall layer,} \quad (B10a)$$

and

$$\mu_e = \mu_e \left( \rho_e U\delta^*, y, \frac{\partial \bar{\rho} \bar{u}}{\partial y} \right) \quad \text{for the defect layer,} \quad (B10b)$$

so that

$$\frac{\mu_e}{\mu} = \phi^* \left( \frac{\kappa^2 y^2}{\mu} \frac{\partial \bar{\rho} \bar{u}}{\partial y} \right), \quad (B11a)$$

$$\frac{\mu_e}{\rho_e U\delta^*} = \phi^* \left( \frac{\kappa^2 y^2}{\rho_e U\delta^*} \frac{\partial \bar{\rho} \bar{u}}{\partial y} \right), \quad (B11b)$$

and in the overlap region

$$\mu_e = \kappa^2 y^2 \frac{\partial \bar{\rho} \bar{u}}{\partial y} \quad . \quad (B12)$$

The correlation  $\overline{u'v'} = \bar{\tau}/\bar{\rho}$  must be very nearly invariant under a stream-wise Galilean transformation as is the hypothesis of equation (8) . However, that is not the case for the example above or for that matter any hypothesis which uses a function of  $(\rho_e U - \bar{\rho} \bar{u})$  in the defect layer or  $\bar{\rho} \bar{u}$  in the wall layer, since both the differential and the integral of these quantities would then depend on the magnitude of the velocity. On the other hand, the differential and integral of  $(U - \bar{u})$  and  $\bar{u}$  are independent of reference frame as is  $\overline{u'v'}$  .

# APPENDIX C. EQUATIONS FOR THE

## RUNGE-KUTTA METHOD

The Runge-Kutta method is a procedure for solving first order differential equations. In order to apply this method to a linear equation of the form

$$\left\{ c_6(\eta) \left[ f'' + c_5(\eta) \right] \right\} = c_3(\eta) f'' + c_2(\eta) f' + c_1(\eta) f + c_4(\eta) \quad , \quad (C1)$$

the equation must be rewritten as a set of first order equations as follows. Let

$$f^{(1)} = f \quad , \quad f^{(2)} = f' \quad , \quad f^{(3)} = c_6(f'' + c_5) \quad . \quad (C2)$$

Then

$$\frac{\partial f^{(1)}}{\partial \eta} = f^{(2)} \quad , \quad \frac{\partial f^{(2)}}{\partial \eta} = \frac{f^{(3)}}{c_6} - c_5 \quad .$$

$$\frac{\partial f^{(3)}}{\partial \eta} = c_3 \left( \frac{f^{(3)}}{c_6} - c_5 \right) + c_2 f^{(2)} + c_1 f^{(1)} + c_4 \quad . \quad (C3)$$

From Hildebrand [ 44 ], if the values of  $f_n^{(i)}$  at  $\eta_n$  are known, the values at  $\eta_{n+1} (= \eta_n + \Delta\eta)$  are given to fourth order accuracy by the relation,

$$f_{n+1}^{(i)} = f_n^{(i)} + \frac{1}{6} \left( a_1^{(i)} + 2a_2^{(i)} + 2a_3^{(i)} + a_4^{(i)} \right) \quad , \quad (C4)$$

where

$$a_1^{(1)} = \Delta\eta f^{(2)} \quad , \quad a_1^{(2)} = \Delta\eta \left( \frac{f^{(3)}}{c_{6n}} - c_{5n} \right) \quad ,$$

$$a_2^{(1)} = \Delta\eta \left( f^{(2)} + \frac{1}{2} a_1^{(2)} \right) \quad , \quad a_2^{(2)} = \Delta\eta \left( \frac{f^{(3)} + \frac{1}{2} a_1^{(3)}}{c_{6_{n+\frac{1}{2}}}} - c_{5_{n+\frac{1}{2}}} \right) \quad ,$$

$$a_3^{(1)} = \Delta\eta \left( f^{(2)} + \frac{1}{2} a_2^{(2)} \right) \quad , \quad a_3^{(2)} = \Delta\eta \left( \frac{f^{(3)} + \frac{1}{2} a_2^{(3)}}{c_{6_{n+\frac{1}{2}}}} - c_{5_{n+\frac{1}{2}}} \right) \quad ,$$

$$a_4^{(1)} = \Delta\eta \left( f^{(2)} + a_3^{(2)} \right) \quad , \quad a_4^{(2)} = \Delta\eta \left( \frac{f^{(3)} + a_3^{(3)}}{c_{6_{n+1}}} - c_{5_{n+1}} \right) \quad ,$$

$$a_1^{(3)} = \Delta\eta \left[ c_{3n} \left( \frac{f^{(3)}}{c_{6n}} - c_{5n} \right) + c_{2n} f^{(2)} + c_{1n} f^{(1)} + c_{4n} \right] \quad ,$$

$$a_2^{(3)} = \Delta\eta \left[ c_{3_{n+\frac{1}{2}}} \left( \frac{f^{(3)} + \frac{1}{2} a_1^{(3)}}{c_{6_{n+\frac{1}{2}}}} - c_{5_{n+\frac{1}{2}}} \right) + c_{2_{n+\frac{1}{2}}} \left( f^{(2)} + \frac{1}{2} a_1^{(2)} \right) \right. \\ \left. + c_{1_{n+\frac{1}{2}}} \left( f^{(1)} + \frac{1}{2} a_1^{(1)} \right) + c_{4_{n+\frac{1}{2}}} \right]$$



$$a_3^{(3)} = \Delta\eta \left[ c_{3_{n+\frac{1}{2}}} \left( \frac{f^{(3)} + \frac{1}{2} a_2^{(3)}}{c_{6_{n+\frac{1}{2}}}} - c_{5_{n+\frac{1}{2}}} \right) + c_{2_{n+\frac{1}{2}}} \left( f^{(2)} + \frac{1}{2} a_2^{(2)} \right) \right. \\ \left. + c_{1_{n+\frac{1}{2}}} \left( f^{(1)} + \frac{1}{2} a_2^{(1)} \right) + c_{4_{n+\frac{1}{2}}} \right] ,$$

$$a_4^{(3)} = \Delta\eta \left[ c_{3_{n+1}} \left( \frac{f^{(3)} + a_3^{(3)}}{c_{6_{n+1}}} - c_{5_{n+1}} \right) + c_{2_{n+1}} \left( f^{(2)} + a_3^{(2)} \right) \right. \\ \left. + c_{1_{n+1}} \left( f^{(1)} + a_3^{(1)} \right) + c_{4_{n+1}} \right] ,$$

$$c_{n+\frac{1}{2}} = \frac{1}{2} (c_n + c_{n+1}) \quad . \quad (C5)$$

# APPENDIX D. ASYMPTOTIC SOLUTION FOR LARGE $\eta$

The turbulent Prandtl number has been assumed to be equal to 1 in the analysis which follows.

For large  $\eta$  ,  $f \rightarrow 1$  ,  $f' \rightarrow 0$  ,  $f'' \rightarrow 0$  ,  $g' \rightarrow 0$  ,  $g'' \rightarrow 0$  ,  $T \rightarrow K \frac{\delta_k^*}{\delta^*}$  ,  $T_h \rightarrow K \frac{\delta_k^*}{\delta^*}$  and from equation (25),

$$\theta \rightarrow 1 + \frac{(\gamma - 1) M_e^2 f' - \left(1 + \frac{\gamma-1}{2} M_e^2\right) Hg'}{1 + (\gamma - 1) M_e^2} , \quad (D1)$$

$$\theta' \rightarrow \frac{(\gamma - 1) M_e^2 f'' - \left(1 + \frac{\gamma-1}{2} M_e^2\right) Hg''}{1 + (\gamma - 1) M_e^2} , \quad (D2)$$

$$\begin{aligned} \delta^* \theta_x &\rightarrow \frac{(\gamma - 1) M_e^2 \delta^* f'_x - \left(1 + \frac{\gamma-1}{2} M_e^2\right) \delta^* Hg'_x}{1 + (\gamma - 1) M_e^2} \\ &+ V \frac{\left[1 + (\gamma - 1) M_e^2\right]^2 - 1}{\left[1 + (\gamma - 1) M_e^2\right]^2} \left(f' + \frac{H}{2} g'\right) . \end{aligned} \quad (D3)$$

Then the asymptotic forms of equations (24a) and (24b) are

$$\frac{\delta_k^*}{\delta^*} K f''' + Q(\eta - 1) f'' - 2V \frac{1 + \frac{\gamma-1}{2} M_e^2}{1 + (\gamma-1) M_e^2} f' - \delta^* f'_x = V \frac{1 + \frac{\gamma-1}{2} M_e^2}{1 + (\gamma-1) M_e^2} Hg' , \quad (D4a)$$

and

$$\frac{\delta^*}{\delta} K g''' + Q(\eta - 1) g'' - \delta^* g'_x = 0 \quad (D4b)$$

In order to insure the satisfaction of the fourth and seventh boundary conditions (28) , the asymptotic solutions of  $f'$  and  $g'$  were assumed in exponential form,

$$f'(\eta, x) = R(x) \exp \left\{ - \frac{(\eta - 1)^2}{2r(x)} \right\} , \quad (D5a)$$

$$g'(\eta, x) = S(x) \exp \left\{ - \frac{(\eta - 1)^2}{2s(x)} \right\} . \quad (D5b)$$

Although strictly speaking  $R$  and  $S$  are functions of  $\eta$  as well as  $x$  , the  $\eta$  dependence is small. Furthermore the outer boundary conditions on  $f'$  and  $g'$  can be satisfied with knowledge of only  $r(x)$  and  $s(x)$  .

$R(x)$  and  $S(x)$  can then be eliminated using  $f'(\eta_1, x)$  and  $g'(\eta_1, x)$  , where  $\eta_1$  is a point far from the wall. Then

$$f'(\eta, x) = f'(\eta_1, x) \exp \left\{ \frac{(\eta_1 - 1)^2 - (\eta - 1)^2}{2r(x)} \right\} \quad (D6a)$$

$$g'(\eta, x) = g'(\eta_1, x) \exp \left\{ \frac{(\eta_1 - 1)^2 - (\eta - 1)^2}{2s(x)} \right\} . \quad (D6b)$$

Then  $r(x)$  and  $s(x)$  may be found by inserting (D5a) and (D5b) into (D4a)

and (D4b) . The coefficients of  $(\eta - 1)^2$  are

$$\frac{\delta^*}{2} r_x + Qr = K \frac{\delta_k^*}{\delta^*} , \quad (D7a)$$

and

$$\frac{\delta^*}{2} s_x + Qs = K \frac{\delta_k^*}{\delta^*} . \quad (D7b)$$

The solution of these equations can easily be shown to be

$$r(x) = \left( \frac{\rho_{e0} U_0 \delta_0^*}{\rho_e U \delta^*} \right)^2 r(x_0) + \frac{2K}{(\rho_e U \delta^*)^2} \int_{x_0}^x \frac{\delta_k^*}{\delta^*} (\rho_e U)^2 \delta^* dx , \quad (D8a)$$

and

$$s(x) = \left( \frac{\rho_{e0} U_0 \delta_0^*}{\rho_e U \delta^*} \right)^2 s(x_0) + \frac{2K}{(\rho_e U \delta^*)^2} \int_{x_0}^x \frac{\delta_k^*}{\delta^*} (\rho_e U)^2 \delta^* dx . \quad (D8b)$$

# APPENDIX E. BOUNDARY LAYER EQUATIONS OF MOTION

## IN AXISYMMETRIC FLOW

Following an argument similar to that in Section II , the boundary layer equations for a steady flow at moderate Mach number and heat transfer for which  $\delta/R_{LAT} = O(1)$  , are

$$\frac{\partial r}{\partial x} \bar{\rho} \bar{u} + \frac{\partial}{\partial y} \left[ r (\bar{\rho} \bar{v} + \overline{\rho'v'}) \right] = 0 \quad , \quad (E1a)$$

$$r \bar{\rho} \bar{u} \frac{\partial \bar{u}}{\partial x} + r (\bar{\rho} \bar{v} + \overline{\rho'v'}) \frac{\partial \bar{u}}{\partial y} = - \frac{dp}{dx} + \frac{\partial r \tau}{\partial y} \quad , \quad (E1b)$$

$$r \bar{\rho} \bar{u} \frac{\partial \bar{h}^o}{\partial x} + r (\bar{\rho} \bar{v} + \overline{\rho'v'}) \frac{\partial \bar{h}^o}{\partial y} = \frac{\partial}{\partial y} \left[ r (\bar{q} + \bar{u} \bar{\tau}) \right] \quad . \quad (E1c)$$

The definitions of  $\bar{\tau}$  and  $\bar{q}$  and the effective viscosity hypothesis are unchanged. The sole difference in the effective viscosity is that in flow with lateral curvature the defect scale becomes

$$U_{\delta k}^* = \int_0^\infty (U - \bar{u}) \frac{r}{R_{LAT}} dy \quad . \quad (E2)$$

As for the two dimensional equations, new variables are introduced,

$$f'(\eta, x) = \Lambda \left( \frac{\rho_e U - \bar{\rho} \bar{u}}{\rho_e U} \right) \quad . \quad (E3a)$$

$$\theta(\eta, x) = \frac{\rho_e}{\bar{\rho}} \quad , \quad (E3b)$$

$$g'(\eta, x) = \frac{h_e^o - \overline{h^o}}{h_e^o - h_r} \quad , \quad (E3c)$$

$$\Lambda = \frac{r}{R_{LAT}} = 1 + \lambda \eta \quad , \quad \lambda = \frac{\delta^*}{R_{LAT}} \quad , \quad (E3d)$$

$$\eta = \frac{y}{\delta^*} \quad , \quad (E3e)$$

$$D = \frac{(R_{LAT})_x \delta^*}{R_{LAT}} \quad , \quad (E3f)$$

$$P = \frac{(\rho_e U)_x \delta^*}{\rho_e U} \quad , \quad (E3g)$$

$$Q = \frac{(R_{LAT} \rho_e U \delta^*)_x}{R_{LAT} \rho_e U} \quad , \quad (E3h)$$

$$V = \frac{U_x \delta^*}{U} \quad . \quad (E3i)$$

When rewritten in terms of these variables, the equations of motion become

$$\begin{aligned}
 & \left\{ \frac{\delta_k^*}{\delta^*} \frac{\Lambda}{\theta} \left[ \theta \left( 1 - \frac{f'}{\Lambda} \right) \right]' \right\} = \left\{ \theta \left[ \frac{Q}{\Lambda} (\eta - f) + \frac{\lambda \eta^2}{2\Lambda} (P + 2\delta_x^*) \right] \right\} f'' \\
 & + \left\{ (V\theta + \delta_{\theta x}^*) \left( \frac{f'}{\Lambda} - 2 \right) + \left( \delta_{\theta x}^{*'} - \frac{\lambda D}{\Lambda} \theta \right) \left( 1 - \frac{f'}{\Lambda} \right) \eta \right. \\
 & + \left. \left( \theta' - \frac{\lambda \theta}{\Lambda} \right) \frac{Q}{\Lambda} (\eta - f) + P \frac{\lambda \eta^2}{2\Lambda} - \eta \frac{\delta_x^*}{\Lambda} \left( 1 - \frac{f'}{\Lambda} \right) \right\} f' \\
 & + \left\{ Q\theta' \right\} f + \left\{ \Lambda V(\theta - 1) + \Lambda \theta \delta_x^* - \theta' \left[ \eta Q + \frac{\lambda}{2} \eta^2 (P + 2\delta_x^*) \right] \right\} \\
 & + \delta_{f_x}^* \left[ \theta' \left( 1 - \frac{f'}{\Lambda} \right) - \theta \frac{f''}{\Lambda} + \frac{\lambda \theta}{\Lambda} \frac{f'}{\Lambda} \right] - \delta_{\theta}^* f_x' \left( 1 - \frac{f'}{\Lambda} \right) = 0 \quad , \quad (E4a)
 \end{aligned}$$

$$\begin{aligned}
 & \left[ \frac{\Lambda}{\theta} \frac{\delta_k^*}{\delta^*} T_h \left\{ -g'' + \frac{\frac{(\gamma-1)M_e^2}{2}}{H \left( 1 + \frac{\gamma-1}{2} M_e^2 \right)} \left[ \frac{T}{T_h} - 1 \right] \left[ \theta^2 \left( 1 - \frac{f'}{\Lambda} \right)^2 \right] \right\} \right] \\
 & = \left\{ Q(\eta - f) + \frac{\lambda \eta^2}{2} (P + 2\delta_x^*) - \delta_{f_x}^* \right\} g'' - (\Lambda - f') \delta_{g_x}^* = 0 \quad , \quad (E4b)
 \end{aligned}$$

$$q = \frac{2(1 + \frac{\gamma-1}{2} M_e^2) (1 - Hg')}{1 + \sqrt{1 + \frac{\gamma-1}{2} M_e^2 (1 - f'/\Lambda)^2} (1 + \frac{\gamma-1}{2} M_e^2) (1 - Hg')} , \quad (E4c)$$

where primes indicate differentiation with respect to  $\eta$  .



# REFERENCES

- [1] Clauser, F., Turbulent boundary layers in adverse pressure gradients, Jour. of Aero. Sci., XXI, 91-108, (1954).
- [2] Clauser, F., The turbulent boundary layer, Advances in Applied Mechanics, Vol. IV, Academic Press, New York, (1956).
- [3] Mellor, G. L. and Gibson, D. M., Equilibrium turbulent boundary layers, Jour. of Fluid Mech., XXIV, 225-253, (1966).
- [4] Mellor, G. L., The effect of pressure gradients on turbulent flow near a smooth wall, Jour. of Fluid Mech., XXIV, 255-274, (1966).
- [5] Mellor, G. L., Turbulent boundary layers with arbitrary pressure gradients and divergent or convergent cross flows, AIAA Journal, Vol. 5, 1570-1579, (1967).
- [6] Prandtl, L., Ueber die ausgebildete Turbulenz, ZAMM 5, 136, (1925) and Proc. Second Int. Congress Appl. Mech., Zurich, (1926).
- [7] Laufer, J., The structure of turbulence in fully developed pipe flow, NACA Report 1174, (1954).
- [8] Van Dyke, M., Perturbation Methods in Fluid Mechanics, Academic Press, New York, (1964).
- [9] Bradshaw, P., Ferriss, D. H. and Atwell, N. P., Calculation of boundary-layer development using the turbulent energy equation, National Physical Laboratory, Aerodynamics Division, Report 1182, (1966).
- [10] Van Driest, E. R., On turbulent flow near a wall, J. Aero. Sci., XXIII, 1007-1011, (1956)
- [11] Townsend, A. A., The Structure of the Turbulent Shear Flow. Cambridge University Press, (1956).
- [12] Millikan, C. B. A., A critical discussion of turbulent flows in channels and circular tubes, Proc. Fifth Int. Congress Appl. Mech., 386-392, (1939).

- [13] Smith, A. M. O. and Clutter, D. W., A general method for solving the compressible laminar boundary layer equations, Douglas Aircraft Division Paper 1699, (1963).
- [14] Coles, D. E., Measurements in the boundary layer on a smooth flat plate in supersonic flow, III. Measurements in a flat-plate boundary layer at the Jet Propulsion Laboratory, Jet Propulsion Laboratory, California Institute of Technology, Pasadena, Calif., Report 20 - 71, (1953).
- [15] Nothwang, G. J., An evaluation of four experimental methods of measuring mean properties of a supersonic turbulent boundary layer, NACA TN 3721, (1956).
- [16] Moore, D. R. and Harkness, J., Experimental investigation of the compressible turbulent boundary layer at very high Reynolds numbers, Ling-Temco-Vought, Research Center Report O-7100/4R-9, (1964).
- [17] Chapman, D. R. and Kester, R. H., Measurements of turbulent skin friction on cylinders in axial flow at subsonic and supersonic velocities, J. Aero. Sci., XX, N. 7, 441-448, (1953).
- [18] Lobb, R. K., Winkler, E. M. and Persh, J., Experimental investigation of turbulent boundary layers in hypersonic flow, Jour. of the Aero. Sci., XXII, 1-9, (1955).
- [19] Dhawan, S., Direct measurements of skin friction, NACA Report 1121, (1953).
- [20] Kuethe, A. M., Some features of boundary layers and transition to turbulent flow, Jour. of Aero. Sci., XXIII, 444-452, (1956).
- [21] Monaghan, R. J. and Johnson, J. E., The measurement of heat transfer and skin friction at supersonic speeds, Aeronautical Research Council C. P. 64, (1952).
- [22] Michel, Roger, Resultats sur la couche limite turbulente aux grandes vitesses, Office National d'Etudes et de Recherches Aéronautiques Mémo Technique 22, (1961).
- [23] Winter, K. G., Smith, K. G. and Rotta, J. C., Turbulent boundary-layer studies on a waisted body of revolution in subsonic and supersonic flow, AGARDograph 97, 933-962, (1965).

- [24] Eskinazi, S. and Yeh, H., An investigation on fully developed turbulent flows in a curved channel, J. Aero. Sci., XXIII, 23-34, Jan. (1956).
- [25] McLafferty, G. H. and Barber, R. E., The effect of adverse pressure gradients on the characteristics of turbulent boundary layers in supersonic streams, J. Aero. Sci., XXIX, 1-10, (1962).
- [26] Rotta, J. C., On the effects of streamwise wall curvature on compressible turbulent boundary layers, Aerodynamische Versuchsanstalt, Gottingen, Report 66A44, (1966).
- [27] Danberg, J. E., Characteristics of the turbulent boundary layer with heat and mass transfer at  $M=6.7$ , U. S. Naval Ord. Lab. Rept. 64-69, (1964).
- [28] Reynolds, W. C., Kays, W. M. and Kline, S. J., Heat transfer in the turbulent incompressible boundary layer; I - Constant wall temperature, NASA MEMO 12-1-58W, (1958).
- [29] Moretti, P. M. and Kays, W. M., Heat transfer to a turbulent boundary layer with varying free-stream velocity and varying surface temperature - an experimental study, Int. J. Heat Mass Transfer, VIII, 1187-1202, (1965).
- [30] Kistler, A. L., Fluctuation measurements in a supersonic turbulent boundary layer, The Physics of Fluids, II, 290-296, (1959).
- [31] Kovasznay, L. S. G., Turbulence in supersonic flow, Jour. of Aero. Sci., XX, 657-675, (1953).
- [32] Rotta, J. C., Turbulent Boundary Layers in Incompressible Flow, Pergamon Press, Oxford. Reprinted from Progress in Aeronautical Sciences, Vol. 2, (1962).
- [33] Lin, C. C. and Shen, S. F., A similarity theory for turbulent boundary layer over a flat plate in compressible flow, NACA Tech. Note 2542, (1951).
- [34] Squire, H. B., Reconsideration of the theory of free turbulence, Phil. Mag. XXXIX, 1-14, (1948).
- [35] Reichardt, H., Vollständige Darstellung der turbulenten Geschwindigkeitsverteilung in glatten Leitungen, Z. Angew. Math. Mech., XXXI, 208-219, (1951).

- [36] Hama, F. R., On the velocity distribution in the laminar sublayer and transition region in turbulent shear flows, J. Aero. Sci., XX, 648-649, (1953).
- [37] von Karman, Th., Mechanische Aehnlichkeit und Turbulenz, Nachr. Ges. Wiss. Gottingen, Math. Phys. Kl., 58-68. NACA TM 611, (1930).
- [38] Stratford, B. S., An experimental flow with zero skin friction throughout its region of pressure rise, Jour. of Fluid Mech., V, 17-35, (1959).
- [39] Bjorgum, O., On the steady turbulent flow along an infinitely long smooth and plane wall, Naturw. rekke, No. 7, Univ. Bergen, Arbok, (1951).
- [40] Deissler, R. G., Analysis of turbulent heat transfer, mass transfer, and friction in smooth tubes at high Prandtl and Schmidt numbers, NACA Rept. 1210, 69-82, (1955).
- [41] Loitsianskii, L. G., The hypothesis of localness in the turbulent motion of a viscous fluid, Prikl. Mat. Mekh., XXII, 560-611. English translation J. Appl. Math. Mech., (1958).
- [42] Maise, G. and McDonald, H., Mixing length and kinematic eddy viscosity in a compressible boundary layer, United Aircraft Research Laboratories Report E211557 - 1, (1966).
- [43] Zakkay, V. and Fox, H., An experimental and theoretical investigation of the turbulent far wake, AIAA Journal, V, 568-574, (1967).
- [44] Hildebrand, F. B., Advanced Calculus for Engineers, Prentice Hall Inc., New York, (1949).
- [45] Young, A. D., The equations of motion and energy and the velocity profile of a turbulent boundary layer in a compressible fluid, College of Aeronautics Report No. 42, Cranfield.
- [46] Morkovin, M. V., Effects of compressibility on turbulent flows, Collogue International sur "La Mecanique de la turbulence", Marseille, 1961.

# ANALYSIS OF SOME SIMPLIFIED MODELS OF TURBULENCE

By Robert G. Deissler

NASA Lewis Research Center  
Cleveland, Ohio

## SUMMARY

The derivation of multipoint correlation and spectral equations for turbulent flow is reviewed, and the physical significance of the various terms in the equations is discussed. Because of the nonlinearity of the Navier-Stokes equations the system of correlation or spectral equations is indeterminate. In order to obtain a solution which illustrates some of the turbulent processes, the system of equations is closed by assuming that the turbulence is moderately weak. The solution assumes homogeneous turbulence with no mean velocity gradients and includes the transfer of turbulent energy between eddy sizes and the dissipation of energy. To illustrate the production of turbulent energy from a mean flow field, the analysis is extended to include a uniform mean velocity gradient. Although the energy transfer between wave numbers due to triple correlations is neglected in this case, an energy transfer associated with the mean velocity gradient occurs. The analysis is carried out for an incompressible fluid, but it can be shown that the same equations apply when mean property gradients are present, provided the gradients are not too large.

## DISCUSSION

In this paper we will be concerned with the analysis of turbulence itself, rather than with compressible or incompressible turbulent boundary layers. A turbulent boundary layer, even when it is of the simplest type, is already exceedingly complicated when we try to analyze it from a fundamental standpoint, that is, by starting with the Navier-Stokes equations. Such an analysis appears to be impracticable to carry out by the analytical and computational tools presently available.

In an attempt to gain some insight into the processes occurring in turbulence and in turbulent boundary layers, we therefore consider some simplified models for which solutions can be obtained. For convenience, the fluid will be considered as incompressible; later we will indicate conditions under which the results are applicable to compressible flows. Some of the processes to be considered are the transfer of energy between eddies of various sizes, dissipation, and production of turbulent energy by mean velocity gradients.

In order to consider the important processes of transfer of turbulent energy between wave numbers or eddy sizes, and turbulent dissipation, we first consider homogeneous turbulence without mean velocity gradients. Such a turbulence will decay with time since no energy is added to the system, and so we must consider

an initial value problem. The turbulence must be generated initially by some means, as by flow through a grid.

We start the analysis by writing the Navier-Stokes equations at two arbitrary points  $P$  and  $P'$  in the turbulent fluid. (See fig. 1. Symbols are defined in the Appendix. A repeated subscript in a term indicates a summation.) Then we multiply the equation at point  $P$  through by a velocity component  $P'$ , and that at  $P'$  by a velocity component at  $P$ , add the equations, take average values, and finally arrive at the equation involving correlations between quantities at the points  $P$  and  $P'$  shown at the bottom of figure 1 (ref. 1). Besides velocity-velocity correlations, the equation contains pressure-velocity correlations and triple-velocity correlations. The equation can be converted to spectral form by taking its Fourier transform, as shown at the top of figure 2. Note that this operation also converts the partial differential equation to an ordinary one. The various terms in the equation can be interpreted by multiplying the equation through by a wave number band of width  $dk$  and referring to the sketch in figure 2.  $E$  is the energy spectrum function and gives contributions from various eddy sizes to the total turbulent energy. The area under the spectrum curve is thus equal to the total turbulent energy  $\overline{u_i u_i}/2$ . The first term in the spectral equation represents the rate of change of turbulent energy in the cross-hatched wave number band. The next term  $W dk$  represents the net rate of transfer of energy into the wavenumber band by nonlinear effects; that is, by the triple correlation terms in figure 1. Finally, the last term  $2\nu k^2 E dk$  represents the rate at which turbulent energy is dissipated within the wave number band by viscous action.

Unfortunately the spectral equation contains two unknowns,  $E$  and  $W$ , so that we cannot in general obtain a solution without more information. That is a consequence of the nonlinearity of the original Navier-Stokes equations. However, if the turbulence is sufficiently weak, the inertia or transfer term  $W$  will be negligible, and we can obtain, subject to particular initial conditions, the simple exponential solution for the energy spectrum shown at the bottom of figure 2 (ref. 1).  $J_0$  and  $t_0$  are constants that depend on initial conditions. In this case the only turbulence process present is viscous dissipation.

Unless the turbulence level is very low, as in the final period of decay, the inertia or transfer effects will not be negligible ( $W \neq 0$ ); thus, we would like to be able to take them into account in some way. A large number of proposals for calculating the transfer function  $W$  have been given, including those of Heisenberg (ref. 2), Kovasznay (ref. 3), and Kraichnan (ref. 4). There are, in fact, almost as many proposals for the transfer function as there have been workers in turbulence. For our purposes it will be sufficient to consider a simple deductive approach which is essentially a perturbation on the solution for the final period of decay (refs. 5 and 6).

In carrying out the analysis we now consider, in addition to the two-point correlations of figure 1, three and four-point correlations. Thus, we write the Navier-Stokes equations at three and four arbitrary points in the turbulent fluid, as in figure 3. We can then construct three-point correlation equations involving triple and quadruple correlations, and four-point equations involving quadruple and quintuple correlations, as shown in the figure (refs. 5 and 6).

However, there are still more unknowns than there are equations, again as a result of the nonlinearity of the Navier-Stokes equations. To make the system of equations determinate, we use an operation similar to that used for the final period, but instead of assuming that the turbulence is weak enough to neglect the inertia term in the two-point equation, we assume only that it is weak enough to neglect the inertia term in the highest order equation considered; in this case the four-point equation (refs. 5 and 6). Thus, neglecting the quintuple correlations in the four-point equation gives a determinate set of equations that should be applicable at times somewhat before the final period.

The resulting dimensionless energy spectra are plotted for various dimensionless times in figure 4. Plotted by using the dimensionless or similarity variables shown (with time included in those variables), the curve for the final period, shown dot dashed, does not change with time. Thus, the curves show how the spectrum changes shape with time and approaches that for the final period. For small time the inertia or transfer terms transfer energy into the high wave number or small eddy region and cause the slopes on the high wave number sides of the spectra to be less steep than they are at larger time, when the spectrum assumes a more or less symmetrical shape. Thus, the function of the inertia terms in the equations is to excite the higher wave number or small eddy regions of the spectrum by transferring energy into those regions. If it were not for inertia effects, those regions of the spectra would be absent, as they are in the final period of decay.

Although the energy transfer by triple correlations, has, of necessity, been discussed for a simplified case of homogeneous turbulence without mean gradients, the same process will occur in turbulent boundary layers, including compressible turbulent boundary layers.

Turning now to a process which is more commonly associated with turbulent boundary layers than is energy transfer between wave numbers, we consider the important process of the production of turbulence by mean velocity gradients. In this case, in order to consider a solvable problem, we use for our model a homogeneous turbulent field with a uniform mean shearing velocity gradient. Since we have already considered the energy transfer process, the turbulence is, in this case, considered weak enough to neglect triple correlation terms. Thus, we need only consider a two-point correlation equation. The analysis is similar to that just described, except that we break the velocity up into mean and fluctuating components (ref. 7).

The resulting equation for the energy spectrum is shown in figure 5. As in the equation at the top of figure 2, the first term gives the rate of change of the energy spectrum function  $E$  at wave number  $\kappa$ . The next term is proportional to the mean shearing velocity gradient, and  $P$  in that term is proportional to a spectral component of the turbulent shear stress. That term is thus interpreted as a production term by which energy is produced at wave number  $\kappa$  by work done by the velocity gradient on a spectral component of the turbulent shear stress.

The third term is also proportional to the mean velocity gradient, but we interpret it as a transfer term rather than as a production term. That is

because if we integrate the term over  $\kappa$  from 0 to  $\infty$ , we get zero as a result (ref. 7). Thus, the term gives zero contribution to the rate of change of the total turbulent energy, but it can transfer energy between wave numbers. Thus, although we neglected triple correlations, we still get an energy transfer which appears to be similar to that produced by triple correlations. The difference between the two cases is that, whereas in the case of triple correlations, the transfer is produced by the nonlinear action of the turbulence on itself, in the present case it is due to the external action of the mean velocity gradient on the turbulence. However, the results in both cases are similar, as shown in figure 6. Since the dimensionless transfer term is primarily negative at low wave numbers and positive at higher ones (net area = 0), the energy transfer is mostly from small to large wave numbers, as is the case for energy transfer by triple correlations. Finally, the last term in the spectral equation in figure 5 is again the dissipation term.

Plots of the energy spectrum, production term, and dissipation term are shown (normalized to the same height) in figure 7. From these we can summarize the history of the turbulent energy as follows: The energy comes into the turbulent field from the mean velocity field mainly through the large eddies. This energy is then transferred from the big eddy region to the small eddy region by the transfer term just discussed. Physically, this transfer might be thought of as being produced by the stretching of turbulent vortex filaments by the mean velocity gradient. Finally, the energy is dissipated in the small eddy region by viscous action. It is physically reasonable that the dissipation should occur mainly in the small eddy region since the shear stress should be greater between the small eddies than between the larger ones. The energy resides in a region between the production and dissipation regions, as shown by the plot of the energy spectrum.

By integrating under the calculated energy spectrum curves we can obtain a plot of the total turbulent energy as a function of time and velocity gradient. Such a plot is shown in dimensionless form in figure 8. Dimensionless turbulent energy is plotted against dimensionless time for various values of dimensionless velocity gradient. As velocity gradient increases, the rate of decrease of the turbulent energy with time decreases because of energy fed into the turbulent field by the mean velocity gradient. Although the changes produced by the velocity gradient are considerable (note that the vertical scale is logarithmic), the turbulence at all times decays. For these curves the initial energy spectrum function  $E$  is assumed to be isotropic and proportional to  $\kappa^4$  so that the total initial energy is infinite. In some recent calculations, we used that initial condition for  $E$  multiplied by a negative exponential in  $\kappa^2$  so that the total initial turbulent energy is finite. In that case the energy increased in some time intervals; thus, more energy was fed into the turbulent field than was dissipated. Still no steady-state solution was obtained for large times. It may be that in order to obtain a steady-state solution, triple correlations or inhomogeneities in the turbulent field will have to be considered.

The curves in figure 8 are plotted with three dimensionless groups in order to show the effects of time and mean velocity gradient separately. The curves



are, however, similar and can be compressed into one by using the proper similarity parameters. The result is shown in figure 9, where  $\frac{v^{5/2}(t-t_0)^{5/2} \overline{u_1 u_1}}{2J_0}$  is plotted against  $(t - t_0) \frac{dU}{dy}$ .

These results have been obtained by using the incompressible, constant property Navier-Stokes equations. However, if the variation of properties over a correlation or mixing length is small, and if the density fluctuations are small (small Mach number of the eddies), then the same correlation equations will apply to a compressible, variable property flow (ref. 8). That will be the case, of course, if the property gradients are not too large. Thus, to a first approximation, figure 9 will apply to a compressible, variable property flow. It is known experimentally and analytically that for a compressible turbulent boundary layer with frictional heating and a given free-stream temperature, the shear stress decreases as the Mach number, or the frictional heating in the boundary layer, increases (ref. 9). It is of interest that the same trend occurs according to figure 9. For frictional heating, as opposed to no frictional heating, the temperature, and thus the kinematic viscosity, will increase. For a given time and velocity gradient, the turbulent energy, and thus the turbulent shear stress, will be decreased by frictional heating so that the parameter in the ordinate remains constant.

#### CLOSING REMARKS

We have considered a number of turbulent processes, including turbulent dissipation, transfer of energy between wave numbers by triple correlations, production of turbulent energy by mean shear, and transfer of energy between wave numbers by mean shear. Although these processes were investigated for simplified models for which solutions could be obtained, the same processes will occur in turbulent boundary layers, including compressible turbulent boundary layers.

In addition to the processes considered here, several others should be mentioned. They are the transfer of energy between directional components by pressure fluctuations, and the spatial diffusion of turbulence by inhomogeneities in the turbulent field. These have been considered for weak turbulence in reference 7. However, for stronger turbulence there can be directional transfer of turbulence due to the simultaneous presence of pressure fluctuations and triple correlations, and spatial diffusion due to the simultaneous presence of triple correlations and inhomogeneities in the turbulent field. These conditions may be important, although at least in the case of spacial diffusion, experiments such as those by Laufer (ref. 10) indicate that diffusion is important only in the region at a distance from the wall, where the velocity gradients are small, and is much smaller in the possibly more important region closer to the wall where the velocity gradients are large.

It is hoped that this discussion will give some insight into the processes occurring in turbulence and in turbulent boundary layers.

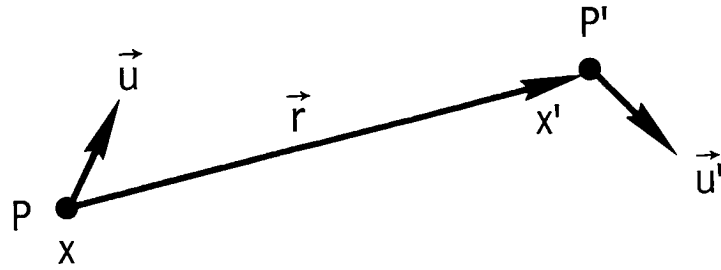
# APPENDIX

## SYMBOLS

$E$	energy spectrum function
$E^*$	dimensionless energy spectrum function, $v^2(t - t_0)^2 E/J_0$
$J_0$	constant depending on initial conditions
$p$	pressure
$P$	function in production term, also a point $P$
$r_1, r_l, r_m$	components of vector separating points $P$ and $P'$
$t$	time
$t_0$	initial time
$t^*$	dimensionless time, $v^{11/9} J_0^{2/9} (t - t_0) / \beta_0^{2/9}$
$T$	function in velocity-gradient transfer term
$T^*$	dimensionless velocity-gradient transfer term, $v^3(t - t_0)^3 T/J_0$
$u_i, u_j, u_k$	components of fluctuating velocity
$U_1$	mean velocity
$W$	transfer term due to triple correlations
$x_i$	position coordinate
$\beta_0$	constant depending on initial conditions
$\kappa$	wave number
$\kappa^*$	dimensionless wave number
$\nu$	kinematic viscosity
$\rho$	density
$'$	at point $P'$
$\overline{\quad}$	overbar on averaged quantities

## REFERENCES

1. Batchelor, George K.: The Theory of Homogeneous Turbulence. Cambridge Univ. Press, 1953.
2. Heisenberg, W.: Zur Statistischen Theorie der Turbulenz. Zeitschrift für Physik, vol. 124, 1948, pp. 628-657.
3. Kovasznay, Leslie S. G.: Spectrum of Locally Isotropic Turbulence. J. Aeronaut. Sci., vol. 15, no. 12, Dec. 1948, pp. 745-753.
4. Kraichnan, Robert H.: Lagrangian-History Closure Approximation for Turbulence. Phys. Fluids, vol. 8, no. 4, Apr. 1965, pp. 575-598.
5. Deissler, Robert G.: On the Decay of Homogeneous Turbulence Before the Final Period. Phys. Fluids, vol. 1, no. 2, Mar.-Apr. 1958, pp. 111-121.
6. Deissler, Robert G.: A Theory of Decaying Homogeneous Turbulence. Phys. Fluids, vol. 3, no. 2, Mar.-Apr. 1960, pp. 176-187.
7. Deissler, Robert G.: Effects of Inhomogeneity and of Shear Flow in Weak Turbulent Fields. Phys. Fluids, vol. 4, no. 10, Oct. 1961, pp. 1187-1198.
8. Deissler, Robert G.: Effect of Uniform Longitudinal Strain Rate on Weak Homogeneous Turbulence in a Compressible Flow. NASA TN D-2800, 1965.
9. Deissler, R. G.; and Loeffler, A. L., Jr.: Analysis of Turbulent Flow and Heat Transfer on a Flat Plate at High Mach Numbers with Variable Fluid Properties. NASA TR R-17, 1959. (Supersedes NACA TN 4262.)
10. Laufer, John: The Structure of Turbulence in Fully Developed Pipe Flow. NACA Rep. 1174, 1954. (Supersedes NACA TN 2954.)



$$\frac{\partial u_i}{\partial t} + \frac{\partial (u_i u_k)}{\partial x_k} = -\frac{1}{\rho} \frac{\partial p}{\partial x_i} + \nu \frac{\partial^2 u_i}{\partial x_k \partial x_k} \Bigg| u'_j$$

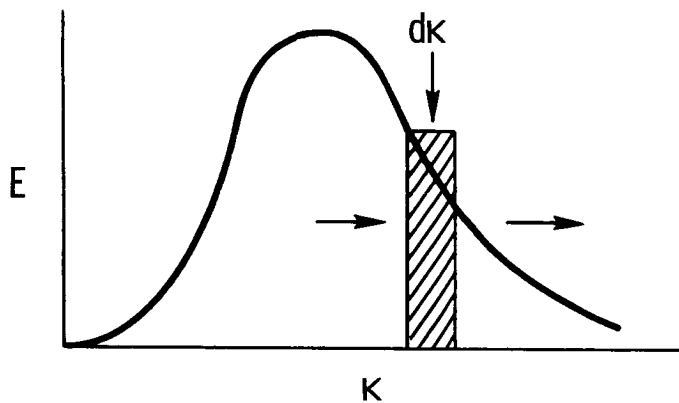
$$\frac{\partial u'_j}{\partial t} + \frac{\partial (u'_j u'_k)}{\partial x'_k} = -\frac{1}{\rho} \frac{\partial p'}{\partial x'_j} + \nu \frac{\partial^2 u'_j}{\partial x'_k \partial x'_k} \Bigg| u_i$$

$$\frac{\partial \overline{u_i u'_j}}{\partial t} + \frac{\partial}{\partial r_k} (\overline{u_i u'_j u'_k} - \overline{u_i} \overline{u'_j u'_k}) = -\frac{1}{\rho} \left( \frac{\partial \overline{p' u_i}}{\partial r_j} - \frac{\partial \overline{p u'_j}}{\partial r_i} \right) + 2\nu \frac{\partial^2 \overline{u_i u'_j}}{\partial r_k \partial r_k}$$

Figure 1. - Two-point correlation equation.

$$\frac{dE}{dt} = W - 2\nu k^2 E$$

$$\frac{d(E dk)}{dt} = W dk - 2\nu k^2 E dk$$

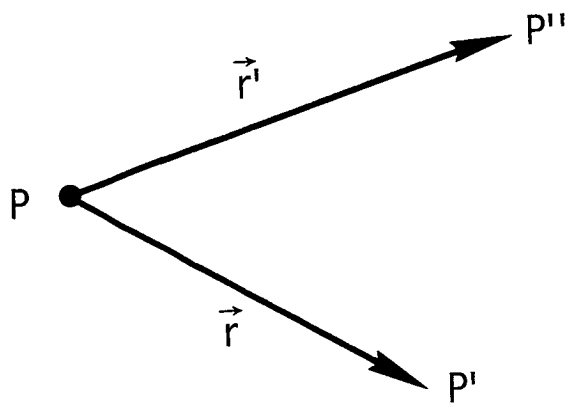


$$\int_0^\infty E dk = \frac{\overline{u_i u_i}}{2} = \frac{1}{2} \overline{u_1^2} + \frac{1}{2} \overline{u_2^2} + \frac{1}{2} \overline{u_3^2}$$

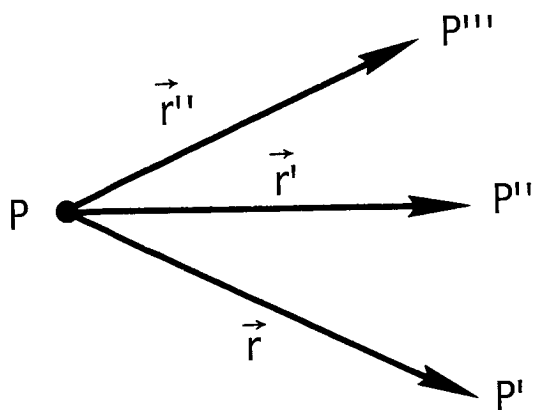
FOR WEAK TURBULENCE,

$$E = J_0 k^4 \text{EXP}[-2\nu k^2(t - t_0)]$$

Figure 2. - Spectral equations and energy spectrum.



$$\frac{\partial}{\partial t} \overline{u_i u_j' u_k''} = \frac{\partial}{\partial r_l} \overline{u_i u_j' u_k'' u_l} + \dots$$



$$\frac{\partial}{\partial t} \overline{u_i u_j' u_k'' u_l'''} = \frac{\partial}{\partial r_m} \overline{u_i u_m u_j' u_k'' u_l'''} + \dots$$

Figure 3. - Three and four point correlation equations.

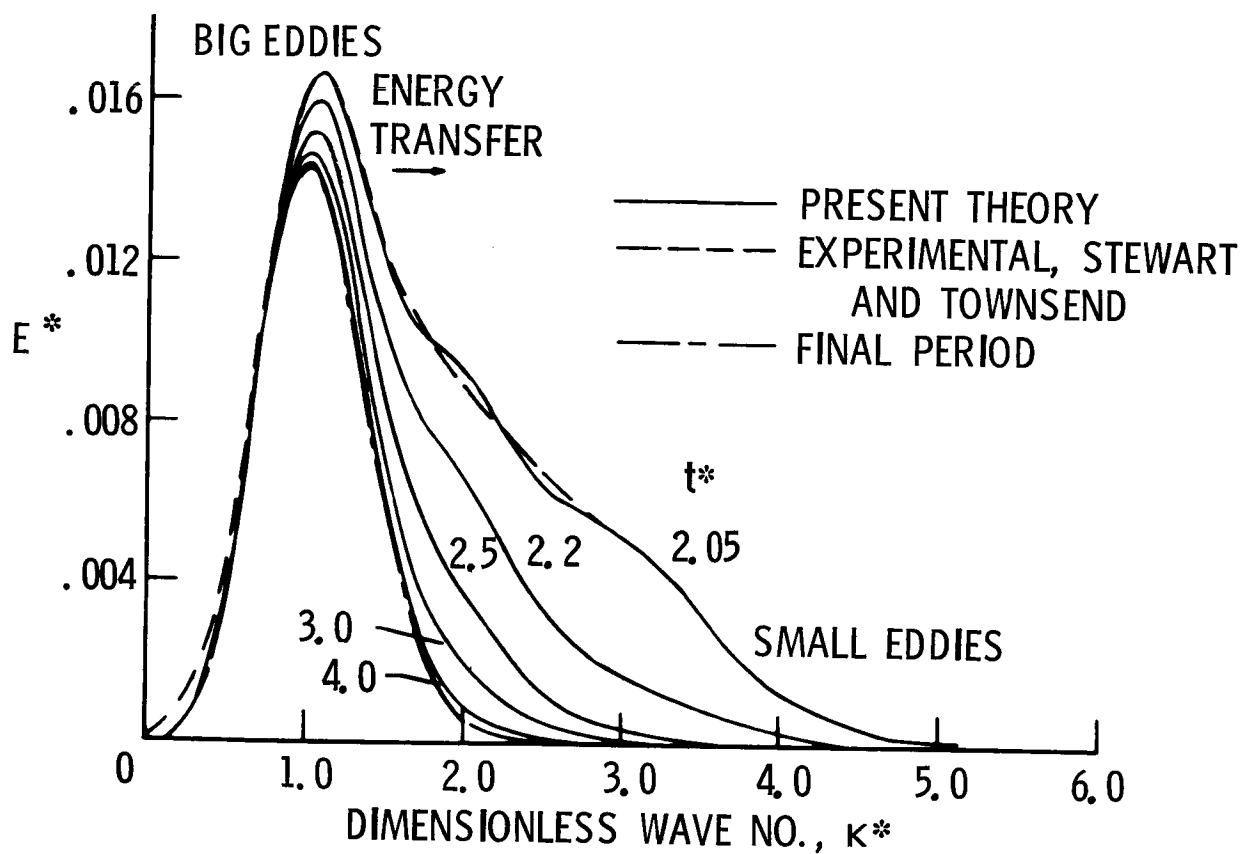


Figure 4. - Variation of dimensionless energy spectrum with time.

$$\frac{\partial E}{\partial t} = P \frac{\partial U_1}{\partial x_2} + T \frac{\partial U_1}{\partial x_2} - 2\nu \kappa^2 E$$

$$\int_0^\infty T(\kappa) d\kappa = 0$$

Figure 5. - Spectral equation for homogeneous turbulence with uniform transverse velocity gradient.



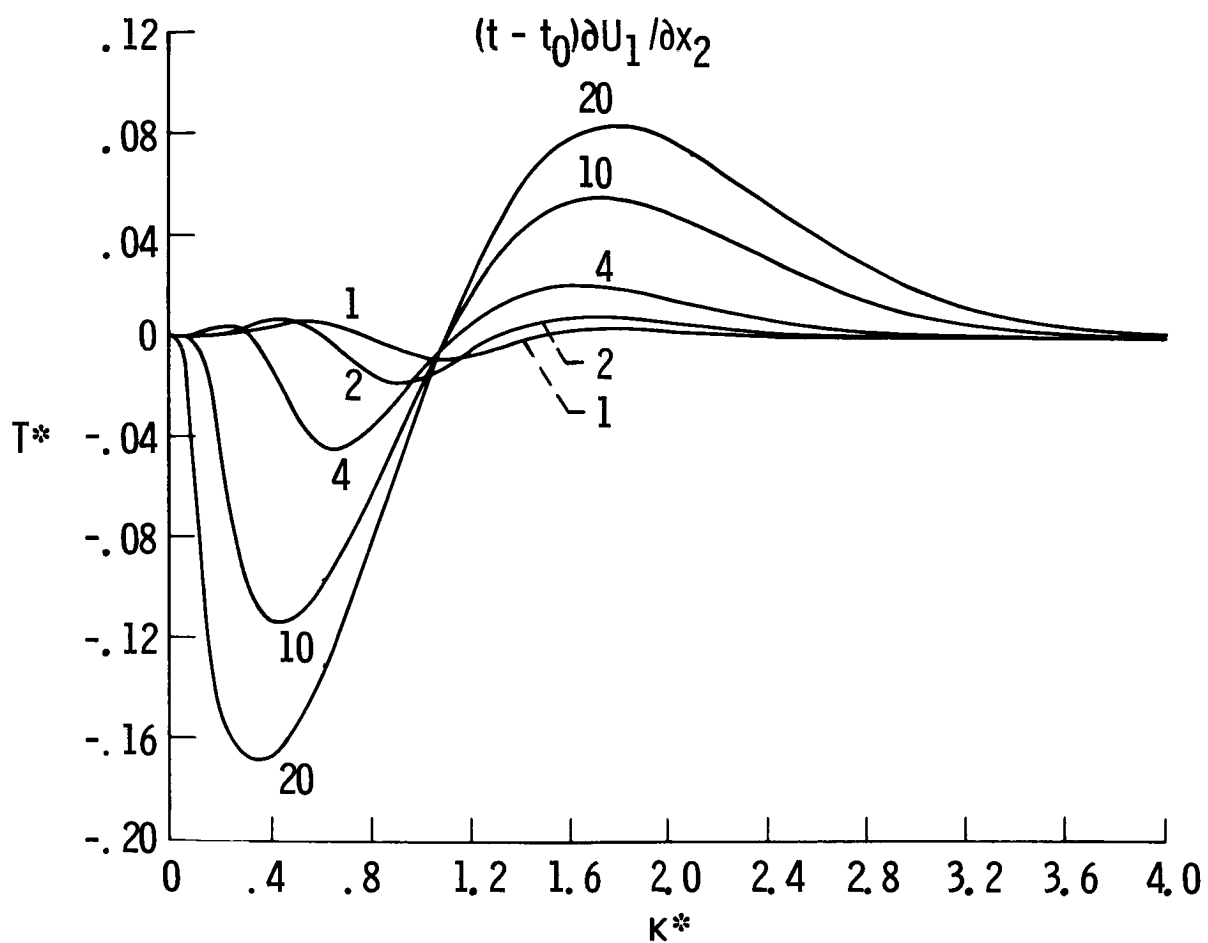


Figure 6. - Spectra of transfer term due to mean velocity gradient.

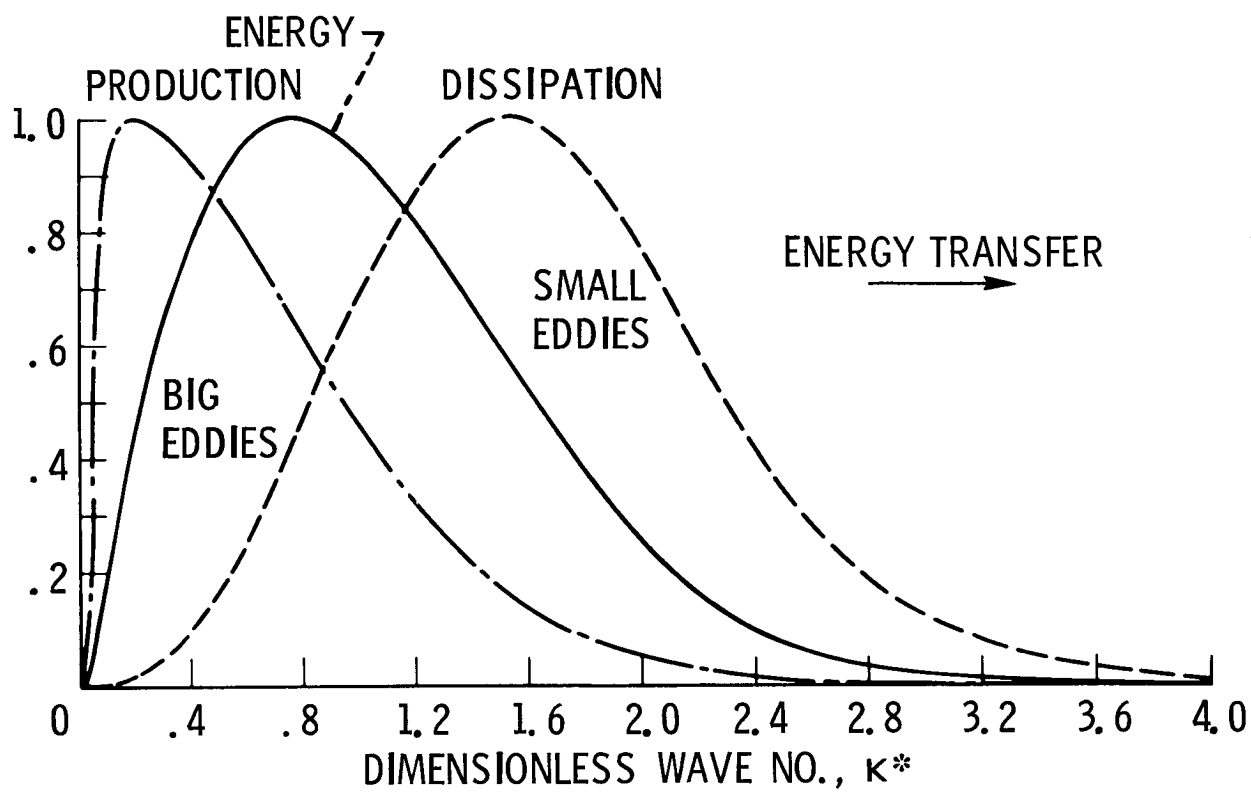


Figure 7. - Production, energy-containing, and dissipation regions.

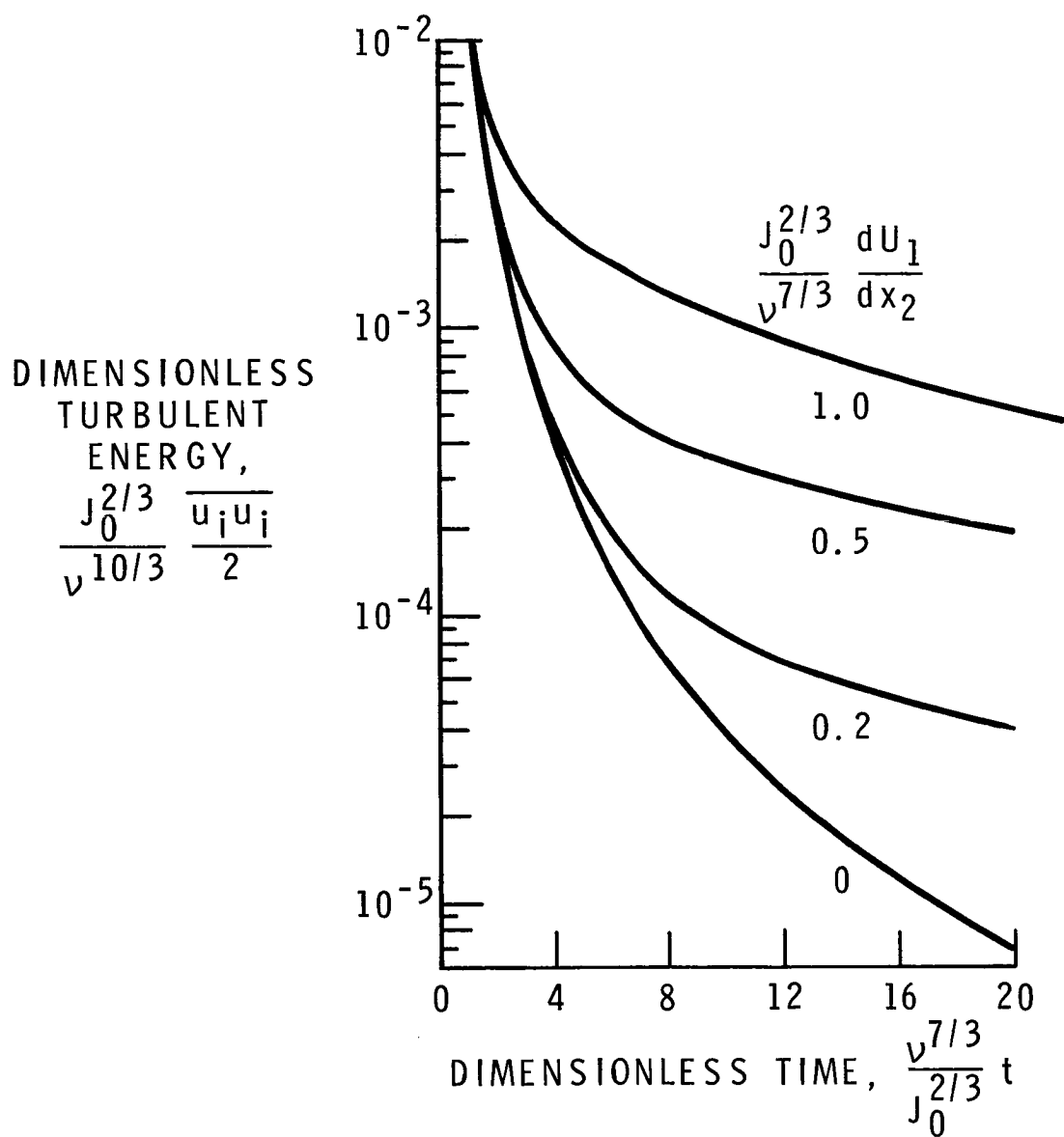


Figure 8. - Effect of uniform shear on decay of turbulent energy.

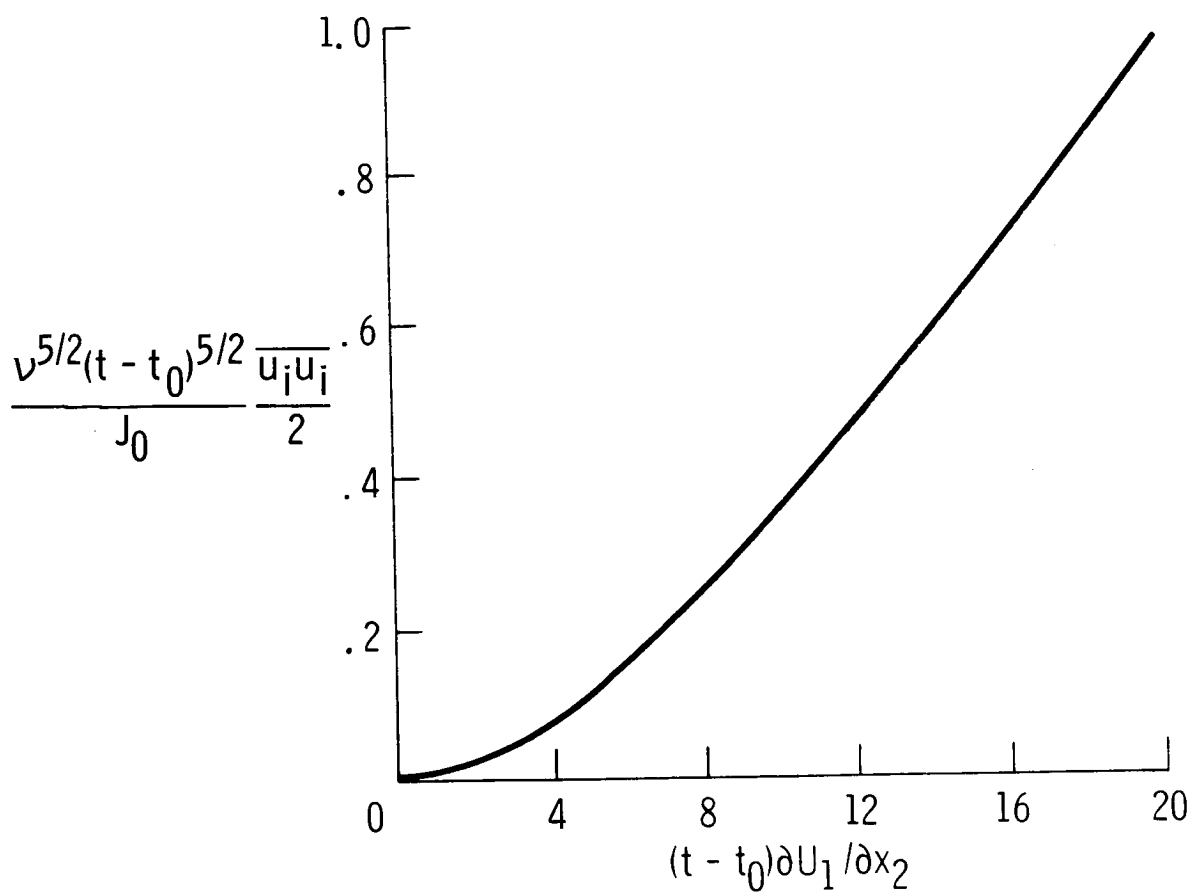


Figure 9. - Effect of uniform shear on turbulent energy. Curves from Figure 8 collapsed into one.

ON THE APPLICABILITY OF TRANSFORMATION THEORY TO VARIABLE  
PROPERTY TURBULENT BOUNDARY LAYERS WITH PRESSURE  
GRADIENT AND HEAT AND MASS TRANSFER\*

By Constantino Economos\*\*

General Applied Science Laboratories, Inc.

SUMMARY

Various properties of the Coles' compressibility transformation when modified and extended to include turbulent boundary layer flows with mass transfer and pressure gradient are examined. First the formulation for the mass transfer case in the absence of pressure gradient is developed and its applicability demonstrated by comparison with experimental data involving both homogeneous and heterogeneous injection as well as chemical reaction. This modified form of the transformation is then applied to the impermeable case and is shown to differ significantly from the earlier Baronti-Libby formulation. In particular, improved agreement with experimental skin friction data obtained under cold wall conditions is demonstrated. The implications of this result with regard to the more general case involving simultaneous mass transfer and pressure gradient are then discussed. In addition to these considerations the inability of the transformation to preserve the "wake component" of the velocity distribution is examined. An empirical method is proposed which provides good correlation of the transformed velocity profiles throughout the viscous layer and more realistic prediction for the streamwise variation of skin friction. Finally, the applicability of this technique to three-dimensional boundary layers is examined. In particular, the appropriate form of the transformation for flow over a swept cylinder is developed.

---

\* This work was partially supported by NASA-Langley Research Center under Contract No. NAS1-8424.

\*\* Supervisor, Thermochemistry and Viscous Flow Section

## INTRODUCTION

For a number of years the Coles compressibility transformation (Ref. 1) has been utilized by many investigators (Refs. 2,3,4,5) in studies related to variable property (VP) turbulent boundary layer flows on impermeable surfaces and at constant pressure. Exploitation of this technique for more complex flow configurations involving pressure gradient and/or mass transfer, on the other hand, has been quite limited. Furthermore, as will be indicated in the subsequent discussion, among those studies which have treated this more general problem (Refs. 6,7,8,9) fundamental differences regarding the properties of the transformation arise.

In the present paper a unified description is formulated by considering, at the outset, the most general problem, i.e., one in which mass transfer and pressure gradient occur simultaneously. The special cases wherein one or both of these disturbing influences vanish are then derived. The properties of the resulting formulations are compared with those derived by a less general approach, and the significant differences which arise are delineated and discussed qualitatively.

In order to provide a more quantitative indication of these effects, various forms of the transformation are applied to a series of zero pressure gradient flow configurations. These include:

- (a) zero heat transfer with homogeneous and heterogeneous mass transfer,
- (b) mass transfer with heat transfer and combustion,
- (c) zero mass transfer with and without heat transfer.

In each case a comparison of the various predictions with experimental results is presented. It is found that one form of the transformation is clearly superior to the others. In particular, improved agreement with skin friction data under cold wall conditions is obtained.

Despite this result, detailed analysis of velocity profiles with this modified approach shows no corresponding improvement regarding the distortion of the "wake component" of the transformed velocity distribution. Accordingly, an empirical method is developed which serves to improve correlation of the transformed

velocity profiles in the outer region. It should be emphasized here however, that this procedure does not represent a fundamental change in the transformation but is simply a "curve fit" of the available data. Accordingly, its applicability to flows involving pressure gradient is questionable at the present time.

Insofar as the gradient case is concerned, results of the type described above are not currently available. However, several velocity profiles obtained on curved ramps are analyzed utilizing the earlier formulation of Baronti-Libby (Ref. 2). The results which are obtained, although of a preliminary nature, are encouraging in that good correlation of profiles in the inner region in terms of the law of the wall is obtained. Further work in this area is continuing under the support of NASA Langley Research Center, Contract No. NAS1-8424.

Finally, the applicability of the transformation technique to three-dimensional boundary layer flows is examined. In particular, the appropriate form of the transformation for flow over a swept infinite cylinder is developed and presented.

#### SYMBOLS

$c_f, \bar{c}_f$	local skin friction coefficients
$F, \bar{F}$	non-dimensionalized transpiration rate - $\frac{(\rho v)_w}{(\rho_e u_e)_o}$
$g_1, g_2, g'_1, g'_2$	thermodynamic functions - see Appendix B
$M$	Mach number
$p, \bar{p}$	pressure
$\dot{q}_w$	heat-transfer rate at wall
$R_y, \bar{R}_y$	Reynolds numbers based on normal coordinate
$R_\delta, \bar{R}_\delta$	Reynolds number based on boundary layer thickness
$R_\delta^*, \bar{R}_\delta^*$	Reynolds number based on displacement thickness
$R_\theta, \bar{R}_\theta$	Reynolds number based on momentum thickness
$T$	temperature
$T_t$	total temperature
$u, \bar{u}$	streamwise (or chordwise) velocity component
$\bar{u}^+$	non dimensional velocity - $\bar{u}/\bar{u}_\tau$

$\bar{u}_\tau$	shearing velocity $(\bar{\tau}_w/\bar{\rho})^{1/2}$
$U_e, \bar{U}_e$	external velocity ratio - $u_e/u_{e_o}, \bar{u}_e/\bar{u}_{e_o}$
$v, \bar{v}$	normal velocity component
$w, \bar{w}$	spanwise velocity component
$x, \bar{x}$	streamwise (or chordwise) coordinates
$y, \bar{y}$	normal coordinates
$\bar{y}^+$	transformed normal coordinate $\bar{\rho} \bar{u}_\tau \bar{y} / \bar{\mu}$
$\eta, \xi, \sigma$	scaling parameters of the transformation
$\tilde{\eta}$	$\eta \rho_e / \bar{\rho}$
$\mu, \bar{\mu}$	coefficients of viscosity
$\pi$	Coles wake parameter
$\rho, \bar{\rho}$	densities
$\tilde{\sigma}$	$\sigma \mu_e / \bar{\mu}$
$\tau, \bar{\tau}$	shear stresses (including Reynolds stresses)
$\chi, \bar{\chi}$	Reynolds number based on distance from arbitrary initial station
$\psi, \bar{\psi}$	stream function
$\nu$	kinematic viscosity

#### Subscripts:

BL	value inferred using form II-B
e	local condition external to boundary layer
M	value inferred using form II-D
o	initial value
R	Reference value (direct measurement or Spalding-Chi)
s	conditions at edge of laminar sub-layer
w	conditions at wall
{ }	variables in the variable property flow
{ - }	variables in the constant property flow
( ~ )	normalization with respect to corresponding external value; e.g., $\tilde{u} = u/u_e$
( )'	differentiation with respect to $\bar{\chi}$



## THEORETICAL CONSIDERATIONS\*

### Fundamental Transformation Relations and Correspondence of Boundary Layer Parameters

The describing differential equations for the velocity field of interest here are assumed to be of the form

$$\frac{\partial \rho u}{\partial x} + \frac{\partial \rho v}{\partial y} = 0 \quad (1)$$

$$\rho u \frac{\partial u}{\partial x} + \rho v \frac{\partial u}{\partial y} = \frac{\partial \tau}{\partial y} - \frac{dp}{dx} \quad (2)$$

It can be shown that this system of equations can be transformed identically to the constant property (CP) form:

$$\frac{\partial \bar{u}}{\partial \bar{x}} + \frac{\partial \bar{v}}{\partial \bar{y}} = 0 \quad (3)$$

$$\bar{\rho} \bar{u} \frac{\partial \bar{u}}{\partial \bar{x}} + \bar{\rho} \bar{v} \frac{\partial \bar{u}}{\partial \bar{y}} = \frac{\partial \bar{\tau}}{\partial \bar{y}} - \frac{d\bar{p}}{d\bar{x}} \quad (4)$$

by introduction of the following transformation relations\*\*

$$\frac{d\bar{x}}{dx} = \xi(x) \quad (5)$$

$$\frac{\bar{\rho} d\bar{y}}{\rho dy} = \eta(x) \quad (6)$$

$$\frac{\bar{\psi} - \bar{\psi}_w}{\psi - \psi_w} = \sigma(x) \quad (7)$$

providing that the following correspondences between gross boundary layer parameters are imposed

\* Only a brief outline of the formal development is presented here. For more detailed derivations see Refs. 6 and 8.

\*\*It is noted here that relation (7) represents a modification from the original Coles' stretching. The significance and motivation for this modification is discussed in Appendix A.

$$(\ln \tilde{\sigma})' - (\ln \tilde{\eta})' - (\ln \tilde{U}_e)' + \left( \frac{d \ln \tilde{U}_e}{d \chi} - \frac{d \ln \nu_e / \nu_{e0}}{d \chi} \right) \chi' = 0 \quad (8)$$

$$\frac{dR_\theta}{d\chi} + R_\theta \left( \frac{R_{\delta^*}}{R_\theta} + 2 \right) \frac{d \ln \bar{U}_e}{d \chi} + R_\theta \frac{d \ln \rho_e / \rho_{e0}}{d \chi} = \frac{c_f}{2} + \frac{F}{U_e} \frac{\rho_{e0}}{\rho_e} \quad (9)$$

$$(R_\theta) + R_\theta \left( \frac{R_{\delta^*}}{R_\theta} + 2 \right) (\ln \bar{U}_e)' = \frac{\bar{c}_f}{2} + \frac{\bar{F}}{\bar{U}_e} \quad (10)$$

$$\frac{u}{u_e} = \frac{\bar{u}}{\bar{u}_e} \equiv \bar{u} \quad (11)$$

$$\frac{c_f}{\bar{c}_f} = \tilde{\sigma} \tilde{\rho}_w \tilde{\mu}_w \quad (12)$$

$$\frac{R_\theta}{R_\theta} = \frac{1}{\tilde{\eta}} \frac{\tilde{\eta}_0}{\tilde{\sigma}_0} \quad (13)$$

$$\frac{R_{\delta^*} - R_\delta}{R_{\delta^*} - R_\delta} = \frac{1}{\tilde{\eta}} \frac{\tilde{\eta}_0}{\tilde{\sigma}_0} \quad (14)$$

$$R_\delta = \frac{1}{\tilde{\eta}} \frac{\tilde{\eta}_0}{\tilde{\sigma}_0} \int_0^{R_\delta} \frac{dR_\theta}{\tilde{\rho}} \quad (15)$$

Here the existence of mass transfer in both flow regimes is manifested by the presence of the terms  $F \equiv \rho_w v_w / \rho_{e0} u_{e0}$  and  $\bar{F} \equiv \bar{\rho} \bar{v}_w / \bar{\rho} u_{e0}$ .

### The CP Solutions

It is obvious that successful exploitation of this transformation approach depends upon the availability of appropriate CP solutions. For purposes of the discussion in this section it is

assumed that such a formulation exists and is of the form\*

$$\tilde{u} = \tilde{u}(R_{\overline{y}}; R_{\overline{\delta}}, \overline{c}_f, \overline{F}, \pi) \quad (16)$$

$$\overline{c}_f = \overline{c}_f(R_{\overline{\delta}}, \overline{F}, \pi) \quad (17)$$

$$R_{\overline{\theta}} = R_{\overline{\theta}}(R_{\overline{\delta}}, \overline{F}, \pi) \quad (18)$$

$$R_{\overline{\delta}^*} = R_{\overline{\delta}^*}(R_{\overline{\delta}}, \overline{F}, \pi) \quad (19)$$

$$R_{\overline{y}_s} = R_{\overline{y}_s}(R_{\overline{\delta}}, \overline{F}, \pi) \quad (20)$$

$$\frac{d\pi}{d\chi} = f(\overline{F}, R_{\overline{\delta}}, \overline{c}_f, \overline{U}_e, \frac{d\overline{U}_e}{d\chi}) \quad (21)$$

Note that an additional parameter  $\pi$  has been introduced in the velocity representation (16) to reflect the dependence of the profiles on the varying external pressure distribution given by  $\overline{U}_e = \overline{U}_e(\chi)$ . Note also that Equation (21) anticipates the possible extension of the arbitrary pressure gradient formulation such as that developed in Refs. 10 or 11, to include the effect of mass transfer.

#### Completion of the System of Working Equations - The Sublayer Hypothesis and the Compatibility Conditions

With regard to the system of Equation (8)-(21) we consider that:

- 1)  $\overline{U}_e, \overline{F}, \rho_e/\rho_{e_0}, \nu_e/\nu_{e_0}$  are prescribed functions of the VP Reynolds number  $\chi$ .
- 2) the initial values of the stretching parameters  $\tilde{\sigma}_0, \tilde{\eta}_0$  can be specified.
- 3) the density (and viscosity) distribution can be prescribed as a function of the local velocity ratio  $\tilde{u}$ ; i.e.,  $\tilde{\rho} = \tilde{\rho}(\tilde{u})$   $\tilde{\mu} = \tilde{\mu}(\tilde{u})$

---

\* Actually very little has been accomplished in the way of developing such a general formulation for the CP case. This situation is compounded by the absence of reliable experimental data at low speeds. It is interesting to note that if the general validity of the transformation technique is ultimately demonstrated, the desire to develop analytical tools which describe the VP behavior may give impetus to extensive work in the low speed area.

Then, examination of this system reveals that a total of 11 equations\* are available for the determination of 14 dependent variables with the CP Reynolds number  $\bar{X}$  considered to be the sole independent variable. Accordingly, three additional equations are required. One is obtained by invoking the sublayer hypothesis which can be written (c.f., Ref. 2 or 6).

$$\tilde{\sigma} = \frac{\tilde{\rho}_s}{\tilde{\mu}_s} \frac{1}{R_{\bar{y}_s}} \int_0^{R_{\bar{y}_s}} \frac{dR_{\bar{y}}}{\tilde{\rho}}$$

In view of the assumptions made above this is an implicit relation of the form

$$\tilde{\sigma} = \tilde{\sigma} (R_{\bar{y}_s}, R_{\bar{\delta}}, \bar{c}_f, \bar{F}, \pi)$$

or in view of Equation (20)

$$\tilde{\sigma} = \tilde{\sigma} (R_{\bar{\delta}}, \bar{c}_f, \bar{F}, \pi)$$

The final two equations are obtained by satisfying the wall compatibility conditions in both flow regimes, i.e., we satisfy the momentum Equations (2) and (4) and their respective  $y$  derivatives at  $y, \bar{y} \rightarrow 0$  taking into account the differentiation rules implied by the transformation and that  $\tau \rightarrow \mu \frac{\partial u}{\partial y}$ ,  $\bar{\tau} \rightarrow \bar{\mu} \frac{\partial u}{\partial \bar{y}}$ , at  $y, \bar{y} \rightarrow 0$ . As a result of this procedure\*\*there are obtained two relations of the form\*\*\*

---

\* Here we have not included Equation (20) nor  $R_{\bar{y}_s}$  as a dependent variable since the latter does not appear within the system at this point.

\*\* This procedure is equivalent to the expansion method utilized by Lewis (Ref. 9) and the relations which are obtained here correspond to the second and third terms of that expansion. The relations which are obtained are not identical however, since in Ref. 9 the expansion is carried out with  $F=\bar{F}=0$ . As a result the final form of the transformation derived therein differs substantially from the one developed here.

\*\*\* See Appendix B for the explicit form of these relations.

$$\bar{F} - \frac{2}{\bar{c}_f} (\ln \bar{U}_e)' = f_1 \left[ F, \frac{d\bar{U}_e}{d\chi} ; \tilde{\rho}_w, \left( \frac{\partial \tilde{\rho}}{\partial \tilde{u}} \right)_w, \left( \frac{\partial^2 \tilde{\rho}}{\partial \tilde{u}^2} \right)_w, \left( \frac{\partial^3 \tilde{\rho}}{\partial \tilde{u}^3} \right)_w, \dots \right] \quad (22)$$

$$\bar{F} \left[ \bar{F} - \frac{2}{\bar{c}_f} (\ln \bar{U}_e)' \right] = f_2 \left[ F, \frac{d\bar{U}_e}{d\chi} ; \tilde{\rho}_w, \left( \frac{\partial \tilde{\rho}}{\partial \tilde{u}} \right)_w, \left( \frac{\partial^2 \tilde{\rho}}{\partial \tilde{u}^2} \right)_w, \dots \right] \quad (23)$$

where the dependence of the right hand side of these relations on the thermodynamic behavior of the VP gas in the vicinity of the wall has been indicated. The properties of this general transformation and in particular, of Equations (22) and (23) are discussed in the next section.

#### COMPARISON OF VARIOUS FORMS OF THE COMPRESSIBILITY TRANSFORMATION

We consider now the possibility of treating the VP case corresponding to an impermeable flat plate with a uniform external pressure field by use of the unified transformation developed in the previous section. We find in this case that Equations (22) and (23) reduce to

$$\bar{F} - \frac{2}{\bar{c}_f} (\ln \bar{U}_e)' = \frac{\bar{c}_f}{2} g'_1 \quad (24)$$

$$\bar{F} \left[ \bar{F} - \frac{2}{\bar{c}_f} (\ln \bar{U}_e)' \right] = \left( \frac{\bar{c}_f}{2} \right)^2 g'_2 \quad (25)$$

where  $g'_1$  and  $g'_2$ , which depend only on the thermodynamic behavior of the gas in the vicinity of the wall, do not vanish identically. It is easy to show that\* for the adiabatic wall case Equations (24) and (25) are singular. On the other hand, for a viscosity temperature dependence of the form  $\tilde{\mu} \sim \tilde{T}$  we find  $g'_1 = g'_2 = 0$  which implies that  $\bar{F} = d\bar{p}/d\chi = 0$ .

It would appear that the special case corresponding to  $\dot{q}_w = F = d\bar{p}/d\chi = 0$  should be treated with  $\bar{F} = d\bar{p}/d\bar{x} = 0$  together with the assumption that  $\tilde{\mu} \sim \tilde{T}$  which is not an unreasonable model. On the other hand, for the heat transfer case a more general formulation is possible and would be of interest in view of some of the

\* See Appendix B for explicit expressions for  $g'_1$  and  $g'_2$ .

quantitative results which will be presented in the next section. However, we will first review briefly a few of the more specialized forms of the transformation which have previously been utilized and indicate how they differ from the present model.

In Reference 2 the case of  $F=dp/dx=0$  was considered and it was tacitly assumed that  $\bar{F}=d\bar{p}/d\bar{x}=0$ . This form has been applied extensively to many cases involving heat transfer (cf., Refs. 2, 3,4). Accordingly, neither compatibility condition is explicitly satisfied by this formulation.

In Reference 8 the problem corresponding to  $dp/dx \neq 0$  has been formulated. In this case it again is assumed that  $\bar{F} = 0$  and the first compatibility condition (i.e., Eq. (22) ) is satisfied to complete the system of describing equations. Thus the second compatibility condition is not satisfied here.

In Reference 6 the problem corresponding to  $F \neq 0$ ,  $dp/dx=0$  is formulated in an analogous way by assuming  $d\bar{p}/d\bar{x} = 0$  and satisfying Equation (22) to complete the system. Again the second compatibility condition is not explicitly satisfied.

The matters discussed in this section have been summarized in Table I.

## COMPARISON OF THEORY WITH EXPERIMENT

### Mass Transfer at Constant Pressure

In Reference 6 the mass transfer case at constant pressure was treated using the form of the transformation listed as IV-D in Table I. The CP solutions utilized were essentially those due to Stevenson (Ref. 12,13) and Crocco Integrals were used to determine energy and or species distributions. This method was extended to a case involving chemical reactions in Reference 14, by utilizing a flame sheet model to describe the chemistry (Ref. 15). Some comparisons of the theoretical predictions with experiment and with earlier prediction techniques are shown in Figure 1. In all cases improved agreement with the data is evident.

## Impermeable Flow at Constant Pressure With and Without Heat Transfer

As indicated in the previous discussion and in Table I, this has been treated extensively utilizing form II-B of the transformation. Here we will compare these results with those obtained utilizing form II-D which follows from IV-D when  $F = 0$ .

To effect this comparison a total of 48 velocity profiles have been analyzed by both methods from the point of view of establishing whether correlation of the inner region by the law of the wall is obtained. These profiles are identified in Table II wherein the skin friction coefficients inferred from the transformed profiles by the two methods have also been listed. Note also that for each case a value of the incompressible blowing parameter  $\bar{\zeta} = 2\bar{F}/\bar{c}_f$  has also been listed. This value follows from Equation (24) with  $\bar{U}' \equiv 0^*$ . The result of this analysis is shown in Figure 2. A typical comparison for a particular profile is shown in Figure 3. It is evident that the two methods give substantially different results particularly with increasing heat transfer. This effect is demonstrated also by the behavior of the parameter  $\bar{\zeta}$  as shown in Figure 4.

It might be conjectured at this point that a similar improvement might be obtained by utilizing form II-C of the transformation which follows from form III-C for  $dp/dx=0$ . That this is not the case is evident since, insofar as the inner region is concerned, it is completely unaffected by non-zero values of  $dp/dx$ . Thus the values of skin friction that would be inferred using either II-B or II-C would be identical.

### Correlation of Wake Parameter

Despite the improved agreement manifested by form II-D in the inner region, no corresponding improvement in the outer region is observed. In particular, following Reference 2 a value

---

\* For both methods we have utilized a Sutherland viscosity relation for evaluation of viscosity and Crocco integral for the total enthalpy variation.

of Coles wake parameter  $\pi$  was inferred\* for each of the profiles examined. These values are also listed in Table II. The considerable distortion which arises is apparent. Further analysis of these data however has revealed the existence of a correlating parameter  $\bar{\rho}_{\min} T_w/T_{t_e}$  as indicated in Figure 5. Here  $\bar{\rho}_{\min}$  represents the minimum density ratio within the boundary layer\*\*. Note that by maintaining the density in this parameter, correlation of the isothermal, low speed helium injection results obtained in Reference 6 is also possible as shown in Figure 5.

### Streamwise Prediction of Skin Friction

The possible improvement in prediction of skin friction variation by use of the modified transformation or the correlation proposed above or both has been examined. Calculations were made for three cases and are compared with the appropriate experimental data in Figures 6 and 7.

In all cases a considerable improvement in the prediction is obtained by use of the correlation. Furthermore the agreement with experimental data is good with the exception of one of the cases of Reference 16. The reason for this large disagreement is not known at this time. One possibility may be that the effective origins for the two data points do not coincide.

### Impermeable Flow With Variable Pressure and Heat Transfer

Here there are available only a few preliminary results obtained using form III-C of the transformation. Several velocity profiles obtained in adverse pressure gradient (Ref. 17) have been transformed and they appear to be correlated well by the law of the wall as shown in Figure 8. However, this result can not be considered conclusive since no direct measurement (or other reliable estimate) is available for comparison with the inferred values of skin friction.

---

\*See Reference 6 for method of calculating  $\pi$  when  $\bar{F} \neq 0$ .

\*\*  $\bar{\rho}_{\min}$  was computed from the Crocco integral by evaluating the temperature ratio at  $d\tilde{T}/d\tilde{u} = 0$ .



COMPRESSIBILITY TRANSFORMATION FOR TURBULENT BOUNDARY LAYER  
FLOW OVER A SWEPT INFINITE CYLINDER

Following Reference 18, the describing equations for the velocity field prevailing in the boundary layer on a swept infinite cylinder are assumed to be

$$\frac{\partial \rho u}{\partial x} + \frac{\partial \rho v}{\partial y} = 0 \quad (26)$$

$$\rho u \frac{\partial u}{\partial x} + \rho v \frac{\partial u}{\partial y} = - \frac{dp}{dx} + \frac{\partial \tau^{(x)}}{\partial y} \quad (27)$$

$$\rho u \frac{\partial w}{\partial x} + \rho v \frac{\partial w}{\partial y} = \frac{\partial \tau^{(z)}}{\partial y} \quad (28)$$

where  $x$  is a (curvilinear) chordwise coordinate,  $y$  a coordinate normal to the surface of the cylinder and  $z$  a spanwise coordinate parallel to the generators of the cylinder. The quantities,  $u$ ,  $v$ ,  $w$ , of course, represent the corresponding velocity components and  $\tau^{(x)}$  and  $\tau^{(z)}$  represent the chordwise and spanwise components of shear, respectively. We now seek a transformation which takes Equations (26)-(28) to a corresponding CP form given by

$$\frac{\partial \bar{u}}{\partial \bar{x}} + \frac{\partial \bar{v}}{\partial \bar{y}} = 0 \quad (29)$$

$$\bar{\rho} \bar{u} \frac{\partial \bar{u}}{\partial \bar{x}} + \bar{\rho} \bar{v} \frac{\partial \bar{u}}{\partial \bar{y}} = - \frac{d\bar{p}}{d\bar{x}} + \frac{\partial \bar{\tau}^{(x)}}{\partial \bar{y}} \quad (30)$$

$$\bar{\rho} \bar{u} \frac{\partial \bar{w}}{\partial \bar{x}} + \bar{\rho} \bar{v} \frac{\partial \bar{w}}{\partial \bar{y}} = \frac{\partial \bar{\tau}^{(z)}}{\partial \bar{y}} \quad (31)$$

For this purpose, we proceed as in Appendix A and relate the chordwise and normal space coordinates and the chordwise and spanwise velocity components through a series of arbitrary stretching parameters according to

$$\frac{d\bar{x}}{dx} = \xi(x) \quad (32)$$

$$\frac{\bar{\rho} d\bar{y}}{\rho dy} = \eta(x) \quad (33)$$

$$\frac{u}{\bar{u}} = f_1(x) \quad (34)$$

$$\frac{w}{\bar{w}} = f_2(x) \quad (35)$$

It is now noted that Equations (26) and (29) are identically satisfied by stream functions defined by

$$\begin{aligned} \rho u &= \frac{\partial \psi}{\partial y} & \rho v &= \frac{\partial \psi}{\partial x} \\ \overline{\rho u} &= \frac{\partial \bar{\psi}}{\partial \bar{y}} & \overline{\rho v} &= \frac{\partial \bar{\psi}}{\partial \bar{x}} \end{aligned}$$

In view of these definitions and Equations (33) and (34) it follows readily that\*

$$\frac{\bar{\psi}}{\psi} = \frac{\int_0^{\bar{Y}} \overline{\rho u} d\bar{y}}{\int_0^Y \rho u dy} = \eta \frac{\int_0^Y \overline{\rho u} dy}{\int_0^Y \rho u dy} = \frac{\eta}{f_1} \equiv \sigma(x)$$

so that

$$\frac{u}{\bar{u}} = \frac{\sigma}{\eta}$$

The normal velocity component can now be transformed according to

$$\rho v = - \frac{\partial \psi}{\partial x} = - \xi \frac{\partial (\bar{\psi}/\sigma)}{\partial \bar{x}} - \frac{\partial \bar{y}}{\partial x} \frac{1}{\sigma} \frac{\partial \bar{\psi}}{\partial \bar{y}} =$$

$$\rho v = \frac{\xi \bar{\psi}}{\sigma^2} \frac{d\sigma}{dx} + \frac{\xi}{\sigma} \overline{\rho v} - \frac{\overline{\rho u}}{\sigma} \frac{\partial \bar{y}}{\partial x}$$

In a similar manner the remaining terms appearing in the VP equations can be transformed and it can be shown that the desired CP form is obtained provided we take

---

\* For the VP flow we consider the swept cylinder to be impermeable. Also for simplicity, it has been arbitrarily assumed here that  $\bar{v}_w = 0$ .

$$\frac{d\bar{p}}{d\bar{x}} = \frac{\bar{\rho}\sigma^2}{\xi\eta^2} \left( \frac{1}{\rho_e} \frac{dp}{dx} + u\tau^2 \frac{d\ln\eta/\sigma}{dx} \right)$$

$$\frac{\partial \bar{\tau}(\bar{x})}{\partial \bar{y}} = \frac{\bar{\rho}\sigma^2}{\xi\eta^2} \left[ \frac{1}{\rho_e} \frac{\partial \tau^{(x)}}{\partial y} - \frac{\psi}{\rho\sigma} \frac{\partial u}{\partial y} \frac{d\sigma}{dx} + \left( \frac{1}{\rho_e} - \frac{1}{\rho} \right) \frac{dp}{dx} + (u_e^2 - u^2) \frac{d\ln\eta/\sigma}{dx} \right]$$

$$f_2 = \text{constant} = \frac{w_e}{\bar{w}_e}$$

$$\frac{\partial \bar{\tau}(\bar{z})}{\partial \bar{y}} = \frac{\bar{\rho}}{\rho} \frac{\bar{w}_e}{w_e} \frac{\sigma}{\xi\eta} \left[ \frac{\partial \tau^{(z)}}{\partial y} - \frac{\psi}{\sigma} \frac{\partial \bar{w}}{\partial y} \frac{d\sigma}{dx} \right]$$

This is the desired result and would provide the means for generating predictions for the VP flow behavior by formulation of an appropriate CP solution (see e.g., Ref. 19).

#### CONCLUDING REMARKS

It is concluded on the basis of the foregoing discussion and results that treatment of a rather wide variety of variable property turbulent boundary layer flows by means of a compressibility transformation is feasible. It appears to be essential however that for any choice of configuration the appropriate form of the transformation be utilized.

#### APPENDIX A

In the original Coles formulation (Ref. 1) the stream function stretching is taken to be

$$\frac{\bar{\psi}}{\psi} = \sigma(x)$$

Taking into account the differentiation rules implied by Equations (5) and (6) and the usual definitions of the respective stream functions it then follows that the normal velocity components in the two flow regimes are related by

$$\rho v = \frac{\xi}{\sigma} \overline{\rho v} + \psi \frac{d \ln \sigma}{dx} - \frac{\overline{\rho u}}{\sigma} \frac{\partial \bar{y}}{\partial x}$$

at  $y, \bar{y} = 0$  this relation yields

$$\rho_w v_w = \frac{\xi}{\sigma} \overline{\rho v}_w + \psi_w \frac{d \ln \sigma}{dx}$$

which appears to be an independent relation for the determination of  $\bar{F}$ . In the original effort to develop an analysis for the transpired case this was indeed utilized as a working equation but was found to introduce a singularity into the system. Accordingly a modified stretching for the stream function was deduced by requiring that

$$\frac{\overline{\rho dy}}{\rho dy} = \eta(x)$$

and

$$\frac{\bar{u}}{u} = f(x)$$

Then it follows immediately that the stream functions are related according to:

$$\frac{\bar{\psi} - \bar{\psi}_w}{\psi - \psi_w} = \frac{\int_0^{\bar{Y}} \overline{\rho u} dy}{\int_0^Y \rho u dy} = \frac{\eta \int_0^Y \rho \bar{u} dy}{\int_0^Y \rho u dy} = \eta f \frac{\int_0^Y \rho u dy}{\int_0^Y \rho u dy}$$

i.e.,

$$\frac{\bar{\psi} - \bar{\psi}_w}{\psi - \psi_w} = \eta f \equiv \sigma(x)$$

and that

$$\frac{\bar{u}}{u} = \frac{\sigma}{\eta}$$

In this case we find that the normal velocity components are related by

$$\rho v - \rho_w v_w = \frac{\xi}{\sigma} (\overline{\rho v} - \overline{\rho v}_w) + (\psi - \psi_w) \frac{d \ln \sigma}{dx} - \frac{\overline{\rho u}}{\sigma} \frac{\partial \bar{y}}{\partial x}$$

which reduces to the zero identity at  $y, y=0$ . It would appear therefore that the original stretch of the stream function is too restrictive for the mass transfer case. In this connection it is interesting to note that Jeromin (Ref.7) retained the original stretching and used as a working equation the relation

$$\frac{\bar{\psi}_w}{\psi_w} = \sigma$$

which was satisfied empirically. He found however, that the resulting formulation did not reduce uniformly to the impermeable case.

## APPENDIX B

Equations (22) and (23) have the explicit form

$$\bar{F} - \frac{2}{\bar{c}_f} (\ln \bar{U}_e)' = \left( \frac{\tilde{\eta}_o}{\tilde{\eta}} \frac{\tilde{\sigma}}{\tilde{\sigma}_o} \frac{\bar{c}_f}{2} \right) \left[ \frac{U_e \nu_{e0}}{\nu_e} g_1 - \left( \frac{2}{c_f} \right)^2 \frac{d \ln U_e}{d \chi} \right]$$

$$\bar{F} \left[ \bar{F} - \frac{2}{\bar{c}_f} (\ln U_e)' \right] = \left( \frac{\tilde{\eta}_o}{\tilde{\eta}} \frac{\tilde{\sigma}}{\tilde{\sigma}_o} \frac{c_f}{2} \right)^2 \left\{ \frac{U_e \nu_{e0}}{\nu_e} g_2 - \left( \frac{2}{c_f} \right)^2 \frac{d \ln U_e}{d \chi} g_3 \right\}$$

where

$$g_1 = \frac{2F}{c_f} \frac{1}{U_e} - \left( \frac{\partial \ln \tilde{\rho} \tilde{\mu}}{\partial \tilde{u}} \right)_w$$

$$g_2 = 3 \left( \frac{\partial \ln \tilde{\rho}}{\partial \tilde{u}} \right)^2 + \left[ \frac{2F}{c_f} \frac{1}{U_e} - \left( \frac{\partial \ln \tilde{\mu}}{\partial \tilde{u}} \right)_w \right] \left[ \frac{2F}{c_f} \frac{1}{U_e} - 3 \left( \frac{\partial \ln \tilde{\mu}}{\partial \tilde{u}} \right)_w - 4 \left( \frac{\partial \ln \tilde{\rho}}{\partial \tilde{u}} \right)_w \right]$$

$$- \left[ \frac{1}{\tilde{\rho}_w} \left( \frac{\partial^2 \tilde{\rho}}{\partial \tilde{u}^2} \right)_w + \frac{1}{\tilde{\mu}_w} \left( \frac{\partial^2 \tilde{\mu}}{\partial \tilde{u}^2} \right)_w \right]$$

$$g_3 = \frac{2F}{c_f} \frac{1}{U_e} - 3 \left( \frac{\partial \ln \tilde{\mu}}{\partial \tilde{u}} \right)_w - 4 \left( \frac{\partial \ln \tilde{\rho}}{\partial \tilde{u}} \right)_w$$

$$\text{also } g_1' = - \left( \frac{\partial \ln \tilde{\rho} \tilde{\mu}}{\partial \tilde{u}} \right)_w$$

$$g_2' = 3 \left( \frac{\partial \ln \tilde{\rho}}{\partial \tilde{u}} \right)_w^2 + \left( \frac{\partial \ln \tilde{\mu}}{\partial \tilde{u}} \right)_w \left[ 3 \left( \frac{\partial \ln \tilde{\mu}}{\partial \tilde{u}} \right)_w + 4 \left( \frac{\partial \ln \tilde{\rho}}{\partial \tilde{u}} \right)_w \right] - \left[ \frac{1}{\tilde{\rho}_w} \left( \frac{\partial^2 \tilde{\rho}}{\partial \tilde{u}^2} \right)_w + \frac{1}{\tilde{\mu}_w} \left( \frac{\partial^2 \tilde{\mu}}{\partial \tilde{u}^2} \right)_w \right]$$

## REFERENCES

1. Coles, D. E.: The Turbulent Boundary Layer in a Compressible Fluid. Rand Corp. Report R-403-PR, Sept. 1962.
2. Baronti, P. O. and Libby, P. A.: Velocity Profiles in Turbulent Compressible Boundary Layers. AIAA J. vol. 4, 1966, pp. 193-202.
3. Bertram, M. H. and Neal, L., Jr.: Recent Experiments in Hypersonic Turbulent Boundary Layers. AGARD Specialists Meeting on Recent Developments in Boundary Layer Research (1965); also NASA TM X-56335 (1965).
4. Watson, R. D. and Cary, A. M. Jr.: The Transformation of Hypersonic Turbulent Boundary Layers to Incompressible Form. AIAA J., vol. 6, no. 6, June 1967, pp. 1202-1203.
5. Rosenbaum, H.: Turbulent Compressible Boundary Layer on a Flat Plate with Heat Transfer and Mass Diffusion. AIAA J., Sept. 1966.
6. Economos, C.: The Compressible Turbulent Boundary Layer with Mass Injection. PIBAL PhD. Dissertation (June 1968). To be presented at the AIAA Winter Meeting, Jan. 1969.
7. Jeromin, L. O. F.: A Transformation for Compressible Turbulent Boundary Layers with Air Injection. J. Fluid Mech., vol. 31, part 1, 1968, pp. 65-94.
8. Libby, P. A. and Baronti, P. O.: A Transformation Theory of the Turbulent Compressible Boundary Layer with Pressure Gradient and Heat Transfer. GASL TR-455, Aug. 1964.
9. Lewis, John E.: Compressible Boundary Layer and Its Low Speed Equivalent. AIAA J., vol. 6, no. 6, June 1968, pp. 1185-1187.
10. Moses, H. L.: The Behavior of Turbulent Boundary Layers in Adverse Pressure Gradients. Gas Turbine Lab., MIT, Report 73, 1964.
11. Baronti, P. O.: An Investigation of the Turbulent Incompressible Boundary Layer. GASL TR-624, Aug. 1966.

12. Stevenson, T. N.: A Law of the Wall for Turbulent Boundary Layers with Suction or Injection. College of Aeronautics Report 166, 1963.
13. Stevenson, T. N.: A Modified Velocity Defect Law for Turbulent Boundary Layers with Injection. Aero. Research Council of London Report 20,501, 1958.
14. Schneider, J.: Missile Phenomenology Studies; ARPA Summary Report for 1967. GASL TR-684, Jan. 1968.
15. Eschenroeder, A. Q.: Combustion in the Boundary Layer on a Porous Surface. J. Aero. Sci. vol. 27, no. 12, 1960, pp. 901-906.
16. Wallace, J. E.: Hypersonic Turbulent Boundary Layer Studies at Cold Wall Conditions. 1967 Heat Transfer and Fluid Mechanics Institute (San Diego, Calif.) June 19-21, 1967. Also detailed profile data supplied to author, courtesy M. Bertram, NASA Langley Research Center.
17. Kepler, C. E. and O'Brien, R. L.: Supersonic Turbulent Boundary Layer Growth over Cooled Walls in Adverse Pressure Gradients. United Aircraft Corp., Aero. Sys. Div., ASD-TDR-62-87, Oct. 1962.
18. Schlichting, H.: Boundary Layer Theory. McGraw Hill Book Co., New York (1955), p. 437.
19. Bradley, R. G.: Approximate Solutions for Compressible Turbulent Boundary Layers in Three-Dimensional Flow. AIAA J., vol. 6, no. 5, May 1968, pp. 859-864.
20. Coles, D. E.: Measurements in the Boundary Layer on a Smooth Flat Plate in Supersonic Flow, III. Measurements in a Flat Plate Boundary Layer at the Jet Propulsion Laboratory. Jet Prop. Lab., Cal. Inst. Tech., Report 20-71, June 1953.
21. Matting, F. W., Chapman, D. R., Nyholm, J. R. and Thomas, A.G.: Turbulent Skin Friction at High Mach Numbers and Reynolds Numbers in Air and Helium. NASA TR R-82, 1961.
22. Stalmach, Charles J., Jr.: Experimental Investigations of the Surface Impact Pressure Probe Method of Measuring Local Skin Friction at Supersonic Speeds. DRL-410 CF-2675 (Contract Nord-16498), Univ. of Texas, Jan. 1958.

23. Schutts, W. H., Harting, W. H. and Weiler, J. R.: Turbulent Boundary Layer and Skin-Friction Measurements on a Smooth, Thermally Insulated Flat Plate at Supersonic Speeds. Univ. of Texas, Defense Res. Labs., DRL-364, CM-823, Jan. 1955.
24. Lobb, R. K., Winkler, E. M. and Persh, J.: Experimental Investigation of Turbulent Boundary Layers in Hypersonic Flow. J. Aero. Sci., vol. 22, Jan. 1955, pp. 1-9 and 50.
25. Winkler, E. M. and Cha, M. H.: Investigation of Flat Plate Hypersonic Turbulent Boundary Layers with Heat Transfer at a Mach Number of 5.2. U. S. Naval Ord. Lab., NAVORD Rept. 6631, Sept. 1959.
26. Hill, F. K.: Turbulent Boundary Layer Measurements at Mach Numbers from 8 to 10. Phys. Fluids, vol. 2, 1959, pp. 668-680.
28. Maddalon, D. V., Rogallo, R. S. and Henderson, A., Jr.: Transition Measurements at Hypersonic Mach Numbers. AIAA J., vol. 3, 1967, pp. 590-591.
29. Samuels, R. D., Peterson, J. B., Jr., and Adcock, J. B.: Experimental Investigation of the Turbulent Boundary Layer at a Mach Number of Six with Heat Transfer at High Reynolds Numbers. NASA Langley Res. Center TN D-3858, 1967.
30. Sterrett, J. B. and Barber, J. B.: A Theoretical and Experimental Investigation of Secondary Jets in a Mach 6 Free Stream with Emphasis on the Structure of the Jet and Separation Ahead of the Jet. AGARD Conference Proceedings 4, Part 2, 1966, pp. 667-700.
31. Harvey, W. D. and Clark, F. L.: Unpublished data supplied to author courtesy M. Bertram, NASA Langley Research Center.
32. Denison, M. R.: The Turbulent Boundary Layer on Chemically Active Ablating Surfaces. J. of Aero. Sci., vol 28, no. 6, June 1961.
33. Rubesin, M. W. and Pappas, C. E.: An Analysis of the Turbulent Boundary Layer Characteristics on a Flat Plate with Distributed Light Gas Injection. NACA TN 4149, Feb. 1958.



34. Rubesin, N. W.: An Analytical Estimation of the Effect of Transpiration Cooling on the Heat Transfer and Skin Friction Characteristics of a Compressible Turbulent Boundary Layer. NACA TN 3341, Dec. 1954.
35. Scott, C. T., et al.: Measurements of Velocity and Concentration Profiles for Helium Injection into a Turbulent Boundary Layer Flowing Over an Axial Circular Cylinder; Part I - Experimental Results. Univ. of Minn. HTL-TR-55, Feb. 1964.
36. Dershin, H., Leonard, C. A. and Gallaher, W. H.: Direct Measurement of Compressible, Turbulent Boundary Layer Skin Friction on a Porous Flat Plate with Mass Injection. AIAA J., vol. 11, 1967, pp. 1934-1939.

TABLE I COMPARISON OF VARIOUS FORMS OF THE COMPRESSIBILITY TRANSFORMATION

Form	Specification of VP Flow Configuration		Assumed CP Flow Configuration		Number of Additional Relations Required	Form of Relations	Comments
	$\frac{dp}{dx}$	F	$\frac{dp}{dx}$	$\bar{F}$			
Unified	I SNZ	SNZ	A ?	?	2	1st & 2nd Compatibility.	-
II-B	II 0	0	B 0	0	0	-	Formulated in Refs. 1,2. Exploited, e.g., in Refs. 1-4.
III-C	III SNZ	0	C ?	0	1	1st compatibility for $\frac{dp}{dx}$ .	Formulated in Ref. 8.
IV-D	IV 0	SNZ	D 0	?	1	1st compatibility for $\bar{F}$ .	Formulated and Exploited in Ref. 6.
II-D	- 0	0	- 0	?	1	1st compatibility for $\bar{F}$ .	Follows from IV-D.
II-C	- 0	0	- ?	0	1	1st compatibility for $\frac{dp}{dx}$ .	Follows from IV-B
II-A	- 0	0	- ?	?	2	1st & 2nd Compatibility.	Follows from Unified Form

SNZ = Specified Non-Zero

TABLE II SUMMARY OF RESULTS-ANALYSIS OF ZERO PRESSURE GRADIENT VELOCITY PROFILES BY  
TRANSFORMATION METHOD

Ref.	M <sub>e</sub>	R <sub>θ</sub> (-3)	$\tilde{T}_w$	T <sub>w</sub> /T <sub>t<sub>e</sub></sub>	C <sub>f<sub>R</sub></sub> (+3)	C <sub>f<sub>BL</sub></sub> (+3)	$\tilde{\tau}$	C <sub>f<sub>M</sub></sub> (+3)	Π
20	1.97	2.98	1.69	.95	2.72	2.48	.016	2.50	.337
	1.98	6.47	1.70	.95	2.18	2.02	.016	2.05	.414
	1.98	8.57	1.70	.95	2.02	1.88	.015	1.90	.431
	2.54	2.19	2.16	.94	2.42	2.42	.019	2.45	.019
	2.57	6.60	2.18	.94	1.81	1.64	.020	1.66	.381
	2.58	10.2	2.18	.94	1.66	1.48	.021	1.50	.392
	3.70	4.10	3.45	.92	1.62	1.50	.026	1.48	-.010
	3.70	7.56	3.44	.92	1.38	1.23	.026	1.22	+.165
	4.51	3.47	4.69	.92	1.48	1.28	.027	1.32	-.123
	4.55	6.59	4.74	.92	1.22	1.06	.026	1.02	-.167
21	2.95	8.05	2.46	.90	1.54	1.60	.036	1.60	+.134
	2.95	21.57	2.50	.91	1.29	1.29	.030	1.30	+.062
	4.20	6.15	3.81	.84	1.27	1.32	.055	1.32	-.339
	4.20	22.75	4.06	.90	.952	.992	.034	.978	-.206
	4.20	37.58	4.03	.89	.868	.880	.040	.820	-.185
	5.19	5.37	8.10	.81	.673	.896	.082	.810	-.57
	1.74	8.43	1.54	.96	2.11	2.06	.017	2.05	+.37
	1.74	12.49	1.53	.95	1.99	1.90	.014	1.80	+.380
	2.96	2.74	2.55	.93	2.16	2.20	.022	2.15	-.160
	2.74	11.90	2.33	.93	1.53	1.50	.024	1.53	+.073
22	3.67	7.99	3.38	.91	1.29	1.22	.031	1.24	+.123
	3.68	10.18	3.40	.92	1.24	1.16	.027	1.15	+.099
	1.74	3.44	1.53	.95	2.56	2.64	.013	2.65	+.134
	2.50	6.08	2.14	.95	1.80	2.03	.017	2.00	0
	2.53	9.64	2.16	.95	1.58	1.82	.017	1.80	-.121
	2.45	18.81	2.09	.95	1.56	1.57	.015	1.55	+.051
23	2.95	8.05	2.46	.90	1.54	1.60	.036	1.60	+.134
	2.95	21.57	2.50	.91	1.29	1.29	.030	1.30	+.062
	4.20	6.15	3.81	.84	1.27	1.32	.055	1.32	-.339
	4.20	22.75	4.06	.90	.952	.992	.034	.978	-.206
	4.20	37.58	4.03	.89	.868	.880	.040	.820	-.185
	5.19	5.37	8.10	.81	.673	.896	.082	.810	-.57
	1.74	8.43	1.54	.96	2.11	2.06	.017	2.05	+.37
	1.74	12.49	1.53	.95	1.99	1.90	.014	1.80	+.380
	2.96	2.74	2.55	.93	2.16	2.20	.022	2.15	-.160
	2.74	11.90	2.33	.93	1.53	1.50	.024	1.53	+.073

TABLE II (Contd)

Ref.	M <sub>e</sub>	R <sub>θ</sub> (-3)	$\tilde{T}_w$	T <sub>w</sub> /T <sub>te</sub>	C <sub>fR</sub> (+3)	C <sub>fBL</sub> (+3)	ζ	C <sub>fM</sub> (+3)	Π
24	5.01	6.48	4.29	.713	1.10	1.14	.120	1.06	-.175
	5.06	7.37	3.27	.533	1.11	1.19	.263	1.10	-.185
	6.78	7.96	4.64	.455	.814	.860	.362	.775	-.175
	6.83	8.55	6.34	.613	.750	.760	.193	.700	-.206
25	5.29	4.30	5.56	.840	1.08	1.09	.055	1.12	-.309
	5.24	3.79	4.97	.765	1.25	1.22	.091	1.16	-2.88
	5.17	1.05	3.89	.615	1.62	1.90	.027	1.50	-.411
26	9.07	2.276	8.3	.475	.725	.874	.333	.775	-.191
3	6.00	49.0	5.3	.63	.646	.638	.168	.62	-.432
	6.00	24.0	5.3	.63	.717	.720	.168	.70	-.432
	6.00	19.0	5.1	.63	.760	.750	.184	.71	-.227
	6.80	30.0	5.1	.50	.620	.610	.305	.57	-.467
	6.80	13.0	5.1	.50	.716	.690	.305	.64	+ .021
3	20.2	5.24	137.	.99	.115	.149	3.213	.149	+1.84
28	7.53	2.05	19.9	1.0	.587	.620	.005	.66	-1.245
29	6.00	12.9	3.7	.45	.865	.930	.373	.82	-.339
30	6.00	7.1	7.3	.89	.830	.800	.034	.78	-.380
31	18.4	1.25	11.3	.16	.313	.564	1.539	.388	-.760
16	7.87	58.0	3.88	.29	.540	.630	.766	.50	-.800
	7.61	14.0	3.69	.29	.620	.820	.751	.65	-.610
	7.16	2.69	.760	.094	1.09	1.65	4.146	.79	-.473
	7.21	3.40	.900	.105	1.09	1.88	3.50	1.02	-.950

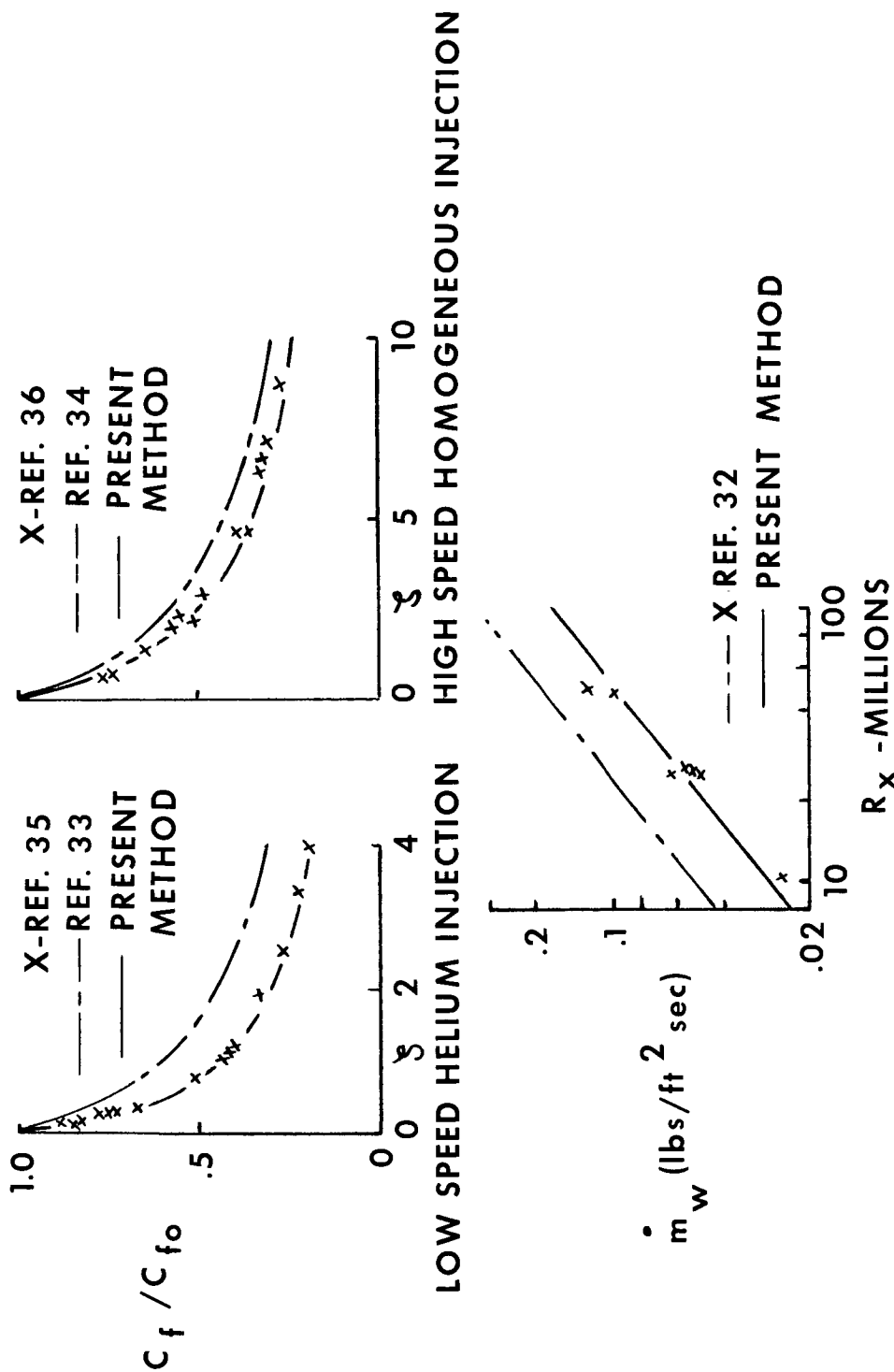


FIGURE 1 - COMPARISON OF THEORY AND EXPERIMENT FOR FLOW WITH MASS TRANSFER AT CONSTANT PRESSURE

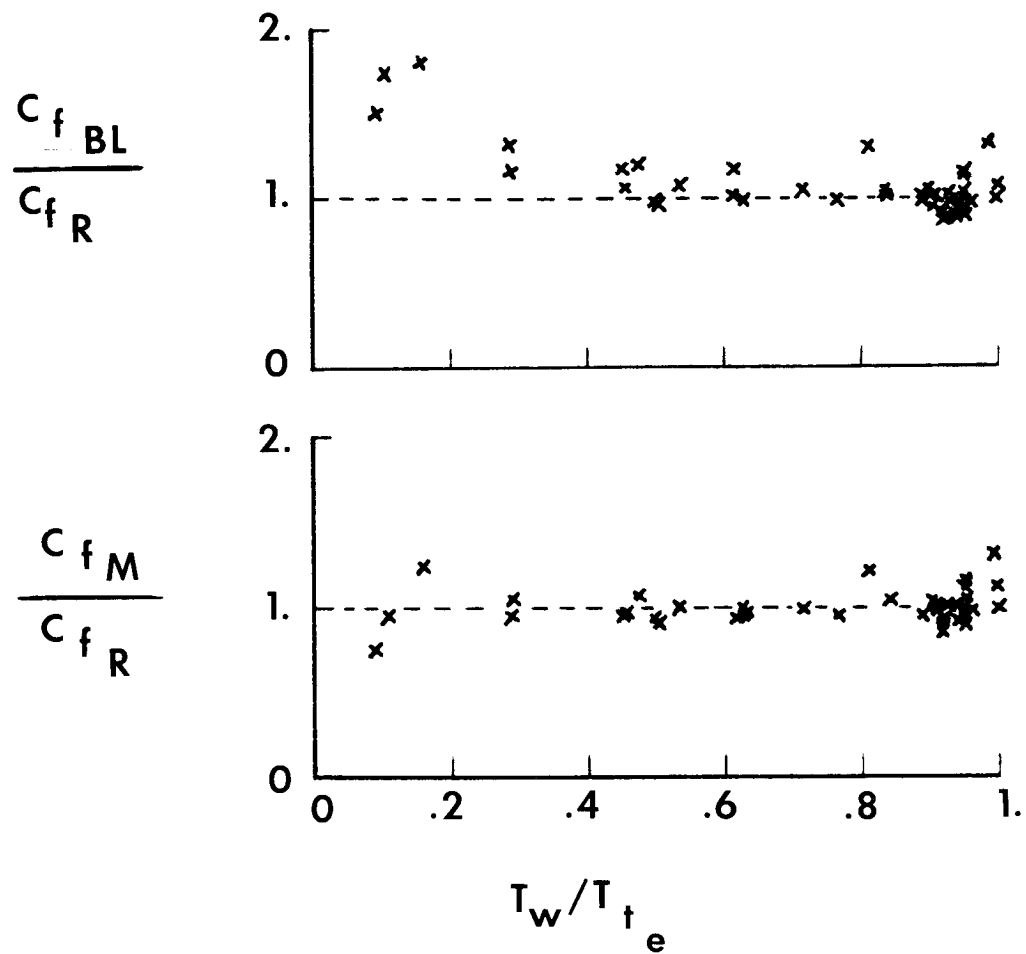


FIGURE 2 - COMPARISON OF SKIN FRICTION INFERRED FROM TWO FORMS OF THE TRANSFORMATION

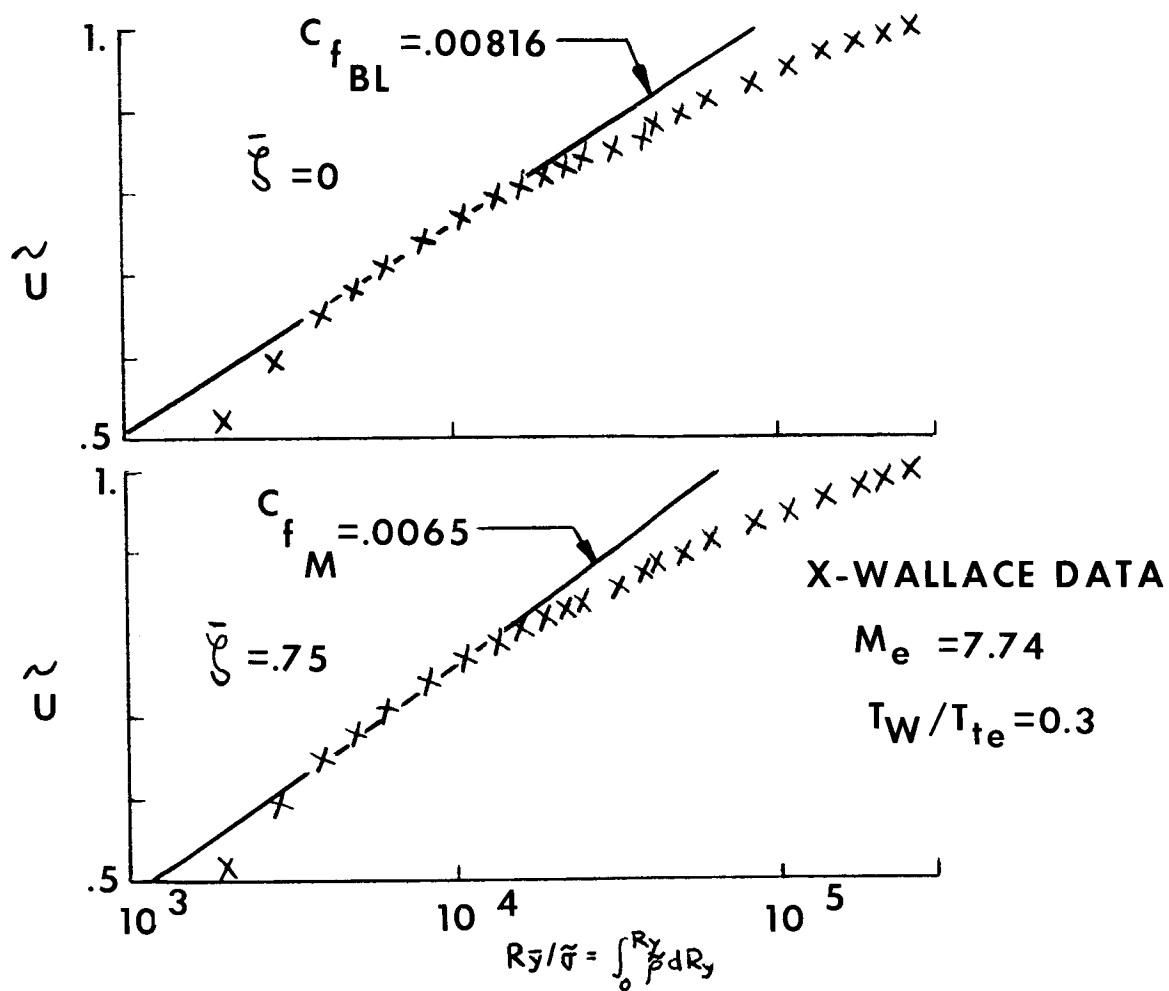


FIGURE 3 - SKIN FRICTION ESTIMATE USING TWO FORMS OF THE TRANSFORMATION

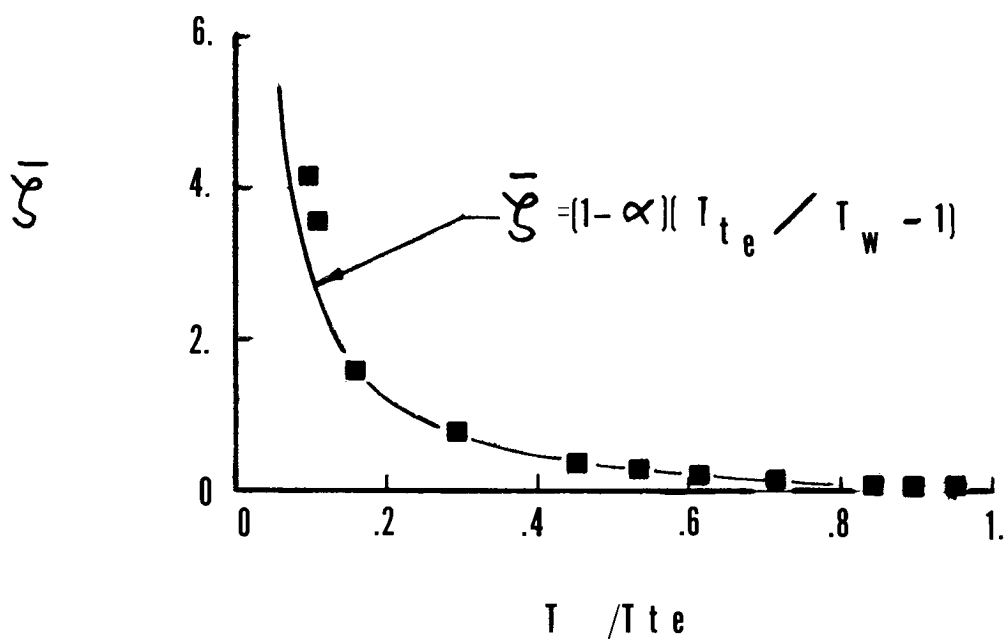


FIGURE 4 - VARIATION OF CP BLOWING PARAMETERS WITH WALL TEMPERATURE



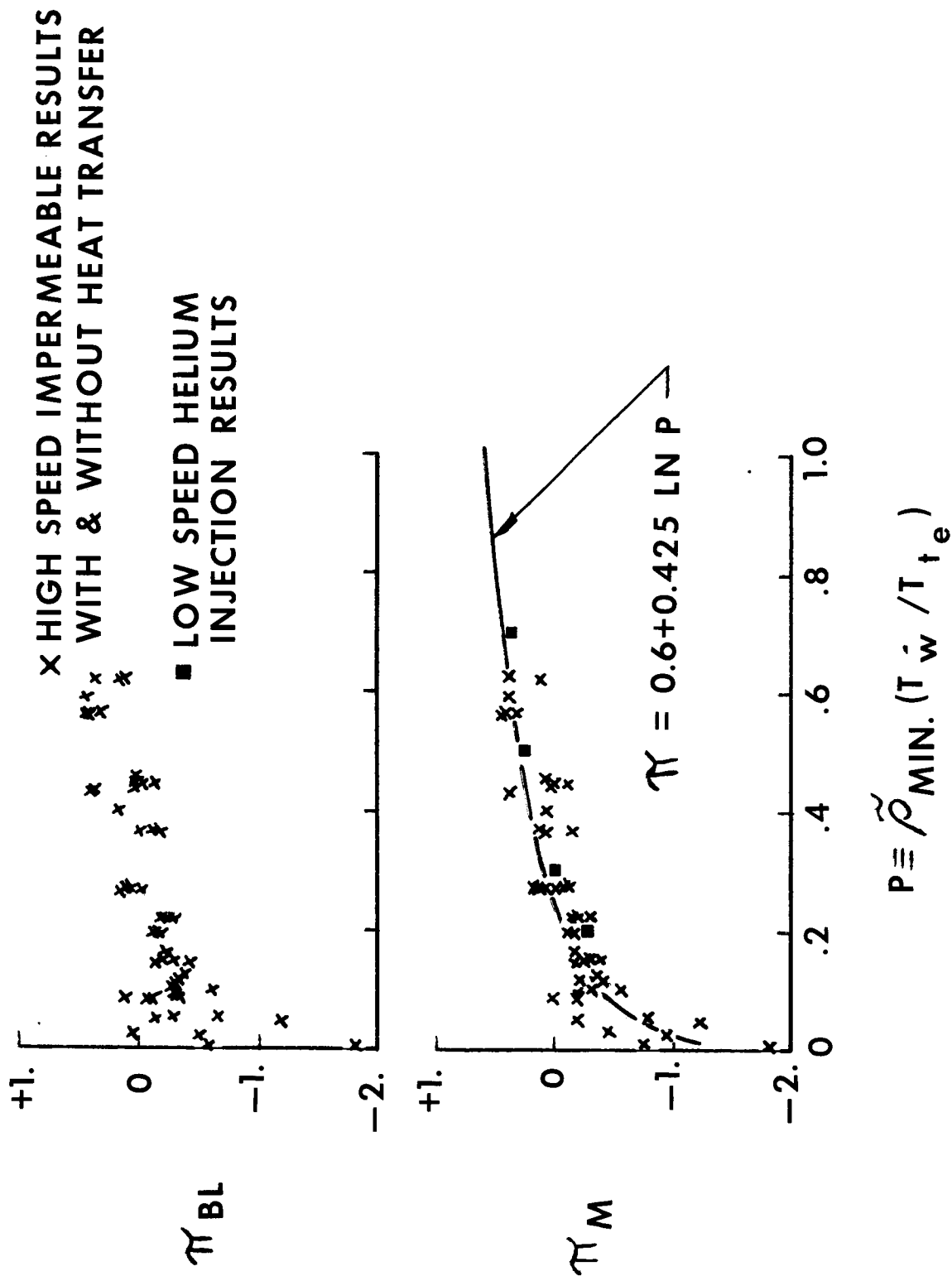


FIGURE 5 - CORRELATION OF THE WAKE PARAMETER

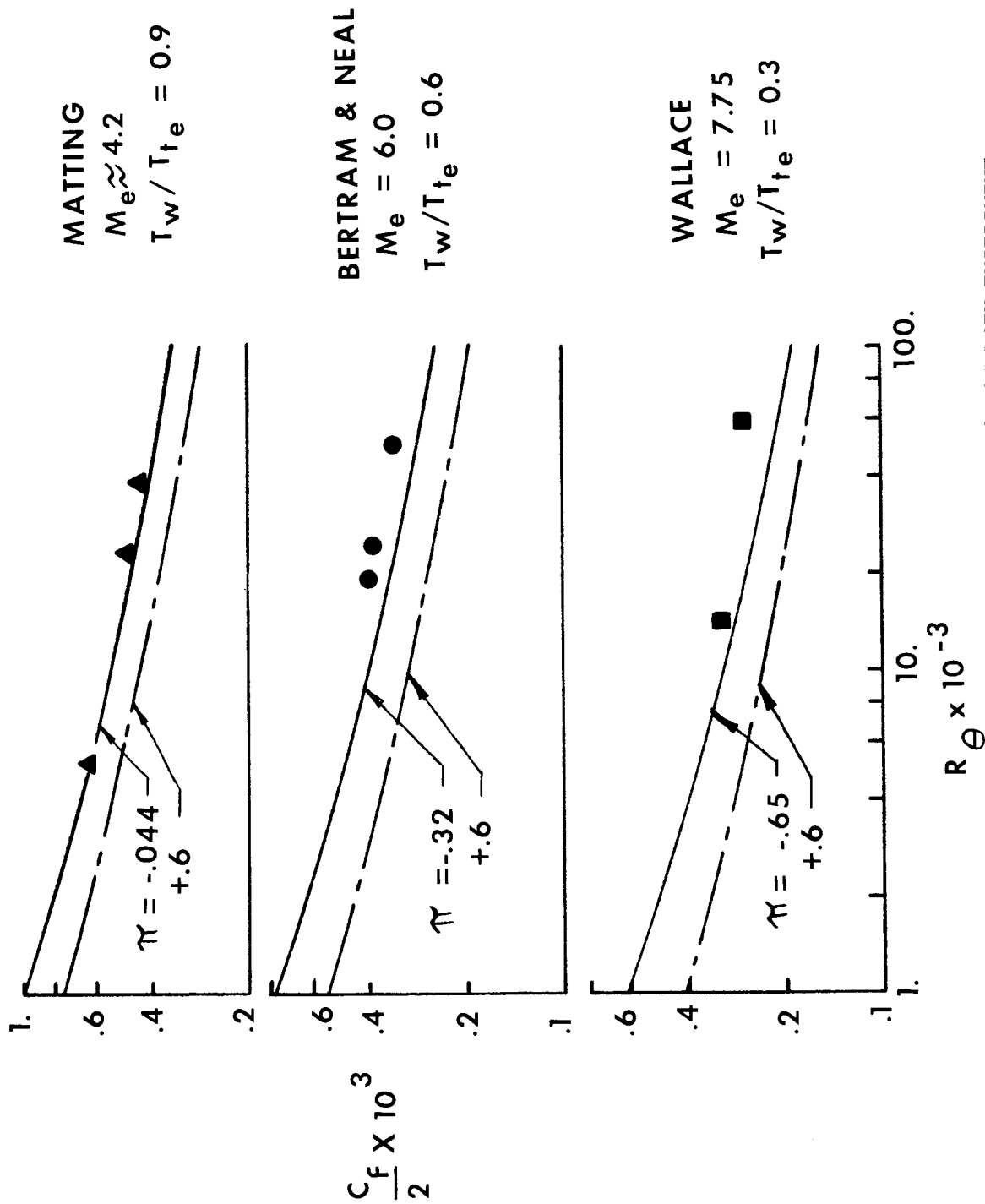


FIGURE 6 - COMPARISON OF SKIN FRICTION PREDICTION WITH EXPERIMENT

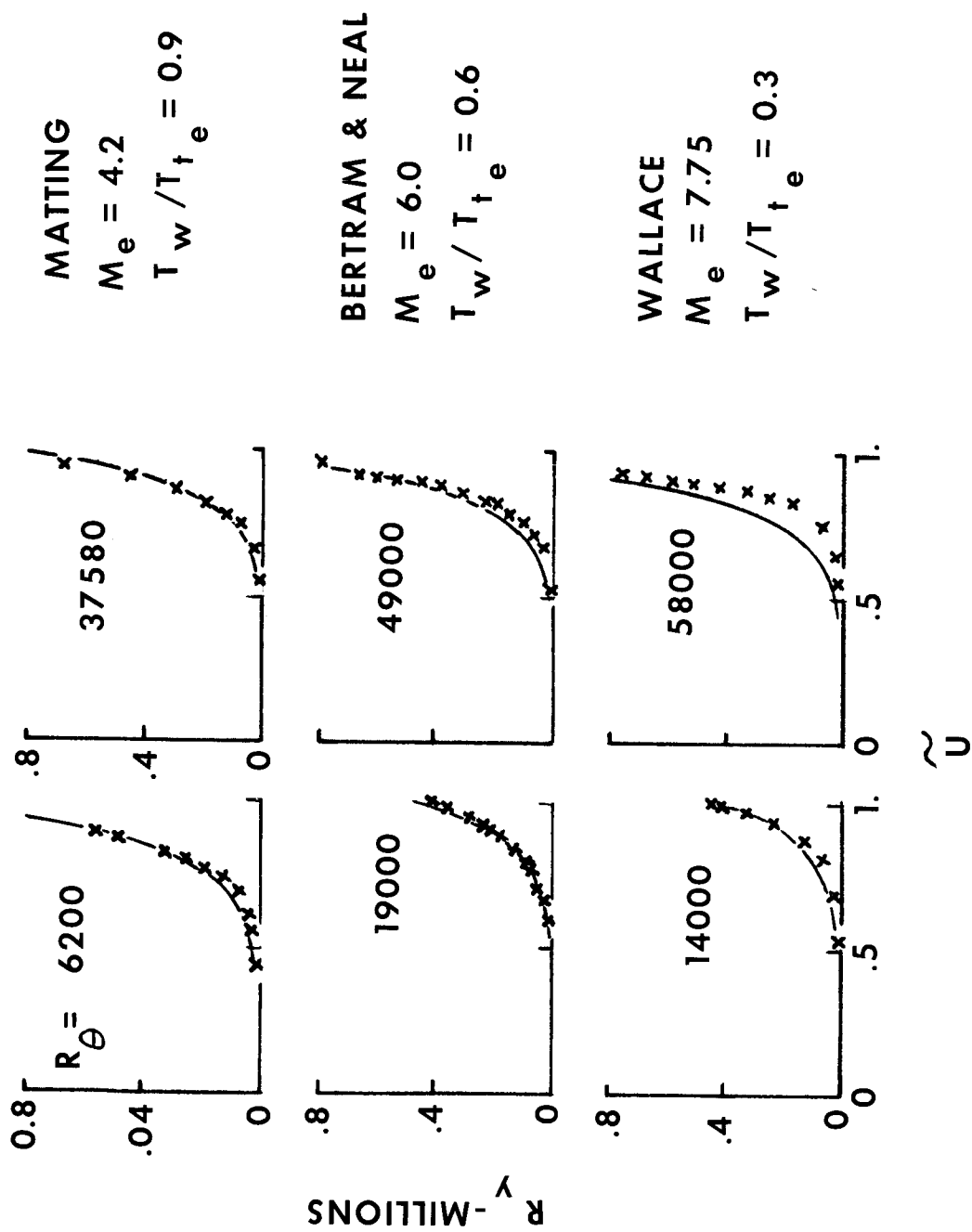


FIGURE 7 - COMPARISON OF VELOCITY PROFILES IN PHYSICAL COORDINATES

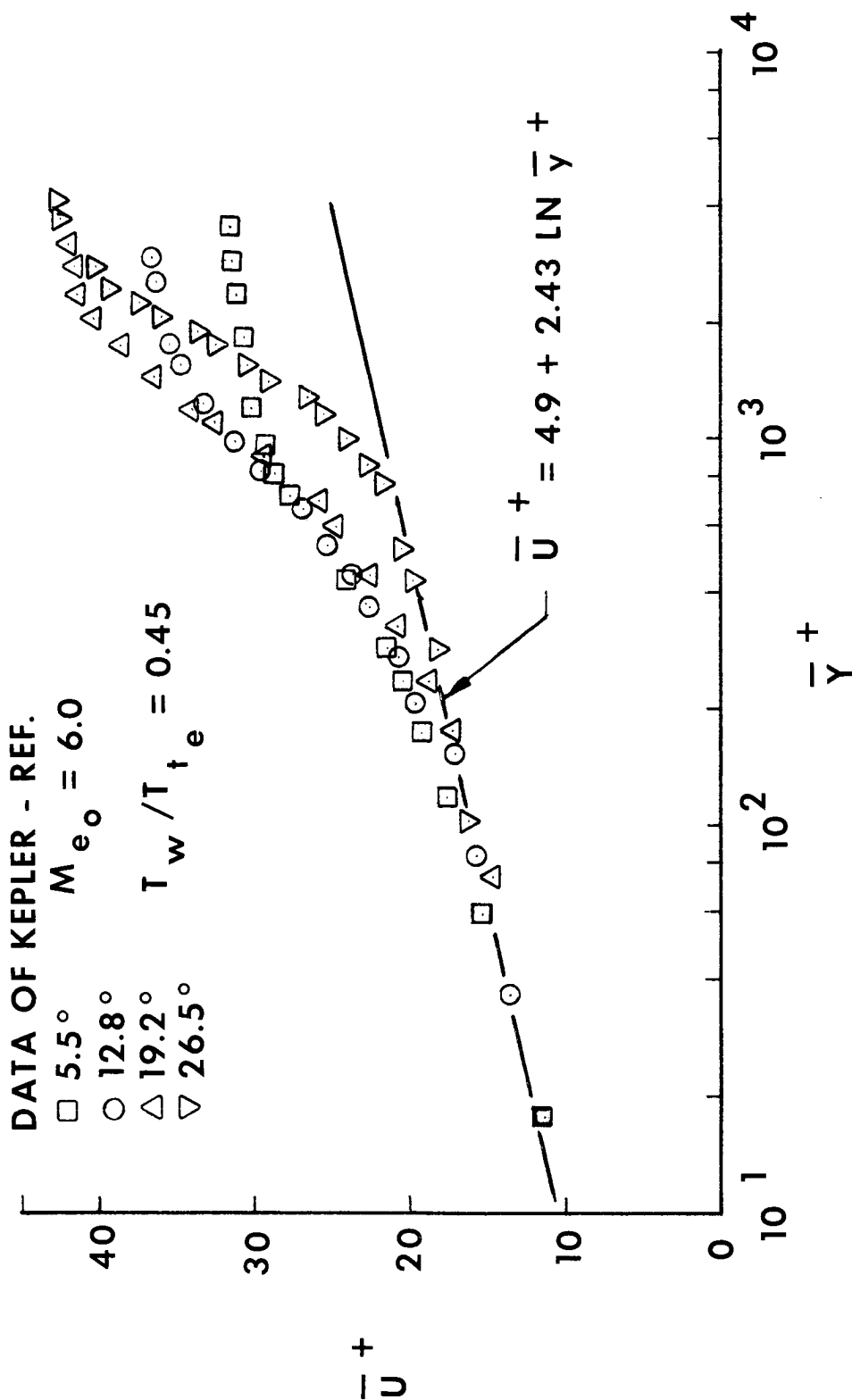


FIGURE 8 - CORRELATION OF VELOCITY PROFILES OBTAINED IN  
VARIABLE PRESSURE FLOWS

An Assessment of Certain Procedures For Computing The  
Compressible Turbulent Boundary Layer Development

by

Henry McDonald  
Supervisor, Theoretical Gas Dynamics  
United Aircraft Research Laboratories,  
East Hartford, Connecticut

SUMMARY

A brief review of the state-of-the-art of predicting the compressible turbulent boundary layer development is presented together with an extensive comparison between the predictions of four selected procedures and the available measurements. Three of the procedures considered are integral methods of computing the boundary layer development and utilize a compressibility transformation to reduce the problem to the more manageable one of predicting the development of an equivalent incompressible turbulent boundary layer. One of the integral procedures takes into account the effect of upstream history on the turbulent shear stress. The fourth procedure considered is a numerical solution to the boundary layer partial differential equations of motion and in this case the turbulent shear stress is described by a simple eddy viscosity model. The results of the comparison between theory and experiment indicate that, relative to incompressible flow, much poorer agreement is obtained when the pressure gradients are pronounced. The cause of the large discrepancies is tentatively attributed to the neglect of the static pressure variation normal to the wall. No significant gain in accuracy of prediction in the present case was found to result from the use of the numerical solution of the boundary layer partial differential equations of motion compared to the less rigorous, but much faster, integral procedures.

The work reported in the present note was sponsored jointly by Pratt & Whitney Aircraft and United Aircraft Research Laboratories.

INTRODUCTION

In designing aerodynamic systems a frequently occurring problem is to accurately predict the boundary layer development throughout these systems. The reasons for requiring an accurate knowledge of the boundary layer behavior are not difficult to

understand, since in most instances the boundary layer plays a key role both in determining the aerodynamic losses which occur in the system and, in addition, determines the possible operating envelope of the system. In the commonly encountered design problems the boundary layer is turbulent and the mean flow velocities are in the compressible flow regime. Although quite a number of procedures which compute the compressible turbulent two-dimensional boundary layer development under the influence of an arbitrary pressure gradient exist, the question arises as to the accuracy of these existing procedures for design purposes.

In a compressible turbulent shear flow, the fluctuating velocity field causes a net transport of momentum and heat normal to the streamlines of the mean flow. The fundamental problem of the turbulent boundary layer is the explicit or implicit description of this transport mechanism. In view of the heavy reliance that compressible calculation procedures place on incompressible theory, it is relevant to the present study to review the status of incompressible prediction methods. In this context it is noted that in recent years Rotta (Ref. 1), Thompson (Ref. 2), and Rotta (Ref. 3) have reviewed the then available procedures and concluded that prior to about 1964 only one procedure for computing the incompressible turbulent boundary layer, that due to Head (Ref. 4), could be relied upon to provide reasonable predictions. Rotta (Ref. 1) attributed the poor performance of most of the other procedures to an inadequate description of the relationship between the momentum transport and the mean velocity.

Partially as a result of the Rotta-Thompson reviews and partially as a result of the re-emergence of the boundary layer as a major aerodynamic problem area, there have been numerous re-analyses of the boundary layer problem since the Rotta-Thompson reviews. These newer contributions have been categorized and assessed in the recent AFOSR-IFP Conference at Stanford (Ref. 5). It is evident from the Stanford meeting that many of the newer procedures can make rapid, accurate predictions of the incompressible two-dimensional turbulent boundary layer flowing in an arbitrary pressure gradient. From an engineering point of view, then, the two-dimensional incompressible development of thin unseparated turbulent boundary layer growing under, but not influencing, a steady inviscid free stream may be considered predictable to a fair degree of accuracy. The present note attempts to ascertain the degree of accuracy which may be expected in the corresponding compressible case. It is felt that such a study would help orient future research as well as provide an accuracy base level to guide users of the existing procedures. Also, it would seem ill-advised to proceed to study more complex flows, such as three-dimensional boundary layers, without first clarifying the position as far as possible in two dimensions.

# LIST OF SYMBOLS

$C_f$	Skin friction coefficient
$C_p$	Specific heat at constant pressure
$H$	Shape factor
$H_0$	Stagnation enthalpy, defined by Eq. (4)
$M$	Mach number
$Pr$	Prandtl number
$p$	Pressure
$T$	Temperature
$u$	Velocity along the wall
$v$	Velocity normal to the wall
$x$	Distance along the wall
$y$	Distance normal to the wall
$\xi, \sigma, \eta$	Transformation scales, see Refs. 9 and 10
$\rho$	Density
$\delta$	Boundary layer thickness
$\delta^*$	Boundary layer displacement thickness $\int_0^{\delta} \left( 1 - \frac{\bar{\rho} \bar{u}}{\rho_e u_e} \right) dy$
$\theta$	Boundary layer momentum thickness $\int_0^{\delta} \frac{\bar{\rho} \bar{u}}{\rho_e u_e} \left( 1 - \frac{\bar{\rho} \bar{u}}{\rho_e u_e} \right) dy$
$\overline{v' T'}$	Turbulent thermal transport correlation
$\overline{u' v'}$	Turbulent apparent shear stress
$\mu$	Molecular viscosity

### Subscripts

- e            Edge of the boundary layer  
w            Wall value  
o            Stagnation value

### Superscripts

- '            Fluctuating quantity  
—            Time mean average

## COMPRESSIBLE TURBULENT BOUNDARY LAYER THEORY

### The Basic Equations

Within the framework of the usual boundary layer approximations, various authors, for example, Schubauer and Tchen (Ref. 6), have reduced the time-averaged Navier-Stokes equations to the compressible boundary layer equations of motion. For steady two-dimensional flow these equations may be written together with the continuity equation in the form

$$\frac{\partial}{\partial x} (\bar{\rho} \bar{u}^2) + \frac{\partial}{\partial y} (\bar{u} \bar{\rho} \bar{v}) = - \frac{\partial \bar{p}}{\partial x} + \frac{\partial}{\partial y} \left( \bar{\mu} \frac{\partial \bar{u}}{\partial y} - \bar{\rho} \overline{u'v'} \right) - \frac{\partial}{\partial x} \left( \bar{\rho} \overline{u'^2} \right) \quad (1)$$

$$\frac{\partial}{\partial x} (\bar{H}_0 \bar{\rho} \bar{u}) + \frac{\partial}{\partial y} (\bar{H}_0 \bar{\rho} \bar{v}) =$$

$$\frac{\partial}{\partial y} \left( \bar{\mu} \frac{\partial \bar{H}_0}{\partial y} - \bar{\rho} C_p \overline{v'T'} \right) + \frac{\partial}{\partial y} \left( \frac{1}{Pr} - 1 \right) \bar{\mu} \frac{\partial}{\partial y} C_p \bar{T} + \bar{\rho} C_p \overline{u'v'} \frac{\partial \bar{u}}{\partial y} \quad (2)$$

and

$$\frac{\partial}{\partial x} \bar{\rho} \bar{u} + \frac{\partial}{\partial y} \bar{\rho} \bar{v} = 0 \quad (3)$$



where

$$\bar{H}_0 = C_p \bar{T}_0 = C_p \bar{T} + \frac{1}{2} (\bar{u}^2 + \bar{v}^2) \quad (4)$$

In the above equations  $u$  and  $v$  are the velocities in the  $x$  and  $y$  directions (i.e., parallel to and normal to the wall). The prime denotes a fluctuating quantity and the bar a time mean average. The stagnation temperature is denoted by  $\bar{T}_0$ , the static temperature  $\bar{T}$  is defined by Eq. (4). The specific heat at constant pressure is denoted by  $C_p$  and the Prandtl number by  $Pr$ . In view of subsequent developments, it is worth noting at this point that under the usual boundary layer approximations the  $y$ -momentum equation reduces to

$$\frac{\partial}{\partial y} \left( \bar{p} + \bar{p} \bar{v}'^2 \right) = 0 \quad (5)$$

which then integrates to give

$$\bar{p} + \bar{p} \bar{v}'^2 = \bar{p}_w \quad (6)$$

where the subscript 'w' denotes conditions at the wall. If, in addition, the usual assumption is made that the longitudinal gradient of Reynolds normal stress contribution to Eq. (1) is negligible, then from Eq. (6) it follows that the static pressure gradient  $\partial p / \partial x$  is constant across the boundary layer. This point will be discussed at length subsequently. Under the terms of these additional assumptions the  $x$ -momentum equation, Eq. (1), becomes

$$\frac{\partial}{\partial x} (\bar{p} \bar{u}^2) + \frac{\partial}{\partial y} (\bar{u} \bar{p} v) = - \frac{d \bar{p}_w}{dx} + \frac{\partial}{\partial y} \left( \bar{\mu} \frac{\partial \bar{u}}{\partial y} - \bar{p} \overline{u' v'} \right) \quad (7)$$

Inspection of Eqs. (2), (3), and (7) together with the equations of state reveals that the only unknowns in the system of equations are the turbulent shear stress  $-\overline{u' v'}$  and the temperature correlation  $-\overline{v' T'}$  (provided of course that  $\mu$ ,  $C_p$ , and  $Pr$  may be expressed in terms of the problem variables, as indeed they usually can be). For

obvious reasons the  $\overline{u'v'}$  and  $\overline{v'T'}$  correlations are often loosely termed the turbulent transport terms. Thus, it can be seen that in going from incompressible to compressible flow the least amount of additional information required is firstly, a knowledge of the relationship between the mean flow variables and the temperature correlation  $\overline{v'T'}$  and secondly, the effect, if any, of temperature on the relationship between the mean velocity field and turbulent shear stress  $-\overline{u'v'}$ . Proposed methods of predicting the compressible turbulent boundary layer can thus be assessed firstly on what basis this additional information on  $-\overline{u'v'}$  and  $\overline{v'T'}$  is introduced and secondly on what additional simplifications, if any, are used in order to obtain a solution to Eqs. (2), (3), and (7).

#### Outline of Approaches

In general, the static pressure distribution  $\overline{p_e(x)}$  is either supposed known a priori or calculable from an additional equation, such as the strong-interaction equation (see Crocco-Lees, Ref. 7). It follows, therefore, that as soon as the turbulent transport terms are related to the mean flow variables, Eqs. (2), (3), and (7), together with the equation of state form a closed set of coupled non-linear, usually parabolic, differential equations. This set of equations may be solved numerically by a number of finite-difference schemes and so the streamwise development of  $\overline{u}(y)$ ,  $\overline{p}(y)$ ,  $\overline{T}(y)$ , and  $\overline{\rho v}(y)$  computed. These numerical solutions can be refined to a high degree of accuracy so that from a practical (as opposed to mathematical) point of view the solutions so obtained are usually regarded as exact. As a result, provided the finite differencing procedures are adequate, this numerical approach can be criticized on two counts only, the first being the accuracy of the usual boundary layer approximations used to reduce the time averaged Navier-Stokes equations and the second being the nature of the specified turbulent transport mechanism. Both of these areas will be discussed in the subsequent work.

As an alternative to the computationally difficult task of numerically solving the partial differential equations of motion by means of a finite-difference procedure the so-called integral methods have been developed. In the integral methods, various moments of the partial differential equations are taken until the number of equations is equal to the number of parameters required to specify the profiles of velocity and temperature. Integration (i.e. averaging) of these partial differential equations across the boundary layer (using assumed temperature and velocity profile families) usually leads to a set of coupled quasi-linear ordinary differential equations which are easily integrated downstream to yield the streamwise distribution of the profile parameters, and hence the profiles themselves. The integration across the boundary layer reduces the sensitivity of the integral procedures to the precise form of the adopted profile families. However, it is apparent that, by assuming velocity and temperature profile families, integral procedures have gained an additional count on which they can be criticized.

In laminar flows the same problem of solving the compressible integral or partial differential equations of motion is greatly simplified by the introduction of a coordinate transformation which uncouples the thermal energy equation from the streamwise momentum equation. These compressibility transformations, as they are termed, effectively reduce the compressible boundary layer to an equivalent incompressible boundary layer which can then be solved by any appropriate procedure. The use of these transformations in laminar flow is a result of their mathematical convenience and at the present time their use is restricted to fluids which satisfy certain requirements on the relationship between the kinematic viscosity and temperature. A number of authors have tried to develop transformations for use in turbulent flows. The central difficulty encountered in this work is that the relationship between the compressible turbulence and the mean flow, which the transformation should retain, is in itself the subject of considerable research. Most authors to date have made an invariance hypothesis concerning some transformation scale and subsequently examined the resulting compressible turbulence-mean velocity relationship. Consequently, the transformation in turbulent flow has been used not as a mathematical convenience but as a device for generating information on compressible turbulence. This point will be developed subsequently but it can be appreciated that use of a compressibility transformation introduces two further possible problem areas, the first being concerned with the mathematical approximations used to obtain the transformation, and secondly the physical constraints introduced into the compressible turbulence-mean velocity relationship.

#### Some General Comments on the Various Approaches

##### Numerical Solutions of the Partial Differential Equations of Motion

On the basis of the previous remarks it will be appreciated that the numerical solutions to the boundary layer partial differential equations of motion are regarded as approximate only insofar as the specification of the turbulent transport mechanism is concerned. Several other points, however, ought to be taken into account. Firstly, the boundary layer approximations may not be valid in the flow situations under study and so the boundary layer equations of motion would in this instance provide a poor description of the flow. This objection would, of course, also apply to the integral procedures. Secondly, it is worth bearing in mind that the numerical scheme of solving the partial differential equations almost always involves representation of derivatives by finite differences. Consequently, the so-called exact solutions of the partial differential equations are in reality only solutions to the finite-difference equations. Unfortunately, in turbulent flow there are no good representative analytic solutions to the boundary layer equations which can be used to assess the various finite-difference schemes, although an estimate of the possible errors involved can be obtained by comparing the solution across a step to the

solution obtained from the momentum integral equation. As a result, speed and not computational accuracy has become almost the sole criterion on which the finite-difference procedures are judged in turbulent flows.

From the point of view of the user, the finite-difference procedures can be very temperamental. Slight changes in geometry or flow conditions can sometimes result in the calculation becoming unstable or quite inaccurate, thus requiring considerable effort on the part of the user to obtain a satisfactory computation. Lastly, both the computer execution time (generally of the order 1 minute per boundary layer) and the computer programming time (generally of the order 1 man year) may either be prohibitive or at best uneconomic on the basis of the desired information. However, there can be little doubt that the potential capability of handling the more complex problems and of changing the boundary conditions such that smooth or rough walls, wall suction or blowing etc. can be treated, makes a finite-difference procedure very attractive.

### Integral Procedures

Integral procedures for computing the compressible turbulent boundary layer fall conveniently into two classes, those which utilize a compressibility transformation and those which do not. In either event the resulting procedures are usually computationally rapid and, as has been pointed out by Reynolds (Ref. 5), require a less specific definition of the turbulence structure. Integral procedures which do not utilize a compressibility transformation require the specification of velocity, temperature and turbulent shear stress profile families. This is obviously a difficult task in compressible flow at the present time and consequently not much progress has been made in developing integral procedures of this type.

The majority of integral procedures developed to date have used a compressibility transformation and solve the resulting incompressible problem by some convenient integral procedure. As mentioned previously, the major problem in applying a compressibility transformation is the basic question of the applicability of such a transformation to the flow under consideration. Early transformations, such as that of Mager (Ref. 8), were subsequently criticized by Coles (Ref. 9) who, while not appearing overly enthusiastic about the transformation, did at least manage to generate a transformation which was formally rigorous and which upon introduction of a scaling parameter,  $\sigma$ , predicted the wall skin friction variation with Mach number and Reynolds number quite well. Coles' transformation was subsequently discussed in detail by Crocco (Ref. 10). However, Libby and Baronti (Ref. 11) noted that using Coles' transformation the predicted shape of the velocity profiles at high Mach number away from the wall did not agree with experiment. Later Clark (Ref. 12) substantiated Libby and Baronti's findings. In addition, Maise and McDonald (Ref. 13) have shown that predictions of the structure made using Coles' transformation could also be considerably in error at high supersonic Mach numbers. In summary, it does not seem that the presently available transformation can withstand a careful scrutiny. This does not preclude the possibility that an acceptable transformation can be developed and indeed it would appear that a simple two-layer transformation might remove many of the present objections to the transformation.

## The Various Structural Hypothesis

Any method of computing the turbulent boundary layer development must contain either an explicit or implicit description of the relationship between the mean velocity field and the turbulent apparent shear stress. In addition, when the flow is compressible or heat is being transferred to or from the fluid, the relationship of the mean velocity field to the turbulent temperature transport correlation coefficient must also be specified, again either explicitly or implicitly. In the numerical solutions to the partial differential equations the relationship between the mean velocity field and the turbulent stress correlations is usually stated explicitly. The limitations of these explicit relationships, such as 'eddy viscosity' or 'mixing length' and turbulent Prandtl number, are now quite well-known in incompressible flow and much current effort is being devoted to determining both the form and limitations of these formulations in compressible flow. The compressibility effect on certain formulations has been obtained from physical arguments (e.g., Bradshaw, Ref. 14), from comparisons between prediction and measurement (e.g., Herring, Ref. 15), from the compressibility transformation (e.g., Ting and Libby, Ref. 16) and in the equilibrium flat plate case, indirectly from experimental evidence (Maise and McDonald, Ref. 13). Certainly, neither the arguments nor the experimental evidence are, at present, conclusive, but on the basis of the available information the existing compressibility transformations would appear to yield the poorest quantitative predictions of the compressibility effects on the various stress-velocity formulations (Maise and McDonald, Ref. 13).

An additional feature of certain stress formulations is the absence, or otherwise, of a lag in the relationship between the mean velocity profile and the turbulent shear stress (the so-called upstream history effect). There can be little doubt that in certain near equilibrium incompressible boundary layers this effect is unimportant (AFOSR-IFP Conference, Ref. 5). The question arises, however, as to the importance of this historic effect in computing the more commonly encountered types of compressible turbulent boundary layers. Consequently, the present investigation sought to answer the question of how important the known failings of the compressible transformations are in making boundary layer predictions and in addition what discernible errors are introduced through the neglect of upstream history on the turbulence.

## The Available Prediction Methods

Methods of computing the compressible turbulent boundary layer available prior to 1965 have been discussed by Rotta (Ref. 3) and Hornung (Ref. 17). Noteworthy of these earlier methods is the fact that all are integral procedures. In the light of the Rotta-Thompson reviews (Refs. 1 and 2) it would be expected that extrapolations to compressible flow of certain incompressible procedures such as have been performed

by Spence (Ref. 18), Stratford and Beavers (Ref. 19), Waltz (Ref. 20), and Reshotko and Tucker (Ref. 21), would be unsatisfactory. The unsatisfactory extrapolation arises as a result of the inaccurate predictions of the basic incompressible procedure. The procedure of Reshotko and Tucker (Ref. 21) is typical of these early methods and was selected for use in the present comparison with experiment since, as well as being in wide spread use, this method has been the subject of considerable development, see for instance Sasman and Cresci (Ref. 22).

Following Thompson's review, however, it would be expected that an extrapolation to compressible flow of the method of Head (Ref. 4), such as has been performed by Standen (Ref. 23) and Stoddart (Ref. 24), using Mager's transformation, might be rewarding. Indeed, predictions obtained using Stoddart's (Ref. 24) application of the Mager transformation to Head's method were examined in some detail by the present author but found on average to be slightly inferior to a very simply modified version of the procedure of Reshotko-Tucker (Ref. 21). This modified version of Reshotko-Tucker is described in Ref. 25 and in adiabatic flow is conceptually identical to the modified procedure of Reshotko and Tucker previously described by Sasman and Cresci (Ref. 22). Since it is apparent the many similarly modified versions of the Reshotko-Tucker procedure are in wide spread industrial use, the modified version of the Reshotko-Tucker procedure described by Flaherty (Ref. 25) was selected for detailed comparison with experiment.

In recent times So (Ref. 26) and Camarata and McDonald (Ref. 27) have applied Coles' transformation to basically quite accurate incompressible procedures, the methods of Head (Ref. 4) and McDonald (see Ref. 5), respectively. The procedure of Camarata and McDonald (Ref. 27) was selected for use in the present study mainly because this procedure could take into account the effect of upstream history on the turbulence and consequently an estimate of the importance of this effect in compressible flow could be made using this particular procedure.

Since the Rotta-Hornung reviews (Refs. 3 and 17) four numerical procedures for computing the compressible turbulent boundary layer have been published, these being the procedures of Herring (Ref. 15), Spalding and Partankar (Ref. 28), Smith and Cebici (Ref. 29), and Bradshaw and Ferriss (Ref. 14). In the light of the performance of the numerical procedures in incompressible flow (Stanford Conf., Ref. 5) no large differences between the methods would be expected to show up, at least, when the methods are applied to predict the presently available experimental evidence\*. Consequently, for use in the present study a similar development to the Herring procedure (Ref. 15) evolved by Fish and McDonald (Ref. 30) was utilized. Although

---

\*(Assuming that a more reasonable compressible outer layer eddy viscosity relationship was used in the Smith-Cebici procedure - See for instance Maise and McDonald Ref. 13.)

the procedure described by Fish and McDonald (Ref. 30) contains an extended turbulence model as well as a number of numerical improvements, in the present study, the Herring eddy viscosity relationship was used. Thus, any differences which might arise between the predictions of the Herring procedure and the Fish-McDonald procedure can at this stage only be attributable to the differences in the numerical techniques employed.

Before going on to discuss the detailed comparisons with experiment it would seem worthwhile to mention, from a users point of view, a few findings concerning the selected procedures. Firstly, the integral procedures were all easily programmed and fast in execution. Starting the calculation was also generally quite simple. Only in a very few cases (not reported here) did any of the integral methods fail to give an answer. It was found that using the transformation of Coles (Ref. 9) as suggested by Crocco (Ref. 10) the predictions were very sensitive to the precise value of the  $\sigma/\eta$  ratio. This sensitivity was also predicted by Green (Ref. 31) and probably featured in So's (Ref. 26) method also. It turned out that the extreme sensitivity, indeed singular behavior, was a consequence of deriving the transformation scale  $\xi$  by simultaneously satisfying the energy and momentum equations at the wall using a laminar Prandtl number invariant under the transformation. The behavior of the resulting expression for the streamwise rate of change of the transformation scale ratio,  $\eta/\sigma$ , indicated that it was obviously impractical to try to satisfy the energy equation at the wall when there was no heat transfer or the Prandtl number was other than unity. In the version of the Coles transformation used in the present report, an alternative procedure was adopted and the  $\eta/\sigma$  scale assumed to be proportional to the static temperature. This assumption is certainly permissible in a zero pressure gradient flow and is used in the laminar flow transformation. Nearly identical predictions were obtained with  $\eta/\sigma$  set equal to a constant, indicating that the theory was not sensitive to these scales provided the singularity was avoided. It follows from the definition of the  $\eta/\sigma$  scale that the satisfaction of the energy equation only requires that the Prandtl number not be a transformation invariant. In addition, several of the suggested  $\sigma$ -scale relationships were tried and found to yield very similar predicted boundary layers, the definition of  $\sigma$  suggested by Libby and Baronti (Ref. 11) being used for the comparisons presented in this note.

Preliminary versions of the Fish-McDonald (Ref. 30) procedure which did not contain the numerical improvements referred to earlier and which was therefore very similar to the Herring procedure, proved to be troublesome to use in routine calculations. Upon introduction of a special starting routine and a novel finite-differencing procedure, this method became much easier to use but was still more troublesome than the integral procedures and on average about two orders slower. It must also be acknowledged that the user obtained almost one order more information from the numerical procedures, and in different circumstances, such as in performing calculations on aerofoil blades, this particular procedure even in unmodified form, performed well.

## THE COMPARISONS BETWEEN THEORY AND EXPERIMENT

### The Experimental Data

Before going on to examine the comparisons between theory and experiment, the available experimental information will be briefly mentioned. First of all, the broad rule was adopted that no experimental data would be considered in the present note if only one boundary layer property, such as skin friction or heat transfer, had been measured. The reasons for this ground rule were simply that any resulting comparisons could be greatly influenced by the choice of the unknown starting conditions for the other required variables and hence the comparisons could become quite meaningless. In addition, the role of fortuitous error cancellation cannot be assessed in boundary layers where only one of the predicted quantities is measured.

Perhaps one of the best sets of experimental information to date on compressible turbulent boundary layers has been reported by Winter, Smith, and Rotta (Ref. 32). In this particular study both the boundary layer velocity profiles and the skin friction were measured for six free-stream Mach numbers. The very large scale of the model used (5 feet) and the high Reynolds number achieved (10 million based on body length) make these results particularly noteworthy. Above about  $M_\infty = 1.4$  there seems to be a suggestion that the transition trip was not fully effective. No mention is made by the investigators concerning the strength of the normal pressure gradient, presumably ignored in reducing the data.

Another important experimental contribution to the study of compressible turbulent boundary layers has been reported by Michel (Ref. 33). Although Michel's measurements were made in a much smaller tunnel (typical boundary layer thicknesses of order 1 cm) Michel examined three very different types of pressure gradients and, probably most important of all, he attempted to measure the transverse static pressure distribution. Michel's three boundary layers were formed in one instance by inserting a concave wall designed to give a linearly decreasing Mach number. In another instance the boundary layer along the tunnel wall was disrupted by placing a 16 deg wedge on the wall and so formed a shock-wave boundary layer interaction. In the third instance, Michel arranged for a deceleration in Mach number by means of a concave-convex tunnel wall. No skin friction measurements were made for the flows in a pressure gradient.

In Ref. 34, McLafferty and Barber have reported a series of measurements, made in a fairly small wind tunnel, of supersonic turbulent boundary layers in a number of severe adverse pressure gradients. Typically McLafferty and Barber's boundary layers were less than 0.5 inches thick and were formed by placing circular arc ramps on varying radii of curvature into a Mach number 3.0 free stream. Large transverse static pressure variations were indicated in these tests. McLafferty and Barber did not measure skin friction in their tests.



More recently Kepler and O'Brien (Ref. 35) extended the investigation of McLafferty and Barber to higher Mach numbers ( $M_{\infty} = 6.0$ ) and also included the effect of heat transfer. Kepler and O'Brien's more detailed investigation was performed on a similar scale and on similar models to those used by McLafferty and Barber. Once again, very large transverse static pressure gradients were indicated and no skin friction measurements were made.

In a study of the flow over axisymmetric afterbodies at  $M_{\infty} = 2$ , Reid and Hastings (Ref. 36) made a number of boundary layer velocity profile surveys. These measurements were taken at quite high Reynolds number ( $2.7 \times 10^5$  per inch) and on quite a large model (typical model diameter 4 in). Only the parabolic afterbodies were sufficiently well detailed for use in the present study and for these bodies the pressure distribution was always favorable.

Seddon (Ref. 37) has measured a very interesting shock wave boundary layer interaction at transonic speed. In this case the boundary layer was typically less than 0.5 in. and once again the transverse static pressure gradient was not negligible. Seddon's boundary layer formed a local separation bubble and upon reattachment developed into an example of the relaxing boundary layers commented upon frequently at the Stanford Conference (Ref. 5). Green later made a much more extensive experimental investigation of this type of flow at supersonic speeds but as yet this information is not generally available, although it is cited in Ref. 31.

Finally, Pasiuk, et al., (Ref. 38) have made some measurements at a Mach number around 2 of the influence of heat transfer on the growth of a compressible turbulent boundary layer in a favorable pressure gradient. In these measurements the boundary layer thicknesses were generally less than 0.5 in. thick and the flow Reynolds number was moderate. Pasiuk, et al.'s., investigation was aimed primarily at obtaining heat transfer information and so details on the transverse static pressure gradient are lacking.

#### Comparison with Experiment

The comparisons between the theories and the experimental evidence are presented in Figs. 1 through 27. Care was taken to ensure that the input data to the various theories was as near identical as possible. Whenever possible the boundary layer momentum thickness and shape factor were matched at the starting point but in the Fish-McDonald (Ref. 30) procedure it was convenient and much less expensive to match only the momentum thickness closely and settle for an approximate match on the shape factor. In certain cases the measured boundary layers at the starting point were inconsistent with the theories. In the event of such inconsistency, the nearest consistent set of starting values were adopted. Identical measured pressure or Mach number distributions were used in performing the calculations, but at least two of

the theories, the modified mixing length - Coles' transformation procedure (Ref. 27) and the finite-difference procedure (Ref. 30), possessed smoothing and interpolating routines to enable a more uniform step size to be used. These smoothing and interpolating routines, although very convenient, did introduce small changes (evidently negligible) into the pressure distributions used. Due to computer time limitations, a number of cases did not proceed completely through the Fish-McDonald (Ref. 30) procedure. If only a small portion of the computation remained to be performed for these incomplete cases and nothing of significance was to be expected, then the cases were not rerun.

## DISCUSSION

It is evident from the comparisons between theory and experiment that the three more recent calculation procedures all perform in a very similar manner for the range of experimental flows measured to date. The same measured boundary layers are surprisingly well predicted by the three procedures, while certain other boundary layers are consistently erroneously predicted. Comparing the performance of the procedures it does not appear that either the compressibility transformation or historic effects on the turbulence are responsible for the observed discrepancies. Instead, it can be readily shown that the boundary layers which are poorly predicted do not satisfy the two-dimensional von Karman momentum integral equation, at least for any reasonable assumed value of the skin friction coefficient. In incompressible flow a disparity of this sort is usually attributed to the three-dimensionality of the experiment. However, in some of the poorly predicted boundary layers examined in the present study the correction to the two-dimensional von Karman momentum integral equation was very large indeed, much larger than was felt could reasonably be attributed to any three-dimensional effects. Doubtless such three-dimensional effects are present in the measurements but an additional possibility is that the normal stress terms, normally neglected in the von Karman equation, were appreciable in some of the flows under consideration. Again, it is difficult to imagine that the normal stress component could be sufficiently large to make up the suspected momentum equation deficit and indeed in some instances the normal stress component would seem to enhance the observed disparity. The remaining possibility is that normal pressure gradient effects were non-negligible and this point is now considered in detail.

The usual two-dimensional von Karman momentum integral equation is obtained by integrating Eq. (7). The corresponding momentum integral equation obtained from Eq. (1) neglecting only the normal stress terms can be written as

$$\frac{d\theta}{dx} + \frac{\theta}{u_e} \frac{du_e}{dx} \left( H + 2 + \frac{u_e}{\rho_e} \frac{d\rho_e}{du_e} \right) + \frac{1}{\rho_e u_e^2} \frac{d}{dx} \left\{ \rho_e \delta - \int_0^\delta \bar{p} dy \right\} = \frac{C_f}{2} \quad (8)$$

where

$$\theta = \int_0^\delta \frac{\bar{p} \bar{u}}{\rho_e u_e} \left( 1 - \frac{\bar{p} \bar{u}}{\rho_e u_e} \right) dy$$

$$H = \delta^* / \theta$$

and

$$\delta^* = \int_0^\delta \left( 1 - \frac{\bar{p} \bar{u}}{\rho_e u_e} \right) dy \quad (9)$$

It is noted that if  $p$  is independent of  $y$  Eq. (8) reduces to the conventional von Karman momentum integral equation. Also, in passing, if the free-stream flow is adiabatic then

$$\frac{u_e}{\rho_e} \frac{d\rho_e}{du_e} = -M_e^2 \quad (10)$$

where the subscript 'e' denotes the inviscid flow. If the outer inviscid flow is of the Prandtl-Meyer type then to the usual boundary layer approximation

$$\left( \frac{\partial p}{\partial x} \right)_e = - \frac{1}{\sqrt{M_e^2 - 1}} \left( \frac{\partial p}{\partial y} \right)_e \quad (11)$$

Using Eq. (11) as a guide it follows that, in supersonic flows, where  $(dp/dx)_e$  is large,  $(dp/dy)_e$  is also very large. Consequently, an appreciable contribution from the integral of  $p$  with respect to  $y$  term in the momentum integral equation can be generally anticipated in a pressure gradient. Michel (Ref. 33) was fully aware that his measured boundary layers could not satisfy the von Karman momentum equation with any reasonable assumed skin friction. In an effort to isolate the source of the discrepancy Michel measured the transverse static pressure variation in his boundary layers and found that the measured static pressure contribution could fully account for the disparity in the momentum equation. Michel's findings in the case of the linear Mach number deceleration are reproduced in Figs. 28 & 29. In the concave-

convex deceleration experiment, Michel noted that normal pressure gradients were not pronounced and suggested that this explained why no great discrepancy in the von Karman momentum equation was observed in this particular test.

From the foregoing it would seem reasonable to conclude that much of the responsibility for the inaccurate predictions can be attributed to the neglect of the static pressure variation normal to the wall. Insofar as taking this variation into account in making predictions of the boundary layer is concerned, once again Michel (Ref. 33) has pointed the way by demonstrating that the static pressure distribution normal to the wall can be estimated by computing the Mach waves emanating from the wall. This essentially inviscid approach for computing the static pressure distribution normal to the wall has been developed more recently (and at length) by Myring and Young (Ref. 39). Based on Michel's and Myring and Young's work it would seem that very reasonable approximate static pressure distribution can, in certain instances, be calculated. Once this static pressure distribution is known it is a straight forward matter to introduce it into the boundary layer equations. If, in addition, it can be ascertained that the turbulence per se is not also affected by the static pressure gradients normal to the wall then some confidence can be expressed in the eventual prediction capability of a boundary layer procedure of this type.

A slightly different approach to the problem of specifying the static pressure distribution normal to the wall has been adopted by McDonald and Shamroth (Ref. 40). In their approach, McDonald and Shamroth introduced a third order polynomial static pressure profile and satisfied four boundary conditions on the pressure; two at the wall and two at the outer inviscid edge. The resulting polynomial pressure profile was used in an integral procedure for computing the near wake development during reattachment. The results of this procedure show some promise for application to the boundary layer problem.

## CONCLUSIONS

1. The three most recent procedures of the four considered in the present note give very similar predictions for the experimental boundary layers. This finding must, however, be treated with caution, since only a very limited number of different types of boundary layers have been measured to date. In reattaching boundary layers, for instance, the indications are that this finding would have to be revised.

2. In severe adverse pressure gradients at supersonic speeds the predictions are usually in poor agreement with the measurements. In moderate pressure gradients the predictions are usually in quite fair agreement with the measurements.

3. While most of the measured boundary layers leave much to be desired it appears that the primary reason for the poor agreement between prediction and measurement in severe adverse pressure gradient flow lies in the neglect of the static pressure gradient normal to the wall in the theories. The indications are that an inviscid approach to calculating the normal static pressure gradient may be adequate. If this is found to be the case it would seem only a matter of time before the theories are corrected.

#### REFERENCES

1. Rotta, J. C.: Turbulent Boundary Layers in Incompressible Flow. Progress in Aeronautical Sciences, Vol. 2, Ed. A. Ferri, et al., Pergamon Press, 1962.
2. Thompson, B. G. J.: A Critical Review of Existing Methods of Calculating the Turbulent Boundary Layer. Aeronautical Research Council 26,109, 1964. Also, Ph.D. Thesis University of Cambridge, 1964.
3. Rotta, J. C.: Recent Developments in Calculation Methods for Turbulent Boundary Layers with Pressure Gradient and Heat Transfer. Journal of Applied Mechanics. Paper No. 66-APM-F, 1966.
4. Head, M. R.: Entrainment in the Turbulent Boundary Layer. Aeronautical Research Council R & M 3152, 1960.
5. Kline, S. J., D. G. Cockrell, and M. V. Morkovin: AFOSR-IFP, Stanford 1968 Conference on Turbulent Boundary Layer Prediction. Vol. I, 1968.
6. Schubauer, G. B., C. M. Tchen: Turbulent Flow. Vol. 5, Princeton Series on High Speed Aerodynamics, 1959.
7. Crocco, L. and L. Lees: A Mixing Theory for Interaction Between Dissipative Flows and Nearly Isentropic Streams. Journal of the Aeronautical Sciences, Vol. 19, No. 10, October 1952.
8. Mager, A.: Transformation of the Compressible Turbulent Boundary Layer. Journal of Aeronautical Sciences, 25, pp 305-3011, 1958.
9. Coles, D. E.: The Turbulent Boundary Layer in a Compressible Fluid. Physics of Fluids, pp 1403-1423, September 1964.

10. Crocco, L.: Transformation of the Compressible Turbulent Boundary Layer with Heat Exchange. AIAA Journal 1, pp 2723-2731, December 1963.
11. Baronti, P. O. and P. A. Libby: Velocity Profiles in Turbulent Compressible Boundary Layers. AIAA Journal 4, pp 193-202, February 1966.
12. Clark, D. R.: Boundary Layers in Hypersonic Flows. Ph.D. Thesis, Linacre College, Oxford, 1966.
13. Maise, G. and H. McDonald: Mixing Length and Kinematic Eddy Viscosity in a Compressible Boundary Layer. AIAA Journal 6, pp 73-80, January 1968.
14. Bradshaw, P. and D. H. Ferriss: Calculation of Boundary Layer Development Using the Turbulent Energy Equation. II Compressible Flow on Adiabatic Walls. National Physical Laboratory Report 1217, November 1966.
15. Herring, H. J.: On the Calculation of Compressible Turbulent Boundary Layers. Princeton University Ph.D. Thesis, 1966. See also, NASA-CR 1144, September 1968. (Co-author: G. L. Mellor).
16. Ting, L. and P. A. Libby: Remarks on the Eddy Viscosity in Compressible Mixing Flows. Journal of Aeronautical Sciences, Vol. 27, pp 797-798, 1960.
17. Hornung, H. G.: A Survey of Compressible Flow Boundary Layers - Theory and Experiment. Australian Aeronautical Research Committee Report ACA 67, February 1966.
18. Spence, D. A.: The Growth of Compressible Turbulent Boundary Layers on Isothermal and Adiabatic Wall. Royal Aircraft Establishment Report Aero. 2619. See also, R & M 3191, 1961.
19. Stratford, B. S. and G. S. Beavers: The Calculation of the Compressible Turbulent Boundary Layer in an Arbitrary Pressure Gradient - A Correlation of Certain Previous Methods. Aeronautical Research Council R. & M. No. 3207, 1959.
20. Waltz, A.: Compressible Turbulent Boundary Layers. Colloques Internationaux CNRS No. 108. Mechanique de la Turbulence, Marseille, pp 299-352, 1961.
21. Reshotko, E. and M. Tucker: Approximate Calculation of the Compressible Turbulent Boundary Layer with Heat Transfer and Arbitrary Pressure Gradient. NACA TN 4154, 1957.

22. Sasman, P. K. and R. J. Cresci: Compressible Turbulent Boundary Layer with Pressure Gradient and Heat Transfer. AIAA Journal 4, pp 19-25, January 1966.
23. Standen, N. M.: A Concept of Mass Entrainment Applied to Compressible Turbulent Boundary Layers in Adverse Pressure Gradients. Proceedings of the Fourth International Congress of the Aeronautical Sciences, pp 1101-1125, 1965.
24. Stoddart, J. A. P.: Unpublished Work, 1966.
25. Flaherty, R. J.: A Method for Estimating Turbulent Boundary Layers and Heat Transfer in an Arbitrary Pressure Gradient. United Aircraft Research Laboratories Report No. UAR-G51, August 1968.
26. So, R. M. C.: An Extension of a Turbulent Incompressible Boundary Layer Theory to Compressible Boundary Layers. McGill University Technical Note 65-6, December 1965.
27. Camarata, F. J. and H. McDonald: A Procedure for Predicting Characteristics of Compressible Turbulent Boundary Layers Which Includes the Treatment of Upstream History. United Aircraft Research Laboratories Report No. G212238-3, August 1968.
28. Spalding, D. B. and S. V. Patankar: Heat and Mass Transfer in Boundary Layers. Morgan-Grampian Books, Ltd., 1967.
29. Smith, A. M. O. and T. Cebici: Numerical Solution of the Turbulent Boundary Layer Equations. Douglas Aircraft Report No. DAC 33735, May 1967.
30. R. W. Fish and H. McDonald: Practical Calculations of Transitional Boundary Layers. United Aircraft Corporation Report UAR H48, March 1969.
31. Green, J. E.: The Prediction of Turbulent Boundary Layer Development in Compressible Flow. Journal of Fluid Mechanics, Vol. 31, part 4, pp 753-778, 1968.
32. Winter, K. G., K. G. Smith, and J. C. Rotta: Turbulent Boundary Layer Studies on a Waisted Body of Revolution in Subsonic and Supersonic Flow. AGARDograph 97, May 1965.
33. Michel, R.: Resultats sur la couche limite turbulente aux grandes vitesses. ONERA Publication 102, 1961.

34. McLafferty, G. H. and R. E. Barber: Turbulent Boundary Layer Characteristics in Supersonic Streams Having Adverse Pressure Gradients. United Aircraft Research Department R-1285-11, September 1959. See also, Journal of Aeronautical Sciences, Vol. 29, pp 1-10, 1962.
35. Kepler, C. E. and R. L. O'Brien: Supersonic Turbulent Boundary Layer Growth Over Cooled Walls in Adverse Pressure Gradients. ASD TDR 62-87, October 1962.
36. Reid, J. and R. C. Hastings: Experiments on the Axisymmetric Flow Over Afterbodies and Bases at  $M = 2.0$ . Royal Aircraft Establishment Report No. Aero. 2628, October 1959.
37. Seddon, J: Flow Produced by Interaction of a Turbulent Boundary Layer with a Normal Shock Wave of Sufficient Strength to Cause Separation. RAE Technical Memo Aero. 667, 1960. See also, R & M No. 3502.
38. Pasiuk, L., S. M. Hastings, and R. Chatham: Experimental Reynolds Analogy Factor for a Compressible Turbulent Boundary Layer with a Pressure Gradient. Naval Ordnance Laboratory Report NOLTR 64-200, November 1964.
39. Myring, D. F. and A. D. Young: The Isobars in Boundary Layers at Supersonic Speeds. The Aeronautical Quarterly, Vol. 19, May 1968.
40. McDonald, H. and S. J. Shamroth: A New Solution to the Near Wake Problem. United Aircraft Research Laboratories Report G212237-2, September 1968.



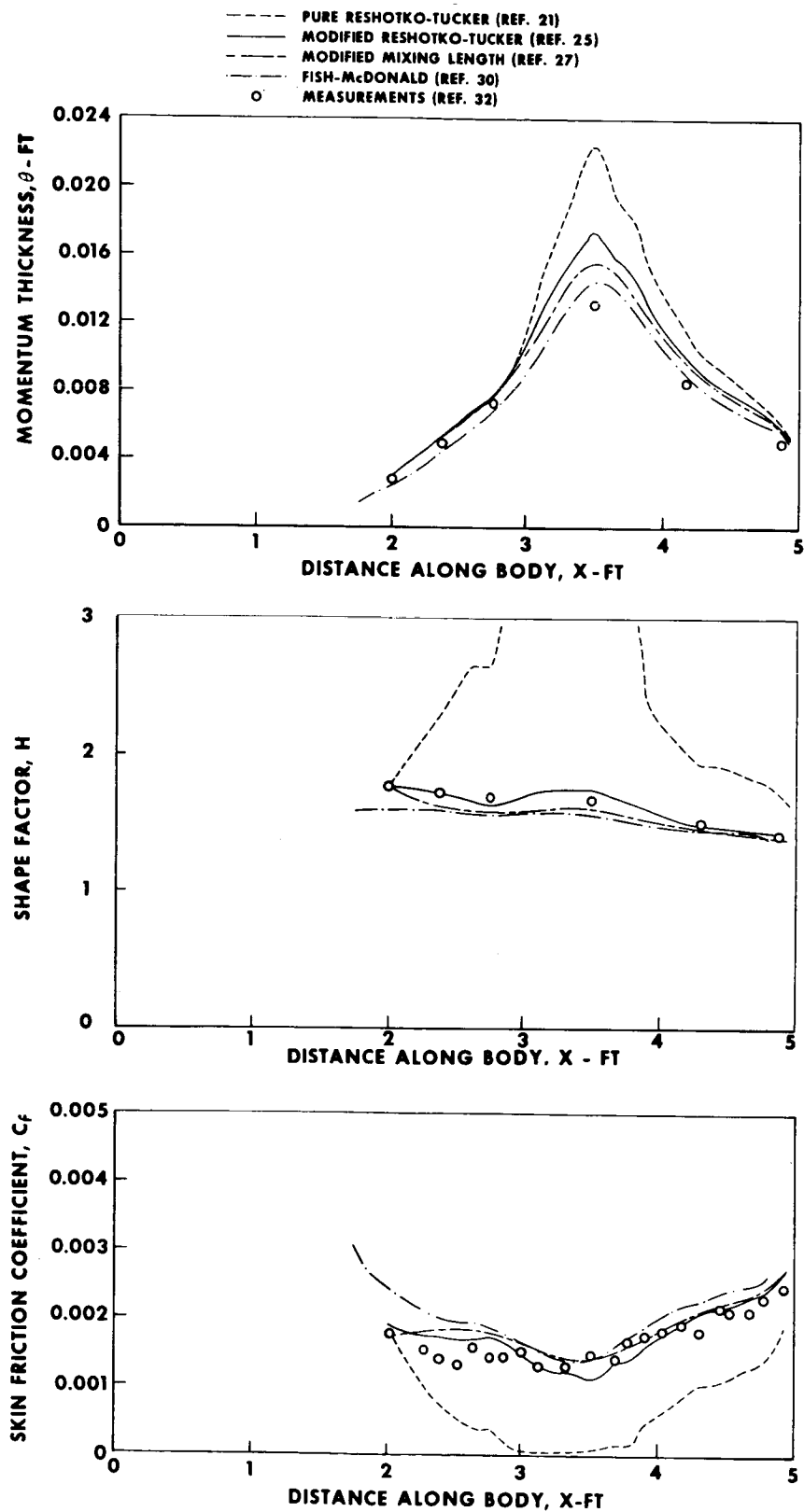


Figure 1.- Comparison between theories and measurements of Winter et al. (ref. 32) at  $M_\infty = 0.6$ .

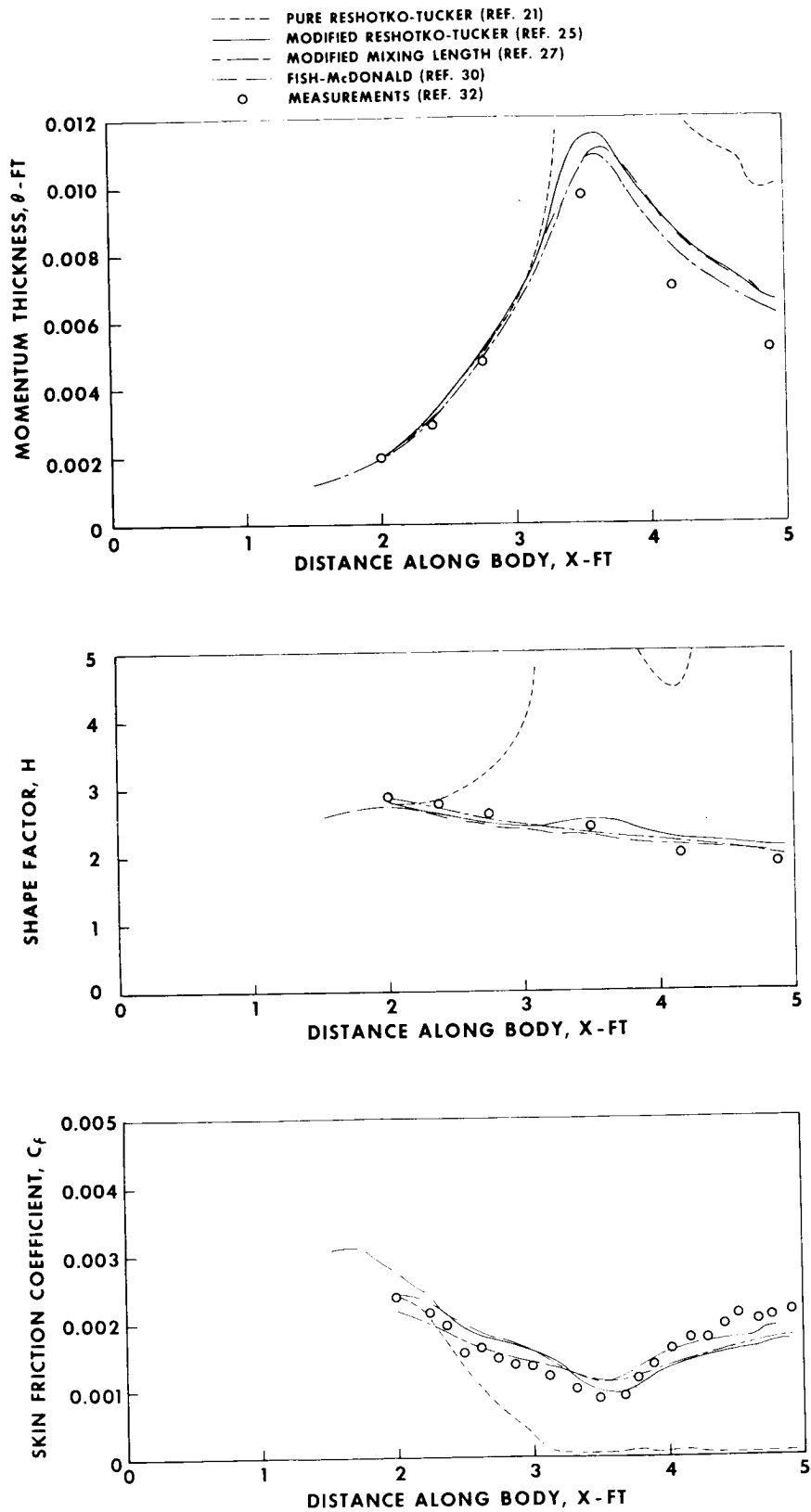


Figure 2.- Comparison between theories and measurements of Winter et al. (ref. 32) at  $M_\infty = 1.4$ .

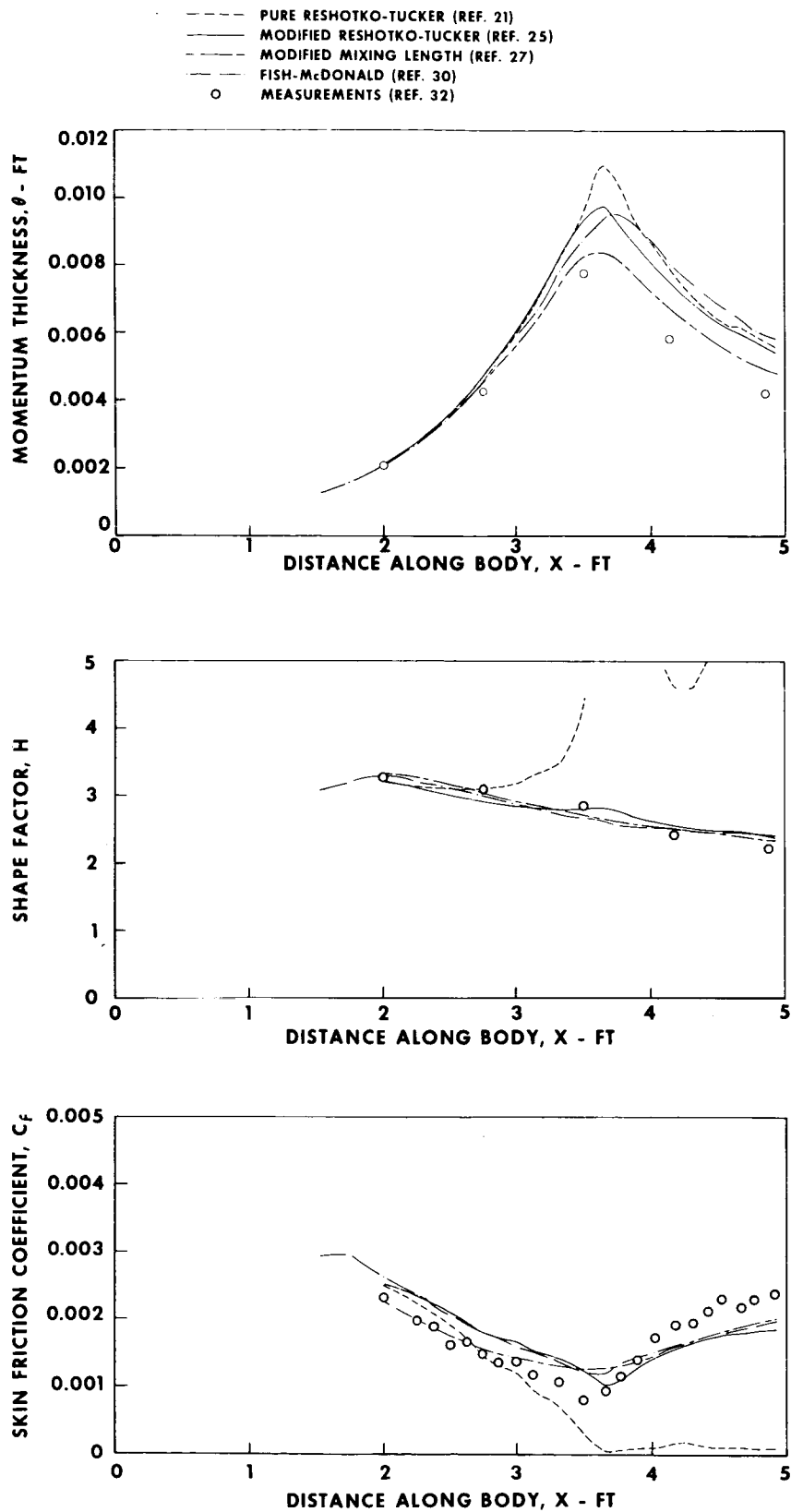


Figure 3.- Comparison between theories and measurements of Winter et al. (ref. 32) at  $M_\infty = 1.7$ .

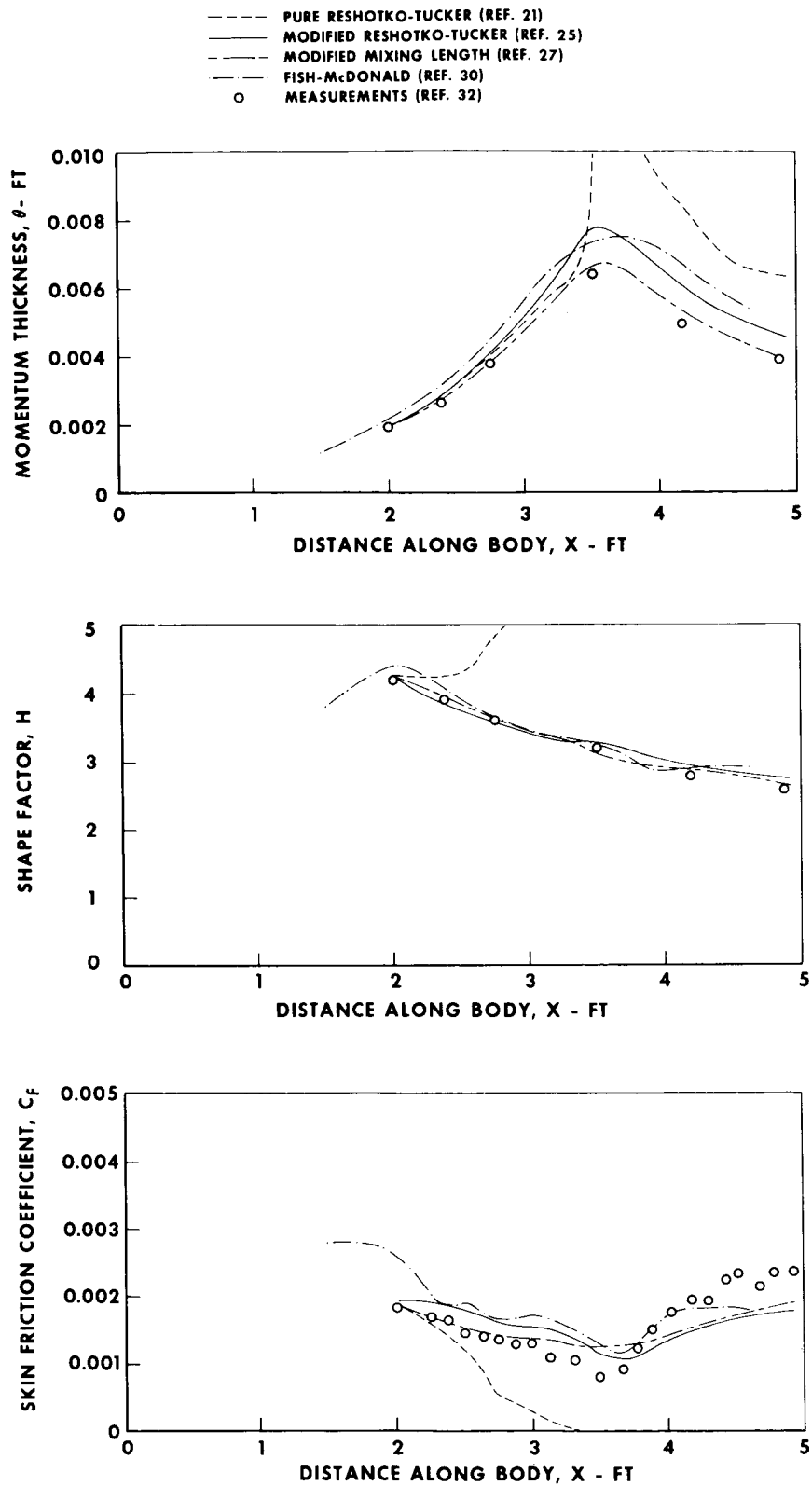


Figure 4.- Comparison between theories and measurements of Winter et al. (ref. 32) at  $M_\infty = 2.0$ .

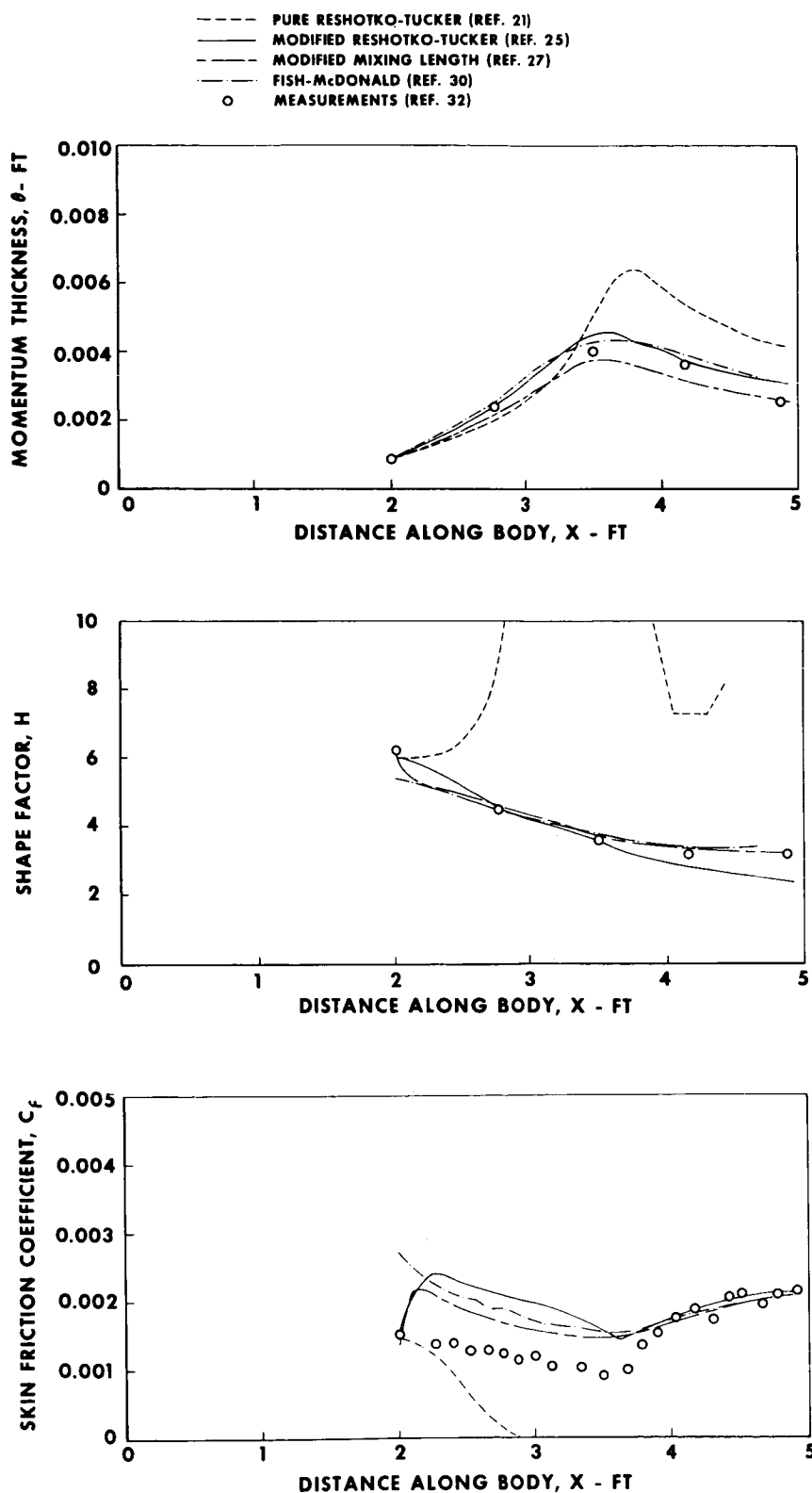


Figure 5.- Comparison between theories and measurements of Winter et al. (ref. 32) at  $M_\infty = 2.4$ .

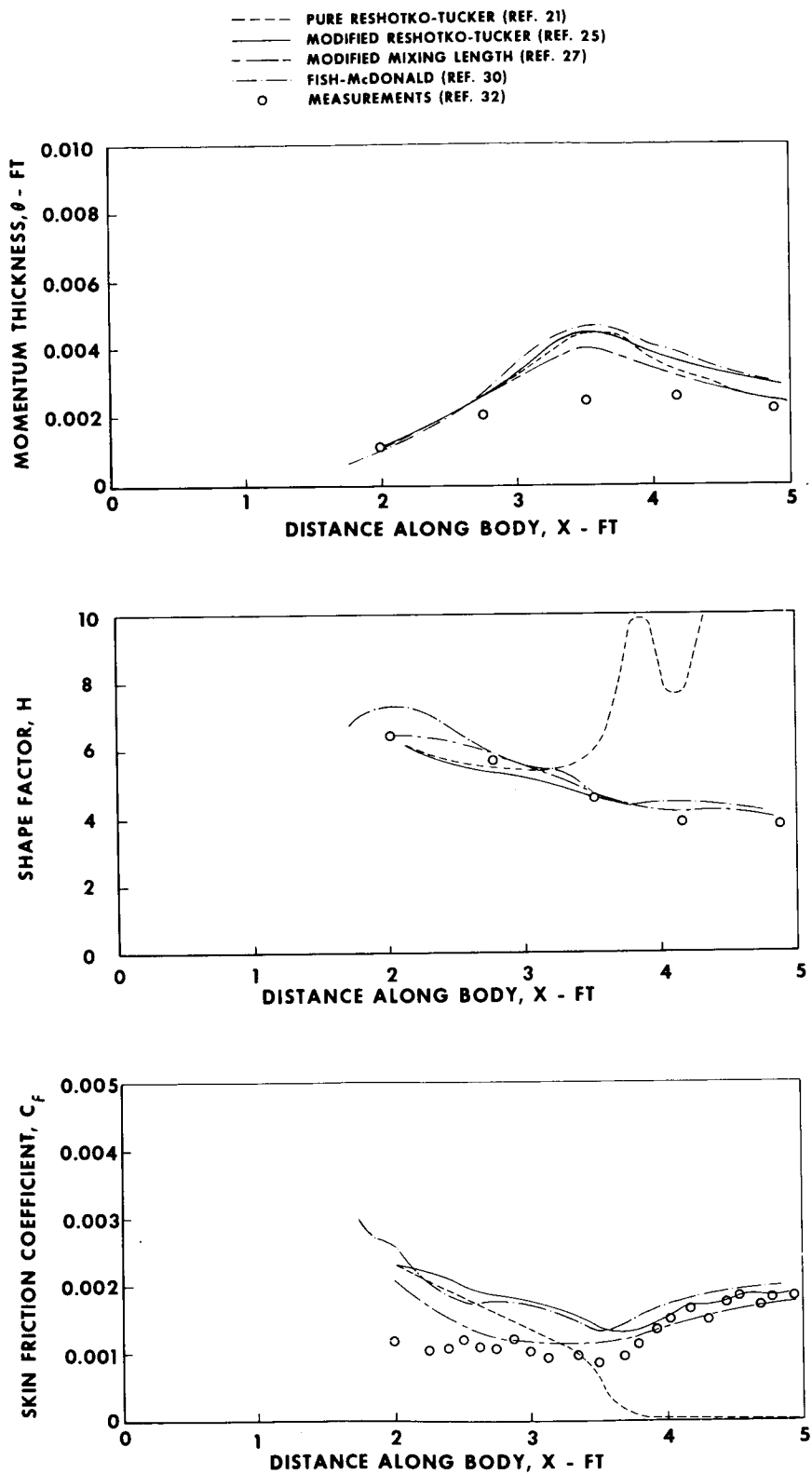


Figure 6.- Comparison between theories and measurements of Winter et al. (ref. 32) at  $M_\infty = 2.8$ .

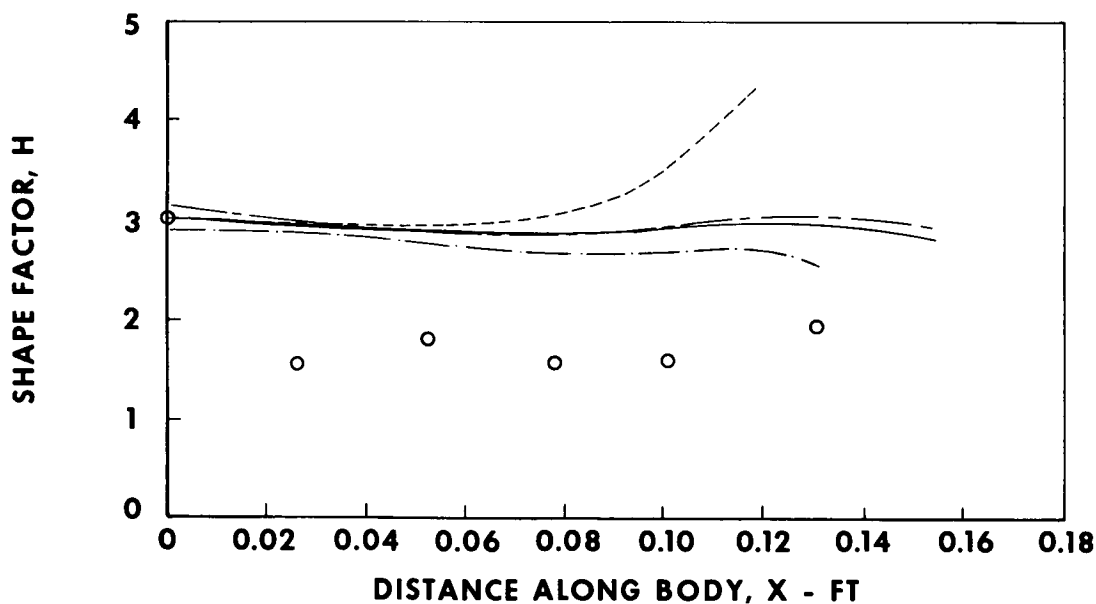
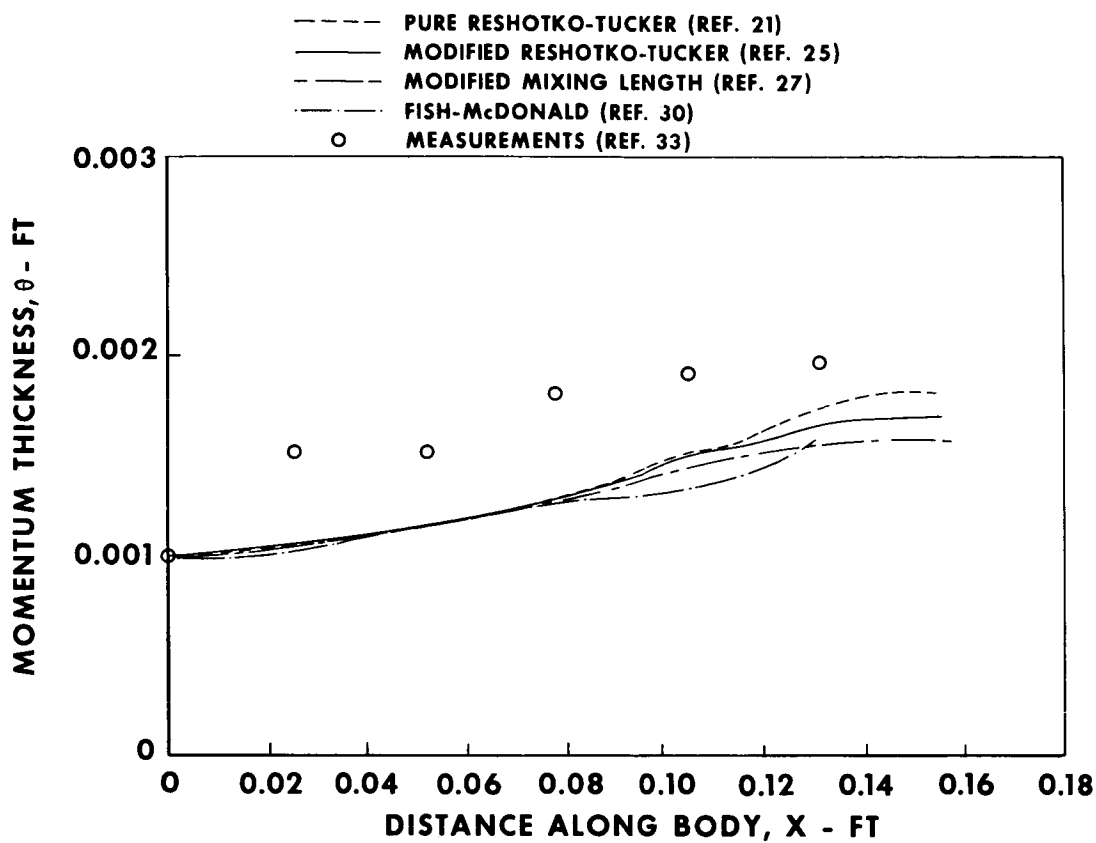


Figure 7.- Comparison between theories and measurements of Michel (ref. 33) linear adverse gradient,  $M_\infty \approx 2.0$ .

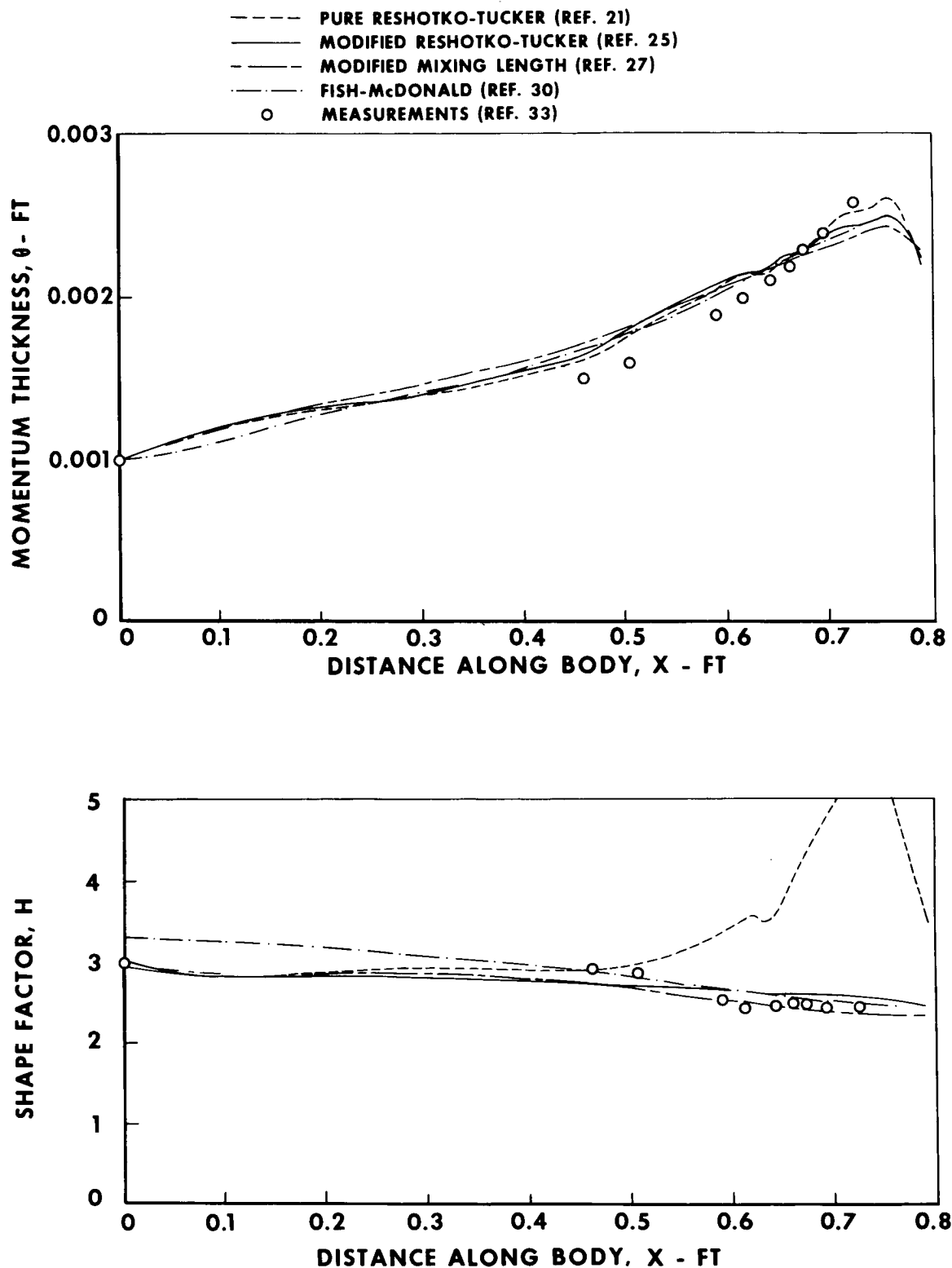


Figure 8.- Comparison between theories and measurements of Michel (ref. 33) convex adverse gradient,  $M_\infty \approx 2.0$ .



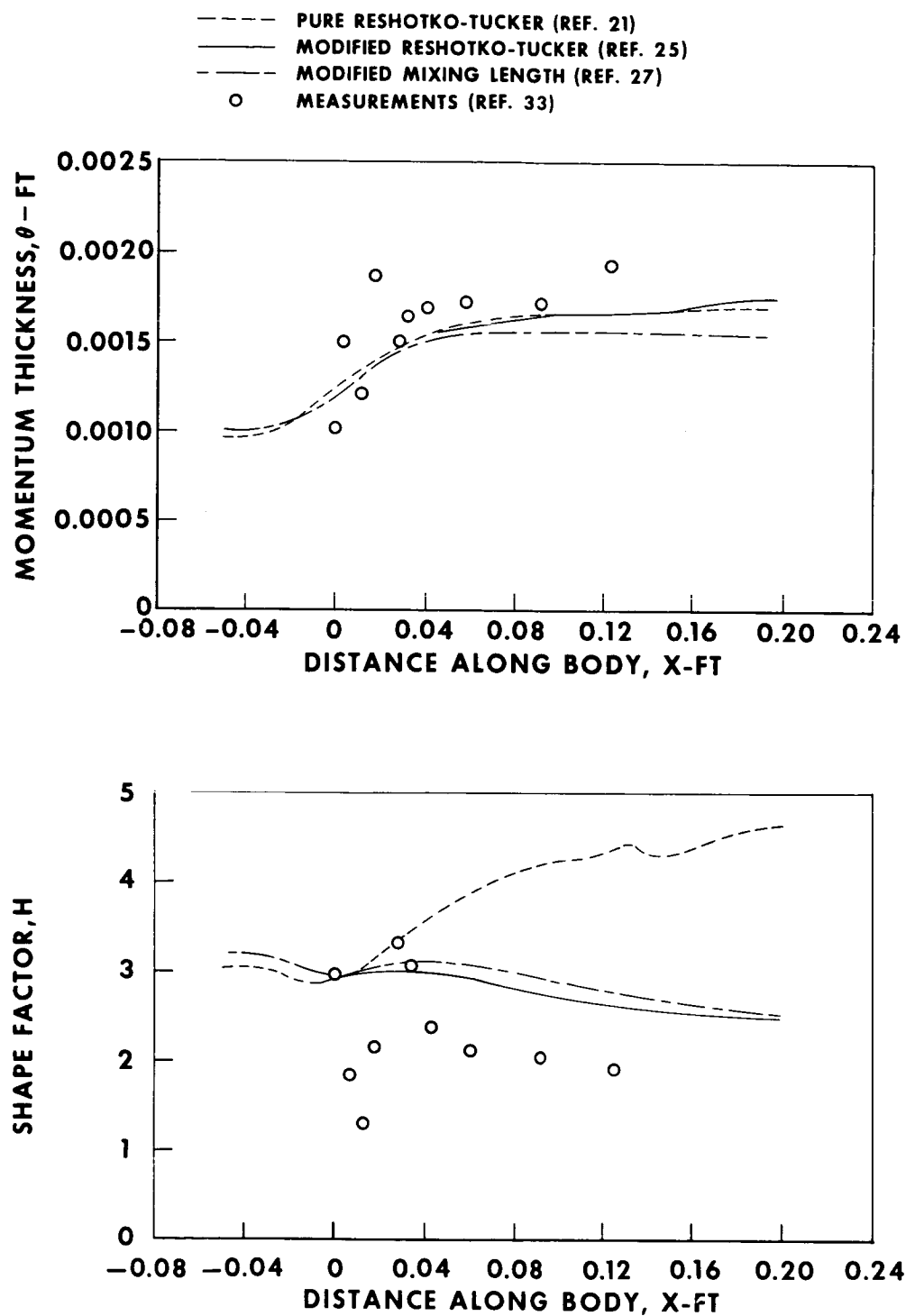


Figure 9.- Comparison between theories and measurements of Michel (ref. 33) shock adverse gradient,  $M_\infty \approx 2.0$ .

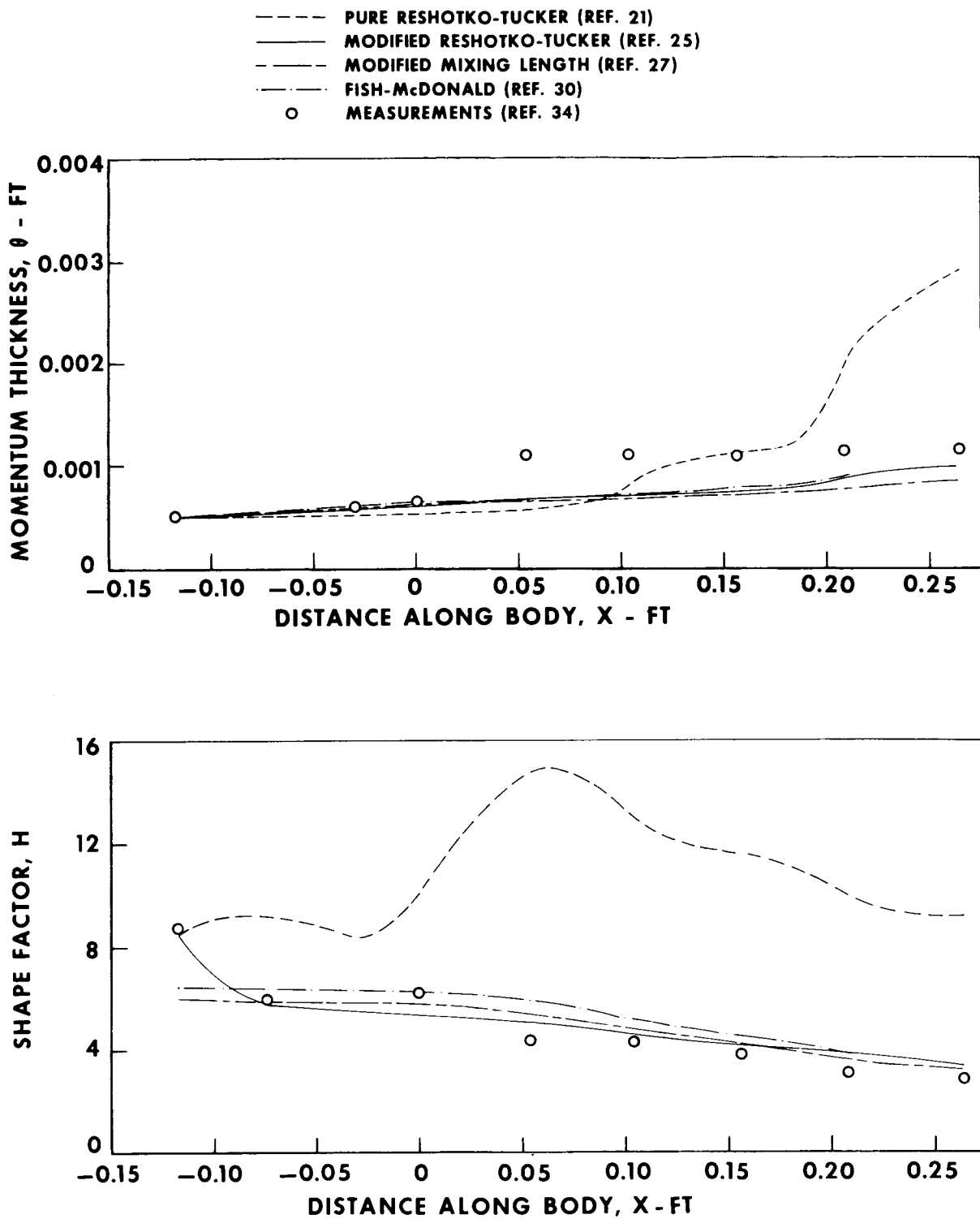


Figure 10.- Comparison between theories and measurements of McLafferty and Barber (ref. 34) for curved surface -  $1R(A)$ ,  $M_\infty \approx 3.0$ .

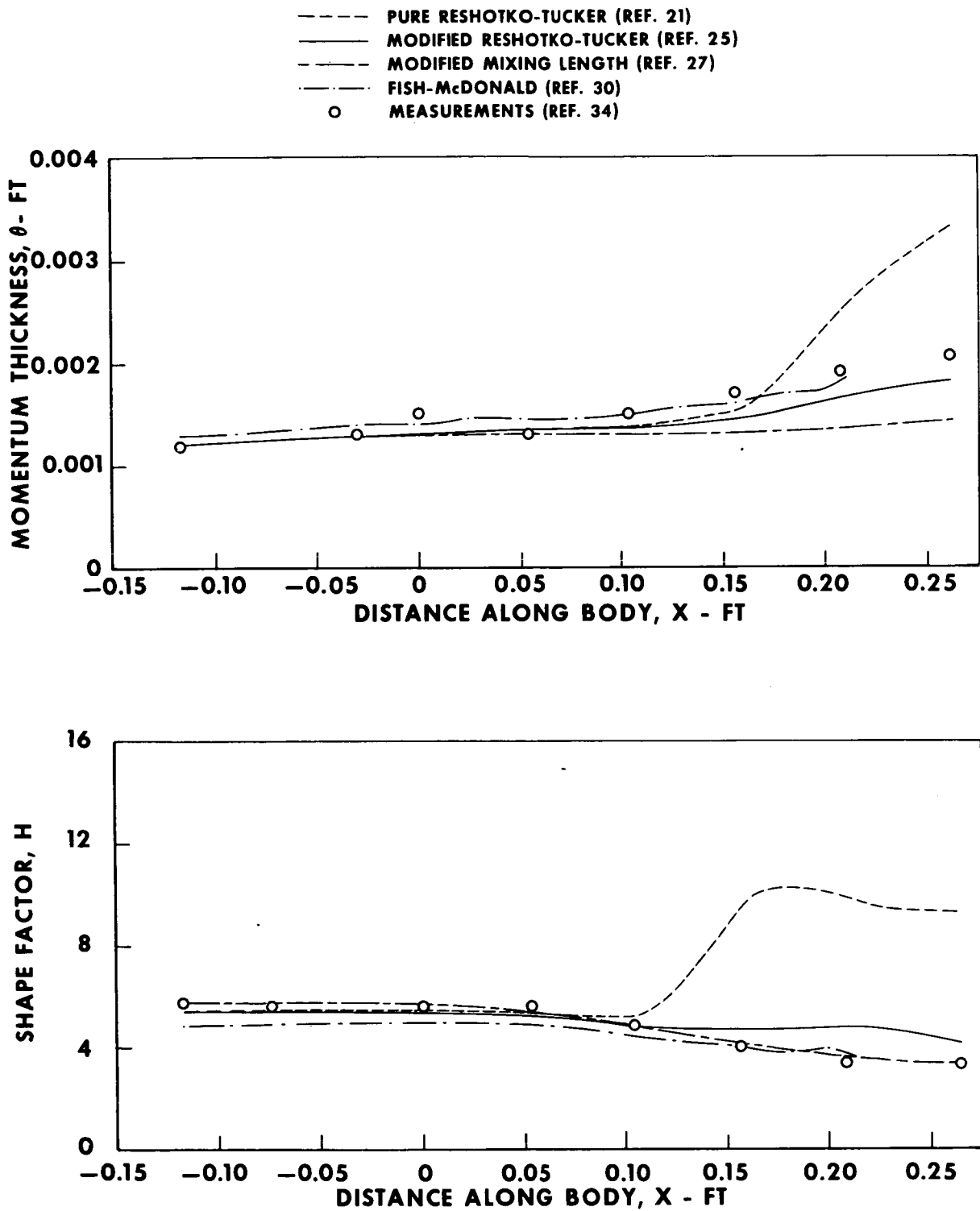


Figure 11.- Comparison between theories and measurements of McLafferty and Barber (ref. 34) for curved surface -  $1R(B)$ ,  $M_\infty \approx 3.0$ .

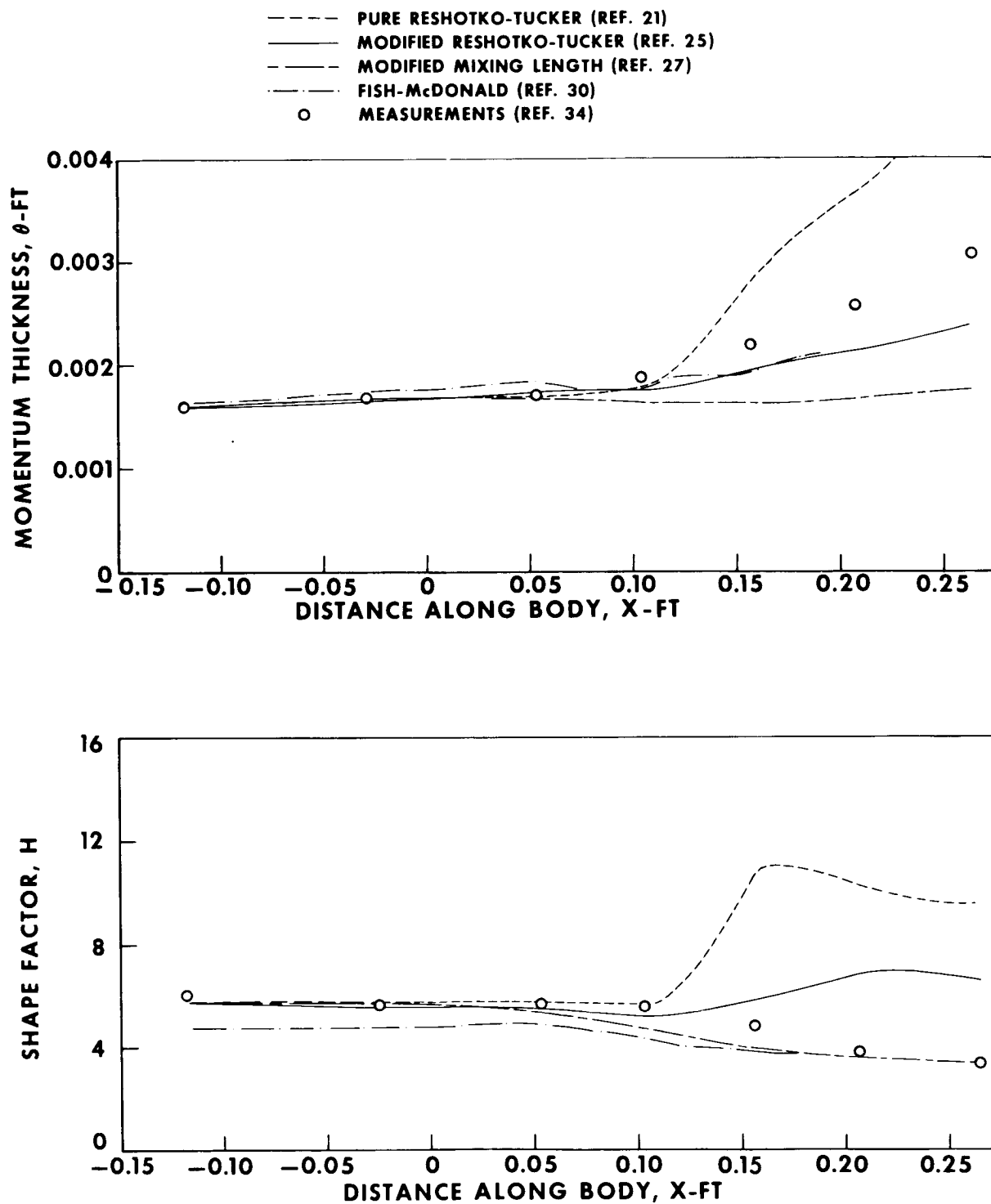


Figure 12.- Comparison between theories and measurements of McLafferty and Barber (ref. 34) for curved surface -  $1R(C)$ ,  $M_\infty \approx 3.0$ .

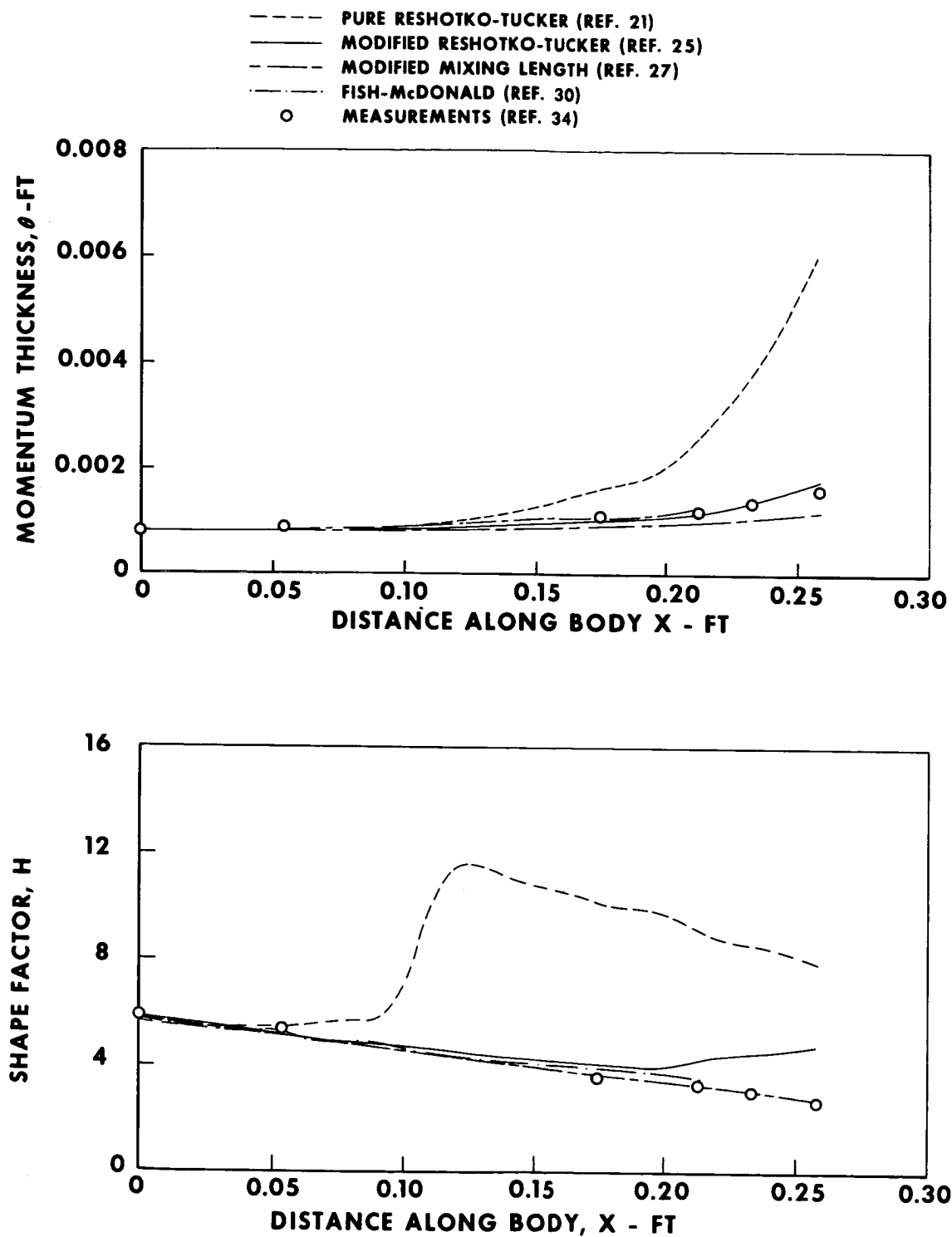


Figure 13.- Comparison between theories and measurements of McLafferty and Barber (ref. 34) for curved surface -  $2R(D)$ ,  $M_\infty \approx 3.0$ .

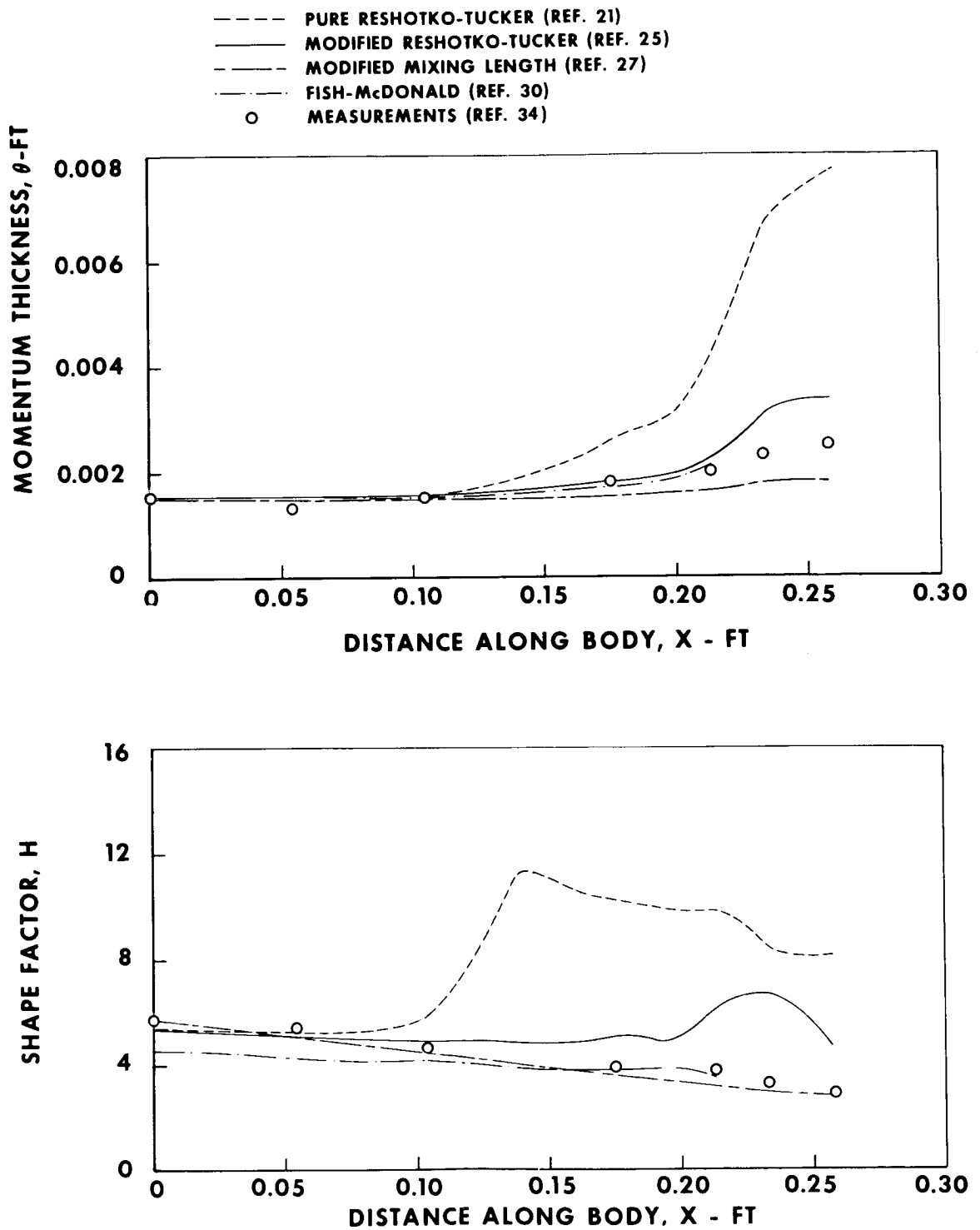


Figure 14.- Comparison between theories and measurements of McLafferty and Barber (ref. 34) for curved surface -  $2R(E)$ ,  $M_\infty \approx 3.0$ .

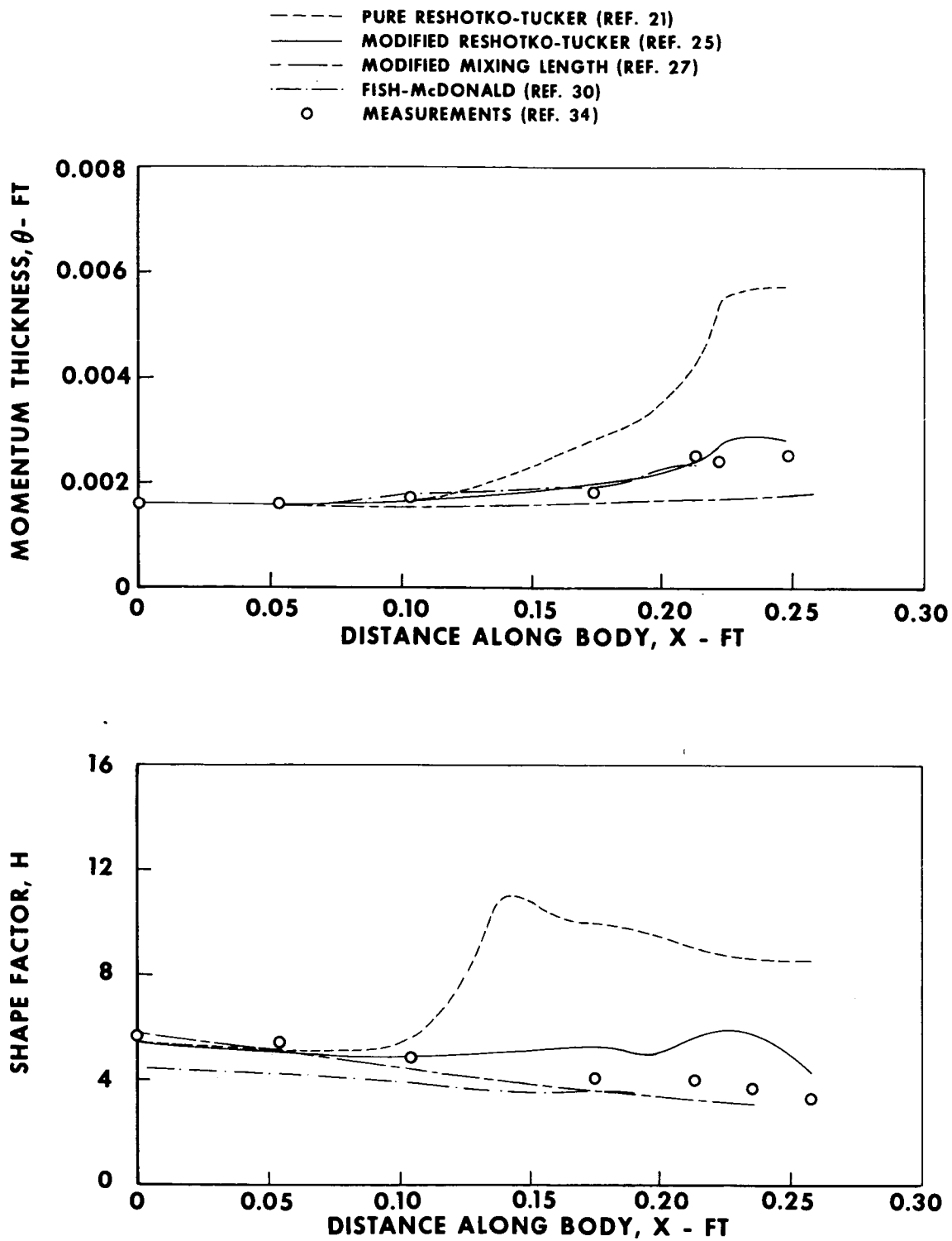


Figure 15.- Comparison between theories and measurements of McLafferty and Barber (ref. 34) for curved surface -  $2R(F)$ ,  $M_\infty \approx 3.0$ .

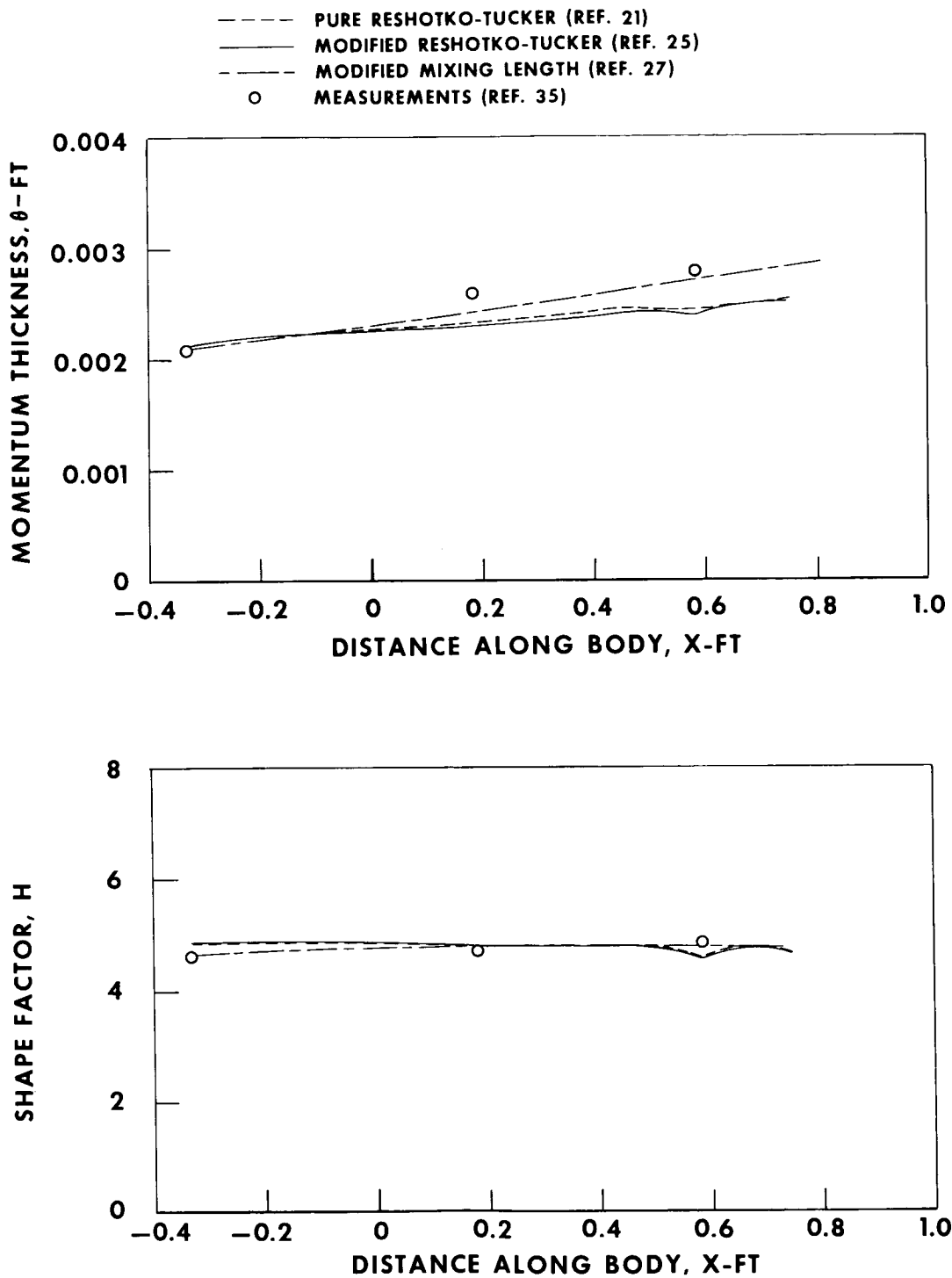


Figure 16.- Comparison between theories and measurements of Kepler and O'Brien (ref. 35) for flat plate, zero heat transfer,  $M_\infty \approx 3.0$ .



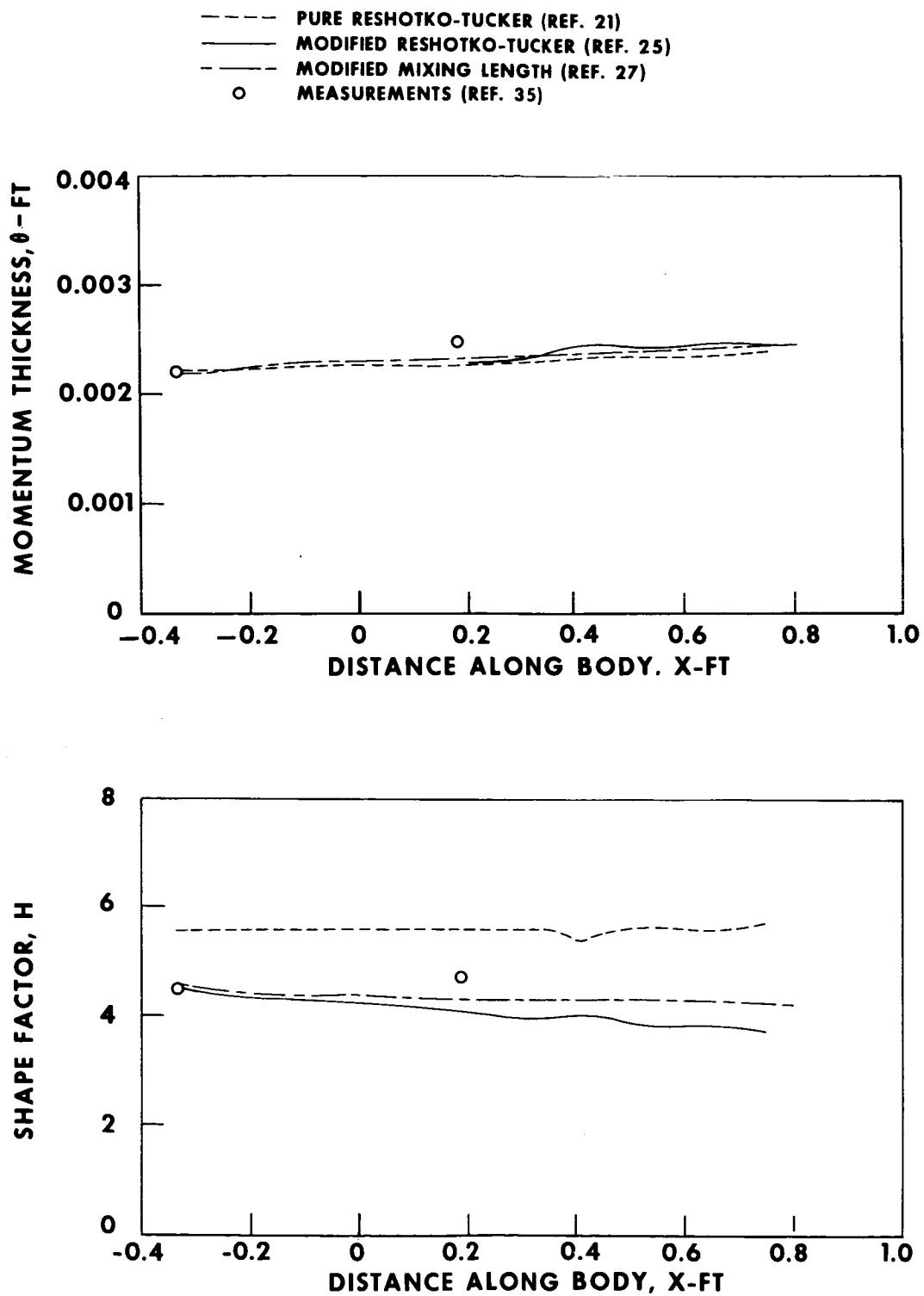


Figure 17.- Comparison between theories and measurements of Kepler and O'Brien (ref. 35) for flat plate, high heat transfer,  $M_\infty \approx 3.0$ .

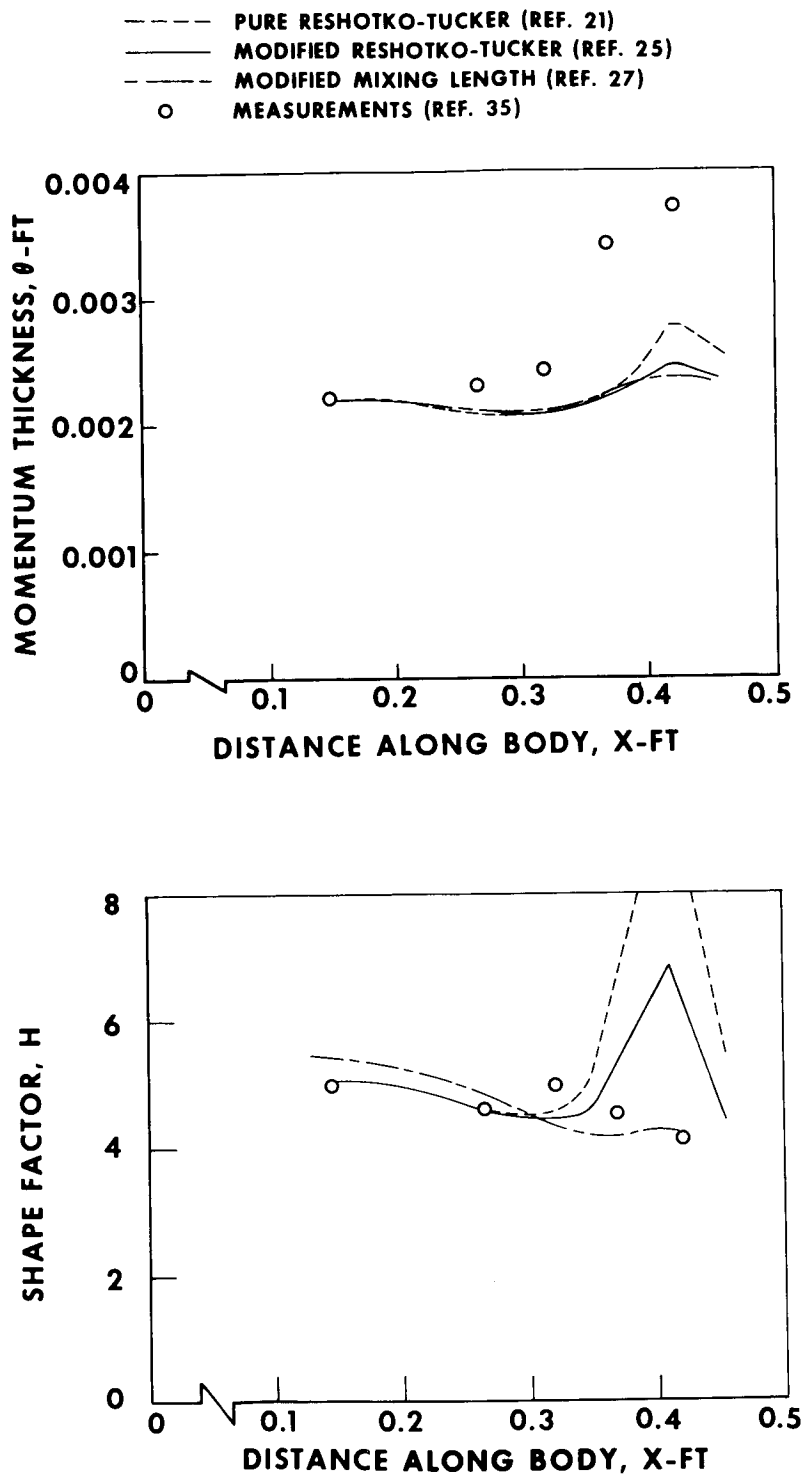


Figure 18.- Comparison between theories and measurements of Kepler and O'Brien (ref. 35) for curved surface, zero heat transfer,  $M_\infty \approx 3.0$ .

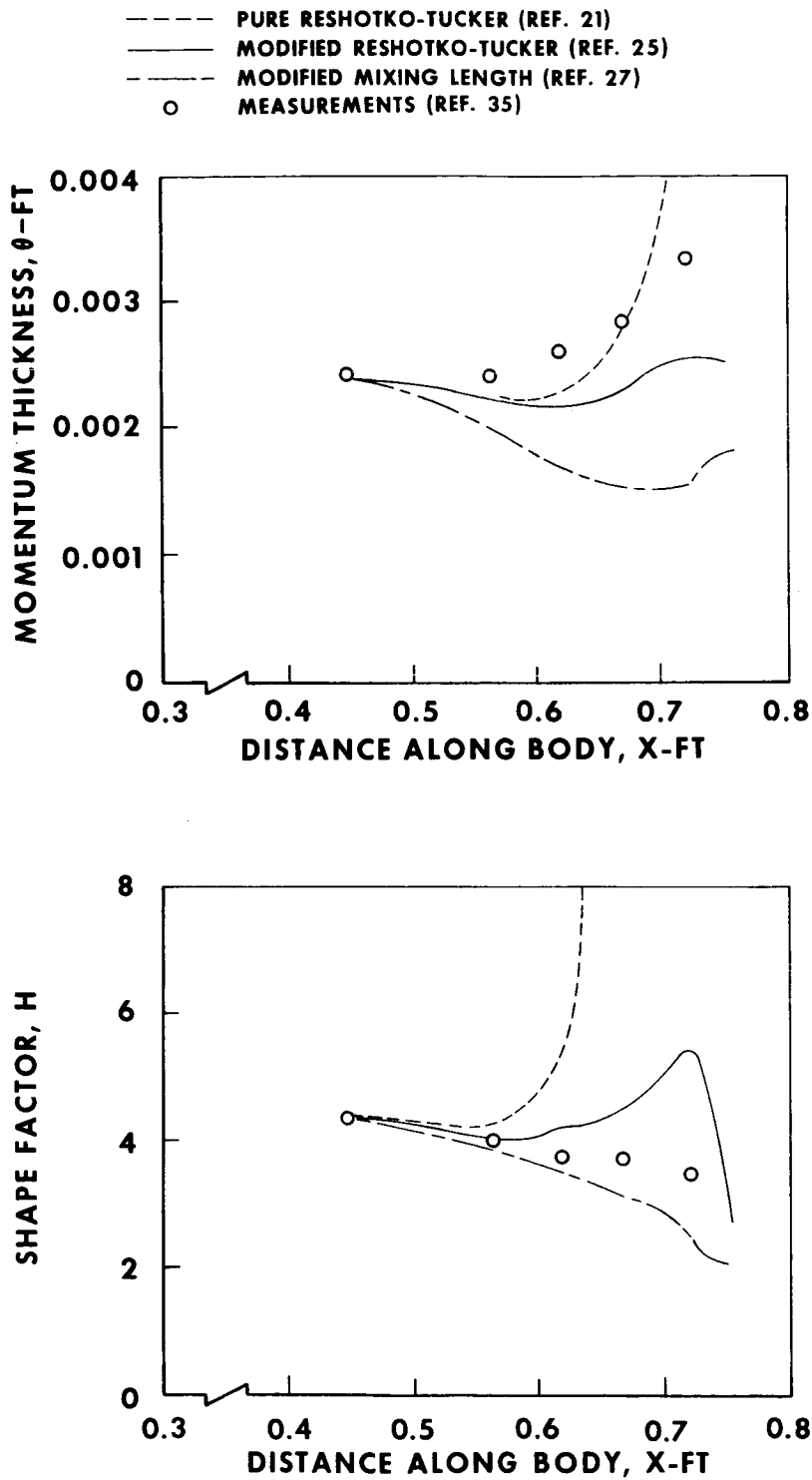


Figure 19.- Comparison between theories and measurements of Kepler and O'Brien (ref. 35) for curved surface, high heat transfer,  $M_\infty \approx 3.0$ .

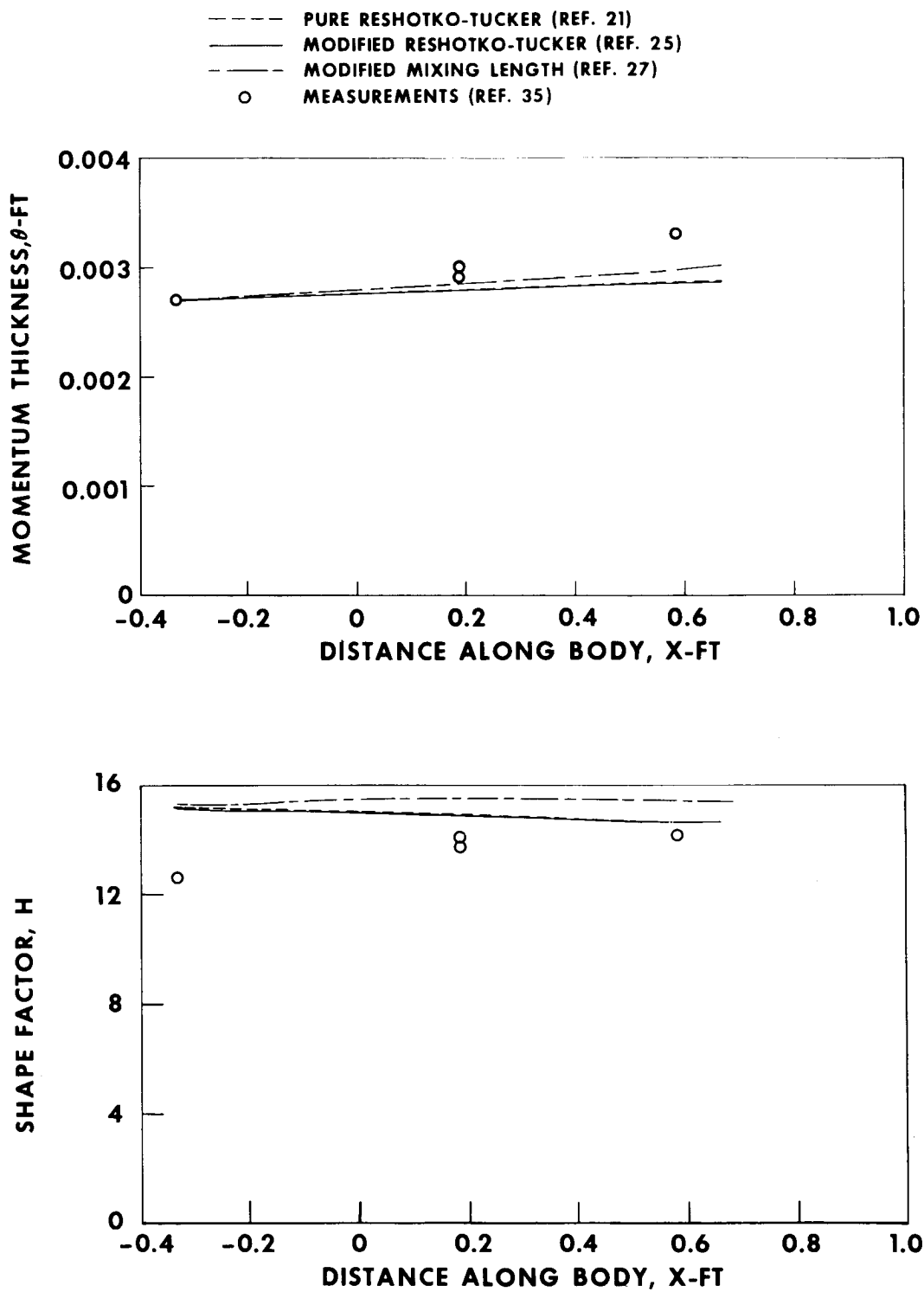


Figure 20.- Comparison between theories and measurements of Kepler and O'Brien (ref. 35) for flat plate, zero heat transfer,  $M_\infty \approx 6.0$ .

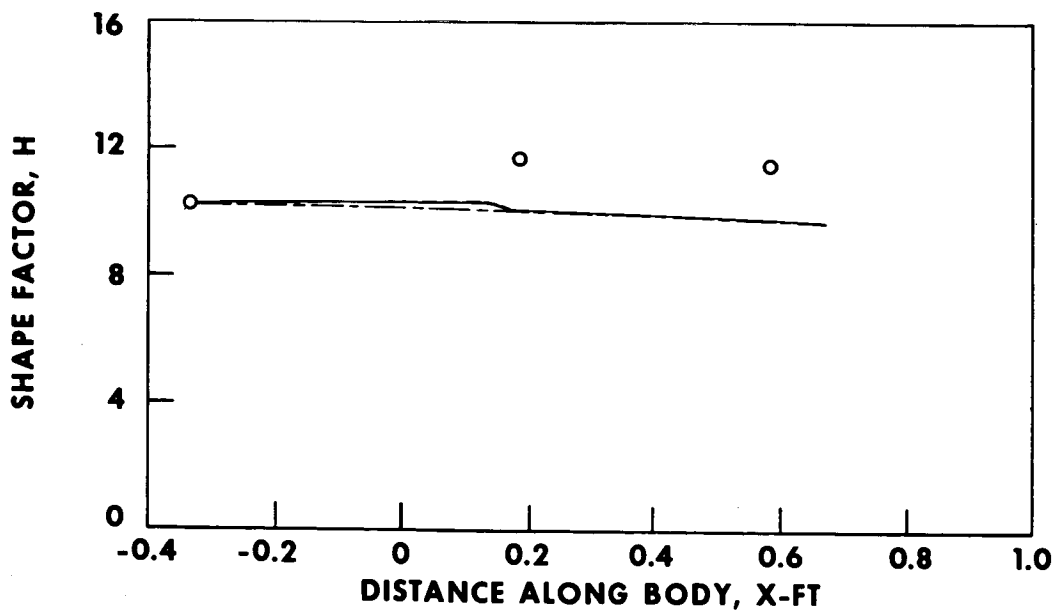
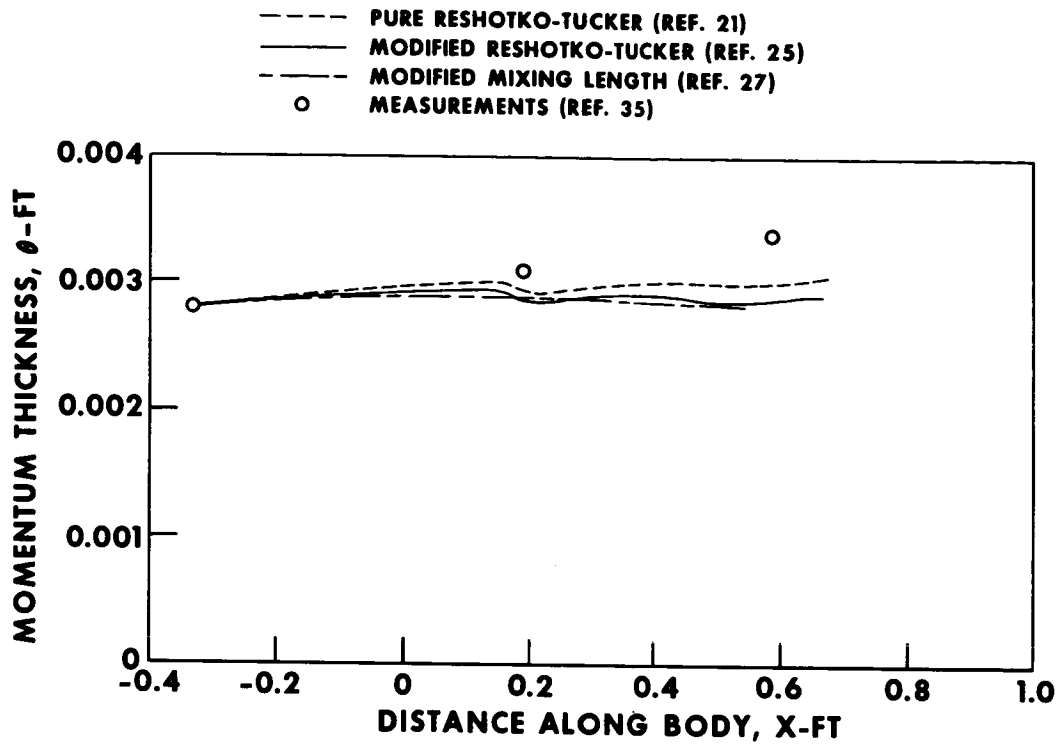


Figure 21.- Comparison between theories and measurements of Kepler and O'Brien (ref. 35) for flat plate, high heat transfer,  $M_\infty \approx 6.0$ .

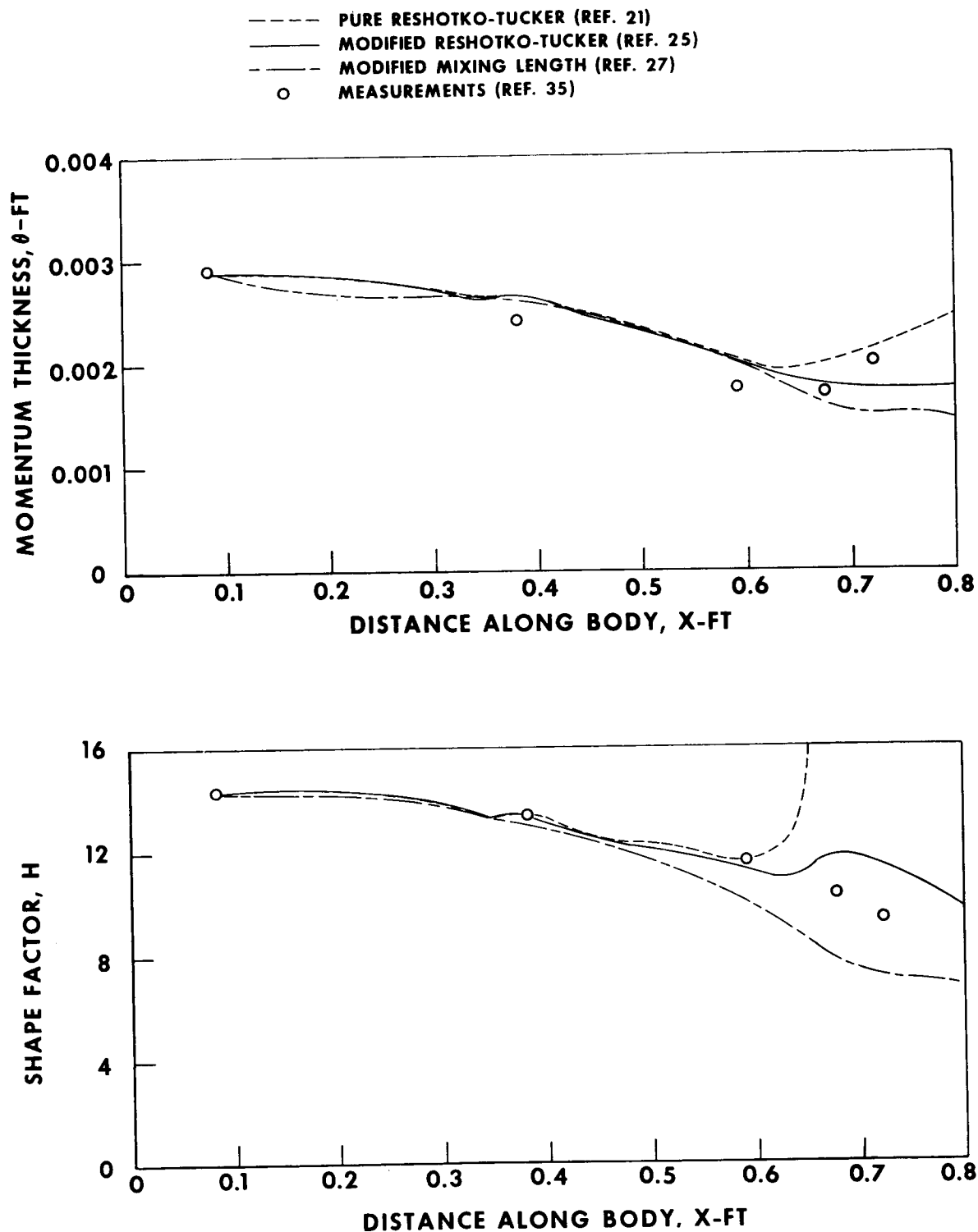


Figure 22.- Comparison between theories and measurements of Kepler and O'Brien (ref. 35) for curved surface, zero heat transfer,  $M_\infty \approx 6.0$ .

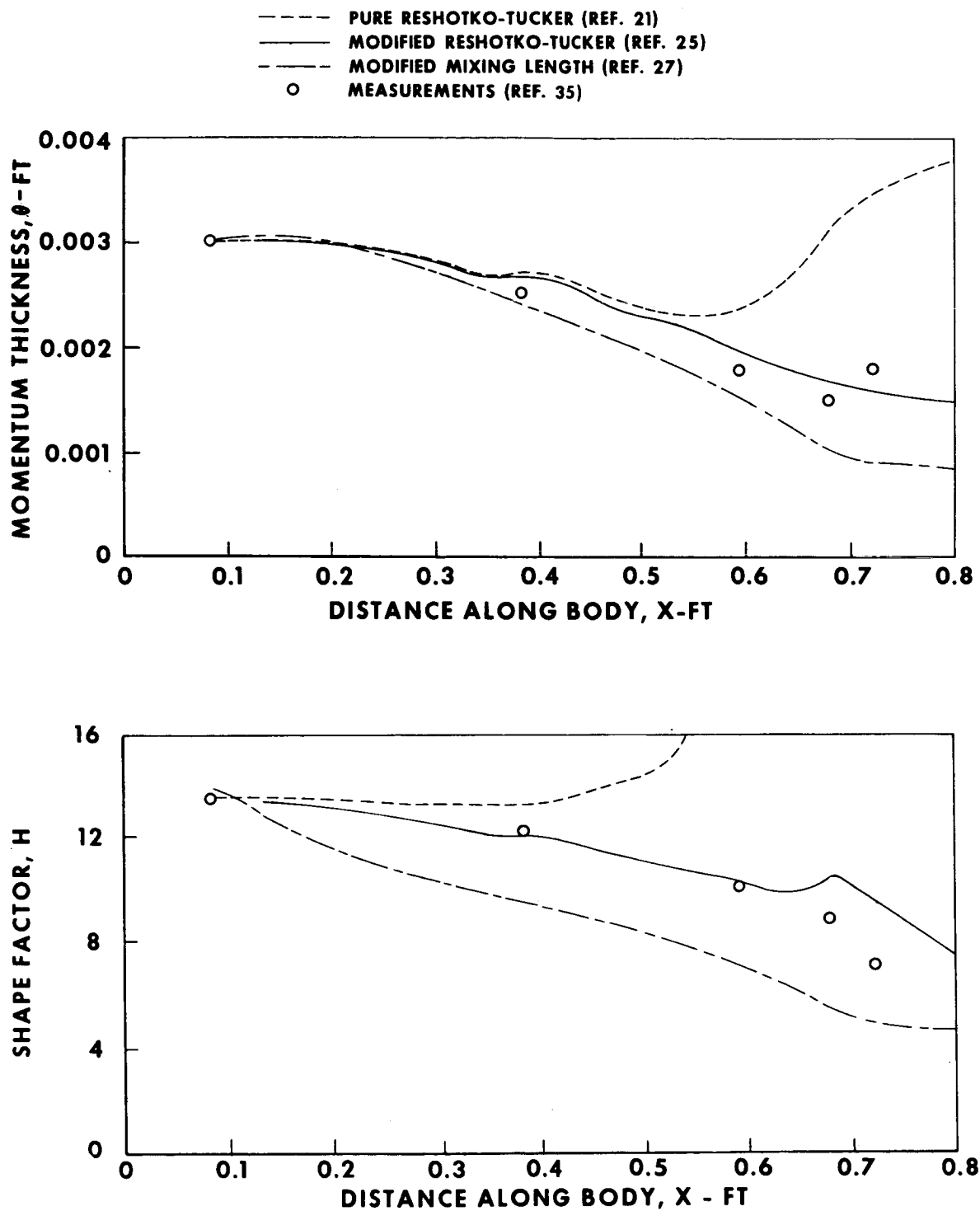


Figure 23.- Comparison between theories and measurements of Kepler and O'Brien (ref. 35) for curved surface, high heat transfer,  $M_\infty \approx 6.0$ .

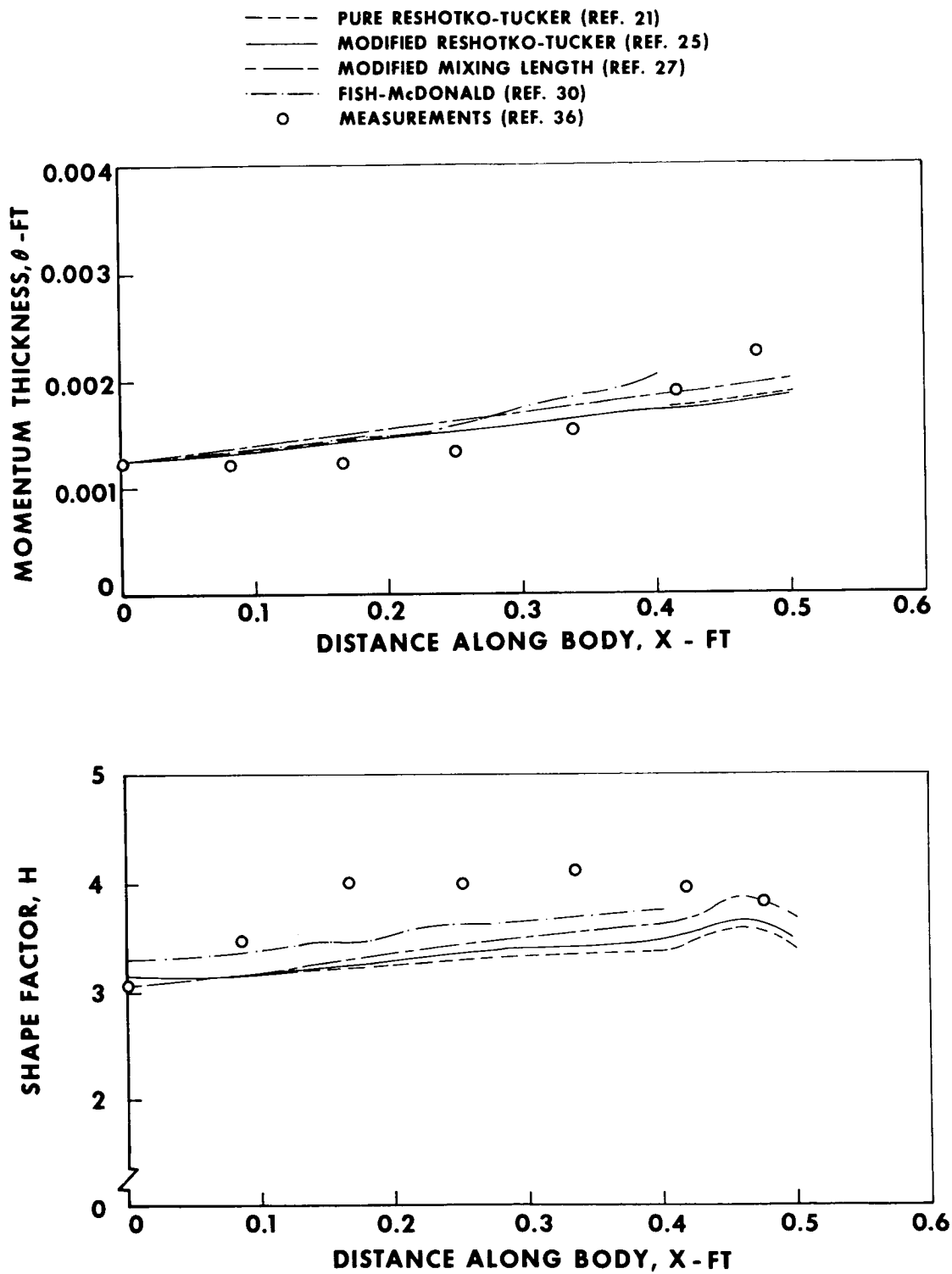


Figure 24.- Comparison between theories and measurements of Reid's (ref. 36) for parabolic afterbody.



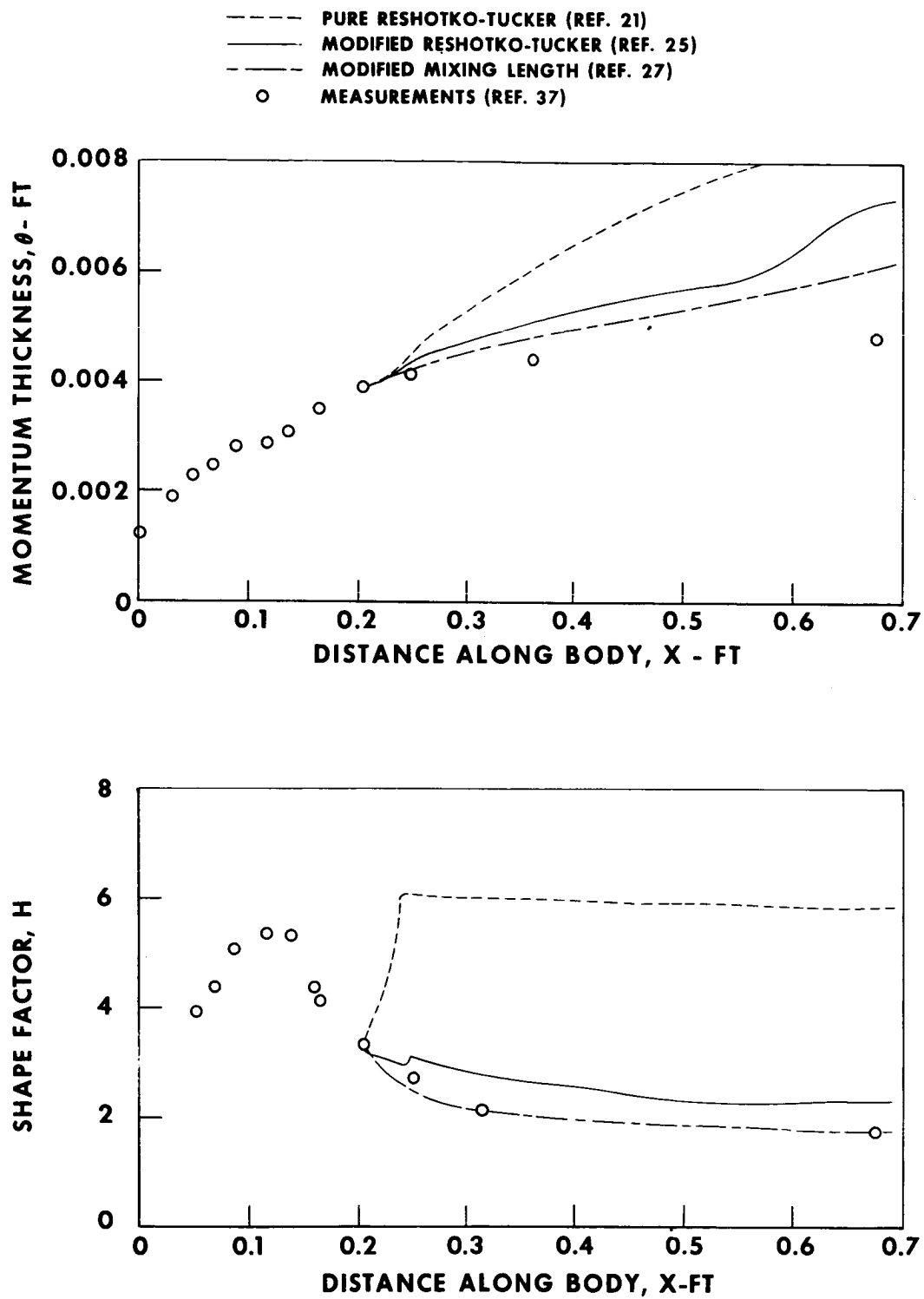


Figure 25.- Comparison between theories and measurements of Seddon (ref. 37),  $M_{\infty} \approx 1.0$ .

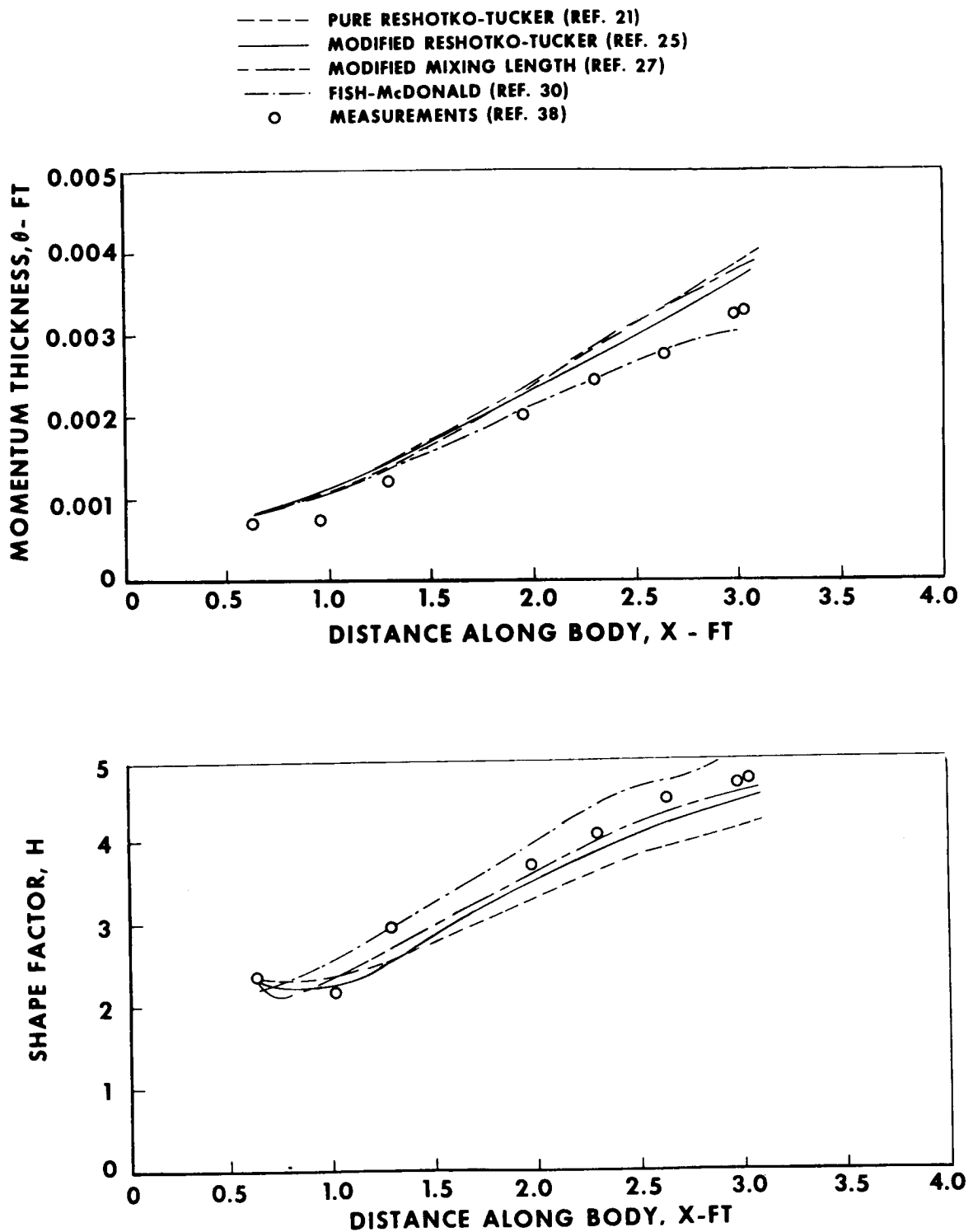


Figure 26.- Comparison between theories and measurements of Pasiuk, Chatham and Hastings (ref. 38) low heat transfer,  $M_\infty \approx 1.5$ .

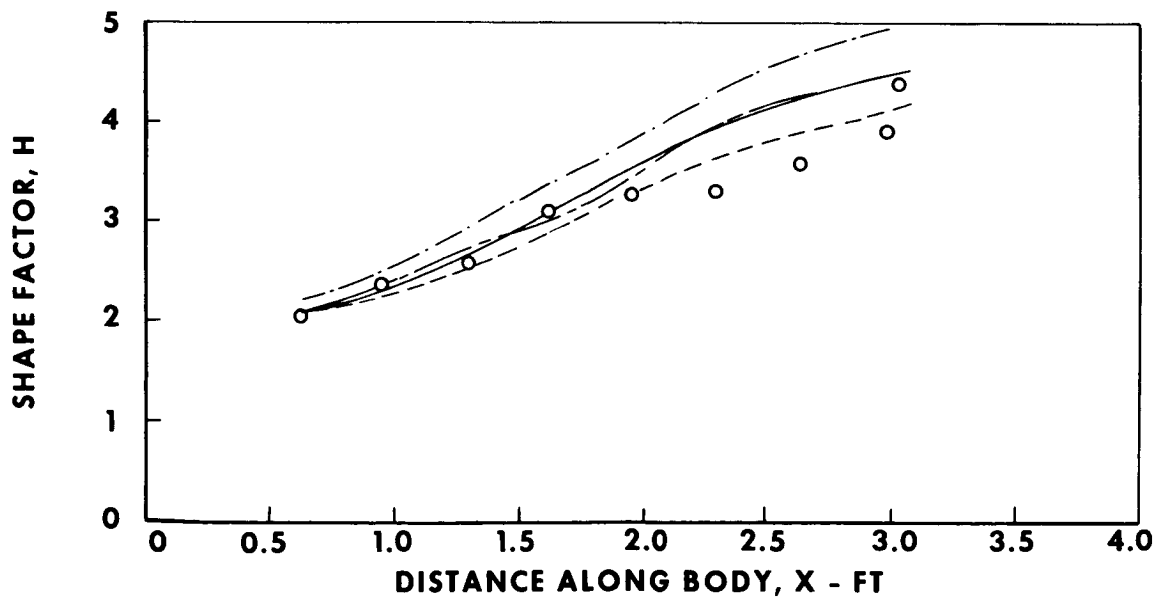
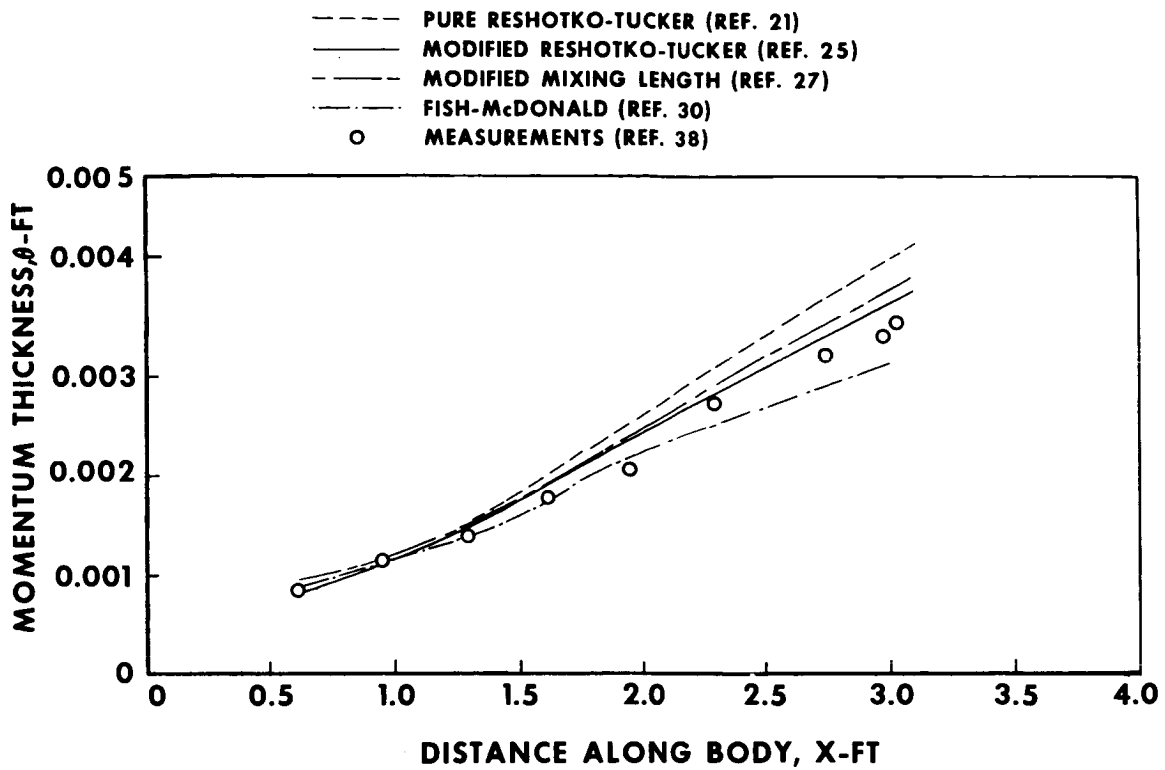


Figure 27.- Comparison between theories and measurements of Pasiuk, Chatham and Hastings (ref. 38) high heat transfer,  $M_\infty \approx 1.5$ .

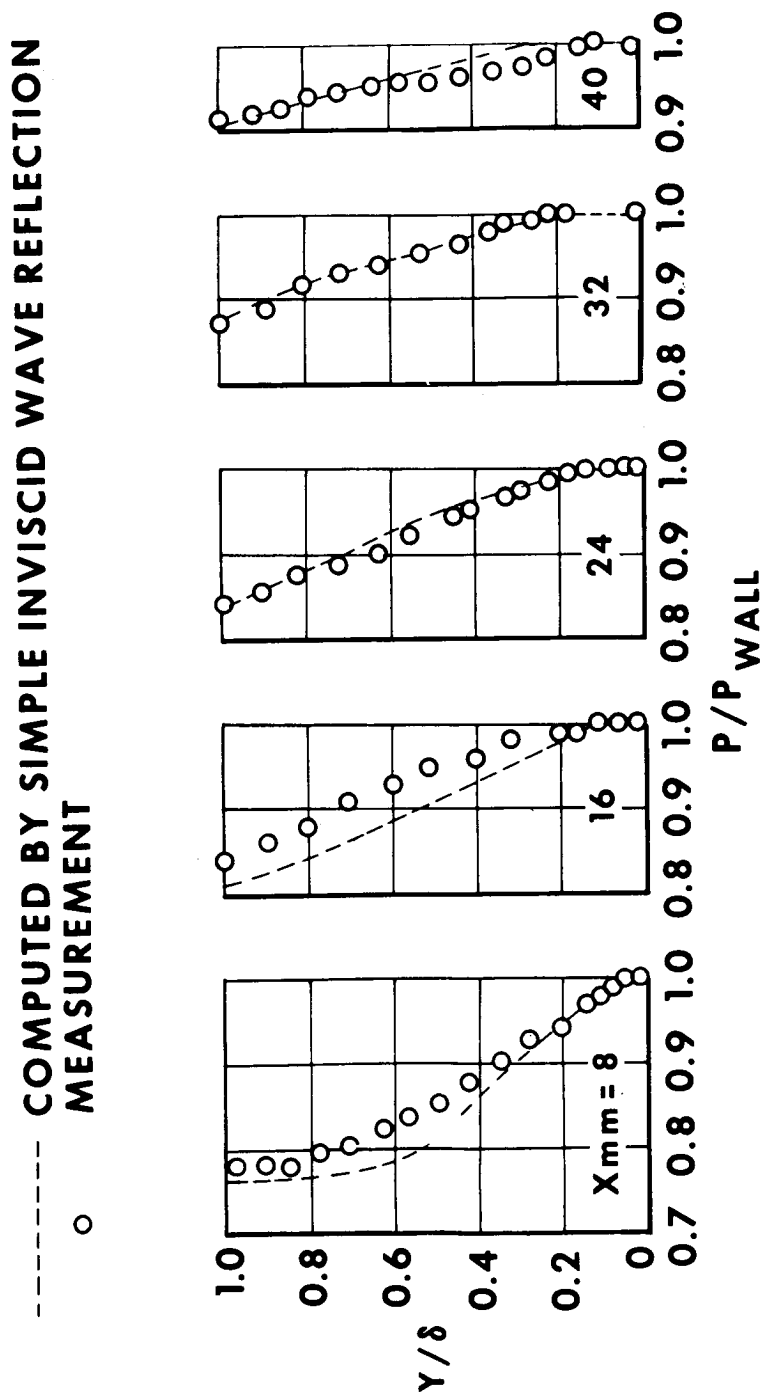


Figure 28.- Static pressure distribution across Michel's (ref. 33) linear adverse gradient boundary layer,  $M_\infty \approx 2.0$ .

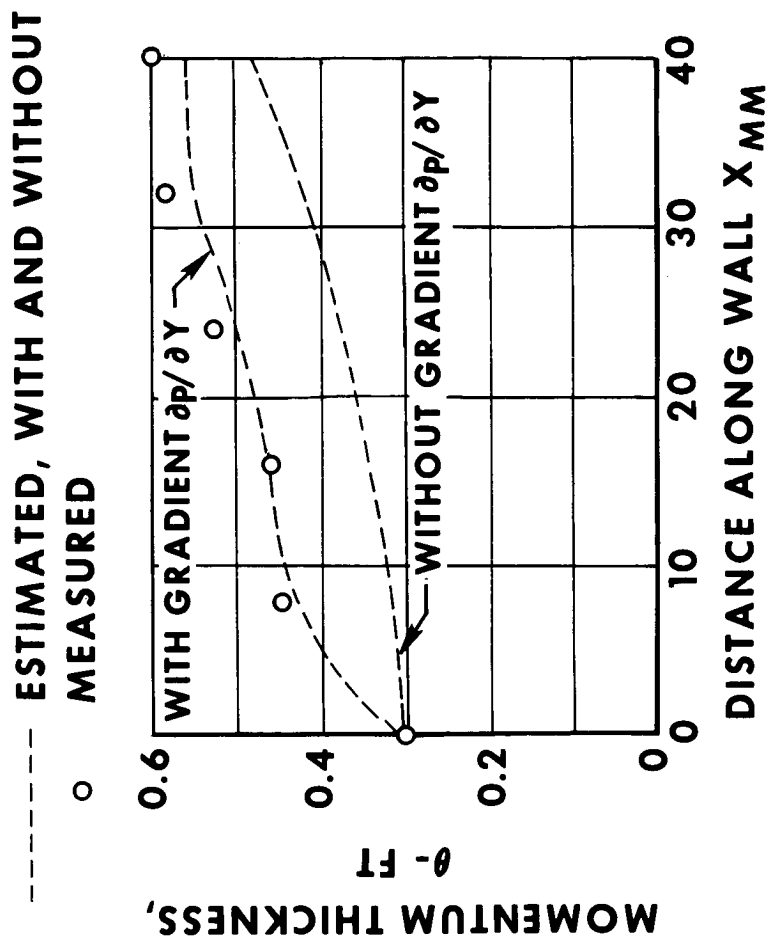


Figure 29.- Effect of the normal static pressure gradient on the estimated momentum thickness growth for Michel's (ref. 33) linear adverse gradient boundary layer,  $M_\infty \approx 2.0$ .

# CALCULATION OF TURBULENT SHEAR FLOWS THROUGH CLOSURE OF THE REYNOLDS EQUATIONS BY INVARIANT MODELING

By Coleman duP. Donaldson and Harold Rosenbaum  
Aeronautical Research Associates of Princeton, Inc.

## INTRODUCTION

This paper presents a progress report on the work carried out by the authors under NASA Contract No. NASW-1777. This work is concerned with the development of a method for computing the characteristics of turbulent shear layers which will not suffer from some of the restrictive assumptions of present methods and which, hopefully, will be applicable to a number of interesting turbulent shearing problems other than the conventional turbulent boundary layer. The method has come to be called the method of invariant modeling since the technique is based on a closure of the equation for the Reynolds stress tensor by means of physical models of the higher order terms in this equation that are invariant under transformation of coordinate systems.

## BACKGROUND

The starting point for all studies of incompressible turbulent fluid motion is the equation derived by Reynolds (ref. 1) for the mean motion  $\bar{u}_i = \bar{u}_i(x^j, t)$  of a fluid in which there are fluctuations in velocity and pressure,  $u_i' = u_i'(x^j, t)$  and  $p' = p'(x^j, t)$ , whose averages are zero. This equation is obtained from the general equation of motion, namely,

$$\frac{\partial}{\partial t} (\rho u_i) + (\rho u^j u_i)_{,j} = - \frac{\partial p}{\partial x^i} + \tau_{i,j}^j \quad (1)^*$$

$$\tau_{ij} = \mu(u_{i,j} + u_{j,i}) \quad (2)$$

---

\*In this report, the notation is that of general tensor analysis in curvilinear coordinates. The metric tensor is indicated by the symbol  $g_{ij}$ . This general notation is used since it facilitates the study of the invariant properties of certain models that will be used in the course of this report.

by substituting  $u_i = \bar{u}_i + u'_i$  and  $p = \bar{p} + p'$  into equation (1) and time-averaging the resulting equation. By this procedure, Reynolds' well-known equation

$$\frac{\partial}{\partial t} (\rho \bar{u}_i) + (\rho \bar{u}^j \bar{u}'_i)_{,j} = - \frac{\partial \bar{p}}{\partial x^i} + (\bar{\tau}^j_i - \overline{\rho u'^j u'_i})_{,j} \quad (3)$$

is obtained. In this equation

$$\bar{\tau}^j_i = g^{jk} \mu (\bar{u}_{i,k} + \bar{u}_{k,i}) \quad (4)$$

and the Reynolds stress

$$T^j_i = - \overline{\rho u'^j u'_i} \quad \text{or} \quad T_{ij} = - \overline{\rho u'_i u'_j} \quad (5)$$

is determined by the value of the correlation between the fluctuating components  $u'_i$  and  $u'_j$ .

For many years it has been customary to attempt a solution of equation (3) through the use of the continuity equation, namely,

$$\bar{u}^j_{,j} = 0 \quad (6)$$

and the notion that an effective eddy viscosity could be determined for roughly parallel shear flows of similar form such that the Reynolds stress could be expressed as

$$T_{ij} = - \overline{\rho u'_i u'_j} = \rho f(n) (\bar{u}_{i,j} + \bar{u}_{j,i}) \quad (7)$$

where  $n$  is the coordinate normal to the surface. This expression reduces for boundary layers, with the usual notation, to

$$T_{xy} = \rho f(y) \frac{\partial \bar{u}}{\partial y} \quad (8)$$

The shortcomings of the expression given above have long been known. For example, the function  $f(y)$  is not even defined everywhere in a wall jet flow since a Reynolds stress can be measured at the point where  $\partial \bar{u} / \partial y = 0$ . The interesting aspect of the expression given in equation (8) is not its shortcoming but the fact that the simple concept of an eddy viscosity has worked so well for flows of boundary layer type, even though the turbulent kinetic energy and actual Reynolds stresses in a

turbulent medium are not tied to the mean velocity profile but have definite dynamics of their own. Presumably the success of equation (8) is due to the fact that, for most boundary layer situations, the dynamics of the various components of the tensor  $\underline{u_i u_j}$  are rapid enough to allow these components to stay in some sort of equilibrium relative to the mean flow.

Most of the eddy viscosity models that are in use today are based on the idea of a mixing length. The idea, originally due to Prandtl (ref. 2), is that the scale of the turbulence in a shear layer must be governed by the scale of the mean motion and/or the distance of a given point in the shear flow from a solid surface. Suppose a scale length  $\Lambda$  is associated with this local scale; one might then expect to find velocity fluctuations of the order of  $\Lambda \partial \bar{u} / \partial y$ . This line of reasoning prompted Prandtl to write as a possible expression for the Reynolds stress

$$T_{xy} = \rho \Lambda^2 \left| \frac{\partial \bar{u}}{\partial y} \right| \frac{\partial \bar{u}}{\partial y} \quad (9)$$

Other expressions similar in form to equations (7), (8), or (9) can be given. The general expression for the Reynolds stress in terms of an eddy viscosity based on the idea of a mixing length can be written

$$T_{ij} = \rho f(\Lambda, \bar{u}_k) (\bar{u}_{i,j} + \bar{u}_{j,i}) \quad (10)$$

More generally, if the idea of an eddy viscosity is abandoned, one might seek a general form for  $T_{ij}$  in terms of the mean velocity and local scale; thus,

$$T_{ij} = \rho f_{ij}(\Lambda, \bar{u}_i) \quad (11)$$

It is obvious that any method which is described by equations (10) or (11) ties the Reynolds stress to the mean velocity profile and, as such, does not really consider the dynamics of the development of the various components of this tensor. As mentioned before, for most boundary layer flows, this does not seem to be a serious omission. However, for certain rapidly changing boundary layer situations, as well as for more difficult geometric problems such as the decay of a free vortex in a turbulent medium, the neglect of the dynamics of the Reynolds tensor leads to serious difficulties.

#### MORE RECENT METHODS

Within recent years, actually since the advent of modern computers, several attempts have been made to account for the fact



that there are actual dynamics associated with the development of the various components of the Reynolds stress tensor. Two methods which are well known should be discussed here. One is due to Glushko (refs. 3 and 4) and the other is due to Bradshaw, Ferriss, and Atwell (ref. 5).

In these two methods, an attempt is made to keep track of the dynamics of the turbulence itself by computing the development of the local turbulent kinetic energy per unit mass

$$E = \overline{u'^i u'^i} / 2 \quad (12)$$

as a shear layer develops and relating the local Reynolds stress to this quantity.

In order to carry out this computation, one needs, in addition to equations (3) and (6), an equation for the turbulent kinetic energy. This may be obtained from the equation for the correlation  $\overline{u'_i u'_k}$  by multiplying this equation by  $g^{ik}$ . The equation for the correlation  $\overline{u'_i u'_k}$  is derived in a number of references (see, for example, ref. 6, pp. 249-255) and is well known, so it will not be derived here. It is

$$\begin{aligned} \rho \frac{\partial}{\partial t} (\overline{u'_i u'_k}) + \rho \bar{u}^j (\overline{u'_i u'_k})_{,j} \\ = -\rho \overline{u'^j u'_k} \bar{u}_{i,j} - \rho \overline{u'^j u'_i} \bar{u}_{k,j} - \rho (\overline{u'^j u'_i u'_k})_{,j} \\ - (\overline{p' u'_i})_{,k} - (\overline{p' u'_k})_{,i} + \overline{p' (u'_{i,k} + u'_{k,i})} \\ + \mu g^{mn} (\overline{u'_i u'_k})_{,mn} - 2\mu g^{mn} \overline{u'_{i,m} u'_{k,n}} \end{aligned} \quad (13)$$

The terms on the left-hand side of equation (13) describe the variation, as a fluid element moves along a streamline, of the correlation  $\overline{u'_i u'_k}$  at the fluid element. The first two terms on the right-hand side of equation (13) are terms which describe the production of the correlation  $\overline{u'_i u'_k}$  as the turbulence interacts with the mean motion. The term  $\rho (\overline{u'^j u'_i u'_k})_{,j}$  describes the diffusion of the correlation  $\overline{u'_i u'_k}$  by the turbulent motion itself. The next two terms,  $(\overline{p' u'_i})_{,k}$  and  $(\overline{p' u'_k})_{,i}$ , are the so-called general pressure diffusion terms and represent both diffusion and second-order production effects. The next term on the right-hand side,  $\overline{p' (u'_{i,k} + u'_{k,i})}$ , is the tendency-towards-isotropy

term. The reason for this nomenclature is that the term drops from the equation for the energy  $\overline{u'^1 u'^1}$  by virtue of the incompressibility condition  $\overline{u'^1} = 0$ . Since the term appears in the equation for each velocity component's contribution to the total turbulent kinetic energy but not in the equation for the total energy itself, it must represent a rearrangement of the turbulent kinetic energy between the various velocity components. The term  $\mu g^{mn} \overline{(u'_i u'_k)_{,mn}} = \mu \nabla^2 \overline{(u'_i u'_k)}$  represents the diffusion of the correlation  $\overline{u'_i u'_k}$  by the action of viscosity. Finally, the last term on the right is called the dissipation term. It is truly dissipative for the energy components of the term  $\overline{u'_i u'_k}$  but is not necessarily always uncorrelative in actual flows for the off-diagonal components of the tensor.

In equation (13) there are four terms which contain unknowns other than  $\overline{u'_i}$  and  $\overline{u'_i u'_k}$ . Thus, at this point, if one wishes to solve the problem posed by equations (3), (6), and (13), one must have some method for closing the system of equations by making four assumptions about the unknown terms in equation (13) so as to express these terms in terms of what is already known. Both Glushko and Bradshaw, et al, reduce the number of assumptions that have to be made in regard to equation (13) by working with the equation for  $\overline{u'^1 u'_i}$  so that the term  $p'(u'_{i,k} + u'_{k,i})$  disappears. Nevertheless, each investigator is required to make an additional assumption in regard to the off-diagonal term  $\overline{u'_1 u'_2}$  which is left in an essentially parallel shear flow.

Before examining the methods proposed by Glushko and Bradshaw, et al, it will be instructive to write out in detail the equations of the turbulent energies and the shear stress for a boundary layer-like flow. We find with coordinates (x,y,z) and velocities ( $\bar{u}, \bar{v}, 0$ ) and ( $u', v', w'$ )

$$\begin{aligned} \rho \frac{D}{Dt}(\overline{u' u'}) = & - 2\rho \overline{u' v'} \frac{\partial \bar{u}}{\partial y} - 2\rho \overline{u' u'} \frac{\partial \bar{u}}{\partial x} - \rho \frac{\partial}{\partial y}(\overline{v' u' u'}) + 2p' \frac{\partial u'}{\partial x} \\ & + \mu \frac{\partial^2}{\partial y^2}(\overline{u' u'}) - 2\mu \overline{\frac{\partial u'}{\partial x} \frac{\partial u'}{\partial x}} \end{aligned} \quad (14)$$

$$\begin{aligned} \rho \frac{D}{Dt}(\overline{v' v'}) = & + 2\rho \overline{v' v'} \frac{\partial \bar{u}}{\partial x} - \rho \frac{\partial}{\partial y}(\overline{v' v' v'}) + 2p' \frac{\partial v}{\partial y} \\ & - 2 \frac{\partial}{\partial y}(\overline{p' v'}) + \mu \frac{\partial^2}{\partial y^2} \overline{v' v'} - 2\mu \overline{\frac{\partial v'}{\partial x} \frac{\partial v'}{\partial x}} \end{aligned} \quad (15)$$

$$\rho \frac{D}{Dt}(\overline{w'w'}) = -\rho \frac{\partial}{\partial y}(\overline{v'w'w'}) + 2\rho \overline{p' \frac{\partial w'}{\partial z}} + \mu \frac{\partial^2}{\partial y^2} \overline{w'w'} - 2\mu \overline{\frac{\partial w'}{\partial x} \frac{\partial w'}{\partial x}} \quad (16)$$

$$\rho \frac{D}{Dt}(\overline{-u'v'}) = \rho \overline{v'v'} \frac{\partial \bar{u}}{\partial y} - \rho \frac{\partial}{\partial y}(\overline{v'(-u'v')}) - \rho \overline{p' \left( \frac{\partial u'}{\partial y} + \frac{\partial v'}{\partial x} \right)} + \frac{\partial}{\partial y}(\overline{p'u'}) + \mu \frac{\partial^2}{\partial y^2}(\overline{-u'v'}) + 2\mu \overline{\frac{\partial u'}{\partial x} \frac{\partial v'}{\partial x}} \quad (17)$$

Summing equations (14), (15), and (16), we obtain an equation for the turbulent kinetic energy  $E$

$$\begin{aligned} \frac{D}{Dt} E = & -\rho \overline{u'v'} \frac{\partial \bar{u}}{\partial y} - (\overline{u'u'} - \overline{v'v'}) \frac{\partial \bar{u}}{\partial x} + \mu \frac{\partial^2 E}{\partial y^2} \\ & - \rho \frac{\partial}{\partial y} \left[ \overline{v' \left( \frac{u'u' + v'v' + w'w'}{2} \right)} \right] - \frac{\partial}{\partial y}(\overline{p'v'}) \\ & - \mu \left( \overline{\frac{\partial u'}{\partial x} \frac{\partial u'}{\partial x}} + \overline{\frac{\partial v'}{\partial x} \frac{\partial v'}{\partial x}} + \overline{\frac{\partial w'}{\partial x} \frac{\partial w'}{\partial x}} \right) \end{aligned} \quad (18)$$

Equation (18) is the basic equation which forms the starting point for the methods of both Glushko and Bradshaw, et al. When making use of equation (18), both the above-mentioned methods neglect the second term on the right. Thereafter, the two methods diverge in detail.

In the method of Glushko, the two diffusive terms, velocity diffusion

$$\rho \frac{\partial}{\partial y} \left[ \overline{v' \left( \frac{u'u' + v'v' + w'w'}{2} \right)} \right]$$

and pressure "diffusion"

$$\frac{\partial}{\partial y}(\overline{p'v'})$$

are lumped into one diffusion term and modeled in the form

$$\rho \frac{\partial}{\partial y} \left[ \overline{v' \left( \frac{p'}{\rho} + \frac{u'u' + v'v' + w'w'}{2} \right)} \right] = \frac{\partial}{\partial y} \left[ f(E, \Lambda) \frac{\partial E}{\partial y} \right] \quad (19)$$

where  $\Lambda$  is a length associated with the integral scale.

The dissipation is modeled as

$$\mu \left( \frac{\partial u'}{\partial x^i} \frac{\partial u'}{\partial x^i} + \frac{\partial v'}{\partial x^i} \frac{\partial v'}{\partial x^i} + \frac{\partial w'}{\partial x^i} \frac{\partial w'}{\partial x^i} \right) = \mu \frac{E}{\lambda^2} \quad (20)$$

where  $\lambda$  is a dissipative length scale different from  $\Lambda$ . In Glushko's work, the two lengths are related by the expression

$$\lambda^2 = \frac{\Lambda^2}{\sqrt{a + bR}} \quad (21)$$

where  $a$  and  $b$  are constants and  $R$  is the Reynolds number defined by

$$R = \frac{\rho \sqrt{E} \Lambda}{\mu} \quad (22)$$

If equations (19) and (20) are substituted into equation (18) after neglecting the second term on the right, all one needs to compute a turbulent boundary layer is some assumption about the shear stress  $-\rho \overline{u'v'}$ . Glushko makes the assumption

$$T = - \overline{\rho u'v'} = \rho f(E, \Lambda) \frac{\partial \bar{u}}{\partial y} \quad (23)$$

and gives expressions for the form of  $f(E, \Lambda)$  as functions of the Reynolds number  $R$ .

We are not interested in the details of Glushko's method here. We note only that five assumptions were necessary to achieve a closed set of equations.

(a) Neglect of the term

$$\overline{(u'u' - v'v')} \frac{\partial \bar{u}}{\partial x}$$

(b) An assumption concerning the velocity diffusion term

$$\rho \frac{\partial}{\partial y} \left[ \overline{v' \left( \frac{u'u' + v'v' + w'w'}{2} \right)} \right]$$

(c) An assumption concerning the pressure diffusion term

$$\frac{\partial}{\partial y} (\overline{p'v'})$$

(d) An assumption concerning the dissipation

(e) Finally, an assumption concerning the nature of the shear stress.

In the method of Bradshaw, Ferriss, and Atwell, the procedure is somewhat different but the same types of assumptions are necessary. Bradshaw, et al, assume that the turbulent stress is given by

$$T = a_1 2\rho E \quad (24)$$

where  $a_1$  is a function of  $y/\delta$  depending on the type of flow. The energy equation, (18), is turned into an equation for the stress  $T$  through the use of equation (24) and by modeling the diffusive and dissipative terms in the equation in terms of the stress  $T$ , a length  $L$ , and a function  $G(y/\delta)$ . The modeling used is

$$\left( \frac{\overline{p'v'}}{\rho} \right) + \frac{1}{2} \overline{v'(u'u' + v'v' + w'w')} = \left( \frac{T_{\max}}{\rho} \right)^{1/2} \frac{T}{\rho} G\left(\frac{y}{\delta}\right) \quad (25)$$

and

$$\mu \left( \frac{\partial u'}{\partial x^i} \frac{\partial u'}{\partial x^i} + \frac{\partial v'}{\partial x^i} \frac{\partial v'}{\partial x^i} + \frac{\partial w'}{\partial x^i} \frac{\partial w'}{\partial x^i} \right) = \frac{(T/\rho)^{3/2}}{L} \quad (26)$$

As was so in the case of Glushko's method, five assumptions were necessary to obtain a closed set of equations for the calculation of turbulent shear layers. Although the assumptions made by Bradshaw, et al, are different in detail from those made by Glushko, the assumptions are, necessarily, of exactly the same general nature, namely,

- (a) Neglect of the term  $(\overline{u'u'} - \overline{v'v'}) \partial \bar{u} / \partial x$  ;
- (b) An assumption concerning the velocity diffusion term;
- (c) An assumption concerning the pressure diffusion term;
- (d) An assumption concerning the dissipation;
- (e) An assumption concerning the nature of the shear stress.

It has been demonstrated (ref. 7) that, with suitable choices for the parameters which are free in the methods of Bradshaw, et al, and Glushko, both methods can be used to predict the

character of reasonably well-behaved boundary layer-like flows. It is the opinion of the authors of this paper that both methods suffer from the same drawback, namely, a lack of generality due to the very restrictive nature of the assumption regarding the shear stress. In the following section, we shall attempt to describe a method which, while closely related to each of the methods just described, does not suffer from this shortcoming.

## THE METHOD OF INVARIANT MODELING

In attempting to develop a new method for computing turbulent shear flows, it was the authors' purpose not only to try to put forward a method that would remove the restrictive assumptions of previous methods concerning the nature of the shear stress but also to develop a method that might be useful for a wider class of shear flows than the usual boundary layer-like flows. The starting point for any such attempt is certainly equation (13). However, depending on how general one wishes to make the result, one can proceed in several ways from this equation. For example, if one were interested only in boundary layer flows, one might start with the set of equations given by equations (14) through (17). Because we wish to follow the dynamics of  $T = -\rho \overline{u'v'}$  itself (surely this is the most important quantity in the development of the mean motion), we must keep equation (17). In this equation,  $\overline{v'v'}$  appears explicitly so we shall have to keep the equation for this quantity, namely, (15). This equation for  $\overline{v'v'}$  does not have a true energy production term such as the term  $-2\rho \overline{u'v'}(\partial \bar{u}/\partial y)$  which occurs in the equation for  $\overline{u'u'}$ . Thus the real contribution to the energy  $\overline{v'v'}$  must come from the pressure interaction terms  $2\overline{p'(\partial v'/\partial y)}$  and  $2\partial(\overline{p'v'})/\partial y$ . To get appropriate expressions for these terms, it will be necessary to keep track of  $\overline{u'u'}$  and  $\overline{w'w'}$  through equations (14) and (16). We are thus faced with the task of solving simultaneously the two equations for the mean motion, namely, momentum (eq. (3)) and continuity (eq. (6)), and the four equations for  $\overline{u'u'}$ ,  $\overline{v'v'}$ ,  $\overline{w'w'}$ , and  $\overline{u'v'}$ , namely, equations (14) through (17).

To accomplish a solution of these six equations, it is necessary to model the unknown terms in equations (14) through (17) in terms of known quantities. Here one might model each of the various unknown terms that occur in these equations separately. This is, in fact, what was done in reference 8. However, from the point of view of generality as well as convenience, it is best not to follow the above procedure when doing this modeling but instead to work with the single equation for the tensor  $\overline{u'_i u'_k}$ , i.e., equation (13). We shall seek to model the unknown terms in this equation in terms of the second-order correlation tensor  $\overline{u'_i u'_k}$  itself and suitable scale lengths  $\Lambda$  and  $\lambda$  so as to form a

closed set of equations. Such a procedure appears to be the logical generalization of the methods of Glushko and Bradshaw, et al. The procedure will only be valid for strongly sheared flows in which the appropriate scales are defined by the scale of the mean motion and the Reynolds number of the turbulence  $R$  (see eq. (22)).

To carry out the procedure outlined above requires only four assumptions:

- (a) A modeling of the velocity diffusion term;
- (b) A modeling of the pressure diffusion term;
- (c) A modeling of the dissipation term;
- (d) A modeling of the tendency-towards-isotropy term.

In order to keep the method as general as possible, we shall require that any model that is used must retain the tensor character of the original term so that the model will be meaningful in any coordinate system.

Many models can be constructed. However, the number of models which can be constructed that are of simple form, that depend only on the two parametric lengths  $\Lambda$  and  $\lambda$ , and that have the required symmetries and other required physical properties is really not very large. In what follows we will set forth one modeling that has been selected for initial programming and is presently under investigation. The model is not presented as that which is thought to be the ultimate choice. It represents merely the starting point for our investigation of the general method of invariant modeling.

Specifically, the presently used modeling is one which expresses the unknown terms, i.e., the pressure diffusion term, the velocity diffusion term, the dissipation term, and the tendency-towards-isotropy term, in terms of the second-order correlation itself  $\overline{u'_i u'_k}$  or operations on this tensor and two scales  $\Lambda$  and  $\lambda$  which are indicative of two scales that may be defined for a particular shear flow. We do not, at present, consider operations on the length scales such as  $\Lambda_{,i}$  or  $\lambda_{,ij}$ .

#### Modeling of the velocity diffusion term

In modeling the velocity diffusion term

$$- \rho(\overline{u'^j u'_i u'_k}),_j \quad (27)$$

we must seek an expression for the mixed tensor

$$A^j_{ik} \equiv \overline{u'^j u'_i u'_k} \quad (28)$$

in terms of the correlation  $\overline{u'_i u'_k}$  and the scalar  $\Lambda$  which we now associate with the integral scale of the turbulence and which we will use as the scale appropriate for modeling the higher order nonviscous terms. If we seek a form for  $A_{ik}^j$  such that the total effect of the term  $-\rho A_{ik,j}^j$  will be a diffusion of the correlation  $\overline{u'_i u'_k}$  with a coefficient of this diffusion that depends on the turbulence level  $\overline{u'_i u'_i}$ , we are led to an expression of the form

$$A_{ik}^j = -\Lambda \sqrt{\overline{u'_m u'_m}} \left[ g^{j\ell} (\overline{u'_i u'_k})_{,\ell} + (\overline{u'^j u'_k})_{,i} + (\overline{u'^j u'_i})_{,k} \right] \quad (29)$$

This expression has the right dimensions and represents a general gradient-dependent flux of the correlation  $\overline{u'_i u'_k}$  whose magnitude is proportional to the square root of the turbulent energy. It consists of three terms because of the symmetry requirements of  $\overline{u'^j u'_i u'_k}$ , namely,

$$\overline{u'^s u'_i u'_t} = g^{sk} g_{jt} \overline{u'^j u'_i u'_k} \quad (30)$$

Thus the total velocity diffusion term is modeled

$$-\rho (\overline{u'^j u'_i u'_k})_{,j} = \rho \left\{ \Lambda \sqrt{\overline{u'_m u'_m}} \left[ g^{j\ell} (\overline{u'_i u'_k})_{,\ell} + (\overline{u'^j u'_i})_{,k} + (\overline{u'^j u'_k})_{,i} \right] \right\}_{,j} \quad (31)$$

Modeling of the tendency-towards-isotropy term

In modeling the tendency-towards-isotropy term

$$p'(\overline{u'_{i,k} + u'_{k,i}}) \quad (32)$$

we seek an expression which will have dimensions  $\rho u^3$ , symmetric in  $i$  and  $k$ , which will represent a tendency for each velocity component's contribution to the total turbulent energy to become equal at a rate that depends on the turbulent energy level and is inversely proportional to the scale of the turbulence. Such an expression was given by Rotta in 1951 (ref. 9), and we will, for the present modeling, use this expression, namely,



$$\overline{p'(u'_{i,k} + u'_{k,i})} = \frac{\rho \sqrt{\overline{u'_m u'_m}}}{\Lambda} \left( g_{ik} \frac{\overline{u'_m u'_m}}{3} - \overline{u'_i u'_k} \right) \quad (33)$$

#### Modeling of the dissipation

In the present modeling, the dissipation is modeled in the same general way as it is modeled in Glushko's work, namely,

$$\mu g^{mn} \frac{\partial u'_i}{\partial x^m} \frac{\partial u'_k}{\partial x^n} = \mu \frac{\overline{u'_i u'_k}}{\lambda^2} \quad (34)$$

Here we have obviously identified the scalar  $\lambda$  with a dissipative length scale. Following Glushko, we assume that the scales  $\Lambda$  and  $\lambda$  are related by the formula

$$\lambda = \frac{\Lambda}{\sqrt{a + bR}} \quad (35)$$

where again  $a$  and  $b$  are constants and  $R$  is the Reynolds number

$$R = \frac{\rho \sqrt{\overline{u'_m u'_m}} \Lambda}{\mu} \quad (36)$$

#### Modeling the pressure diffusion term

At the present time, a final model for the pressure diffusion term has not been settled upon. The invariant model chosen has been one that treats this term as an extra gradient-dependent diffusion term similar to that used for velocity diffusion. The model chosen expresses the vector  $\overline{p' u'_k}$  as

$$\overline{p' u'_k} = - \rho \sqrt{\overline{u'_m u'_m}} \Lambda (\overline{u'^l u'_k})_{,l} \quad (37)$$

so that the total pressure diffusion term is modeled as

$$\begin{aligned}
(\overline{p'u'_k})_{,i} + (\overline{p'u'_i})_{,k} = & - \left[ \rho \sqrt{\overline{u'^m u'_m}} \Lambda(\overline{u'^l u'_k})_{,l} \right]_{,i} \\
& - \left[ \rho \sqrt{\overline{u'^m u'_m}} \Lambda(\overline{u'^l u'_i})_{,l} \right]_{,k}
\end{aligned} \quad (38)$$

### Final equations

If the results presented above in equations (31), (33), (34), and (38) are substituted into equation (13) and one uses equations (3) and (6) for the mean flow, a closed system of equations for computing turbulent shear flows is obtained. This set of equations is displayed below for the sake of convenience.

$$\bar{u}_{,j}^j = 0 \quad (39)$$

$$\rho \frac{\partial \bar{u}}{\partial t} + \rho \bar{u}^j \bar{u}_{i,j} = - \frac{\partial \bar{p}}{\partial x^i} + (\bar{\tau}_i^j - \rho \overline{u'^j u'_i})_{,j} \quad (40)$$

$$\begin{aligned}
\rho \frac{\partial}{\partial t} (\overline{u'_i u'_k}) + \rho \bar{u}^j (\overline{u'_i u'_k})_{,j} = & - \overline{\rho u'^j u'_k} \bar{u}_{i,j} - \overline{\rho u'^j u'_i} \bar{u}_{k,j} \\
& + \rho \left\{ \Lambda \sqrt{\overline{u'^m u'_m}} \left[ g^{jl} (\overline{u'_i u'_k})_{,l} + (\overline{u'^j u'_i})_{,k} + (\overline{u'^j u'_k})_{,i} \right] \right\}_{,j} \\
& + \rho \left\{ \left[ \Lambda \sqrt{\overline{u'^m u'_m}} (\overline{u'^l u'_i})_{,l} \right]_{,k} + \left[ \Lambda \sqrt{\overline{u'^m u'_m}} (\overline{u'^l u'_k})_{,l} \right]_{,i} \right\} \\
& + \frac{\rho \sqrt{\overline{u'^m u'_m}}}{\Lambda} \left( g_{ik} \frac{\overline{u'^m u'_m}}{3} - \overline{u'_i u'_k} \right) \\
& + \mu g^{mn} (\overline{u'_i u'_k})_{,mn} - 2\mu \frac{\overline{u'_i u'_k}}{\lambda^2}
\end{aligned} \quad (41)$$

In these equations,

$$\bar{\tau}_{ij} = \mu (\bar{u}_{i,j} + \bar{u}_{j,i}) \quad (42)$$

and the scale parameter  $\Lambda$  is to be chosen in some fashion depending on the nature and scale of the mean velocity profile. The dissipation scale  $\lambda$  is chosen according to equation (35).

The above-noted system of equations is obviously an oversimplification of turbulent flow. The general method of closure should, however, for the proper modeling, be valid for those strongly sheared flows for which the scale of the dominant fraction of the turbulent kinetic energy is determined by the scale of the mean velocity profile. The normal turbulent boundary layer is such a flow. Hopefully, other flows of more complicated geometry, such as a turbulent vortex, may also be found to fall in this category. In this case, the proper equations for computing such flows can be obtained from a general set of equations such as those given above.

### PRELIMINARY RESULTS FOR BOUNDARY LAYERS

For normal time-independent boundary layer flows with velocity components  $(\bar{u}, \bar{v}, 0), (u', v', w')$  in a coordinate system  $(x, y, z)$ , equations (39) through (41) become, with  $q^2 = \overline{u'^2 + v'^2}$ ,

$$\frac{\partial \bar{u}}{\partial x} + \frac{\partial \bar{v}}{\partial y} = 0 \quad (43)$$

$$\rho \frac{D\bar{u}}{Ds} = - \frac{\partial \bar{p}}{\partial x} + \frac{\partial}{\partial y} \left( \mu \frac{\partial \bar{u}}{\partial y} - \rho \overline{u'v'} \right) \quad (44)$$

$$\begin{aligned} \rho \frac{D\overline{u'u'}}{Ds} = & - 2\rho \overline{u'v'} \frac{\partial \bar{u}}{\partial y} - 2\rho \overline{u'u'} \frac{\partial \bar{u}}{\partial x} + \rho \frac{\partial}{\partial y} \Lambda \sqrt{q^2} \frac{\partial}{\partial y} (\overline{u'u'}) \\ & + \frac{\rho \sqrt{q^2}}{\Lambda} \left( \frac{q^2}{3} - \overline{u'u'} \right) + \mu \frac{\partial^2}{\partial y^2} (\overline{u'u'}) - 2\mu \frac{\overline{u'u'}}{\lambda^2} \end{aligned} \quad (45)$$

$$\begin{aligned} \rho \frac{D\overline{v'v'}}{Ds} = & + 2\rho \overline{v'v'} \frac{\partial \bar{u}}{\partial x} + 5\rho \frac{\partial}{\partial y} \Lambda \sqrt{q^2} \frac{\partial}{\partial y} (\overline{v'v'}) \\ & + \frac{\rho \sqrt{q^2}}{\Lambda} \left( \frac{q^2}{3} - \overline{v'v'} \right) + \mu \frac{\partial^2}{\partial y^2} (\overline{v'v'}) - 2\mu \frac{\overline{v'v'}}{\lambda^2} \end{aligned} \quad (46)$$

$$\rho \frac{D\overline{w'w'}}{Ds} = \rho \frac{\partial}{\partial y} \Lambda \sqrt{q^2} \frac{\partial}{\partial y} (\overline{w'w'}) + \frac{\rho \sqrt{q^2}}{\Lambda} \left( \frac{q^2}{3} - \overline{w'w'} \right) + \mu \frac{\partial^2}{\partial y^2} (\overline{w'w'}) - 2\mu \frac{\overline{w'w'}}{\lambda^2} \quad (47)$$

$$\rho \frac{D\overline{u'v'}}{Ds} = -2\overline{v'v'} \frac{\partial \bar{u}}{\partial y} + 3\rho \frac{\partial}{\partial y} \Lambda \sqrt{q^2} \frac{\partial}{\partial y} (\overline{u'v'}) - \frac{\rho \sqrt{q^2}}{\Lambda} \overline{u'v'} + \mu \frac{\partial^2}{\partial y^2} (\overline{u'v'}) - 2\mu \frac{\overline{u'v'}}{\lambda^2} \quad (48)$$

This set of equations has been programmed for simultaneous solution on a digital computer. The scale function  $\Lambda$  can be chosen an arbitrary function of  $y$ , the distance from the surface on which the boundary layer is growing. The dissipation scale  $\lambda$  is computed by means of equation (35).

To compute a given boundary layer flow, an initial boundary layer profile at some point in the flow ( $x = x_0$ ) must be given together with the distributions of  $\overline{u'u'}$ ,  $\overline{v'v'}$ ,  $\overline{w'w'}$ , and  $\overline{u'v'}$  at this station. The pressure gradient on the surface, i.e., the mean velocity external to the boundary layer, must be given. In general, we take  $\overline{u'u'} = \overline{v'v'} = \overline{w'w'} = \overline{u'v'} = 0$  at  $y = \infty$  and at  $y = 0$ . If the initial boundary layer chosen is laminar but contains some small initial disturbance, say  $\overline{u'u'} = \overline{v'v'} = \epsilon_0(y)$ , a kind of transition to a turbulent flow takes place. The character of this turbulent boundary layer is independent of the initial conditions which started the transition at sufficient distances downstream from  $x = x_0$ .

Calculations of turbulent boundary layers according to the scheme outlined are presently under way, and attempts are being made to refine the choice of the function  $\Lambda(y)$  and to determine the best choices for the constants  $a$  and  $b$  which appear in the expression for  $\lambda$ .

The first calculations made with equations (43) through (48) were made allowing the programmer to choose the functions  $\Lambda(y)$  and  $\lambda(y)$  independently. This enabled one to investigate the effect of varying each of these parameters separately. Most of these early runs were made selecting

$$\begin{aligned} \Lambda &= k_1 y & 0 < y < \frac{k_2}{k_1} \delta \\ \Lambda &= k_2 \delta & \frac{k_2}{k_1} \delta < y < \infty \end{aligned}$$

and

$$\begin{aligned}\lambda &= k_3 y & 0 < y < \frac{k_4}{k_3} \delta \\ \lambda &= k_4 \delta & \frac{k_4}{k_3} \delta < y < \infty\end{aligned}$$

As an example of the types of mean velocity and turbulence profiles generated by the method just outlined, some typical results obtained in the first phase of this study are presented. The results shown are for one of the oversimplified choices of  $\Lambda$  and  $\lambda$  that were first studied, namely,

$$\Lambda = 1.32 y \quad 0 < y < 0.056 \delta$$

$$\Lambda = 0.074 \delta \quad 0.056 \delta < y < \infty$$

and

$$\lambda = 0.23 y \quad 0 < y < 0.056 \delta$$

$$\lambda = 0.013 \delta \quad 0.056 \delta < y < \infty$$

The profiles are plotted for this case at the position downstream from  $x_0$  where the skin friction coefficient was that appropriate to the local Reynolds number (in this case,  $R_\delta = \rho u_e \delta / \mu = 6 \times 10^4$ ).

The profiles shown are only indicative of the type of profiles that the program develops, since no choice of  $\lambda$  relative to  $\Lambda$  which is not a function of Reynolds number can achieve the proper relationship between skin friction coefficient and Reynolds number as the boundary layer growth is followed.

Figure 1 shows a typical mean velocity profile plotted in the form of the law of the wall. The results are compared with both the results of Clauser (ref. 10) and Coles (ref. 11). Figure 2 shows the distribution of turbulent Reynolds stress through the boundary layer. The calculated distribution is compared with the experimental results of Klebanoff obtained at  $R_\delta = 8 \times 10^4$  (ref. 12). Figures 3, 4, and 5 show the distributions of

$$\sqrt{u'^2}, \quad \sqrt{v'^2}, \quad \sqrt{w'^2}$$

that were calculated and also the experimental results obtained by Klebanoff. The general agreement of the character of these results with known experimental results is encouraging. It is the authors' belief that through proper choice of the scale function

$\Lambda$  and the relation between  $\Lambda$  and the dissipation length  $\lambda$ , the known characteristics of turbulent boundary layers can be closely approximated. At present, our efforts are directed towards accomplishing this end with the simplest possible choice of the function  $\Lambda$ . The first choice we have made and which is presently under investigation is

$$\begin{aligned}\Lambda &= k_1 y & 0 < y < \frac{k_2}{k_1} \delta \\ \Lambda &= k_2 \delta & \frac{k_2}{k_1} \delta < y < \infty\end{aligned}$$

This choice for the function  $\Lambda$  and the use of equation (35) for  $\lambda$ , namely,

$$\lambda = \frac{\Lambda}{\sqrt{a + bR}}$$

reduces the description of turbulent boundary layers to the choice of the four constants  $k_1$ ,  $k_2$ ,  $a$ , and  $b$ . Whether or not this can be accomplished is the substance of our current research effort.

### CONCLUSIONS

In this short progress report, we have outlined the basis for a method of calculating turbulent shear flows that removes the basic drawback of previous methods that make some strong assumptions on the nature of the turbulent shear stress. One particular model of this general method, which has been called the method of invariant modeling, has been chosen to illustrate the technique. Some very preliminary results have been given which illustrate the type of results given by the method, and the general thrust of our research in the near future has been indicated.

### REFERENCES

1. Reynolds, O.: On the Dynamical Theory of Incompressible Viscous Fluids and the Determination of the Criterion. Phil. Trans. Roy. Soc. London, A 186, 1895, pp. 123-164.
2. Prandtl, L.: Bericht über Untersuchungen zur ausgebildeten Turbulenz. ZAMM, vol. 5, 1925, pp. 136-139.

3. Glushko, G.S.: Turbulent Boundary Layer on a Flat Plate in an Incompressible Fluid. Bull. Acad. Sci. USSR, Mech. Ser., no. 4, 1965, pp. 13-23.
4. Beckwith, I.E. and Bushnell, D.M.: Detailed Description and Results of a Method for Computing Mean and Fluctuating Quantities in Turbulent Boundary Layers. NASA TN D-4815, 1968.
5. Bradshaw, P., Ferriss, D.H., and Atwell, N.P.: Calculation of Boundary Layer Development Using the Turbulent Energy Equation. J. Fluid Mech., vol. 28, pt. 3, 1967, pp.593-616.
6. Hinze, J.O.: Turbulence. McGraw Hill Book Co., Inc., 1959.
7. Anon.: Proceedings Computation of Turbulent Boundary Layers - 1968 AFOSR-IFP-Stanford Conference. Aug. 1968.  
     Vol. I - Methods, Predictions, Evaluation and Flow Structure, Kline, S. J., Morkovin, M. V., Sovran, G., and Cockrell, D. J., eds.  
     Vol. II - Compiled Data, Coles, D. E. and Hirst, E. A., eds.
8. Donaldson, C. duP.: A Computer Study of an Analytical Model of Boundary Layer Transition. AIAA J., vol. 7, Feb. 1969, pp. 271-278.
9. Rotta, J.: Statistische Theorie nichthomogener Turbulenz. Z. Physik, vol. 129, 1951, pp. 547-572.
10. Clauser, F. H.: Turbulent Boundary Layers in Adverse Pressure Gradients. J. Aero. Sci., vol. 21, 1954, pp. 91-108.
11. Coles, D.: Measurements in the Boundary Layer on a Smooth Flat Plate in Supersonic Flow. I. The Problem of the Turbulent Boundary Layer. JPL Report No. 20-69, 1953.
12. Klebanoff, P. S.: Characteristics of Turbulence in a Boundary Layer with Zero Pressure Gradient. NACA Rep. 1247, 1955.

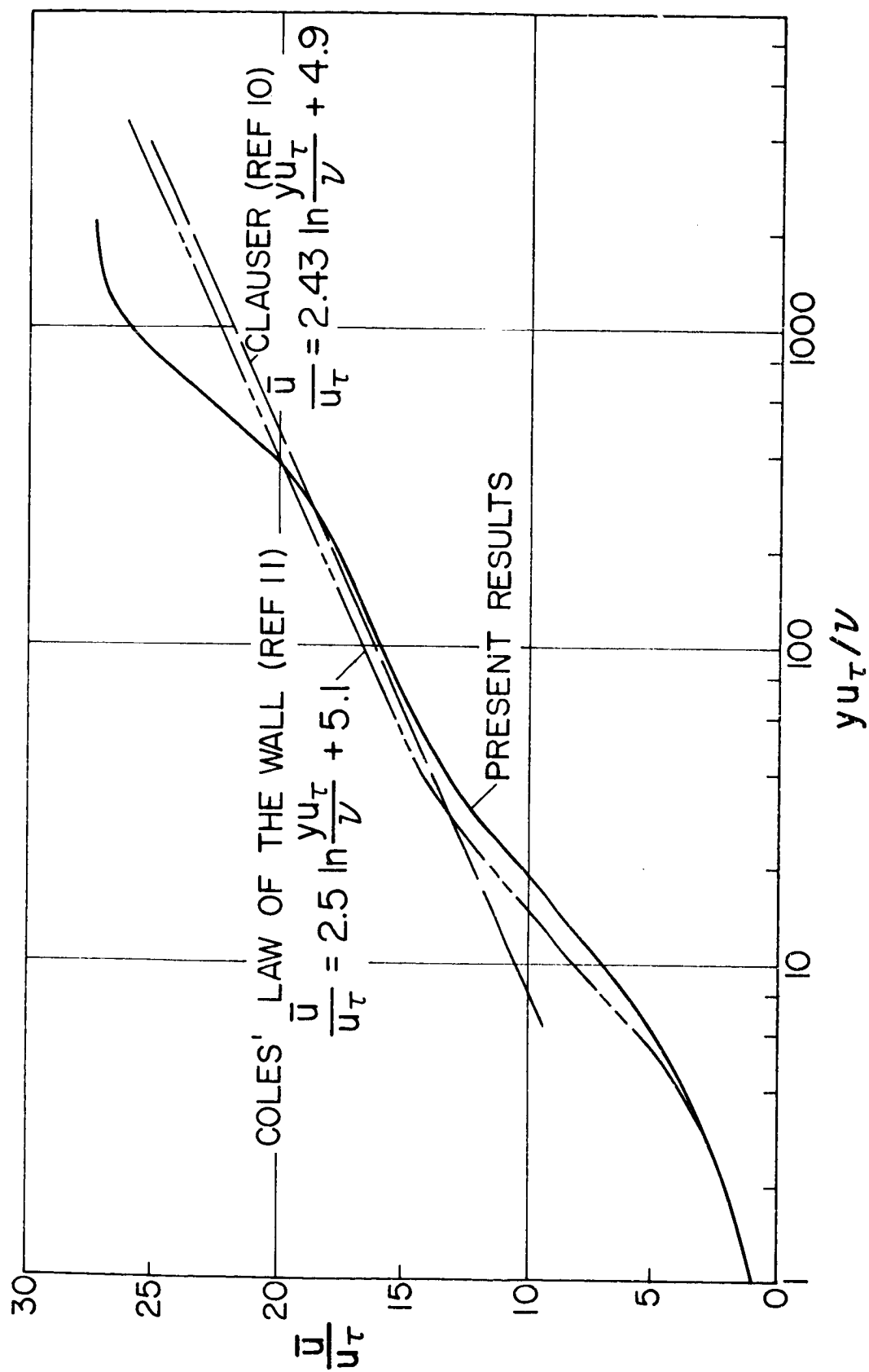


Figure 1.- Velocity profile compared with law of the wall.



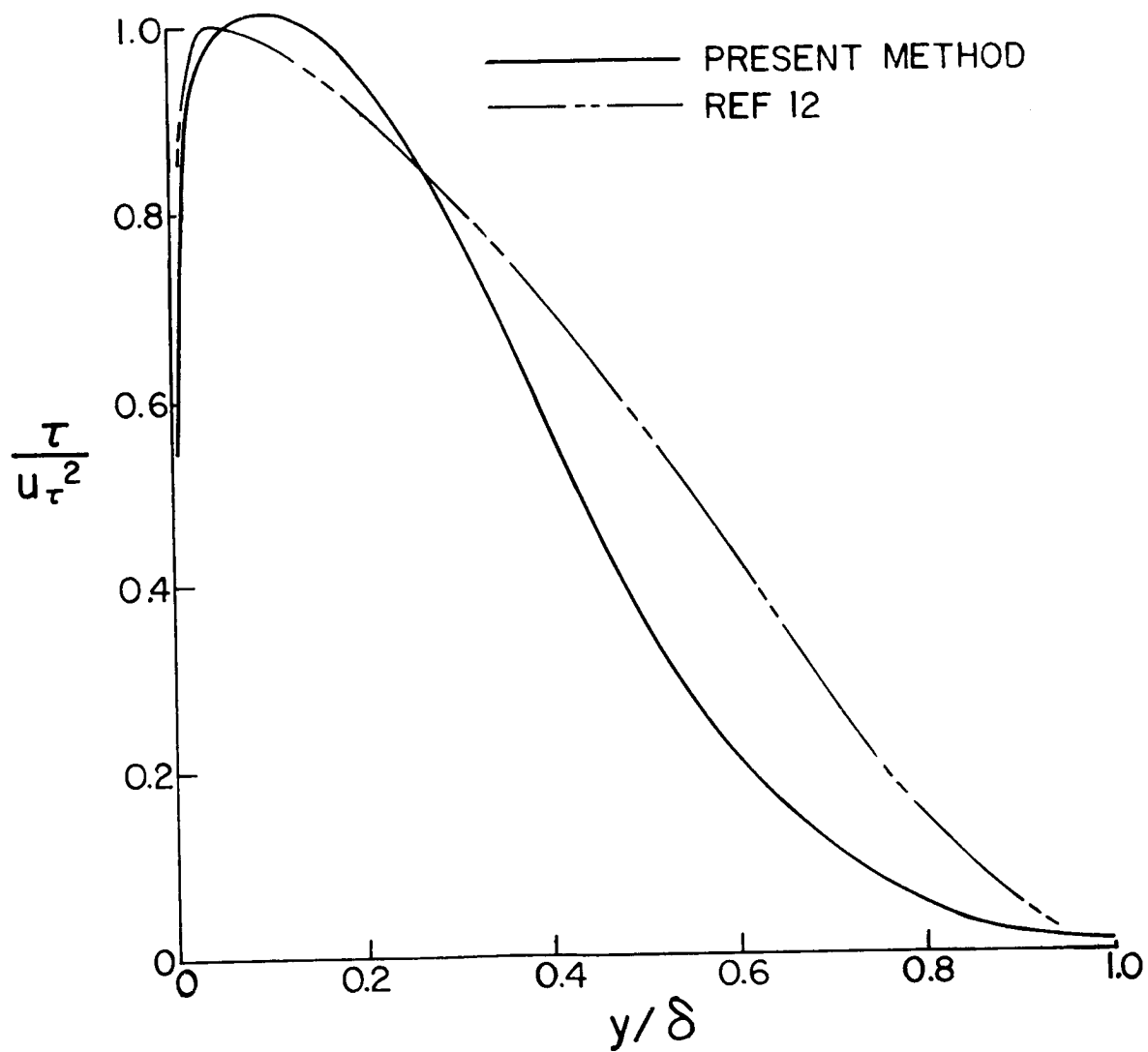


Figure 2.- Distribution of turbulent shear stress.

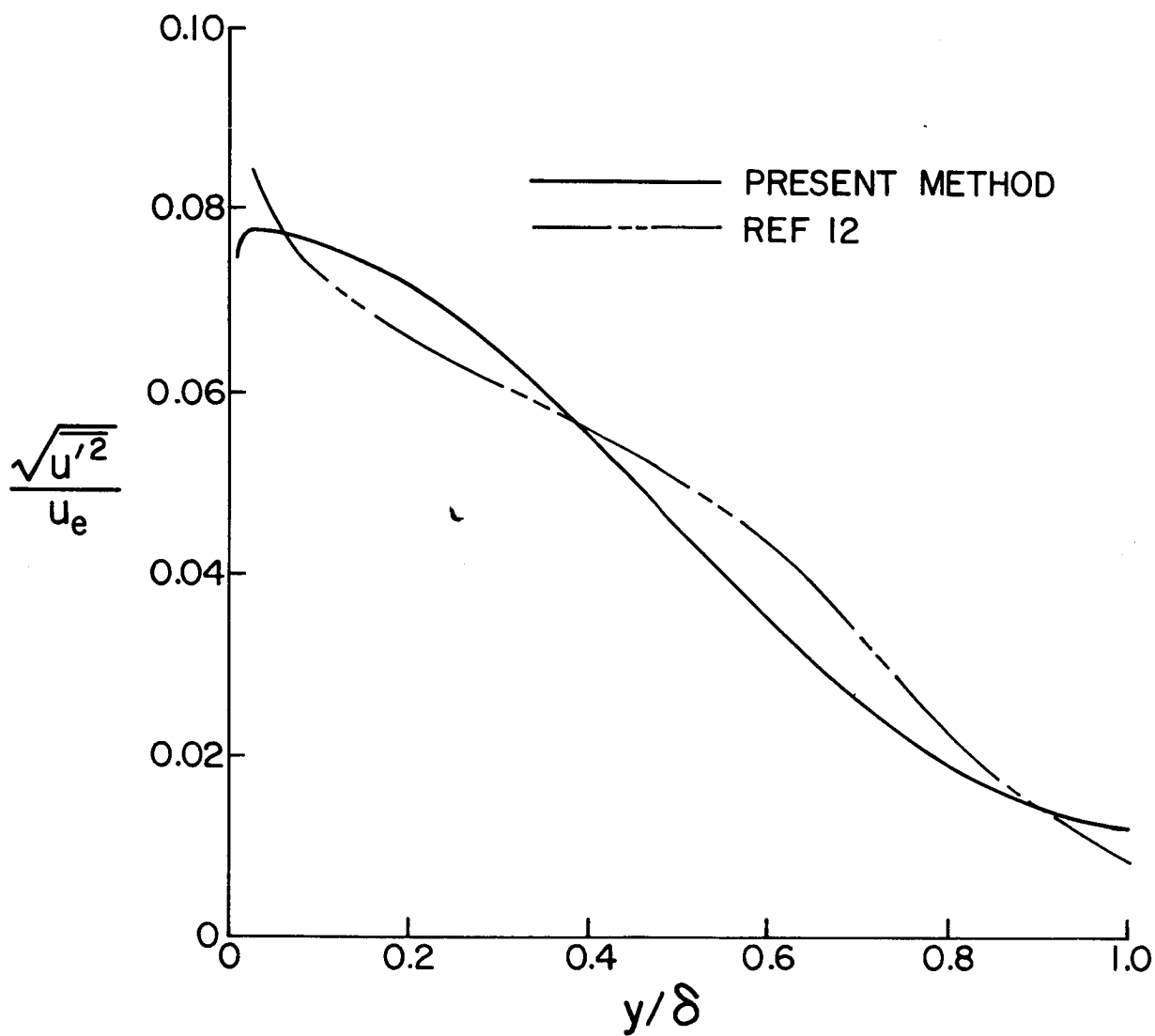


Figure 3.- Distribution of rms value of longitudinal fluctuation  $u'$  .

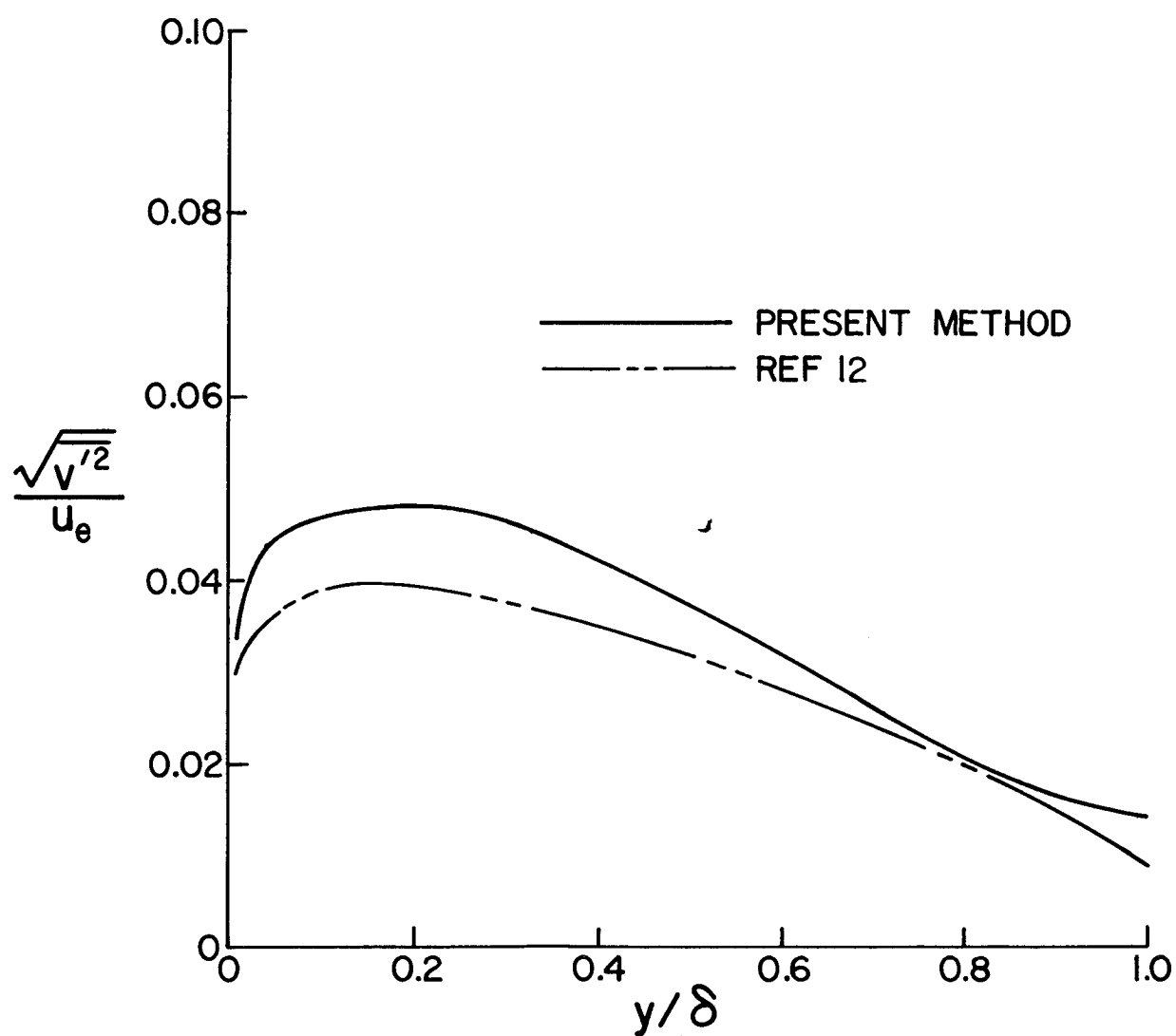


Figure 4.- Distribution of rms value of normal fluctuation  $v'$  .

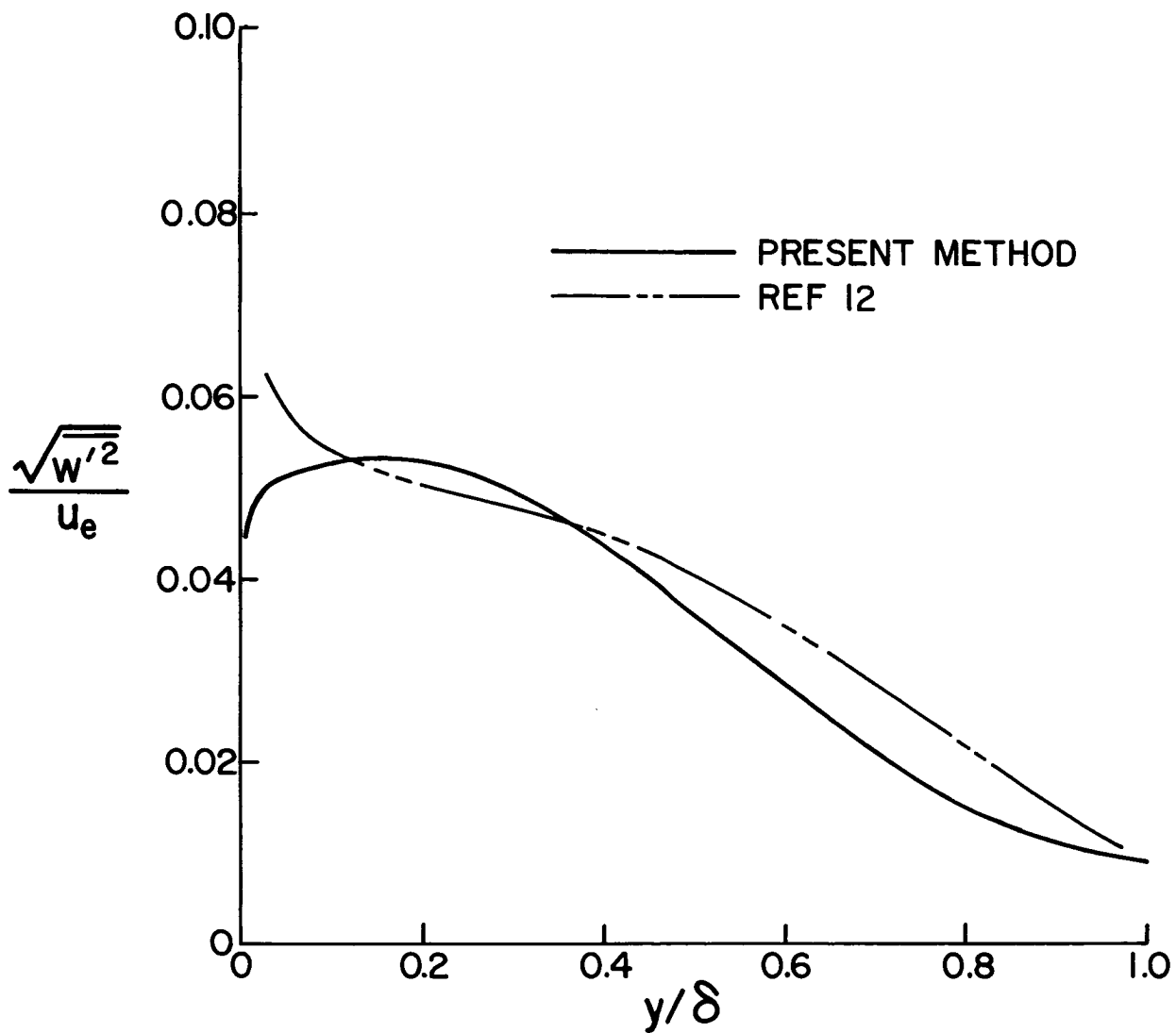


Figure 5.- Distribution of rms value of transverse fluctuation  $w'$  .

# HYPERSONIC TURBULENT BOUNDARY-LAYER MEASUREMENTS USING

## AN ELECTRON BEAM\*

J. E. Wallace

Cornell Aeronautical Laboratory, Inc.

### SUMMARY

An experimental study has been made of hypersonic, turbulent boundary layers developed on a shock-tunnel nozzle wall at cold-wall conditions. The electron beam fluorescence technique was used to obtain distributions of local mean density and also density fluctuations across the boundary layer. In addition to density, simultaneous measurements were made of boundary-layer pitot pressure distributions and of wall heat transfer, skin friction, and static pressure. Since the measured values of static pressure at the wall were found to agree with free-stream static pressures, the measured densities are exactly the inverse of static temperatures in the boundary layer. The resulting profiles of static temperature inferred from the density measurements are far below the values predicted by the classical Crocco integral and its conventional modifications for turbulent flows.

Both the density measurements and the accompanying pitot pressure measurements indicate peak fluctuations intensities quite close to the wall and an inflection in the fluctuation intensity in the mid-region of the boundary layer.

The direct measurements of skin friction and heat transfer on the nozzle wall were compared with the Spalding and Chi theory. Agreement is poor for skin friction as a function of momentum thickness Reynolds number unless the density data are ignored and the Crocco relation used in conjunction with the pitot pressure profiles to obtain the boundary-layer profiles, in which case the data and Spalding and Chi theory are in good agreement.

---

\* Paper 8 is also available as Cornell Aeronautical Laboratory Technical Report CAL No. AN-2112-Y-1, Aug. 1968.

# LIST OF SYMBOLS

$C_f$	Local skin friction coefficient, $\tau_w / (\frac{1}{2} \rho_\infty u_\infty^2)$
$D$	Film density
$E$	Exposure
$F_c$	Spalding and Chi Factor, $F_c C_f = C_{f_i}$
$F_{R_x}$	Spalding and Chi Factor, $F_{R_x} Re_x = Re_{x_i}$
$F_{R_\theta}$	Spalding and Chi Factor, $F_{R_\theta} Re_\theta = Re_{\theta_i}$
$h$	Static enthalpy
$H$	Total enthalpy
$M$	Mach number
$n$	Power law exponent
$p$	Pressure
$p_s$	Pitot pressure
$\dot{q}$	Heat transfer rate
$r$	Radial coordinate in nozzle; also recovery factor
$Re$	Reynolds number
$St$	Stanton number, $\dot{q} / \rho_\infty u_\infty (H_r - h_w)$
$T$	Temperature
$u$	Velocity
$y$	Coordinate normal to surface of nozzle wall
$\sigma$	Ratio of specific heats
$\delta$	Boundary-layer thickness (based on pitot pressure profile)
$\delta_*$	Boundary-layer displacement thickness
$\mu$	Viscosity coefficient
$\theta$	Boundary-layer momentum thickness

## LIST OF SYMBOLS (Cont.)

$\rho$	Density
$\sigma$	Prandtl number
$\tau$	Skin friction

## SUBSCRIPTS

$o$	Reservoir conditions
$AW$	Adiabatic wall condition
$i$	Incompressible, constant density case
$r$	Recovery
$s$	Stagnation point (behind normal shock on pitot probes)
$w$	Wall
$\infty$	Freestream (in these experiments, conditions computed at the edge of the boundary layer from measured pitot pressure)

## I. INTRODUCTION

Despite the considerable analytical and experimental work on compressible turbulent boundary layers which has been performed in recent years, a satisfactory and general description of turbulent flow is still lacking. The basic complexity of turbulent flow has led those seeking to describe the compressible case to hypothesize similarities between the compressible boundary layer and the constant density boundary layer, where at least a larger body of experimental measurements is available. Attempts to compare the theoretical work with compressible turbulent flow experiments have been limited by the lack of data at cold wall conditions (low values of  $h_w/H_o$ , or large heat transfer to the wall), by the lack of direct measurements of skin friction, and by incomplete experimental definition of the mean profiles and fluctuations across the boundary layer in high-speed compressible flows. Furthermore, the linear relation between total enthalpy and velocity required by the unit-Prandtl-number Crocco relation has often been assumed but not thoroughly checked for validity under the conditions of interest.

No attempt will be made here to review the numerous investigations of compressible turbulent flow which have been made in recent years; however, mention of some recent references for background is in order. The work by Spalding and Chi<sup>1</sup> included a rather comprehensive review of current theoretical methods as well as a new, semi-empirical theory. The transformation approach developed by Coles<sup>2</sup> has been modified by Crocco<sup>3</sup> and extended and applied by Baronti and Libby<sup>4</sup>. Extensions to compressible flow of Head's entrainment theory<sup>5</sup> have been published by Standen<sup>6</sup> and Green<sup>7</sup>, for example. Published results of direct skin friction measurements for turbulent flow include those reported by Neal<sup>8</sup> and Wallace<sup>9</sup>.

Upon examination it will be found that all the theoretical and semi-empirical approaches rely, for a relation between static temperature (or density) and velocity in the boundary layer, upon the assumption of conservation of energy in the mean values of  $h$  and  $u$  and of the Crocco relation for unit Prandtl number,  $\frac{H-h_w}{H_\infty-h_w} = \frac{u}{u_\infty}$ , or a slight modification of



it, e.g., replacement of the total enthalpy by an effective enthalpy ( $H_r = h + r \frac{1}{2} u^2$  where  $r$  is a recovery factor) or by addition of a weak quadratic term in velocity. Discussions of these relationships are legion (Refs. 3, 10-14, for example), but direct measurements of enough boundary layer quantities to assess the relations assumed are relatively few (Refs. 15-19) and are limited to a range of  $h_w/H_e$  between 0.5 and 1.0 (adiabatic wall). With the exception of the data reported in Ref. 17 static temperatures inferred from measurements of total temperature and pitot pressure have been observed to agree with the Crocco relation only for the adiabatic wall case and have otherwise been found to be lower than predicted. This divergence appears, on the basis of the limited data available, to become greater with larger freestream Mach numbers and with decreasing values of  $h_w/H_e$ . Viewed in terms of the total enthalpy profile, the summary of experimental results reported by Bertram and Neal<sup>20</sup> indicates consistently lower values of total enthalpy in the turbulent boundary layer than either the unit-Prandtl-number Crocco relation or its modifications.

The objective of the present investigation has been to obtain a full complement of boundary layer measurements at low hypersonic, cold-wall conditions for a determination of the boundary layer profiles and their relationship to wall shear and heat transfer under these conditions. An electron beam luminescence probe has been used to measure the density in the turbulent boundary layer on a shock tunnel nozzle wall. In conjunction with measured pitot pressures in the boundary layer the density measurements have been used to compute the boundary layer profiles for the other thermodynamic and gasdynamic variables, in order to compare them with the Crocco relation. Simultaneous measurements of wall heat transfer and skin friction have also been made.

## II. TEST PROGRAM

### 1. Test Configuration

The contoured expansion nozzle (nominal Mach number of 8) of the Cornell Aeronautical Laboratory 48-Inch Hypersonic Shock Tunnel<sup>21</sup> was instrumented to record skin friction, heat transfer, and pressure on the nozzle wall and to record pitot pressure and static density in the nozzle-wall boundary layer. A discussion of the design, operation and calibration of the electron beam is included in the Appendix. Figure 1 is a photograph of the instrumented nozzle wall in the vicinity of the station at which a 40 kV electron beam was projected through an orifice in the nozzle wall. A graphite cup, used to collect the beam current (approximately 1 milliampere), has been removed in the view shown to avoid obscuring the wall instrumentation. Hidden from view in Fig. 1 are the two stations instrumented with skin friction, pressure, and heat transfer gages upstream from the electron beam station. Figure 2 is a schematic drawing of the instrumentation arrangement and the optics for viewing the electron beam luminescence. The optics system, discussed further in the Appendix, was designed to obtain samples of the beam luminescence at 13 points over the boundary layer thicknesses of 5 to 6 inches. A set of miniaturized pitot probes was used to obtain pitot pressure data at 12 points within the boundary layer thickness.

### 2. Instrumentation

#### 2.1. Pitot Probes

The boundary-layer pitot pressure transducers used in this program are described in Ref. 22. The basic transducer is 1/8-inch in diameter with an exposed diaphragm. Diaphragm deflections, in response to pressure forces, are mechanically transmitted to a cantilever beam of piezoceramic by means of a drive pin. To ensure dimensional stability of the transducer in the presence of temperature gradients, the diaphragm, the drive pin, the beam holder, and the case are fabricated from Invar, a material having a low

coefficient of thermal expansion. The transducing beam consists of two layers of Sonotite 101 piezoceramic which are cemented together, oppositely poled, and series-connected electrically to achieve first order insensitivity to temperature. A second transducing beam (unattached to the diaphragm) provides an electrical signal that is used to achieve acceleration compensation. The entire force-sensing system, comprising the diaphragm, transducing beams, and holder constitutes a very small assembly which is placed at the probe tip where bending stresses are low. Nominally two inches long, the probe case is designed so that it may be extended to any desired length without disturbance to the force-sensing system or the electronic components. The probe incorporates a field-effect transistor and other necessary circuit elements to act as a cathode follower and preamplifier with a gain of approximately 2. Typical sensitivity is 50 mv/psi.

In the development of the pitot probe it was considered important to devise thermal protection for the diaphragm and crystal elements to avoid inducing false signals from temperature gradients in these materials. The best mode of protection developed was that of a labyrinth-path cap, consisting of an 0.035-inch diameter orifice in the outer cap, followed by a multiorifice plate, which in turn was followed by another 0.035-inch diameter orifice plate over the gage diaphragm. This configuration offered protection from convective heating, from radiative heating, and from possible damage by particles in the post-test flow. All but two of the twelve probes used in the present tests were of the labyrinth-path cap configuration. On the remaining two, the gage diaphragm was covered only by a thin layer (0.005 inch) of sheet rubber. The apparent adequacy of the thermal protection provided by this covering was attested by the good agreement between this configuration and the labyrinth-path cap configuration when all probes were placed in the uniform core flow of the nozzle. It was found that the dynamics of the signal fluctuations in the two types of probes do not differ significantly, i.e., the labyrinth-path cap does not seriously damp or mask the predominant oscillations in the flow impinging on the probe.

## 2.2 Wall Instrumentation

Skin friction gages developed at Cornell Aeronautical Laboratory for

shock tunnel measurements<sup>23</sup> were used in the present program. A 1/4-inch diameter Invar sensing diaphragm is mounted flush with the instrumented surface and has a gap of approximately 0.010 inches around the diaphragm. The diaphragm is supported on two lead-zirconium-titanate crystals that are sensitive in a bending mode and insensitive in a compression mode. This provides the necessary sensitivity to tangential loading and insures a minimum response to normal loading. A third crystal is mounted within the case and loaded with a dummy mass to provide partial acceleration compensation. In the nozzle-wall application, where large accelerations of the wall are produced by the bursting of the shock tube diaphragm and by the reflection of the incident shock at the throat station, it was necessary to supplement the internal acceleration compensation of the gage by using the output of accelerometers mounted on the skin friction gage case to cancel the acceleration-induced signals in the skin friction gage. The matching of accelerometer output with that of the skin friction gage was accomplished on a shake table for three orthogonal axes. The base of the transducer contains a field effect transistor and other circuit elements that act as a cathode follower and preamplifier with a gain of approximately 2. Typically, the sensitivity for this instrument is 20 volts/psi.

Heat transfer and pressure instrumentation used in the present experiments was that now conventional for shock tunnel measurements. The heat transfer gages<sup>24</sup> were thin-film platinum strips on a pyrex substrate. Pressure gages<sup>25</sup> on the nozzle wall were shock isolated by mounting the transducer on a suspended mass and connecting the transducer with the orifice in the nozzle wall by a short length of flexible tubing. The response time of the pressure transducers, as well as that of the other transducers used, was comparable to the flow establishment time.

### 3. Test Conditions

A summary of the test conditions for the experimental program is provided as Table 1. Shock-tunnel reservoir enthalpy in the stagnated gas behind the reflected shock was computed for equilibrium air using the measured velocity of the incident shock. Reservoir pressure (behind the reflected shock) was measured directly. Free-stream conditions in the test section were

Table 1  
TEST CONDITIONS

SYM.	$H_o(ft^2/sec^2)$	$T_o(^{\circ}R)$	$P_o(psia)$	$P_{s_{\infty}}(psia)$	$M_{\infty}$	$Re_{\infty}/ft$	$\rho_{\infty}(slugs/ft^3)$	$T_{\infty}(^{\circ}R)$
○	$2.43 \times 10^7$	3580	375	1.60	8.80	$1.82 \times 10^5$	$5.43 \times 10^{-6}$	245
△	$2.41 \times 10^7$	3550	390	1.61	8.87	$1.89 \times 10^5$	$5.51 \times 10^{-6}$	240
◊	$2.40 \times 10^7$	3540	370	1.59	8.81	$1.85 \times 10^5$	$5.47 \times 10^{-6}$	240
▽	$2.44 \times 10^7$	3590	385	1.61	8.82	$1.84 \times 10^5$	$5.45 \times 10^{-6}$	245
□	$4.41 \times 10^7$	5815	845	3.35	8.22	$1.54 \times 10^5$	$6.22 \times 10^{-6}$	506
◻	$4.40 \times 10^7$	5805	845	3.30	8.25	$1.52 \times 10^5$	$6.13 \times 10^{-6}$	502
◇	$2.60 \times 10^7$	3795	240	1.10	8.62	$1.10 \times 10^5$	$3.48 \times 10^{-6}$	272
◊	$1.92 \times 10^7$	2920	290	1.29	8.89	$2.12 \times 10^5$	$5.56 \times 10^{-6}$	189

$T_{WALL} = 525^{\circ}R$ ,  $h_{WALL} = 3.16 \times 10^6 ft^2/sec^2$  IN ALL CASES

calculated assuming an equilibrium air expansion to the measured test section pitot pressure. The narrow range in Reynolds number and total enthalpy encompassed by the test conditions is attributable to the lower limits on total enthalpy and reservoir pressure for which stable, fully developed nozzle flows are available and to the upper limits in density set by the onset of collision quenching of the electron beam-stimulated radiation and by spreading of the electron beam at the higher densities. The upper limit on density (2 Torr at room temperature or approximately  $6 \times 10^{-6}$  slugs/ft<sup>3</sup>) was ultimately set by the requirement to protect the filament in the electron gun chamber from pressures above  $10^{-5}$  Torr during calibration (see Appendix).

Precautions were taken to validate the choice of test conditions and of the configuration of the test hardware. The expansion nozzle consisted of a cylindrical throat of 0.964-inch diameter with a one-inch radius transition to a conical section with a 10.5-degree half angle, followed by a contoured wall. The wall contour is designed to cancel the expansion waves generated in the throat and conical section and to yield nearly parallel flow at the exit. Although the original nozzle had been cut off at 125 inches from the throat (with a wall angle of 0.76 degree at the exit), for the present experiments the original design contour was continued with a contoured extension for approximately three feet. The nozzle station at which the primary instrumentation was located was then 135 inches from the throat where the local wall angle is 0.58 degree. The additional extended nozzle length was provided to minimize end effects on the measurements. Because the nozzle had to be operated at local Mach numbers slightly in excess of the design Mach number of 8 in order to produce sufficiently low densities, the possibility of uncanceled waves reaching the test section had to be checked with measurements of pitot pressure in the inviscid core. The required uniform flow at the test station is attested by the shape of the radial profiles of pitot pressure shown in Fig. 3. The boundary-layer pitot pressure measurements, made after the nozzle calibration measurements, join smoothly with the profiles in the inviscid core. The results shown are representative of the four test conditions used in the program.

The correspondence between the present nozzle-wall boundary layer and that on a sharp flat plate may, of course, be influenced by the difference between the nozzle flow history and the uniform flow over a flat plate or by the small axial pressure gradient along the wall. However, any upstream disturbances of the boundary layer by wave systems would be expected to be rapidly diffused through the turbulent layer by turbulent mixing. In addition, good agreement in surface measurements has been found<sup>9</sup> in comparisons between sharp plate data and nozzle wall data obtained with the same nozzle as the present measurements, with the exception of the nozzle extension.

Wall pressures measured at three stations indicated a very small axial pressure gradient as shown in Fig. 4. The absence of any significant normal pressure gradients is indicated by a comparison of these values of measured static pressure at the wall with the free-stream static pressure computed from measured pitot pressure (Fig. 4), which reveals good agreement between the measured and computed static pressures and which also suggests that the nozzle expansion is isentropic (free of shocks). For reference purposes, Fig. 4 also includes the values of skin friction and heat transfer measured on the nozzle wall.

The assurance that the boundary-layer flow was turbulent in the instrumented region of the nozzle wall lies in the boundary layer profiles and the wall measurements themselves. However, it can be noted that in a shock tunnel test program with reservoir conditions comparable to the present ones, Burke<sup>26</sup> found that the throat Reynolds numbers were high enough to achieve transition to turbulent flow in the throat region. Furthermore, the Reynolds numbers based on local conditions and nozzle length were relatively high -- in the range of  $1 \times 10^6$  to  $3 \times 10^6$ .

Several possible types of interference were evaluated. Possible interference between the pitot probes and the wall instrumentation was assessed by operating the shock tunnel at a given condition with and without the pitot probe rake in position. No perceptible difference in measured pressure, heat transfer, or skin friction was observed. Possible wall interference with the pitot probe measurement closest to the wall was minimized by placing the lower edge of that probe just above the subsonic portion of the boundary layer.

The possibility of disturbances in the wall measurements from the viewing-optics port was explored by making identical shock tunnel runs with the viewing-optics port open and with it closed by a cover contoured to the nozzle wall geometry. No differences in wall data were observed.

Finally, a check was made of the background radiation by recording the light received by the photomultiplier during a shock tunnel run with the electron beam turned off. The received light was completely negligible compared with the light levels recorded during runs with the electron beam on.



### III. EXPERIMENTAL RESULTS

#### 1. Measured Boundary Layer Profiles

Typical shock tunnel records of the density measurements obtained in the nozzle-wall boundary layer are shown in Fig. 5. The oscilloscope pictures of the beam fluorescence are of particular interest because of the details revealed in the signal dynamics. The magnitude of the fluctuations in the photomultiplier output is seen to vary from very small fluctuations near the wall to large fluctuations in the interior of the boundary layer and back to very small fluctuations as the free-stream core flow is approached. The consistent variation in the relative amplitude of the fluctuations and the degree of correlation of the details of the signal dynamics for adjacent points along the beam suggest that the fluctuations seen are real variations in the local light intensity; hence, these fluctuations presumably represent real variations in density within the gas volume viewed by the optics systems (see Appendix). This feature of the records suggests that detailed measurements of the turbulence-induced fluctuations would be feasible and could yield information on the turbulence structure in compressible turbulent boundary layers.

For present purposes a simple analysis of the oscilloscope records has been made to determine the root-mean-square value of the fluctuations from the mean density level during the first four milliseconds of quasi-steady flow.\* In view of the small degree of nonlinearity in the relationship between the photomultiplier output and the gas density (see Appendix), the fluctuations in the photomultiplier signal are taken to represent density fluctuations. Barred symbols will be used to indicate average values; symbols

---

\* The digitizing of the analog data and computing of the RMS values of the fluctuations were performed at the NASA Langley Research Center under the supervision of Messrs. Ivan E. Beckwith and William D. Harvey. Each analog record was digitized at 100 points per millisecond of record over a period of four milliseconds.

with a prime will be used to indicate the fluctuating component. Figure 6 is a summary plot of the variation across the boundary layer in the intensity of density fluctuations, defined as the ratio of the root-mean-square of the fluctuations to the local mean value,  $(\overline{\rho'^2})^{1/2}/\bar{\rho}$ . The peak fluctuation intensity occurs near the wall ( $y/\delta \cong 0.05$ ), as had been previously inferred in other investigations of turbulent boundary layers<sup>27, 28</sup>, but without direct measurements of density. A curious phenomenon is observed in the present data, however, in the form of an inflection at approximately  $0.2 < y/\delta \leq 0.5$  in the curve of fluctuation intensities. This behavior would doubtless have been attributed to random scatter and brushed aside had it not been for a similar occurrence in the variation of both the density and the pitot pressure fluctuation intensities.

Samples of the pitot pressure records are included in Fig. 7. These indicate that the pitot-pressure fluctuations are much larger in relative magnitude than the density fluctuations. (The apparent "stepped" character of the pitot pressure records is caused by the data recording system used to obtain the pitot data. This system samples a given signal every 50 microseconds, stores it on a drum during the run, and after the run displays the signal on a strip-chart recorder.) Once again it is observed that the largest fluctuations occur in the boundary layer relatively close to the wall and diminish toward the edge of the boundary layer. However, the inflection point is again observed when the RMS value of the fluctuations from the mean in pitot pressure is computed and plotted against boundary layer position as in Fig. 8. Whether this phenomenon is, in fact, a general characteristic of compressible turbulent boundary layers at cold wall conditions remains for further investigation.

In Fig. 9 the mean values of density inferred from the electron beam measurements are presented. Densities in the interior of the boundary layer are normalized by the values at the edge of the boundary layer. Edge values of density were obtained by extrapolation to the boundary-layer edge obtained from the pitot pressure profiles. (The determination of the location of the boundary layer edge was based on subjectively identifying the point on the pitot pressure profiles at which the freestream pitot pressure was reached.

Simultaneous changes in Mach number, Reynolds number and total temperature produced approximately the same thickness, 5.9 inches, for the last two test conditions.) Points shown at the wall represent the wall density as computed from the freestream static pressure and the pre-run wall temperature (nominally 525 °K). Test durations are so short that there is no significant rise in the nozzle wall temperature during the test period. Data points for the first condition shown represent the average of data from two shock tunnel runs.

Because of apparently spurious records, three of the photomultiplier channels were discarded. The remaining data scatter was such that a point-to-point following of the data did not seem realistic; consequently, the smooth curves shown faired through the data in Fig. 9 were used in the further calculations of boundary layer profiles. A more exact following of the density data points would not alter the qualitative observations made later with regard to temperature and velocity profiles. It is noted, however, that there is a possible inflection in the mean density profiles in the same region of the boundary layer at which inflections are observed in the profiles of the fluctuation intensity for both density and pitot pressure.

Pitot pressure profiles are presented in Fig. 10. The plotted points represent averages from four runs at the first test condition and from two runs at the third test condition. The free-stream static pressure was used to obtain points at the wall. The present nozzle boundary-layer profiles are seen to be qualitatively similar to profiles obtained<sup>19</sup> on an entirely different geometry -- a hollow cylinder.

## 2. Computed Boundary Layer Profiles

Using the measured density and pitot pressure results, profiles of temperature, velocity and total enthalpy have been computed and are presented in Figs. 11, 12 and 13. Since the measured wall static pressure is in good agreement with the free-stream static pressure computed from measured pitot pressure, the assumption of constant pressure across the boundary layer is justified. For an ideal gas the equation of state then yields  $T/T_\infty = \rho_\infty/\rho$ , where the density ratio is taken from the faired

curves in Fig. 9.

The velocity ratio,  $u/u_\infty$ , is obtained by using the measured pitot pressure and density profiles. Denoting conditions at the stagnation point on the pitot probe by subscript, "s", conditions behind the standing normal shock by subscript "1" (all probes were in the supersonic portion of the boundary layer), and conditions ahead of the normal shock with no subscript, the normal shock relations

$$\frac{p_1}{p} = 1 + \frac{2\gamma(M^2-1)}{\gamma+1} \quad (1)$$

and

$$\frac{\rho}{\rho_1} = \frac{\gamma-1}{\gamma+1} + \frac{2}{(\gamma+1)M^2} = \frac{u_1}{u} \quad (2)$$

are substituted in the incompressible-flow Bernoulli equation for the subsonic region behind the shock

$$p_s = p_1 + \frac{1}{2} \rho_1 u_1^2 \quad (3)$$

to obtain

$$\left(\frac{u}{u_\infty}\right)^2 = \frac{p_s}{p_{s_\infty}} \frac{\rho_\infty}{\rho} \frac{1 - \frac{1}{2} \frac{\gamma-1}{\gamma+1} + \frac{1}{\gamma(\gamma+1)M_\infty^2}}{1 - \frac{1}{2} \frac{\gamma-1}{\gamma+1} + \frac{1}{\gamma(\gamma+1)M^2}} \quad (4)$$

The term with local Mach number in this expression is a small correction except for the low supersonic region. Values for local Mach number were first obtained from the ideal gas NACA tables<sup>29</sup> as a function of  $p_\infty/p_s$  in the boundary layer, then revised from  $M/M_\infty = (u/u_\infty)(T/T_\infty)^{1/2}$  in cases near the wall where iteration was necessary. The resulting velocity profiles are presented in Fig. 11. For purposes of comparison, power law profiles of  $u/u_\infty = (y/\delta)^n$  are shown. Turbulent boundary-layer velocity profiles are usually associated with small values of  $n$ , typically  $n = 1/7$  to  $1/10$ . However, it is clear that the present results agree best with larger values of  $n$ ,

typically  $n = 1/3$ . It should be noted that more conventional velocity profiles result if, as shown in Fig. 11 for the  $1.85 \times 10^5/\text{ft}$  unit Reynolds number case, the measured density is ignored and the velocity profile computed from the measured pitot pressure and the Crocco energy relation  $\frac{u}{u_\infty} = \frac{H-h_w}{H_\infty-h_w}$ . This approach was necessary in previous studies<sup>9</sup> of turbulent boundary layers at higher Reynolds numbers, when pitot pressure was the only variable measured directly. The results of such a computation are shown only for one test condition; but the resulting profile does indicate that the boundary layer under study would be adjudged typically turbulent in view of its favorable comparison with the 1/10th power law profile.

A presentation of the static temperature ratio,  $T/T_\infty$ , (inverse of density ratio) versus computed velocity in Fig. 12 clearly indicates the divergence of the present measurements from the temperature profile predicted by the Crocco relation (in conjunction with the energy equation)

$$\frac{T}{T_\infty} = \frac{T_w}{T_\infty} + \left( \frac{H_\infty}{h_\infty} - \frac{T_w}{T_\infty} \right) \frac{u}{u_\infty} - \left( \frac{H_\infty}{h_\infty} - 1 \right) \left( \frac{u}{u_\infty} \right)^2 \quad (5)$$

Profiles of total enthalpy as a function of velocity are presented in Fig. 13. These further illustrate the divergence from the Crocco relation. The cross-hatched area on Fig. 13 represents a summary<sup>20</sup> of previous data obtained from experimental pitot pressure and total temperature measurements, which are substantially in agreement with the present results. Purely as an empiricism, a curve for  $\frac{H-h_w}{H_\infty-h_w} = \left( \frac{u}{u_\infty} \right)^2$  is drawn in Fig. 13 and is seen to describe much more adequately the experimental results than the classical, linear Crocco relation. Other more rational, but less successful, modifications of the Crocco relation are discussed in Ref. 9. It is noted in both Fig. 12 and Fig. 13 that, within the limited range of unit Reynolds numbers developed, the divergence of the experimental results from the Crocco theory appears to increase with increasing Reynolds number. However, the same trend is observed with higher ratios of  $h_w/H_\infty$ , despite the fact that in the adiabatic wall case ( $h_w/H_\infty = 1$ ) agreement with the Crocco relation is known to be good. The apparent trends with Reynolds number and wall cooling may thus be within the experimental error.

### 3. Profile Integrations

Appropriate integrations have been performed to obtain the usual boundary-layer profile parameters, displacement thickness and momentum thickness. The axisymmetric forms of the expressions for displacement and momentum thicknesses<sup>9</sup> have been used, because the boundary layer thickness is roughly half the nozzle radius. Density and velocity values from the experimental data have been substituted in

$$\frac{\delta_*}{\delta} = \frac{1 - \left\{ 1 - 2 \frac{\delta}{r_w} \left[ 1 - \frac{\delta}{2r_w} - \int_0^\delta \frac{\rho u}{\rho_\infty u_\infty} \left( 1 - \frac{y}{r_w} \right) dy \right] \right\}^{1/2}}{\delta / r_w} \quad (6)$$

and

$$\frac{\theta}{\delta} = \frac{1 - \left[ 1 - 2 \frac{\delta}{r_w} \int_0^\delta \frac{\rho u}{\rho_\infty u_\infty} \left( 1 - \frac{u}{u_\infty} \right) \left( 1 - \frac{y}{r_w} \right) dy \right]^{1/2}}{\delta / r_w} \quad (7)$$

where  $r_w$  denotes the local radius (11.63 inches) of the nozzle. For purposes of comparison with results based only on pitot pressure data, the first case has also been computed using the velocity and density obtained from the measured pitot pressure plus the Crocco relation. These results are shown in parentheses and are found to compare favorably with previous data<sup>9</sup>. The complete results from the present experiments are tabulated in Table 2. Values have been grouped for the repeat conditions listed in the test conditions, Table 1.

Table 2  
BOUNDARY LAYER THICKNESS

$T_o(^{\circ}R)$	$M_\infty$	$Re_\infty / ft$	$\delta_*' / \delta'$	$\theta / \delta$	$\delta_*' / \theta$
3560	8.82	$1.85 \times 10^5$	0.335(0.279)	0.0778(0.0213)	4.305(13.1)
5810	8.24	$1.53 \times 10^5$	0.319	0.0890	3.59
3790	8.62	$1.10 \times 10^5$	0.357	0.0688	5.19
2920	8.89	$2.12 \times 10^5$	0.329	0.0873	3.77

The only further use made of these results in the present work is in the comparison of measured values of skin friction with shear laws based on momentum thickness Reynolds numbers.

#### 4. Wall Data

In the present results the measurements of heat transfer and skin friction on the wall are used primarily as a verification that the nozzle boundary layer is turbulent. On the basis of its successful application in the author's previous studies<sup>9</sup> the compressible turbulent boundary layer theory of Spalding and Chi<sup>1</sup> has been relied upon for purposes of comparison. It should be noted, however, that in the development of the Spalding and Chi theory the mixing-length related parameter,  $F_c$ , was computed using a slightly modified Crocco relation, as noted in Ref. 9. It has been shown that the experimental results differ significantly from the Crocco relation. When the Spalding and Chi theory is applied to the present heat transfer and skin friction data, the resulting comparison, as shown in Fig. 14, yields results comparable to those reported previously<sup>9</sup> for higher unit Reynolds number flows with the same basic experimental set-up as the present one (excepting the nozzle extension). (Two heat transfer curves are shown - one for the unit Prandtl number Reynolds analogy,  $2St = C_f$ , and one for the Colburn modification of Reynolds analogy,  $2St = \sigma^{-2/3} C_f$ .) Thus, despite the low unit Reynolds numbers required in the present experiments to remain within the operating range of the electron beam, the flow is still a turbulent one.

For the case in which the Crocco relation was used in conjunction with measured pitot pressures to obtain profiles for the momentum thickness integration, the resulting momentum thickness Reynolds number was used to compare the experimental value of the skin friction coefficient with Spalding and Chi theory. The resulting data point is less than ten per cent above the Spalding and Chi theory, as had been the case for the nozzle measurements reported previously<sup>9</sup>. This comparison is consistent with the way in which Spalding and Chi developed their theory. However, when the density profiles from the present experiments are used to calculate the value of the coefficient

for  $C_f$ ,

$$F_c = \left[ \int_0^1 \left( \frac{\rho}{\rho_\infty} \right)^{1/2} d \frac{u}{u_\infty} \right]^{-2}$$

the value for  $F_c$  becomes 1.72 compared to the Spalding and Chi value of 3.62. Since the  $F_c$  value is involved in the Spalding and Chi error minimization used in choosing the momentum thickness Reynolds number coefficient,  $FR_\theta$ , it is not possible to locate within the Spalding and Chi results a value of  $FR_\theta$  consistent with the values of  $F_c$  and  $R_\theta$  taken directly from the present experiments. Thus, as a prediction method the Spalding and Chi formulation is internally consistent and provides consistently good predictions. But as an actual description of the relationship between compressible, cold-wall turbulent boundary layers and the constant density turbulent boundary layer, the Spalding and Chi formulation fails to incorporate the apparent discrepancies observed here between the Crocco relation and measurements obtained at cold wall conditions.



#### IV. CONCLUSIONS

It has been demonstrated in a series of measurements with an electron beam probe in the boundary layer of a shock-tunnel nozzle wall that direct measurements of densities and density fluctuations can be obtained in a turbulent boundary layer. Both the density measurements and accompanying pitot pressure measurements indicate peak fluctuation intensities quite near the wall.

The direct measurement of boundary layer density in the present experiments, in conjunction with measured pitot pressures, has confirmed the substantial deviation from the simple Crocco energy relation of actual turbulent hypersonic turbulent boundary layers at cold wall conditions. The degree of deviation in temperature and total enthalpy from the Crocco relation has marked effects upon the integrated boundary layer thicknesses. As a result the attempted comparison with the Spalding and Chi theory failed, except when the Crocco relation was invoked instead of using the measured density.

## V. REFERENCES

1. Spalding, D.B. and Chi, S.W., "The Drag of a Compressible Turbulent Boundary Layer on a Smooth Flat Plate with and without Heat Transfer," Journal of Fluid Mechanics, Vol. 18, Part I, 1964, pp. 117-143.
2. Coles, D.E., "The Turbulent Boundary Layer in a Compressible Fluid," RAND Corp. Rept. R-403-PR, September 1962.
3. Crocco, L., "Transformation of the Compressible Turbulent Boundary Layer with Heat Exchange," AIAA Journal, Vol. 1, No. 12, December 1963, pp. 2723-2731.
4. Baronti, P.O. and Libby, P.A., "Velocity Profiles in Turbulent Compressible Boundary Layers," AIAA Journal, Vol. 4, No. 2, February 1966, pp. 193-202.
5. Head, M.R., "Entrainment in the Turbulent Boundary Layer," Aeronautical Research Council (G.B.) R&M 3152, 1958.
6. Standen, N.M., "A Concept of Mass Entrainment Applied to Compressible Turbulent Boundary Layers in Adverse Pressure Gradients," AIAA Paper No. 64-584, 1964.
7. Green, J.E., "The Prediction of Turbulent Boundary Layer Development in Compressible Flow," Journal of Fluid Mechanics, Vol. 34, Part 4, 1968, pp. 753-778
8. Neal, Luther, Jr., "Pressure Heat Transfer and Skin Friction Distributions over a Flat Plate Having Various Degrees of Leading Edge Bluntness at a Mach Number of 6.8," NASA TN D-3312, April 1966.
9. Wallace, J.E., "Hypersonic Turbulent Boundary-Layer Studies at Cold Wall Conditions," Proceedings of the 1967 Heat Transfer and Fluid Mechanics Institute, Paul A. Libby, et al., editors, Stanford University Press, 1967, pp. 427-451.

10. Cohen, N.B., "A Method for Computing Turbulent Heat Transfer in the Presence of a Streamwise Pressure Gradient for Bodies in High-Speed Flow," NASA Memo I-2-59L, March 1959.
11. Spence, D.A., "Some Applications of Crocco's Integral for the Turbulent Boundary Layer," Proceedings of the 1960 Heat Transfer and Fluid Mechanics Institute, D.M. Mason et al., editors, Stanford University Press, 1960, pp. 62-76.
12. Kutateladze, S.S. and Leont'ev, A.I. (Translated by D.B. Spalding), Turbulent Boundary Layers in a Compressible Gas, New York: Academic Press, 1964, pp. 25-29.
13. Walz, A. "Compressible Turbulent Boundary Layers," in The Mechanics of Turbulence, New York: Gordon and Breach Science Publishers, Inc., 1964 (Proceedings of Colloque International Sur, "La Mechanique de la Turbulence," Marseille, August 28 to September 2, 1961), pp. 299-350.
14. Rotta, J.C., "Heat Transfer and Temperature Distributions in Turbulent Boundary Layers at Supersonic and Hypersonic Flow," in "Recent Developments in Boundary Layer Research," AGARDograph 97, Part I, May 1965, pp. 35-63.
15. Lobb, R.K., Winkler, E.M. and Persh, S., "Experimental Investigation of Turbulent Boundary Layers in Hypersonic Flows," Journal of Aeronautical Sciences, Vol. 22, No. 1, 1955, pp. 1-9, 50.
16. Hill, F.K., "Turbulent Boundary Layer Measurements at Mach Numbers of 8 to 10," Physics of Fluids, Vol 2, 1959, pp. 668-680.
17. Winkler, E.M. and Cha, M., "Investigation of Flat Plate Hypersonic Turbulent Boundary Layers with Heat Transfer at a Mach Number of 5.2," NAVORD Rept. 6631, 1959, U.S. Naval Ordnance Lab., White Oak, Md.
18. Danberg, J.E., "Characteristics of the Turbulent Boundary Layer with Heat and Mass Transfer at  $M = 6.7$ ," NOLTR 64-99, October 1964, Naval Ordnance Lab., White Oak, Md.

19. Samuels, R.D., Peterson, J.B., Jr. and Adcock, J.B.,  
"Experimental Investigation of the Turbulent Boundary Layer at a  
Mach Number of 6 with Heat Transfer at High Reynolds Numbers,"  
NASA TN D-3858, March 1967.
20. Bertram, M. H. and Neal, L., Jr., "Recent Experiments in  
Hypersonic Turbulent Boundary Layers," NASA TMX-56335, May 1965.
21. "Cornell Aeronautical Laboratory Hypersonic Shock Tunnel ,  
Description and Capabilities," April 1968, Cornell Aeronautical Lab.,  
Buffalo, N.Y.
22. MacArthur, R.C., "The Development of High Output Pressure  
Transducers for Shock Tunnel Testing," Rept. TR-68-37, April 1968,  
Air Force Aero Propulsion Laboratory, (Cornell Aeronautical Lab.,  
Buffalo, N.Y.).
23. MacArthur, R. C. , "Contoured Skin Friction Transducer, " Rept.  
AN-2403-Y-1, August 1967, Cornell Aeronautical Lab., Buffalo, N. Y.
24. Vidal, R.J., "Transient Surface Temperature Measurements, "  
Rept. 114, March 1962, Cornell Aeronautical Lab., Buffalo, N.Y.
25. Martin, J.F., Duryea, G.R. and Stevenson, L.M., "Instrumentation  
for Force and Pressure Measurements in a Hypersonic Shock Tunnel,"  
Advances in Hypervelocity Techniques, Plenum Press, 1962,  
(Cornell Aeronautical Laboratory Rept. No. 113).
26. Burke, A. F. , "Turbulent Boundary Layers on Highly Cooled Surfaces  
at High Mach Numbers, " in Symposium on Aerothermoelasticity,  
Dayton, Ohio, October 3 to November 1, 1961, Air Force Aeronautical  
Systems Div., TR 61-645, pp. 704-741.
27. Kistler, A. L. , "Fluctuation Measurements in a Supersonic Turbulent  
Boundary Layer, " Physics of Fluids, Vol. 2, No. 3, 1959, pp. 290-  
296.
28. Morkovin, M. V. , "Effects of Compressibility on Turbulent Flows, "  
in The Mechanics of Turbulence, New York: Gordon and Breach  
Science Publishers, Inc., 1964, pp. 367-380.

29. "Equations, Tables, and Charts for Compressible Flow," NACA Rept. 1135.
30. Llinas, J. and Rustay, W. C., "Temperature and Density Measurements in the Base Region of a Clustered Rocket Model Using an Electron-Beam Technique," Rept. HM-2107-Y-1, July 1966, Cornell Aeronautical Lab., Buffalo, N. Y.
31. Muntz, R. P., Abel, S. J. and Maguire, B. L., "The Electron Beam Fluorescence Probe in Experimental Gas Dynamics," Supplement to IEEE Transactions on Aerospace, Vol. AS-3, No. 2, June 1965, pp. 210-222.
32. Davidson, G. and O'Neil, R., "The Fluorescence of Air and Nitrogen Excited by 50 keV Electrons," Rept. AFCRL-64-466, May 1964, Air Force Cambridge Research Labs. (also American Science and Engineering, Inc. Rept. ASE-512 and DDC No. AD 608058).
33. Camac, M., "Boundary Layer Measurements with an Electron Beam," Research Rept. 275, July 1967, AVCO Corp., Everett Research Lab., Everett, Mass. (prepared for Bell Telephone Labs., Inc.).

## APPENDIX

### ELECTRON-BEAM DENSITY PROBE

#### 1. Electron-Beam Density Probe

The electron-beam density-probe technique is based on the stimulation of emission from a gas by collisional excitation using a beam of energetic electrons (energies usually greater than 10 kV). Inelastic collisions between the gaseous molecules and the beam electrons result in the production of electronically excited molecules or molecular ions and the subsequent radiative transition to the electronic ground state of the molecule or ion, which produces a gaseous fluorescence coincident with the electron beam. If the radiative transition is unaffected by gas-kinetic collisions, the local emitted intensity is directly proportional to the local gas number density of molecules (such other conditions as beam current and beam voltage held constant). With the fluorescent light yield detected at a number of points along the beam with photomultipliers and with the beam continuously in operation during the test event, spatially and temporally resolved measurements can be made.

To achieve a luminescence which is linear with the number density of molecules, one desires that the particular emission to be used result from a direct excitation-emission sequence and that the excited state involved in the transition be reached by direct excitation from the ground state of the neutral molecule. In the case of nitrogen, which has been studied extensively in the application of the electron beam probe to number density and temperature measurements in gas flows, the most prominent system excited is the first negative system of  $N_2^+$  with spectral emission located approximately in the 3800 Å to 4300 Å band. Investigations have been conducted at Cornell Aeronautical Laboratory using both nitrogen and air.<sup>30</sup> The present study used air exclusively as the test gas. The mean lifetime of the excited state of  $N_2^+$  is only about  $6 \times 10^{-8}$  sec., so that the extent to which the flow carries radiating molecules away from the region viewed (that is, the region

of initial excitation by the beam) is negligibly small. The spatial resolution is limited only by the beam diameter and length of beam selected for observation.

In addition to the inelastic collisions, elastic collisions between molecules and beam electrons can occur; these elastic collisions contribute primarily to scattering of the electron beam which causes a spreading of the light emanating from the region of the beam (See Figure 15). Scattering increases with number density and causes a loss of spatial resolution in density measurements, since it is necessary to observe the total emission. A measure of control over scattering is possible by increasing the beam accelerating voltage, since electron-neutral collision cross sections decrease with increasing electron energy. However, a reduction in emission intensity (for a given beam current) also occurs due to the concurrent reduction in the number of inelastic collisions. Muntz<sup>31</sup> has pointed out that the improvements resulting from the use of beam energies exceeding 50 kV to counteract beam spreading are small, especially in view of the rapidly increasing cost and complexity of operating equipment above that voltage level and the increased radiation (X-ray) hazards to operating personnel. The present beam was operated at 40 kV.

The measurement of molecular number density is conceptually simple. Emission intensity is measured from the full width and some arbitrary length of the beam together with a simultaneous measurement of beam current. Since emission intensity is directly proportional to beam current, accurate measurement of current is of fundamental importance, and corrections for any variation in beam current during the test interval are necessary. In addition, the sensing optics must accommodate the full beam width; this consideration is especially important if accurate density measurements are to be obtained in the presence of appreciable beam spreading. The length of beam observed will generally be determined a compromise between need to achieve satisfactory signal-to-noise ratios in the optical sensors at low densities and the requirements of spatial resolution.

For nitrogen densities equivalent to room temperature pressures of

less than about 500 microns Hg, emission intensity is directly proportional to number density. With increasing density, collisional de-excitation (quenching) becomes important and the linear relation between density and emission intensity is lost, as is ultimately the sensitivity of emission intensity to changes in density.

## 2. Equipment

For a schematic drawing of the electron beam installation used in the present program, reference is again made to Figure 2. The 40 kV electron beam was projected through the nozzle wall and collected in a graphite cup. The electron gun is an air-cooled, grid-controlled, electrostatically focused RCA J1694 unit with a directly heated tungsten cathode. The electron gun control unit and power supply is an RCA VX2207 unit. The electron beam is projected through a series of orifices (apertures) to generate a collimated beam of electrons. The orifices serve both to collimate the beam and to isolate the beam generating apparatus into a series of chambers that are differentially pumped to provide the necessary pressure buffering between the high vacuum required for the electron gun and the higher pressure of the shock tunnel test section.

The upper limit in density was ultimately set by the maximum pressure buildup allowable in the electron gun chamber, viz.  $10^{-5}$  Torr. It was found during calibration that a final orifice diameter of 0.028 inch had to be used in the drift tube for the gun chamber pressure to remain within this limit for test section pressures up to 2 Torr. This orifice size limited the beam current during calibration to 200 microamps. For shock tunnel runs the gun chamber was isolated from the test section pressure after the useful test period by closing a pneumatically-operated ball valve. This arrangement permitted the use of a larger diameter 0.060 inch for the final orifice in the drift tube, which in turn yielded a beam current of one milliampere for the shock tunnel runs.

To avoid a small ac ripple in the beam current, the filament heater circuit was opened by a trigger from the shock tube just prior to shock



tunnel flow in the nozzle. The filament thus operated during the run entirely on thermal inertia. Steadiness of the current during the test time was checked by observing the current after filament shut-off without flow in the nozzle. The current would continue for the four to six millisecond period typical of shock tunnel test time at a steady level within three to five percent of the pre-shut-off level. In addition, the scattered current collected on the interior of the end of the drift tube was monitored during shock tunnel operation and was found to remain steady.

Since the shock-tunnel test section is evacuated to a pressure of a few microns of mercury prior to the test, it was considered important to avoid suction of the boundary layer through the orifice provided for the beam in the nozzle wall. To minimize this potential disturbance in the boundary layer being traversed by the electron beam, a series of relief holes were incorporated in the nozzle wall just downstream from the electron beam orifice. These were designed to allow rapid filling (within one millisecond) of a small, enclosed volume surrounding the path of the beam between the end of the electron beam drift tube and the orifice in the nozzle wall.

The electron beam fluorescence was viewed through a port cut into the nozzle wall such that the edge of the port closest to the beam was approximately nine inches from the beam (or one-eighth of the nozzle circumference). Although this arrangement set the axis of the viewing optics system at 20 degrees away from normal to the beam, it was adopted to avoid possible disturbances in the instrumented region of the wall and of the boundary layer. The option of using a viewing system with an axis normal to the beam, but looking upstream, was discarded because of potential errors which could be produced by radiation from the hot gas in the nozzle throat or from the shock system which would have formed over the viewing optics hardware.

The image of the electron beam fluorescence was formed at a distance of 39 inches from the beam with a one-to-one optical system using a pair of 3.1-inch diameter f/6.3, coated, achromatic lenses. The luminescence at points along the beam image was picked up by fiber optics (light guide) bundles and transmitted through them to conventional photomultipliers. Six points close to the nozzle wall (within 1.2 inches) were viewed with

fiber optics bundles six inches in length and having a rectangular end at the beam image 0.1 inch along the beam and 0.125 inch across the beam. Seven additional points over the range 1.8 to 5.85 inches from the wall were viewed with one-foot long bundles having a rectangular cross section 0.1 inch (along the beam) by 0.475 inch. The fiber optics bundles, supplied by American Optical, were circular at the end connected to the photomultipliers. Glass filters (Corning No. 5-58), having peak transmission at  $4100 \text{ \AA}$  and dropping to ten percent of peak transmission at  $3600$  and  $4600 \text{ \AA}$ , were placed between the light guide ends and the photomultiplier cathode to select radiation primarily from the 0,0 and 0,1 bands of the  $\text{N}_2$  + first negative system (with band heads centered at  $3914$  and  $4278 \text{ \AA}$ , respectively).<sup>32</sup> The peak spectral response of the photomultiplier units (Dumont 6467 with an S11 cathode) occurs at  $4400 \text{ \AA}$ . The fiber optics bundles are known to have reduced transmittance in the blue region of the spectrum (dropping sharply for wavelengths below  $4000 \text{ \AA}$ ), but the units used were not specifically calibrated to measure the transmission efficiency. It is simply assumed that the effect is consistent, independent of possible temperature effects on the intensity distribution, within each of the bands and is therefore adequately incorporated in the beam calibration, especially since the temperatures encountered in the test program were comparable to the calibration temperature.

### 3. Beam Calibration

The use of electron-beam-induced luminescence to infer gas density requires that the relationship between total received light, beam current, and density be known. In its present application the entire electron beam system, including viewing optics, was calibrated with dry air as the test gas over the range 0.18 (Torr) to 2.15 Torr at room temperature ( $0.55$  to  $6.6 \times 10^{-6}$  slugs/ft<sup>3</sup> in density). The accelerating potential for the electron beam was held constant at 40 kV.

Collection of the beam current presented something of a challenge. Although the portion of the beam intended for use was the segment within six inches of the shock tunnel nozzle wall, earlier experience with the

electron beam system had shown that the glow around a current collection cup could interfere with the measurement of beam luminescence at points along the beam which are too close to the current cup. Consequently, in the present program -- both for calibration and during the shock tunnel runs -- the current collection cup was located at 13.65 inches from the nozzle wall, near the axis of the nozzle. The cup, sketched in Figure 2, was made from graphite stock. To take into account the spreading of the electron beam encountered in the density range of the present program, a device was installed in the tunnel during calibration to permit a current cup to be extended to intercept the beam at the wall (close to the orifice in the nozzle wall) and then to be retracted to permit measurement of the current collected by the remote current cup. In this way a calibration of the total beam current and of the current scattered outside the remote, one-inch diameter cup could be made as a function of the gas density, as shown in Figure 16.

In the actual shock tunnel runs the test section was evacuated prior to the run to a pressure of less than 5 microns of mercury. In this case the beam spreading is negligible, and the total beam current is collected by the remote collection cup. During the shock tunnel run the beam traverses gas at the freestream core density over most of its path and, therefore, spreads such that a smaller, but steady, current is collected during the run. The ratio of the current collected during the run to the pre-flow current is also shown in Figure 16 as a function of the gas density in the freestream core. It can be seen that the current loss is somewhat greater in the flowing case despite the fact that, for the present test conditions, the gas densities in the boundary layer were lower than the density in the nozzle core. The effect of density changes is seen to produce similar changes in collected current for both the static calibration and the measurements with gas flow. In the present experiments the primary current measurement during static calibration was made by using the remote one-inch cup (at 13.65 inches from the wall). At each level of air density in the static calibration the output voltage of the photomultiplier for each viewing channel was normalized by the total beam current inferred from the measured cup current and Figure 16.

The lower curve was used because it yielded better agreement between the density calibration curve (Figure 17) and the absolute value of freestream density during the tests. The relative variation in density across the boundary layer is unaffected by the choice of curves from Figure 16, since the two curves are in a constant ratio.

Figure 17 is a typical calibration curve for air with one of the two outermost viewing channels. Some nonlinearity is noted over the entire range of the calibration, but not enough to affect resolution of density variations at the upper range.

Although the primary objective of the shock tunnel tests was the observation of the relative variation in density across the boundary layer, it is of interest to note the accuracy of the absolute value of density as inferred from the light received from a point in the freestream. The experimental output for the photomultiplier whose static calibration is shown in Figure 17 was divided by the indicated pre-flow current and entered on Figure 17 at the value of freestream density computed from the measured freestream pitot pressure for each of the shock tunnel runs. The points at densities of approximately  $6 \times 10^{-6}$  slugs/ft<sup>3</sup> lie slightly below the static calibration, while the single point at  $3 \times 10^{-6}$  slugs/ft<sup>3</sup> is slightly higher than the calibration curve. Although the source of the observed differences is not known, beam spreading, as considered in the following discussion, is not believed to be responsible.

#### 4. Beam Profiles

A primary concern in applying the electron beam to the measurement of density is that of accounting correctly for the total light generated at a given station along the beam and of including the full beam current which produces the beam luminescence. One method of assessing beam characteristics is that of interpreting photographs of the beam luminescence. Photographs taken of the beam at two pressures (0.82 and 1.6 Torr) have been analyzed to determine the distribution of light intensity at several stations along the beam. A print of the photograph taken at 0.85 Torr is included as Figure 15. The spot seen at one end of the beam is associated with the

exposed end of the drift tube and apparently results from scattering through the final orifice, which is 0.060 inch in thickness. During shock tunnel runs a cover plate with a relatively large hole (0.15 inch diameter) for the beam was in place, as seen in the configuration photograph, Figure 1, and screened the spot from the view of the optics. The negatives of the two photographs were scanned on a microdensitometer with an effective viewing rectangle 20 microns wide (across the beam) and 0.115 inch long (along the beam) in the actual scale of the experiment. A film calibration of the Royal Pan film with an exposure step table indicated that except for very low exposures the dependence of film density,  $D$ , on exposure,  $E$ , is  $\Delta D = \Delta \log E$ . Since exposure is the product of light intensity and time and since the exposure time is constant for a given photograph, the change in film density is therefore equal to the change in the logarithm of the local light intensity.

Several important characteristics of the beam could be inferred from the film scans, samples of which are shown in Figure 18. Light intensity as calculated from film density is shown on the ordinate in Figure 18; the abscissa represents the actual scale of the cylindrical radius from the center of the beam. The decrease in peak intensity and the spreading of the profile along the beam as a result of beam spreading are clearly shown. At each station three beam characteristics were determined:

- 1) total light (found by integrating the total area under the intensity vs. radial distance plot).
- 2) integrated light within the width viewed by the fiber optics at each station
- 3) the half intensity width,  $w_{1/2}$  (width at which the light intensity is half the peak intensity at that station).

The results of these measurements are shown in Figure 19. At the top of the figure is shown the ratio of the integrated total light at a given position along the beam to the integrated total light at the wall (actually 0.2 inch from the wall position when the cover plate is in place). Within the reading and integration error, there is not significant attenuation in total light (or total beam current) along the 5 1/2 inches of the beam photographed. The

indicated increase in (total light)/(total light at wall) with distance along the beam for the 1.6 Torr case is unrealistic and is believed to be a result of reading and integration errors involved in reading the photographs. In the lower curves at the top of the figure the fraction of total light found to be within the viewing width of the fiber optics bundles seems alarmingly low because it falls in the range of 50 to 70 percent of the total light. However, closer inspection reveals two important characteristics, viz., that the fraction of light viewed changes little with either distance along the beam or pressure (density) level, both of which should have an effect on spreading the beam. It should be noted here that the photographs from which these measurements were made were obtained with an unfiltered system, that is, with a conventional camera viewing the beam through a clear glass plate. Radiation from systems other than the  $N_2^+$  first negative may therefore have been included in the photograph although excluded in the actual filtered optics system used in calibration and test. For example, there exists some evidence<sup>33</sup> that excitation and radiation of neutral  $N_2$  molecule is mainly produced by low-energy secondary electrons and might, therefore, produce a wider profile than the  $N_2$  radiation. The test data were therefore reduced without any attempt to account for "missed light" in either calibration or test. This approach seems to be validated by the fact that the boundary layer density determined in this way shows no step change at the adjacent points in the boundary layer (at 1.3 inches from the wall) viewed by adjacent optics channels with viewing widths of 0.125 inch and 0.475 inch, respectively.

Finally, Figure 19 also presents the readings of the half-intensity widths as a function of distance along the beam. The fiber optics widths are shown by solid lines. It is interesting to note that the beam remains effectively focused for the first inch or two after it passes through the nozzle wall, then begins to spread rapidly. Probably more by coincidence than by actual duplication, the beam spreading in the outer portion of the beam follows very well the empirical correlation of beam spreading reported by Camac.<sup>33</sup> The effect of gas density on beam spreading seems to be slightly greater in the present measurements, however, than in the Camac correlation. The primary

core of the beam is seen to remain well within the width of the viewing optics, with the possible exception of the outermost point at the 1.6 Torr condition. The beam calibrations and shock tunnel readings have been used directly without attempts to account for the apparently small relative differences in beam spreading between the calibration (at constant density) and the shock tunnel run (with density variations in the boundary layer thickness of just less than six inches and with constant density over the remaining path to the current collection cup).

The spectral distribution of the beam luminescence from the  $N_2^+$  first negative system is a function of the vibrational temperature of the gas at elevated temperatures. Thus a possible discrepancy can arise if the calibration is made at room temperature and the test made at a higher gas temperature. In the present case, however, the maximum static temperature in the boundary layer is approximately  $1000^\circ R$ . Even if the vibrational excitation level freezes in the nozzle expansion, the maximum vibrational temperature would be approximately  $1500^\circ R$ , which is well below the range at which the  $N_2^+$  first negative band intensities are affected to a detectable degree by the vibrational temperature of the gas.

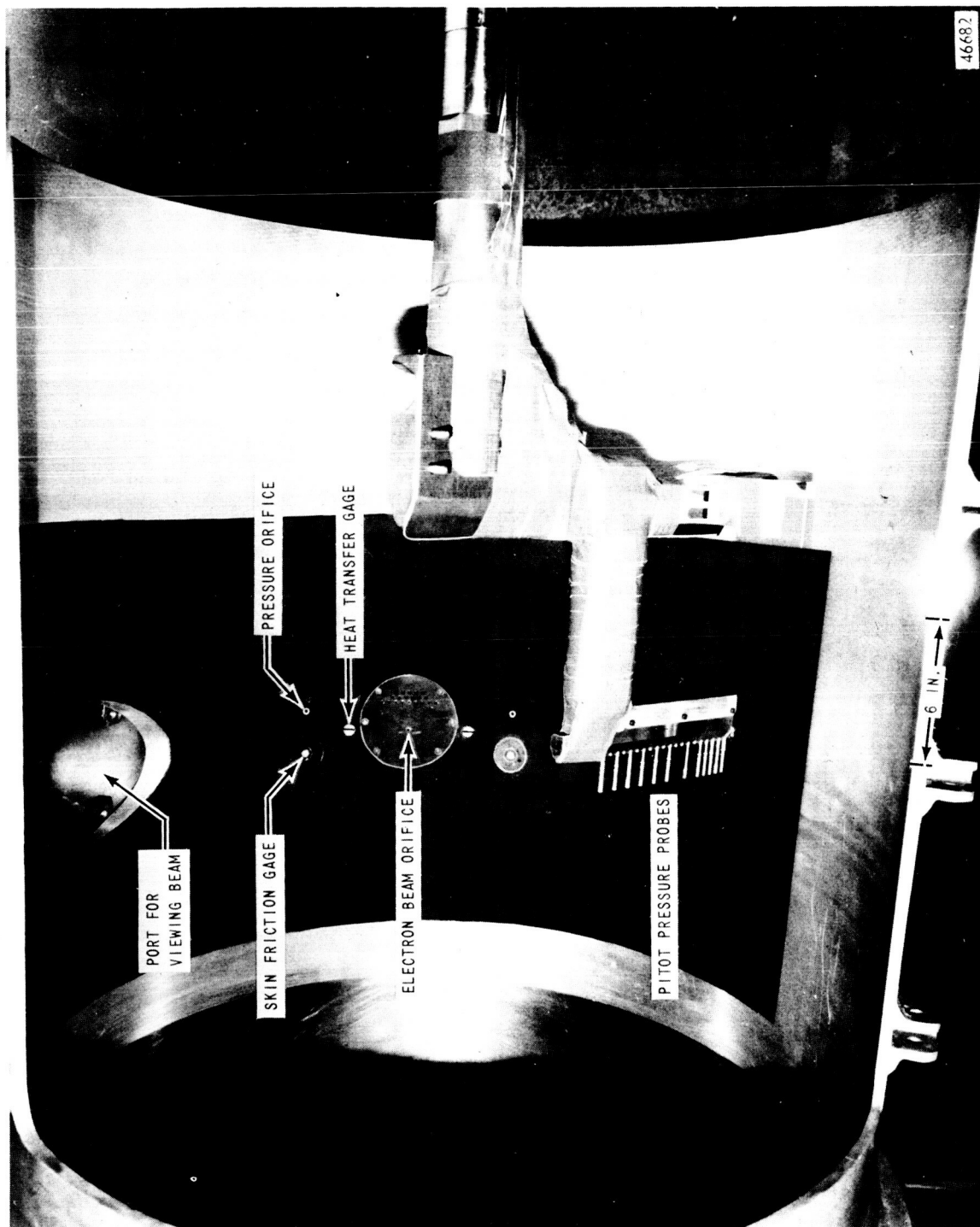


Figure 1 NOZZLE INSTRUMENTATION FOR TURBULENT BOUNDARY LAYER EXPERIMENTS



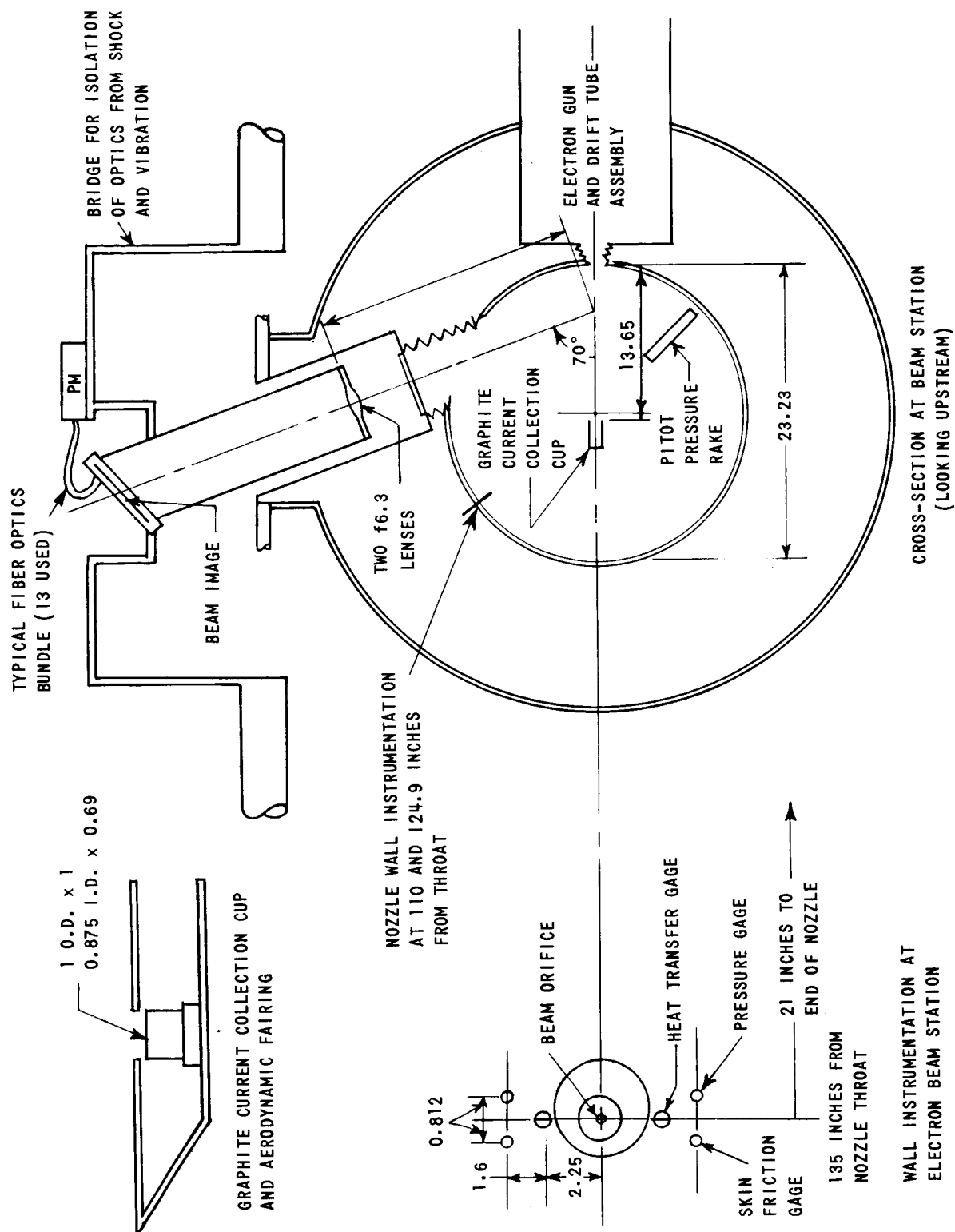


Figure 2 NOZZLE INSTRUMENTATION AND VIEWING OPTICS (NOT TO SCALE - ALL DIMENSIONS IN INCHES)

(CONTOURED, MACH 8 NOZZLE, THROAT DIAMETER = 0.964 INCHES)

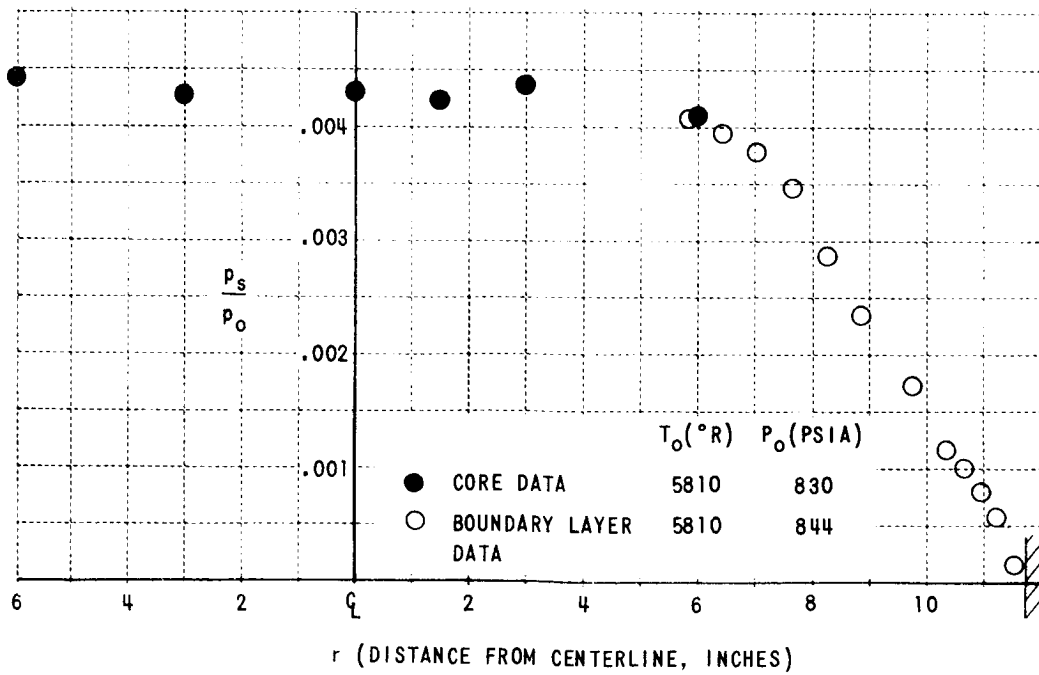
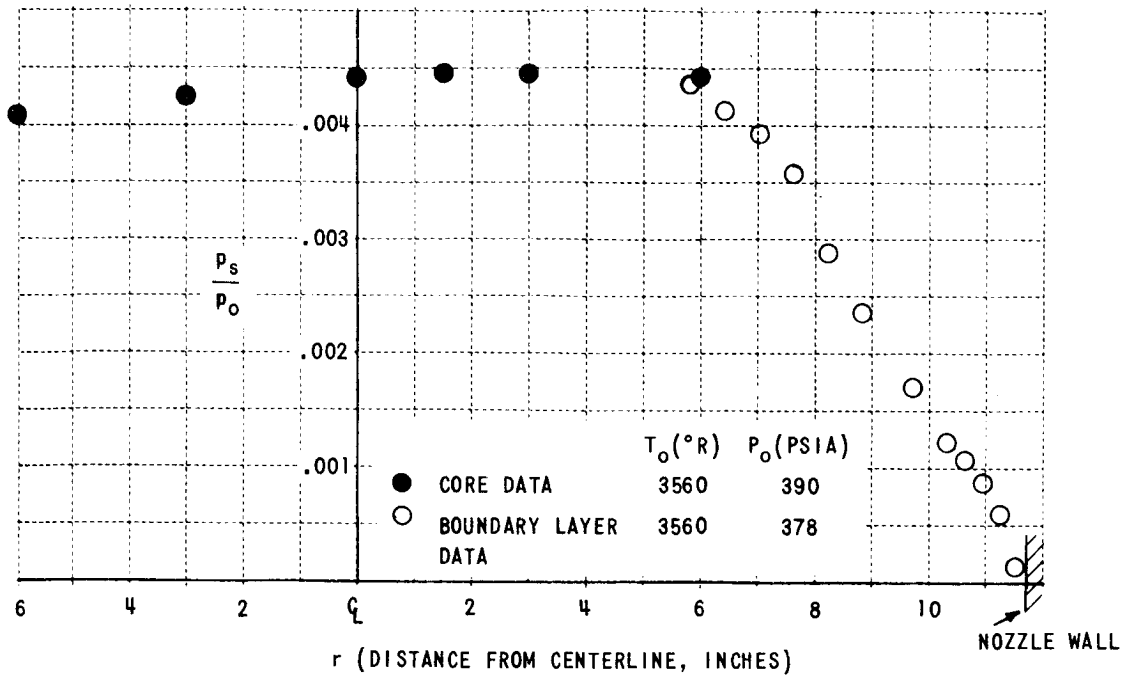


Figure 3 NOZZLE PITOT PRESSURE DISTRIBUTIONS

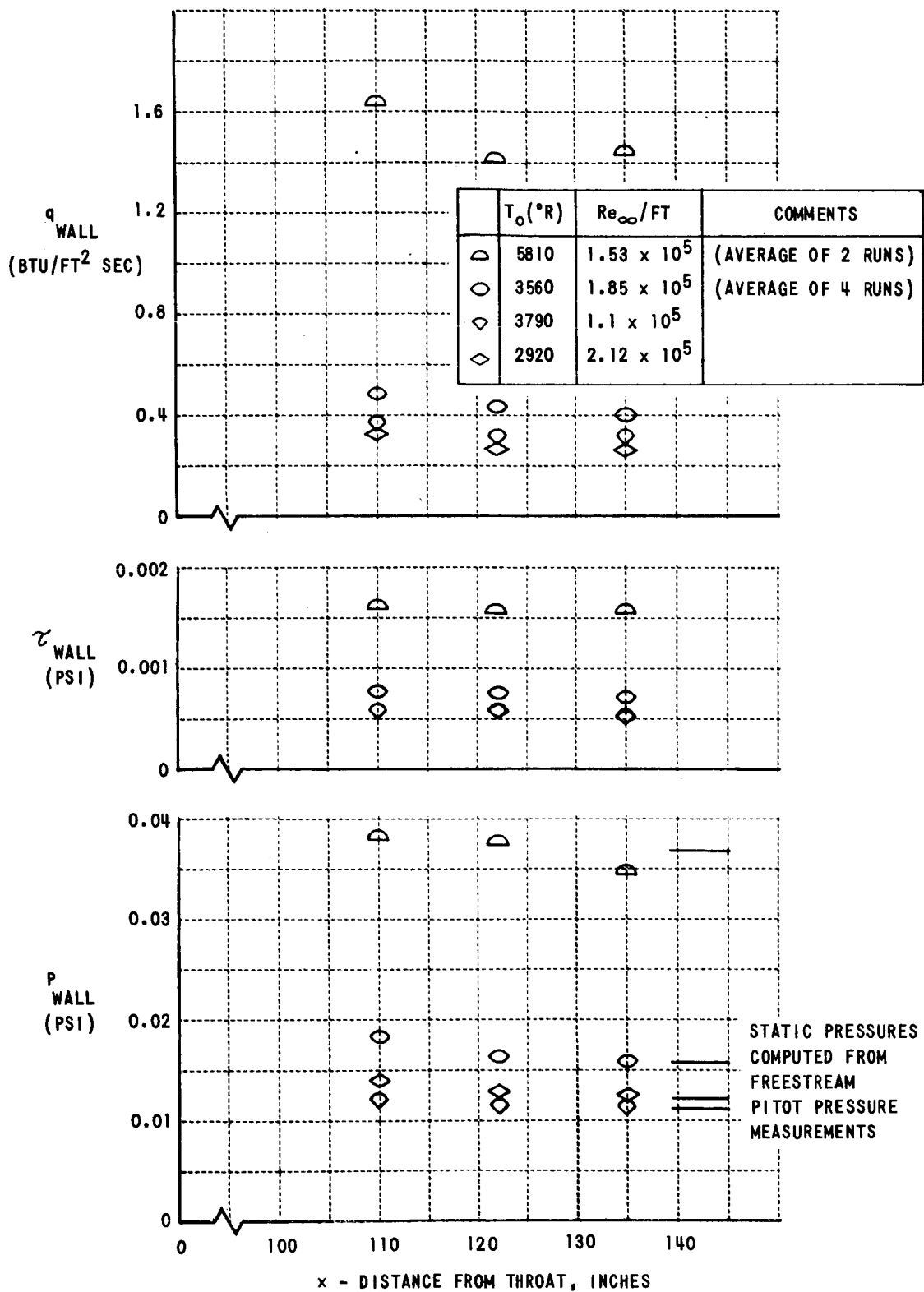


Figure 4 EXPERIMENTAL DATA ON THE NOZZLE WALL

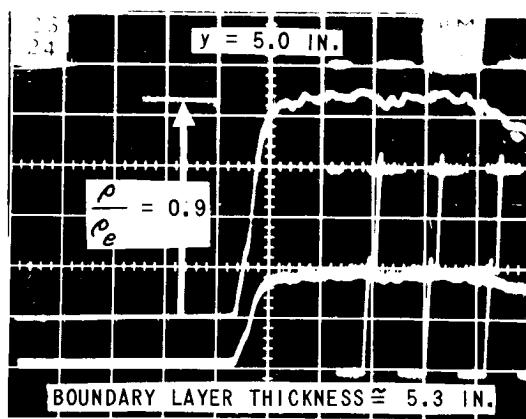
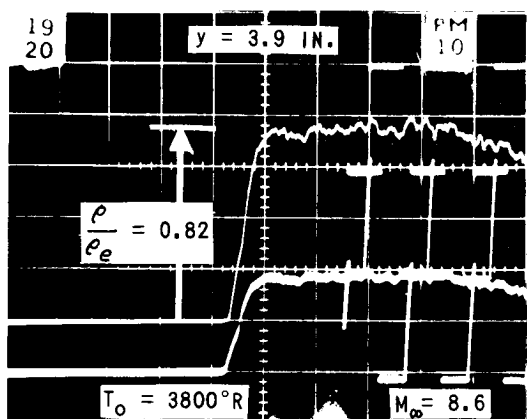
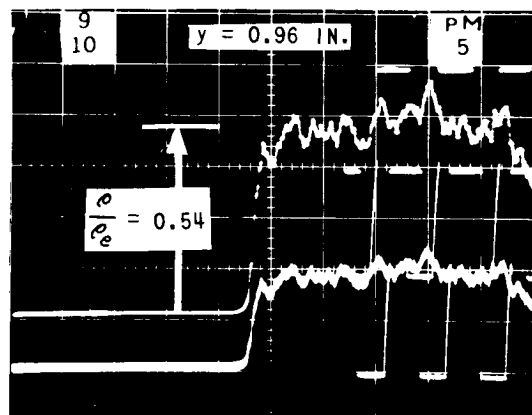
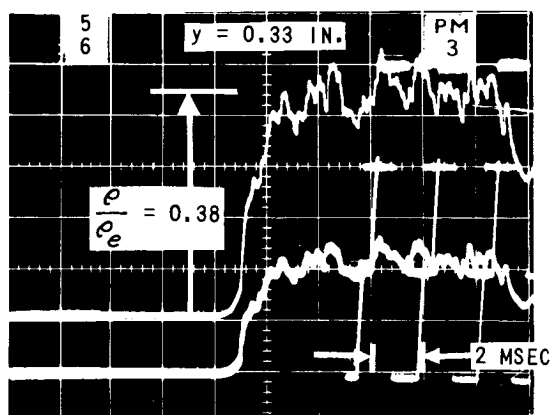
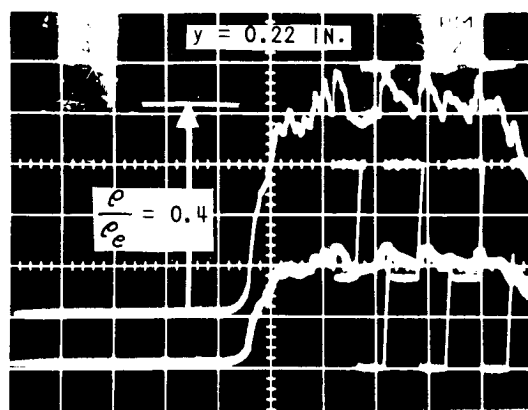
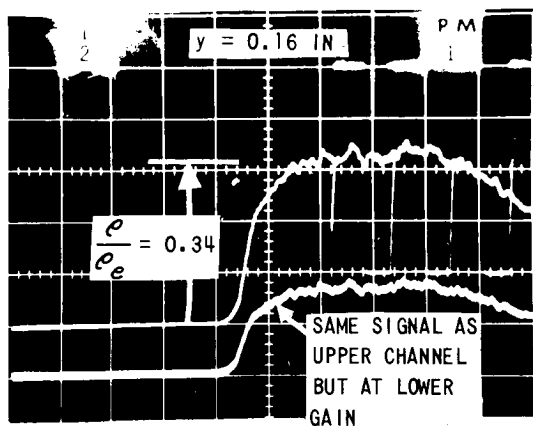


Figure 5 PHOTOMULTIPLIER RECORDS FROM ELECTRON BEAM LUMINESCENCE IN A TURBULENT BOUNDARY LAYER

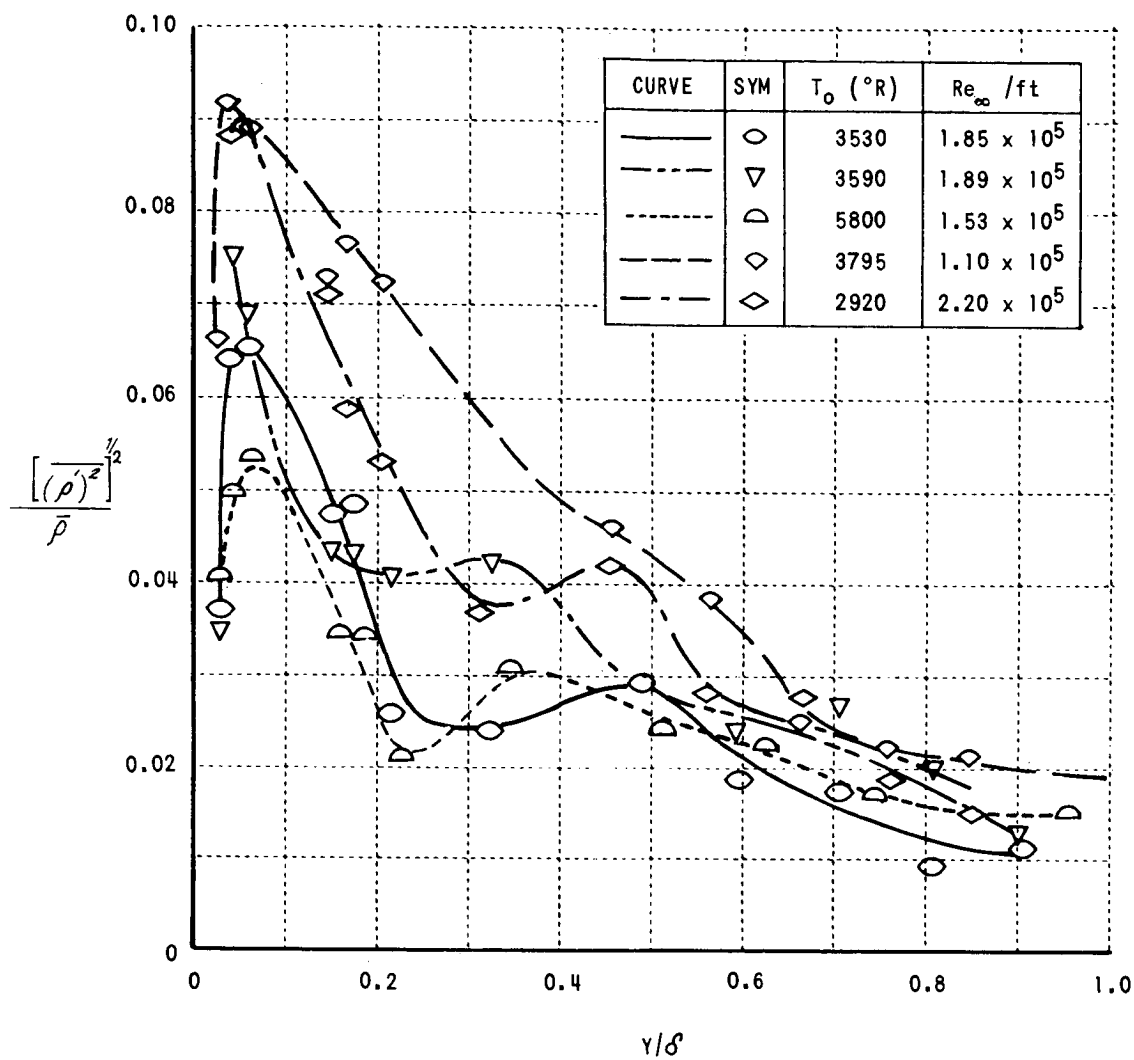
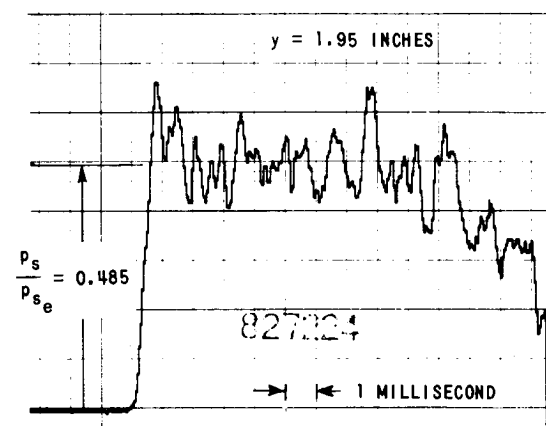
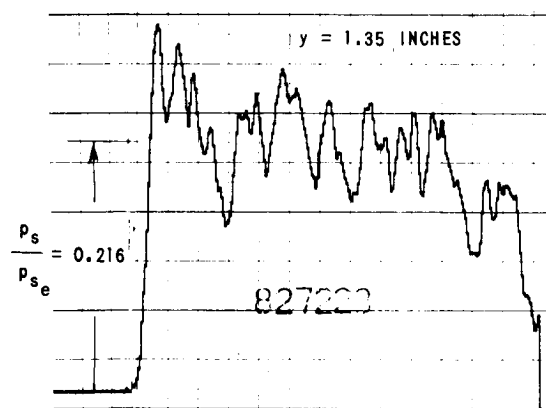
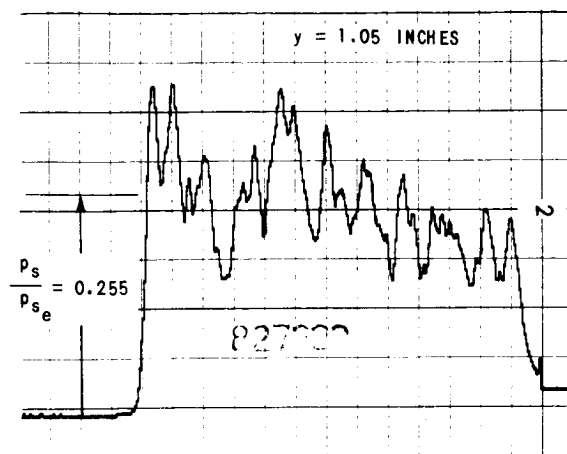
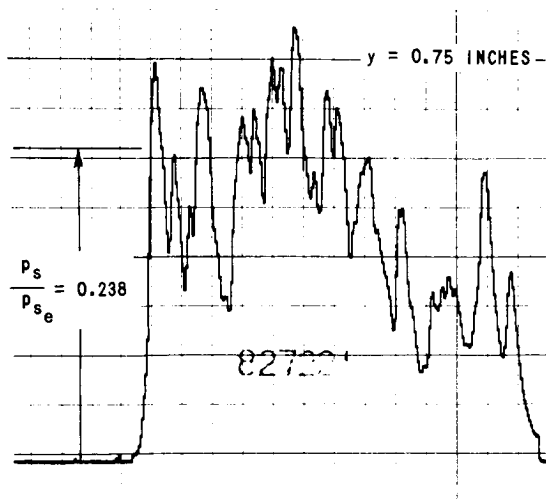


Figure 6 INTENSITY OF DENSITY FLUCTUATIONS FROM PHOTOMULTIPLIER RECORDS



THIN RUBBER CAP OVER DIAPHRAGM (ALL OTHER PROBES SHOWN HAVE LABYRINTH-PATH CAP)

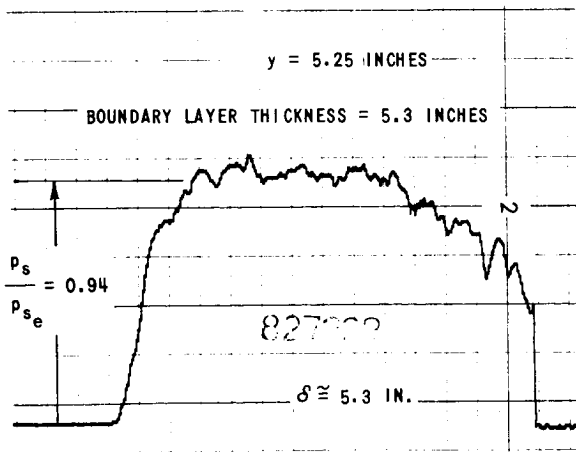
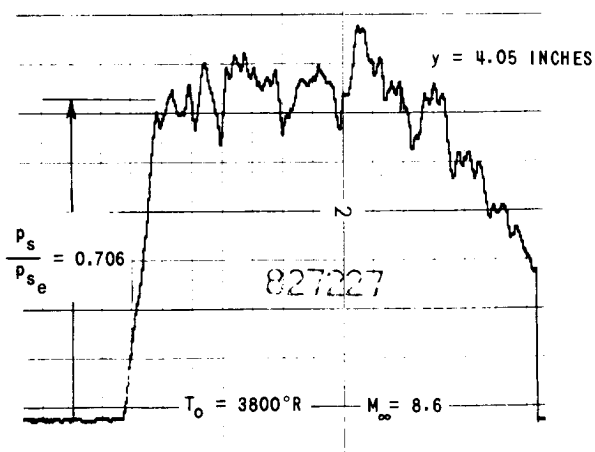


Figure 7 RECORDS OF PITOT PRESSURE IN A TURBULENT BOUNDARY LAYER

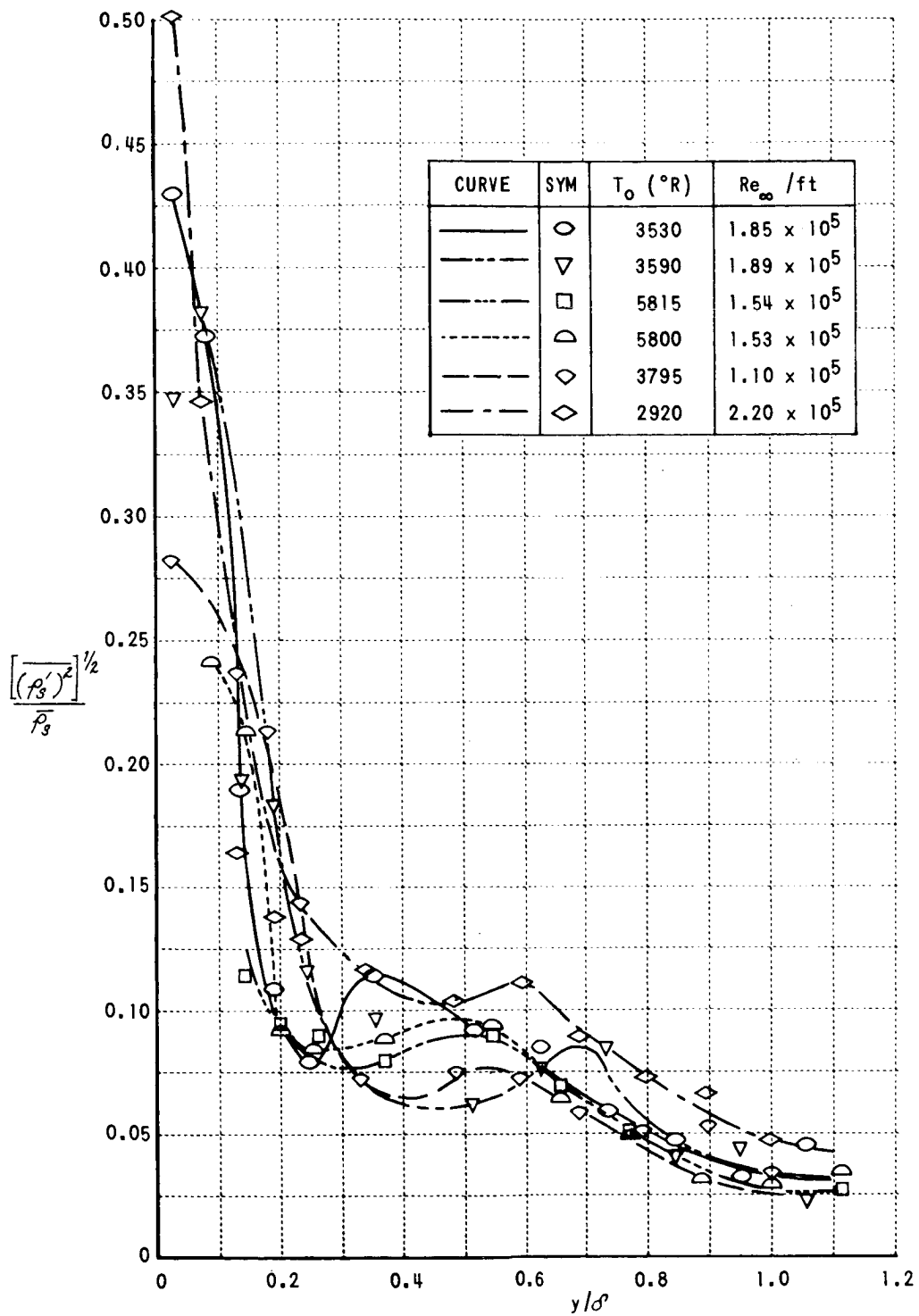


Figure 8 INTENSITY OF PITOT PRESSURE FLUCTUATIONS

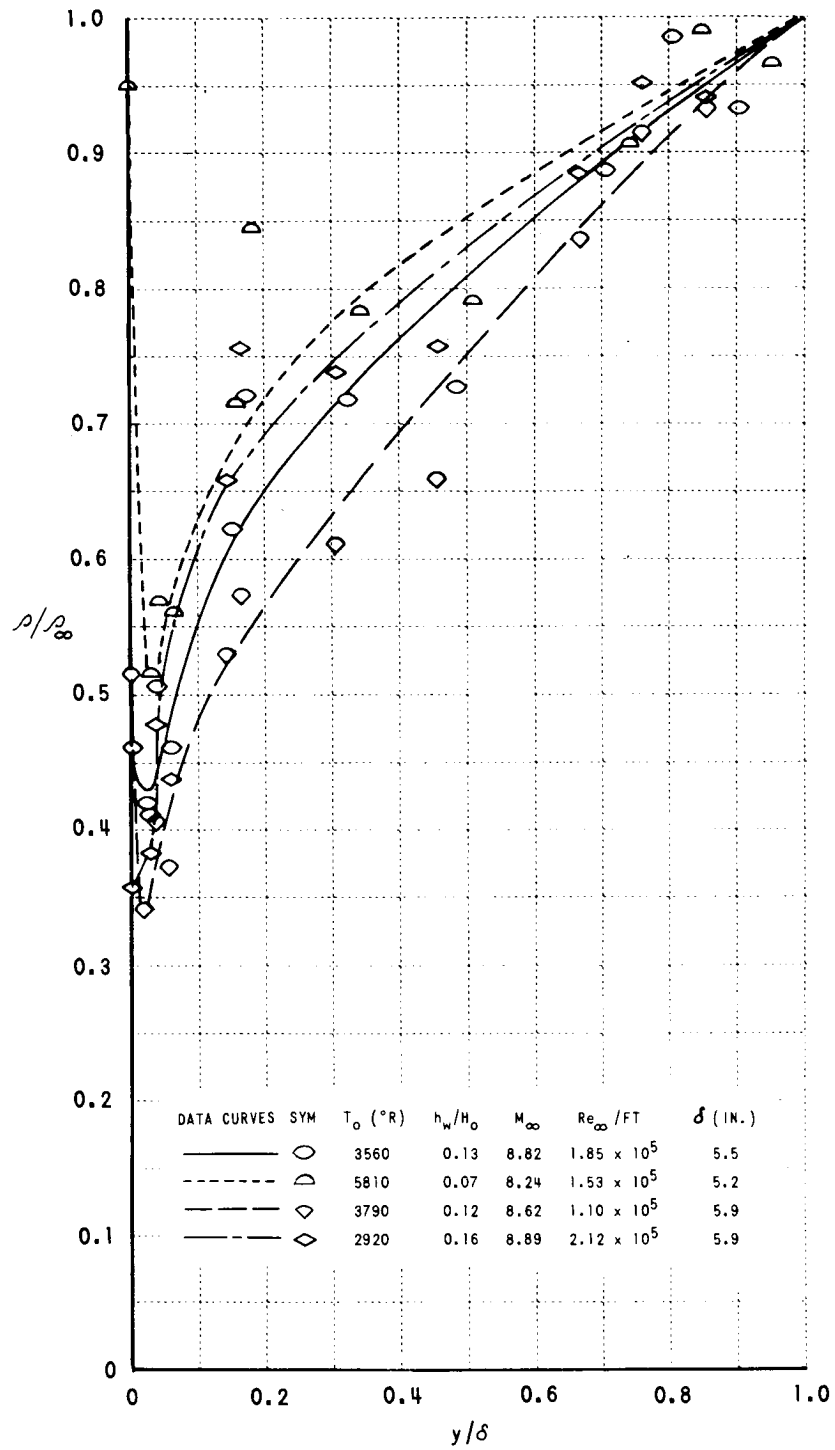


Figure 9 MEASURED DENSITY PROFILES



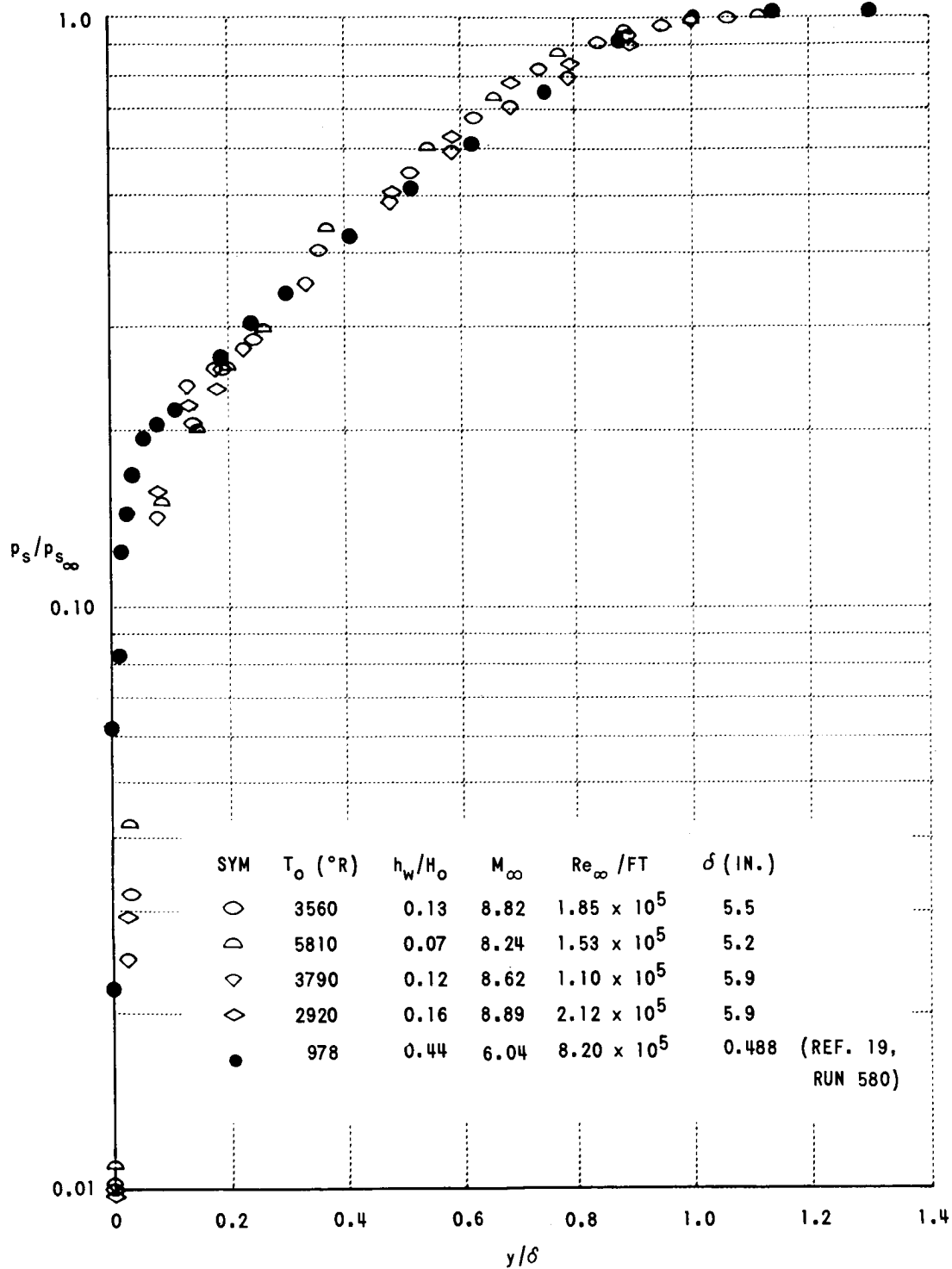


Figure 10 MEASURED PITOT PRESSURE PROFILES

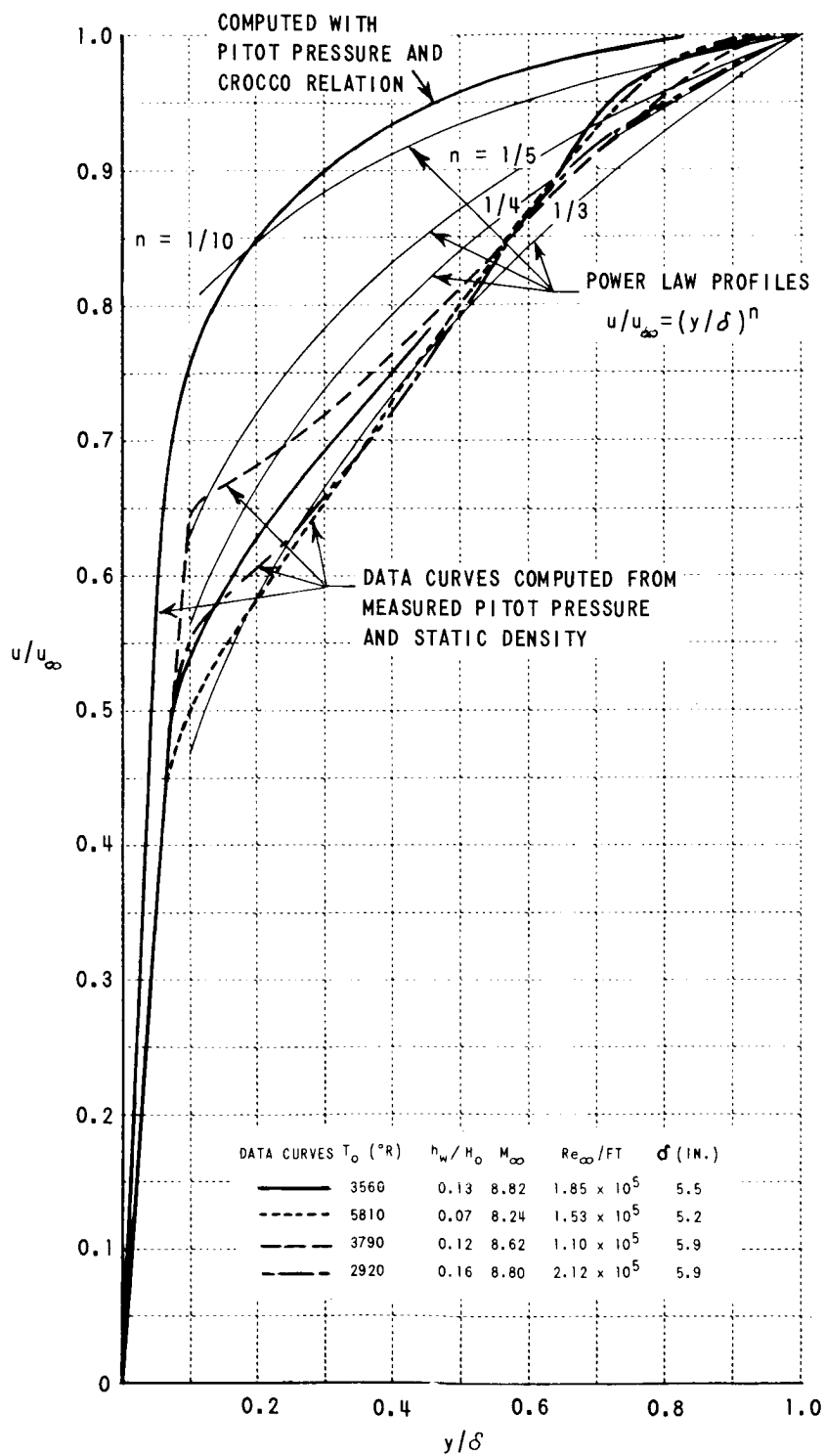


Figure 11 COMPARISON OF COMPUTED EXPERIMENTAL VELOCITY PROFILES  
WITH POWER LAW PROFILES

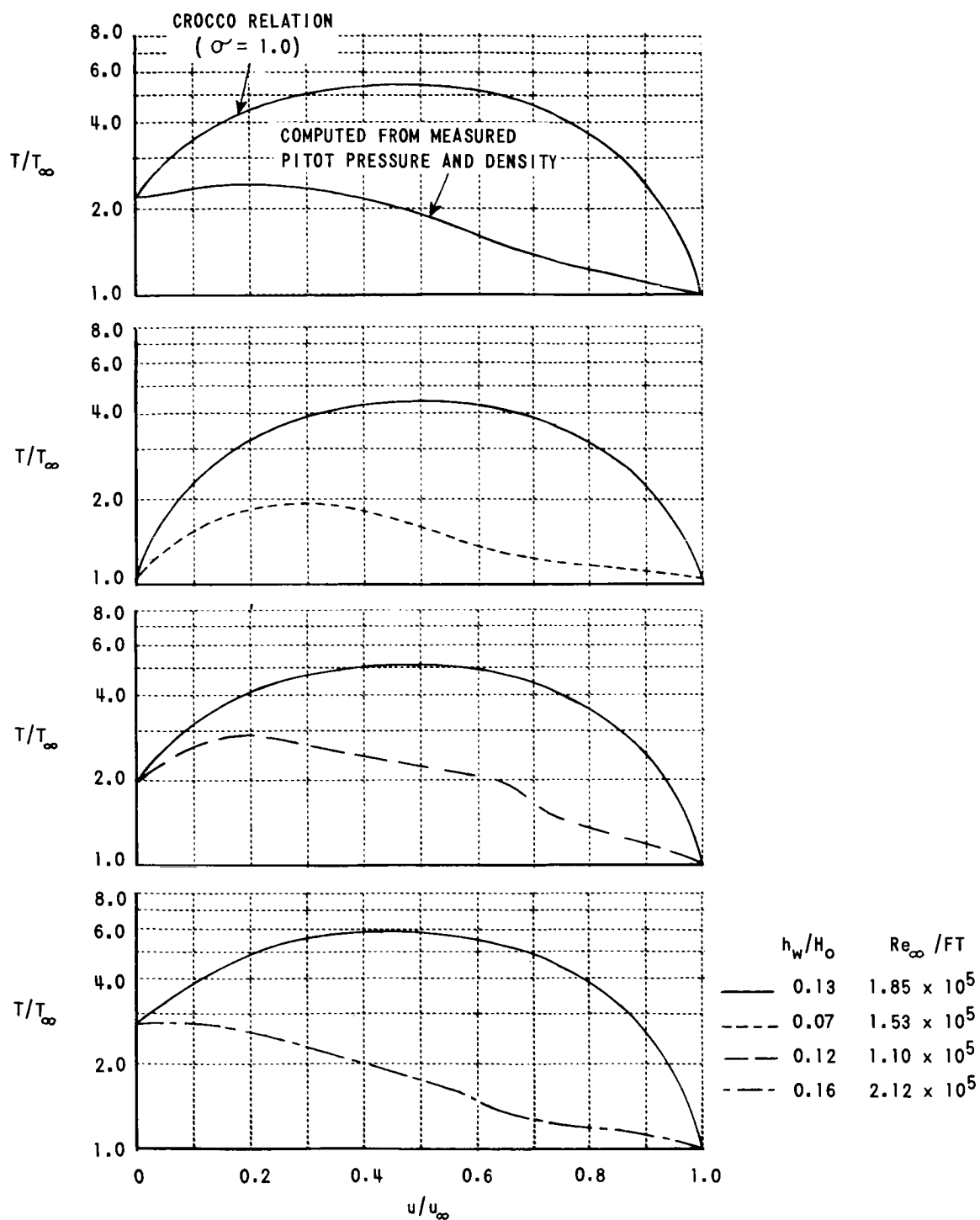


Figure 12 COMPARISON OF EXPERIMENTAL TEMPERATURE PROFILES  
WITH CROCCO THEORY

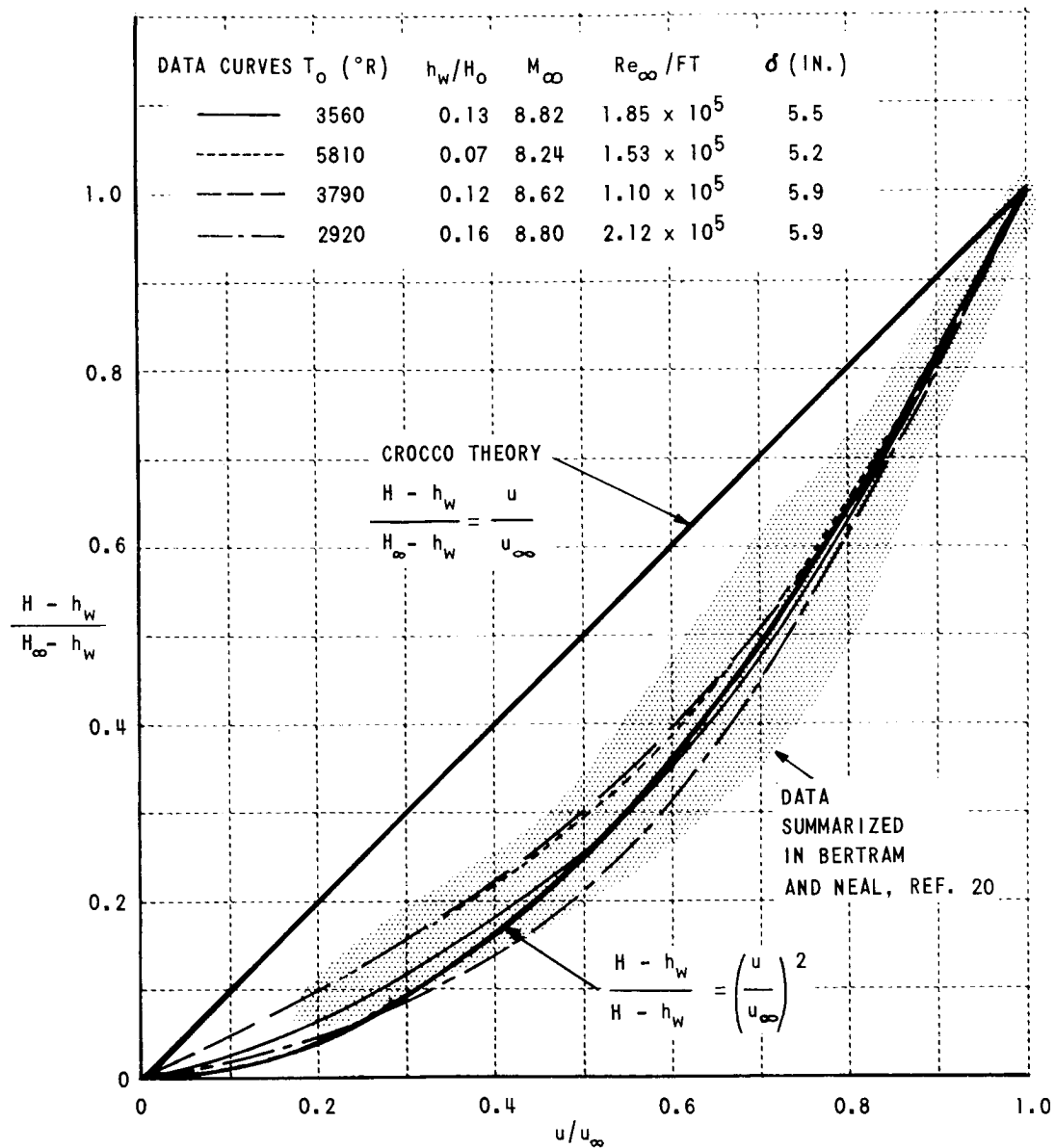


Figure 13 COMPARISON OF TOTAL ENTHALPY PROFILE WITH CROCCO THEORY

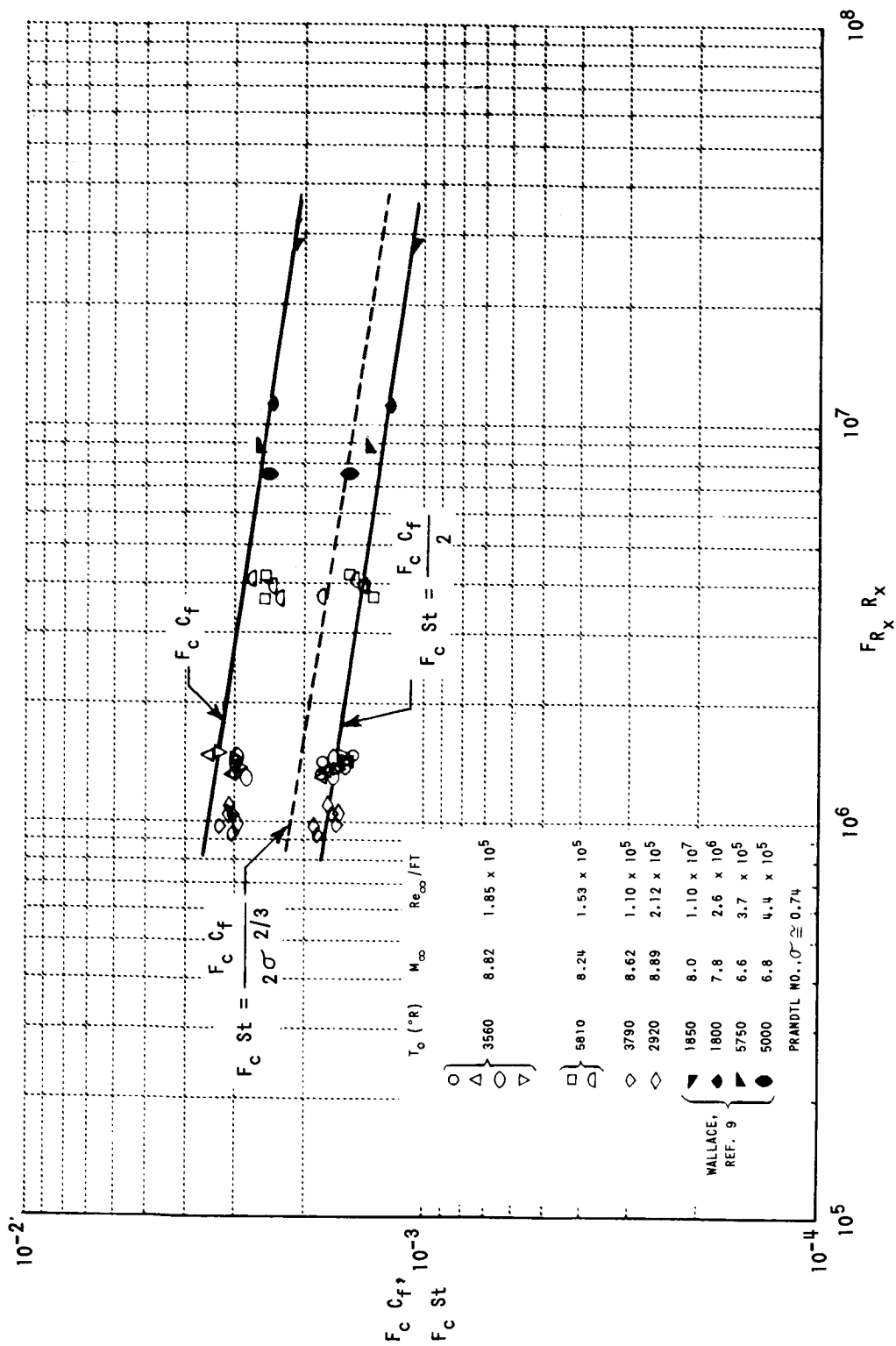


Figure 14 COMPARISON OF TURBULENT BOUNDARY LAYER SKIN FRICTION AND HEAT TRANSFER WITH SPALDING AND CHI THEORY

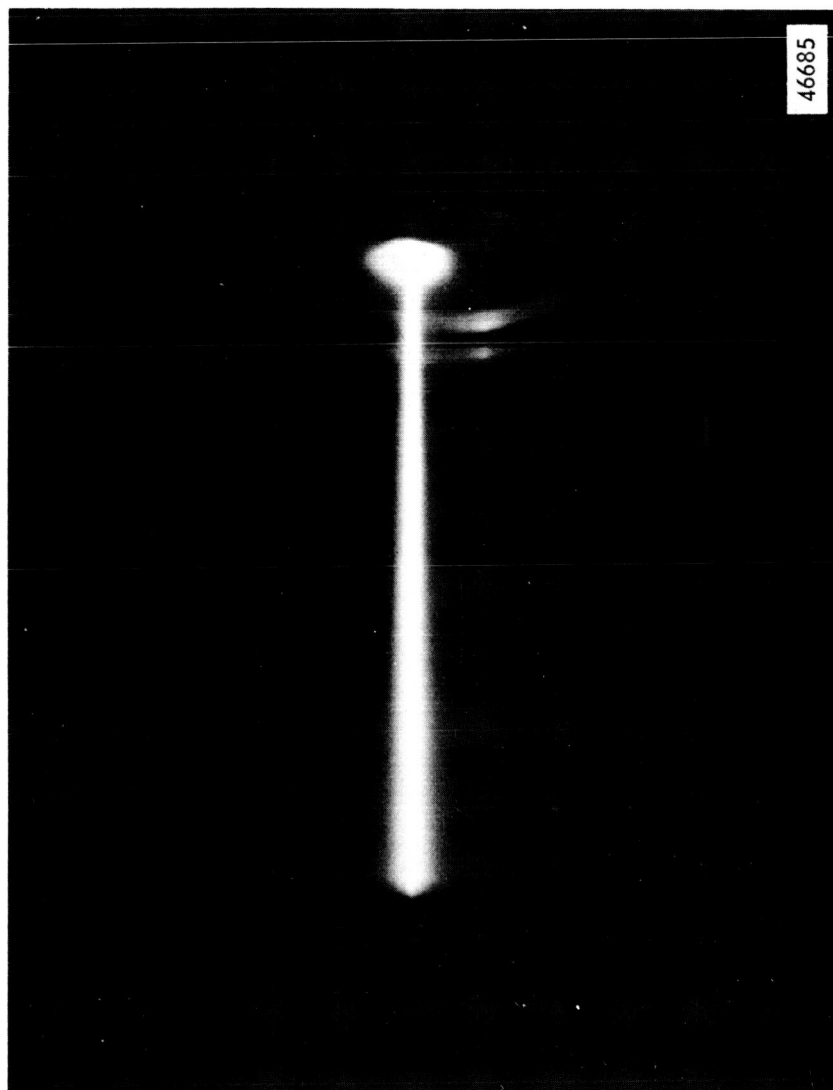


Figure 15 ELECTRON BEAM IN SHOCK-TUNNEL NOZZLE CONFIGURATION  
(BEAM LENGTH 6 INCHES, PRESSURE = 0.85 Torr)

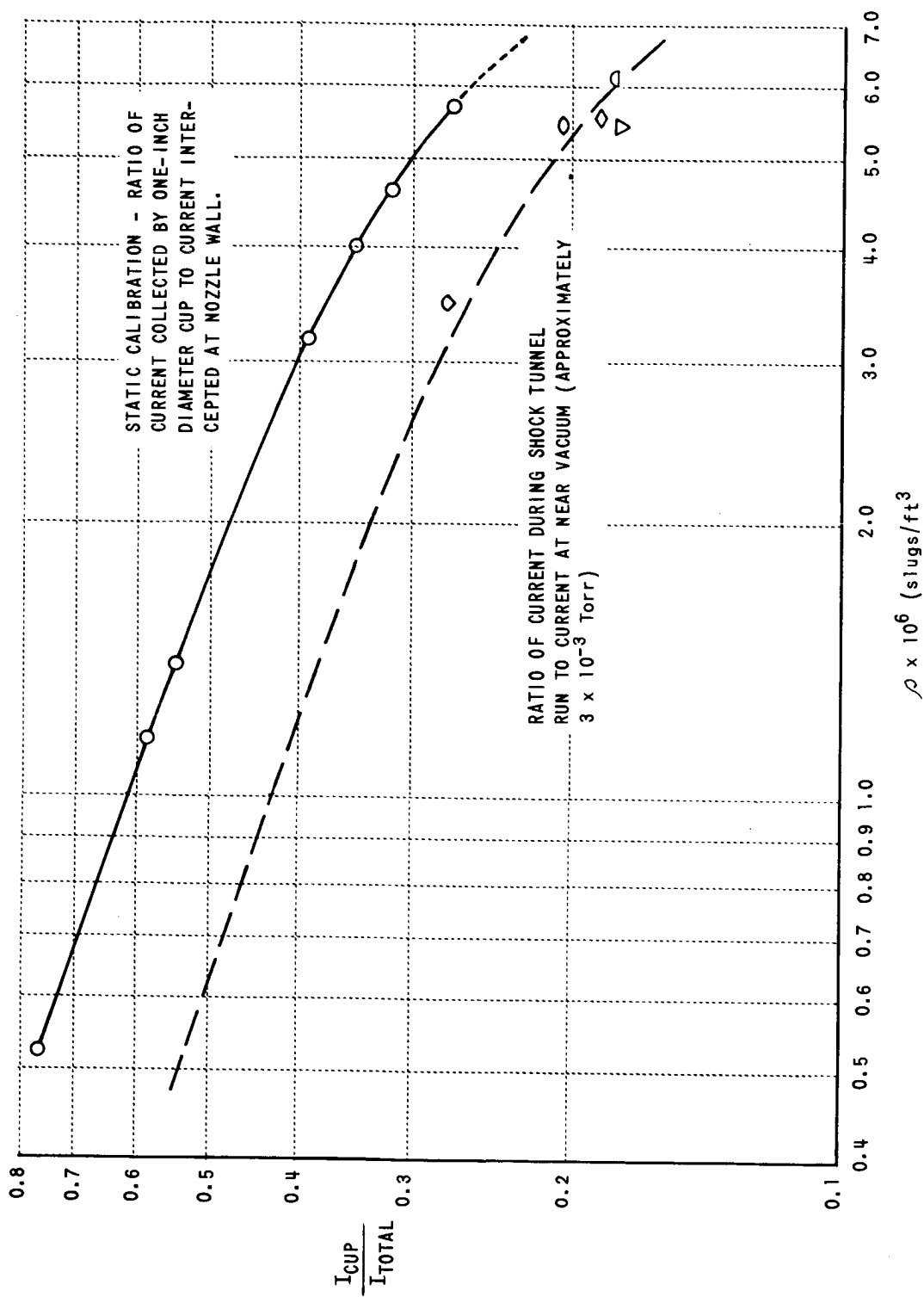


Figure 16 EFFECT OF BEAM SPREADING ON CURRENT COLLECTION

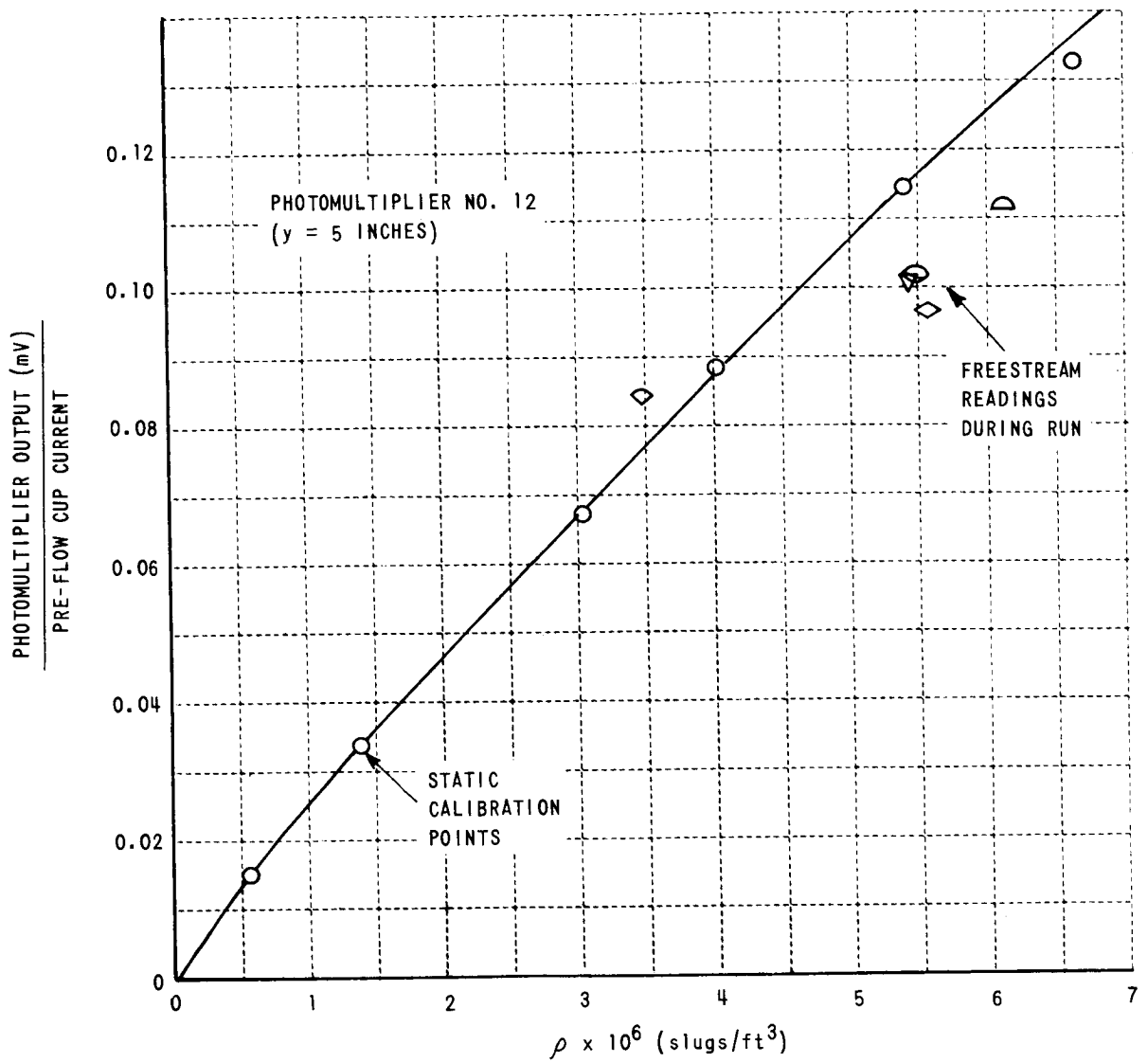


Figure 17 DENSITY CALIBRATION CURVE



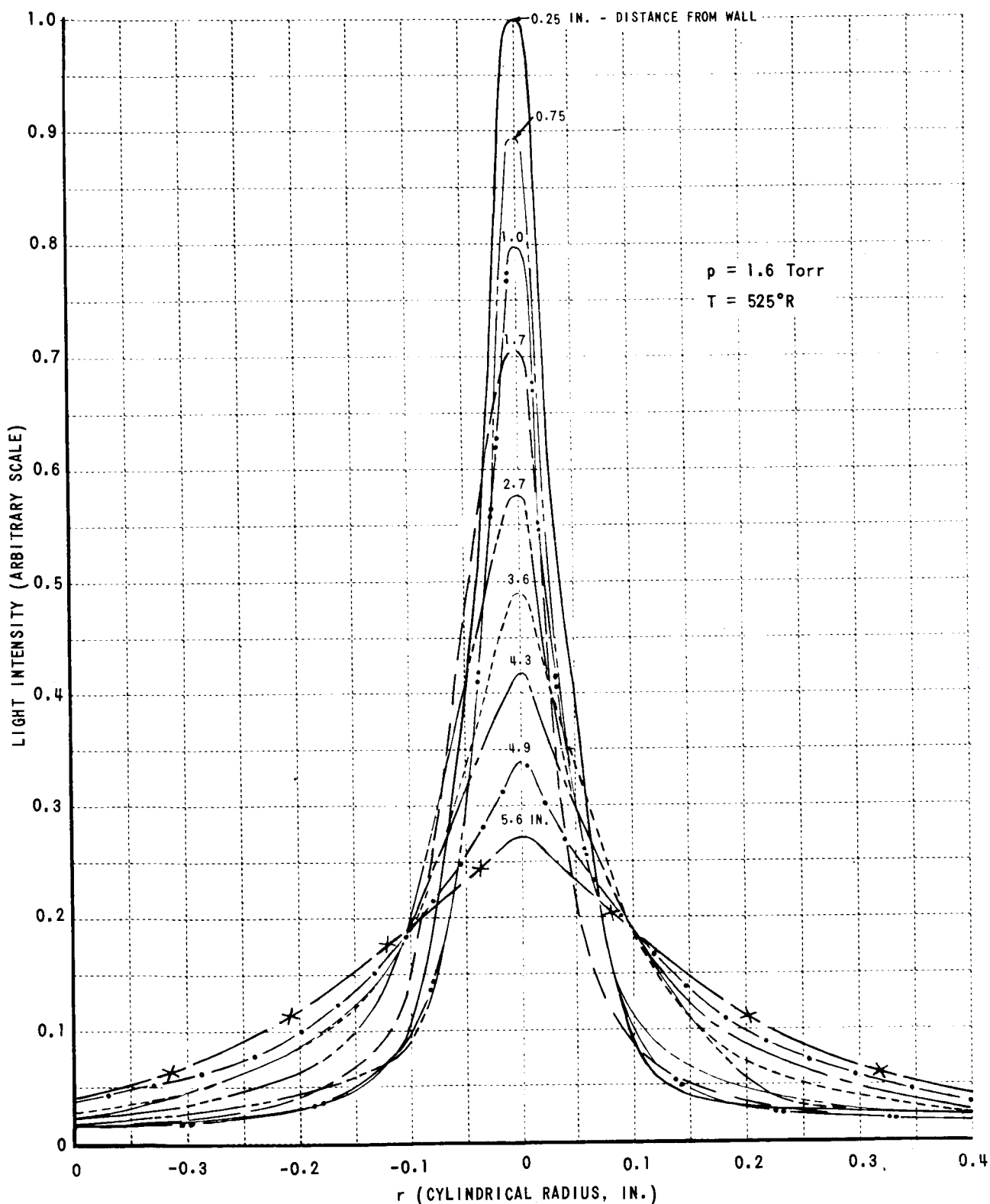


Figure 18 ELECTRON BEAM LUMINESCENCE PROFILES CALCULATED FROM DENSITOMETER READINGS OF BEAM PHOTOGRAPH

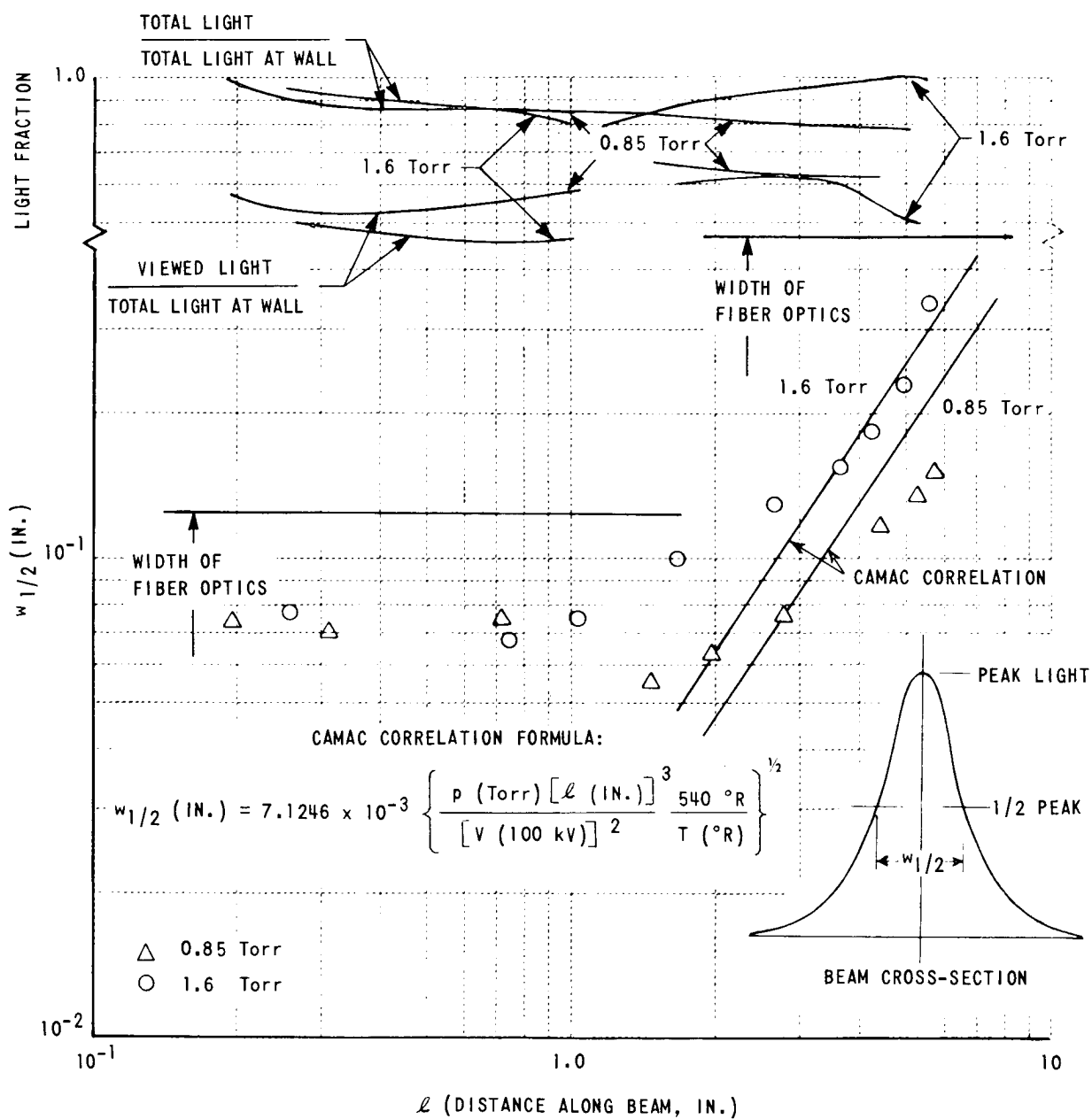


Figure 19 ELECTRON BEAM CHARACTERISTICS FROM DENSITOMETER READINGS OF BEAM PHOTOGRAPHS

# COMMENTS ON HYPERSONIC TURBULENT BOUNDARY-LAYER

## MEASUREMENTS USING AN ELECTRON BEAM

By William D. Harvey and Dennis M. Bushnell

NASA Langley Research Center

### SUMMARY

Estimates of the root-mean-square velocity fluctuation level and trend at Mach 8.5 were made by utilizing the experimental fluctuating density and pitot pressure measurements of Wallace. Also, fair estimates of both the magnitude and trend of the fluctuating density and velocity can be made by using a mixing length type of approach. Present indications are that for zero pressure gradient the intensity of the fluctuating velocity in a boundary layer may be independent of Mach number.

### INTRODUCTION

Most of the available experimental data on compressible turbulent boundary layers are limited primarily to the mean properties of the flow. In order to obtain a more thorough understanding of such flows and ultimately to advance theoretical prediction methods, it is necessary to study the statistical properties of the turbulent flow.

Measurements of mass flow and total temperature fluctuations in supersonic turbulent shear layers have been made with hot wires (refs. 1 to 3). Recent measurements of the mean and fluctuating density and pitot pressure across a turbulent boundary layer on a shock tunnel wall at a Mach number of 8.5 have been reported by Wallace (ref. 4). The density measurements were obtained with a 40-kV electron beam and the pitot pressure data were obtained with piezo-electric crystals. The purpose of this paper is to present an estimate of the intensity of the velocity fluctuations, based directly on the fluctuating data of Wallace (ref. 4), and to evaluate a mixing length approach to compute indirectly the magnitude and trends of density and velocity fluctuations from measurements of mean flow quantities.

### SYMBOLS

- A correlation coefficient,  $\frac{\overline{\rho' u'}}{\left( \overline{\rho'^2} \overline{u'^2} \right)^{1/2}}$
- G function of Mach number (see eq. (2))
- $H_o$  total enthalpy

$h_w$  static enthalpy

$\ell$  mixing length

$M$  Mach number

$$P = \sqrt{p_t'^2} / \bar{p}_t$$

$p_t$  pitot pressure

$R$  Reynolds number

$$r = \sqrt{\rho'^2} / \bar{\rho}$$

$T_o$  total temperature

$$U = \sqrt{u'^2} / \bar{u}$$

$u$  instantaneous longitudinal velocity component,  $\bar{u} + u'$

$y$  normal distance from tunnel wall

$\rho$  instantaneous density,  $\bar{\rho} + \rho'$

$\delta$  nominal boundary-layer thickness

Subscripts:

$e$  edge value

$\delta$  based on boundary-layer thickness

Bar over symbol indicates time mean value.

Prime with symbol denotes fluctuating value.

## RESULTS AND DISCUSSION

### Density and Pitot Pressure Fluctuations

Figures 6 and 8 of reference 4 show the variation in the ratio of the root-mean-square density and pitot pressure fluctuations to the local mean values across a Mach 8 turbulent boundary layer. These data of reference 4 were computed at the NASA Langley Research Center by digitizing the original oscilloscope records at time intervals of  $10^{-5}$  second. Because of the way the data were obtained and reduced, the ratios of the root-mean-square values to the respective mean values are essentially independent of the absolute levels of

density or pitot pressure. Consequently, the accuracy of these fluctuation intensity data is believed to be better than the accuracy of the corresponding mean data. Therefore, the fairings for each run shown on the figures of reference 4 probably indicate actual data trends. These fluctuating density and pitot pressure data have been used herein to determine the intensity of the velocity fluctuations.

### Density and Longitudinal Velocity Fluctuations

Figure 1 shows the original data for the ratios of mean density to the density at the edge of the boundary layer as reported by Wallace (ref. 4). Fairings of the data for the four test runs as used herein are also shown. Fluctuations in temperature and velocity have previously been modeled by a mixing length type of formulation for incompressible flow (refs. 5 and 6) and velocity fluctuations for compressible flow (ref. 7). A mixing length expression for the root-mean-square fluctuating density may be written as

$$\frac{\sqrt{\overline{\rho'^2}}}{\overline{\rho}} = \left( \frac{\rho_e}{\overline{\rho}} \right) \left( \frac{\ell}{\delta} \right) \left| \frac{d(\overline{\rho}/\rho_e)}{d(y/\delta)} \right| \quad (1)$$

where, in accordance with Prandtl's mixing length concept and recent calculations (refs. 6 and 7),

$$\ell = 0.4 y \quad (0 \leq y/\delta \leq 0.2)$$

$$\ell = 0.08 \delta \quad (0.2 \leq y/\delta \leq 1.0)$$

Shown in figure 2 are the root-mean-square density fluctuations using the faired mean density profiles of figure 1 in equation (1) and the direct measurements of reference 4. The bands include results for the four test runs. Comparison of results from equation (1) with the data indicates that the magnitude of the fluctuating density through the boundary layer can be estimated to within roughly a factor of 2 by using the mixing length approach although the values obtained obviously depend on the particular fairings used in figure 1. One of the interesting features in the fluctuating density and pitot pressure profiles of reference 4 is that there appears to be a definite minimum in the distributions at values of  $y/\delta$  from about 0.2 to 0.5. This minimum would follow from the faired profiles of mean density and pitot pressure (ref. 4) and a mixing length assumption like equation (1).

The extension to compressible flows of recent calculation methods (refs. 8 and 9) for incompressible flows which utilize the turbulent kinetic energy equation is, to a large extent, dependent upon a knowledge of the root-mean-square variations of the fluctuating quantities for compressible flows. The magnitude and variation of the root-mean-square fluctuation velocity through a turbulent boundary layer are the more important quantities required in such methods.

An approximate equation giving the relationship of the instantaneous velocity, density, and pitot pressure may be written as

$$\rho u^2 \approx G(M) p_t \quad (2)$$

where, for  $M > 2$ ,  $G(M)$  is a slowly varying function of the local Mach number so that  $G'$  may be neglected. Substitution of mean and fluctuating quantities into equation (2) and taking the average then gives

$$\overline{G p_t} = \overline{\rho} \overline{u^2} + \overline{\rho} \overline{u'^2} + 2 \overline{u} \overline{\rho' u'} \quad (3)$$

where third and higher order correlations of fluctuating quantities are neglected. Now, first squaring both sides of equation (2), then substituting mean and fluctuating quantities, and finally taking the average results in

$$\frac{\overline{G^2 p_t^2}}{\overline{\rho^2 u^4}} \left( 1 + \frac{\overline{p_t'^2}}{\overline{p_t^2}} \right) = 1 + 6 \frac{\overline{u'^2}}{\overline{u^2}} + 8 \frac{\overline{\rho' u'}}{\overline{\rho u}} + \frac{\overline{\rho'^2}}{\overline{\rho^2}} \quad (4)$$

Elimination of  $G$  by the use of equation (3) and the introduction of the correlation coefficient  $A$  then gives the following expression for the intensity of the fluctuating velocity as a function of the intensities of pitot pressure and density fluctuations:

$$U = \left[ -2Ar \left( 1 - P^2 \right) + \sqrt{4A^2 r^2 \left( 1 - P^2 \right)^2 + 2 \left( 2 - P^2 \right) \left( P^2 - r^2 \right)} \right] / 2(2 - P^2) \quad (5)$$

This equation applies over most of the hypersonic turbulent boundary layer except near the wall where  $M \leq 2.0$ , say. The Mach number profiles given by Wallace (ref. 4) show that the Mach number is greater than 2.5 for  $y/\delta \geq 0.1$ ; hence equation (2) can be expected to give reasonable estimates for this range of  $y/\delta$ .

A mixing length expression for the root-mean-square velocity fluctuations may be written as

$$\frac{\sqrt{\overline{u'^2}}}{u_e} = \left( \frac{\ell}{\delta} \right) \left| \frac{d(\overline{u}/u_e)}{d(y/\delta)} \right| \quad (6)$$

This expression was applied to Wallace's data (ref. 4) by using the same values of  $\ell/\delta$  as were used in equation (1). Velocity derivatives were obtained from fairings of velocity profiles as computed from the faired density profiles of figure 1 and  $p_t$  data as given by Wallace (ref. 4).

The longitudinal velocity fluctuation intensities determined from equations (5) and (6) are compared in figure 3. Again the bands include results for the four test runs. The value of  $A$  used in equation (5) to obtain the results shown was taken as 1.0; however, calculations made with  $A = 0.5$  indicated a maximum 5-percent deviation in the velocity fluctuations. Kistler's data (ref. 3) would give a value of  $A \approx 0.7$  since static pressure fluctuations were neglected. The results from the mixing length approach of equation (6) agree to within a factor of 2 or 3 with the other method that uses measured quantities in equation (5). Also shown for comparison are data of Kistler (ref. 3), Schloemer (ref. 10), and Serafini (ref. 11), all of which are for essentially zero pressure gradient. The data of Kistler (ref. 3) have been normalized by the velocity at the edge of the boundary layer  $u_e$  which reduces the spread between the data at the three Mach numbers to about 10 percent, so that a single curve which represents the mean of Kistler's data (ref. 3) is presented in figure 3. The general agreement in the data shown in figure 3 for the outer portion of the boundary layer indicates that within the probable errors of the data, the intensity of the longitudinal velocity fluctuations may be independent of Mach numbers.

Near the wall the inferred fluctuation levels for Mach 8.5 show a large increase to a peak value that is presumably in the vicinity of the sublayer edge which appears to be considerably farther from the wall than the corresponding peaks for the low speed data (refs. 10 and 11). Since the theory of reference 9 predicts an inverse relationship between  $\sqrt{u'^2}/u_e$  and  $R_\delta$ , it might be expected that the present data should be at a higher level (for the same  $y/\delta$ ) than the other data of figure 3 since the  $R_\delta$  values for the Wallace data are smaller. The values of  $\sqrt{u'^2}/u_e$  in the range  $0.2 < y/\delta < 0.6$  are lower than previous data, as predicted by a mixing length assumption (eq. (6)) and as based on data and equation (2), either because of a Mach number effect or some anomaly in the experimental conditions of Wallace (ref. 4).

#### CONCLUDING REMARKS

Estimates of the root-mean-square longitudinal velocity fluctuation level and trend were made by utilizing the fluctuating density and pitot pressure data of Wallace along with the assumption that pitot pressure is proportional to the mass flow. Reasonable estimates of both the magnitude and trend of the root-mean-square density and velocity fluctuations can be made by using a mixing length type of approach and faired profiles of mean density and velocity. Present indications are that for zero pressure gradient, the level and trends of the root-mean-square fluctuating velocity divided by the local mean velocity may be fairly independent of Mach number in the outer part of the boundary layer and thereby the validity of Morkovin's hypotheses is extended to the low hypersonic speed range.

## REFERENCES

1. Morkovin, Mark V.: Fluctuations and Hot-Wire Anemometry in Compressible Flows. AGARDograph 24, Nov. 1956.
2. Kovásznay, Leslie S. G.: Turbulence in Supersonic Flow. J. Aeronaut. Sci., vol. 20, no. 10, Oct. 1953, pp. 657-674, 682.
3. Kistler, Alan L.: Fluctuation Measurements in a Supersonic Turbulent Boundary Layer. Phys. Fluids, vol. 2, no. 3, May-June 1959, pp. 290-296.
4. Wallace, J. E.: Hypersonic Turbulent Boundary Layer Measurements Using an Electron Beam. CAL Rep. No. AN-2112-Y-1 (Contract No. NSR33-009-029), Cornell Aeronaut. Lab., Inc., Aug. 1968.
5. Rust, J. H.; and Sesonske, Alexander: Turbulent Temperature Fluctuations in Mercury and Ethylene Glycol in Pipe Flow. Int. J. Heat Mass Transfer, vol. 9, no. 3, Mar. 1966, pp. 215-227.
6. Escudier, M. P.; and Spalding, D. B.: A Note on the Turbulent Uniform-Property Hydrodynamic Boundary Layer on a Smooth Impermeable Wall; Comparisons of Theory With Experiment. Brit. A.R.C. 27 302, Aug. 1965.
7. Maise, George; and McDonald, Henry: Mixing Length and Kinematic Eddy Viscosity in a Compressible Boundary Layer. AIAA J., vol. 6, no. 1, Jan. 1968, pp. 73-80.
8. Glushko, G. S.: Turbulent Boundary Layer on a Flat Plate in an Incompressible Fluid. Bull. Acad. Sci. USSR, Mech. Ser., no. 4, 1965, pp. 13-23.
9. Beckwith, Ivan E.; and Bushnell, Dennis M. (With appendix C by Carolyn C. Thomas): Detailed Description and Results of a Method for Computing Mean and Fluctuating Quantities in Turbulent Boundary Layers. NASA TN D-4815, 1968.
10. Schloemer, Howard H.: Effects of Pressure Gradients on Turbulent Boundary-Layer Wall-Pressure Fluctuations. USL Rep. No. 747, U.S. Navy, July 1, 1966.
11. Serafini, John S.: Wall-Pressure Fluctuations and Pressure-Velocity Correlations in a Turbulent Boundary Layer. NASA TR R-165, 1964.



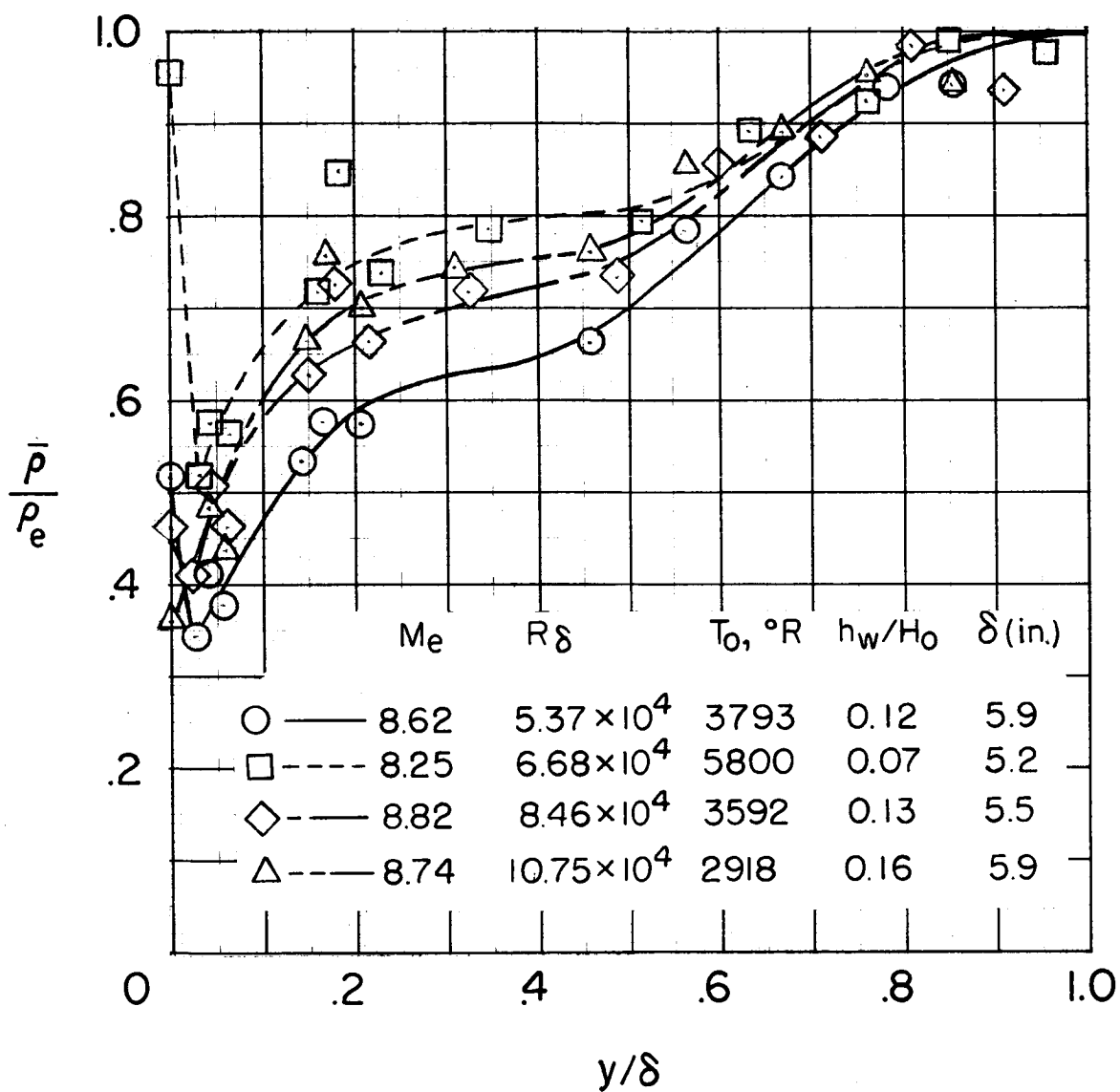


Figure 1.- Measured mean density profiles.

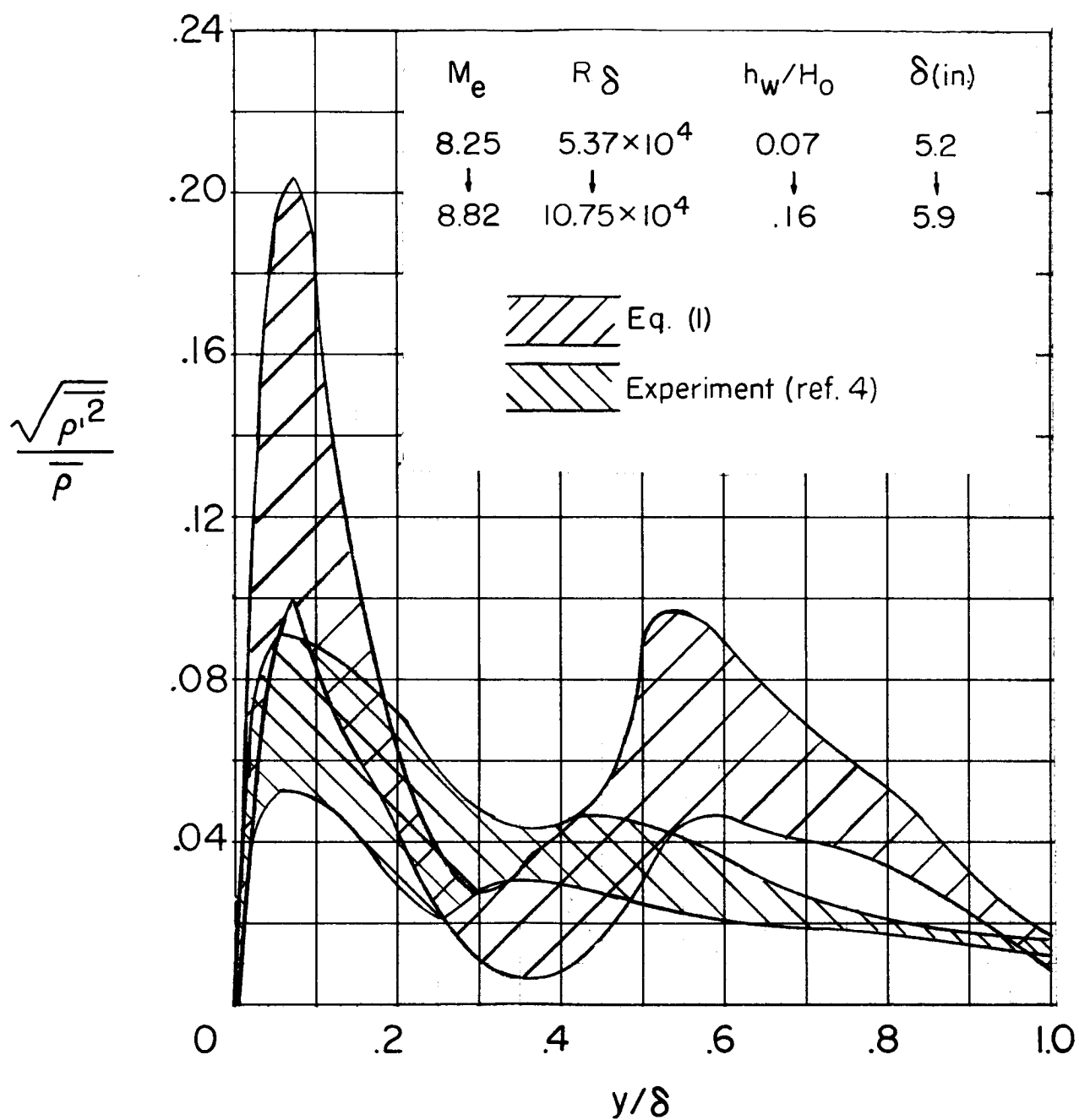


Figure 2.- Intensity of density fluctuations.

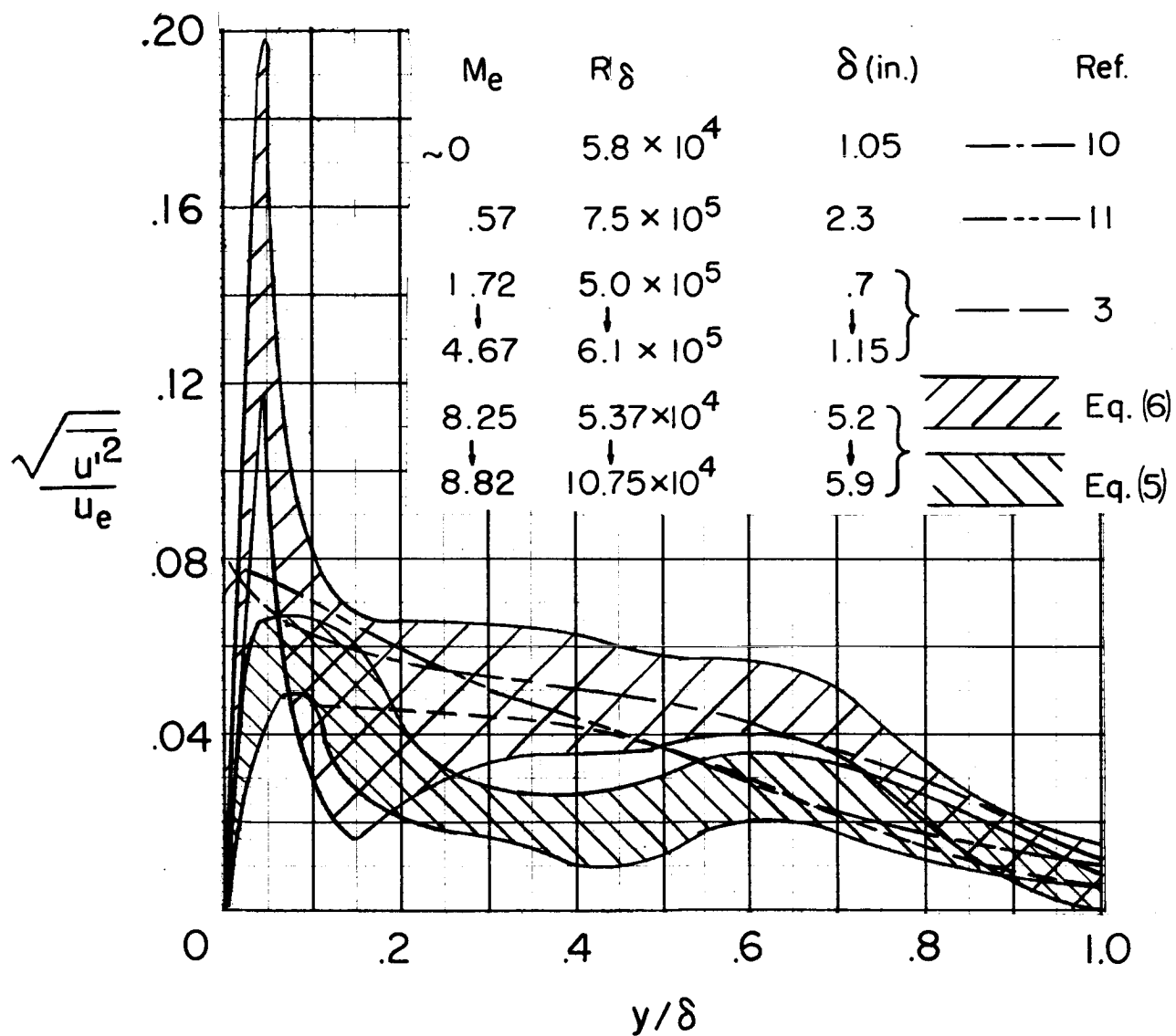


Figure 3.- Comparison of present velocity fluctuations with previous results.

# SUMMARY AND CORRELATION OF SKIN-FRICTION AND

## HEAT-TRANSFER DATA FOR A HYPERSONIC

### TURBULENT BOUNDARY LAYER

#### ON SIMPLE SHAPES<sup>1</sup>

By Edward J. Hopkins, Morris W. Rubesin, Mamoru Inouye,  
Earl R. Keener, George C. Mateer, and Thomas E. Polek

Ames Research Center

#### SUMMARY

Local skin-friction and heat-transfer data were directly measured in air for turbulent boundary layers on flat plates, cones, and a wind-tunnel wall. The Mach number at the edge of the boundary layer ranged between 5 and 7.4 and the wall to adiabatic wall temperature ratio varied between 0.1 and 0.6.

The skin-friction and heat-transfer data are compared with other data obtained by direct measurement of surface shear with balances and accompanied by boundary-layer surveys. The use of momentum-thickness Reynolds number in the skin-friction comparison avoids the need for arbitrary location of the virtual origin of the turbulent boundary layer. A boundary-layer energy thickness obtained from integration of the heat-flux distribution up to a test station proved useful in correlating the local heat flux at that station in a manner analogous to the use of momentum thickness.

Adiabatic and cold wall data are employed to assess four theories for predicting turbulent skin friction. The theories examined are those of Sommer and Short, Spalding and Chi, Van Driest II, and Coles.

Analysis of the skin-friction data indicates that the theory of either Van Driest II or Coles gives the best predictions for wall to adiabatic wall temperature ratios above 0.3, generally within about  $\pm 10$  percent of the measured values. Although Coles' theory gives results generally comparable to those of the Van Driest II theory, at high Reynolds numbers it underpredicts the results by more than 10 percent. At Mach numbers near 6 and above, theories of Sommer and Short or Spalding and Chi generally underpredict the measured skin friction by 20 to 30 percent. At wall to adiabatic wall temperature ratios below 0.3, none of the theories give the proper trend with wall to adiabatic wall temperature ratio.

The heat-transfer analysis for nonadiabatic wall conditions generally substantiates the skin-friction analysis, favoring the theory of either Van Driest II or Coles, provided the Reynolds analogy factor of 1.0 (containing an assumed recovery factor of 0.9) measured in the present investigation is employed.

---

<sup>1</sup>Paper No. 10 also available as NASA TN D-5089.

## INTRODUCTION

Accurate knowledge of skin friction and heat transfer is required to predict the performance and structural requirements of supersonic and hypersonic aircraft. Generally, calculations are relied upon to provide estimates of either wind-tunnel or flight values of skin friction since it is impractical to measure these values over the entire configuration. Similarly, the thermal design of airplane structures and the selection of material depend largely on predictions of the incoming convective heat flux over the various surface elements. Supersonic and hypersonic aircraft will operate with skin temperatures near the radiative equilibrium temperature, where the incoming convection is balanced by radiation to the surroundings. At supersonic speeds ( $M \approx 3$ ), the radiation equilibrium temperature is almost equal to the adiabatic wall temperature. At hypersonic speeds ( $M \approx 7$ ), however, the external surfaces will generally have wall to adiabatic wall temperature ratios between 0.3 and 0.5 as a result of considerable radiative cooling and internal heat transfer.

Previous evaluations of turbulent skin-friction theories may have questionable accuracy at hypersonic Mach numbers for lack of many direct measurements by skin-friction balances. These evaluations include numerous indirect measurements from (1) heat transfer with an assumed Reynolds analogy factor, (2) rate of change of momentum thickness with longitudinal distance, (3) velocity gradient at the surface, or (4) velocity profile. Examples of such evaluations are those of Spalding and Chi (ref. 1), Hopkins and Keener (ref. 2) and Peterson (ref. 3). Spalding and Chi examined 20 theories and showed that the theories of Van Driest II (ref. 4) and Sommer and Short (ref. 5) gave root-mean-square deviations of about 11 and 14 percent, respectively, compared with 10 percent for their semiempirical theory. Independent studies of references 2 and 3 indicate that for the adiabatic-wall case the theories of Van Driest II and Sommer and Short bracket nearly all the experimental results. For the non-adiabatic wall case, Peterson's analysis also favors Sommer and Short's theory up to a Mach number of 6. Miles and Kim (ref. 6) show that Coles' theory (ref. 7), not considered in the other analyses, is competitive with Spalding and Chi's theory for the nonadiabatic wall case.

Heat-transfer data for flat plates are compared by Bertram et al. (refs. 8 and 9) with theoretical values derived from skin-friction theory through an extension to compressible flow of the von Kármán form of the Reynolds analogy factor. Bertram's analysis and later results of Cary (ref. 10) suggest best agreement with the prediction method of Spalding and Chi.

Recently, a skin-friction balance became available that can be used on models in hypersonic facilities with elevated stagnation temperatures. However, preliminary skin-friction measurements at Mach number 6.5 were not in accord with the cited heat-transfer results in indicating the best theory for predictions. Consequently, the present investigation was undertaken to obtain both heat-transfer measurements on flat plates and cones and skin-friction measurements on flat plates and a wind-tunnel wall, all surfaces being nonadiabatic. This investigation was conducted in the Ames 3.5-Foot Hypersonic Wind

Tunnel at Mach numbers between 5 and 7.4. Skin friction and heat transfer were measured simultaneously at one of the longitudinal stations on a flat plate to determine the Reynolds analogy factor. The results were then employed to reevaluate the theories of Sommer and Short (ref. 5), Spalding and Chi (ref. 1), Van Driest II (ref. 4), and Coles (ref. 7).

#### NOTATION

- $C_f$  local skin-friction coefficient,  $\frac{\tau}{q_e}$
- $C_F$  average skin-friction coefficient,  $\frac{2\theta}{x}$  for a flat plate
- $C_h$  local Stanton number,  $\frac{\dot{q}_w}{\rho_e U_e (H_w - H_{aw})}$
- $F_c$  transformation function for  $C_f (\bar{C}_f = F_c C_f)$ , reference 1
- $H$  total enthalpy
- $M$  Mach number
- $p$  pressure
- $Pr$  Prandtl number
- $q$  dynamic pressure
- $\dot{q}_w$  rate of heat transfer from the surface per unit area
- $r$  local-cone radius, wind-tunnel radius, or temperature recovery factor
- $Re_x$  Reynolds number based on distance to virtual origin of turbulent flow,  
 $\frac{\rho_e U_e x}{\mu_e}$
- $Re_\Gamma$  Reynolds number based on energy thickness,  $\frac{\rho_e U_e \Gamma}{\mu_e}$
- $Re_\theta$  Reynolds number based on momentum thickness,  $\frac{\rho_e U_e \theta}{\mu_e}$

s	distance along surface from cone apex or flat-plate leading edge
T	absolute temperature
U	velocity
x	distance along surface from either leading edge or virtual origin
$x_L$	distance along surface from leading edge to peak Stanton number location
$x_T$	distance along surface from virtual origin of turbulent flow to peak Stanton number location
y	distance normal to surface
$\alpha$	angle of attack
$\Gamma$	energy thickness $\int_0^\delta \frac{\rho U}{\rho_e U_e} \left( \frac{H}{H_w} - \frac{H_e}{H_e} \right) dy$ , also see equation (6)
$\delta$	boundary-layer thickness
$\theta$	momentum thickness $\int_0^\delta \frac{\rho U}{\rho_e U_e} \left( 1 - \frac{U}{U_e} \right) dy$ for flat plates or $\int_0^\delta \frac{\rho U}{\rho_e U_e} \left( 1 - \frac{U}{U_e} \right) \left( \frac{r - y}{r} \right) dy$ for circular wind-tunnel walls
$\mu$	coefficient of viscosity
$\rho$	mass density
$\tau$	shear stress
$(\bar{\phantom{x}})$	variable transformed to equivalent constant property case

#### Subscripts

aw	adiabatic wall
e	boundary-layer edge
exp	experimental

i     incompressible  
l     local station  
L     laminar  
max   maximum  
t     total  
T     turbulent  
the   theoretical  
w     wall

#### Superscript

$\epsilon$      index ( $\epsilon = 0$  for flat plate and  $\epsilon = 1$  for cone)

### APPARATUS AND TEST

#### Wind Tunnel

The experimental investigation was conducted in air in the Ames 3.5-Foot Hypersonic Wind Tunnel. This facility is a "blow-down" type wind tunnel in which the air is heated by a hot pebble bed to temperatures ranging from about 1000° to 2100° R. The throat and nozzle walls are cooled by helium injection ahead of the throat, the helium remaining within the wind-tunnel boundary layer as confirmed by surveys. The Mach number 5.4 and 7.4 contoured nozzles were used, and the stagnation pressure was varied from about 7 to 120 atmospheres. The present tests used both a quick-insert mechanism and a fixed-support system for holding models.

#### Models and Instrumentation

Flat plates.- Two flat plates, 18 inches wide by 47 inches long, were tested. The leading edge of each plate was 0.004 inch thick and was unswept. Both flat plates were used to obtain skin friction and momentum thickness at a station 39 inches from the leading edge under nearly isothermal wall conditions. The first flat plate was sting supported with the test surface at an angle of 3° windward to the airstream. Both pitot-pressure and total-temperature boundary-layer profiles were obtained at the skin-friction test station. The second flat plate was mounted on the injection mechanism to obtain heat-transfer distributions on the surface. Thin-skin heat-transfer gages were installed in the heavy-walled steel plate along the centerline and also off center at several locations. Pitot-pressure profiles and skin friction were measured at the station 39 inches from the leading edge. This plate



was tested at angles of  $0^\circ$  and  $3.1^\circ$  windward to the airstream. Cross flow was minimized by fences 1 inch high at the trailing edge and tapering to zero at the leading edge.

Cones. - The conical heat-transfer models had half-angles of  $5^\circ$  and  $15^\circ$  and surface lengths of approximately 28 and 20 inches, respectively. These models were of thin-walled (0.033 in.) electroformed nickel and instrumented with thermocouples spot-welded to the interior surface. The  $5^\circ$  cone had a single row of 22 thermocouples spaced at 1-inch intervals along one conical ray. Tip radii were 0.005 and 0.0025 inch for the  $5^\circ$  and  $15^\circ$  models, respectively.

The wall-to-recovery-temperature ratio was varied by changing both the total temperature and the wall temperature. The preinjection value of the wall temperature was either the ambient value or  $160^\circ$  R. The latter value was obtained by externally cooling the model with liquid nitrogen before the model was injected into the airstream.

Test-section wall. - Skin-friction measurements and surveys of pitot pressure and total temperature were made on the test-section wall in the region of zero axial pressure gradient 27.5 feet from the nozzle throat and 8.5 feet behind the beginning of the test section. The local Mach number was 7.4 at the edge of the 8-inch-thick boundary layer. Normally, helium is injected ahead of the throat to cool the throat and the nozzle walls. During this test, however, the helium was shut off for periods up to 30 seconds while data were obtained with an air boundary layer. Five triple-shielded thermocouple total-temperature probes were used to survey the boundary layer at heights from 1 to 14 inches from the wall.

Skin-friction balance. - The skin friction was directly measured with floating-element balances manufactured by the Kistler Instrument Corporation. Four different balances were used, one at a time. The first measurement was made on the sting-mounted stationary flat plate with a balance having a 0.370-inch element diameter. Two balances, each 0.500 inch in diameter, were used consecutively with the injected flat plate. A fourth balance, 0.500 inch in diameter and contoured to fit the curved surface of the wind tunnel, was used in the test-section wall. The statically balanced elements of each balance were self-nulling to the center position with a perimetrical gap of 0.003 inch. The current required to produce the nulling force was calibrated against known weights. Electrical components were maintained at temperatures below  $200^\circ$  F by a water jacket. A test coil in the gage was used to simulate an external friction force and to check the calibration between each test run.

## DATA REDUCTION

### Flat Plates and Cones

Local flow conditions were calculated from the measured free-stream conditions for a two-dimensional wedge and a cone. Compressible flow relations were used in the calculations, including corrections for real gas

effects for calorically imperfect, thermally perfect air. Momentum thicknesses of the boundary layers on the flat plates were calculated from both the pitot-pressure profiles and an assumed Crocco linear total-temperature distribution with velocity ( $Pr = 1$ ), which was found to agree with the measured total-temperature distributions. Energy thicknesses were obtained by integration of the measured heat-transfer rate along the plate. Viscosity was calculated by Keyes' equation.<sup>2</sup>

Test-section-wall data reduction was similar to that for the flat plates, except that the measured total-temperature profile was used in the calculations.

## ACCURACY

The estimated probable uncertainties of the pertinent recorded and calculated quantities are as follows:

Free-stream $p_t$	$\pm 1$ percent
Free-stream $T_t$	$\pm 50^\circ$ R
Free-stream flow angle	$\pm 0.2^\circ$
Local flow angle	$\pm 0.3^\circ$
$\tau_w$	$\pm 5$ percent
$T_w$	$\pm 10^\circ$ R
$p_e$	$\pm 5$ percent
$M_e$	$\pm 0.17$
$q_e$	$\pm 2$ percent
$\rho_e U_e / \mu_e$	$\pm 7$ percent
$Re, \theta$ or $Re, \Gamma$	$\pm 8$ percent
Pitot-probe pressure	$\pm 2$ percent
Boundary-layer total temperature	$\pm 50^\circ$ R
$y$	$\pm 0.005$ in.
$\theta$ or $\Gamma$	$\pm 5$ percent
$\dot{q}_w$	$\pm 5$ percent

## DISCUSSION OF RESULTS

### Skin Friction

The skin-friction data obtained in these tests at cold-wall conditions are summarized in tables I and II. The flat-plate data were obtained with and without boundary-layer trips. Because the data are in the form  $C_f(Re, \theta)$ , there is no need to define a virtual origin of turbulent boundary-layer flow in the analysis of the data.

<sup>2</sup>See note in Journal of Spacecraft and Rockets, vol. 4, no. 2, Feb. 1967, pp. 287-288 by Mitchel H. Bertram entitled "Comment on 'Viscosity of Air'."

An evaluation of the representative theories<sup>3</sup> of Sommer and Short (ref. 5), Spalding and Chi (ref. 1), Van Driest II (ref. 4), and Coles (ref. 7) for local turbulent skin friction is made by comparing the difference between experimental and theoretical skin friction for specified free-stream conditions and surface temperature. Most of the data was taken in the moderate Reynolds number range,  $3 \times 10^3 < R_{e,\theta} < 30 \times 10^3$ . Data taken at higher Reynolds numbers will be marked by high flags, data at lower Reynolds numbers by low flags. Adiabatic and nonadiabatic data are treated separately to discern the effects of Mach number and wall temperature independently. In addition, non-adiabatic wind-tunnel-wall data are treated separately from flat-plate data for reasons to be discussed.

Adiabatic-wall conditions.— Only skin-friction data in air from flat plates and wind-tunnel walls for which  $C_f$  was directly measured and  $R_{e,\theta}$  was evaluated from boundary-layer surveys were chosen for the comparisons<sup>4</sup> presented in figure 1. For some of the test data, it was assumed that the total temperature was constant across the boundary layer in evaluating  $R_{e,\theta}$ . This assumption is valid for the adiabatic wall case because  $R_{e,\theta}$  is relatively unaffected by differences in the assumed temperature distribution (ref. 11). The data are from references 2 and 12 through 19.

Comparisons presented in figure 1 indicate that at Mach numbers below 4 all the theories give about the same prediction for the data obtained at low and moderate Reynolds numbers ( $R_{e,\theta} < 30 \times 10^3$ ). At high Reynolds numbers ( $R_{e,\theta} > 30 \times 10^3$ ), however, Coles' theory tends to underpredict the experimental results by 10 to 15 percent. This Reynolds number effect in Coles' theory is related to the Reynolds number dependence of the temperature computed from the substructure hypothesis. As the Mach number is increased above 4, there is a tendency for the theories of Spalding and Chi and Sommer and Short to underpredict the data, reaching underpredictions of 20 and 30 percent, respectively, for Korkegi's data (ref. 19) near Mach number 6. Theories of Van Driest II and Coles predict the data within about 8 percent at the higher Mach numbers.

Nonadiabatic wall - flat plates.— Only skin-friction data for which  $C_f$  was directly measured on flat plates or circular cylinders (representative of flat plates) at Mach numbers between 5.6 and 7.4 were used in the comparisons presented in figure 2. The dashed lines represent fairings through the data, which include the unpublished data from Ames Research Center and the data from references 5 and 19 through 21. Sommer and Short (ref. 5) obtained their data from hollow circular cylinder models fired down a ballistic range. The local skin friction was calculated from the average skin friction of reference 5 by

<sup>3</sup>The transformed values of measured  $R_{e,\theta}$  as given by each theory were used in the incompressible Kármán-Schoenherr equation of  $\bar{C}_f$  as a function of  $\bar{R}_{e,\theta}$  (ref. 2) to calculate the theoretical values of  $C_f$ . For Van Driest's theory, a temperature recovery factor of 0.9 was assumed in a manner similar to Spalding-Chi (ref. 1).

<sup>4</sup>Each symbol in figure 1 stands for a representative average of several data points taken over a limited Reynolds number range at the particular Mach number of a given experiment.

assuming that  $C_f/C_{f,i} = C_F/C_{F,i}$ . The analysis of Ames and Korkegi's data was based on the measured momentum-thickness Reynolds number; therefore, it was not necessary to derive a virtual origin of turbulent flow for these data. Examination of the Ames data indicates that any effect of boundary-layer trips on  $C_f(R_{e,\theta})$  was within the experimental accuracy (compare the open circles with the solid circles). In addition, the results from the injected model (flagged solid symbols) agree with those for the stationary model (solid symbols).

The effect of two different choices for virtual origin of turbulent flow is also shown in figure 2. Theoretical local skin-friction coefficients for the data of Wallace and McLaughlin (ref. 21) and of Neal (ref. 20), for which the momentum-thickness Reynolds number was not measured, were calculated for Reynolds numbers obtained by two current methods for determining the virtual origin of turbulent flow. In the first method, the virtual origin was taken to be located at the position of maximum Stanton number (dashed symbols). In the second method, the virtual origin was derived by assuming that the momentum thickness for turbulent and laminar flow at the end of transition is equal  $(x_T)(C_{F,T}) = (x_L)(C_{F,L})$ , for which  $x_L$  was taken at the point where the Stanton number was maximum (regular symbols). Results from this latter method for Neal's data appear to be in better agreement with the Ames data.

For  $T_w/T_{aw} > 0.3$ , the theories of Van Driest II and Coles predict the skin friction within about 10 percent, whereas theories of Spalding and Chi and Sommer and Short underpredict the skin friction by 20 to 30 percent. At the lower temperature ratios, none of the theories predict the experimental variation of skin friction with wall to adiabatic wall temperature ratio.

Nonadiabatic wall - tunnel walls. - Measurements of nonadiabatic skin friction on wind-tunnel walls are treated separately because of the significant difference in measured temperature distributions presented in figure 3. For the flat plate, the Crocco linear temperature distribution ( $Pr = 1.0$ ) as a function of velocity ratio represents the data, but for the tunnel side wall, the results lie closer to a quadratic temperature distribution. A similar difference between the temperature distributions on free-flight models and on a nozzle wall was noticed previously by Seiff and Short (ref. 22). They suggested that the history of the rapid expansion in the nozzle to high Mach numbers results in a boundary layer that is not in equilibrium with the local edge conditions.

The wind-tunnel-wall skin-friction data for  $dp/dx \approx 0$  are compared with predicted values based on flat-plate theory in figure 4. Note that the theories of Spalding and Chi, Van Driest II, and Coles are based on the Crocco linear temperature distribution; however, the data reflect the side-wall boundary-layer temperature distributions indicated in figure 3. In general, figure 4 shows that the theories of Sommer and Short, Spalding and Chi, and Van Driest II give about the same ratios of  $(C_f)_{exp}/(C_f)_{the}$  at  $T_w/T_{aw} \approx 0.4$  on the wind-tunnel wall as on the flat plates (dashed lines). Coles' theory predicts these ratios from 20 to 30 percent below the data at  $T_w/T_{aw} > 0.3$  (similar to the high Reynolds number data in fig. 1), which further indicates

that Coles' theory might be inherently incorrect at the higher Reynolds numbers. Wallace's data from two separate tests appear to be self-consistent within about  $\pm 10$  percent and generally agree with the Ames data at  $T_w/T_{aw} \approx 0.3$ . It is interesting that a flat-plate theory (in this case, Van Driest II) correlates the wall data at  $T_w/T_{aw} > 0.3$ .

### Heat Transfer

The analysis of the heat-transfer data parallels that for skin friction where it was found that expressing the data as

$$C_f = f(R_e, \theta, M_e, T_w/T_{aw}) \quad (1)$$

was useful in eliminating an arbitrarily assigned origin for the turbulent boundary layer. The local skin-friction coefficient is related to the momentum thickness and length Reynolds numbers by the momentum-integral equation

$$\frac{C_f}{2} \equiv \frac{\tau_w}{\rho_e U_e^2} = \frac{dR_{e,\theta}}{dR_{e,s}} + \frac{R_{e,\theta}}{r^\epsilon} \frac{dr^\epsilon}{dR_{e,s}} \quad (2)$$

where  $\epsilon = 0$  for a flat plate,  $\epsilon = 1$  for a cone, and the momentum thickness is defined as

$$\theta \equiv \int_0^\delta \frac{\rho U}{\rho_e U_e} \left(1 - \frac{U}{U_e}\right) dy \quad (3)$$

The results of boundary-layer pitot and total temperature surveys were introduced into equation (3) to evaluate the momentum thickness in the skin-friction analysis.

In an analogous manner, the local Stanton number is related to the energy thickness and length Reynolds numbers by the energy-integral equation ( $H_w = \text{const}$ )

$$C_h \left( \frac{H_w - H_{aw}}{H_w - H_e} \right) \equiv \frac{\dot{q}_w}{\rho_e U_e (H_w - H_e)} = \frac{dR_{e,\Gamma}}{dR_{e,s}} + \frac{R_{e,\Gamma}}{r^\epsilon} \frac{dr^\epsilon}{dR_{e,s}} \quad (4)$$

where the energy thickness is defined as

$$\Gamma \equiv \int_0^\delta \frac{\rho U}{\rho_e U_e} \left( \frac{H - H_e}{H_w - H_e} \right) dy \quad (5)$$

Instead of boundary-layer surveys, the local heat-flux distribution was employed to evaluate  $\Gamma$  from

$$\Gamma = \frac{\int_0^{s_1} \dot{q}_w(s) r^\epsilon(s) ds}{\rho_e U_e (H_w - H_e) r_1^\epsilon} \quad (6)$$

which results from the integration of equation (4). In the evaluation of equation (6), the boundary layer ahead of the first thermocouple station was assumed laminar with  $\dot{q}_w \sim s^{-1/2}$ . In a few tests in which both boundary-layer surveys and heat-flux distributions were obtained, it was found that  $\Gamma$  from equations (5) and (6) agreed within 7 percent.

Prediction of turbulent-boundary-layer heat transfer from skin-friction theories,  $C_f(R_{e,\theta})$ , requires the assumption of a Reynolds analogy factor and a recovery factor. Choices for these factors are based either on extensions of the now classic constant-property theories or on past experimental results. If these quantities are uniform along the surface,  $C_h$  and  $C_f/2$ , and  $R_{e,\Gamma}$  and  $R_{e,\theta}$  are related as follows:

$$(C_h)_{the} = \left( \frac{C_h}{C_f/2} \right) \left( \frac{C_f}{2} \right)_{the}$$

$$R_{e,\theta} = \frac{R_{e,\Gamma}}{\left( \frac{C_h}{C_f/2} \right) \left( \frac{H_w - H_{aw}}{H_w - H_e} \right)}$$

where  $C_h/(C_f/2)$  is the Reynolds analogy factor, and  $r$ , the recovery factor, is introduced into the adiabatic wall enthalpy

$$H_{aw} = H_e - (1 - r) \frac{U_e^2}{2}$$

Typical variations of  $C_h$  with  $R_{e,\Gamma}$  for a  $5^\circ$  cone and a flat plate with nearly the same conditions of  $M_e$  and  $T_w/T_{aw}$  are shown in figure 5. A recovery factor of 0.85 was used for laminar flow and 0.9 for turbulent flow, with a linear interpolation in the transition region. Although the transition location differs for the two shapes, the Stanton number for the fully turbulent flow is essentially the same for a given value of  $R_{e,\Gamma}$ .

The heat-transfer results are presented in figure 6 in a form analogous to the skin friction (see fig. 2(b)). Shown are recent Ames data for  $5 < M_e < 7.4$  obtained on two cones with a wall-temperature-ratio range of  $0.11 < T_w/T_{aw} < 0.6$  and on a flat plate with  $T_w/T_{aw} \approx 0.3$ . To relate the heat-transfer results to the skin-friction theories, either as  $(\dot{q}_w)_{exp}/(\dot{q}_w)_{the}$  or  $(C_h)_{exp}/(C_h)_{the}$ , it is necessary to assume values for the recovery and Reynolds analogy factors. For figure 6, the values assumed are  $r = 0.9$  and  $C_h/(C_f/2) = 1.16$ , which are characteristic of supersonic flow and

moderate cooling rates. From these results, it would be concluded that the Spalding and Chi theory agrees best with the experimental results. This conclusion, however, is inconsistent with the findings of the skin-friction data, where the Van Driest II and Coles theories are favored. Thus, the skin-friction and heat-transfer experiments lead to different conclusions regarding the accuracy of prediction theories, at least when the usually accepted values of  $r = 0.9$  and  $C_h/(C_f/2) = 1.16$  are used.

To reconcile the dichotomy between the skin-friction and heat-transfer results, a short series of tests was conducted in which simultaneous measurements were made of local heat flux and skin friction on a flat plate with  $T_w/T_{aw} \approx 0.3$ . It was found that the heat flux shear ratio,  $\dot{q}_w U_e / [\tau_w (H_w - H_e)]$ , varied between 0.84 and 0.94, depending on the Reynolds number, whereas, at this wall temperature, the ratio calculated for  $r = 0.9$  and  $C_h/(C_f/2) = 1.16$  is 1.02. Furthermore, substituting  $Pr = 0.72$  and  $Pr_T = 1.0$  into the von Kármán Reynolds analogy factor and the corresponding recovery factor expression by Van Driest resulted in a heat flux shear ratio of 1.06 over the Reynolds number range of the tests. Thus, for the conditions of these tests, there is about a 10 to 20 percent reduction in heat transfer relative to skin friction from values expected from past experiments and theory. The data are too limited to permit evaluating the Reynolds analogy and recovery factors individually from the measured heat flux shear ratios. Therefore, it is necessary to rely on theory or a hypothesis to distinguish the effects of each factor. The von Kármán Reynolds analogy and Van Driest recovery factor expressions can be forced to agree with the heat flux shear ratio data by imposing a turbulent Prandtl number of 0.7 and arriving at  $r = 0.7$  and  $C_h/(C_f/2) = 1.4$ . Alternatively, as shown in figure 7, the hypothesis that the recovery factor remains equal to 0.9 requires that  $C_h/(C_f/2) \approx 1.0$ , which is 15 to 20 percent lower than the value usually employed. This is illustrated by the dashed line, which represents the von Kármán Reynolds analogy factor ( $Pr = 0.725$ ,  $Pr_T = 1.0$ ) extended to compressible flows (ref. 8).

To test the surface temperature range where the preceding values of  $r$  and  $C_h/(C_f/2)$  remain valid, the data cited in figure 8(a) were analyzed with  $r = 0.7$ ,  $C_h/(C_f/2) = 1.4$  and with  $r = 0.9$ ,  $C_h/(C_f/2) = 1$ . It was found that the latter set of values caused the heat-transfer data (open symbols) to be more consistent with the skin-friction data (solid symbols) over the entire wall-temperature range shown in figure 8(b). With  $r = 0.9$  and  $C_h/(C_f/2) = 1$ , the theories of Van Driest II and Coles predict the heat flux to within  $\pm 10$  percent at  $T_w > 0.3T_{aw}$ . The Spalding and Chi method generally under-predicted the heat-transfer data by 20 percent over the entire wall-temperature range.

#### CONCLUDING REMARKS

The turbulent boundary-layer skin-friction theories of Sommer and Short, Spalding and Chi, Van Driest II, and Coles have been evaluated on the basis

of directly measured skin friction on flat plates and wind-tunnel side walls. The use of momentum-thickness Reynolds number in the skin-friction comparisons avoids the need for arbitrarily locating the virtual origin of the turbulent boundary layer. At Mach numbers below 4, all the theories agree well with adiabatic wall data. On flat plates, at Mach numbers between 5.6 and 7.4 and wall to adiabatic wall temperature ratios down to 0.3, theories of Van Driest II and Coles give the best skin-friction predictions. For these temperatures, the theories of Sommer and Short or Spalding and Chi underpredict the skin friction by 20 to 30 percent. At lower wall temperatures, none of the theories gives the proper effect of wall-temperature level on the skin friction; however, the amount of data available is quite limited.

For the fully turbulent portions of the boundary layer on a wind-tunnel side wall at reduced temperatures, measured total temperature distributions were more nearly quadratic than linear with velocity as is characteristic of boundary layers on flat plates. This reflects the growth of the boundary layer in a favorable pressure gradient upstream of the test station. Even with these effects, when the measured profiles are used to evaluate the local momentum-thickness Reynolds number, values of  $C_f(R_{e,\theta})$  on the side wall agree fairly well with the Van Driest II flat-plate theory.

The above theories have also been evaluated on the basis of heat-transfer measurements on cones and flat plates with boundary-layer-edge Mach numbers between 5 and 7.4 and wall to adiabatic wall temperature ratios between 0.1 and 0.6. A boundary-layer energy thickness obtained from integration of the heat-flux distribution up to a test station proved useful in correlating the local heat flux at that station, in a manner analogous to the use of momentum thickness. The theory of Spalding and Chi was in best agreement with the data, provided values of recovery factor equal to 0.9 and Reynolds analogy factor equal to 1.16 were used. Simultaneous measurements of heat transfer and skin friction on a flat plate at a single temperature ( $T_w/T_{aw} = 0.3$ ) yielded heat flux shear ratios about 10 to 20 percent lower than the usually predicted values, the Reynolds analogy factor being unity if the recovery factor is assumed to remain constant at 0.9. Use of these values in the heat-transfer predictions at wall-temperature ratios between 0.2 and 0.8 produced results consistent with the skin-friction data. For wall to adiabatic wall temperature ratios greater than 0.3, the theories of Van Driest II and Coles predicted the heat-transfer data within  $\pm 10$  percent. The theory of Spalding and Chi generally underpredicted the heat-transfer data by 20 percent over the complete wall-temperature range.

Although the assumptions cited in the previous paragraph caused the comparisons between heat-transfer data and theories to be consistent with those for skin friction, caution should be exercised in generalizing the results beyond the range of variables of this investigation. Turbulent-boundary-layer theory that admits changes in the Reynolds analogy factor invariably requires a change in the recovery factor. It was found that ignoring the latter change yielded the best correlation of the present data. Additional simultaneous heat-transfer and skin-friction data over a large range of surface temperatures are needed to distinguish the individual behavior of the Reynolds analogy and recovery factors as Mach number is increased and the



walls are highly cooled. Further, an understanding of these effects will require careful probing of the boundary layer to establish the distribution of quantities such as the turbulent Prandtl number.

Ames Research Center

National Aeronautics and Space Administration

Moffett Field, Calif., 94035, Feb. 18, 1969

129-01-08-24-00-21

#### REFERENCES

1. Spalding, D. B.; and Chi, S. W.: The Drag of a Compressible Turbulent Boundary Layer on a Smooth Flat Plate With and Without Heat Transfer. *J. Fluid Mech.*, vol. 18, pt. 1, Jan. 1964, pp. 117-143.
2. Hopkins, Edward J.; and Keener, Earl R.: Study of Surface Pitots for Measuring Turbulent Skin Friction at Supersonic Mach Numbers - Adiabatic Wall. NASA TN D-3478, 1966.
3. Peterson, John B., Jr.: A Comparison of Experimental and Theoretical Results for the Compressible Turbulent-Boundary-Layer Skin Friction With Zero Pressure Gradient. NASA TN D-1795, 1963.
4. Van Driest, E. R.: Problem of Aerodynamic Heating. *Aero. Aspects Sessions, Natl. Summer Meeting, IAS, Los Angeles, June 1956.* (Also *Aeron. Eng. Rev.*, Oct. 1956, pp. 26-41.)
5. Sommer, S. C.; and Short, B. J.: Free-Flight Measurements of Turbulent Boundary-Layer Skin Friction in the Presence of Severe Aerodynamic Heating at Mach Numbers From 2.8 to 7.0. NACA TN 3391, 1955. (Also *J. Aeron. Sci.*, vol. 23, no. 6, June 1956.)
6. Miles, John B.; and Kim, Jong Hyun: Evaluation of Coles' Turbulent Compressible Boundary-Layer Theory. *AIAA J.*, vol. 6, no. 6, June 1968, pp. 1187-1189.
7. Coles, Donald: The Turbulent Boundary Layer in a Compressible Fluid. *Phys. Fluids*, vol. 7, no. 9, Sept. 1964, pp. 1403-1423. (Also Rand Rep. R-403-PR, 1962.)
8. Bertram, Mitchel H.; and Neal, Luther, Jr.: Recent Experiments in Hypersonic Turbulent Boundary Layers. NASA TM X-56335, 1965. (Also AGARD Specialists' Meeting on Recent Developments in Boundary-Layer Research, Naples, Italy, May 10-14, 1965.)

9. Bertram, Mitchel H.; Cary, Aubrey M., Jr.; and Whitehead, Allen H., Jr.: Experiments With Hypersonic Turbulent Boundary Layers on Flat Plates and Delta Wings. AGARD Specialists' Meeting on Hypersonic Boundary Layers and Flow Fields, London, England, May 1-3, 1968.
10. Cary, Aubrey M., Jr.: Turbulent Boundary-Layer Heat Transfer and Transition Measurements for Cold-Wall Conditions at Mach 6. AIAA J., vol. 6, no. 5, May 1968, pp. 958-959.
11. Adcock, Jerry B.; Peterson, John B., Jr.; and McRee, Donald I.: Experimental Investigation of a Turbulent Boundary Layer at Mach 6, High Reynolds Numbers, and Zero Heat Transfer. NASA TN D-2907, 1965.
12. Smith, Donald W.; and Walker, John H.: Skin-Friction Measurements in Incompressible Flow. NASA TR R-26, 1959.
13. Hakkinen, Raimo J.: Measurements of Turbulent Skin Friction on a Flat Plate at Transonic Speeds. NACA TN 3486, 1955.
14. Shutts, W. H.; Hartwig, W. H.; and Weiler, J. E.: Final Report on Turbulent Boundary-Layer and Skin-Friction Measurements on a Smooth, Thermally Insulated Flat Plate at Supersonic Speeds. Rep. DRL-364, CM-823, Univ. of Texas Defense Res. Lab., 1955.
15. Stalmach, Charles J., Jr.: Experimental Investigation of the Surface Impact Pressure Probe Method of Measuring Local Skin Friction at Supersonic Speeds. Rep. DRL-410, CR-2675, Univ. of Texas Defense Res. Lab., 1958.
16. Coles, Donald: Measurements in the Boundary Layer on a Smooth Flat Plate in Supersonic Flow III. Rep. 20-71, Jet Propulsion Lab., Calif. Inst. of Tech., 1953.
17. Moore, D. R.; and Harkness, J.: Experimental Investigations of the Compressible Turbulent Boundary Layer at Very High Reynolds Numbers. AIAA J., vol. 3, no. 4, April 1965, pp. 631-638.
18. Matting, Fred W.; Chapman, Dean R.; Nyholm, Jack R.; and Thomas, Andrew G.: Turbulent Skin Friction at High Mach Numbers and Reynolds Numbers in Air and Helium. NASA TR R-82, 1961.
19. Korkegi, Robert H.: Transition Studies and Skin-Friction Measurements on an Insulated Flat Plate at a Mach Number of 5.8. J. Aeron. Sci., vol. 23, no. 2, Feb. 1956, pp. 97-107, 192.
20. Neal, Luther, Jr.: A Study of the Pressure, Heat Transfer, and Skin Friction on Sharp and Blunt Flat Plates at Mach 6.8. NASA TN D-3312, 1966.

21. Wallace, J. E.; and McLaughlin, E. J.: Experimental Investigations of Hypersonic, Turbulent Flow and Laminar, Leeward-Side Flow on Flat Plates. Tech. Rep. AFFDL-TR-66-63, Vol. I, Cornell Aeronautical Lab., July 1966.
22. Seiff, Alvin; and Short, Barbara J.: An Investigation of Supersonic Turbulent Boundary Layers on Slender Bodies of Revolution in Free Flight by Use of a Mach-Zehnder Interferometer and Shadowgraphs. NACA TN 4364, 1958.
23. Wallace, J. E.: Hypersonic Turbulent Boundary-Layer Studies at Cold Wall Conditions. Proceedings of the 1967 Heat Transfer and Fluid Mechanics Institute, Univ. of Calif., San Diego, June 19-21, 1967, pp. 427-451.
24. Wallace, J. E.: Hypersonic Turbulent Boundary-Layer Measurements Using an Electron Beam. Tech. Rep. CAL AN-2112-Y-1, Cornell Aeronautical Lab., Aug. 1968.
25. Van Driest, E. R.: Investigation of Laminar Boundary Layer in Compressible Fluids Using the Crocco Method. NACA TN 2597, 1952.

TABLE 1.- SKIN-FRICTION DATA FOR FLAT PLATES IN THE AMES 3.5-FOOT WIND TUNNEL

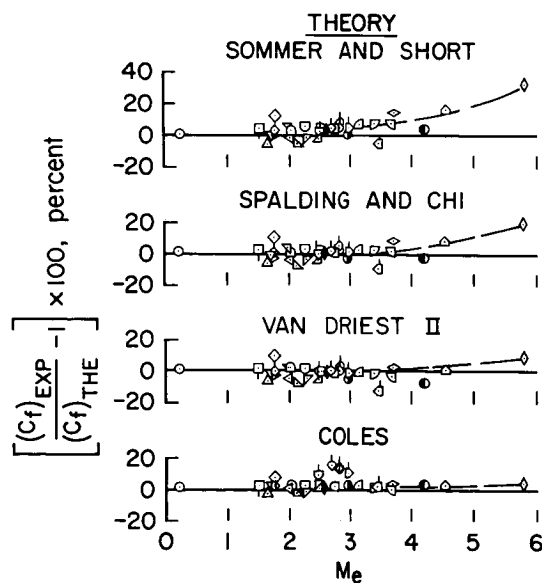
Me	$(\rho_e U_e / \mu_e) \times 10^{-6}$ , ft <sup>-1</sup>	$(Re, \theta) \times 10^{-3}$	T <sub>t,e</sub> , °R	T <sub>w</sub> , °R	T <sub>e</sub> , °R	T <sub>w</sub> /T <sub>aw</sub>	(C <sub>f</sub> ) × 10 <sup>3</sup>	Boundary- layer trips	Source
6.5	1.70	2.26	1850	583	205	0.34	1.57	Off	Hopkins and Keener, stationary flat plate
	2.62	4.56	1960	587	218	.32	1.22	On	
	1.64	3.30	1410	551	153	.43	1.25	On	
	2.37	5.90	1477	564	161	.42	1.20	On	
	1.49	2.39	1474	559	160	.41	1.52	Off	
	2.82	3.82	1376	561	149	.45	1.23	Off	
	1.26	2.19	1158	537	124	.51	1.41	On	
	1.81	3.89	1250	543	130	.50	1.35	On	
	4.01	8.33	1240	572	133	.51	1.00	On	
	4.07	6.42	1231	572	132	.51	1.06	Off	
7.4	2.39	3.01	1963	560	172	.31	1.26	Off	Keener and Polek, injected flat plate
7.4	4.53	5.67	1983	573	172	.31	1.08	Off	

TABLE II.- SKIN-FRICTION DATA FOR SIDE WALL OF THE AMES 3.5-FOOT WIND TUNNEL

$M_e$	$(\rho_e U_e / \mu_e) \times 10^{-6}$ , ft <sup>-1</sup>	$(R_{e,\theta}) \times 10^{-3}$	$T_{t,e}$ , °R	$T_w$ , °R	$T_e$ , °R	$T_w / T_{aw}$	$(C_f) \times 10^4$
7.4	2.95	52.4	1359	543	114	0.44	6.84
	3.86	56.4	1340	555	112	.46	6.50
	1.16	20.5	1273	544	109	.47	7.14
	1.97	40.2	1250	552	105	.49	6.76
	2.73	48.1	1404	558	118	.44	6.70
	4.01	62.6	1328	568	111	.47	6.30
	.91	18.7	1453	554	125	.42	8.08
	1.88	31.7	1363	567	113	.46	7.26
	.69	16.4	1595	546	133	.39	8.86
	1.44	28.4	1561	558	129	.40	7.82
	2.09	52.6	1637	557	139	.37	7.33
	2.98	53.0	1564	568	132	.40	7.12
	.71	21.1	1686	552	146	.35	9.12
	1.34	30.1	1685	562	144	.36	7.97
	.63	13.2	1812	554	158	.33	9.45
	1.23	33.0	1795	564	155	.34	8.43
	1.66	42.1	1879	558	162	.32	8.13

SYMBOL	$M_e$	$(R_{e,\theta}) \times 10^{-3}$	SOURCE
○	0.22	7	SMITH AND WALKER, REF. 12
□	1.50	2	HAKKINEN, REF. 13
△	1.63	12	SHUTTS et al., REF. 14
▽	1.68	20	
◇	1.73	13	
○	1.75	2	HAKKINEN, REF. 13
○	1.75	8	STALMACH, REF. 15
▽	1.97	6	COLES, REF. 16
△	2.00	13	SHUTTS et al., REF. 14
○	2.01	8	STALMACH, REF. 15
△	2.11	14	SHUTTS et al., REF. 14
□	2.23	7	STALMACH, REF. 15
▽	2.25	13	SHUTTS et al., REF. 14
△	2.46	12	
○	2.46	68	HOPKINS AND KEENER, REF. 2
□	2.49	7	STALMACH, REF. 15
◆	2.56	6	COLES, REF. 16
○	2.67	690	MOORE AND HARKNESS, REF. 17
○	2.80	360	
○	2.80	81	
□	2.72	7	STALMACH, REF. 15
□	2.95	7	
●	2.95	15	MATTING et al., REF. 18
○	2.96	61	HOPKINS AND KEENER, REF. 2
△	3.16	7	STALMACH, REF. 15
▽	3.39	7	
○	3.45	56	HOPKINS AND KEENER, REF. 2
○	3.67	6	STALMACH, REF. 15
◇	3.69	5	COLES, REF. 16
●	4.20	13	MATTING et al., REF. 18
△	4.53	5	COLES, REF. 16
◇	5.79	3	KORKEGI, REF. 19

(a) Data identification.



(b) Comparison of data with theory.

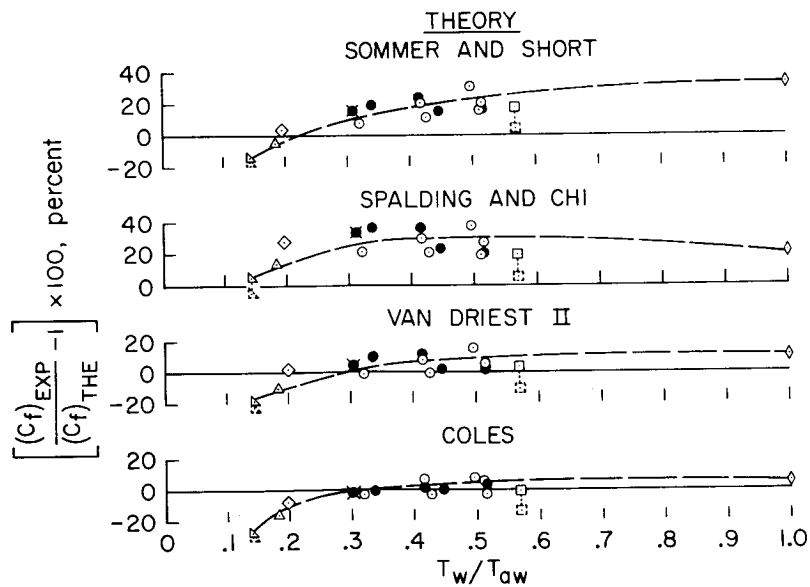
Figure 1.- Adiabatic-wall skin friction;  $C_f$  and  $R_{e,\theta}$  directly measured.

SYM	$M_e$	B.L. TRIPS	$(R_{e,\theta}) \times 10^{-3}$	$(R_{e,x}) \times 10^{-6}$	SOURCE
○	6.5	ON	5		AMES 3.5 ft W.T.* (HOPKINS AND KEENER, UNPUBLISHED)
●	6.5	OFF	4		
■	7.4	OFF	4		(KEENER AND POLEK, UNPUBLISHED)
□	6.8	OFF		3	NEAL, REF. 20**
◻	6.8	OFF		2	
△	7.0	ON		1	SOMMER AND SHORT, REF. 5
◇	5.6	ON		8	
▴	7.4	OFF		18	WALLACE AND McLAUGHLIN, REF. 21**
◊	7.4	OFF		13	
◊	5.8	ON	3		KORKEGI, REF. 19

\* THE TWO DIFFERENT MODELS CAN BE IDENTIFIED AS STATIONARY (○,●) AND INJECTED MODEL (■)

\*\* REGULAR SYMBOLS REPRESENT VIRTUAL ORIGIN CALCULATED FROM  $(X_L)(C_{F,L}) = (X_T)(C_{F,T})$   
DASHED SYMBOLS REPRESENT VIRTUAL ORIGIN AT  $C_{h,MAX}$

(a) Data identification.



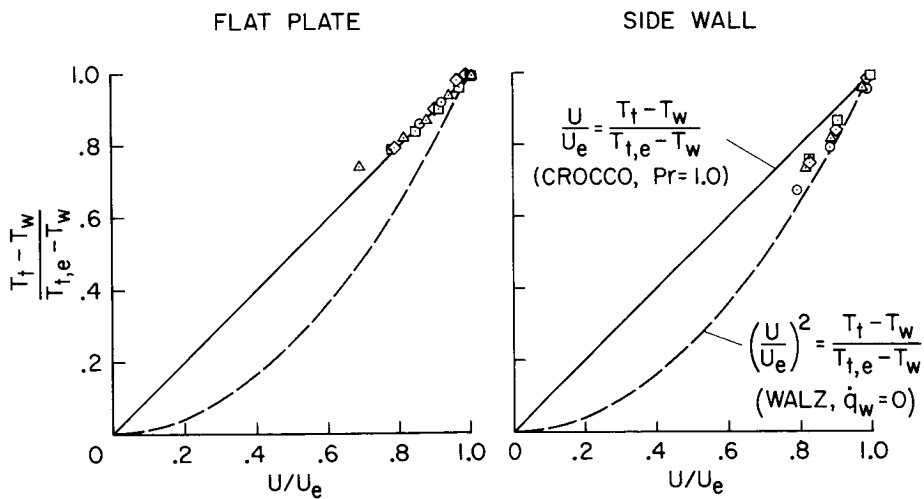
(b) Comparison of data with theory.

Figure 2.- Nonadiabatic-wall skin friction for flat plates;  $C_f$  directly measured.

FLAT PLATE					
SYM	$Me$	$(Re, \theta) \times 10^{-3}$	$T_w/T_{t,e}$	$T_{t,e}, ^\circ R$	B.L. TRIPS
○	6.5	2.26	0.315	1850	OFF
□	6.5	4.56	.300	1960	ON
◇	6.5	3.30	.391	1410	ON
△	6.5	5.90	.382	1477	ON

SIDE WALL					
SYM	$Me$	$(Re, \theta) \times 10^{-3}$	$T_w/T_{t,e}$	$T_{t,e}, ^\circ R$	
○	7.4	40.2	0.442	1250	
□	7.4	52.4	.400	1359	
◇	7.4	53.0	.363	1564	
△	7.4	47.5	.304	1881	

(a) Data identification.



(b) Comparison of data with theory.

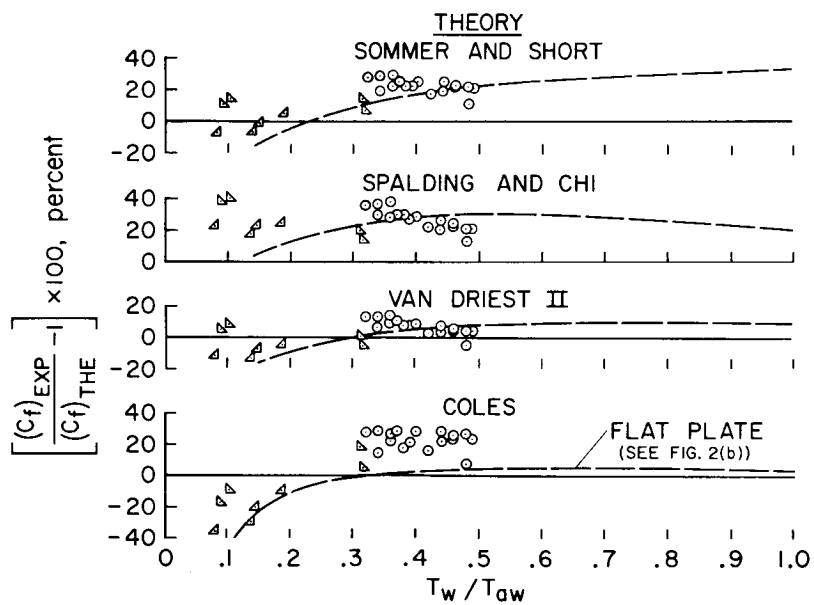
Figure 3.- Temperature-velocity profiles measured in the Ames 3.5-Foot Wind Tunnel by Hopkins and Keener; nonadiabatic wall.



SYMBOL	$Me$	$(Re_{\theta}) \times 10^{-3}$	SOURCE
○	7.4	37	HOPKINS AND KEENER, UNPUBLISHED
△	7.5	44	WALLACE, REF. 23*
◀	8.6	6	WALLACE, REF. 24

\* DATA RECALCULATED WITH A QUADRATIC TEMPERATURE DISTRIBUTION ASSUMED

(a) Data identification.



(b) Comparison of data with theory.

Figure 4.- Nonadiabatic-wall skin friction for wind-tunnel walls;  $C_F$  and  $Re_{\theta}$  directly measured.

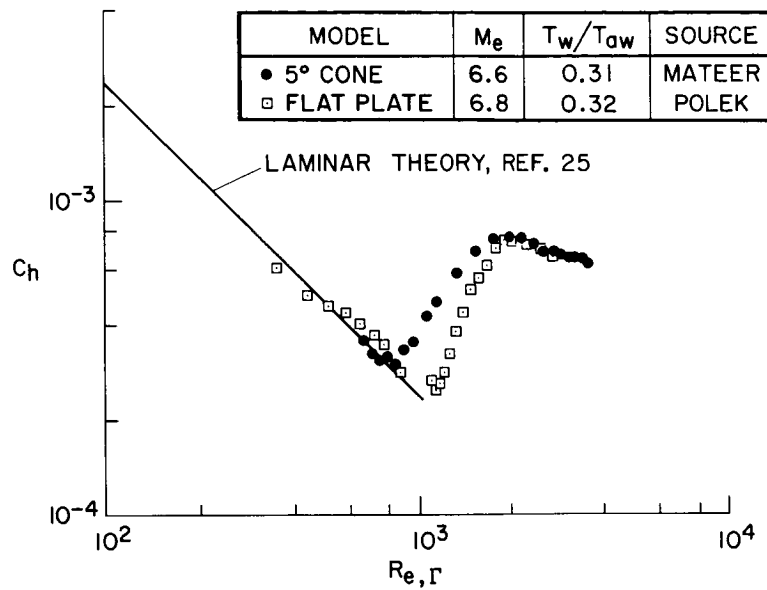
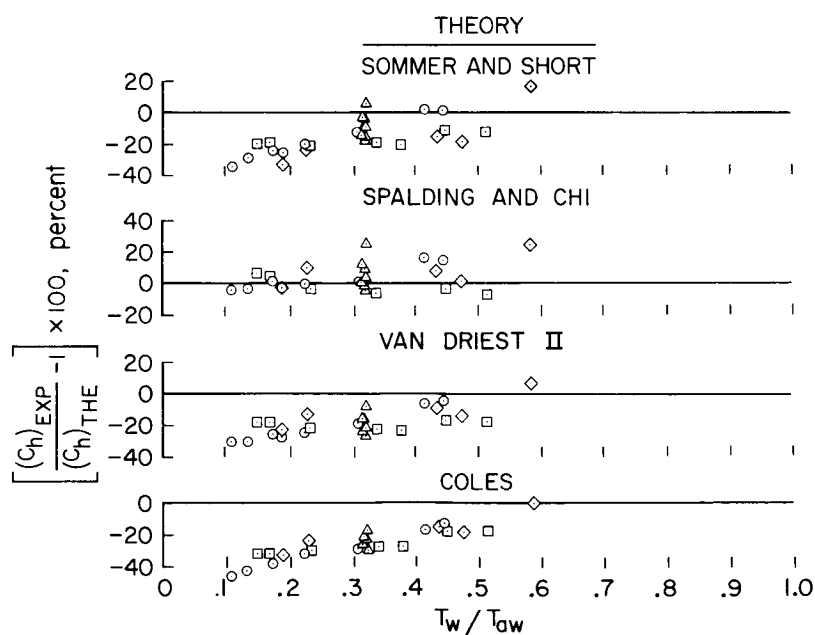


Figure 5.- Stanton number variation with energy-thickness Reynolds number;  
Ames 3.5-Foot Wind Tunnel.

SYM	$M_e$	$(Re, \Gamma) \times 10^{-3}$	MODEL	SOURCE
○	6.6	4	5° CONE	MATEER, UNPUBLISHED
□	4.9	4	15° CONE	
◇	5.0	4	5° CONE	
△	7.4-6.8	5	FLAT PLATE ( $\alpha = 0$ AND $3.1^\circ$ )	POLEK, UNPUBLISHED

(a) Data identification.



(b) Comparison of data with theory;  $C_h / (C_f / 2) = 1.16$  and  $r = 0.9$ .

Figure 6.- Nonadiabatic-wall heat-transfer data; Ames 3.5-Foot Wind Tunnel.

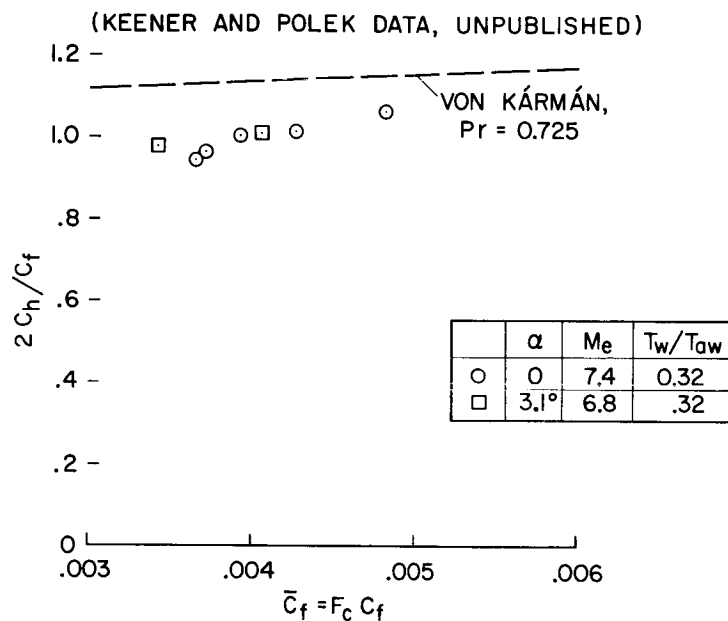
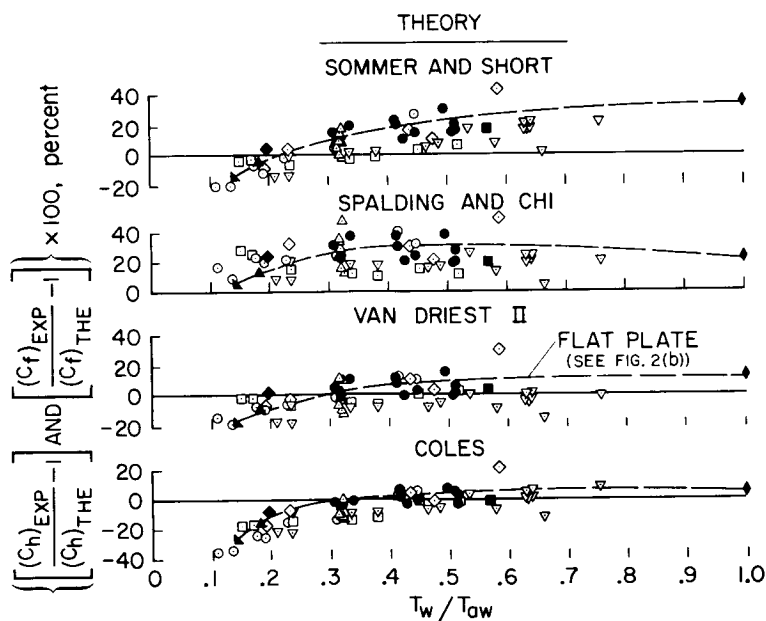


Figure 7.- Reynolds analogy factors measured for a flat plate; Ames 3.5-Foot Wind Tunnel;  $r = 0.9$ .

SYM	M <sub>e</sub>	MODEL	(Re,θ)×10 <sup>-3</sup> OR (Re,Γ)×10 <sup>-3</sup>	(Re,x)×10 <sup>-6</sup>	SOURCE
●	6.5	FLAT PLATE	5		HOPKINS AND KEENER, UNPUBLISHED
■	6.8	FLAT PLATE		3	NEAL, REF. 20
▲	7.0	CYLINDER		1	SOMMER AND SHORT, REF. 5
◆	5.6	CYLINDER		8	
▴	7.4	FLAT PLATE		18	WALLACE AND Mc LAUGHLIN, REF. 21
♦	5.8	FLAT PLATE	3		
◊	6.6	CONE	4		MATEER, UNPUBLISHED
□	4.9	CONE	4		
◇	5.0	CONE	4		
△	6.8-7.4	FLAT PLATE	5		POLEK, UNPUBLISHED
▽	6.0	FLAT PLATE	5		CARY, REF. 10

TYPE DATA  
 OPEN SYMBOL - HEAT TRANSFER  
 SOLID SYMBOL - SKIN FRICTION

(a) Data identification.



(b) Comparison of data with theory;  $C_h/(C_f/2) = 1.0$  and  $r = 0.9$ .

Figure 8.- Nonadiabatic-wall skin-friction and heat-transfer data.

COMPARISON OF PREDICTION METHODS AND STUDIES OF  
RELAXATION IN HYPERSONIC TURBULENT  
NOZZLE-WALL BOUNDARY LAYERS\*

By Dennis M. Bushnell, Charles B. Johnson,  
William D. Harvey, and William V. Feller  
Langley Research Center

SUMMARY

Recent turbulent boundary-layer measurements on axisymmetric nozzle walls at Mach numbers of 6, 8, and 19 are presented and compared with the predictions of two theoretical methods. One of the methods was of the integral type; the other was a finite-difference solution to the governing differential equations. The integral method gave good predictions of the data at Mach 6 and 8 and a reasonable prediction at Mach 19. Results for the finite-difference approach were available only at Mach 8, for which good agreement with data was obtained.

A survey of boundary-layer data indicates that the variation of total temperature with velocity for flat-plate type of flows can be represented within the scatter of the data by the linear Crocco relation, whereas for nozzle-wall flows, this relation is generally more nearly quadratic. A finite-difference solution for the Mach 8 nozzle-wall boundary layer resulted in a quadratic-type temperature-velocity relation in the strong favorable pressure-gradient region downstream of the throat. However, near the nozzle exit the theoretical solution tended to approach the linear variation of Crocco. Apparently, the observed quadratic variation in nozzle boundary layers can be at least partly accounted for by the pressure-gradient history of the flow.

Profile measurements along a straight pipe extension downstream of the nozzle exit of the Mach 6 tunnel indicate that at a distance of the order of 60 boundary-layer thicknesses, the flow tended to relax toward the linear temperature-velocity variation.

INTRODUCTION

Because of the difficulty of obtaining fully developed turbulent boundary-layer flows on flat plates and hollow cylinders at hypersonic speeds (ref. 1), turbulent boundary layers

---

\*Paper no. 11 also available as NASA TN D-5433, 1969.

on nozzle walls have been surveyed extensively. Also, more accurate measurements can be obtained on tunnel-wall boundary layers because of their comparatively larger thickness. There have been only a limited number of comparisons made between the measured profiles and integral thicknesses with the results of theoretical methods wherein the nozzle pressure-gradient history is taken into account. (See, for example, refs. 2, 3, and 4.) Therefore, there is some question as to the magnitude of the effects of the favorable pressure-gradient history on the profiles measured at the nozzle exit. That is, because of past history, the boundary layer at the nozzle exit (where the pressure gradient is usually small locally) may not have the same characteristics as a boundary layer which developed in a zero-pressure-gradient situation.

On the basis of skin-friction and heat-transfer data obtained on both a flat plate and a tunnel wall, Wallace (ref. 5) concluded that the two flows tend to have a close correspondence as far as surface phenomena are concerned. However, discussion in references 6, 7, and 8 (based on limited profile measurements) indicates that the temperature and velocity profiles for the nozzle-wall boundary layer are appreciably different from those for the flat-plate case.

The purpose of this paper is to present some recent nozzle-wall turbulent-boundary-layer measurements at Mach numbers of 6, 8, and 19, and to compare the results obtained with two theories which utilize the upstream pressure history in computing the flow. One of the theories is of the conventional integral type, and the assumptions used are examined as to relative applicability in flat-plate and nozzle flows. The other approach is a nonsimilar numerical solution of the governing differential equations and hence should be able to give an indication of the effects of the upstream favorable pressure gradient on the profiles at the nozzle exit. Numerical procedures for solving the differential equations have previously been developed by A. M. O. Smith (ref. 9) and others.

## SYMBOLS

$A$	constant in eddy viscosity expression (eq. (4))
$c_p$	specific heat
$C_f$	skin-friction coefficient
$H$	total enthalpy
$H^*$	form factor, $\delta^*/\theta$

$l$	mixing length (eq. (4))
$M$	Mach number
$N$	index in velocity profile (eq. (6))
$p$	pressure
$N_{Pr}$	Prandtl number
$N_{Pr,t}$	turbulent Prandtl number
$R$	Reynolds number
$r$	radius
$T$	temperature
$u,v$	velocity components in x- and y-directions, respectively
$x,y$	Cartesian coordinates along and normal to surface, respectively
$\alpha$	exponent in total-temperature-velocity relationship (eq. (5))
$\rho$	density
$\epsilon$	eddy viscosity
$\kappa$	eddy conductivity
$\mu$	viscosity
$\tau$	shear stress
$\delta$	boundary-layer thickness taken where $\frac{u}{u_e} = 0.995$
$\delta^*$	displacement thickness
$\theta$	momentum thickness



$$\bar{\theta} = \frac{T_t - T_w}{T_{t,\infty} - T_w}$$

Subscripts:

t            total

w            wall

$\infty$            local free stream

e            local external to boundary layer

A prime denotes a fluctuating quantity.

## DESCRIPTION OF THEORIES

### Finite-Difference Approach

The finite-difference method solves the compressible turbulent-boundary-layer equations in terms of mean flow quantities (ref. 10). With the following assumptions for the Reynolds stress and heat transfer

$$-\rho \overline{u'v'} = \epsilon \frac{\partial u}{\partial y}$$

$$-\rho \overline{v'T'} = \kappa \frac{\partial T}{\partial y}$$

and the definition of turbulent Prandtl number

$$\frac{c_p \epsilon}{\kappa} = N_{Pr,t}$$

the governing equations become

For continuity:

$$\frac{\partial}{\partial x}(\rho u r^j) + \frac{\partial}{\partial y}(\rho v r^j) = 0 \quad (1)$$

where  $j = 1$  for axisymmetric flows and  $j = 0$  for two-dimensional flows

For conservation of momentum:

$$\rho u \frac{\partial u}{\partial x} + \rho v \frac{\partial u}{\partial y} = - \frac{dp}{dx} + \frac{\partial}{\partial y} \left[ \mu \left( 1 + \frac{\epsilon}{\mu} \right) \frac{\partial u}{\partial y} \right] \quad (2)$$

For conservation of energy:

$$\rho u \frac{\partial H}{\partial x} + \rho v \frac{\partial H}{\partial y} = \frac{\partial}{\partial y} \left\{ \frac{\mu}{N_{Pr}} \left[ \left( 1 + \frac{\epsilon}{\mu} \frac{N_{Pr}}{N_{Pr,t}} \right) \frac{\partial H}{\partial y} - \left( 1 - N_{Pr} + \frac{\epsilon}{\mu} N_{Pr} \frac{1 - N_{Pr,t}}{N_{Pr,t}} \right) u \frac{\partial u}{\partial y} \right] \right\} \quad (3)$$

The assumption is made that the eddy viscosity can be represented by the simple Prandtl mixing-length concept across the entire boundary layer. A Van Driest modification (ref. 11) is used near the wall, gas properties being evaluated at wall conditions. The expression for  $\epsilon$  is thus

$$\epsilon = \rho l^2 \left[ 1 - \exp\left(\frac{y}{A}\right) \right]^2 \left| \frac{\partial u}{\partial y} \right| \quad (4)$$

where

$$A = -26 \frac{\mu_w}{\rho_w} \left( \frac{\rho_w}{\tau_w} \right)^{1/2}$$

The variation of  $l/\delta$  with  $y/\delta$  was based on results from reference 12 and was assumed to be invariant with Mach number. The numerical values used in the present work are given in table I. For the calculations shown herein,  $N_{Pr,t}$  was taken as 0.9 (ref. 13) and was assumed to be constant.

The method of solution of equations (1), (2), and (3) is similar to that used in reference 14 and is essentially a linearized form of the implicit finite-difference numerical method of reference 15. As in reference 14, a variable step size in the y-direction is used.

### Integral Approach

In the integral method the momentum integral equation for axisymmetric flow (eq. (42), ch. 9 of ref. 16) is solved by a variable-step-size fifth-order Runge-Kutta numerical scheme. In order to solve this equation,  $H^*$  and  $C_f$  variations must be specified. In the outer part of the boundary layer, a temperature-velocity relationship of the form

$$\bar{\theta} \equiv \frac{T_t - T_w}{T_{t,\infty} - T_w} = \left( \frac{u}{u_e} \right)^\alpha \quad (5)$$

is assumed where the value of  $\alpha$  depends on the flow configuration for which calculations are being made. Further discussion of the values assigned to  $\alpha$  is given in a subsequent section. Near the wall the total-temperature—velocity relation is obtained from the Colburn form of the Reynolds analogy. The wall total-temperature—velocity relationship is joined to equation (5) by an intermediate linear relationship which matches the wall equation at  $\frac{u}{u_e} = 0.01$  and equation (5) at  $\frac{u}{u_e} = 0.10$ .

The velocity profiles were assumed to be

$$\frac{u}{u_e} = \left( \frac{y}{\delta} \right)^{1/N} \quad (6)$$

where  $N$  is a specified function of  $Re_{\theta}$  and  $T_w/T_t$ . For calculations of the nozzle-wall boundary layers, this function was taken as the solid line through the data shown in figure 1. The data shown are taken from references 4, 18 to 22. The wall-temperature factor used in the correlation is based on flat-plate type of data at the same Mach number and  $Re_{\theta}$  values but at different  $T_w/T_t$  values. Since the present objective is the calculation of air and nitrogen axisymmetric nozzle-wall boundary layers, the data used to define an  $N$  variation are limited to these conditions. For those cases where only pitot data were available (shown flagged), the velocity profiles were obtained by using a value of 2 for  $\alpha$  in equation (5). (See next section.) The velocity and temperature distributions just described (eqs. (5) and (6)) were used to obtain  $H^*$ .

The skin-friction-coefficient expression of Spalding and Chi (ref. 17) was used directly, without any attempt to account for the effects of pressure gradient.

## RESULTS AND DISCUSSION

### Dependence of Temperature-Velocity Relation on Flow History

As mentioned in the Introduction, the relation between total temperature and velocity may be different for flat-plate and nozzle-wall boundary layers. (See refs. 6, 7, and 8.) A possible cause of this difference is the favorable pressure-gradient history of the nozzle flows. In order to investigate this difference further, all available data where heat transfer was present and the pressure gradient small locally, are shown plotted in figures 2 and 3 in the usual "Crocco" variables  $(\bar{\theta} \text{ and } \frac{u}{u_e})$ . In figure 2 are shown the data which have been obtained on the flat-plate type of configurations, that is, flat plates, hollow cylinders, and in flows where the upstream pressure gradient was small (refs. 24 to 32). Included are unpublished measurements obtained on a flat plate at Mach 6.5 by Hopkins and Keener of NASA Ames Research Center. The amount of scatter exhibited by the data is appreciable, and this scatter may be due to the difficulty

of obtaining accurate measurements in the relatively thin boundary layers usually present in this class of configuration. Also, "flat-plate-flow" experiments do not always achieve the uniform conditions implied in the name. Effects due to induced pressures, wall-temperature variations, secondary flows, and proximity of the measuring station to transition may contribute to the scatter in the available data. However, the mean of the data is perhaps adequately represented for engineering purposes by the linear relation shown. As is well known, this linear variation is a solution to the governing differential equations for the special case of zero pressure gradient and turbulent Prandtl number equal to 1. Since the turbulent Prandtl number is probably of the order of 1 (ref. 13, for example), the "agreement" between the flat-plate data and the linear relationship seems to be reasonable.

Shown in figure 3 are the available data (refs. 8, 20 to 22, and 33 to 37) from the "nozzle wall" class of configuration, that is, data obtained on wind-tunnel walls or flat plates and cones where a nozzle type of upstream pressure history was imposed. Included in this figure are the results of the present Mach 8 and 19 measurements. It is apparent that, in contrast to the data in figure 2, the nozzle data are better represented by a quadratic type of relationship ( $\alpha = 2$ ). R. K. Matthews of Arnold Engineering Development Center indicated that unpublished nozzle wall data at Mach 6, 8, and 10 from Arnold Engineering Development Center are also in general agreement with this quadratic trend, as are the data from reference 23.

An indication of possible effects of the upstream pressure gradient history that might account for the apparent difference between the nozzle-wall and flat-plate temperature-velocity relation can be obtained from the present finite-difference calculation method. Calculations were made for the boundary-layer development down the contour of the nozzle from which the Mach 8 data were obtained. The calculation was initiated at the nozzle throat and carried through to the nozzle exit. The variation down the nozzle of the parameters needed for the calculation is shown in figure 4.

Computed total temperature and velocity profiles are shown plotted in figures 5 and 6 for several positions along the nozzle. The input profiles for both  $u/u_e$  and  $\bar{\theta}$  at the throat were assumed to be 1/7-power-law profiles, that is, the input total-temperature-velocity relation was linear. These profiles are indicated in figures 5 and 6. Downstream of the throat in the favorable pressure-gradient region at  $x \approx 5$  inches (12.7 cm) (station 2) the velocity profile has bulged outward, but the total-temperature profile has actually become less full. As can be seen from figure 6, these results lead to a temperature-velocity variation similar to that measured further downstream on the nozzle walls. (See fig. 3.) At the measuring station near the nozzle exit, where the pressure gradient is locally small, the velocity profile is still considerably fuller than the total-temperature profile. This condition perhaps indicates that the

boundary layer has not yet relaxed to an equilibrium state. Profiles computed downstream indicate that the temperature-velocity relation tends to approach the linear variation with increasing downstream distance. (Further calculations have indicated that the predicted temperature-velocity relation at the nozzle exit is not a strong function of the input profiles at the throat.)

There is another mechanism present in at least some of the available nozzle-wall investigations which could produce a decrease in the total temperature in the wall boundary layer. In the Mach 6 measurements reported herein, it was found that there was a layer of air adjacent to the settling chamber liner which was much cooler than the rest of the flow. If this thermal layer expands down the nozzle without mixing, the nozzle-wall boundary layer would be growing in a cooler effective free stream until the cool-layer mass flow is absorbed or swallowed in the wall boundary. Estimates of this "swallowing" distance give values of up to half the nozzle length for some cases, and it is possible that the effect within the boundary layer of the cooled mass could persist downstream much farther.

The previous discussion has indicated that turbulent boundary layers on nozzle walls at positions where measurements are usually made may not be in equilibrium in the sense that the effects of upstream pressure gradients and/or thermal layers can persist for large downstream distances. However, the nozzle data are useful for at least two purposes: (1) The data can be used to improve prediction methods for boundary-layer displacement effects in hypersonic nozzle design; and (2) these data can provide valuable test cases for the development of nonsimilar finite-difference methods. That is, the numerical solutions for nozzle flows can be used to evaluate the range of conditions for which models of the turbulent shear term (usually based on equilibrium data) are applicable.

#### Application of Theories to Mach 6, 8, and 19 Nozzle-Wall Data

Mach 8 measurements at nozzle exit.- Pitot-pressure and total-temperature measurements have been obtained by William V. Feller and Robert A. Jones of Langley Research Center in the wall boundary layer at the nozzle exit of the Langley Mach 8 variable-density wind tunnel which is described briefly in reference 38. These data in the form of velocity and Mach number profiles and plots of  $\bar{\theta}$  against  $u/u_e$  are shown in figures 7, 8, and 9. Predictions from the integral and finite-difference methods are also indicated. (A tabulation of the faired experimental profiles is given in table II.)

The measured and theoretical velocity distributions are plotted in figure 7 as a function of  $y$ , the physical distance from the wall. Both methods predict the velocity profile data with acceptable engineering accuracy. As can be seen in the table included in the figure, both theories give a fair prediction of the integral parameters  $\theta$  and  $\delta^*$ .

The corresponding experimental Mach number profile shown in figure 8 is predicted accurately by the integral theory over most of the boundary layer. The finite-difference theory underpredicts the Mach number through most of the boundary layer and indicates that the theoretical total-temperature profile is too full since the velocity prediction was correct. The total-temperature—velocity plots for the Reynolds number range of the tests are shown in figure 9. All the data are more or less in agreement with the quadratic type of temperature-velocity relationship. Also, within the data scatter there seems to be little effect of Reynolds number. The finite-difference theory predicts too rapid a recovery toward the linear variation (or a final total-temperature profile that is too full). This result is reasonable since the eddy viscosity model used (eq. (4)) is based on equilibrium data and hence might be expected to drive the flow toward equilibrium too rapidly. (Further evaluation of the present eddy viscosity model is presented in ref. 39.) However, the additional mechanism referred to previously (enthalpy deficit in settling chamber flow) could cause reduced total temperatures within the boundary layer and hence might be partly responsible for the disagreement between theory and data.

Mach 19 measurements at nozzle exit.— Pitot-pressure and total-temperature measurements at Mach 19 have been obtained by William D. Harvey and Frank L. Clark of Langley Research Center in the wall boundary layer at the nozzle exit of the hypersonic nitrogen facility at the Langley Research Center which is described in reference 40. Velocity and Mach number profiles and total temperature-velocity plots obtained from these data are shown in figures 10, 11, and 12 along with the predictions of the integral method. (A tabulation of the faired experimental profiles is given in table III.)

In the outer section of the velocity profile shown in figure 10, the prediction of the integral theory agrees with the measurements. However, in the inner region the prediction deviates from the data considerably. This discrepancy is due to the fact that a power-law representation of the profile is not valid in the viscous sublayer which, for the present conditions, extends out to values of  $y$  that are from 20 to 40 percent of the boundary-layer thickness. The accuracy of the present integral method is therefore limited by the assumption of a power-law velocity profile. The prediction of the integral theory for the Mach number profile shown in figure 11 is not very satisfactory. The reason for disagreement in the inner region of the boundary layer is probably the overprediction of the velocity as seen in figure 10. The variation of total temperature with velocity indicated by the data is shown in figure 12. The data are seen to be above the quadratic variation.

Mach 6 measurements at and downstream of nozzle exit.— Pitot-pressure and total-temperature measurements have been obtained by William V. Feller and Robert A. Jones of Langley Research Center in the boundary layer of the Langley Mach 6 high Reynolds

number tunnel both at the nozzle exit and at several stations along a straight-pipe extension downstream of the nozzle exit. This facility has recently become operational and has a contoured axisymmetric nozzle with a  $6^\circ$  maximum turning angle and a nominal test-section diameter of 12 inches (30.48 cm). Velocity and Mach number profiles at the nozzle exit are shown in figures 13 and 14, whereas the temperature-velocity data for the various stations along the straight extension are shown in figure 15.

The velocity profile data shown in figure 13 are in good agreement with the integral-theory prediction, as are the integral parameters  $\theta$  and  $\delta^*$ . (See table in fig. 13.) The predicted Mach number profile shown in figure 14 is also in reasonable agreement with the data.

The variations of total temperature with velocity are shown in figure 15 for various positions along the straight-pipe extension. The data at the first three measuring stations (94 in. (238.7 cm), 124 in. (315 cm), and 172 in. (436.7 cm) downstream of the throat) are seen to be nearly the same and are in general agreement with quadratic variation. However, the data at the last measuring station, which is some 60 boundary-layer thicknesses (using an average  $\delta$  of 2 in. (5.08 cm)) downstream of the nozzle exit, show a tendency towards the linear variation. In an unpublished U.S. Naval Ordnance Laboratory investigation by Lee and Yanta at some 30 boundary-layer thicknesses downstream of their nozzle exit (start of  $dp/dx \approx 0$  flow along straight section), they were unable to detect any tendency toward a linear variation. Thus large distances may be necessary in nozzle flows before recovery toward a linear temperature-velocity variation occurs.

### CONCLUDING REMARKS

Comparison of available flat-plate and nozzle-wall turbulent-boundary-layer data indicates that the variation of total temperature with velocity is generally different in the two types of flow. Data for the flat-plate flows show considerable scatter but the average exhibits a linear type of relationship as opposed to the more quadratic variation always found in the nozzle data. Results of nonsimilar finite-difference calculations for the nozzle flows indicate that at least part of this difference is caused by the favorable pressure-gradient history.

Profile measurements along a straight section downstream of the nozzle exit of a Mach 6 tunnel indicate that a distance on the order of 60 boundary-layer thicknesses may be necessary before the flow begins to revert (or relax) toward a linear temperature-velocity variation which is perhaps typical of flat-plate type of flows.

The simple integral method used herein includes correlations taken from nozzle wall data and gives results in good agreement with nozzle profile measurements at Mach 6 and 8 and in reasonable agreement at Mach 18.

## REFERENCES

1. Sterrett, James R.; Morrisette, E. Leon; Whitehead, Allen H., Jr.; and Hicks, Raymond M.: Transition Fixing for Hypersonic Flow. NASA TN D-4129, 1967.
2. Sivells, James C.; and Payne, Robert G.: A Method of Calculating Turbulent-Boundary-Layer Growth at Hypersonic Mach Numbers. AEDC-TR-59-3, DDC Doc. No. AD208774, Arnold Eng. Dev. Center, Mar. 1959.
3. Persh, Jerome; and Lee, Roland: A Method for Calculating Turbulent Boundary Layer Development in Supersonic and Hypersonic Nozzles Including the Effects of Heat Transfer. NAVORD Rep. 4200 (Aeroballistic Res. Rep. 320), U.S. Naval Ord. Lab. (White Oak, Md.), June 7, 1956.
4. Michel, R.: Developpement de la Couche Limite Dans Une Tuyere Hypersonique. The High Temperature Aspects of Hypersonic Flow, Wilbur C. Nelson, ed., Pergamon Press, c.1964, pp. 693-716.
5. Wallace, J. E.: Hypersonic Turbulent Boundary-Layer Studies at Cold Wall Conditions. Proceedings of the 1967 Heat Transfer and Fluid Mechanics Institute, Paul A. Libby, Daniel B. Olfe, Charles W. Van Atta, eds., Stanford Univ. Press, c.1967, pp. 427-451.
6. Seiff, Alvin; and Short, Barbara J.: An Investigation of Supersonic Turbulent Boundary Layers on Slender Bodies of Revolution in Free Flight by Use of a Mach-Zehnder Interferometer and Shadowgraphs. NACA TN 4364, 1958.
7. Rotta, J. C.: Recent Developments in Calculation Methods for Turbulent Boundary Layers With Pressure Gradients and Heat Transfer. Trans. ASME, J. Appl. Mech., vol. 33, ser. E., no. 2, June 1966, pp. 429-437.
8. Bertram, Mitchel H.; and Neal, Luther, Jr.: Recent Experiments in Hypersonic Turbulent Boundary Layers. Presented to the AGARD Specialists Meeting on Recent Developments in Boundary-Layer Research (Naples, Italy), May 10-14, 1965.
9. Smith, A. M. O.; and Cebeci, T.: Numerical Solution of the Turbulent-Boundary-Layer Equations. Report No. DAC 33735 (Contract NOw 66-0324-C), Douglas Aircraft Co., Inc., May 29, 1967.
10. Schubauer, Galen B.; and Tchen, C. M.: Free Turbulent Flows. Turbulent Flows and Heat Transfer. Vol. V of High Speed Aerodynamics and Jet Propulsion, C. C. Lin, ed., Princeton Univ. Press, 1959, pp. 158-184.
11. Van Driest, E. R.: On Turbulent Flow Near a Wall. J. Aeron. Sci., vol. 23, no. 11, Nov. 1956, pp. 1007-1011.



12. Maise, George; and McDonald, Henry: Mixing Length and Kinematic Eddy Viscosity in a Compressible Boundary Layer. AIAA J., vol. 6, no. 1, Jan. 1968, pp. 73-80.
13. Morkovin, Mark V.: Effects of Compressibility on Turbulent Flows. The Mechanics of Turbulence, Gordon and Breach Science Publ., c.1964, pp. 367-380.
14. Beckwith, Ivan E.; and Bushnell, Dennis M. (With appendix C by Carolyn C. Thomas): Detailed Description and Results of a Method for Computing Mean and Fluctuating Quantities in Turbulent Boundary Layers. NASA TN D-4815, 1968.
15. Blottner, F. G.: Nonequilibrium Laminar Boundary-Layer Flow of Ionized Air. AIAA J., vol. 2, no. 11, Nov. 1964, pp. 1921-1927.
16. Fluid Motion Sub-Committee of the Aeronautical Research Council: Modern Developments in Fluid Dynamics. High Speed Flow. Vol. I, L. Howarth, ed., Clarendon Press (Oxford), 1953.
17. Spalding, D. B.; and Chi, S. W.: The Drag of a Compressible Turbulent Boundary Layer on a Smooth Flat Plate With and Without Heat Transfer. J. Fluid Mech., vol. 18, pt. 1, Jan. 1964, pp. 117-143.
18. Persh, Jerome: A Theoretical Investigation of Turbulent Boundary Layer Flow With Heat Transfer at Supersonic and Hypersonic Speeds. NAVORD Rep. 3854, U.S. Naval Ord. Lab. (White Oak, Md.), May 19, 1955.
19. Burke, Andrew F.: Turbulent Boundary Layers on Highly Cooled Surfaces at High Mach Numbers. Proceedings of Symposium on Aerothermoelasticity, ASD Tech. Rep. 61-645, U.S. Air Force, 1961, pp. 704-741.
20. Hill, F. K.: Appendix II - Skin Friction and Heat Transfer Measurements at Mach Numbers From 8-10 in Turbulent Boundary Layers. Bumblebee Aerodynamics Panel. TG-14-37, vol. I, Appl. Phys. Lab., John Hopkins Univ., May 1959, pp. 15-26.
21. Perry, J. H.; and East, R. A.: Experimental Measurements of Cold Wall Turbulent Hypersonic Boundary Layers. AGARD CP No. 30, May 1968, pp. 2-1 - 2-19.
22. Scaggs, Norman E.: Boundary Layer Profile Measurements in Hypersonic Nozzles. ARL 66-0141, U.S. Air Force, July 1966.
23. Shall, Paul Joseph, Jr.: A Boundary Layer Study on Hypersonic Nozzles. M.S. Thesis, U.S. Air Force Institute of Technology, Mar. 1968. (Available from DDC as AD 833236.)
24. Winkler, Eva M.; and Cha, Moon H.: Investigation of Flat Plate Hypersonic Turbulent Boundary Layers With Heat Transfer at a Mach Number of 5.2. NAVORD Rep. 6631, U.S. Nav. Ord. Lab., Sept. 15, 1959.

25. Danberg, James E.: Characteristics of the Turbulent Boundary Layer With Heat and Mass Transfer: Data Tabulation. NOLTR 67-6, U.S. Naval Ordnance Laboratory (White Oak, Md.), Jan. 23, 1967. (Available from DDC as AD 650272.)
26. Samuels, Richard D.; Peterson, John B., Jr.; and Adcock, Jerry B.: Experimental Investigation of the Turbulent Boundary Layer at a Mach Number of 6 With Heat Transfer at High Reynolds Numbers. NASA TN D-3858, 1967.
27. Danberg, James E.: Measurement of the Characteristics of the Compressible Turbulent Boundary Layer With Air Injection. NAVORD Report 6683, U.S. Nav. Ord. Lab., Sept. 3, 1959.
28. Softley, Eric J.; and Sullivan, Robert J.: Theory and Experiment for the Structure of Some Hypersonic Boundary Layers. AGARD CP No. 30, May 1968, pp. 3-1 - 3-18.
29. Swanson, Andrew G.; Buglia, James J.; and Chauvin, Leo T.: Flight Measurements of Boundary-Layer Temperature Profiles on a Body of Revolution (NACA RM-10) at Mach Numbers From 1.2 to 3.5. NACA TN 4061, 1957.
30. Hoydysh, Walter G.; and Zakkay, Victor: An Experimental Investigation of Hypersonic Turbulent Boundary Layers in Adverse Pressure Gradient. AIAA J., vol. 7, no. 1, Jan. 1969, pp. 105-116.
31. Watson, E. C.; Gnos, A. V.; Gallo, W. F.; and Latham, E. A.: Boundary Layers and Hypersonic Inlet Flow Fields. AIAA Paper No. 66-606, June 1966.
32. Stroud, J. F.; and Miller, L. D.: An Experimental and Analytical Investigation of Hypersonic Inlet Boundary Layers. Volume II. Data Reduction Program and Tabulated Experimental Data. AFFDL-TR-65-123 - Vol. II, U.S. Air Force, Aug. 1965. (Available from DDC as AD 621344.)
33. Lobb, R. Kenneth; Winkler, Eva M.; and Persh, Jerome: Experimental Investigation of Turbulent Boundary Layers in Hypersonic Flow. J. Aeronaut. Sci., vol. 22, no. 1, Jan. 1955, pp. 1-9, 50.
34. Lee, Roland E.; Yanta, William J.; and Leonas, Annette C.: Velocity Profile, Skin Friction Balance and Heat Transfer Measurements of the Turbulent Boundary Layer at Mach 5. Proceedings of the 1968 Heat Transfer and Fluid Mechanics Institute, Ashley F. Emery and Creighton A. Depew, eds., Stanford Univ. Press, c.1968.
35. Pasiuk, Lionel; Hastings, Samuel M.; and Chatham, Rodney: Experimental Reynolds Analogy Factor for a Compressible Turbulent Boundary Layer With a Pressure Gradient. NOL TR 64-200, U.S. Naval Ordnance Lab. (White Oak, Md.), Nov. 27, 1964.

36. Sheer, R. E., Jr.; and Nagamatsu, H. T.: Methods for Distinguishing Type of Hypersonic Boundary Layer in Shock Tunnel. AIAA Paper No. 68-50, Jan. 1968.
37. Wallace, J. E.: Hypersonic Turbulent Boundary Layer Measurements Using an Electron Beam. CAL Rep. No. AN-2112-Y-1, Cornell Aeronaut. Lab., Inc., Aug. 1968.
38. Schaefer, William T., Jr.: Characteristics of Major Active Wind Tunnels at the Langley Research Center. NASA TM X-1130, 1965.
39. Bushnell, D. M.; and Beckwith, I. E.: Calculation of Nonequilibrium Hypersonic Turbulent Boundary Layers and Comparisons With Experimental Data. AIAA Preprint No. 69-684, 1969.
40. Clark, Frank L.; Ellison, James C.; and Johnson, Charles B.: Recent Work in Flow Evaluation and Techniques of Operations for the Langley Hypersonic Nitrogen Facility. NASA paper presented at Fifth Hypervelocity Techniques Symposium (Denver, Colo.), Mar. 28-30, 1967.

TABLE I.- MIXING LENGTH VARIATION USED  
IN FINITE-DIFFERENCE THEORY

$y/\delta$	$l/\delta$
0	0
.05	.02
.1	.04
.15	.055
.2	.063
.25	.0725
.3	.08
.35	.083
.4	.0875
.45	.09
.5	.09
.55	.09
.6	.09
.65	.09
.7	.09
.75	.09
.8	.09
.85	.09
.9	.09
.95	.09
1.0	.09
1.4	.09

TABLE II.- DETAILS OF MACH 8 PROFILE




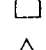
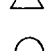



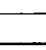
$$\left[ M_{\infty} = 7.99, \quad \theta = 0.239 \text{ cm}, \quad \delta^* = 2.609 \text{ cm}, \right. \\ \left. T_w/T_{t,\infty} = 0.43, \quad R_{e,\theta} = 3.1 \times 10^4 \right]$$

y, cm	u/u <sub>e</sub>	M	T <sub>t</sub> /T <sub>t,∞</sub>
0	0	0	0.43
.254	.67	2.61	.725
.381	.715	2.94	.755
.635	.766	3.36	.791
1.27	.827	4.06	.830
1.90	.864	4.67	.855
2.54	.895	5.26	.881
3.18	.918	5.86	.90
3.81	.935	6.41	.915
4.44	.951	6.90	.932
5.08	.966	7.32	.95
5.72	.980	7.63	.971
6.35	.990	7.80	.986
6.98	.996	7.90	.995
7.62	.999	7.98	.999
8.26	1.0	7.99	1.0

TABLE III.- DETAILS OF MACH 19 PROFILE

$$\left[ M_{\infty} = 19.47, \quad \theta = 0.185 \text{ cm}, \quad \delta^* = 4.84 \text{ cm}, \right. \\ \left. T_w/T_{t,\infty} = 0.177, \quad R_{e,\theta} = 5.14 \times 10^3 \right]$$

y, cm	u/u <sub>e</sub>	M	T <sub>t</sub> /T <sub>t,∞</sub>
0	0	0	0.177
.202	.074	.33	.254
.634	.260	1.25	.281
1.142	.464	2.55	.377
1.650	.586	3.35	.489
2.158	.683	4.40	.579
2.666	.761	5.50	.667
3.174	.810	6.75	.720
3.682	.838	8.00	.748
4.190	.859	9.20	.773
4.698	.881	10.4	.801
5.206	.877	11.60	.789
5.714	.889	12.70	.806
6.222	.928	13.85	.872
6.730	.939	14.95	.890
7.238	.965	16.00	.937
7.746	.974	17.10	.954
8.254	.981	18.85	.964
8.762	.999	19.05	.999
9.270	1.000	19.45	1.000

	$M_\infty$	$T_w/T_t$	Reference
	8.2 - 16	.12	19
	8 - 10	.45	20
	8.8 - 11.6	.28	21
	11.4	.3	22
	6.5	.3 - .4	22
	9.6 - 11.0	.27	4
	8	.42	Present data
	19.47	.17	
	6	.66	

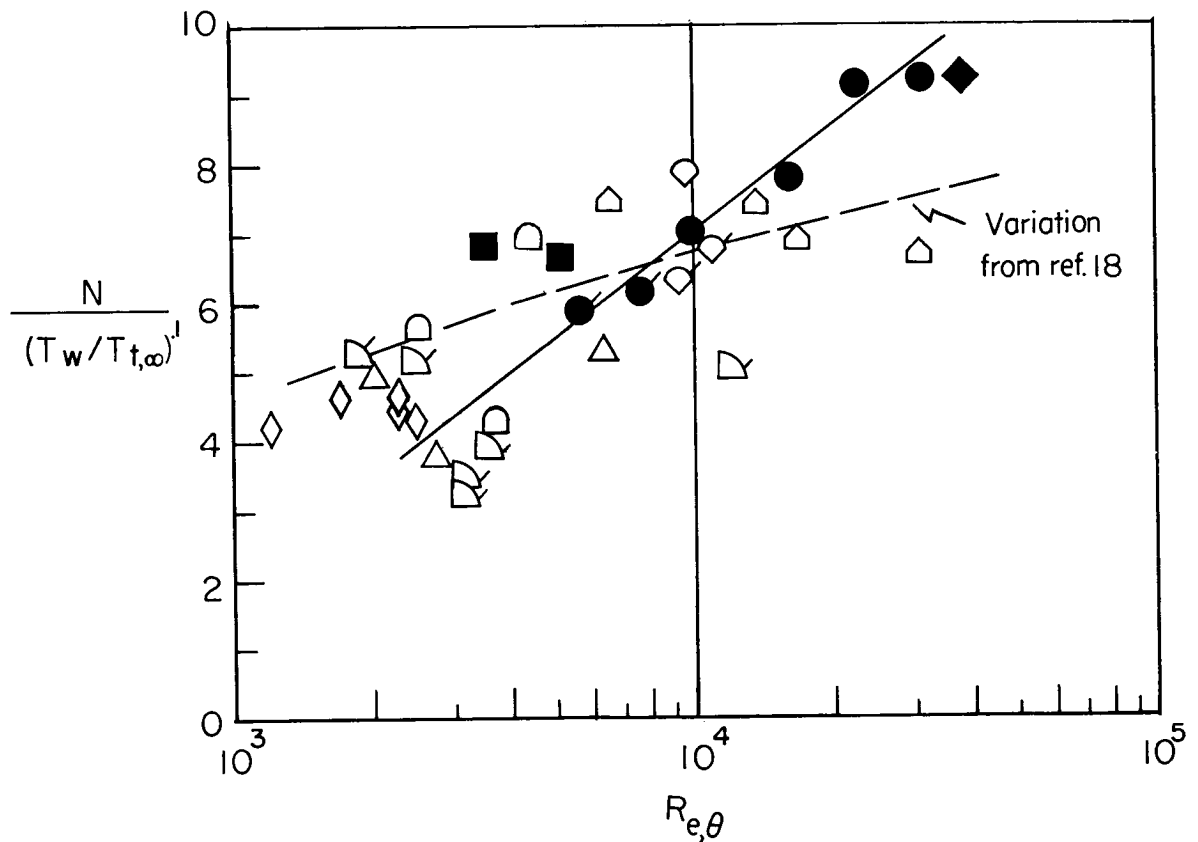


Figure 1.- Variation of  $N$  with  $Re_\theta$  for axisymmetric air and nitrogen nozzle data. Flagged symbols are data reduced from pitot by using  $\alpha = 2.0$ .  $6 \leq M_\infty \leq 18$ ;  $0.1 \leq \frac{T_w}{T_{t,\infty}} \leq 0.7$ .

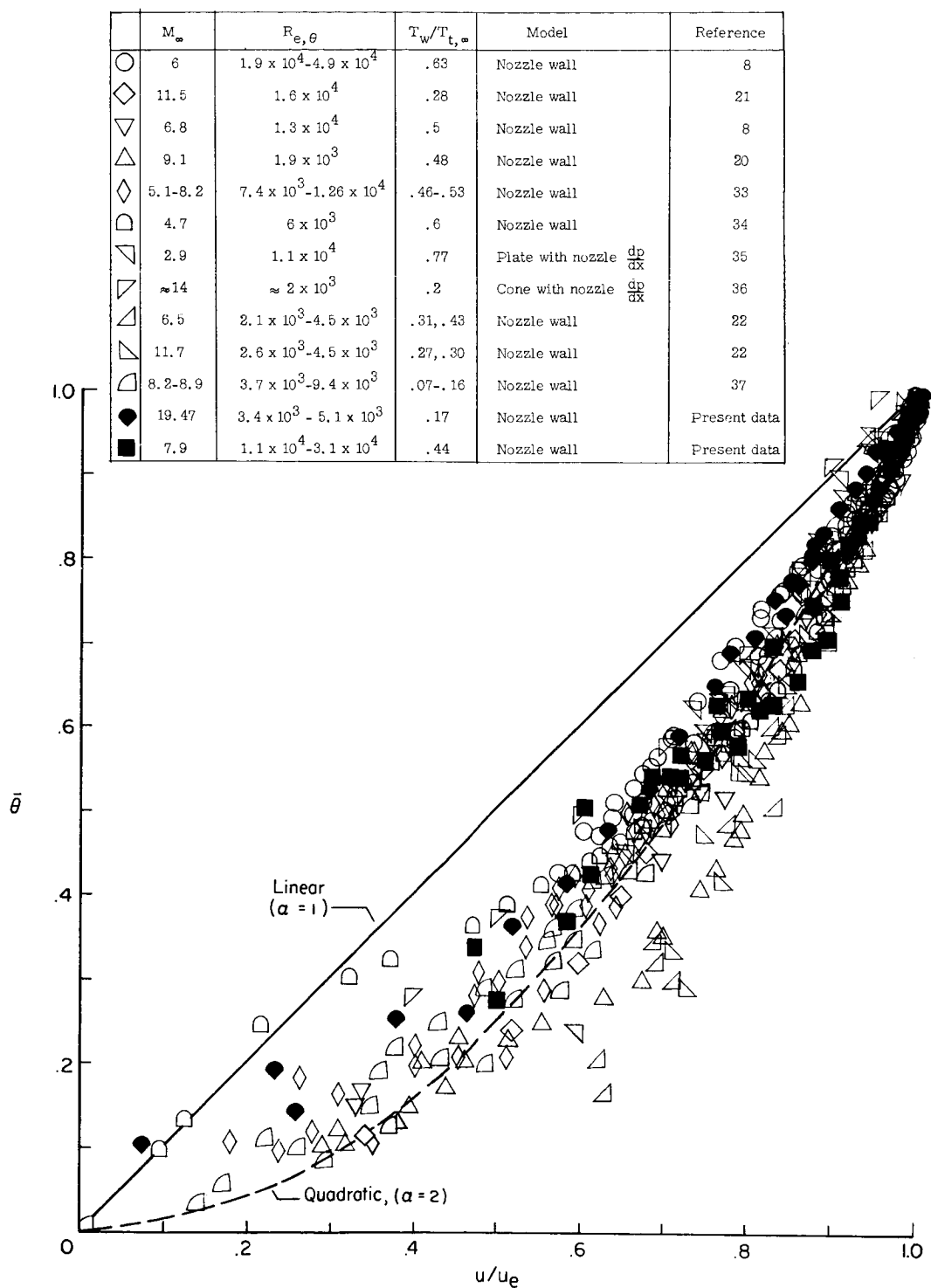


Figure 3.- Total temperature-velocity data for "nozzle wall" flows.  $3 \leq M_\infty \leq 19$ ;  $0.1 \leq \frac{T_w}{T_{t,\infty}} \leq 0.8$ .



	$M_\infty$	$R_{e,\theta}$	$T_w/T_{t,\infty}$	Model	Reference
○	5.2	$1.7 \times 10^3 - 3.6 \times 10^3$	.56 - .84	Flat plate	24
◇	6.4	$6 \times 10^3$	.52	Flat plate	25
△	6.0	$1.1 \times 10^4$	.36, .49	Hollow cylinder	26
◇	8.1	$3.1 \times 10^3 - 4.0 \times 10^3$	.72 - .83	Flat plate	27
⊖	10.2	$2.3 \times 10^3$	.28	Cone	28
⊖	3.67	$9 \times 10^4$	.42	Parabolic, fineness ratio of 10	29
△	5.75	$3.8 \times 10^4$	.63	Hollow cylinder	30
⊖	10.5	$1.3 \times 10^3$	.3	Flat plate	31
⊖	8, 6, 8	$2 \times 10^2 - 1.3 \times 10^4$	.4 - .7	Hollow cylinder	32
◇	6.5	$2.2 \times 10^3 - 8.9 \times 10^3$	.3 - .58	Flat plate	Unpublished Ames data (Hopkins and Keener)

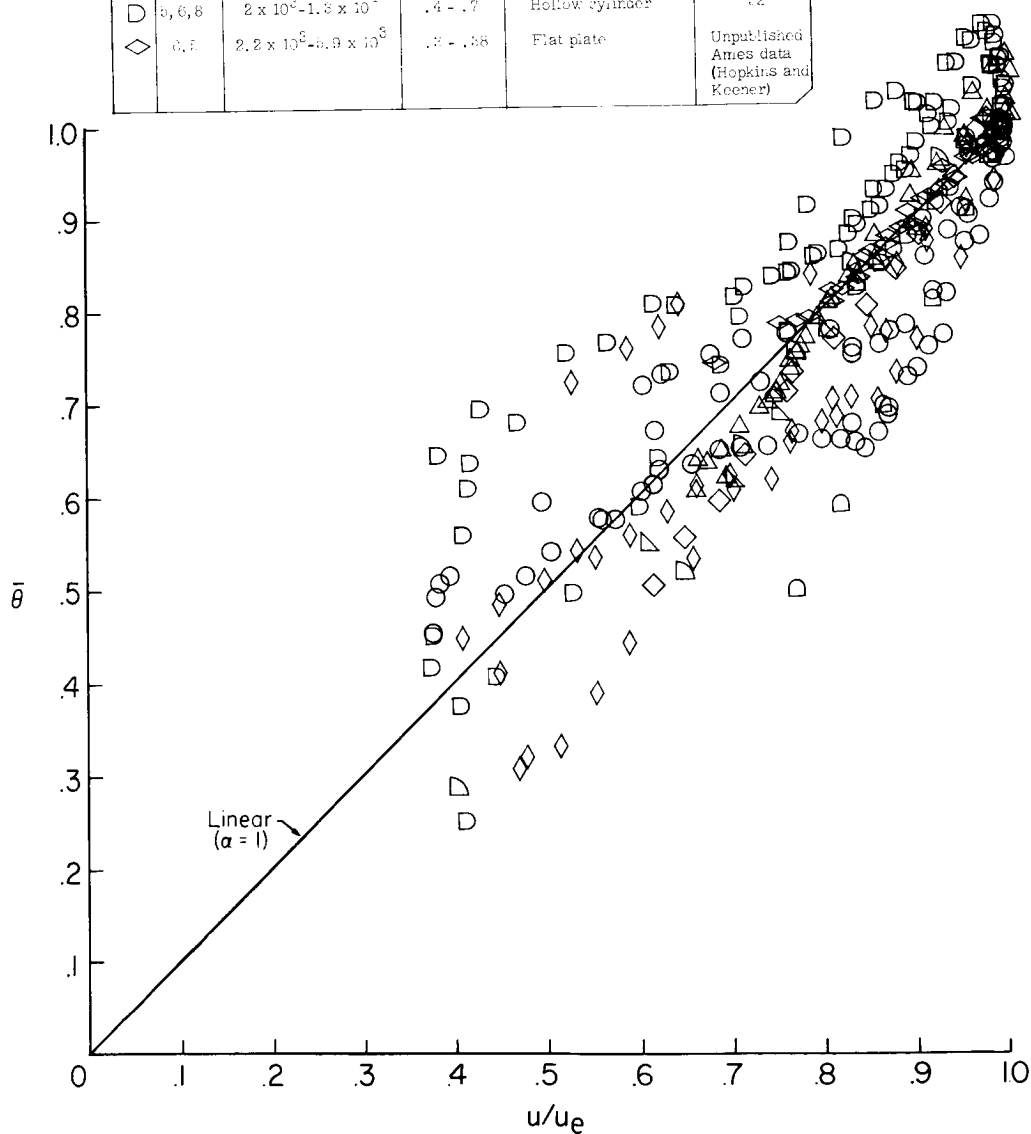


Figure 2.- Total temperature-velocity data for "flat plate" flows.  $3.67 \leq M_\infty \leq 10.5$ ;  $0.28 \leq \frac{T_w}{T_{t,\infty}} \leq 0.84$ .

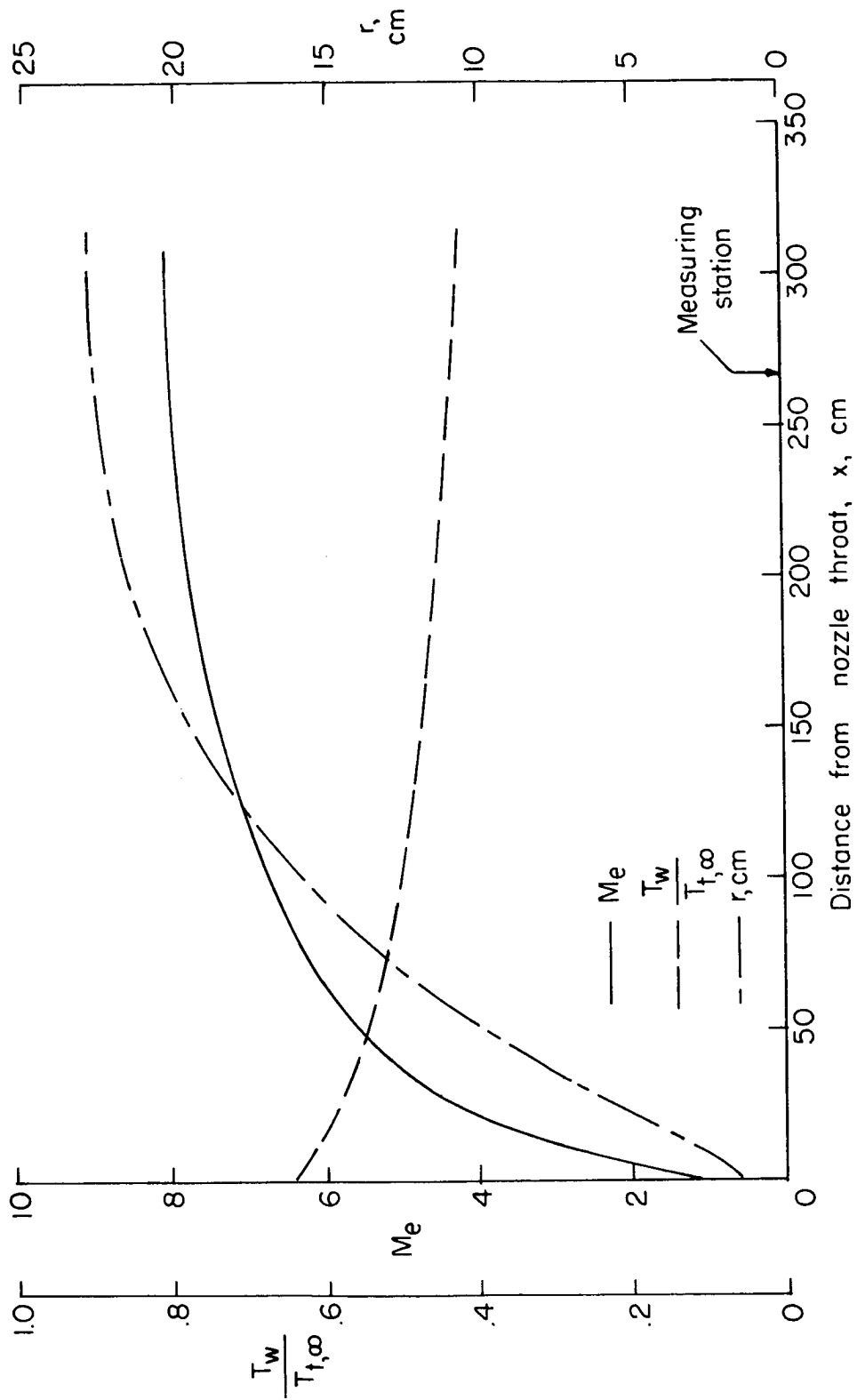


Figure 4.- Parameters for Mach 8 nozzle calculation.

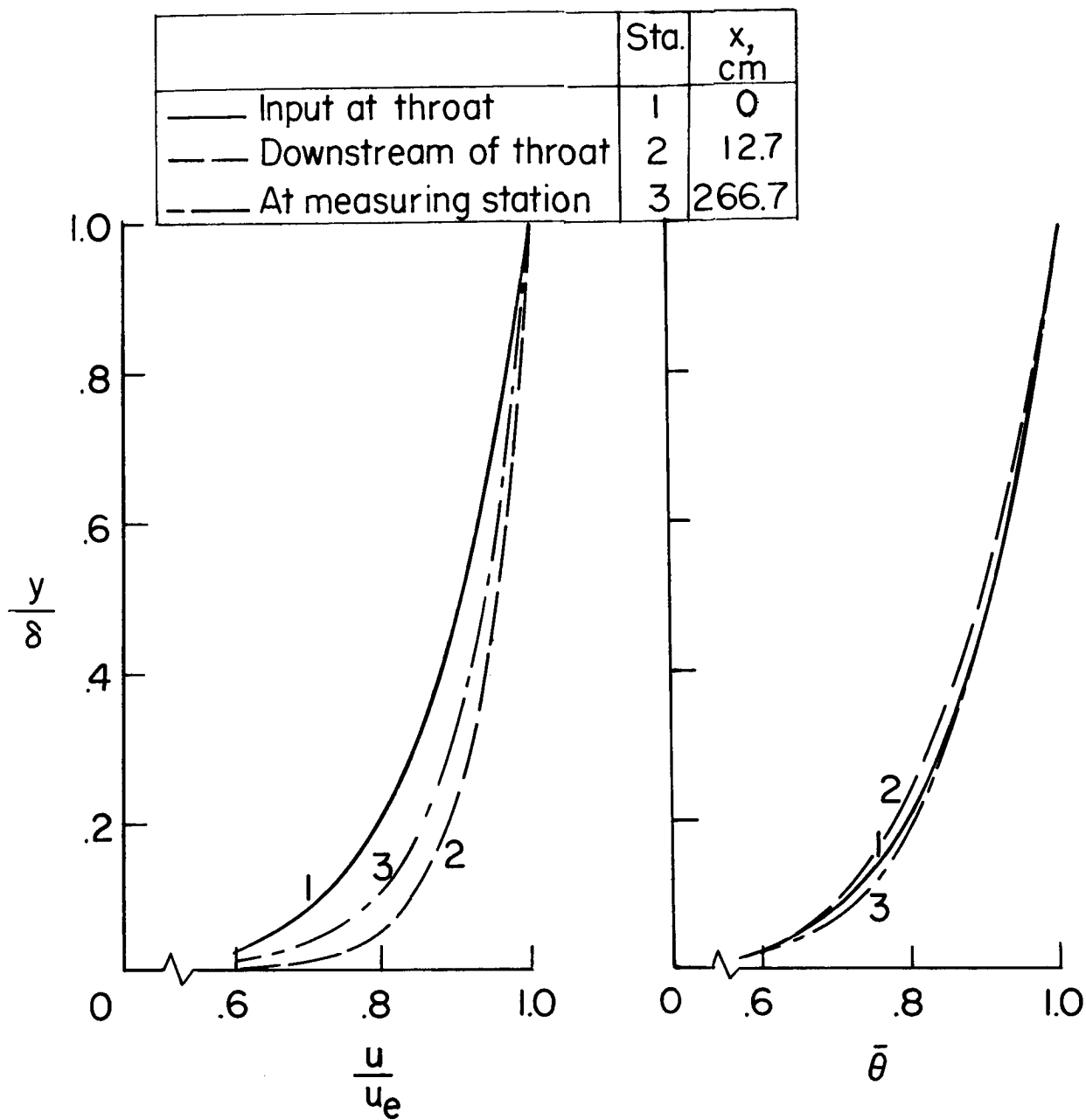


Figure 5.- Velocity and total temperature profiles predicted by finite-difference theory for various positions along Mach 8 nozzle.

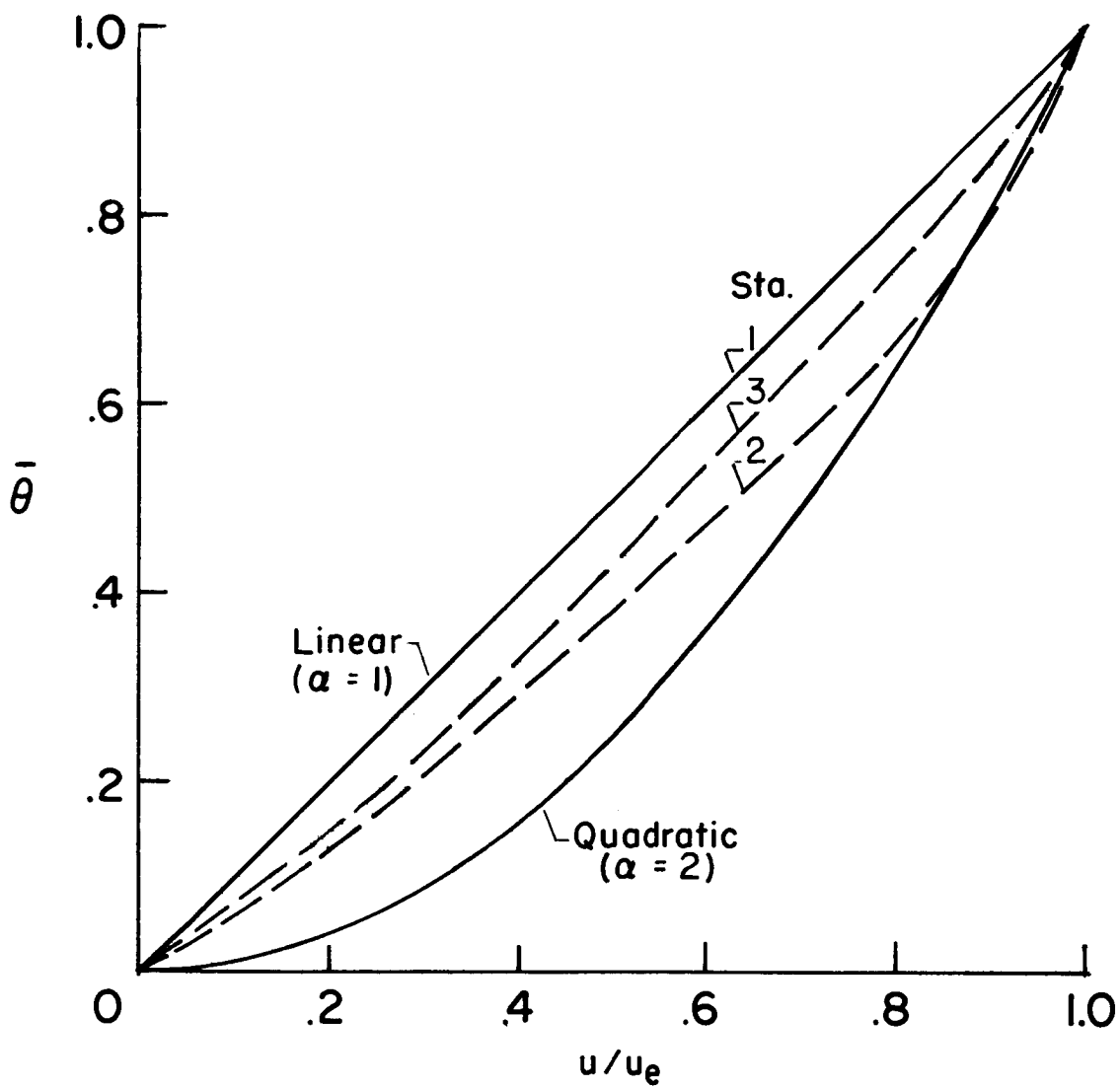


Figure 6.- Predicted total temperature-velocity relationships for Mach 8 nozzle flow from finite-difference theory. Stations are the same as those of figure 5.

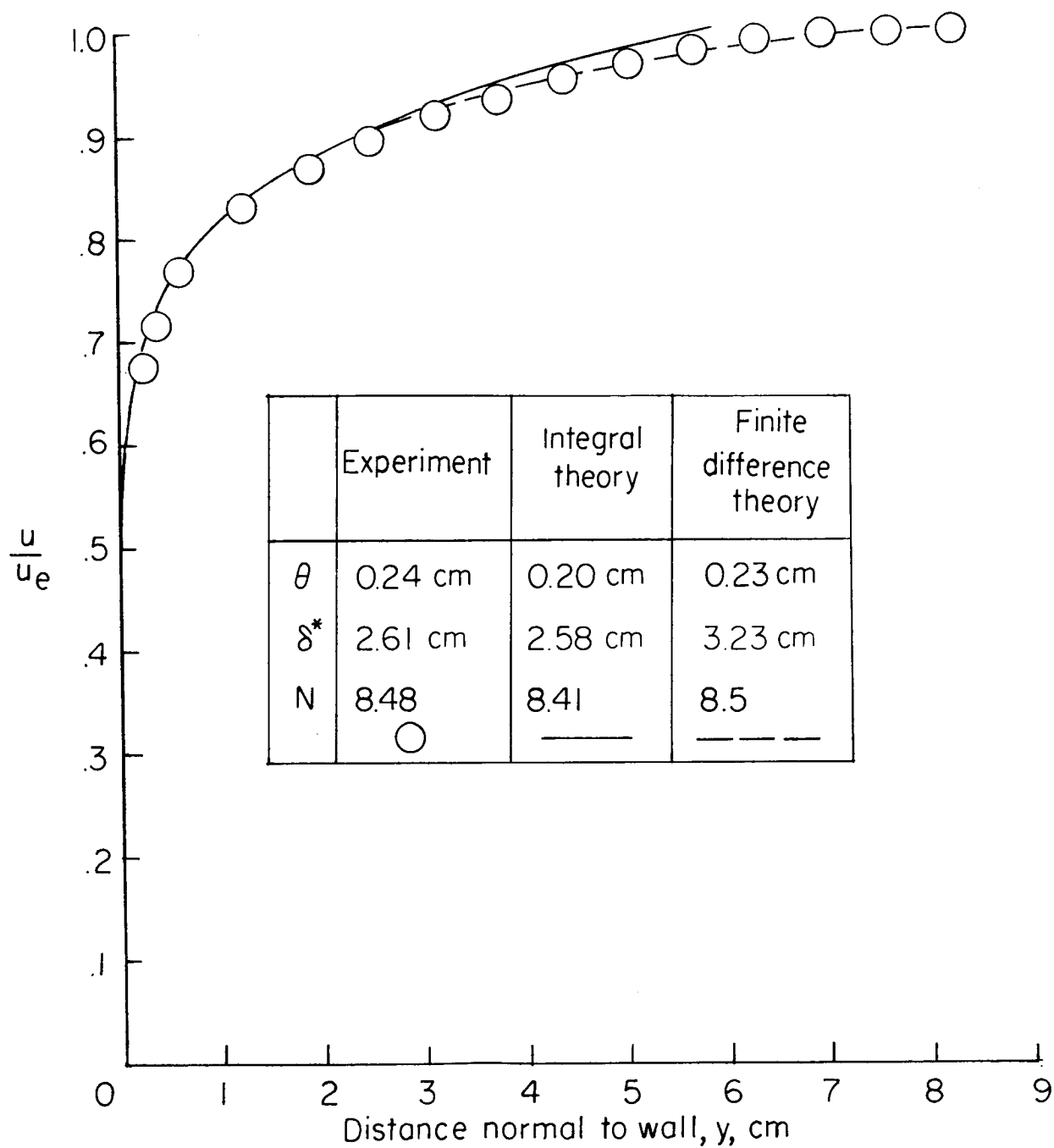


Figure 7.- Turbulent boundary-layer velocity profile at exit of Mach 8 contoured axisymmetric tunnel.  $R_{e,\theta} = 3.1 \times 10^4$ ;  $M_\infty = 7.99$ ;  $\frac{T_w}{T_{t,\infty}} = 0.43$ .

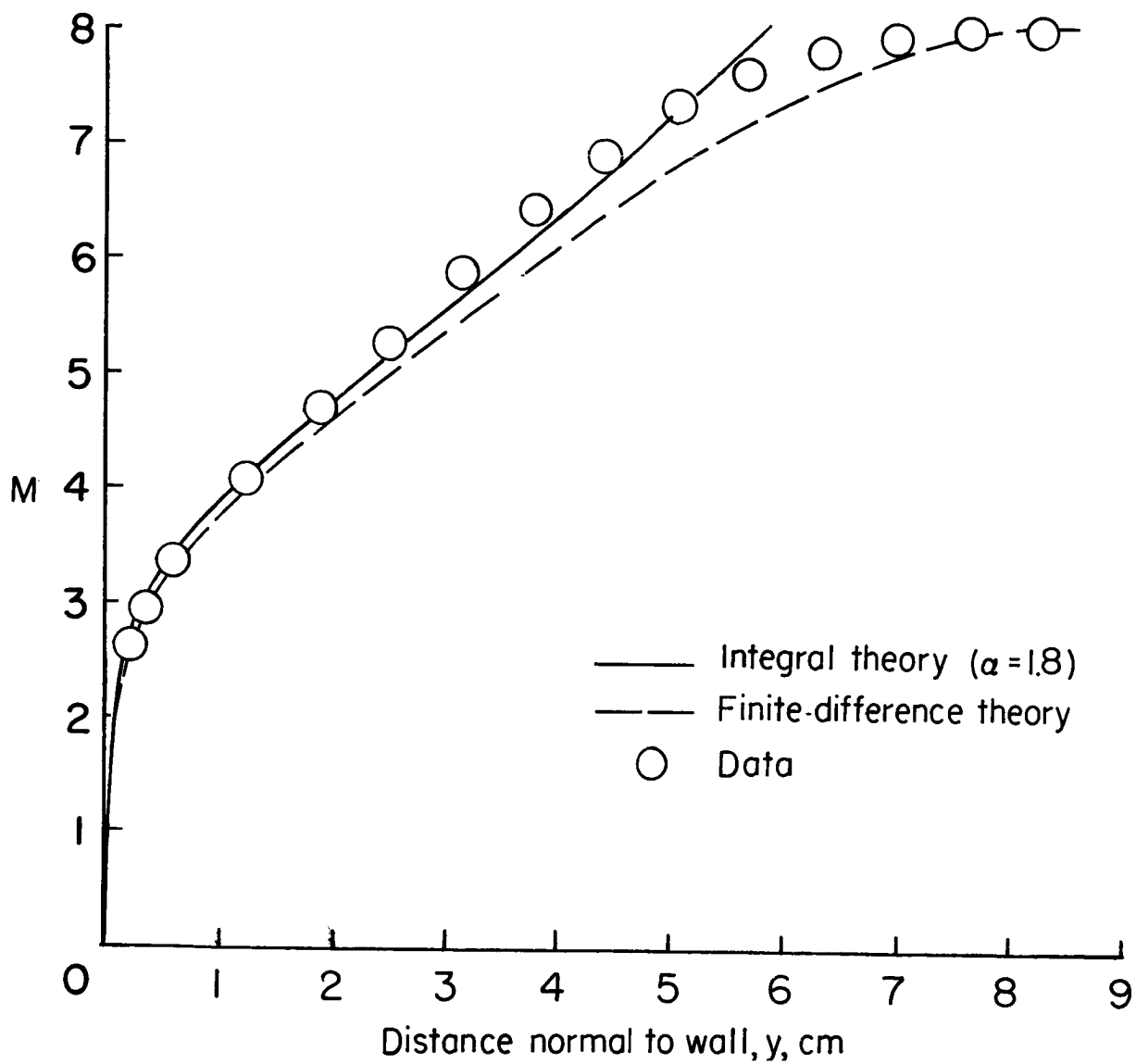


Figure 8.- Mach number profile at exit of Mach 8 nozzle.  $R_{e,\theta} = 3.1 \times 10^4$ ;  $M_\infty = 7.99$ ;  $\frac{T_w}{T_{t,\infty}} = 0.43$ .

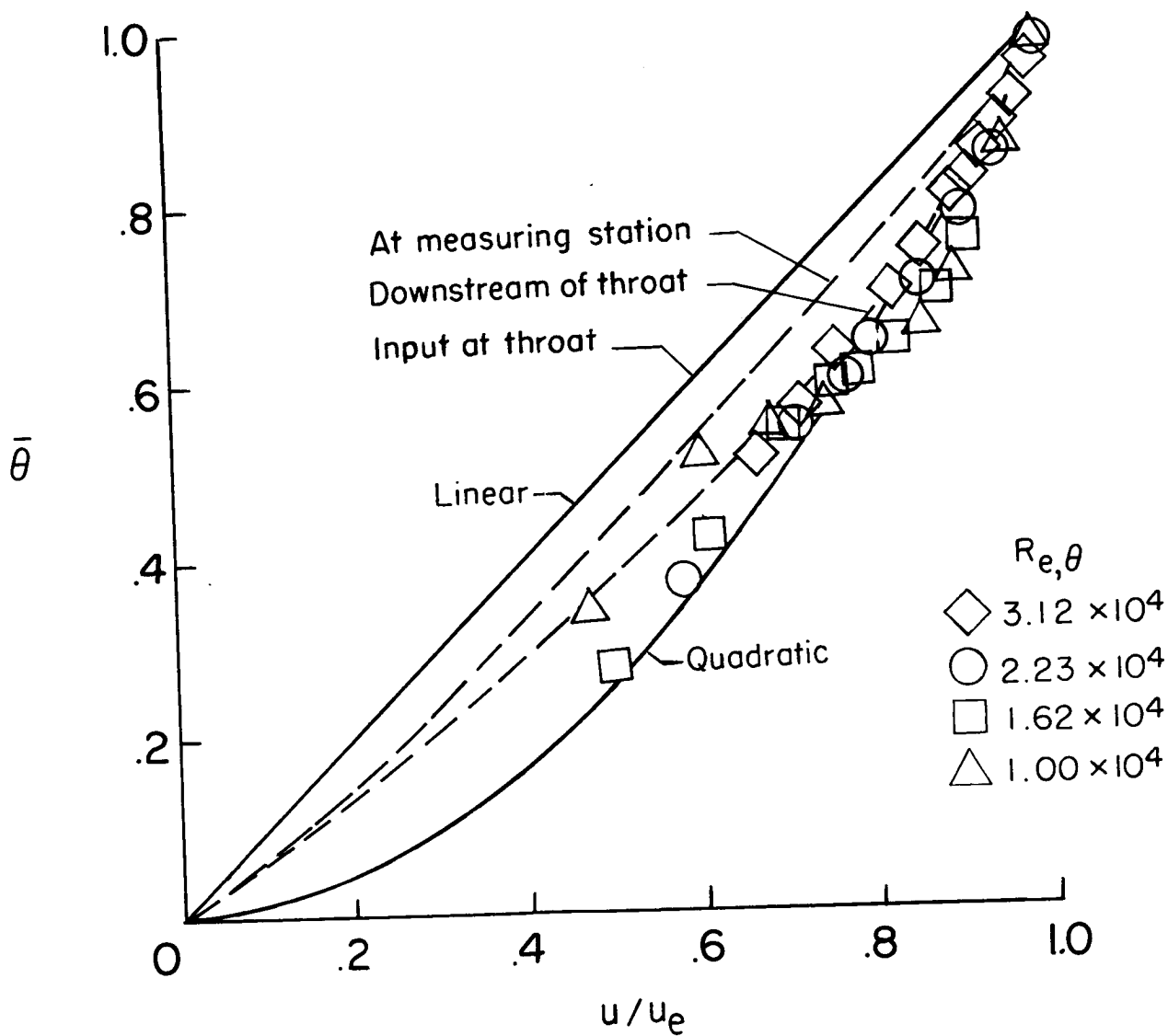


Figure 9.- Total temperature-velocity relationship at Mach 8 nozzle exit for various Reynolds numbers.  $\frac{T_w}{T_{t,\infty}} = 0.42$ . Finite-difference theory shown for  $R_{e,\theta} = 3.12 \times 10^4$  at stations indicated.

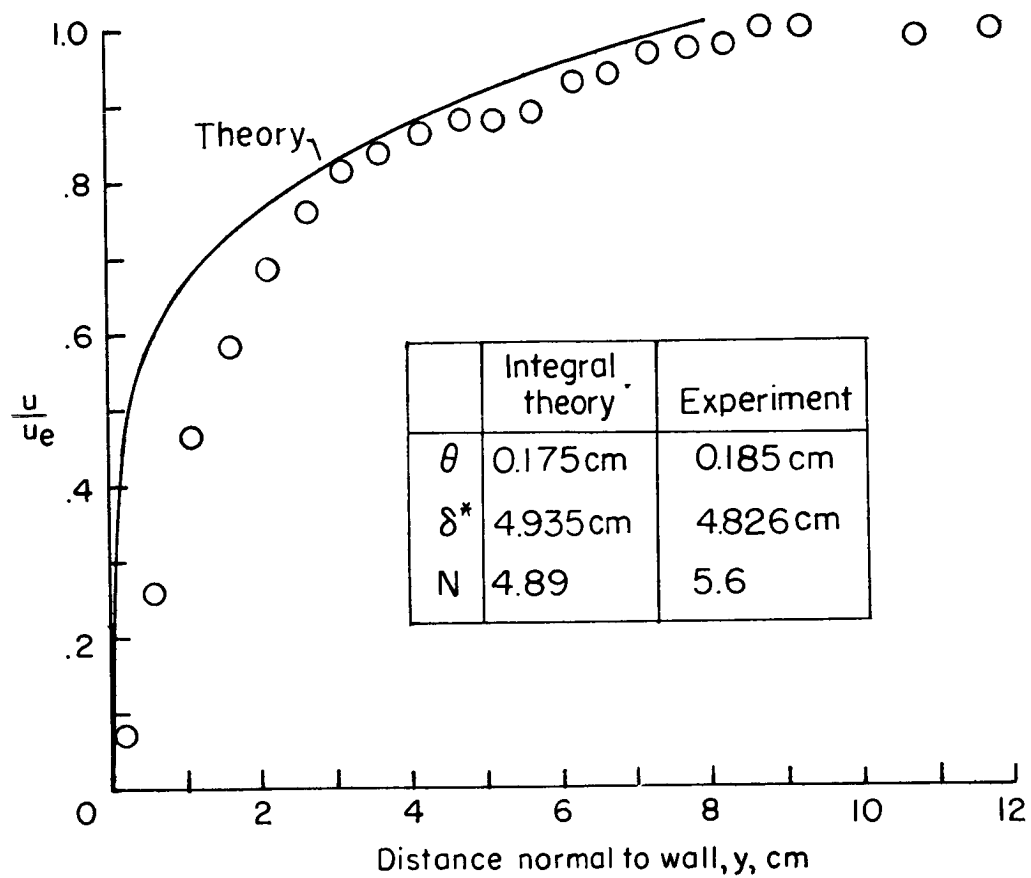


Figure 10.- Measured turbulent boundary-layer velocity profile at exit of Mach 19 contoured axisymmetric tunnel compared with prediction of integral theory using  $\alpha = 2.0$ ;  $R_{e,\theta} = 5.17 \times 10^3$ ;  $\frac{T_w}{T_{t,\infty}} = 0.17$ .



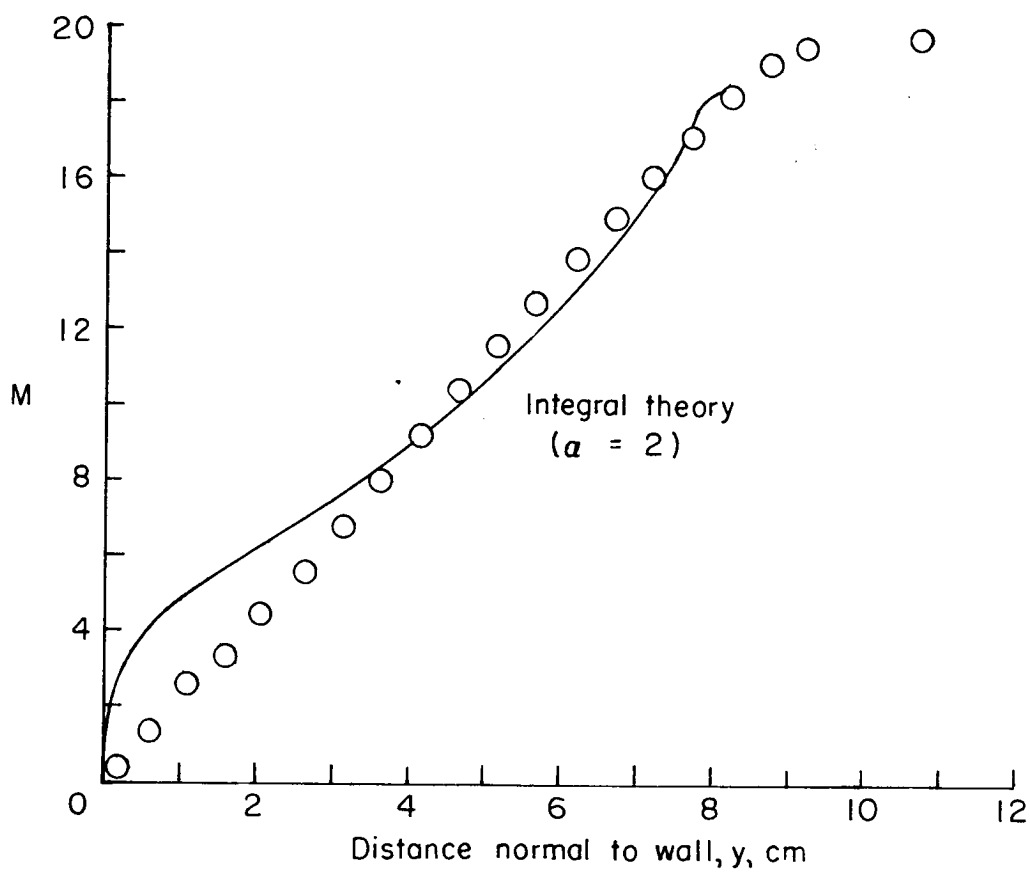


Figure 11.- Mach number profile at exit of Mach 19 nozzle.  $R_{e,\theta} = 3.97 \times 10^3$ ;  $\frac{T_w}{T_{t,\infty}} = 0.17$ .

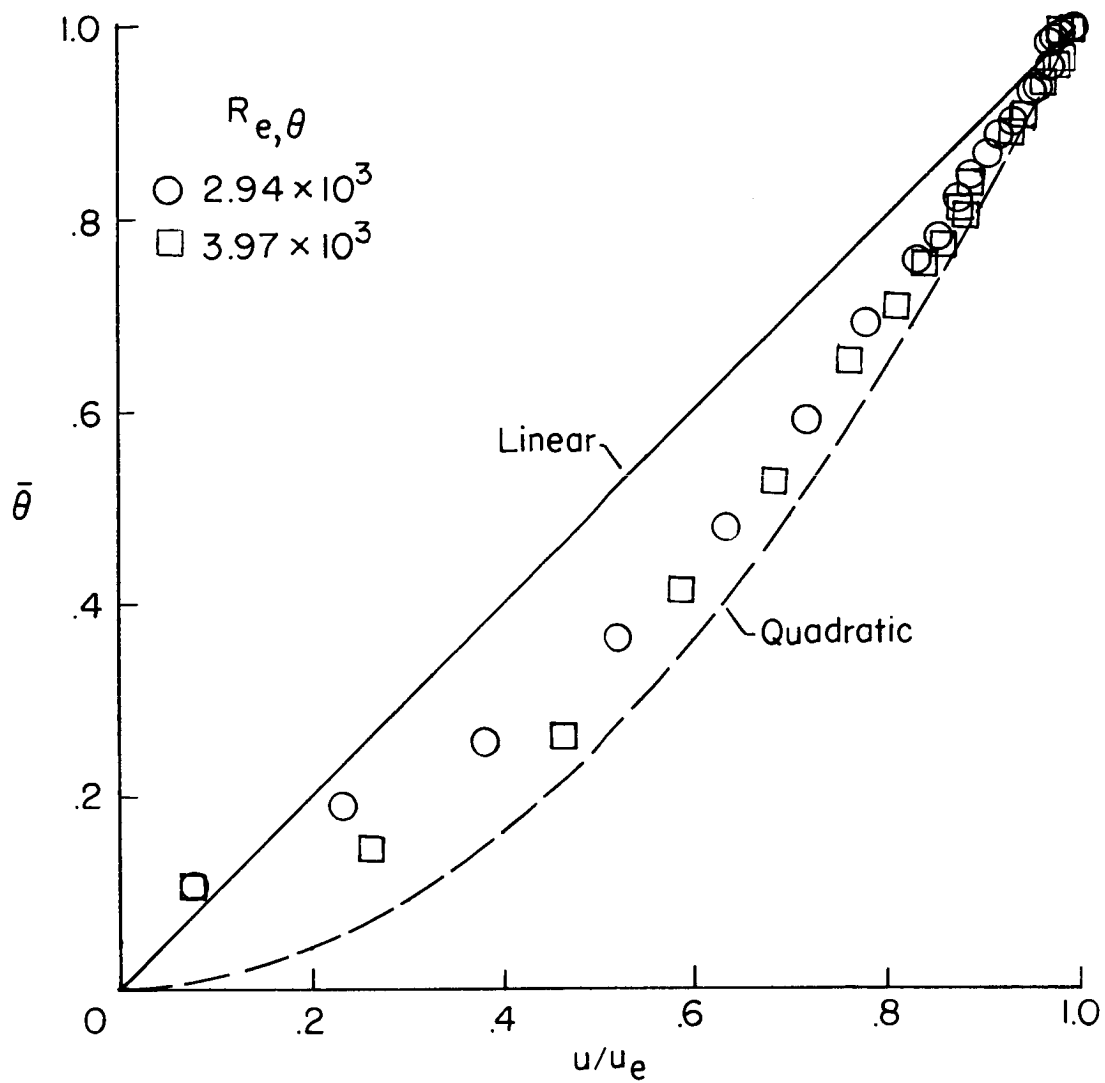


Figure 12.- Total temperature-velocity relationship at Mach 19 nozzle exit.  $\frac{T_w}{T_{t,\infty}} \approx 0.17$ .

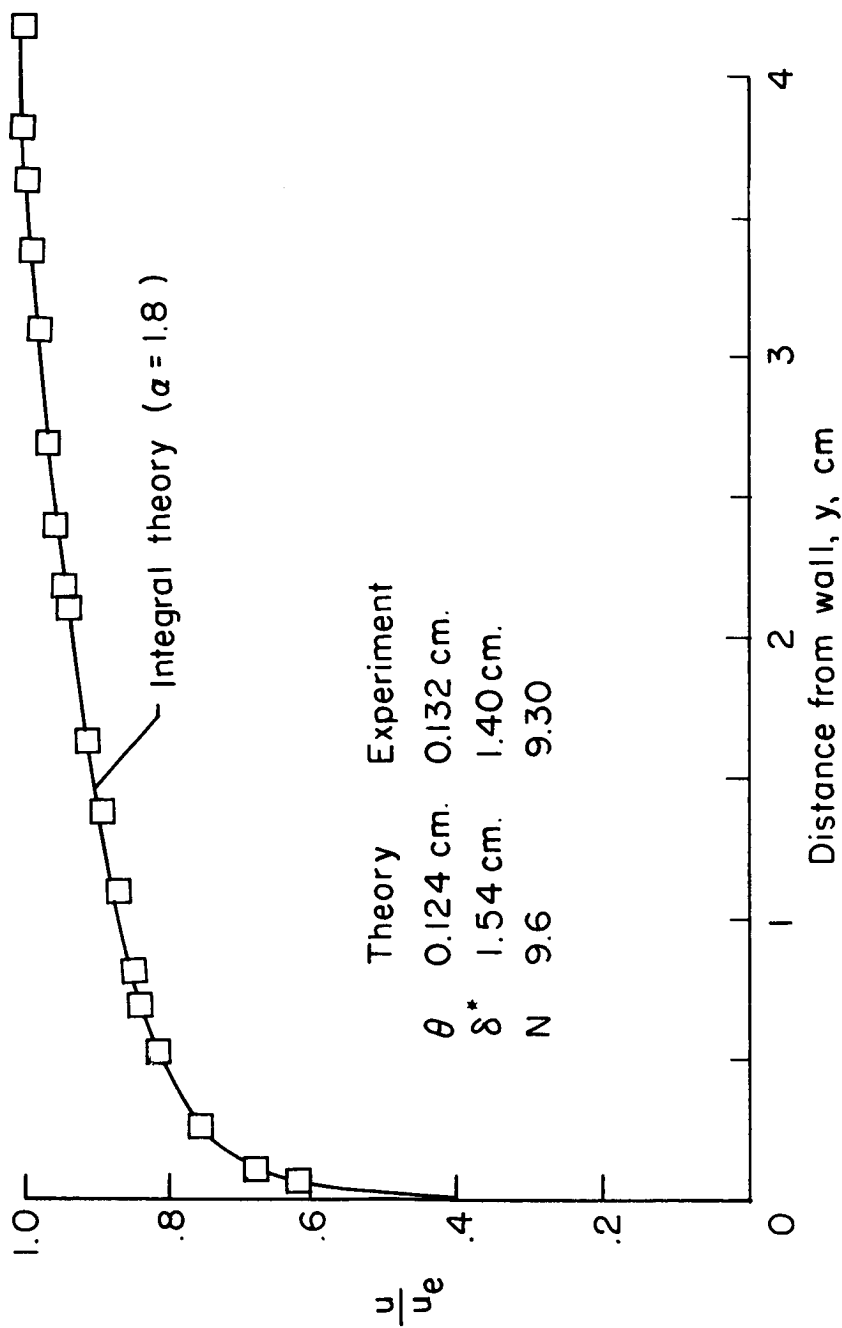


Figure 13.- Turbulent boundary-layer velocity profile at exit of Mach 6 contoured axisymmetric tunnel.  $R_{e,\theta} = 3.8 \times 10^4$ ;  $\frac{T_w}{T_\infty} = 0.66$ .

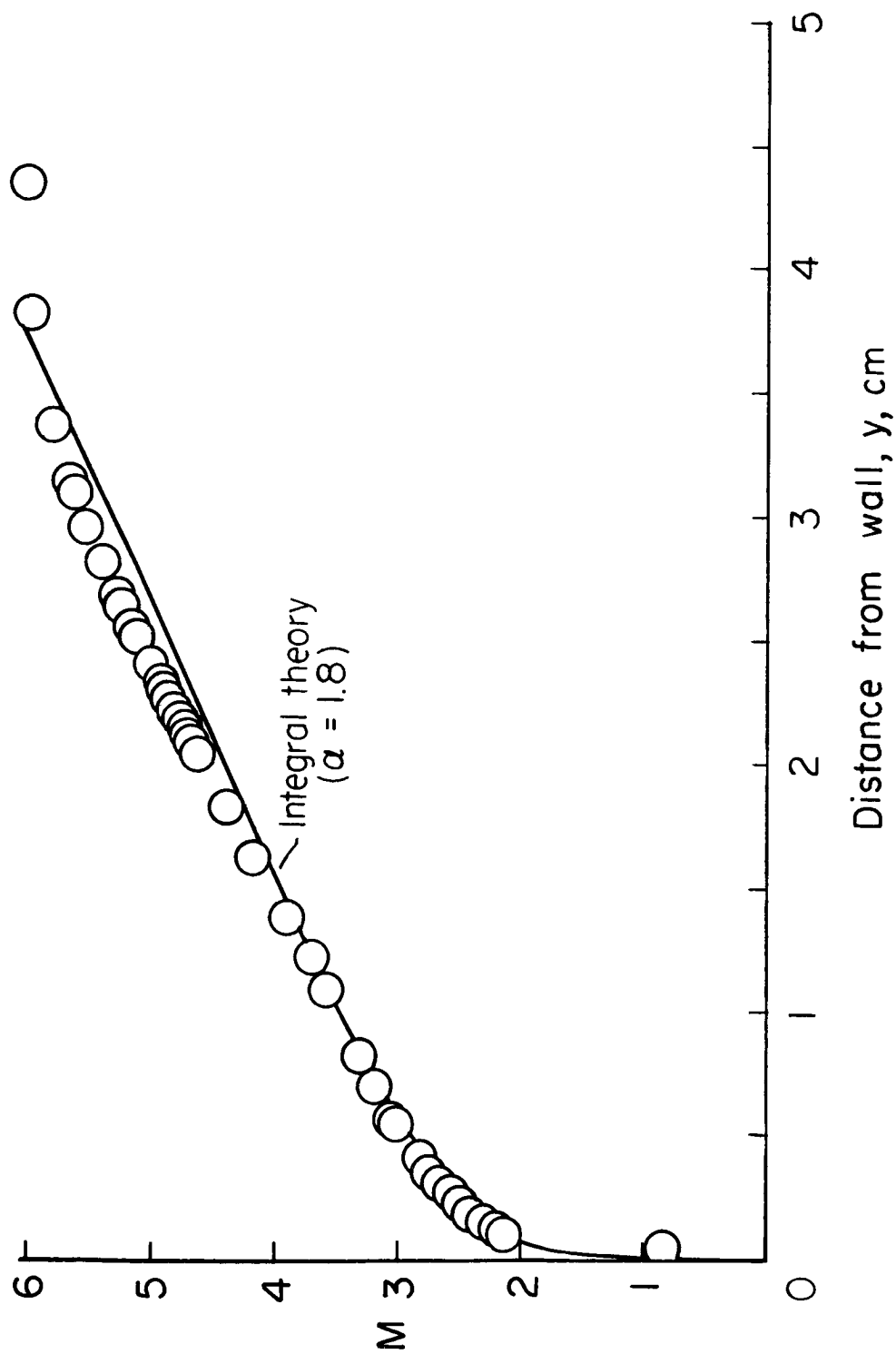


Figure 14.- Mach number profile at exit of Mach 6 nozzle.  $R_{e,\theta} = 3.8 \times 10^4$ ;  $\frac{T_{w_0}}{T_{t,\infty}} = 0.66$ .

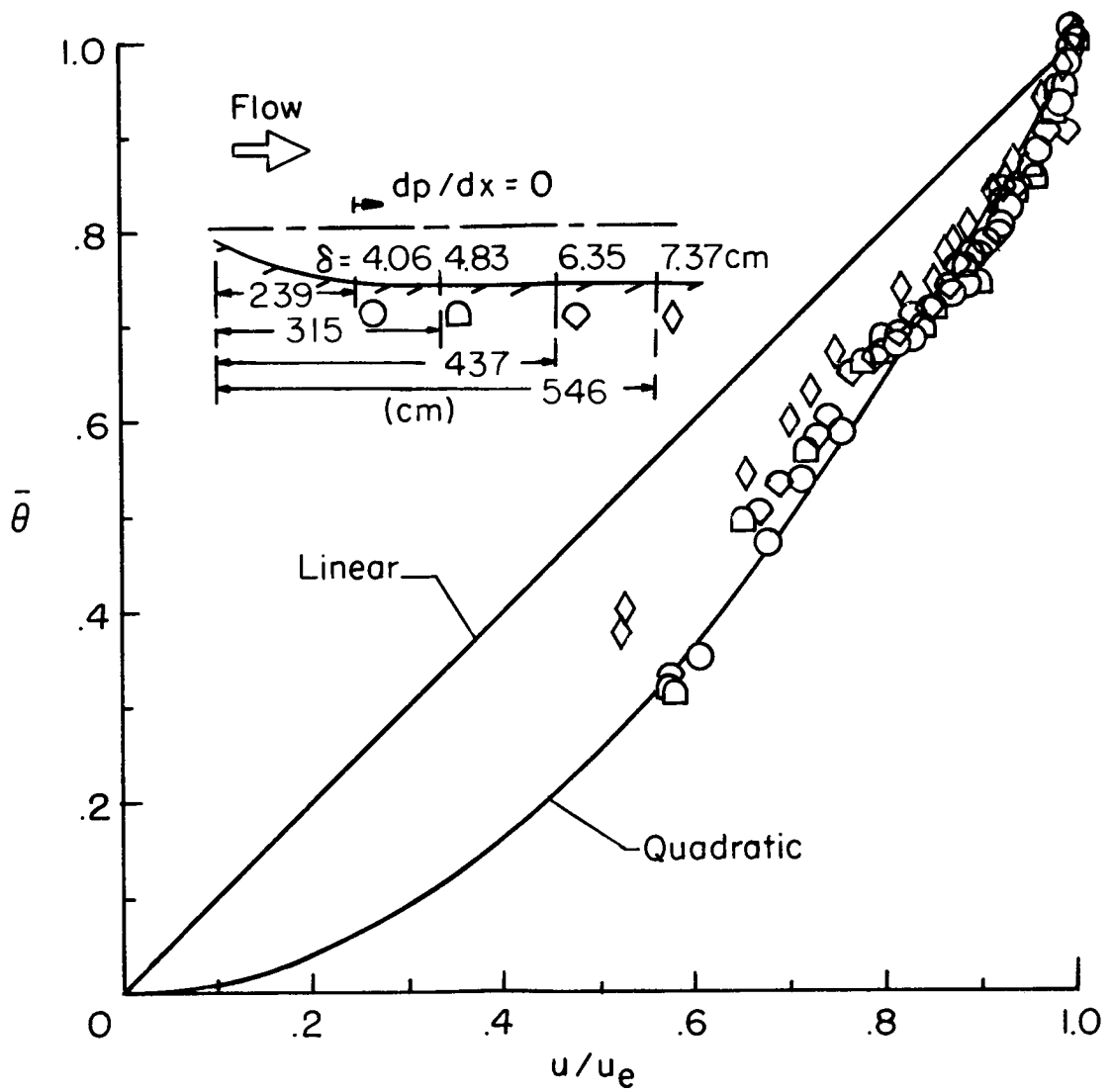


Figure 15.- Total temperature-velocity relationship at various distances downstream of Mach 6 nozzle throat.  $\frac{T_w}{T_{t,\infty}} \approx 0.66$ ;  $p_t \approx 40$  atmospheres.

A COMMENT ON COMPARISON OF PREDICTION METHODS AND STUDIES  
OF RELAXATION IN HYPERSONIC TURBULENT BOUNDARY LAYERS

By Robert A. Jones

NASA Langley Research Center

12

The preceding paper alluded to another mechanism which may account for at least a part of the difference between the linear velocity-temperature relationship generally found for flat-plate boundary layers and the more nearly second degree curve variation found for the Mach 6 tunnel wall data. This mechanism was revealed by a recent survey of the flow in the stagnation chamber of the facility.

A sketch of the Mach 6 high Reynolds number facility is shown in figure 1. The nozzle is axisymmetric and contoured with a maximum flow turning angle of only  $6^\circ$  to reduce the longitudinal pressure gradients. The 8-foot-long nozzle is followed by a 13-foot-long straight-pipe section of 12-inch diameter. Boundary-layer surveys were made at various longitudinal stations as indicated in the sketch. This stagnation chamber is of conventional design with a thin liner (inside diameter 20 inches) to insulate the flow from the heavy pressure vessel and a diffusing cone followed by a series of screens to straighten the flow. Before making a data run, the liner and nozzle throat are preheated by hot air flow. Approximate stagnation conditions for the data presented in the preceding paper were  $450^\circ\text{ F}$  and 550 psig with a corresponding flow velocity in the stagnation chamber of 4.8 ft/sec. Two total-temperature probes were mounted in the stagnation chamber as indicated in the sketch. One was fixed at a position very near the center line and the other was movable.

The results of a detailed total temperature survey in the stagnation chamber are shown in figure 2 where  $y$  is the distance from the inside wall of the liner. Note that the total temperature was uniform over the entire chamber except for the region very near the liner ( $y \leq 0.8$  inch). In this region a rather large temperature deficiency existed. The estimated laminar boundary-layer thickness at this position was only 0.060 inch based on the local conditions and a flow length of 1 foot from the screen. A similar estimate for the turbulent boundary-layer thickness gave 0.20 inch. Since turbulent mixing should not occur outside the dynamic or velocity boundary layer in the entrance section of the nozzle, it is thought that the nozzle boundary layer grows in a layer of air having a lower total temperature than the central core of the flow. A crude mass flow calculation indicated that this lower temperature layer of air is "swallowed" by the boundary layer about half-way down the nozzle and in the test-section boundary layer at a position 172 inches downstream of the throat about half of the boundary layer could be influenced by the low temperature layer.

A similar total-temperature distribution was found in the Mach 8 variable density tunnel. The stagnation chambers of both these facilities are very similar to those of most hypersonic facilities; thus, it is believed that most of

the high Mach number tunnel wall boundary-layer data presently available were taken under similar conditions and may have been influenced to an undetermined extent by settling chamber flow anomalies. It is believed that these low temperature layers can be eliminated by electrically heating the entire stagnation chamber, connecting piping, and nozzle throat, and that new boundary-layer surveys can be made in the absence of such effects.

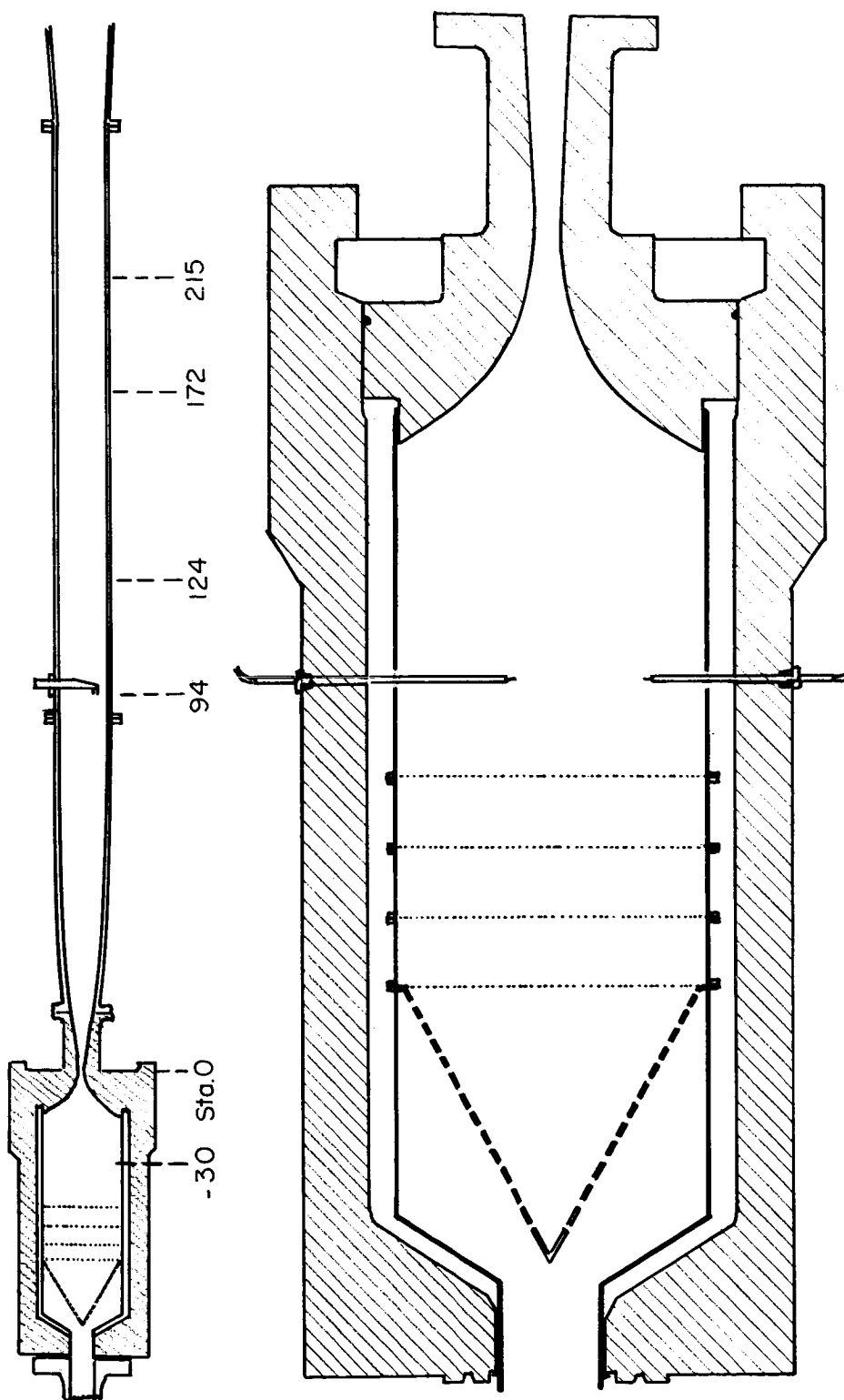


Figure 1.- Mach 6 high Reynolds number facility.



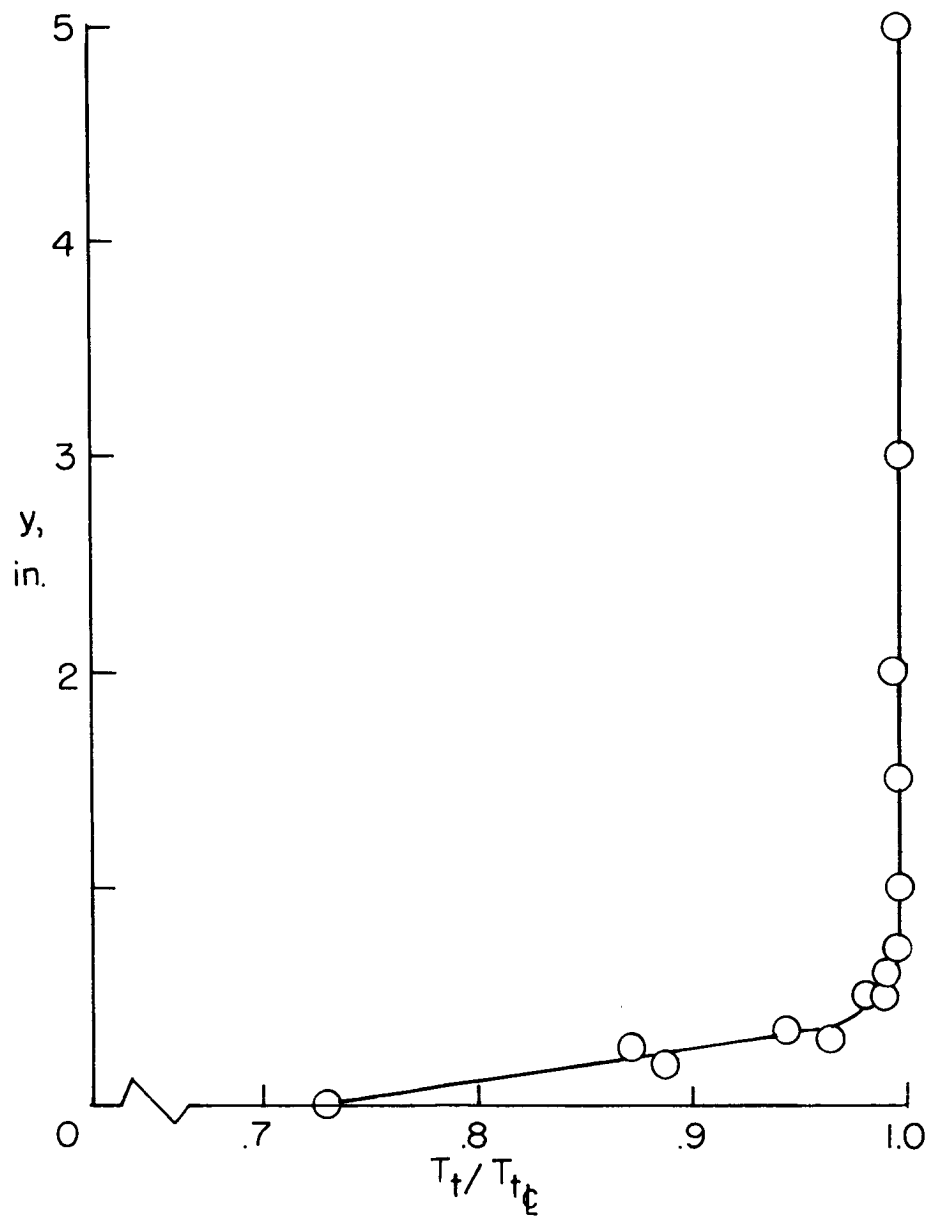


Figure 2.- Stagnation-chamber total-temperature survey.

## CROSSHATCHING

By Howard K. Larson and Philip R. Nachtsheim

NASA Ames Research Center

The subject of crosshatched ablation patterns has received considerable attention recently. The knowledge concerning this phenomenon as of June 27, 1968, is summarized in reference 1 which gives the highlights of a technical interchange meeting held at Aerospace Corporation, San Bernardino, California. At this meeting the results of many theoretical and experimental studies aimed at explaining crosshatching were presented. Several of these presentations resulted from work that had been previously or was subsequently published. See for example, references 2, 3, 4, and 5.

Based on the presentations, two significant factors became apparent to the authors:

(1) All the wind-tunnel models on which crosshatching had been observed had significant surface roughness on the ablated surface upstream of the cross-hatched region. It was felt that this fact was related to the controversial point as to whether the crosshatch pattern was moving or was body fixed.

(2) All the theoretical gasdynamic approaches to the explanation of the crosshatching phenomenon, with the exception of the approach presented in reference 5, were not coupled to the ablation process. In reference 5 the gas-dynamics is coupled to the ablation process via a melt layer. Experimental verification of this coupling would entail testing different materials in the same gasdynamic environment. It was for these reasons that the authors felt that an experiment should be conducted in a facility that provided smooth ablation on models made of different materials.

Hence, several right circular cones made of various types of Teflon were tested in the stream produced by a 4,000-pound-thrust model rocket engine fueled with gaseous hydrogen and liquid oxygen at the NASA Marshall Space Flight Center Test Laboratory, Huntsville, Alabama. The approximate dimensions of the cones were a base diameter of 3 inches and a length of 12 inches, with an initial tip radius of 1/16 inch. The rocket was operated at a stagnation pressure of 1000 psia, an oxygen-fuel ratio of 5, a characteristic velocity of 7500 feet per second, an expansion ratio of 8.5, and had an exit diameter of slightly greater than 5 inches. The models were exposed to the stream for 3.5 seconds by means of a rapidly actuated flame shield. Figure 1 shows a typical model prior to test and figures 2 to 6 show the post run results from five different materials. It is fully recognized that testing models of this size in such a small diameter exhaust results in a very nonuniform stream. The gross shape change is interpreted as resulting from boundary-layer transition. The minimum change in model radius occurs at the beginning of transition with the maximum change in radius occurring at the end of transition or the beginning of turbulent flow. This leads to the necked-down appearance of the models. The cross-hatched pattern begins downstream of the "neck" originating as imperceptibly

shallow grooves. No surface roughness is observed to initiate the pattern and there is no perceptible evidence of either streamwise grooving or transition wedges. The subdued appearance of the patterns in figures 5 and 6 is misleading due to the photographic technique used in making the pictures. The light source is pointed down on the model tip from above the cone axis. It is the translucent nature of the model materials in figures 5 and 6 that subdues the patterns which are physically more evident than those on the model shown in figure 2.

#### REFERENCES

1. Swigart, Rudolph J.: Summary and Highlights of Technical Interchange Meeting on Crosshatched Patterns (Striations) in Ablative Materials held June 27, 1968. Aerospace Corporation Document SA-68-0000-02358, San Bernardino, California, July 8, 1968.
2. Larson, H. K.; and Mateer, G. G.: Cross-Hatching - A Coupling of Gas Dynamics with the Ablation Process. AIAA Paper No. 68-670, June 1968.
3. Laganelli, A. L.; and Nestler, D. E.: Surface Ablation Patterns. A Phenomenology Study. AIAA Paper No. 68-671, June 1968.
4. Canning, Thomas N.; Wilkins, Max E.; and Tauber, Michael E.: Ablation Patterns on Cones Having Laminar and Turbulent Flows. AIAA J., vol. 6, no. 1, Jan. 1968, pp. 174-175.
5. Nachtsheim, Philip R.: Analysis of the Stability of a Thin Liquid Film Adjacent to a High-Speed Gas Stream. NASA TN D-4976, 1969.

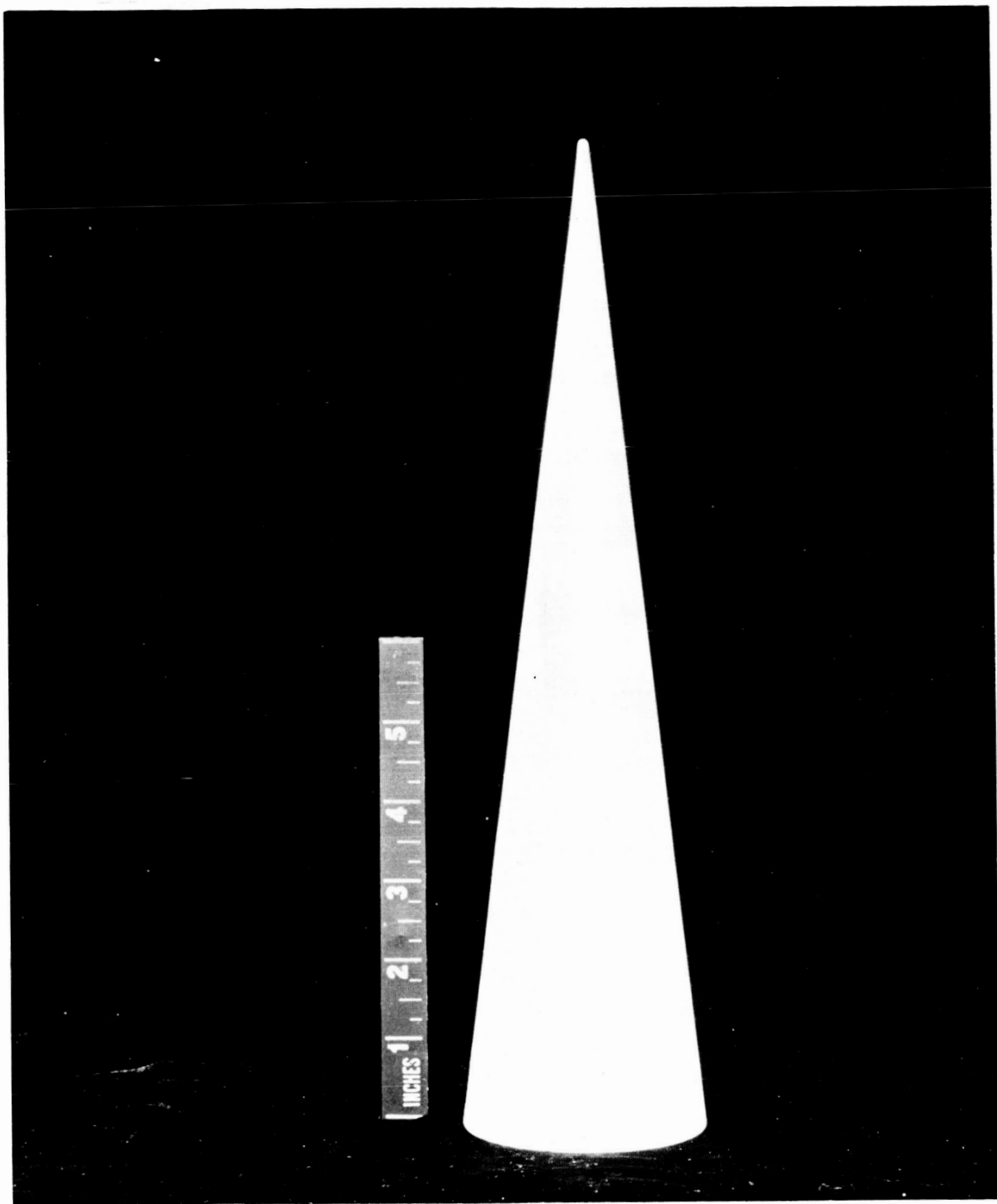


Figure 1.-TFE Teflon before test. Ames  
slide No. A-41315.

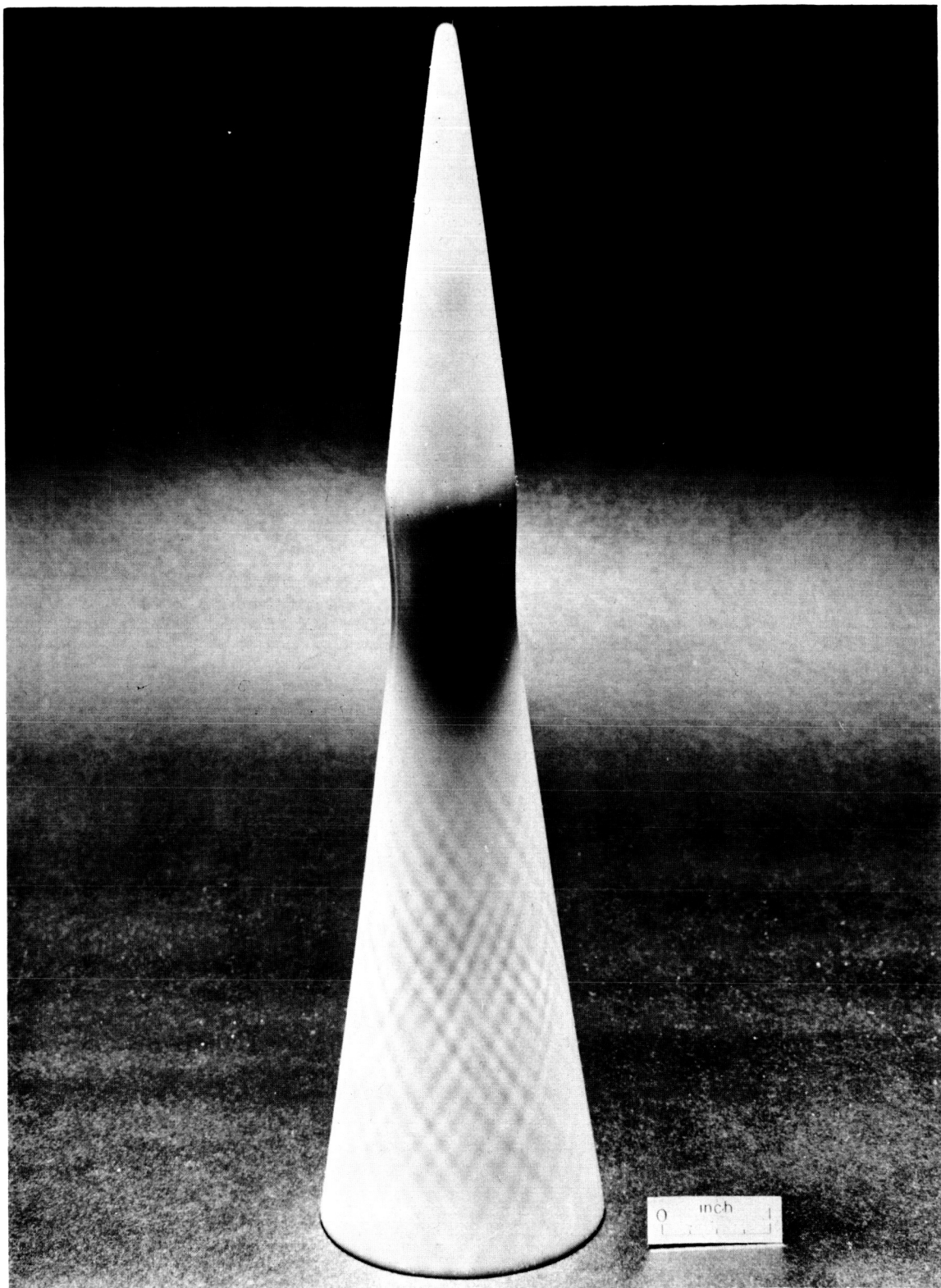


Figure 2.-TFE Teflon; post test, Ames slide  
No. A-41773.

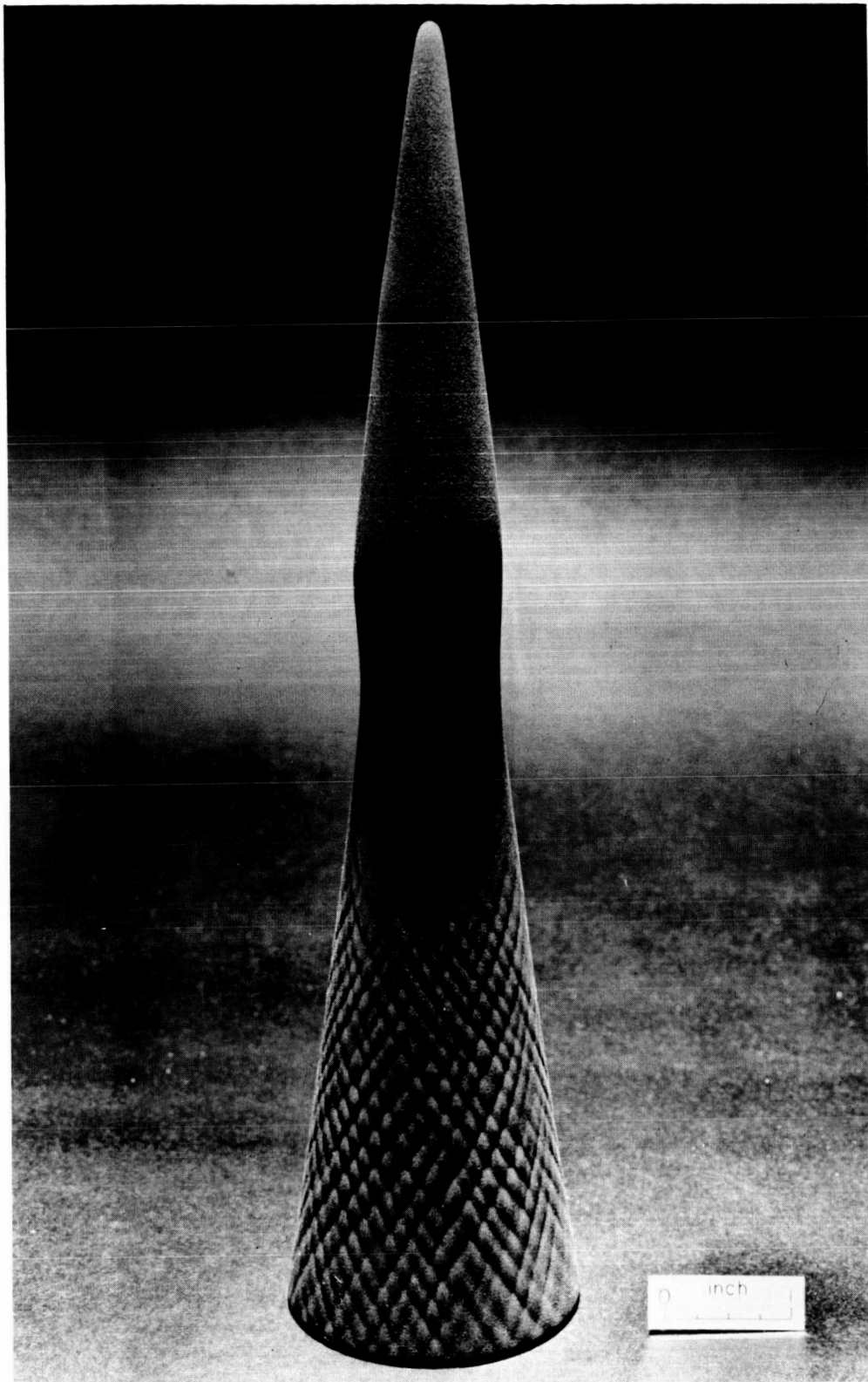


Figure 3.-Utility Teflon + 5% glass; post  
test, Ames slide No. A-41774.

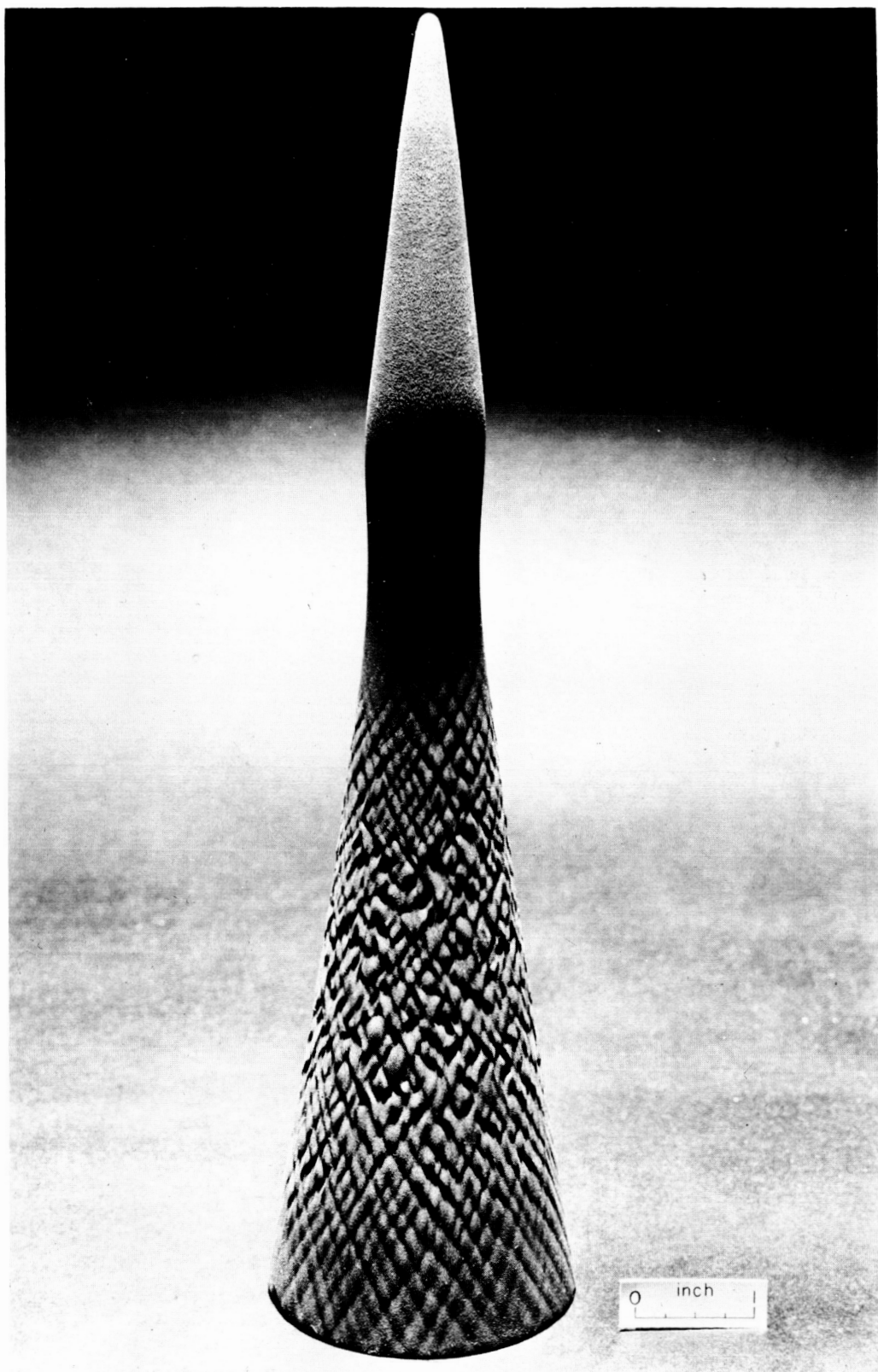


Figure 4.-TFE Teflon + 25% Graphite fill;  
post test, Ames slide No. A-41775.

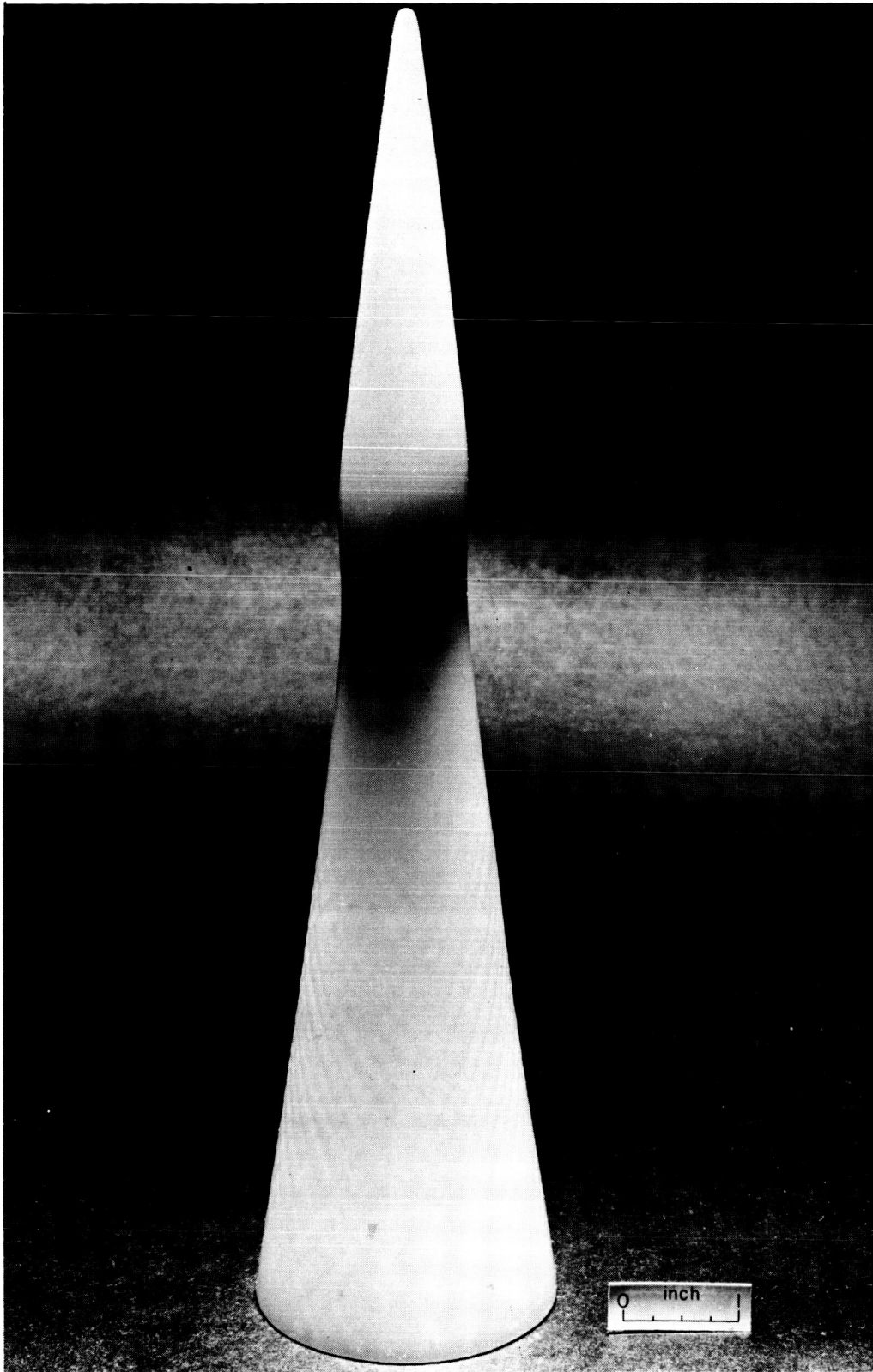


Figure 5.-FEP Teflon; Ames slide No. A-41776.



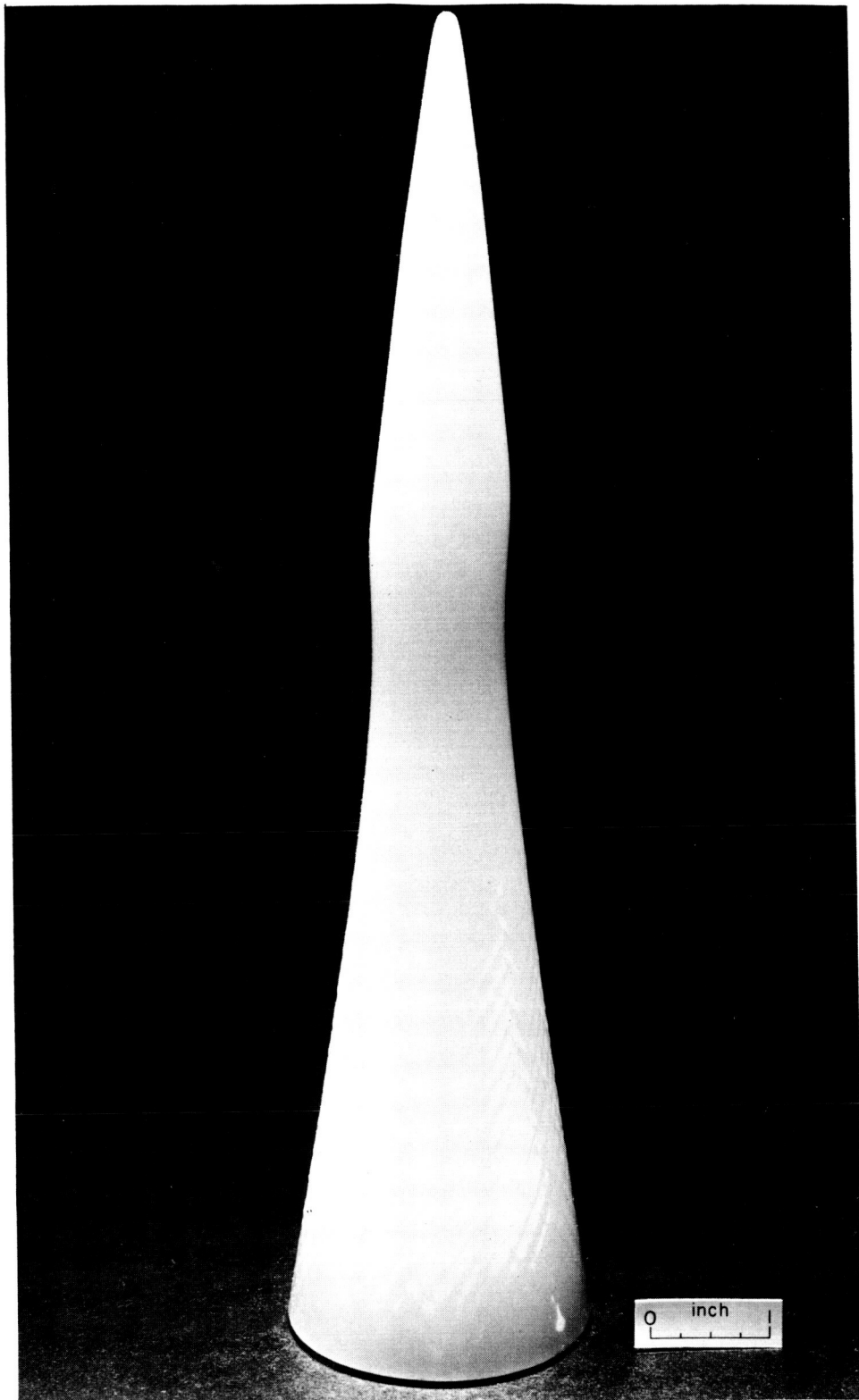


Figure 6.-KEL-F Thermoplastic, Ames slide  
No. A-41777.

RECENT APPLICATIONS OF THE METHOD OF INTEGRAL RELATIONS TO  
TURBULENT BOUNDARY LAYERS WITH HEAT TRANSFER  
AND PRESSURE GRADIENTS

By Jack N. Nielsen and  
Gary D. Kuhn

Nielsen Engineering & Research, Inc.

SUMMARY

The method of integral relations used extensively to study laminar boundary layers, attached and separated, has been extended to compressible turbulent boundary layers with heat transfer and pressure gradients. A brief outline is given of the method, which requires as its only empirical input an eddy-viscosity model. A computer program based on the method has been applied to three illustrative cases. In the first case it is shown that the variation of flat-plate skin-friction coefficient with Mach number and surface temperature is predicted well by the method. In the second case, one of interaction between a hypersonic flat-plate boundary layer and an oblique shock wave, fair to good agreement is obtained between experiment and theory. The third case involves hypersonic flow past an axisymmetric compression flare with appreciable pressure gradients normal to the flare surface. By adjusting the measurements for the normal pressure gradients, good agreement between boundary-layer theory and experiment is obtained. An engineering method of adjusting boundary-layer theory for the normal pressure gradients is also presented.

INTRODUCTION

The method of integral relations (ref. 1) has been extensively applied to laminar boundary layers, attached and separated, by a number of investigators (refs. 2 through 16). The method has also been applied to a lesser extent to turbulent boundary layers for the incompressible case (refs. 17 through 20) and for the compressible case with heat transfer and pressure gradients (refs. 21 through 23). Its application to turbulent incompressible boundary layers has been successful for constant pressure and accelerating flows, but less successful for decelerating flows especially those culminating in separation. This is due in part to the fact that applications of the method to turbulent boundary layers to date have not been formulated to handle the separation point singularity as has successfully been done for the laminar case. Also, some of

the data do not obey the two-dimensional momentum equation approaching separation. This report describes the application of the general Dorodnitsyn method to high-speed turbulent layers with heat transfer and prescribed pressure gradients. Cases of boundary-layer, shock-wave interaction are investigated, as well as axially symmetric compression surfaces with large normal pressure gradients. Greater detail on some of the results may be found in references 21 and 22. The research was accomplished in part under contract to the Air Force Flight Dynamics Laboratory and in part under contract to Ames Research Center.

#### SYMBOLS

$a_{ij}$	coefficients in equation (2)
$c_1, c_2, c_3, \dots$	functions defining velocity gradient in equation (1)
$\dot{c}_1, \dot{c}_2, \dot{c}_3, \dots$	derivatives with respect to $\xi$
$M$	free-stream Mach number
$M_0$	edge Mach number at beginning of pressure rise
$p$	static pressure
$p_0$	static pressure at beginning of pressure rise
$p_w$	static pressure at surface of body
$P_i$	eddy-viscosity integrals, equation (3)
$R_1, R_2, R_3$	nonhomogeneous terms in equation (2)
$R_x/l$	free-stream Reynolds number per unit length at edge of boundary layer at beginning of pressure rise
$s$	distance along surface of compression flare starting at end of cylinder
$T_{t_0}$	total temperature at edge of boundary layer (assumed constant)
$T_w$	wall absolute temperature
$u$	local velocity
$\bar{u}$	ratio of local axial velocity in boundary layer to value at the edge of the boundary layer
$u'_w$	velocity at edge of boundary layer if edge pressure is raised to the wall pressure isentropically
$x$	axial distance along plate measured from leading edge

y	distance normal to the surface
$\delta$	boundary-layer thickness
$\delta^*$	boundary-layer displacement thickness: when $\frac{\partial p}{\partial y} = 0$ , $\delta^* = \int_0^\delta \left(1 - \frac{\rho u}{\rho_\delta u_\delta}\right) dy$ when $\frac{\partial p}{\partial y} \neq 0$ , $\delta^* = \int_0^\delta \left(1 - \frac{\rho u}{\rho_w' u_w'}\right) dy$
$\epsilon$	turbulent eddy viscosity
$\theta$	boundary-layer momentum thickness: when $\frac{\partial p}{\partial y} = 0$ , $\theta = \int_0^\delta \frac{\rho u}{\rho_\delta u_\delta} \left(1 - \frac{u}{u_\delta}\right) dy$ when $\frac{\partial p}{\partial y} \neq 0$ , $\theta = \int_0^\delta \frac{\rho u}{\rho_w' u_w'} \left(1 - \frac{u}{u_w'}\right) dy$
$\theta_w$	wedge angle of oblique shock generator
$\xi, \eta$	coordinates in Dorodnitsyn plane parallel and perpendicular to surface, respectively
$\rho$	local density
$\rho_w'$	density at edge of boundary layer if edge static pressure is brought up to wall pressure isentropically
$\tau$	shear stress in boundary layer
Subscripts:	
i	incompressible
o	beginning of pressure rise
$\delta$	edge of boundary layer

## GENERAL DESCRIPTION OF METHOD

The method of integral relations is a mathematical technique for solving partial differential equations which has been applied to the laminar boundary-layer equations by Dorodnitsyn (ref. 1).

The boundary-layer equations for compressible flow with heat transfer and pressure gradients are first transformed to an incompressible form by the Stewartson transformation, and then to a form independent of viscosity by the Dorodnitsyn transformation. The solution is obtained in the Dorodnitsyn plane with coordinates  $\xi$  and  $\eta$ . First the normal velocity gradient,  $\partial \bar{u} / \partial \eta$  is represented as a function of  $\bar{u}$  with a prescribed number of arbitrary parameters. The following relationship has been used.

$$\frac{\partial \bar{u}}{\partial \eta} = \frac{(1 - \bar{u})}{c_1 + c_2 \bar{u} + c_3 \bar{u}^2 + \dots} \quad (1)$$

where the parameters  $c_1, c_2, c_3, \dots$  are functions of  $\xi$ , the streamwise coordinate in the Dorodnitsyn plane. The differential equations of continuity, momentum, and energy are combined linearly in certain simplifying ways through the use of weighting functions. These functions are functions only of  $\bar{u}$  with certain mathematical properties to avoid singularities and to guarantee linear independence. The equations resulting from the linear combinations are then integrated with respect to  $\bar{u}$  across the boundary layer. The integration produces an independent ordinary differential equation for each weighting function. As many equations are generated as arbitrary parameters are utilized in the normal velocity-gradient representation. In principle, if a proper representation is used together with linearly independent weighting functions, convergence will result. Convergence has been demonstrated for many exact solutions to the laminar equations. For turbulent layers generally there are no exact solutions to demonstrate such convergence.

The method applied to turbulent boundary layers yields ordinary differential equations in terms of the coefficients  $c_1, c_2, c_3, \dots$  which define the velocity profile. The equations have the form

$$\left. \begin{aligned} a_{11} \dot{c}_1 + a_{12} \dot{c}_2 + \dots + a_{1n} \dot{c}_n &= R_1 \\ a_{21} \dot{c}_1 + a_{22} \dot{c}_2 + \dots + a_{2n} \dot{c}_n &= R_2 \\ \vdots & \\ a_{n1} \dot{c}_1 + a_{n2} \dot{c}_2 + \dots + a_{nn} \dot{c}_n &= R_n \end{aligned} \right\} \quad (2)$$

where the dot indicates differentiation with respect to the streamwise direction and the coefficients  $a_{ij}$  are constants. The non-homogeneous terms  $R_1, R_2, R_3, \dots$  contain skin-friction terms, pressure-gradient terms, and shear integrals of the form

$$P_i = \int_0^1 \frac{\partial \bar{u}}{\partial \eta} \bar{u}^{(i-1)} d\bar{u} \quad (3)$$

The shear and the eddy viscosity are related by

$$\tau = \epsilon \frac{\partial u}{\partial y} \quad (4)$$

Thus, an eddy-viscosity model is all that is needed to integrate equation (2) starting from given initial conditions. The incompressible viscosity model used in the inner part of the boundary layer is based on the law of the wall together with the classical Prandtl assumption of constant shearing stress in the inner layer. The eddy viscosity in the outer layer is taken as constant in accordance with the result of Clauser (ref. 24). The compressible eddy viscosity in the inner layer was obtained with the help of the Baronti-Libby transformation (ref. 25) and in the outer layer by simple density scaling of the Clauser result. For complete details, see reference 21.

A computer program has been written (ref. 23) for calculating solutions to compressible, turbulent, boundary-layer flow over two-dimensional or axisymmetric bodies subject to prescribed pressure distributions. The program, based on the use of three parameters in the velocity profile, contains the following assumptions:

- (1) The laminar and turbulent Prandtl numbers are unity.
- (2) The surface temperature is uniform.
- (3) The flow at the edge of the boundary layer is isentropic.
- (4) The Chapman-Rubesin constant is unity.
- (5) The specific heat ratio and the specific heats are constant.
- (6) The slope of the body with respect to the free-stream direction is not large.

#### COMPARISONS BETWEEN EXPERIMENT AND THEORY FOR FLAT PLATES

In order to verify the general correctness of the method, it has been applied to the prediction of the variation of skin-friction coefficient with Reynolds number, Mach number, and

temperature ratio. In order to start the integration it is necessary to determine initial values of the parameters  $c_1$ ,  $c_2$ , and  $c_3$  characterizing the initial velocity profiles. Approximate values were obtained by fitting experimental profiles by the method of least squares. The solution generated from such initial conditions soon developed asymptotic trends demonstrating a "locked-in" solution. The skin-friction coefficients determined by this method are shown in figure 1 for a range of Mach numbers and wall temperature ratios for a fixed Reynolds number. The wall temperature ratio is that of the wall temperature to the total temperature at the edge of the boundary layer assuming a Prandtl number of unity. Also shown are the predicted skin-friction coefficients from two empirical methods; the T' method of Rubesin (ref. 26) and the Spalding-Chi method (ref. 27). The general agreement is good so that the main effects of compressibility and heat transfer are predicted well by the method.

Some turbulent velocity-profile data were taken on a flat plate during the course of the experimental investigation reported in reference 28. Two velocity profiles for a turbulent boundary layer on a 4-foot flat plate are shown in figure 2. The agreement between the experimental and theoretical velocity profiles is considered good.

#### BOUNDARY-LAYER, SHOCK-WAVE INTERACTION

The flat plate discussed above was used for a boundary-layer, shock-wave experiment. For the same test conditions as those of figure 2, an oblique shock generator with a  $5^\circ$  wedge angle was used to cause shock impingement between the first and second measuring stations shown in figure 3. The boundary-layer development was computed by the computer program using the experimental wall pressure distribution. The variation of displacement thickness with  $x$  distance is in good agreement with theory both with and without shock impingement. The variation of the theory and experiment for momentum thickness  $\theta$  is fair for no shock impingement, but the effect of shock impingement in reducing the momentum thickness is overestimated. The theory is based on the assumptions that the pressure is constant across the boundary layer and that the flow at the edge of the layer is isentropic. It is known that for turbulent boundary layers the shock wave penetrates deeply into the boundary layer (ref. 29) causing pressure gradients normal to the surface and introducing entropy changes at the edge of the boundary layer. Accordingly, the method cannot be expected to predict the shock-structure in the outer part of the boundary layer (above the  $M = 1$  line) in the interaction region. If proper account is taken of the entropy changes, it might be expected that the boundary-layer theory would give fairly good results downstream of the interaction region when the pressure has become fairly uniform across the layer.

The actual wall pressure distribution for the case of figure 3 is shown in figure 4(a). The values of  $\delta^*$  and  $\theta$  shown in the previous figure for the impinging shock case correspond to an axial position of 2.17 feet from the leading edge at a position near the end of the pressure rise. The velocity profile at this station is shown in figure 4(b). It is seen that the velocity profile has not yet filled out to a fully turbulent profile, although it is fairly close to this condition considering the fact that the pressure rise is not complete.

## AXISYMMETRIC COMPRESSION SURFACES

The method has been applied to an axisymmetric compression surface tested by Hoydysh and Zakkay (reference 30) at a Mach number of 5.75. The model was a hollow circular cylinder culminating in a compression flare as shown in figure 5(a). The measured surface pressure distribution is shown in figure 5(b) together with the pressure distribution at the edge of the boundary layer. The static pressure drop across the boundary layer is large; the pressure drop is essentially an inviscid effect due to the sharp curvature of the compression surface. Since the boundary-layer data are thus influenced by large normal pressure gradients due to curvature, some basis for comparison between experiment and boundary-layer theory must be arrived at. In the first approach consider that the boundary-layer data are to be adjusted for the effect of normal pressure gradient and compared with conventional boundary-layer theory. In the second approach consider that adjustments are to be made to a boundary-layer theory so that a predictive method is obtained. In the first approach the measured values of  $\delta^*$  and  $\theta$  may be adjusted by incremental values of these quantities which account for normal pressure gradients. Consider an inviscid, isentropic flow with the measured static pressure distribution. Its velocity and density profiles would be known, and inviscid values of  $\delta_i^*$  and  $\theta_i$  for these profiles could be calculated. Assuming superposition, the values of  $\delta_i^*$  and  $\theta_i$  would be subtracted from the measured values of  $\delta^*$  and  $\theta$  to yield values for comparison with predictions of boundary-layer theory.

Figures 6 and 7 show comparison between the predicted and measured values of  $\delta^*$  and  $\theta$ . The circles in figure 6 represent the displacement thickness as measured, and the squares represent the measured values adjusted for normal pressure gradient as described above. It is seen that the corrections are sometimes larger than the measured values. The agreement between theory and the adjusted experiment is very good. In fact, the agreement is remarkable in view of the size of the corrections and the assumption of superposition for a nonlinear flow problem. The angles appearing in this and subsequent figures denote the local slope of the flare surface. Comparisons similar to those for displacement



thickness are shown for momentum thickness in figure 7. The corrections are relatively not so great as for displacement thickness. The correction improves the agreement with adjusted experiment only at the very high ramp angles.

In addition to the boundary-layer measurements the local heat-transfer rates were measured on the flare. The experimental results are shown in figure 8 as the ratio of the local rate to that at the beginning of the flare. The comparison between the predictions and the data shows very good agreement. Hoydysh and Zakkay were able to obtain skin-friction coefficients by correlating their velocity profile measurements on the basis of the law of the wall and the Baronti-Libby transformation. The skin-friction coefficients so obtained were in good agreement with those predicted by Reynolds analogy using the measured heat-transfer rates. Since it was possible to predict the local heat-transfer rates with the present method which neglects normal pressure gradients, it follows that normal pressure gradients have little influence on the skin-friction coefficient provided the wall pressure distribution is used in the boundary-layer calculation.

The previous method of adjusting boundary-layer measurements for normal pressure gradients in order to compare it with boundary-layer theory does not constitute a predictive method. Also, it is based on measured static pressure profiles and on known boundary-layer thicknesses. A predictive method was presented in reference 22 together with suggested improvements which have been carried out herein. In essence the method starts with the predicted boundary-layer quantities neglecting normal pressure gradients and adds increments to account for normal gradients. The first step of the predictive method is to calculate the boundary-layer gross quantities and its velocity profiles using the present computer program with the wall pressure distribution determined on the basis of any appropriate theory. The normal pressure gradients are then calculated from inviscid flow theory as the second step. A simple approximate relation for such normal gradients can be obtained in terms of flare curvature and Mach number at the edge of the boundary layer. Alternately, the normal gradients can be obtained by the method of characteristics.

In the third step it is assumed that the static pressure at any point in the velocity profile now falls isentropically from wall pressure to the value it would have with normal pressure gradients. The boundary-layer velocity thus increases everywhere, especially at the outer edge, where the pressure drop is largest. At the same time the density drops everywhere in the boundary layer, and the boundary layer thickens in accordance with continuity. The corrections  $\Delta\delta^*$  or  $\Delta\theta$  to be added to the boundary layer values can be easily calculated as the differences between  $\delta^*$  and  $\theta$  for the boundary layer after pressure drop and before pressure drop.

The foregoing prediction method was applied to the preceding compression flare to test its validity. In applying the method the experimental normal pressure distributions were used. The results of the prediction method are shown in figure 9 for displacement thickness. The very considerable increases in displacement thickness are fairly well predicted by the theory for small flare angles but for large flare angles the predicted correction is not large enough. The comparison is shown in figure 10 for momentum thickness. Fair agreement between theory and experiment is seen. The relatively smaller corrections for  $\theta$  than for  $\delta$  are noteworthy. It is considered that the proposed method is a simple engineering method for making approximate adjustments to boundary-layer theory for normal pressure gradients in lieu of more exact solutions properly accounting for the simultaneous non-linear effects of normal pressure gradients and viscosity.

### CONCLUDING REMARKS

A description has been given of the application of the method of integral relations (ref. 1) to the calculation of compressible turbulent boundary-layer characteristics with pressure gradients and heat transfer. The detailed method is described in reference 22, and a computer program to do the calculation is described in reference 23. The method is applicable to two-dimensional or axially symmetric bodies, and the computer program has been written for isentropic conditions at the edge of the boundary layer and arbitrary pressure distributions.

Three example applications of the computer program have been shown. In the first example it was shown that the general method properly accounts for the effects of compressibility and heat transfer on skin-friction coefficient with only the present eddy-viscosity model as empirical input. In the second example the method has been applied to a case of interaction between an oblique shock wave and a turbulent boundary layer which was not separated. The quantities at the downstream edge of the pressure rise were predicted fairly well. The third application of the method was to an axisymmetric compression surface attached to a hollow cylinder tested at hypersonic speed. The normal pressure gradients were such as to invalidate the usual assumptions of boundary-layer theory. However, when the experimental displacement and momentum thicknesses were adjusted to account for normal pressure gradients, the comparisons between experiment and boundary-layer theory were good. The comparison between experiment and theory for local heat-transfer rates was good without accounting for normal gradients. A predictive method is presented based on adjusting boundary-layer theory for normal pressure gradients. Fair agreement between the predicted and measured gross boundary-layer properties is found.

## REFERENCES

1. Dorodnitsyn, A. A.: General Method of Integral Relations and Its Application to Boundary Layer Theory. Advances in Aeronaut. Sci., vol. 3, Von Kármán, Ed., c.1962.
2. Abbott, D. E.: Dorodnitsyn's General Method of Integral Relations and Its Application to the Solution of Incompressible Laminar Boundary Layers. Purdue Univ., School of Mech. Engr., Fluid Mech. Group, Tech. Note FMN-65-1, 1965.
3. Bethel, H. E.: Solution of the Laminar Boundary-Layer Equations with Mass Transfer by the GKD Multi-Moment Method. Aerospace Research Labs., ARL 67-0045, Mar. 1967.
4. Bethel, H. E.: On the Convergence and Exactness of Solutions of the Laminar Boundary-Layer Equations Using the N-Parameter Integral Formulation of Galerkin-Kantorovich-Dorodnitsyn. Ph.D. Dissertation, Purdue Univ., 1966. (Also published by Aerospace Research Labs., ARL66-0090.)
5. Bethel, H. E.: On a Convergent Multi-Moment Method for the Laminar Boundary Layer Equations. Reprinted from the Aeronautical Quarterly, Vol. XVIII, Nov. 1967, published by the Royal Aeronautical Society.
6. Bethel, H. E.: On the GKD Multi-Moment Method for Laminar Boundary Layers. Presented at the 10th Midwestern Mechanics Conf., Colorado State Univ., 21-23 Aug. 1967.
7. Bethel, H. E.: Comments on "Approximate Solution of Second-Order Boundary-Layer Equations." AIAA J., vol. 4, no. 10, 1966, pp. 1882-1883.
8. Bethel, H. E., and Abbott, D. E.: On the Convergence and Exactness of Solutions of the Laminar Boundary-Layer Equations Using the N-Parameter Integral Formulation of Galerkin-Kantorovich-Dorodnitsyn. School of Mech. Engr., Fluid Mech. Group, Purdue Univ., Tech. Rep. FMTR-66-2, Apr. 1966.
9. Crawford, D. R.: Supersonic Separated Flow Downstream of a Backward Facing Step. College of Engineering, Univ. of Calif. Berkeley, Rep. AS-65-9, May 1967.
10. Goodwin, F. K., Nielsen, J. N., and Iynes, L. L.: Calculation of Laminar Boundary Layer-Shock Wave Interaction on Cooled Walls by the Method of Integral Relations. NEAR Rep. TR 2, July 1967.
11. Holt, M.: Separation of Laminar Boundary Layer Flow Past a Concave Corner. AGARD Conf. Proc., no. 4, Rhode-Saint-Genése, Belgium.
12. Holt, M.: Applications of the Method of Integral Relations to Laminar Boundary-Layer Flows - A Review of Recent Research in the U.S.S.R. Vidya Rep. No. 125, Jan. 1964.

13. Nielsen, Jack N., Lynes, Larry L., and Goodwin, Frederick K.: Calculation of Laminar Separation With Free Interaction by the Method of Integral Relations. Part I - Two-Dimensional Supersonic Adiabatic Flow. AFFDL-TR-65-107, U.S. Air Force, Oct. 1965. (Available from DDC as AD 626 160.)
14. Nielsen, Jack N., Lynes, Larry L., and Goodwin, Frederick K.: Calculation of Laminar Separation With Free Interaction by the Method of Integral Relations. Part II - Two-Dimensional Supersonic Nonadiabatic Flow and Axisymmetric Supersonic Adiabatic and Nonadiabatic Flows. AFFDL-TR-65-107, U.S. Air Force, Jan. 1966. (Available from DDC as AD 630 765.)
15. Nielsen, J. N., Lynes, L. L., and Goodwin, F. K.: Theory of Laminar Separated Flows on Flared Surfaces Including Supersonic Flow with Heating and Cooling. AGARD Conf. Proc., no. 4, Part 1, proceedings of AGARD Fluid Dynamics Panel held in Rhode-Saint-Genèse, Belgium, 10-13 May 1966.
16. Nielsen, J. N., Lynes, L. L., Goodwin, F. K., and Holt, M.: Calculation of Laminar Separation With Free Interaction by the Method of Integral Relations. AIAA Paper No. 65-50, Jan. 1965.
17. Deiwert, G. S., and Abbott, D. E.: On the Analysis of the Turbulent Boundary Layer by the Method of Weighted Residuals. School of Mech. Engr., Fluid Mech. Group, Purdue Univ., Tech. Rep. FMTR-67-2, Nov. 1967.
18. Deiwert, G. S., and Abbott, D. E.: Application of the Method of Weighted Residuals to the Turbulent Boundary-Layer Equations. Part II - A Two Parameter Prediction Technique. Paper presented at AFOSR-IFP-Stanford 1968 Conf. on Turbulent Boundary Layer Prediction, Aug. 18-25, 1968.
19. Abbott, D. E., Deiwert, G. S., Forsnes, V. G., and Deboy, G. R.: Application of the Method of Weighted Residuals to the Turbulent Boundary-Layer Equations. Part I - The Method of Weighted Residuals as a Solution Technique. Paper presented at AFOSR-IFP-Stanford 1968 Conf. on Turbulent Boundary Layer Prediction, Aug. 18-25, 1968.
20. Murphy, J. D., and Rose, W. C.: Application of the Method of Integral Relations to the Calculation of Incompressible Turbulent Boundary Layers. Paper presented at AFOSR-IFP-Stanford 1968 Conf. on Turbulent Boundary Layer Prediction, Aug. 18-25, 1968.
21. Lynes, L. L., Nielsen, J. N., and Goodwin, F. K.: Inhibition of Flow Separation at High Speed. Vol. I - Supersonic Turbulent Boundary Layers. Air Force Flight Dynamics Lab. Tech. Rep. AFFDL-TR-68-119, Mar. 1969.
22. Lynes, L. L., Nielsen, J. N., and Kuhn, G. D.: Calculation of Compressible Turbulent Boundary Layers with Pressure Gradients and Heat Transfer. NEAR TR 6, Aug. 1968. (Also available as NASA CR-1303.)
23. Kuhn, G. D., Lynes, L. L., and Nielsen, J. N.: Computer Program for Turbulent Boundary Layers on Nonadiabatic Two-Dimensional or Axisymmetric Bodies with Prescribed Pressure Distributions. NEAR TR 7, Aug. 1968.

24. Clauser, Francis H.: The Turbulent Boundary Layer. Vol. IV of Advan. Appl. Mech., H. L. Dryden and Th. von Kármán, eds., Academic Press, Inc., 1956, pp. 1-51.
25. Baronti, Paolo O., and Libby, Paul A.: Velocity Profiles in Turbulent Compressible Boundary Layers, AIAA J., vol. 4, no. 2, Feb. 1966, pp. 193-202.
26. The Vidya Staff: Effects of Supersonic and Hypersonic Aircraft Speed Upon Aerial Photography. Vidya Rep. No. 37, Jan. 1961.
27. Spalding, D. B., and Chi, S. W.: The Drag of a Compressible Turbulent Boundary Layer on a Smooth Flat Plate With and Without Heat Transfer. J. Fluid Mech., vol. 18, pt. I, Jan. 1964, pp. 117-143.
28. Kutschenreuter, P. H., Jr., Brown, D. L., Hoelmer, W., et al.: Investigation of Hypersonic Inlet Shock-Wave Boundary Layer Interaction. Part II - Continuous Flow Test and Analyses. AFFDL-TR-65-36, Apr. 1966. AD 636 981.
29. Watson, E. C., Murphy, J. D., and Rose, W. C.: Shock-Wave, Boundary-Layer Interactions in Hypersonic Inlets. NASA Conf. on Hypersonic Aircraft Tech., Ames Research Center, May 16-18, 1967.
30. Hoydysh, W. G., and Zakkay, V.: An Experimental Investigation of Hypersonic Turbulent Boundary Layers in Adverse Pressure Gradient. AIAA J., vol. 7, no. 1, Jan. 1969, pp. 105-116.

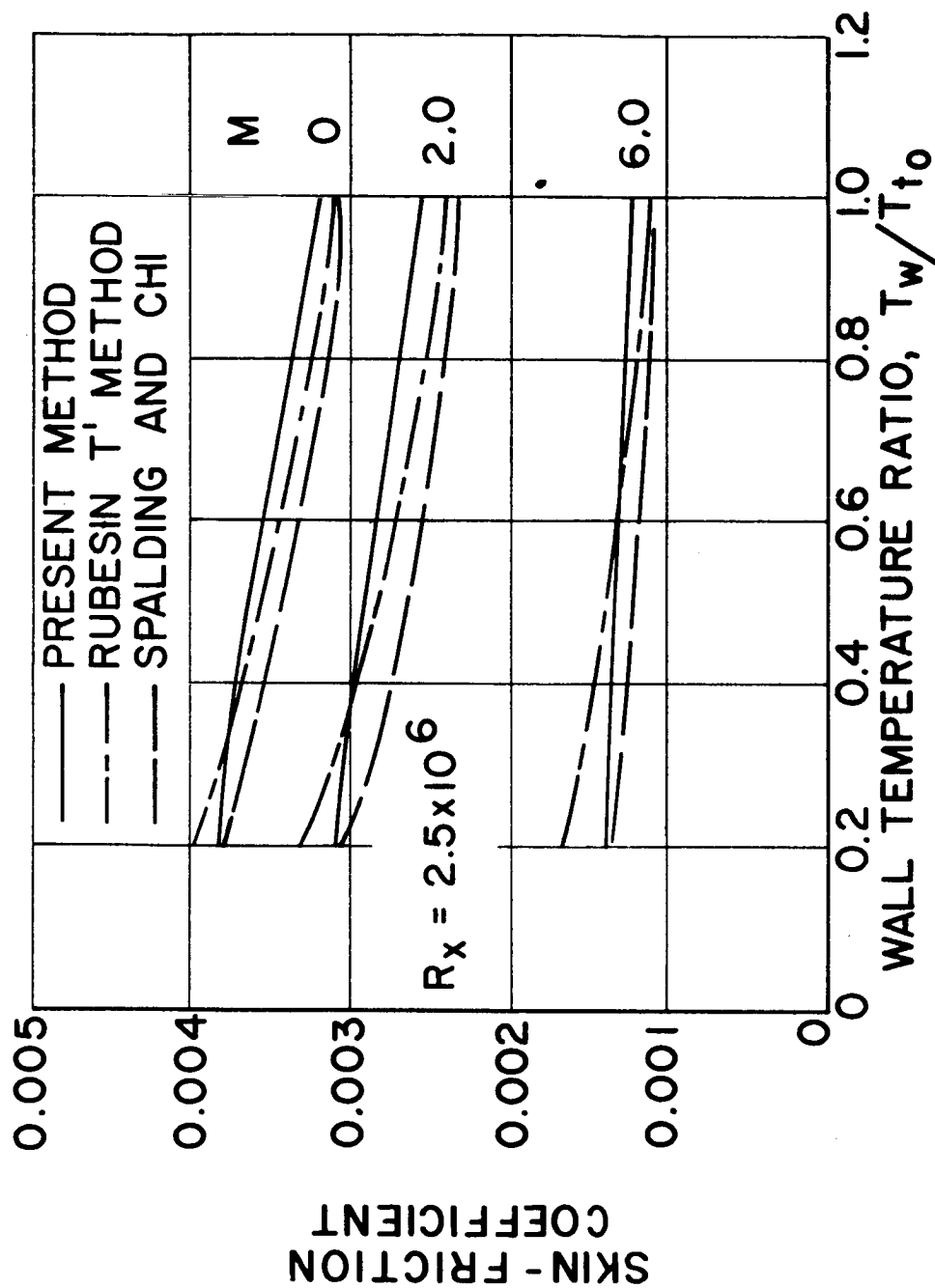


Figure 1.1.- Effect of wall temperature ratio and Mach number on skin-friction coefficient.

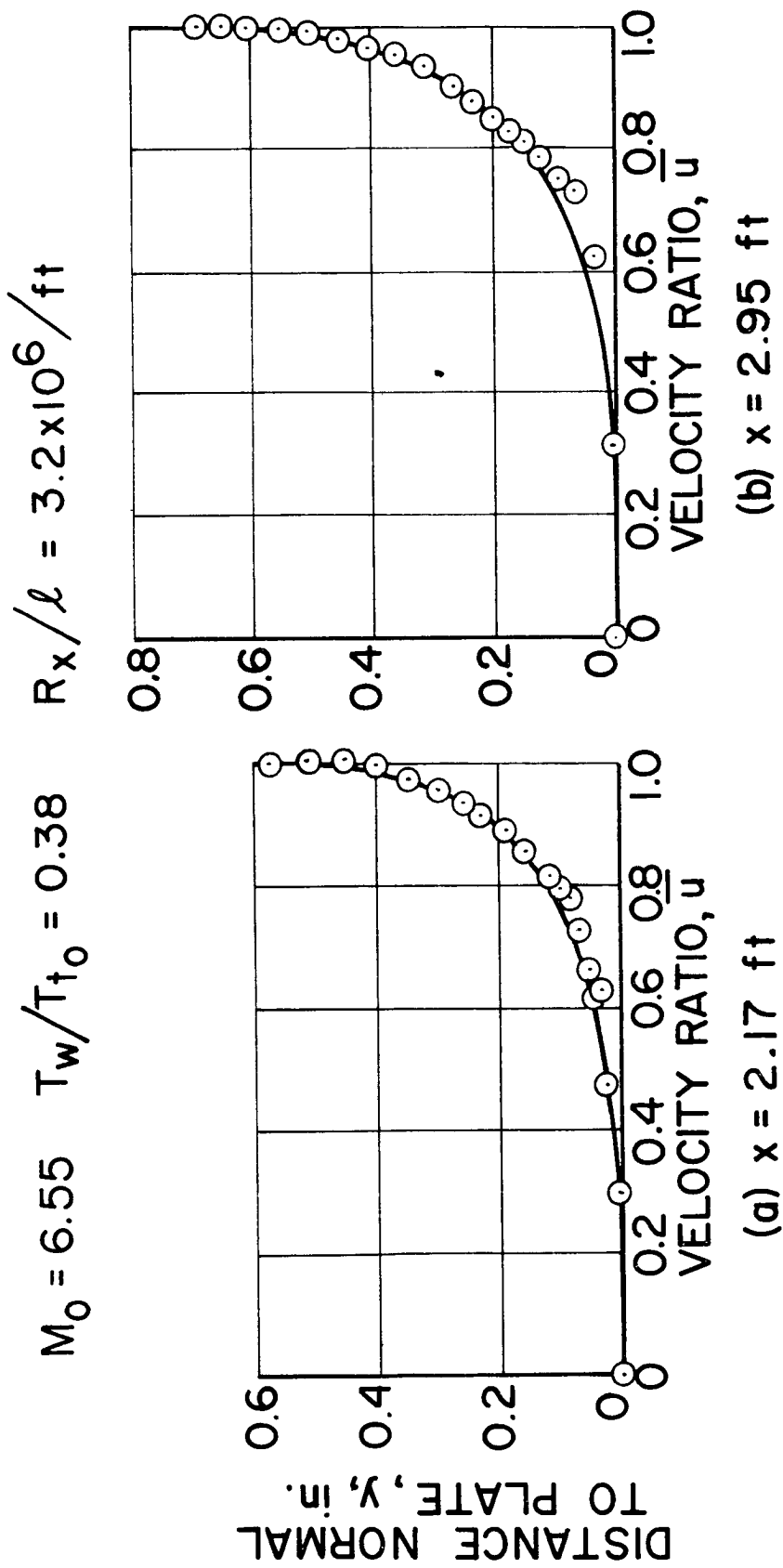
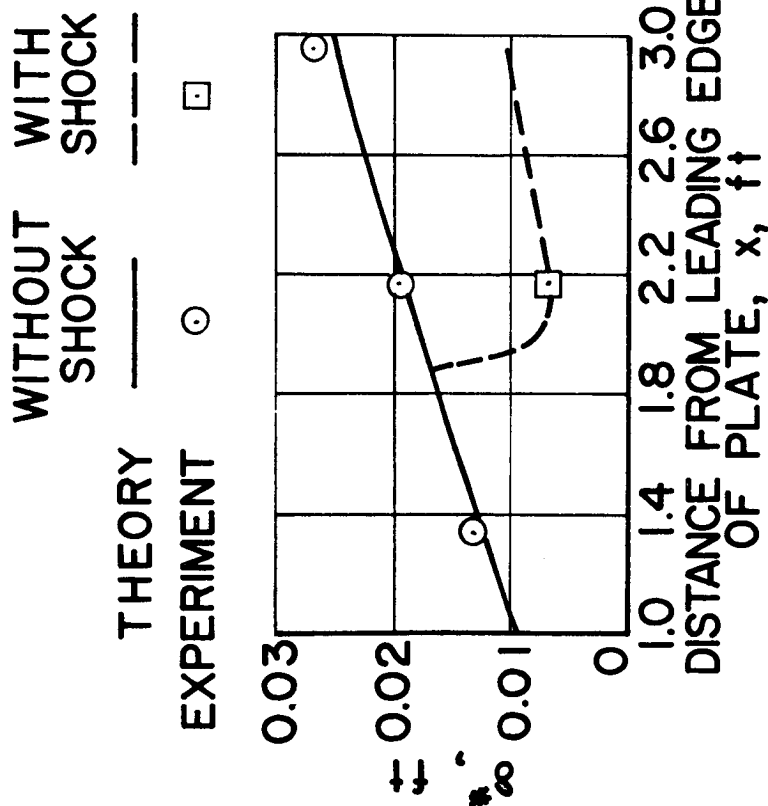
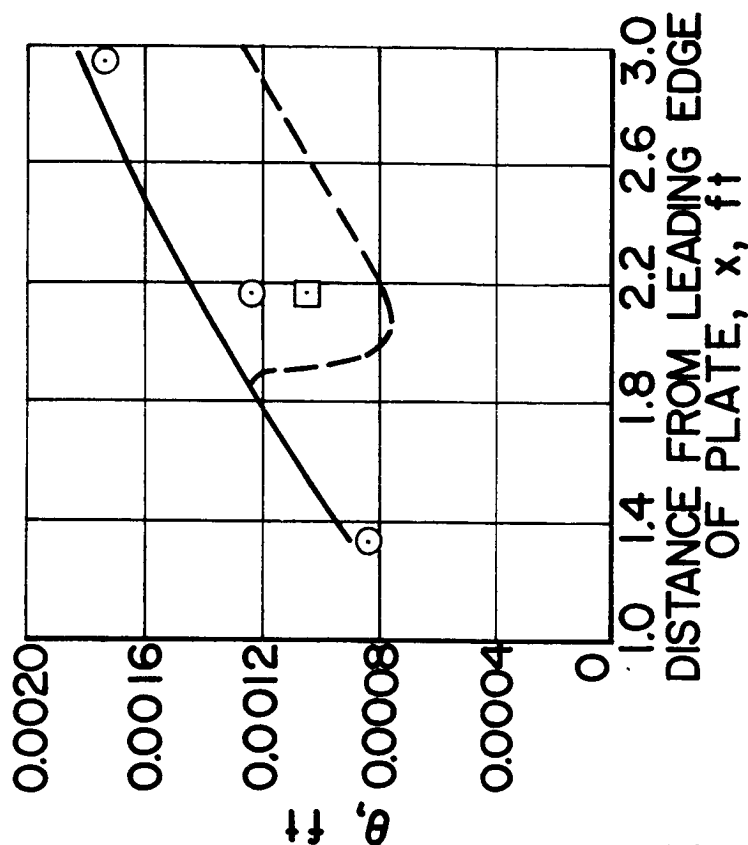


Figure 2.- Comparison between theoretical and experimental turbulent velocity profiles on flat plate.

$$M_0 = 6.55 \quad T_w/T_{t0} = 0.38 \quad R_x/l = 3.2 \times 10^6/\text{ft} \quad \theta_w = 5^\circ$$



(a) DISPLACEMENT THICKNESS



(b) MOMENTUM THICKNESS

Figure 3.- Experimental and theoretical boundary-layer quantities with and without oblique shock impingement on flat plate.



$$M_0 = 6.55 \quad T_w/T_{t0} = 0.38 \quad R_x/l = 3.2 \times 10^6 / \text{ft}$$

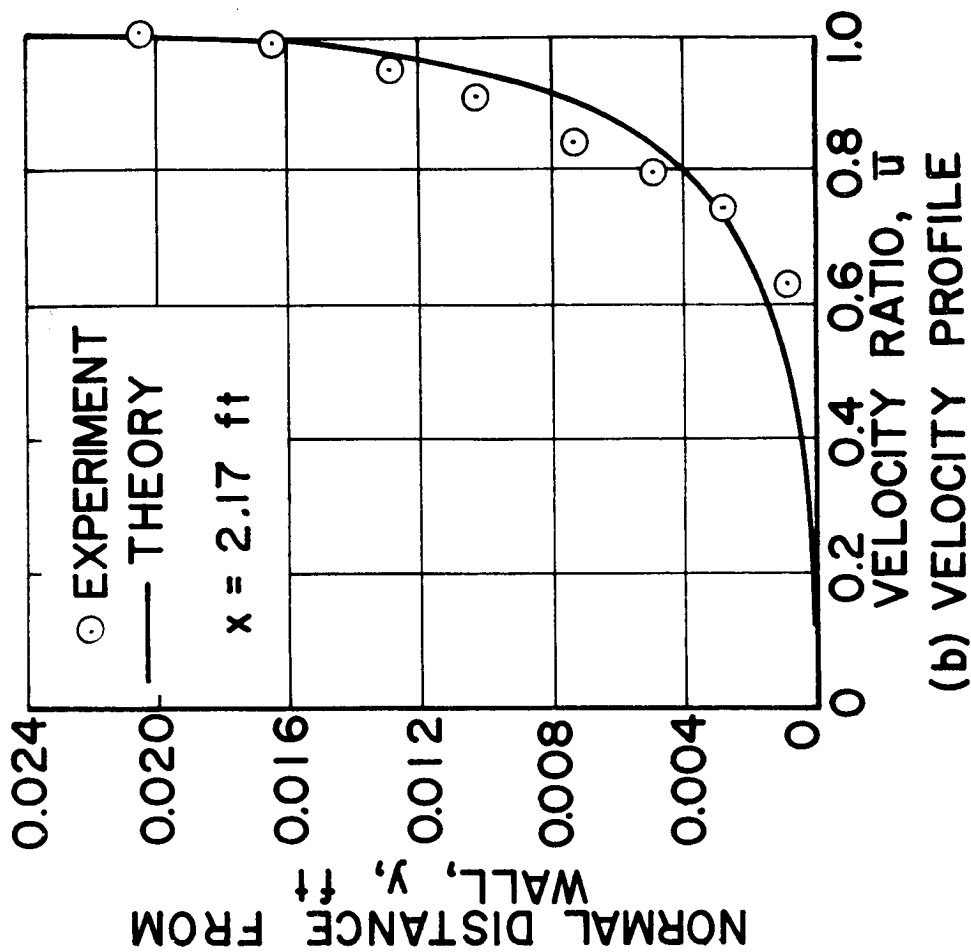
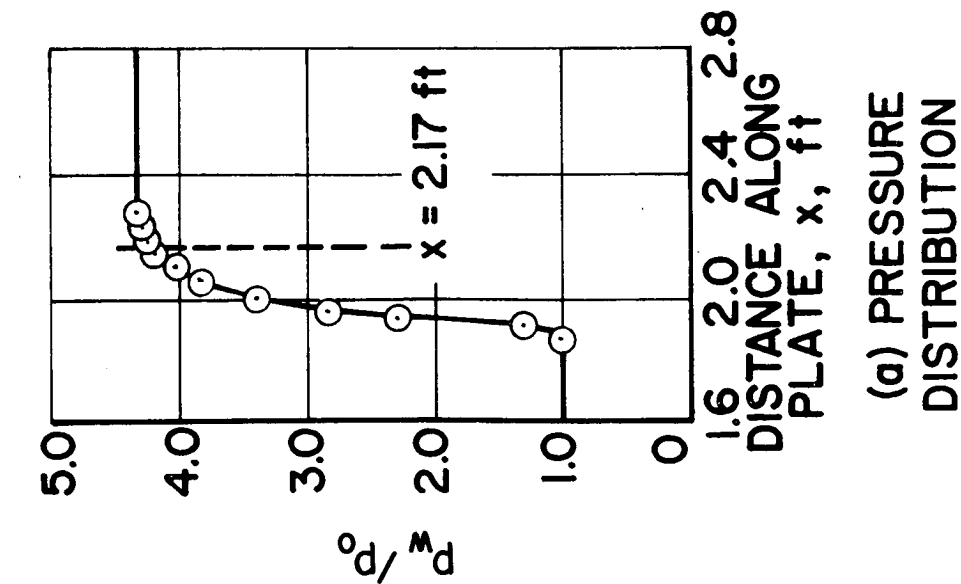
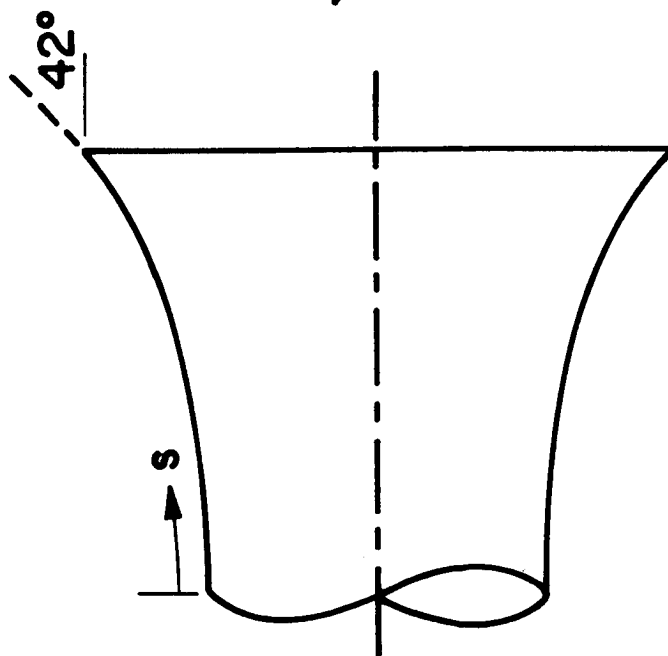
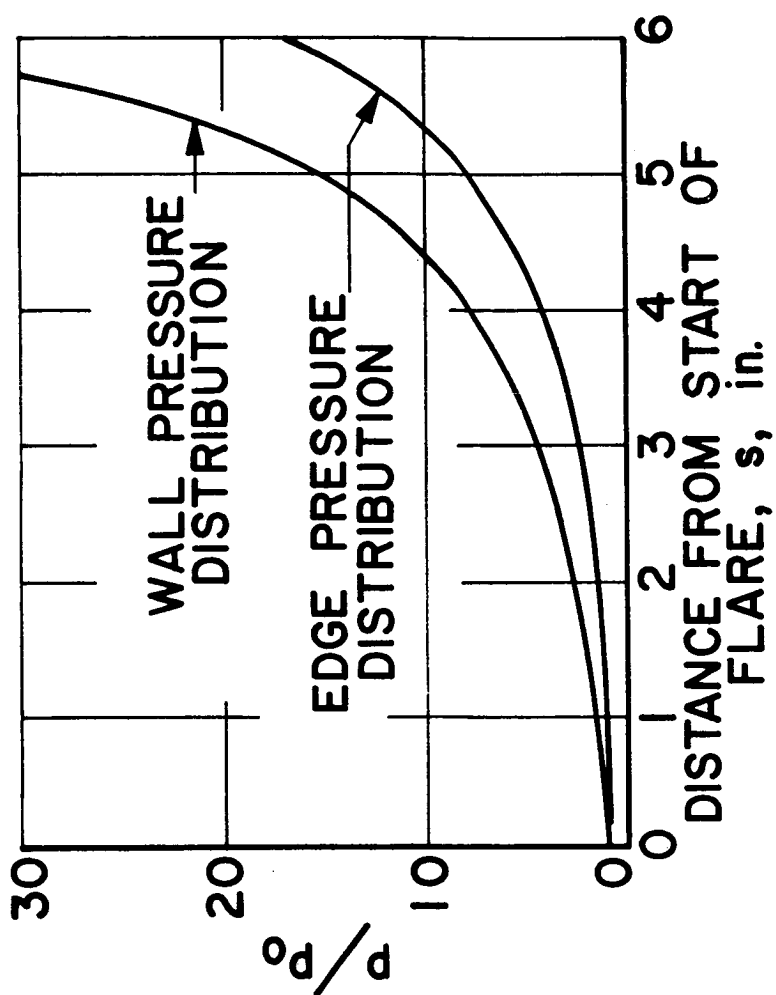


Figure 4.- Velocity profile near downstream end of interaction region.

$$M_0 = 5.75$$



(a) FLARE SHAPE



(b) PRESSURE DISTRIBUTION

Figure 5.- Shape and pressure distribution of axisymmetric compression surface.

$$M_0 = 5.75 \quad T_w/T_{t0} = 0.634 \quad R_x/l = 3.6 \times 10^7 / ft$$

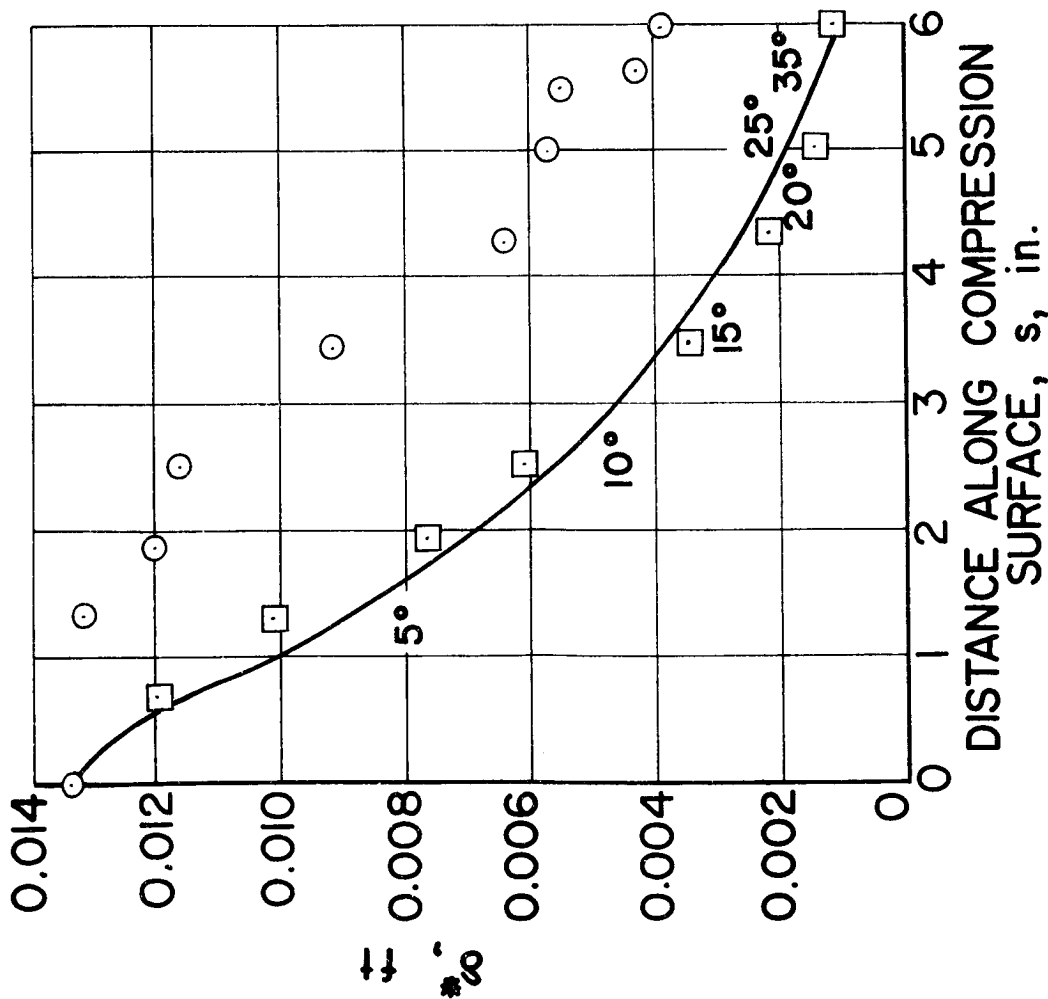


Figure 6.- Displacement thickness for turbulent layer on axisymmetric compression surface.

$$M_0 = 5.75 \quad T_w / T_{t_0} = 0.634 \quad R_x / l = 3.6 \times 10^7 / \text{ft}$$

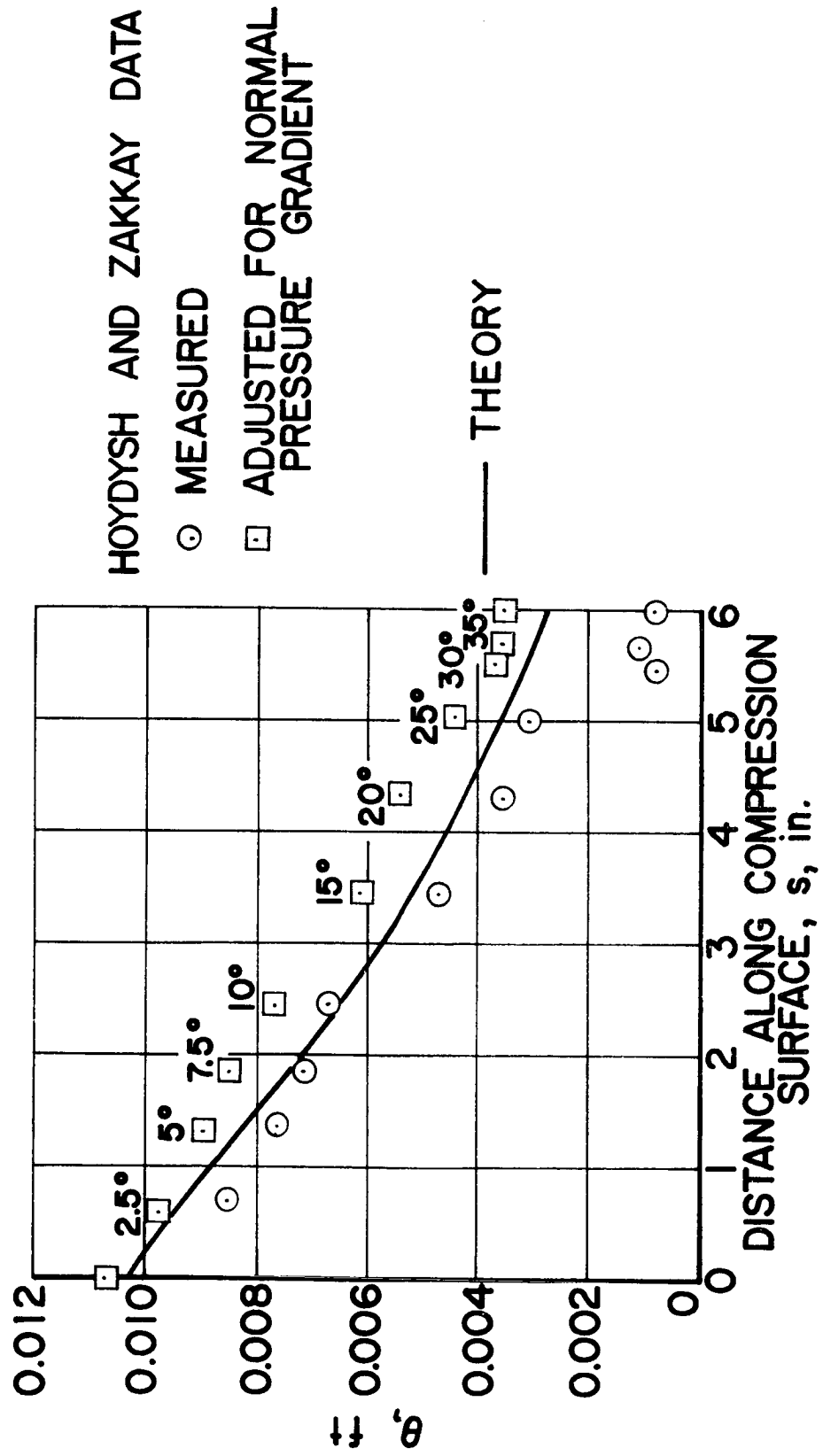


Figure 7.- Momentum thickness for turbulent layer on axisymmetric compression surface.

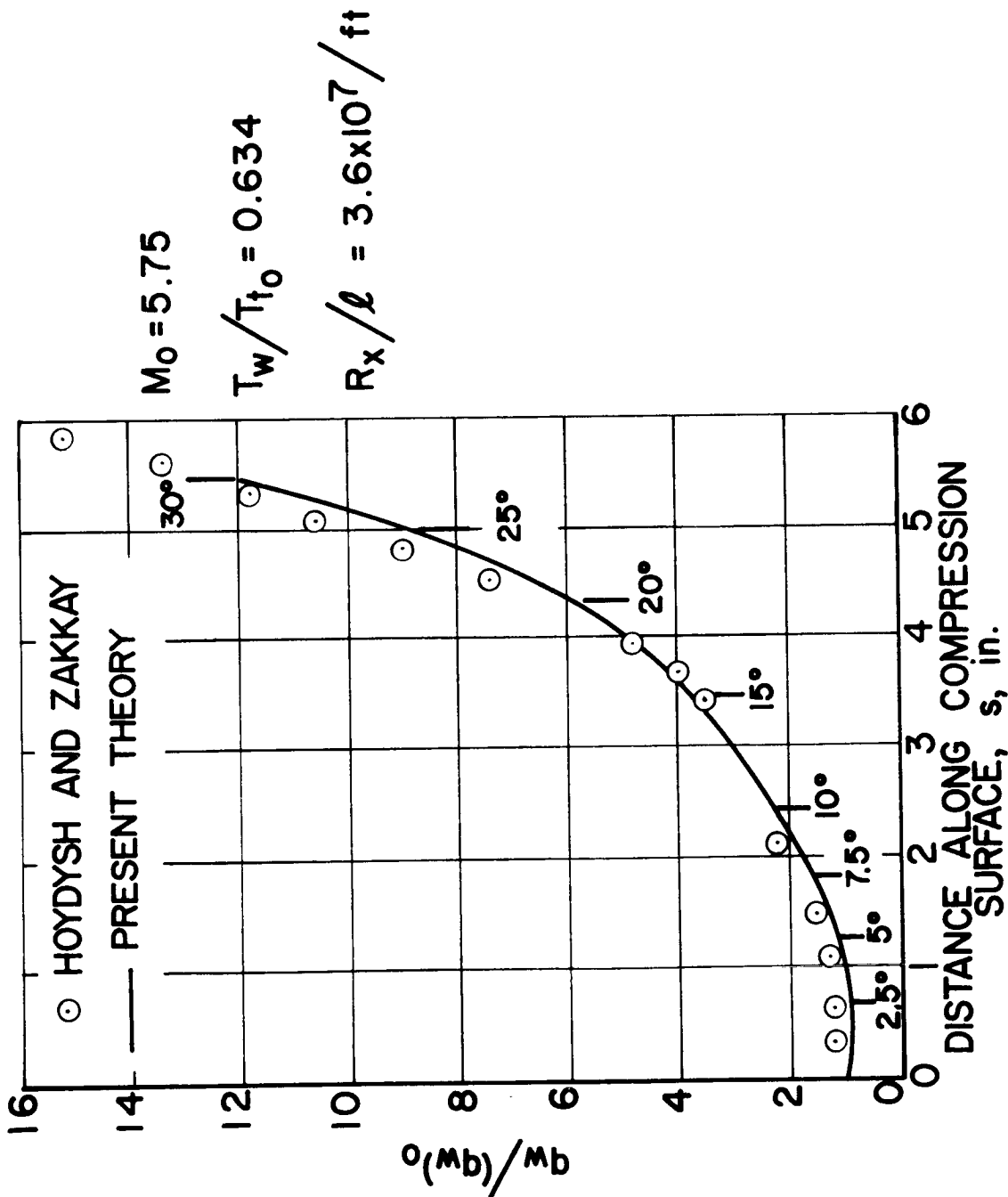


Figure 8.- Surface heat-transfer rates for turbulent boundary layer on axisymmetric compression surface.

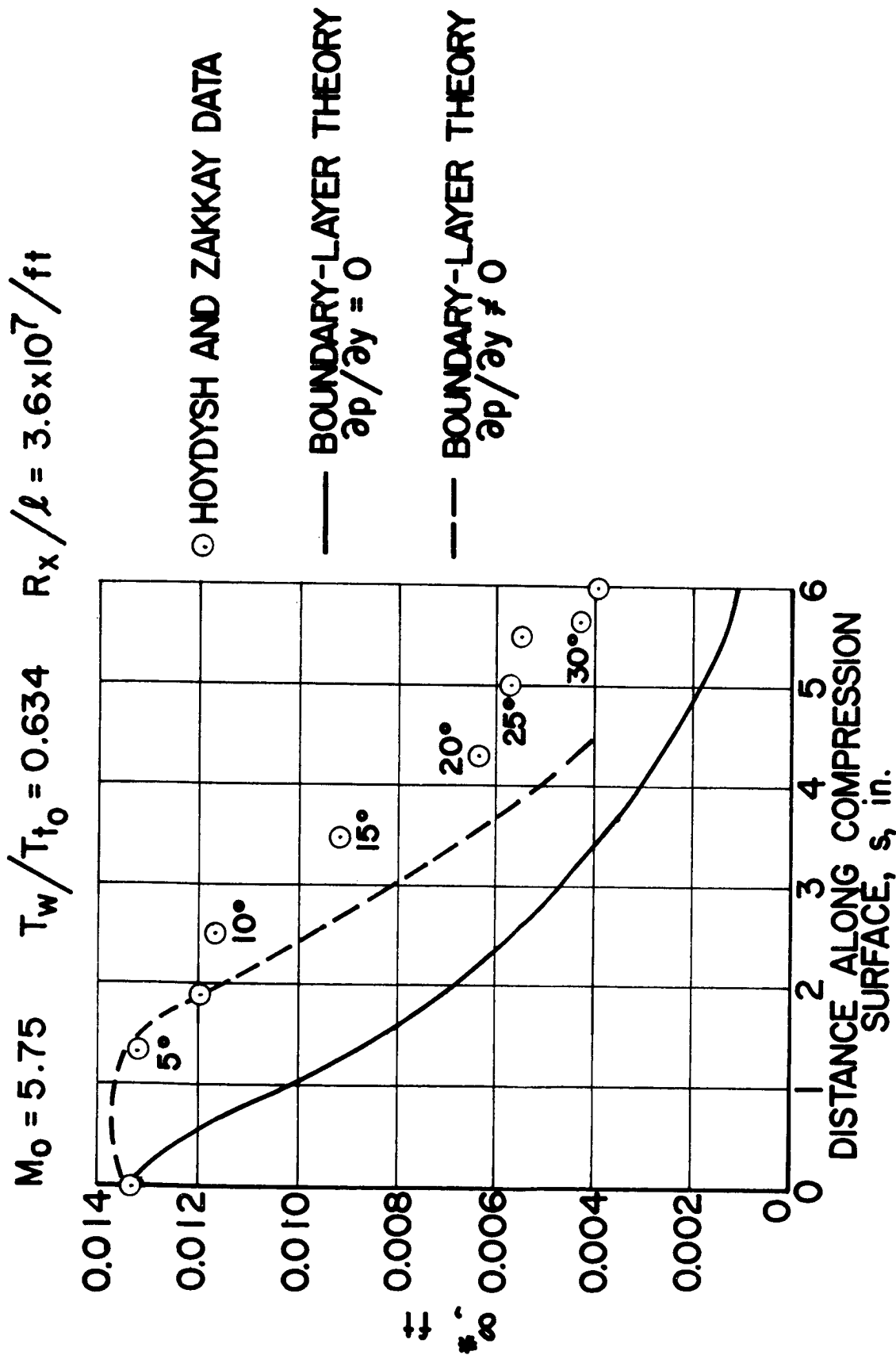


Figure 9.- Prediction of boundary-layer displacement thickness including effect of normal pressure gradients.

$$M_0 = 5.75 \quad T_w / T_{t_0} = 0.634 \quad R_x / \ell = 3.6 \times 10^7 / \text{ft}$$

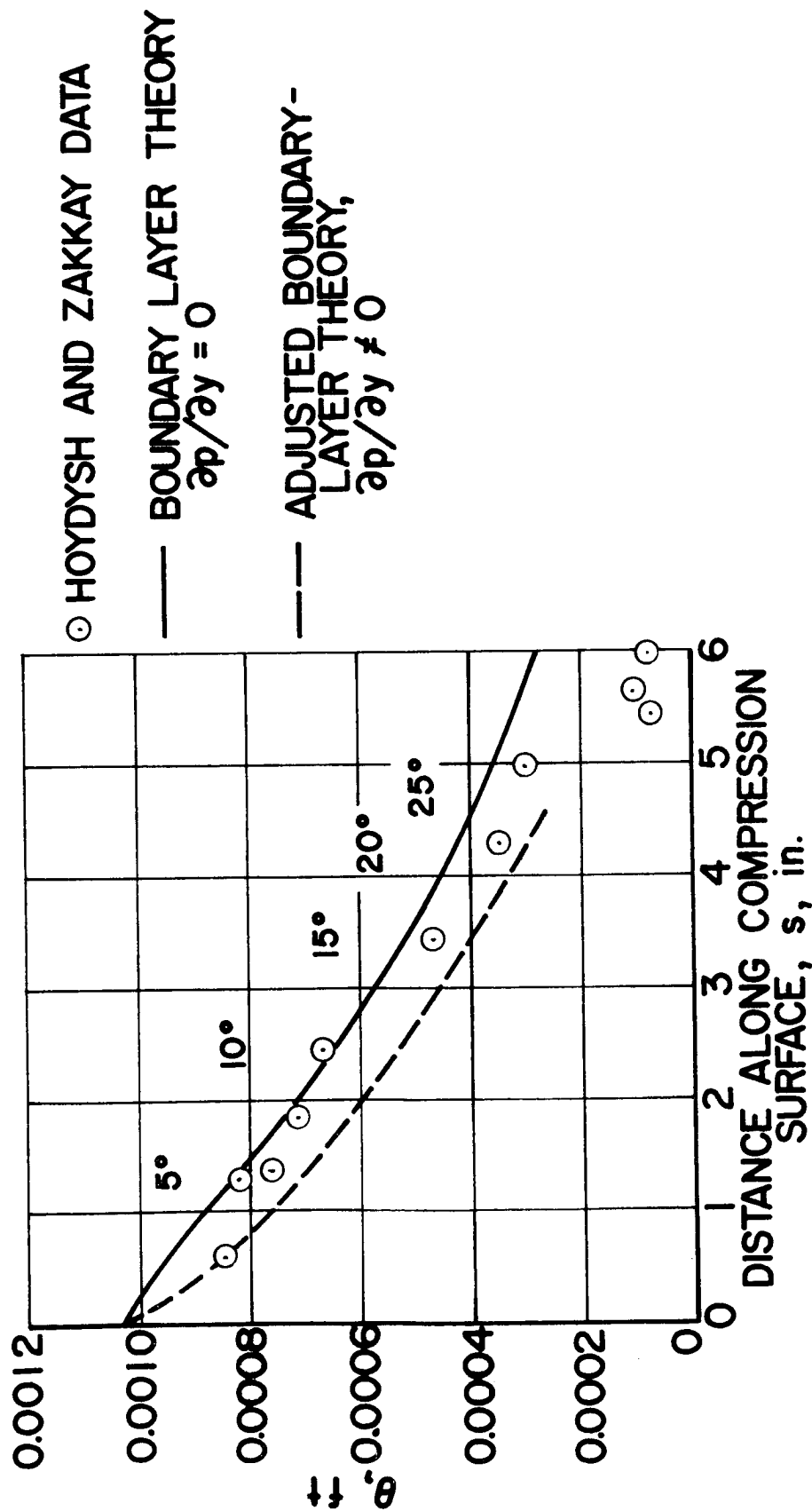


Figure 10.- Prediction of boundary-layer momentum thickness including effects of normal pressure gradients.

# SOME RECENT WORK ON COMPRESSIBLE TURBULENT BOUNDARY

## LAYERS AND EXCRESCENCE DRAG

By K.G. Winter and L. Gaudet

Royal Aircraft Establishment, Bedford, U.K.

### SUMMARY

The analysis, leading to a simple method of calculating skin friction and profiles, of boundary layer characteristics at high Reynolds number and Mach numbers between 0.2 and 2.8 measured on the sidewall of the 8ft x 8ft tunnel is described. An extension to include the effects of surface roughness is indicated. Some results are also given for the drag of discrete excrescences immersed in a turbulent boundary layer.

### INTRODUCTION

This note summarises some of the recent work undertaken in the Royal Aircraft Establishment with the aim of improving the estimation of the surface friction drag of aircraft including the effects of distributed surface roughness and discrete excrescences. The major experiment has been the measurement of the surface shearing stress and boundary layer characteristics on the sidewall of the 8ft x 8ft wind tunnel, in which situation large Reynolds numbers can be achieved. Some results of this experiment have been published but it is considered that the subsequent analysis of the results described herein has revealed characteristics of turbulent boundary layers at compressible speeds which are of general interest. Since the preparation of ref.1 further data has been obtained. This together with the reanalysis of the experiment has led to some modification of the conclusions of ref.1.

A tentative extension of the method for calculating flat plate turbulent boundary layers to include the effects of distributed roughness is proposed and compared with measurements of the drag of roughened cones.

The measurements made on the tunnel sidewall have been extended to the drag of discrete excrescences totally or partially immersed in the boundary layer. Some preliminary results are given.



# SYMBOLS

$C_1$	defined by equation (3)
$C_2$	defined by equation (4)
$c_f$	local skin friction coefficient
$C_F$	mean skin friction coefficient
$C_D$	drag coefficient
$C_L$	lift coefficient
$f$	roughness function
$F$	velocity defect function
$F_c$	compressibility factor on skin friction
$F_\delta$	compressibility factor on momentum thickness
$F_k$	compressibility factor on roughness Reynolds number
$H_{12}$	boundary layer shape factor = $\delta_1/\delta_2$
$H_{12}^i$	'incompressible' boundary layer shape factor = $\delta_1^i/\delta_2^i$
$k$	roughness height
$M$	Mach number
$r$	recovery factor
$Re_k$	roughness Reynolds number = $u_\delta k/\nu_\delta$
$Re_x$	streamwise length Reynolds number = $u_\delta x/\nu_\delta$
$Re_{\delta_2}$	momentum thickness Reynolds number = $\frac{u_\delta \delta_2}{\nu_\delta}$
$T$	ambient temperature
$T_t$	total temperature
$u$	velocity

$u_\tau$	friction velocity
$x$	longitudinal distance
$y$	distance from wall
$\delta$	boundary layer thickness
$\delta_1$	displacement thickness = $\int_0^\delta \left(1 - \frac{\rho u}{\rho_\delta u_\delta}\right) dy$
$\delta_2$	momentum thickness = $\int_0^\delta \frac{\rho u}{\rho_\delta u_\delta} \left(1 - \frac{u}{u_\delta}\right) dy$
$\delta_1^i$	= $\int_0^\delta \left(1 - \frac{u}{u_\delta}\right) dy$
$\delta_2^i$	= $\int_0^\delta \frac{u}{u_\delta} \left(1 - \frac{u}{u_\delta}\right) dy$
$\Delta$	energy thickness = $\int \frac{\rho u}{\rho_\delta u_\delta} \left(\frac{T_t}{T_{t\delta}} - 1\right) dy$
$\varphi$	wake function
$\kappa$	mixing length constant
$\nu$	kinematic viscosity
$\mu$	viscosity
$\rho$	density

Superscript i refers to equivalent incompressible conditions

Subscript w refers to wall conditions

Subscript  $\delta$  refers to conditions at edge of boundary layer

## FLAT PLATE TURBULENT BOUNDARY LAYERS AT HIGH REYNOLDS NUMBER

### Measurements

The measurements were made on the sidewall of the RAE 8ft x 8ft Wind Tunnel over a Mach number range from 0.2 to 2.8. A preliminary

description of the experiment has been given in ref.1.

The measurements consisted of surface shearing stress obtained directly using a force balance and velocity and temperature profiles. All the measurements were taken at one station, with a range of Reynolds numbers obtained by variation of stagnation pressure. The effective run of the boundary layer was determined as about 40 feet at subsonic speeds and about 30 feet at supersonic speeds, giving Reynolds numbers up to about 200 million at low speed ( $M = 0.2$ ) and up to about 100 million in supersonic flow.

### Analysis

The basis of the analysis is the observation, illustrated in Fig.1, that for the Mach number range of the experiment (up to  $M = 2.8$ ), the boundary layer shape parameter is uniquely related to the Reynolds number based on momentum thickness, provided the parameters are evaluated as though the boundary layers were incompressible. That is

$$H_{12}^i = H_{12}^i \left( \frac{\rho_\delta u_\delta \delta_2^i}{\mu_\delta} \right) \quad (1)$$

where superscript  $i$  denotes that density is taken to be constant, and subscript  $\delta$  denotes conditions at the edge of the boundary layer.

By utilising the concept of a velocity defect function the shape parameter can be related to the local skin friction coefficient (in the form of  $u_\tau^i$ , the 'incompressible' friction velocity, the definition of which for compressible flow has still to be determined) as follows:

$$\frac{u_\delta - u}{u_\tau^i} = F\left(\frac{y}{\delta}\right) \quad (2)$$

$$\text{hence} \quad C_1 = \frac{u_\delta}{u_\tau^i} \frac{\delta_1^i}{\delta} = \int_0^1 F\left(\frac{y}{\delta}\right) d\left(\frac{y}{\delta}\right) \quad (3)$$

$$C_2 = \left(\frac{u_\delta}{u_\tau^i}\right)^2 \frac{\delta_1^i - \delta_2^i}{\delta} = \int_0^1 F^2\left(\frac{y}{\delta}\right) d\left(\frac{y}{\delta}\right) \quad (4)$$

$$\text{and} \quad \frac{1}{H_{12}^i} = 1 - \frac{u_\tau^i}{u_\delta} \frac{C_2}{C_1} \quad (5)$$

Taking a velocity profile of the form

$$\frac{u_i}{u_\tau} = \frac{1}{\kappa} \log \left( \frac{y u_\tau^i}{\nu_\delta} \right) + \varphi \left( \frac{y}{\delta} \right) \quad (6)$$

and evaluating at the edge of the boundary layer gives

$$\frac{u_\delta}{u_\tau} = \frac{1}{\kappa} \log \left( \frac{\delta u_\tau^i}{\nu_\delta} \right) + \varphi(1) \quad (7)$$

Hence a momentum thickness Reynolds number can be expressed in terms of the friction velocity by using equations (3) and (7) to give

$$Re_{\delta_2}^i = \frac{C_1}{H_{12}^i} e^{-\kappa\varphi(1)} e^{\frac{\kappa u_\delta}{u_\tau^i}} \quad (8)$$

and eliminating the friction velocity by using equation (5) gives

$$Re_{\delta_2}^i = C_1 e^{-\kappa\varphi(1)} \frac{1}{H_{12}^i} e^{\frac{\kappa C_2}{C_1} \frac{1}{1 - \frac{1}{H_{12}^i}}} \quad (9)$$

An evaluation of equation (9) is shown on Fig.1, with the following values of the constants:

$$\begin{aligned} \frac{C_2}{C_1} &= 6.55 \\ \kappa &= 0.38 \\ C_1 e^{-\kappa\varphi(1)} &= 0.389 \end{aligned} \quad (10)$$

The first of these constants was derived from a least-squares fit of data at  $M = 0.2$  to equation (5). The values for the other two were derived from a least-squares fit of all the experimental data to equation (9).

Apart from scatter at low Reynolds numbers where the data is inaccurate the form of the variation of  $H_{12}^i$  with  $Re_{\delta_2}^i$  is well represented by equation (9).

By elimination of  $H_{12}^i$  from equation (8) by means of (5) the following skin friction equation results

$$\text{Re}_{\delta_2^i} = C_1 e^{-\kappa \Phi(1)} \left( 1 - \frac{u_\tau^i}{u_\delta^i} \frac{C_2}{C_1} \right) e^{\frac{\kappa u_\delta^i}{u_\tau^i}} \quad (11)$$

In order to make use of equation (11) as a skin friction law in compressible flow, it is necessary to determine factors as a function of Mach number to relate  $u_\tau^i$  to  $u_\tau$  and  $\delta_2^i$  to  $\delta_2$ . We define

$$F_c = \left( \frac{u_\tau^i}{u_\tau} \right)^2 \quad (12)$$

and

$$F_\delta = \frac{\delta_2^i}{\delta_2} \quad (13)$$

$F_c$  was determined using equation (5) with measured values of  $u_\tau$ . Its variation with Mach number is shown in Fig. 2a. A plot of  $F_\delta$  against Mach number using equation (13) is given in Fig. 2b. The points plotted in these figures are for a range of Reynolds number at Mach numbers of 1.4, 2.2, and 2.8 but for a single Reynolds number only at other speeds. An appreciable scatter for  $F_c$  at  $M = 1.4$  is apparent, and a scatter for  $F_\delta$  at  $M = 2.2$ , with  $F_\delta$  decreasing as Reynolds number is increased.

The excellent correlation of local skin friction measurements with momentum thickness Reynolds number on the basis of equation (11) and the factors  $F_c$  and  $F_\delta$  is shown in Fig. 3.

For practical application both local and mean skin friction are required in terms of a Reynolds number based on streamwise length. Writing now  $\left( \frac{c_f^i}{2} \right)^{\frac{1}{2}} = \frac{u_\tau^i}{u_\delta^i}$ , the mean skin friction coefficient can be obtained from equation (11) as

$$c_F^i \text{Re}_x^i = 2C_1 e^{-\kappa \Phi(1)} \left[ 1 - \left( \frac{c_f^i}{2} \right)^{\frac{1}{2}} \frac{C_2}{C_1} \right] e^{\kappa \left( \frac{2}{c_f^i} \right)^{\frac{1}{2}}} \quad (14)$$

An approximate equation for local skin friction is the Von Karman formula in the form given by Coles<sup>2</sup>:

$$c_f^i \text{Re}_x^i = 2C_1 e^{-\kappa \Phi(1)} e^{\kappa \left( \frac{2}{c_f^i} \right)^{\frac{1}{2}}} \left[ 1 - \left( \frac{c_f^i}{2} \right)^{\frac{1}{2}} \left( \frac{2}{\kappa} + \frac{C_2}{C_1} \right) + \frac{1}{\kappa} c_f^i \left( \frac{1}{\kappa} + \frac{C_2}{C_1} \right) \right] \quad (15)$$

Where for compressible flow

$$\begin{aligned}
 c_f^i &= F_c c_f \\
 C_F^i &= F_c C_F \\
 Re_{\delta_2}^i &= F_\delta Re_{\delta_2} \\
 Re_x^i &= \frac{F_\delta}{F_c} Re_x
 \end{aligned}
 \tag{16}$$

Measurements at four Mach numbers are compared with equations (14) and (15) using the factors (16) in Fig.4 and can be seen to be in excellent agreement.

The good correlation of Fig.4 is, of course, to be expected since the data has been used to define the skin friction formulae. It is therefore interesting to compare with data from other sources. This has been done in Fig.5 where most of the available data for Mach numbers up to about 4, in which skin friction has been directly measured, has been plotted. The scatter is considerably increased compared with Fig.4 but it is difficult to discern any consistent trends of disagreement with the calculated line shown.

The results of the experiment at selected Mach numbers are compared in Fig.6 with some existing methods of estimating skin friction. In Fig. 6a mean skin friction is shown as a function of streamwise length Reynolds number as calculated by the Spalding and Chi<sup>22</sup> and Sommer and Short<sup>23</sup> methods. As can be seen there is little to choose between the various proposals but contrary to the previous conclusion of ref.1 the data at supersonic speed are better fitted to Sommer and Short than to Spalding and Chi. In Fig.6b the measured local skin friction, as a function of momentum thickness Reynolds number, is shown to agree well with the prediction of Coles<sup>24</sup> at low speed but is increasingly underestimated as Mach number increases.

### Velocity profiles

The velocity profiles are not shown. The variation in slope of the linear portion (in the usual semi-logarithmic plot) with Mach number is in good agreement with that predicted by equation (6). It is of interest, however, to check that the wake component in the velocity profile is independent of Mach number in the form of equation (6). From the profiles the wake component  $\frac{\Delta u}{u_\tau} = \phi\left(\frac{y}{\delta}\right)$  has been extracted and is shown in Fig.7.

Fig.7a shows that at a Mach number of 0.2, though there is some scatter, there is no systematic variation with Reynolds number. Fig.7b shows that the wake component is indeed independent of Mach number when expressed in

terms of the equivalent incompressible friction velocity  $u_\tau^i$ . A simple expression which fits the data in Fig.7 in the range  $0.13 < \frac{y}{\delta} < 1$  is

$$\frac{\Delta u}{u_\tau^i} = 0.89 \left[ 1 + \sin \pi \left( \frac{y/\delta - 0.483}{0.707} \right) \right] \quad (17)$$

This expression is more satisfactory than the 'cosine' wake component commonly used, in that when summed with the logarithmic component, zero slope of the velocity profile is obtained at the edge of the boundary layer. It is very similar in form to that suggested by Clauser<sup>12</sup> for constant pressure but its magnitude is only about two-thirds.

#### Temperature profiles

In calculating integral parameters from measured velocity profiles in experiments where the temperature profile has not been measured, a common assumption is that the modified Crocco profile obtains. For zero heat transfer this may be written in the form

$$\frac{\frac{1}{T} - \frac{1}{T_w}}{\frac{1}{T_\delta} - \frac{1}{T_w}} = \left( \frac{M}{M_\delta} \right)^2 \quad (18)$$

Measured temperatures for all profiles at a Mach number of 2.2 together with data from other sources are plotted in the manner suggested by equation (18) in Fig.8. The modified Crocco form in fact leads to an energy deficit in a boundary layer, and so, as expected in a boundary layer with zero heat transfer, the measured data fall below the Crocco line. There is reasonable agreement between the various data. A line of slope 0.98 times that of the Crocco line, though incorrect at the edge of the boundary layer, fits the data well and could be of practical use in calculating boundary layer profiles.

Fig.9a illustrates, for a typical point at a Mach number of 2.2, the distribution of relative energy flux across the boundary layer thickness. The compensation of the reduced energy flux near the wall by an increase over the outer part of the boundary layer is clearly shown. In Fig.9b values of energy thickness obtained for boundary layers over a range of Mach number from 1.4 to 2.8 are shown. There is scatter but the energy thickness is clearly shown to be small. To give a scale to the figure the energy thickness for the profile shown in Fig.9a has been calculated for a Crocco type temperature profile. This calculation gives a value of  $\frac{\Delta}{\delta} = -6 \times 10^{-3}$  ie. in excess of any of the values shown in Fig.9b.

As has been pointed out by Adcock et al,<sup>13</sup> the temperature assumption used in calculating the properties of a turbulent boundary layer from pitot pressure measurements alone can have a large effect on the integral parameters. This is illustrated for the present measurements and also for those of Adcock et al in Fig.10, where are plotted the errors incurred in  $\delta_2$ ,  $\delta_2^i$ ,  $H_{12}$ ,  $H_{12}^i$  for assumptions of either constant total temperature or the modified Crocco distribution with  $r = 0.89$ , compared with measured temperature distributions. The important point is that with  $r = 0.89$  momentum thickness will be in error by about 5% at  $M = 3$  and 10% at  $M = 6$ , but that with constant total temperature the errors are small. The 'incompressible' shape parameter  $H_{12}^i$  is however better calculated taking  $r = 0.89$ .

## EFFECT OF DISTRIBUTED ROUGHNESS

### Extension of calculation method

For incompressible flow the velocity profile, over a surface with roughness height  $k$ , can be expressed as

$$\frac{u}{u_\tau} = \frac{1}{\kappa} \log\left(\frac{yu_\tau}{\nu}\right) + \phi\left(\frac{y}{\delta}\right) + f\left(\frac{\kappa u_\tau}{\nu}\right) \quad (19)$$

where the function  $f$  is in fact negative and, as shown by Clauser<sup>12</sup>, its form is dependent upon the type of roughness. In the present calculations the form derived by Nikuradse<sup>17</sup> has been assumed.

It has been shown by Hama<sup>16</sup> that equation (5) is applicable to boundary layers on rough walls, hence, the skin friction law is given by a modified form of equation (11) as

$$Re_{\delta_2} = C_1 e^{-\kappa\phi(1)} \left(1 - \frac{u_\tau}{u_\delta} \frac{C_2}{C_1}\right) e^{\frac{\kappa u_\tau}{u_\delta} - \kappa f} \quad (20)$$

By use of this equation with a Nikuradse type function  $f$ , together with a numerical integration,

$$Re_x = 2 \int \frac{1}{c_f} d(Re_{\delta_2}) \quad (21)$$

calculations have been made of the boundary layer development on a flat plate in incompressible flow. It is convenient to use as a parameter in these calculations a roughness Reynolds number

$$Re_k = \frac{\kappa u_\delta}{\nu_\delta} \quad (22)$$



$$\text{so that for incompressible flow } \frac{ku\tau}{\nu} = Re_k \left(\frac{\rho f}{2}\right)^{\frac{1}{2}} \quad (23)$$

Fig.11 shows the results of the calculations in terms of the ratio of the mean skin friction coefficient of a rough surface to that of a smooth surface as a function of  $Re_k$  for a range of Reynolds number based on streamwise length.

The results of Fig.11 are for incompressible flow. For compressible flow equivalent values of the various parameters are required. We have shown that the incompressible profile for a smooth wall is applicable to compressible flow, provided that an effective friction velocity  $u^i$  is used. It is suggested that the factors  $F_o$  and  $F_\delta$  are still valid in compressible flow over a rough wall. However, it is likely that conditions at the wall control the behaviour of the roughness function

$$f = f \left( \frac{ku\tau_w}{\nu_w} \right) \quad (24)$$

Hence it is proposed that the equivalent value of  $Re_k$  is that to give the same value of  $\frac{ku\tau_w}{\nu_w}$  as for incompressible flow. We therefore define a roughness

factor  $F_k$  where

$$Re_k^i = F_k Re_k \quad (25)$$

$$\text{with } F_k = \left(\frac{\rho\delta}{\rho_w}\right)^{\frac{1}{2}} \left(\frac{\nu\delta}{\nu_w}\right) \frac{1}{(F_o)^{\frac{1}{2}}} \quad (26)$$

The inset graph in Fig.11 shows the variation of  $F_k$  with Mach number.

#### Comparison with experiment

A comparison with measurements made in the RAE 8ft x 8ft wind tunnel of the drag of cones of various surface finish has been made. (Though this comparison only is shown, it should be remarked that the calculations are in fair agreement with the measurements of Fenter<sup>25</sup>. The predicted skin friction is somewhat lower than he obtained for roughened plates but the predicted ratio of the drag of rough to smooth plates is in good agreement with his measurements). The cones were of 10 degree total angle, 5 feet long. One cone had a smooth surface, three others had the steel surface photo-etched over the middle 3 foot length of the cone. In fact the smooth rear frustum, of length 1 foot, was common to all cones. The depth of etching was 0.002, 0.004 and 0.010 in., leaving a raised pattern of triangles which was geometrically similar for the three depths and gave a ratio of raised surface area to total surface area of between 10 and 15%. The cones were mounted on a balance via a sting support, which also carried a block close behind the base of the cones and extending the conical surface. It was hoped in this way that the pressure forces on the cones would be small. However, the pressure in the slit at the cone base was found to be very sensitive to the boundary layer conditions on

the cone surface, and the accuracy of the measurement of skin friction was degraded by the necessity to apply a large and varying pressure drag correction.

A transition trip of eight glass beads of 0.020 in. diameter was fixed 0.5 in. from the apex of the cones. It is of interest firstly to compare the skin friction drag of the cones with that predicted by the method described in the previous section. In order to calculate the drag the boundary layer momentum equation, including a divergence term, was integrated step by step, with the local skin friction being given by equation (11). It was thus assumed that the boundary layer shape parameter is unaffected by divergence of the flow in the absence of pressure gradient. As can be seen in Fig.12 the predictions are good within the accuracy of the measurements, which is probably no better than about 10%. The establishment of fully turbulent flow is in good agreement with the correlation suggested by Evans<sup>18</sup>. The predicted drag variation with partially laminar flow using the transition position observed by schlieren corresponds reasonably well with the measured drag. A useful result obtained from the calculations is that the mean skin friction coefficient is the same as that on a flat plate with the Reynolds number factored by 0.82.

To calculate the friction drag of the cones with roughened surfaces a similar procedure has been adopted as for the smooth surface but with the local skin friction coefficient given by equation (20). At the start and finish of the rough region continuity of momentum thickness has been taken but an abrupt change in local skin friction coefficient has been assumed to occur. The calculations are compared with the measurements in Fig.13. It should be noted that the calculated drag for the smooth cone in Fig.13 is very slightly smaller than that in Fig.12 because of different starting conditions taken in the integration procedure. The calculated curves in Fig.13 for various roughness are self consistent.

The measured skin friction coefficients with roughness are even less satisfactory than for the smooth cones. The presence of the roughness on the model surface prevented accurate measurement of the pressure force and the values found for the smooth cones have also been applied to all cones. Because of the lack of accuracy in the experiments it is difficult to draw any firm conclusions. For a fully rough surface the drag will become independent of Reynolds number. For the cones, which have part of their surface only roughened, there is to be expected a small reduction in drag with increase of Reynolds number even when the roughened portion is in the fully rough régime. Except at  $M = 1.4$  the predicted rate of reduction of drag is exhibited by the experiments, giving some confirmation of the calculation method. Clearly, however, the experiments cannot be used as a definitive check of the proposals of the previous section, nor can a roughness function, which may be different from that for sand grain roughness because of the nature of the surface, be adequately described.

#### DRAG OF EXCRESCENCES

Subsequent to the measurement of the boundary layer characteristics on the sidewall of the 8ft x 8ft tunnel an extension to the work has been initiated<sup>19</sup> in which the drag is measured of various excrescences totally or

partially immersed in the boundary layer. The excrescences, which are intended to be typical of those found on aircraft, include two-dimensional forms such as steps and ridges and three-dimensional forms such as circular cylinders and half bodies of revolution. The excrescences are mounted on strain gauge balances of the type used to measure skin friction and the experiments cover a Mach number range from 0.2 to 2.8 and a range of Reynolds numbers.

Some preliminary results for the drag of a ridge of square section are given in Fig.14. It is shown that the drag coefficient based on frontal area of ridges of various heights, but which are small compared with the boundary layer thickness, can be correlated in terms of the local skin friction coefficient as a function of a roughness Reynolds number evaluated at the wall. The correlation is however Mach number dependent.<sup>20</sup> The results at a Mach number of 0.2 are in good agreement with Wieghardt's results at low speed.

As a check of the application of a magnification factor for the drag of local excrescences in pressure gradients as proposed by Nash and Bradshaw<sup>21</sup>, measurements of the drag increment of a similar ridge mounted separately on the upper and lower surfaces of an aerofoil have been made by T.A. Cook. The ridge height was 0.14% of the chord length in both cases, corresponding to three times the local boundary layer momentum thickness for the upper surface, and to the same as the momentum thickness for the lower surface, where the ridge was mounted further aft.

The local increments in drag coefficient, estimated from a correlation of the type shown in Fig.14, varied slightly with the angle of incidence of the aerofoil but were approximately 0.001 for the upper surface and 0.0008 for the lower surface, so that experimentally determined magnification factors varied between about 1.5 and 3.5. The estimate on Fig.15 which uses magnification factors from Ref.21 is seen to be in good agreement with the measurements.

#### CONCLUDING REMARKS

The simple method described of calculating compressible turbulent boundary layers at constant pressure and without heat transfer describes very precisely the measurements from which it was derived. It is not in conflict with published data up to a Mach number of 4. Boundary layer measurements with heat transfer occurring have not yet been studied. It will be interesting to determine whether the simple relationship proposed for shape parameter is still valid for flows with heat transfer.

Further study is also needed to validate the proposed method of calculation for flows over rough surfaces.

It is shown that a correlation of the drag of an isolated ridge immersed in a flat plate turbulent boundary layer can be applied locally to a flow with a pressure gradient but that the total drag increment must take account of the pressure gradient.

## REFERENCES

1. Winter, K. G.; Smith, K. G.; and Gaudet, L.: Measurements of Turbulent Skin Friction at High Reynolds Numbers at Mach Numbers of 0.2 and 2.2. AGARDograph 97, May 1965, pp. 97-124.
2. Coles, Donald: Measurements of Turbulent Friction on a Smooth Flat Plate in Supersonic Flow. J. Aeronaut. Sci., vol. 21, no. 7, July 1954, pp. 443-448.
3. Smith, Donald W.; and Walker, John H.: Skin-Friction Measurements in Incompressible Flow. NASA TR R-26, 1959. (Supersedes NACA TN 4231.)
4. Schultz-Grunow, F.: New Frictional Resistance Law for Smooth Plates. NACA TM 986, 1941.
5. Kempf, G.: Weitere Reibungsergebnisse an ebenen glatten und rauhen Flächen. Hydromechanische Probleme des Schiffsantriebs, 1932, pp. 74-82.
6. Dhawan, Satish: Direct Measurements of Skin Friction. NACA Rep. 1121, 1953. (Supersedes NACA TN 2567.)
7. Monta, William J.; and Allen, Jerry M.: Local Turbulent Skin-Friction Measurements on a Flat Plate at Mach Numbers From 2.5 to 4.5 and Reynolds Numbers up to  $69 \times 10^6$ . NASA TN D-2896, 1965.
8. Matting, Fred W.; Chapman, Dean R.; Nyholm, Jack R.; and Thomas, Andrew G.: Turbulent Skin Friction at High Mach Numbers and Reynolds Numbers in Air and Helium. NASA TR R-82, 1961.
9. Moore, D. R.; and Harkness, J.: Experimental Investigations of the Compressible Turbulent Boundary Layer at Very High Reynolds Numbers. AIAA J., vol. 3, no. 4, Apr. 1965, pp. 631-638.
10. Shutts, W. H.; Hartwig, W. H.; and Weiler, J. E.: Final Report on Turbulent Boundary-Layer and Skin-Friction Measurements on a Smooth, Thermally Insulated Flat Plate at Supersonic Speeds. DRL-364, CM-823 (Contract NOrd-9195), Univ. of Texas, Jan. 5, 1955.
11. Jackson, Mary W.; Czarnecki, K. R.; and Monta, William J.: Turbulent Skin Friction at High Reynolds Numbers and Low Supersonic Velocities. NASA TN D-2687, 1965.
12. Clauser, Francis H.: The Turbulent Boundary Layer. Vol. IV of Advances in Applied Mechanics, H. L. Dryden and Th. von Kármán, eds., Academic Press, Inc., 1956, pp. 1-51.
13. Adcock, Jerry B.; Peterson, John B., Jr.; and McRee, Donald I.: Experimental Investigation of a Turbulent Boundary Layer at Mach 6, High Reynolds Numbers, and Zero Heat Transfer. NASA TN D-2907, 1965.

14. Nothwang, George J.: An Evaluation of Four Experimental Methods for Measuring Mean Properties of a Supersonic Turbulent Boundary Layer. NACA Rep. 1320, 1957. (Supersedes NACA TN 3721.)
15. Bradfield, W. S.: Conical Turbulent Boundary Layer Experiments and a Correlation With Flat Plate Data. Trans. ASME, Ser. C.: J. Heat Transfer, vol. 82, no. 2, May 1960, pp. 94-100.
16. Hama, Francis R.: Boundary-Layer Characteristics for Smooth and Rough Surfaces. Trans. Soc. Nav. Architects Mar. Eng., vol. 62, 1954, pp. 333-358.
17. Nikuradse, J.: Laws of Flow in Rough Pipes. NACA TM 1292, 1950.
18. Evans, J. Y. G.: Transition Fixing Techniques and the Interpretation of Boundary Layer Conditions on Slender Wings in Supersonic Wind Tunnels. AIAA Aerodynamic Testing Conference, Mar. 1964, pp. 50-58.
19. Winter, K. G.; and Gaudet, L.: A Programme of Tests on the Drag of Excrescences Proposed for the 8 ft x 8 ft Wind Tunnel and a Brief Analysis of Some Previous Measurements. Unpublished Mintech Report.
20. Wieghardt, K.: Increase of the Turbulent Frictional Resistance Caused by Surface Irregularities. Rep. Transl. No. 103, Brit. M.A.P. Völkenrode, June 15, 1946.
21. Nash, J. F.; and Bradshaw, P.: The Magnification of Roughness Drag by Pressure Gradients. J. Roy. Aeronaut. Soc. (Tech. Notes), vol. 71, no. 673, Jan. 1967, pp. 44-46.
22. Spalding, D. B.; and Chi, S. W.: The Drag of a Compressible Turbulent Boundary Layer on a Smooth Flat Plate With and Without Heat Transfer. J. Fluid Mech., vol. 18, pt. 1, Jan. 1964, pp. 117-143.
23. Sommer, Simon C.; and Short, Barbara J.: Free-Flight Measurements of Turbulent-Boundary-Layer Skin Friction in the Presence of Severe Aerodynamic Heating at Mach Numbers From 2.8 to 7.0. NACA TN 3391, 1955.
24. Coles, D. E.: The Turbulent Boundary Layer in a Compressible Fluid. U.S. Air Force Proj. RAND Rep. R-403-PR, RAND Corp., Sept. 1962.
25. Fenter, Felix W.: Analysis and Direct Measurement of the Skin Friction of Uniformly Rough Surfaces at Supersonic Speeds. Preprint No. 837, Inst. Aeronaut. Sci., July 1958.

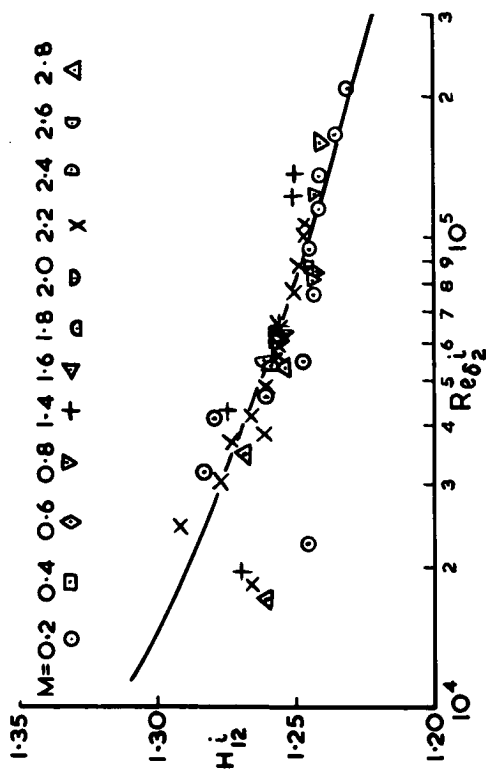
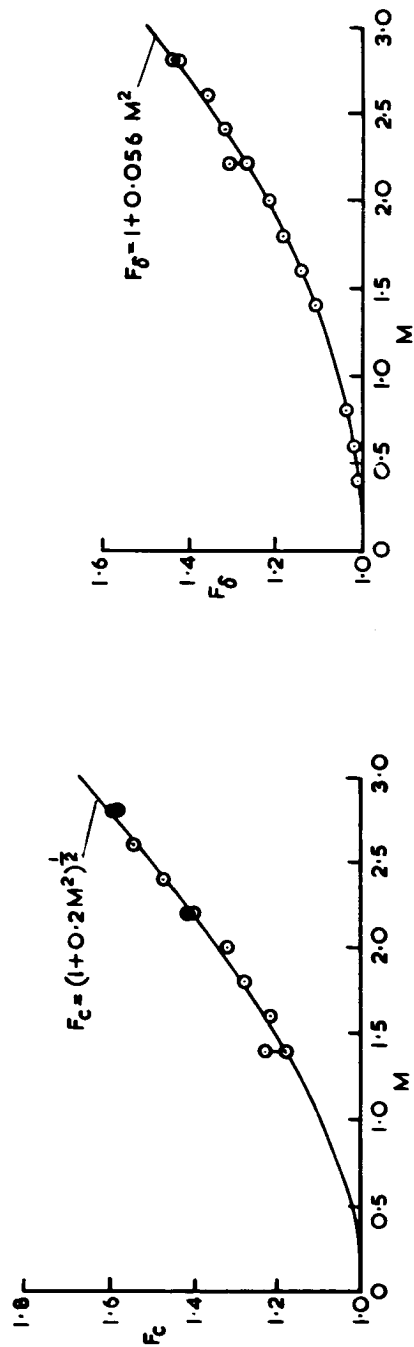


Figure 1.- Variation of 'incompressible' shape parameter with Reynolds number.



(a) For skin friction.

(b) For momentum thickness.

Figure 2.- Compressibility factors.

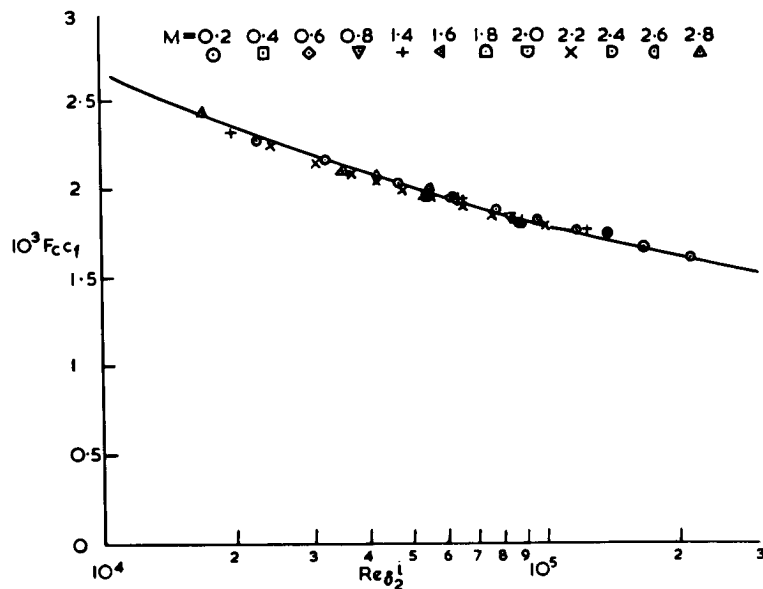


Figure 3.- Correlation of local skin friction with 'incompressible' momentum thickness Reynolds number.

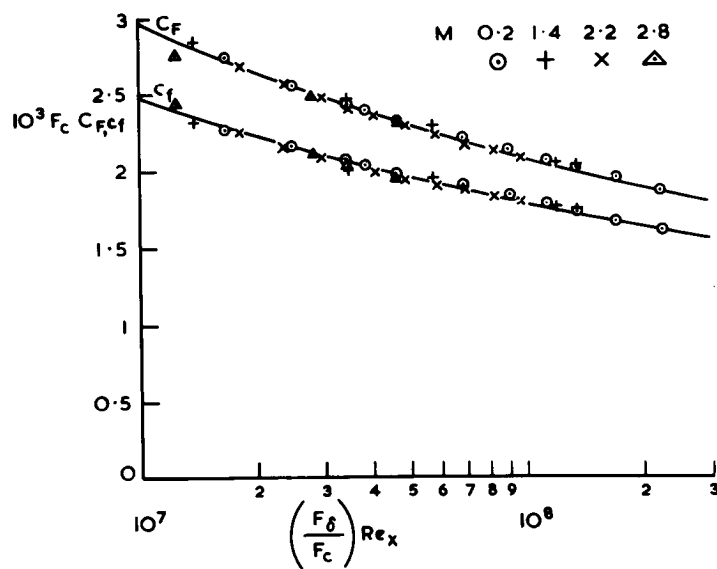


Figure 4.- Local and mean skin friction coefficients in terms of streamwise length Reynolds number.

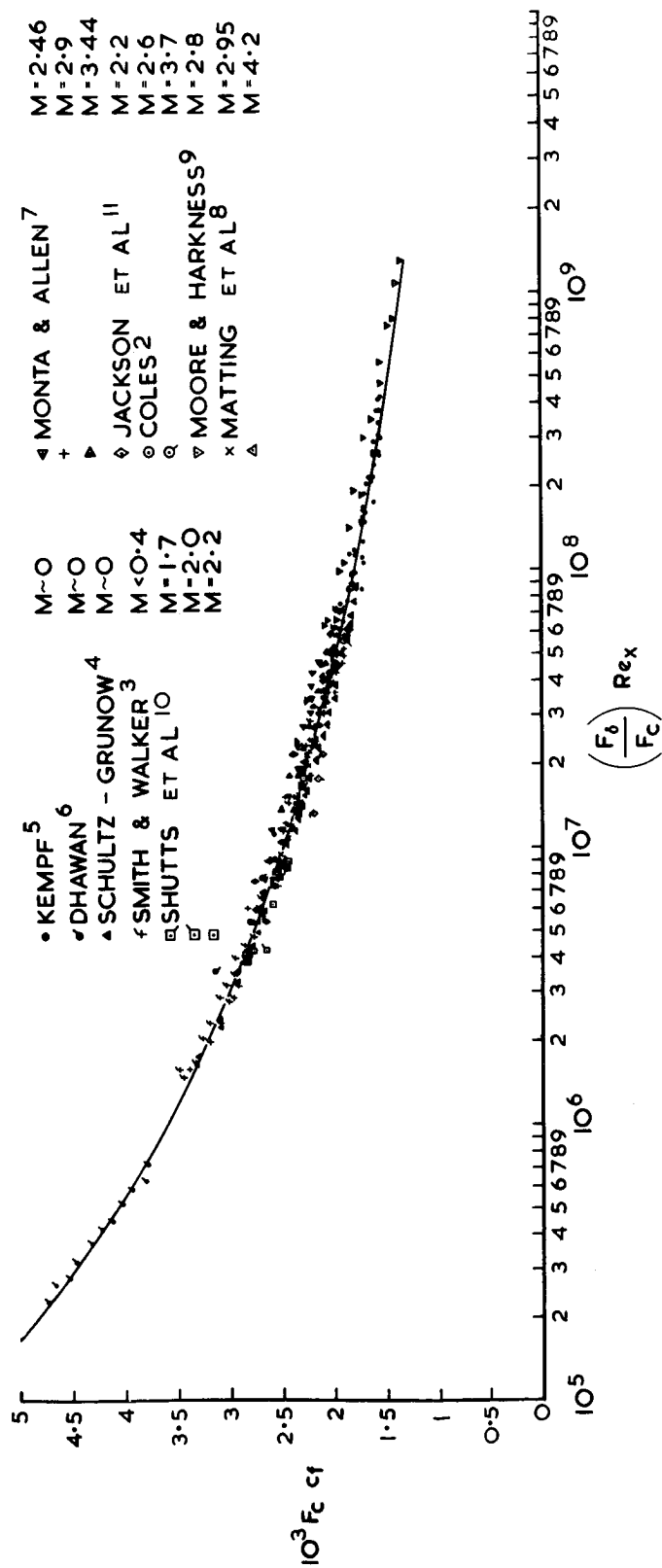
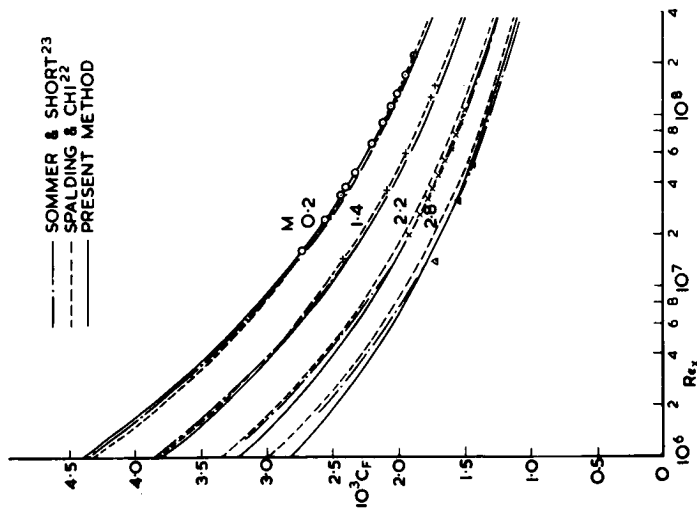
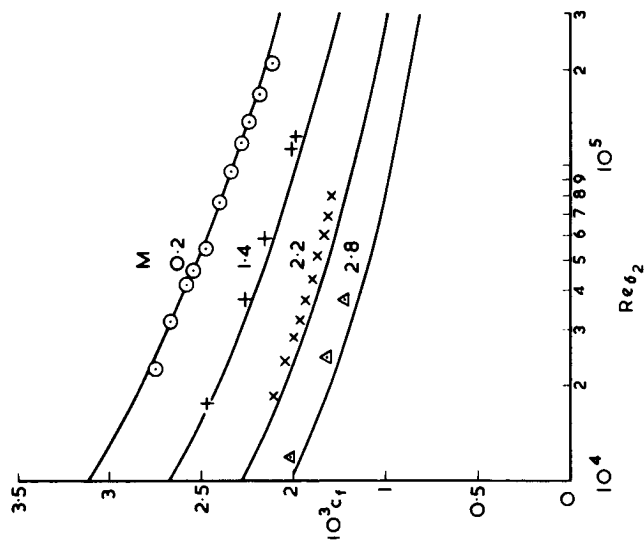


Figure 5.- Comparison of skin friction balance data with proposed correlation.



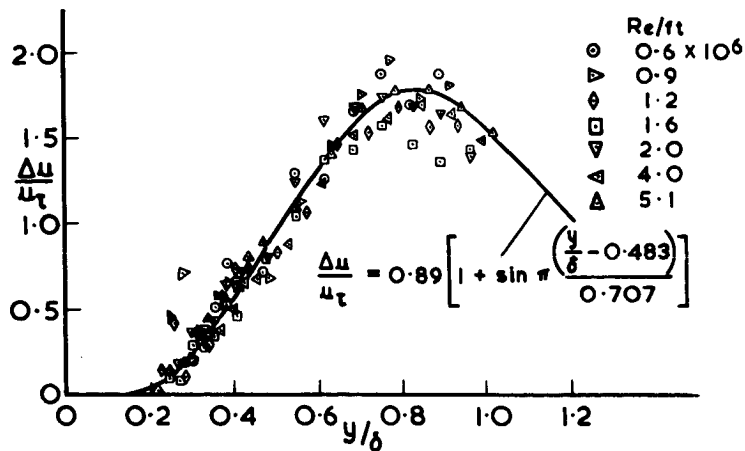


(a) Mean skin friction measurements compared with various methods.

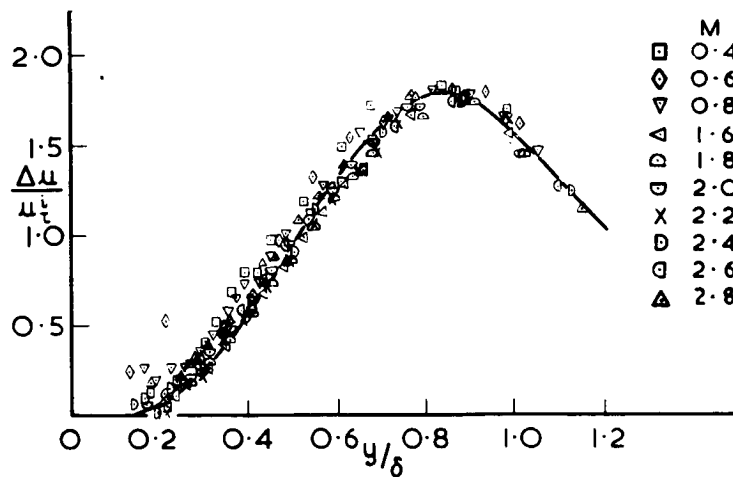


(b) Local skin friction measurements compared with Coles' predictions<sup>24</sup>.

Figure 6.- Comparison of skin friction measurements and various prediction methods.



(a) Range of Reynolds number,  $M = 0.2$ .



(b) Range of Mach number,  $Re/ft = 2 \times 10^6$ .

Figure 7.- Wake component of velocity profile.

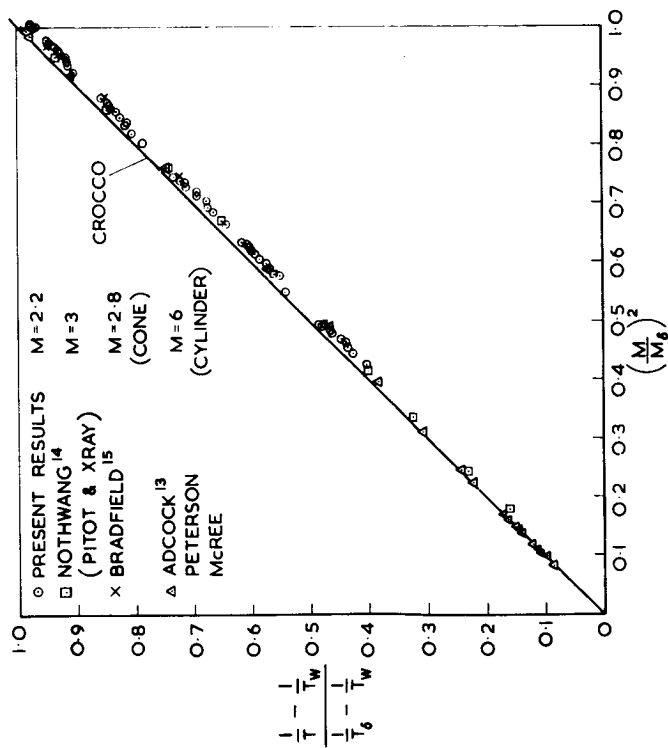


Figure 8.- Temperature - Mach number relationship.

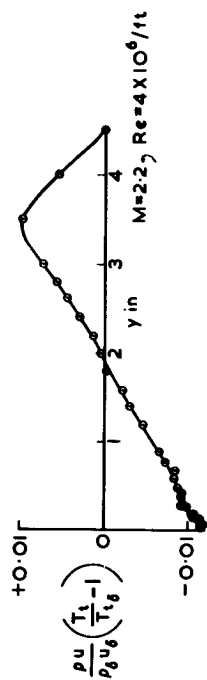


Figure 9(a).- Example of distribution of energy flux.

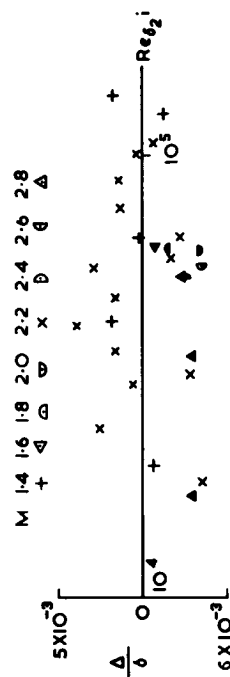


Figure 9(b).- Energy thickness.

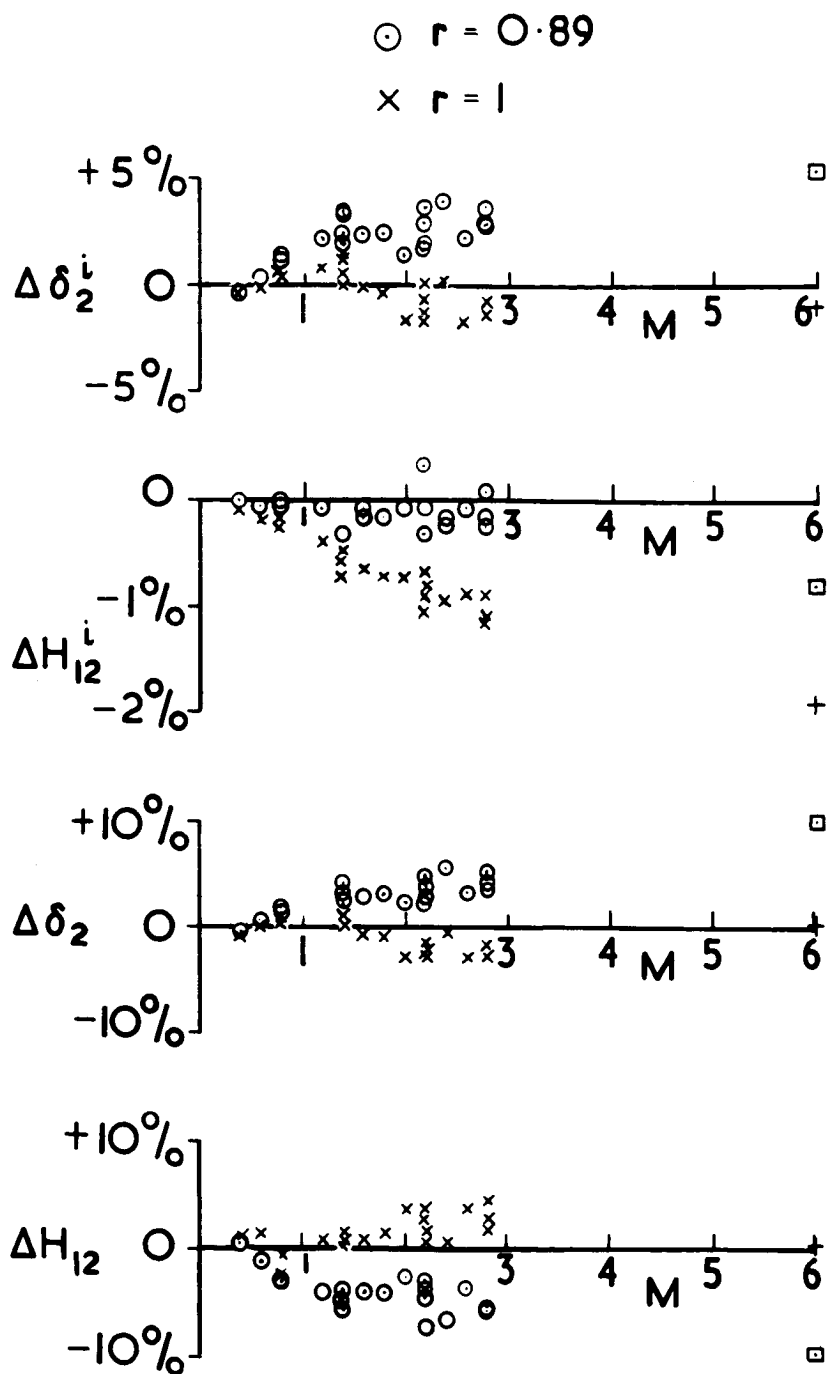


Figure 10.- Effect of assumed temperature distribution on momentum thickness and shape parameter.

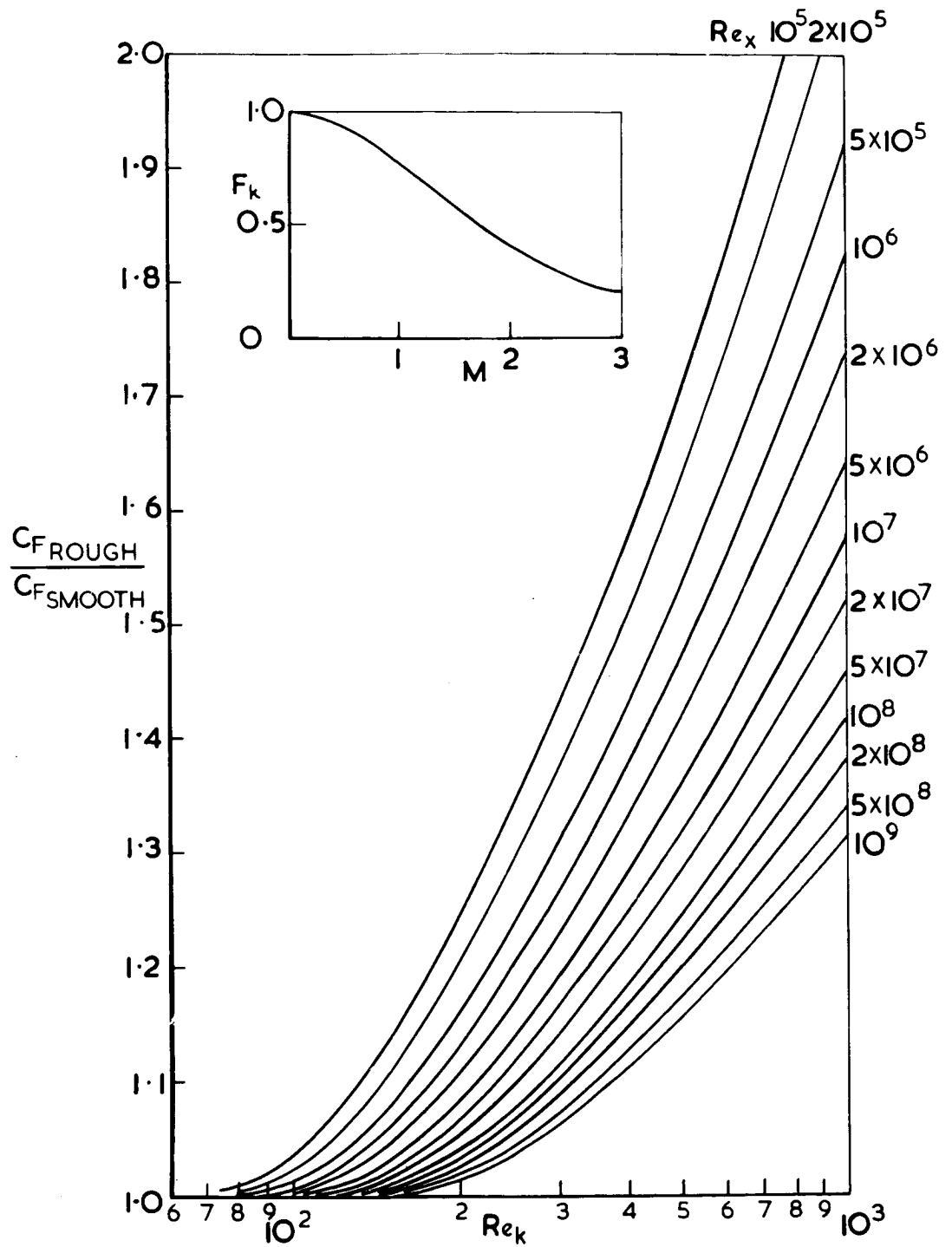
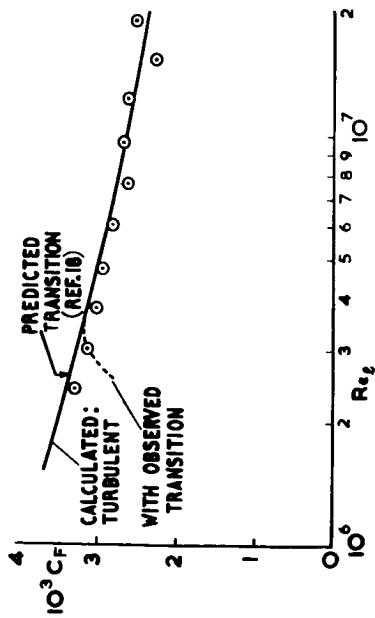
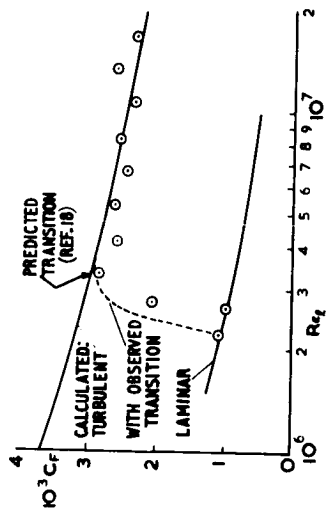


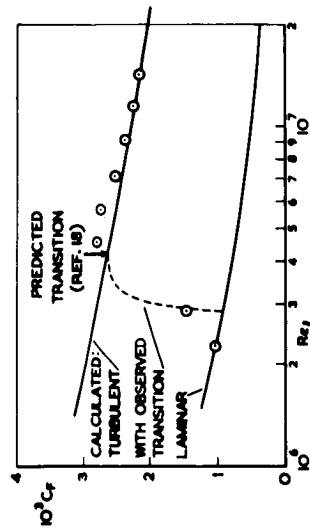
Figure 11.- Variation of increment in mean skin friction coefficient with roughness Reynolds number.



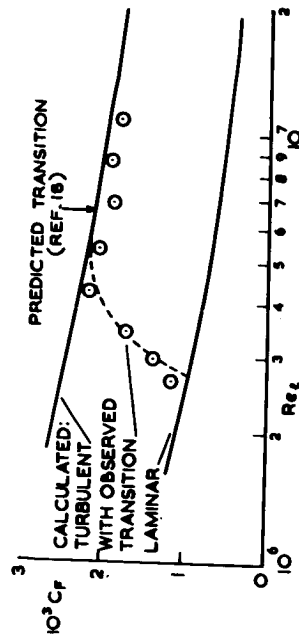
(a)  $M_\infty = 1.4$ .



(b)  $M_\infty = 1.8$ .



(c)  $M_\infty = 2.2$ .



(d)  $M_\infty = 2.8$ .

Figure 12.- Skin friction drag of 10 degree cone (smooth).  
 $Re_l$  is Reynolds number based on length.

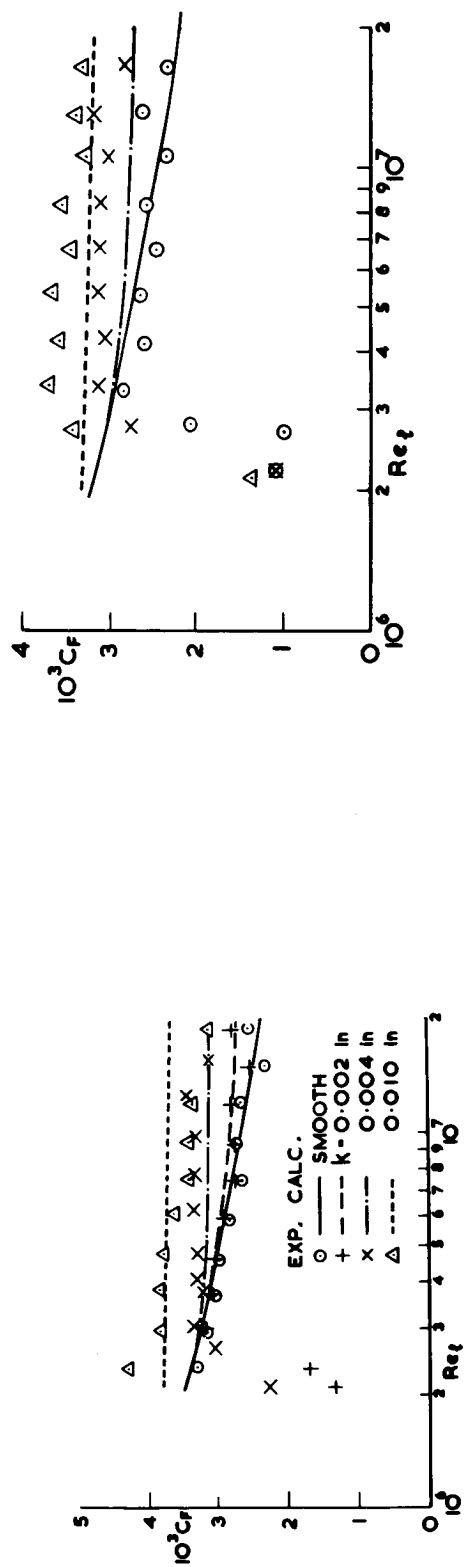
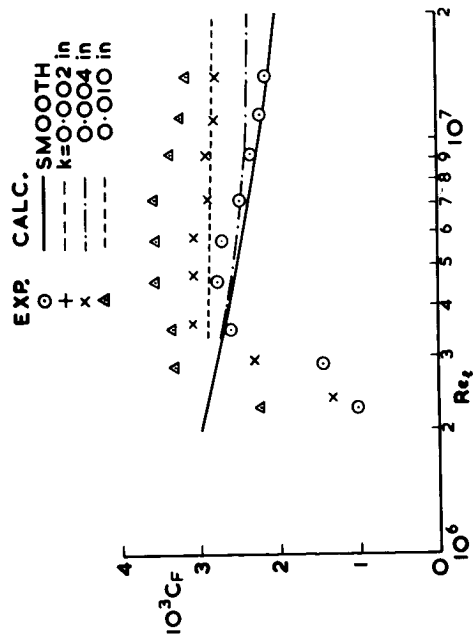
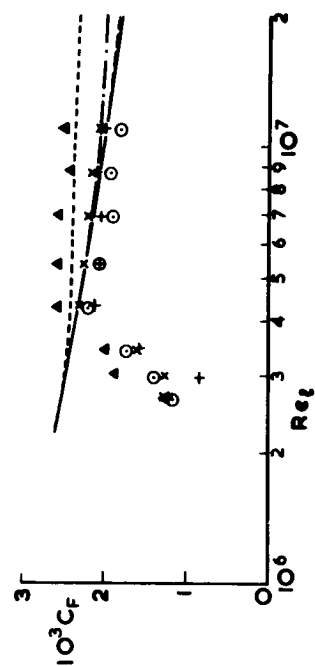
(a)  $M_\infty = 1.4$ .(b)  $M_\infty = 1.8$ .(c)  $M_\infty = 2.2$ .(d)  $M_\infty = 2.8$ .

Figure 13.- Skin friction drag of 10 degree cones with partially rough surfaces.  
 $Re_l$  is Reynolds number based on length.

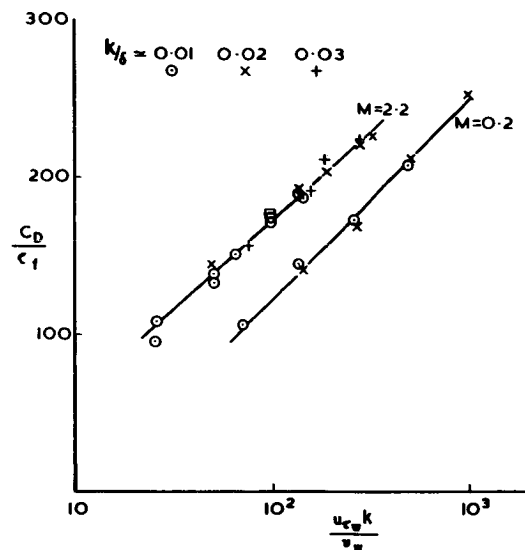


Figure 14.- Drag of square ridges immersed in a turbulent boundary layer.

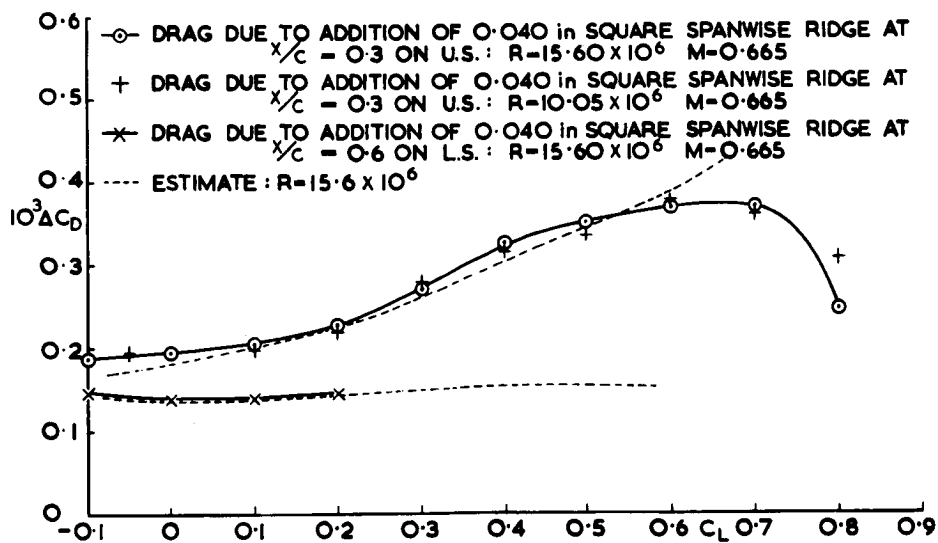


Figure 15.- Incremental drag due to square section 'ridge' excrecence on an aerofoil section.



## DOWNSTREAM EFFECTS OF BOUNDARY-LAYER

### TRIPS IN HYPERSONIC FLOW

By E. Leon Morrisette, David R. Stone,  
and Aubrey M. Cary, Jr.

NASA Langley Research Center

#### SUMMARY

Flow-field and boundary-layer surveys (pitot and total temperature) are shown for flow downstream of spherical roughness trips on a flat plate at near-adiabatic wall conditions in Mach 8.5 flow. The trips are shown to cause large distortions of the flow field and outer portion of the boundary layer. A method for minimizing these distortions is suggested. The nature of the tripping mechanism is discussed. Spherical and air jet trips are compared, and surface heating downstream of both types is presented.

#### INTRODUCTION

Boundary-layer trips have been successfully used in subsonic and moderate supersonic flows as a means of increasing the extent of turbulent flow on wind-tunnel models. The low unit Reynolds numbers and small sizes usually associated with hypersonic wind tunnels have made the use of trips a necessity in many test programs. The required roughness size has been found to increase rapidly through the supersonic regime until at hypersonic speeds the roughness size is at least twice the boundary-layer thickness. The associated element pressure drag can be a significant part of the measured drag of the model ( $\geq 15$  percent). The large size of these elements at hypersonic speeds gives rise to the possibility of distorting the inviscid flow field as well as the boundary layer about the model. The present paper examines the effects of selectively sized spherical roughness elements on the boundary layer and flow field and indicates some of the problems associated with the use of trips in hypersonic flows.

Boundary-layer surveys (pitot and total temperature) are shown for the zero-pressure-gradient case at near-adiabatic wall conditions downstream of roughness elements and with naturally turbulent conditions. Information concerning flow tripped by air jets is also presented. The nature of the three-dimensional disturbances downstream of roughness elements is discussed.

# SYMBOLS

$C_f$	skin-friction coefficient
$k$	height of roughness element
$M$	Mach number
$m_j$	mass flow of air jets per unit span
$N_{St}$	Stanton number
$R$	Reynolds number per centimeter, $\frac{U}{\nu}$
$R_k$	trip-height Reynolds number based on conditions at edge of boundary layer, $\frac{U_e k}{\nu_e}$
$R_{k,eff}$	effective trip-height Reynolds number
$R_V$	Reynolds number based on distance from virtual origin
$R_{x,k}$	Reynolds number based on chordwise distance from leading edge to trip position, $\frac{U_e x_k}{\nu_e}$
$T$	temperature
$T_T$	local total temperature
$U$	velocity in the x-direction
$U_\tau$	friction velocity, $\sqrt{\frac{\tau_w}{\rho}}$
$x$	chordwise distance from leading edge
$x_k$	chordwise distance from leading edge to roughness elements
$x_t$	chordwise distance from leading edge to position where boundary layer becomes turbulent
$x_V$	chordwise distance from leading edge to virtual origin
$y$	vertical distance from plate surface
$z$	spanwise distance from center line of model

$\delta$	undisturbed boundary-layer thickness at the location of roughness element
$\delta^*$	undisturbed displacement thickness at the location of jet trip
$\zeta$	nondimensional distance from plate surface, $\frac{U_{\tau}y}{\nu}$
$\nu$	dynamic viscosity
$\rho$	density
$\tau$	shearing stress

Subscripts:

aw	referred to adiabatic wall conditions
e	conditions at boundary-layer edge
w	wall
$\infty$	free-stream condition

All barred symbols refer to incompressible quantities.

## RESULTS AND DISCUSSION

Before discussing the downstream effects of roughness elements, some comments and observations about the flow field around tripping elements themselves and the efficiency of various types of tripping devices are in order. An understanding of the flow field around a tripping element would hopefully give some insight into the tripping mechanism permitting the development of smaller, more efficient trips. Hot-wire surveys of the near flow field of spherical roughness elements were obtained, but because of the complexity of the flow and the long wire lengths relative to the roughness element size, little useful information was derived. The most fruitful source of information for the present investigation has been the surface oil-flow patterns obtained about the elements at Mach 4.7 and 5.5 by Whitehead at the Langley Research Center. A typical example of such a pattern about a spherical element (fig. 1) indicates that pairs of vortices are generated in the separation region ahead of the element and are swept downstream. It is thought that these vortices introduce the disturbances which cause transition. While the exact mechanism is not known, breakdown of the vortices may occur and introduce turbulence directly into the boundary layer as suggested by Hall (ref. 1) for incompressible flow. This breakdown is further indicated by the disappearance of the traces of the vortices from the surface oil-flow pattern in the transition region. A vortex shedding phenomenon behind trips was found by Van Driest and McCauley (ref. 2) at supersonic speeds, and thus a new mechanism, or flow model, for boundary-layer tripping at hypersonic speeds

as suggested by Van Driest and Blumer (ref. 3) may not be necessary. Other trip shapes (triangular prisms, pinheads, etc.) investigated had similar surface oil-flow patterns. In reference 4 it was shown that the various trips showed no major differences in transition position for a given trip size as long as a major portion of the trip frontal area was in the outer portion of the boundary layer. It appears that trip shape is relatively unimportant to the tripping mechanism; however, certain shapes exhibit advantageous drag characteristics. (See ref. 4.)

Discrete jets were suggested in reference 5 as a means of tripping hypersonic boundary layers with less disturbance to the flow field than solid trips; they have the additional property of directly adding normal momentum to the flow. A comparison of heat-transfer distributions obtained in this investigation for discrete sonic-jet trips and spherical-element trips is shown in figure 2. The jet pressure was regulated so that transition occurred at approximately the same position for the jet trip as for the spherical trip. While the mass injected was small, the disturbance size ( $k/\delta$ , where  $k$  for the jet was assumed to be, for comparison purposes, the jet penetration height obtained from the results of Torrence in ref. 6) was about the same for both trips. However, recent surveys of the flow field downstream of the jet trip (not presented) indicate a marked reduction in flow-field distortion as compared with the spherical trip for the same transition location.

In figure 2 and throughout this study, the transition position refers to the location of peak heating. The surface heating in the laminar and transitional region with the tripped boundary layer (fig. 2) is similar to the surface heating with the untripped boundary layer, but with higher values. This high laminar and transitional heating is typical of tripped hypersonic boundary layers. (See refs. 7 and 8.) The surface-heating distributions in the fully turbulent flow, however, agree well with the modified Spalding-Chi theory (ref. 9) and distributions obtained with natural transition.

It is of interest to indicate just how large the roughness elements must be to cause little or no further forward movement of transition by increasing the roughness height at hypersonic speeds. An indication of the effective roughness height would be the effective roughness Reynolds number ( $R_{k,eff}$ ). This Reynolds number is based on local conditions at the boundary-layer edge and the roughness height at which a further increase in height causes no significant forward movement of transition. This effective-roughness-height Reynolds number, adjusted in each case to adiabatic wall conditions, is shown in figure 3 plotted against the local roughness-position Reynolds number for the data of this investigation at  $M_e = 6$  and 8, and for the data of Raymond M. Hicks of Ames Research Center at  $M_e = 2.91$ . (See ref. 4.) The adjustment for wall-temperature ratio is based on the empirical relationship of Van Driest and Blumer (ref. 3) in the form presented in reference 4. A comparison from figure 3 indicates that effective trips for hypersonic flow are an order of magnitude larger than effective trips for supersonic flow. Although a large body of data from reference 4 might have been included in figure 3, the results shown are typical.

Another salient feature in figure 3 is the rapid increase of roughness height with roughness-position Reynolds number at  $Me = 8$ ; this increase is substantially smaller for  $Me = 2.91$  or  $Me = 6$ . It thus appears that at Mach 8 a significant decrease in the effective roughness height can be achieved by moving the roughness closer to the leading edge.

It is desirable to use the smallest roughness height which will still be effective not only because of the obvious advantage of lower drag, but also because the smaller roughness height may introduce less disturbances into the flow downstream of the roughness. A comparison obtained with trips located at the positions indicated in figure 4 and sized to give the same transition position indicates that there is less distortion in the surface-heating distribution in the transition region with the smaller trip. However, the instrumentation is not located as close to the small trip as to the large trip. Note that both trips are approximately the same size relative to the boundary-layer thickness ( $k/\delta$ ). While data for longitudinal rows of thermocouples at several spanwise locations show no discernible spanwise striations in surface heating (fig. 4), the thin-skin calorimeter method of measuring heat transfer used in the present investigation is probably incapable of detecting subtle variations of spanwise heating. The spanwise heating distributions in the present investigation, however, show that the average heating in the turbulent-flow region agrees with both theory and surface heating obtained with natural transition. In reference 10 Stainback found that where large striations occurred, the average heating was always higher than theory and heating obtained with naturally turbulent flow. Stainback's results also showed that large striations occur only for roughness sizes larger than the effective size. All the data of the present study are for roughness sizes which are effective or smaller.

So far, the results indicate no major problems associated with the use of trips at hypersonic speeds, with the exception that the required large trips have a large pressure drag. Neither the surface-heating distributions nor the surface oil-flow patterns show any discernible three-dimensionality in the regime of fully turbulent flow. However, when a compression surface is introduced into the flow field, a three-dimensional pattern again appears in the surface oil-flow pattern (fig. 5). The traces of the vortices shed by the roughness elements apparently disappear from the surface oil-flow in the transition region and subsequently reappear on the wedge surface, thus indicating that while the lower portion of the boundary layer on the plate may not be distorted, the outer portion of the flow is probably three-dimensional. The heat-transfer data obtained on the compression surface (fig. 5) indicate that the roughness trails do not significantly affect the surface heating on the wedge; however, this may again be a limitation of the thin-skin calorimeter technique.

Since three-dimensional disturbances were indicated behind some roughness elements, an experimental investigation of the flow field downstream of the effective roughness trips was undertaken. Two roughness-position Reynolds numbers ( $R_{x,k} = 2.6 \times 10^5, 9.1 \times 10^5$ ) in Mach 8.5 flow were selected as test cases. The boundary-layer-edge Mach number is approximately 8.0. (See fig. 3.) Mach number profiles for the flow at several positions downstream

of the larger trip ( $R_{x,k} = 9.1 \times 10^5$ ) are presented in figure 6. (Fairings of a large number of data points are used for clarity.) The profile nearest the roughness is significantly distorted; the ensuing profiles indicate that the disturbances are diminishing with distance downstream from the roughness. The profile at the most rearward position has no significant distortion remaining; however, this profile is approximately 135 roughness diameters downstream of the trip position and beyond the region of interest in many tests utilizing trips. The measured wall static pressure was used to reduce the pitot pressures to Mach numbers and the static pressure gradient normal to the wall was assumed to be zero. The profile at the rear station in untripped flow has approximately the same turbulent Reynolds number as the mid-profile with the trip, and the boundary-layer thickness is about the same.

To investigate the possibility of spanwise variations in the flow downstream of the roughness, surveys of the same x-location were made both directly behind a roughness element and halfway between two roughness elements (fig. 7). These profiles indicate no differences in the lower portion of the boundary layer, but in the outer portion of the boundary layer and in the flow field, these curves exhibit a distinct three-dimensional character which diminishes in the downstream direction. These distortions, while not evident on the plate surface, apparently influence the surface flow over the wedge and are responsible for the wedge oil-flow patterns of figure 5.

For the same turbulent Reynolds number, the Mach number through most of the boundary layer is higher for the naturally turbulent profile than for the tripped profile; the boundary-layer thickness for both profiles appears to be about the same. Remember measured surface heating obtained under similar flow conditions with cold walls showed good agreement between the surface heating for the tripped and untripped cases, indicating similar agreement for the temperature profiles near the wall.

The outer flow-field structure can be greatly improved by using smaller trips nearer the leading edge as illustrated in figure 8. While there is good agreement between the two profiles for the large and the small roughness elements in the lower portion of the boundary layer, the profile for the smaller roughness is obviously less distorted in the outer flow region. In fact, the profile of the smaller trip has only small, and for many purposes inconsequential, distortions in the outer flow field. If the magnitude of the flow distortion downstream of the trips scales in roughness diameters, then the small trip would cause less distortion at the lower Reynolds number station (175 roughness diameters) than the large trip at the higher Reynolds number station (135 roughness diameters). This appears to be true for the data of figure 8. Thus, there is an advantage in using trips close to the leading edge in hypersonic flows. There is, of course, a limit as to how close to the leading edge that trips can be placed and still satisfy the criteria for roughness sizing.

Since the objective of using trips is to produce a turbulent boundary layer which is the same as a naturally turbulent boundary layer at some higher Reynolds number, comparisons of the tripped profiles with naturally turbulent profiles are of interest. Turbulent boundary-layer profiles, unlike laminar

profiles, have no strongly defined basis for comparison. One approach to the comparison is shown in figure 9, where the boundary-layer profiles from this investigation for the naturally turbulent case and the small and large roughness cases are compared in temperature-velocity coordinates. All the profiles approximate an empirical quadratic relation in the outer region and approach the linear Crocco relation near the wall. The tripped profiles are slightly less full than the untripped profile; however, since the x-location of the profiles is constant, each profile corresponds to a different turbulent Reynolds number.

Additional profiles (not presented in fig. 9) for the large and the small trip at lower Reynolds number were slightly less full than the tripped profiles shown in figure 9; thus, it appears that the tripped profiles are approaching the untripped profile as the Reynolds number is increased. At all Reynolds numbers, the agreement between tripped and untripped profiles is better when the smaller trip was used.

Many published flat-plate profiles measured at near-adiabatic wall conditions (refs. 9 and 11) are found to approximate the linear Crocco relation, and the sizable deviation of the present profiles (tripped or untripped) from this relation is unexpected. It is possible that at high Mach numbers the quadratic variation of temperature with velocity is realistic since the available higher Mach number data (the present data and data of Softley and Sullivan in ref. 12 at Mach 10) follow the quadratic relation. The resolution of this question awaits the availability of more high Mach number data.

A second comparison between the tripped and untripped profiles is to transform the profiles to the incompressible plane by using the Baronti-Libby transformation (ref. 13), as shown in figure 10. The profiles can then be compared in the incompressible plane with the classical incompressible results, and the compressible skin-friction estimate which results from the transformation can be compared with predictions from a reliable method. The measured temperature distributions were used for the calculation of the velocity profiles, and the Crocco relation was used for the calculation of the density integral through the boundary layer used in the transformation. The transformed profiles are shown compared with the constant-density results in the upper part of figure 10. Obviously, the agreement between the transformed experimental profiles and the incompressible prediction is imperfect, but the correlation of these profiles is typical of the high Mach number results reported in other investigations. (See refs. 13 and 14.)

The compressible skin-friction coefficients obtained from the transformation are compared with the Spalding-Chi prediction in the lower part of figure 10. Previous investigators (refs. 13 and 14) have found that for the conditions of this investigation their skin-friction coefficients from the transformation were approximately 10 percent higher than the Spalding-Chi theory; this is the case for the untripped profile and the tripped profiles at the higher Reynolds number (fig. 10). Skin friction for the tripped profiles at the lower Reynolds number deviate from the established pattern in that the Spalding-Chi prediction is equal to or above the skin-friction values. The profile obtained with the large trip shows the greatest deviation. While the skin-friction coefficients obtained from the transformation are different

for the tripped and untripped profiles at the lower Reynolds number, heat-transfer measurements for these cases showed good agreement.

#### CONCLUDING REMARKS

Surveys in the flow field behind roughness elements in hypersonic flow have shown that large distortions of the outer boundary layer and flow field can occur. Thus, a configuration utilizing trips and having controls (flaps, ailerons, etc.) may not simulate the results obtained with naturally turbulent flow. These flow-field distortions probably account for the reappearance of striations in the oil-flow patterns found on flap surfaces when roughness trips were used. It should be noted that even when flow-field distortions occur for properly sized roughness, the surface-heating distributions and skin friction are generally in agreement with turbulent theory. There were no obvious three-dimensional effects in the lower portion of the boundary layer using properly sized roughness. It was found that flow-field distortions could be minimized by using small trips close to the leading edge. Jet trips were found to require penetration heights approximately equal to conventional spherical roughness heights to produce the same transition position; however, recent experimental data (not presented) indicate that downstream flow-field disturbances are smaller for the jet trip. It is a conclusion of this investigation that it is desirable to produce turbulent flow by a process other than trips on a model surface. Until such a technique is developed, conventional trips will undoubtedly be used; however, they must be used with discretion and a full awareness of the potential problems associated with their presence. Each test will have to be evaluated individually to determine the applicability of trips.



## REFERENCES

1. Hall, G. R.: Interaction of the Wake From Bluff Bodies With an Initially Laminar Boundary Layer. AIAA J., vol. 5, no. 8, Aug. 1967, pp. 1386-1392.
2. Van Driest, E. R.; and McCauley, W. D.: The Effect of Controlled Three-Dimensional Roughness on Boundary-Layer Transition at Supersonic Speeds. J. Aero/Space Sci., vol. 27, no. 4, Apr. 1960, pp. 261-271, 303.
3. Van Driest, E. R.; and Blumer, C. B.: Summary Report on Studies on Boundary Layer Transition for Years 1963-64. SID 64-2191 (Contract AF 49(638)-1178), N. Amer. Aviat. Inc., Dec. 1964.
4. Morrisette, E. Leon; Stone, David R.; and Whitehead, Allen H., Jr.: Boundary-Layer Tripping With Emphasis on Hypersonic Flows. Viscous Drag Reduction, C. Sinclair Wells, ed., Plenum Press, 1969, pp. 33-51.
5. Korkegi, R. H.: Transition Studies and Skin-Friction Measurements on an Insulated Flat Plate at a Mach Number of 5.8. J. Aeronaut. Sci., vol. 23, no. 2, Feb. 1956, pp. 97-107, 192.
6. Torrence, Marvin G.: Concentration Measurements of an Injected Gas in a Supersonic Stream. NASA TN D-3860, 1967.
7. Holloway, Paul F.; and Sterrett, James R.: Effect of Controlled Surface Roughness on Boundary-Layer Transition and Heat Transfer at Mach Numbers of 4.8 and 6.0. NASA TN D-2054, 1964.
8. Richards, Bryan E.: Transitional and Turbulent Boundary Layers on a Cold Flat Plate in Hypersonic Flow. Aeronaut. Quart., vol. XVIII, pt. 3, Aug. 1967, pp. 237-257.
9. Bertram, Mitchel H.; and Neal, Luther, Jr.: Recent Experiments in Hypersonic Turbulent Boundary Layers. Presented at the AGARD Specialists' Meeting on Recent Developments in Boundary-Layer Research (Naples, Italy), May 10-14, 1965.
10. Stainback, P. Calvin: Some Effects of Roughness and Variable Entropy on Transition at a Mach Number of 8. AIAA Paper No. 67-132, Jan. 1967.
11. Bushnell, D. M.; Johnson, C. B.; Harvey, W. D.; and Feller, W. V.: Comparison of Prediction Methods and Studies of Relaxation in Hypersonic Turbulent Nozzle-Wall Boundary Layers. NASA TN D-5433, 1969. (Also paper no. 11 in the present conference.)

12. Softley, Eric J.; and Sullivan, Robert J.: Theory and Experiment for the Structure of Some Hypersonic Boundary Layers. Hypersonic Boundary Layers and Flow Fields, AGARD CP No. 30, May 1968, pp. 3-1 - 3-18.
13. Baronti, Paolo O.; and Libby, Paul A.: Velocity Profiles in Turbulent Compressible Boundary Layers. AIAA J., vol. 4, no. 2, Feb. 1966, pp. 193-202.
14. Bertram, Mitchel H.; Cary, Aubrey M., Jr.; and Whitehead, Allen H., Jr.: Experiments With Hypersonic Turbulent Boundary Layers on Flat Plates and Delta Wings. Hypersonic Boundary Layers and Flow Fields, AGARD CP No. 30, May 1968, pp. 1-1 - 1-21.



## OIL FLOW PHOTOGRAPH AND INTERPRETATION

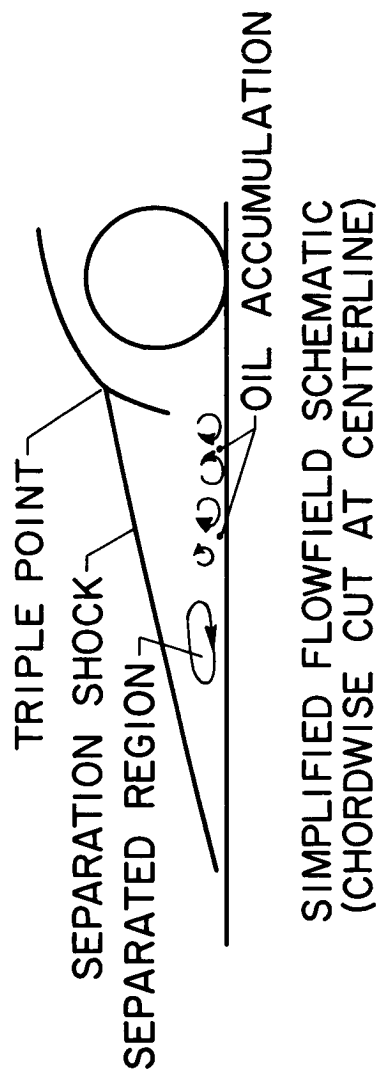


Figure 1.- Flow field about spherical element.  $M_e = 5.5$ ;  
 $R = 0.6 \times 10^5$  per cm;  $k/\delta = 2$ .

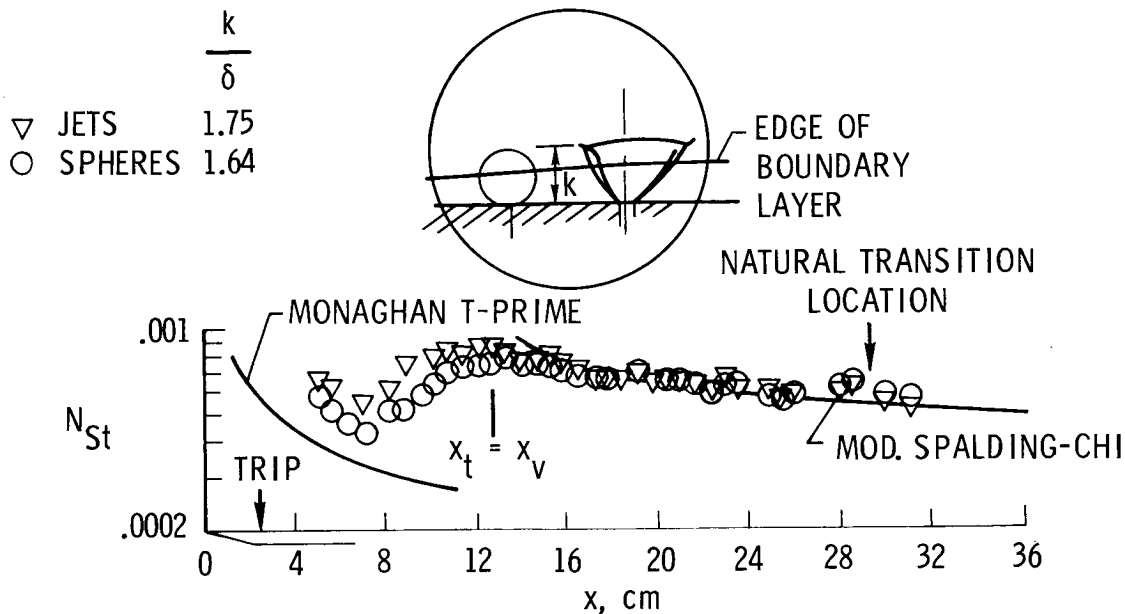


Figure 2.- Comparison of heat-transfer distribution for the jet and spherical element trips.  $M_e = 8.0$ ;  $R = 2.15 \times 10^5$  per cm; jet,  $x_k = 2.54$  cm and  $m_j/\rho_e U_e \delta^* = 0.04$ ; sphere,  $x_k = 2.29$  cm.

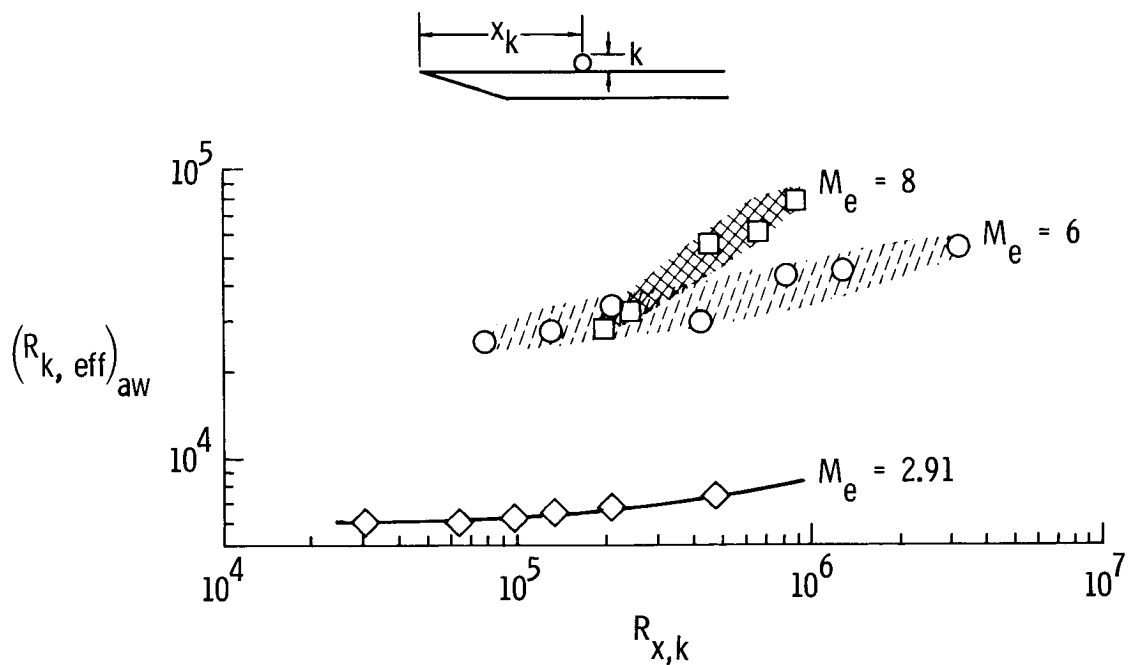
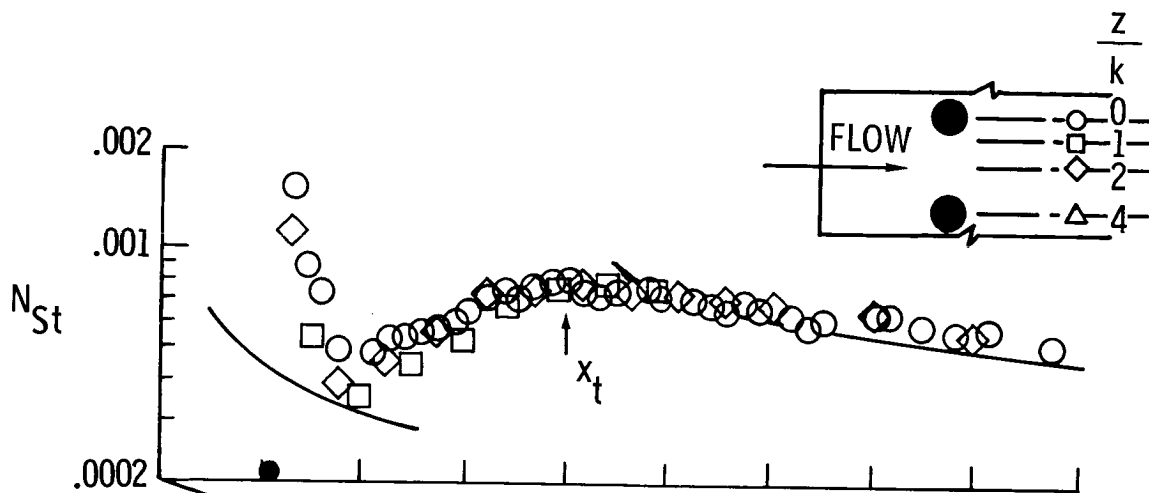
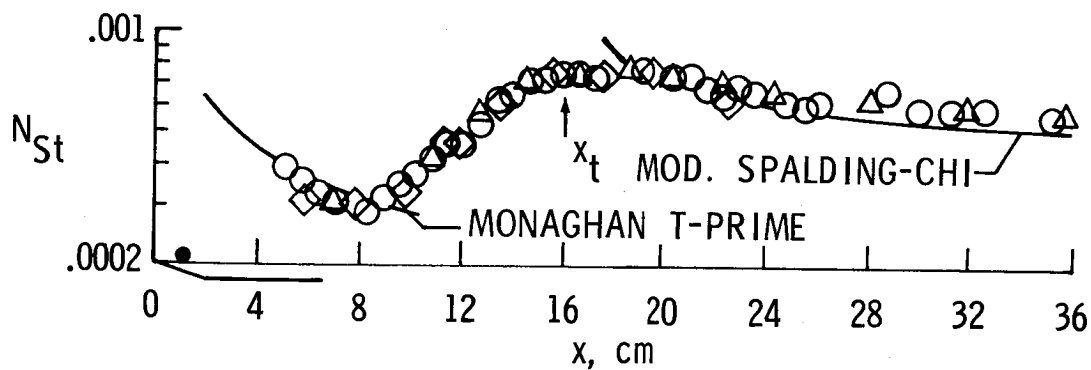


Figure 3.- Effective roughness Reynolds numbers for spherical trips on a flat plate.



(a)  $R_{x,k} = 9.1 \times 10^5$ ;  $R_k = 3.25 \times 10^4$ ;  $k/\delta = 1.57$ .



(b)  $R_{x,k} = 2.57 \times 10^5$ ;  $R_k = 1.61 \times 10^4$ ;  $k/\delta = 1.40$ .

Figure 4.- Effect of roughness location on surface heating.  
 $R = 2.03 \times 10^5$  per cm.

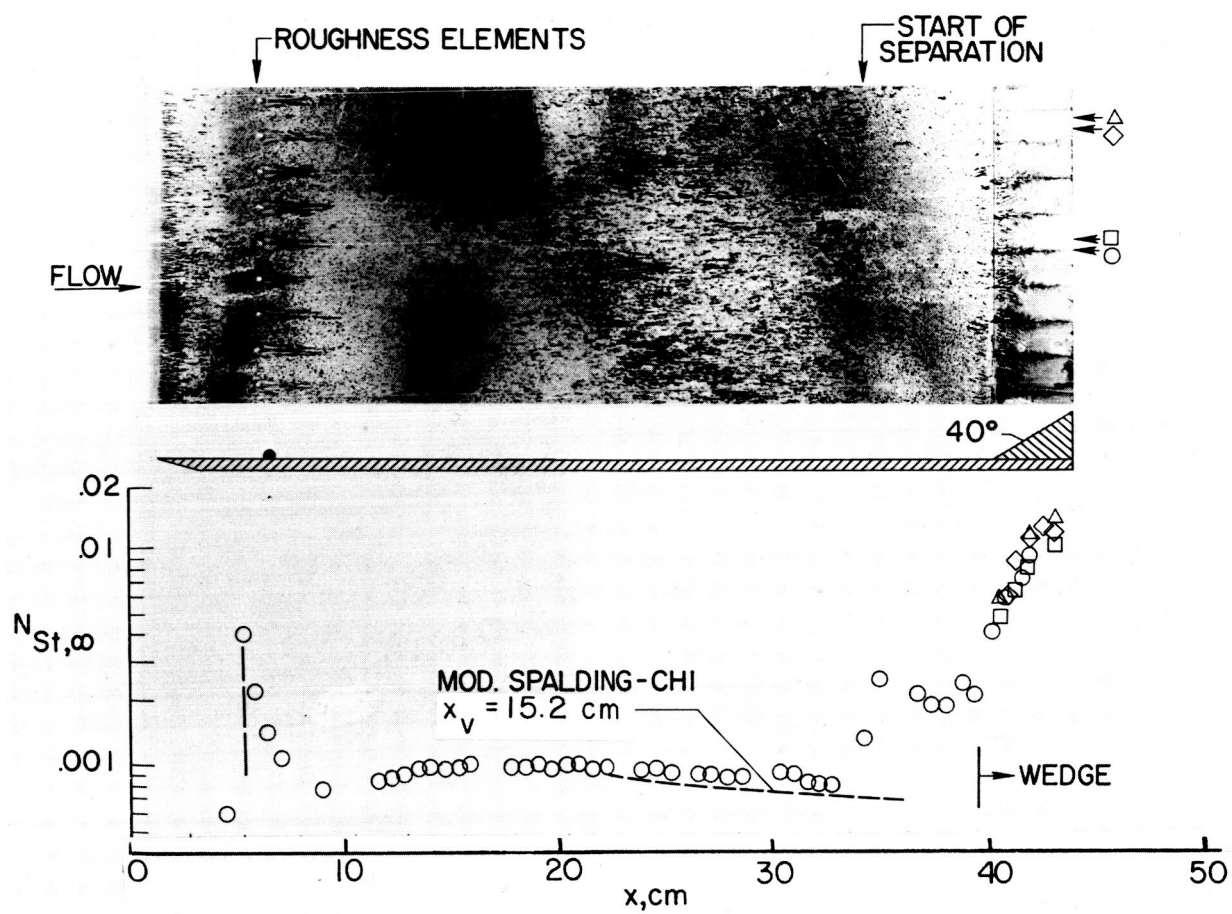


Figure 5.- Oil-flow patterns downstream of roughness elements.

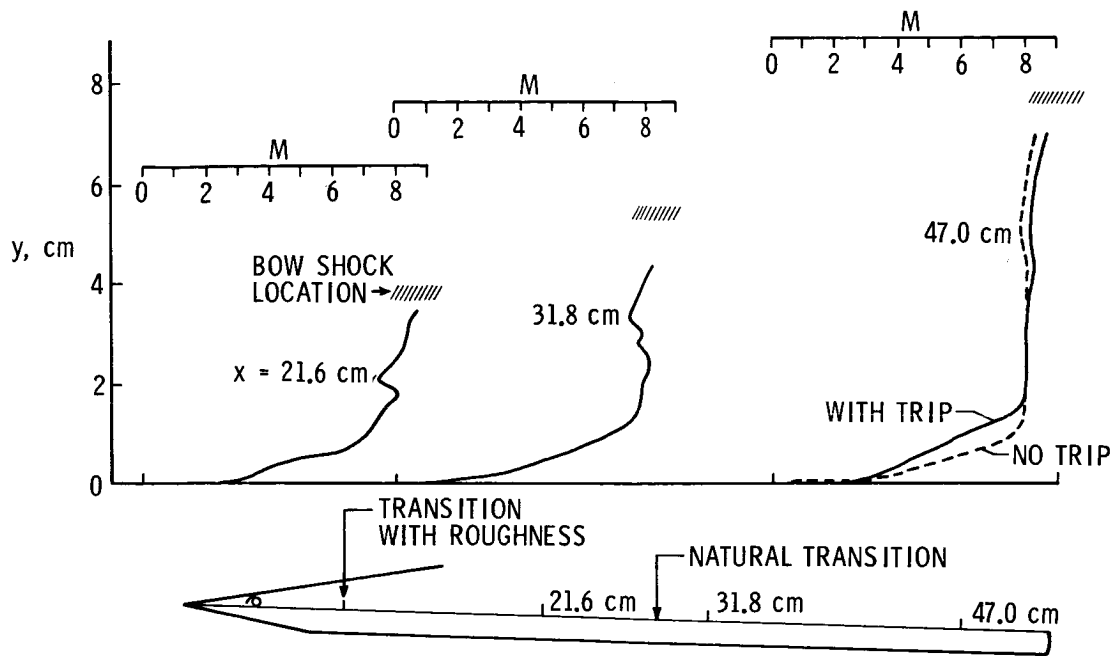


Figure 6.- Flow development downstream of trip.  $M_e = 8.0$ ;  
 $R = 2.05 \times 10^5$  per cm;  $x_k = 4.45$  cm;  $k = 0.318$  cm;  
 $k/\delta = 2.16$ ;  $R_{x,k} = 9.1 \times 10^5$ .

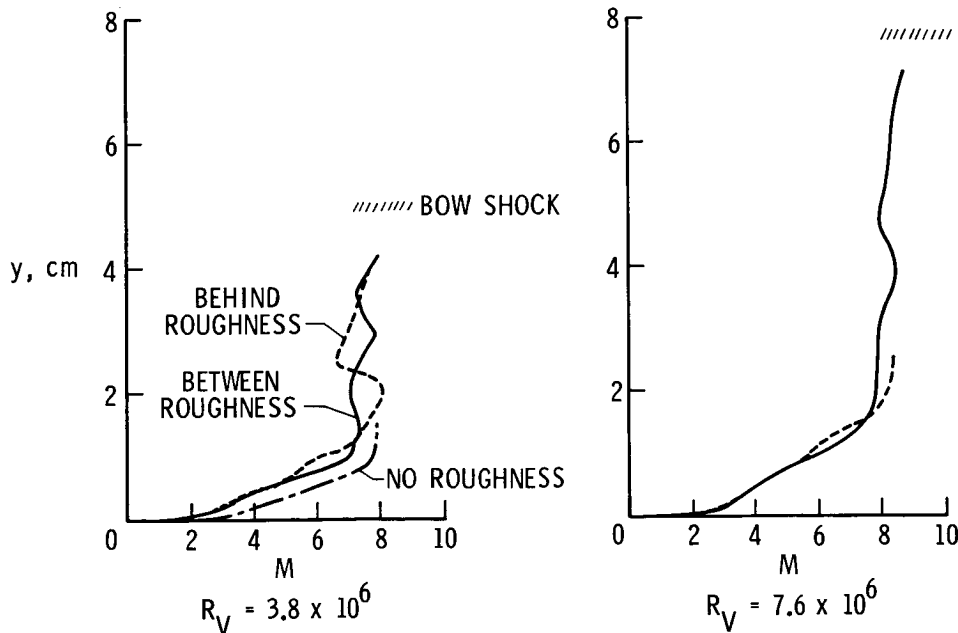


Figure 7.- Spanwise effect of roughness on the downstream flow.  
 $M_e = 8.0$ ;  $R = 2.05 \times 10^5$  per cm;  $x_k = 4.45$  cm;  $k = 0.318$  cm;  
 $k/\delta = 2.16$ .

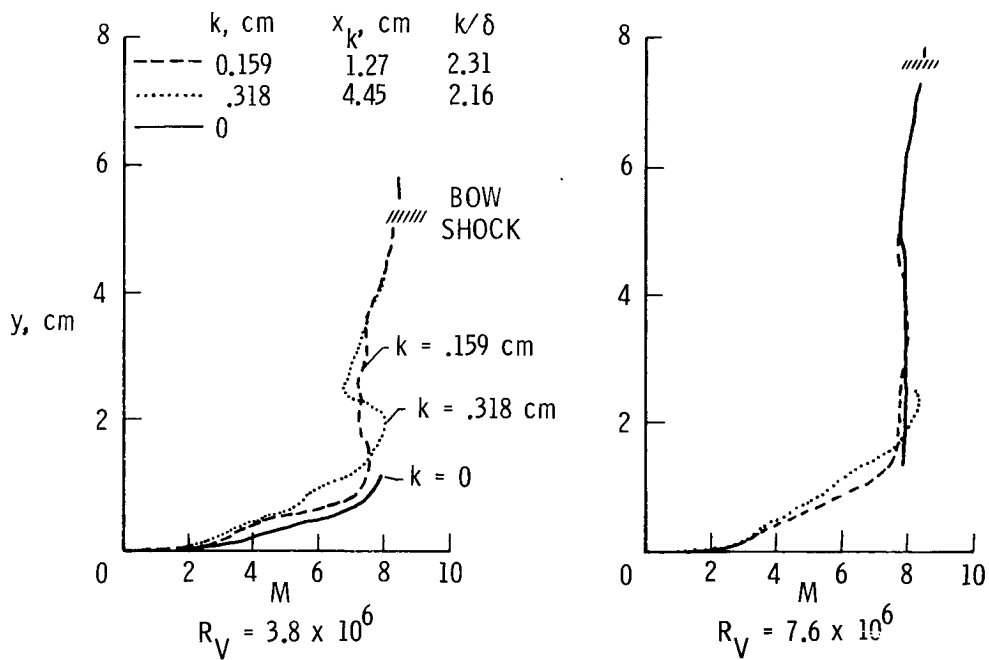


Figure 8.- Effect of roughness size on the downstream flow.  
 $M_e = 8.0$ ;  $R = 2.05 \times 10^5$  per cm.

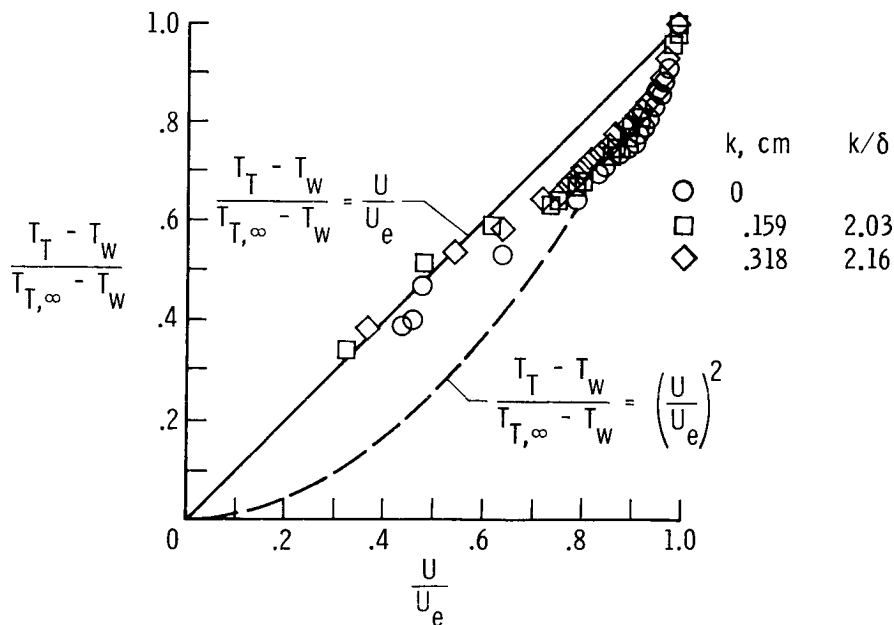


Figure 9.- Effect of roughness on temperature-velocity relationship through the boundary layer.  $M_e = 8.0$ ;  $T_W/T_{T,\infty} = 0.70$  to  $0.73$ ;  $R = 2.05 \times 10^5$  per cm; survey position, 47 cm.



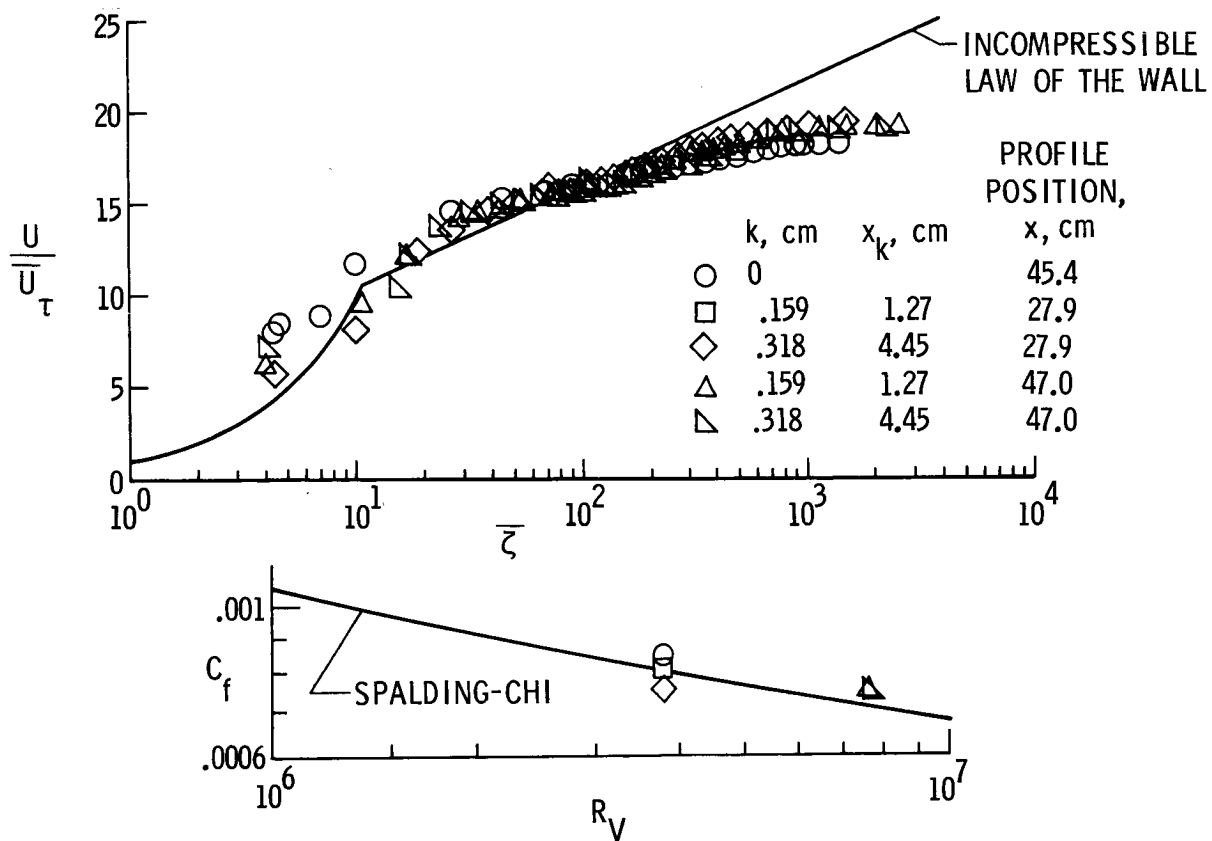


Figure 10.- Tripped profiles in the incompressible plane using the Baronti-Libby transformation.  $Me = 8.0$ ;  $R = 2.05 \times 10^5$  per cm.

# MEASUREMENTS OF TURBULENT HEAT TRANSFER ON CONES

## AND SWEEPED PLATES AT ANGLE OF ATTACK

By Thomas E. Polek and George G. Mateer

NASA Ames Research Center

### SUMMARY

Heat transfer measurements are presented for cones ( $5^\circ$  and  $15^\circ$  half angle) and swept flat plates ( $0^\circ$ ,  $70^\circ$ ,  $75^\circ$  sweepback) at angle of attack having turbulent boundary layers resulting from natural transition. Results are for air at a Mach number of 7.4 and Reynolds numbers ranging from  $3 \times 10^6$  to  $14 \times 10^6$ . The ratio of model wall temperature to stream total temperature ranged from .3 to .4. Results for the cones indicate a moderate dependence of the ratio of heating rates ( $\dot{q}/\dot{q}_{\alpha=0}$ ) on the

surface distance. At angle of attack, heating rates to the windward ray of the cone are predictable by a theory based on calculated inviscid edge conditions. Heating rates on the windward ray of the cone were found to vary linearly with angle of attack. However, for the flat plates, the variation was nonlinear with angle of attack. The heating rates measured on the unswept, sharp plate establish an upper limit for the heating rates on both the sharp and blunt swept plates.

### INTRODUCTION

Measurements of heat transfer to cones and flat plates at angle of attack having turbulent boundary layers resulting from natural transition have been made at Mach number 7.4. Results are presented for cones having semi-vertex angles of  $5^\circ$  and  $15^\circ$  and for flat plates having 0, 70 and 75 degrees of sweepback with both sharp and blunt leading edges.

### APPARATUS AND TESTS

#### Wind Tunnel

The tests were conducted in the Ames 3.5-foot hypersonic wind tunnel. This tunnel is a blowdown type equipped with three interchangeable nozzles contoured to produce Mach numbers of 5.2, 7.4 and

10.4, respectively. The airstream is heated by passing it through a bed of aluminum oxide pebbles heated by natural gas burners. Insulation of the nozzle walls from the hot airstream is accomplished by injecting helium into the nozzle-flow boundary-layer through slots in the nozzle upstream of the throat. The wind tunnel is equipped with a mechanism for quickly inserting models into and retracting them from the airstream. Each of these actions require about 0.3 seconds.

The present tests were conducted by allowing the wind-tunnel flow to reach preselected steady-state test conditions, inserting a model into the test stream for the required length of exposure to the flow and then retracting it from the stream before turning the wind tunnel off.

### Models and Test Conditions

Cones.- Dimensions of the models used in this investigation are shown in figure 1. The models were constructed of thin-walled (0.033 in.) electroformed nickel. They were instrumented with thermocouples spot welded to the interior surfaces. The  $5^\circ$  cone had a single row of 22 thermocouples spaced at 1-inch intervals along one conical ray. One quadrant of the  $15^\circ$  angle cone was instrumented along conical rays spaced  $30^\circ$  apart; 12 thermocouples were placed on each ray. The  $15^\circ$  half-angle cone was tested at a constant total pressure of 1765 psia. The total temperature was  $1460^\circ\text{R}$  for tests at angles of attack ranging from  $0$  to  $6^\circ$  and  $1885^\circ\text{R}$  for the tests at  $10^\circ$  angle of attack. The  $5^\circ$  half-angle cone was tested at total pressures ranging from 900 to 1800 psia at a nominal total temperature of  $1500^\circ\text{R}$ . These test conditions resulted in Reynolds numbers based on cone lengths ranging from  $3.4 \times 10^6$  to  $14.0 \times 10^6$ . The ratio of model wall temperature to free-stream total temperature ranged from about 0.3 to 0.4 for these tests.

Flat plates.- Three different flat-plate models were tested - the planforms are shown in figure 1. The one having an unswept leading edge has a length of 47 inches and a span of 17 inches. Fences were attached to the streamwise edges to minimize cross-flow effects at angle of attack. The fences are 1-inch high at the trailing edge and tapered to zero height at the leading edge. The triangularly shaped model has leading edge sweep of  $75^\circ$ . Its root chord is 32.2 inches long and the span is about 17 inches. The asymmetrically clipped-tip model has a leading edge sweep angle of  $75^\circ$ , a root chord 47 inches and 70 percent of one semispan is removed. The two swept plates had sharp prows. The asymmetric model was constructed to obtain the longest model compatible with the constraints imposed by the wind-tunnel test section and quick-insert mechanism. Data obtained at geometrically similar locations on the clipped and unclipped  $75^\circ$  swept planforms show no discernible differences.

All of the flat-plate models were constructed of stainless steel. They were instrumented with stainless steel calorimeter disks (0.625 in. diam., 0.015 in. thick) placed at  $1\frac{1}{4}$ -inch intervals along chords at several spanwise stations. They were finished flush with the model surface and thermocouples were spot-welded to the interior surface. The leading edge bluntness of each model could be varied by use of interchangeable copper leading edges. A sharp leading edge (less than 0.002-inch radius) with a  $30^\circ$  wedge angle on the uninstrumented side of the plate and a 0.500-inch radius cylindrical leading edge were available for each model. These shall be referred to as the sharp and blunt leading edges, respectively. A 0.750-inch radius cylindrical leading edge also was available for the full-delta planform model.

The flat plates were tested at a total pressure of 1500 psia and a total temperature of  $1900^\circ\text{R}$ . These test conditions resulted in Reynolds numbers based on instrumented chord lengths ranging from  $3.2 \times 10^6$  to  $13.4 \times 10^6$ . The ratio of model wall temperature to free-stream total temperature was about 0.3 for all of the tests.

## RESULTS AND DISCUSSION

Examples of the data obtained for both the cones and plates are shown in figure 2. Results for each type of boundary-layer flow (laminar, transitional and turbulent) are readily identified by the almost linear variations of the data on the logarithmic plot. Only those data downstream of the maximum heating location which are representative of turbulent boundary-layer flow will be considered herein. The data to be presented for the cones at angle of attack are normalized by the values for zero angle of attack. The data to be presented for the plates are normalized by the results given by the fairing ( $\dot{q}_{\text{REF}}$ ) through the data shown in figure 2.

### Cones

The influence of angle of attack on the turbulent heating rates to the cones is shown in figure 3 wherein normalized values are presented as a function of length along the model surface. The turbulent heat-transfer rates are increased on the windward ray and decreased on the leeward ray relative to values at zero angle of attack. These results would be expected considering the changes in local pressure and boundary-layer edge Mach number accompanying the changes in angle of attack. In addition, the cross-flow at angle of attack thins the boundary layer on the windward ray and thickens it on the leeward ray resulting in heating rate increases and decreases, respectively. The

results of figure 3 also show that the dependence of heating rate on distance along the model surface is only moderately influenced by angle of attack. This result also might be expected since the inviscid theory of reference 1 predicts the flow properties to be constant along rays of the cones at angle of attack just as for zero angle of attack.

At  $2^\circ$  angle of attack there is approximately a 25% difference between the relative heating rates on the leeward rays of the  $5^\circ$  and  $15^\circ$  cones. In order to effect a 25% difference between these rates on the windward ray the angle of attack must be increased to  $10^\circ$ . This makes it appear like a different relationship exists between heating rate, angle of attack, and cone angle for the windward and leeward rays. However, the aforementioned trends can be estimated fairly accurately as will be shown later.

As was mentioned earlier, only data downstream of peak heating are considered. However, the location of peak heating is not constant over the surface of a cone at angle of attack (ref. 2). For example, the location of peak heating moves upstream on the leeward ray and downstream on the windward ray as the angle of attack increases while at zero angle of attack the location of peak heating is constant around the cone. As a result, the ratio of heating rates would be expected to be a function of the relative locations of peak heating. It was found, however, that the movement of the location of peak heating changed the total length of turbulent flow by only a small percentage (10%-15%) for the majority of the data presented. Therefore, data at the rearmost station is not greatly affected by changes in location of peak heating. Consequently, only those data at the 21.8 inch station will be considered in the remaining figures.

To more clearly show the meridional distribution of turbulent heating, results of figure 3 for the rearmost station are replotted in figure 4 as a function of meridian angle  $\phi$ . Although not shown, the curves can be approximated by a cosine function.

An explicit effect of angle of attack on turbulent heating is illustrated in figure 5. Again the data are for the rearmost station of the  $15^\circ$  cone. For clarity only results for four of the meridian angles are shown. The windward and leeward heating rates appear to be linear functions of angle of attack, whereas, the data for other meridian angles show a slightly nonlinear dependence on angle of attack.

Theoretical predictions of windward and leeward heating rates that did not depend upon a knowledge of the streamline pattern were made. The boundary-layer edge conditions were calculated for the cone at angle of attack (ref. 1) and then the method of reference 3 was applied. Briefly, in reference 3, the local energy thickness Reynolds number is formed from the integration of the local heating rate and

edge conditions. A particular theory is applied using the premise that experimental and theoretical Stanton numbers correlated on an energy thickness Reynolds number basis are independent of body shape. In this instance the theory "Van Driest II" was applied.

The results of the calculations are shown as lines in figure 5. The theoretical prediction of windward heating is in good agreement with the experimental result. The leeward heating, however, cannot be predicted as well.

### Swept Flat Plates

The turbulent heating rates at selected locations along the centerline of the sharp and blunt unswept flat plates are presented in figure 6 as a function of angle of attack. Positive angle of attack indicates that the surface of the plate is windward. The effect of angle of attack on the windward surface heating is nonlinear for the flat plate, whereas, it was shown to be linear for the cone. Within the accuracy of the experiment there is no variation of normalized heating rate with chordwise location on both the sharp and blunt flat plates. This indicates a negligible change in cross flow as the angle of attack is varied. Values of heating rates for the blunt plate are 65 to 75 percent of the values for the sharp plate.

The effects of bluntness and angle of attack on heating rate at a fixed point on the  $75^\circ$  swept plate are shown in figure 7. Comparison of these results with those of the previous figure shows the effect of bluntness on the swept plate is not as pronounced as it is on the unswept plate. For angles of attack larger than six degrees there is less than a 10% variation in the heating rate between the sharp and the 0.750-inch radius leading-edge plates. For angles of attack less than 6 degrees, increasing the nose bluntness decreases the heating rate. This reduction amounts to approximately 20 percent at zero degrees angle of attack.

The effect of sweepback angle on the heating rates at points (defined in the sketches on the figure) on sharp and blunt plates is shown in figure 8. For the sharp leading edge models, increasing the sweep angle decreases the local heating rate. This reduction is a minimum at  $\alpha = 3^\circ$  and increases as the angle of attack is either increased or decreased from this value.

The opposite effect exists on the blunt plates, where increasing the sweep angle increases the local heating rate. The increase is negligible for angles of attack less than three degrees. As the

cylindrical leading edge is swept back it presents a less blunt shape to the flow, so that the bluntness effect on the swept plate should be less than that on the unswept plate.

The indicated effects of sweepback angle, near  $\alpha = 0^\circ$ , for the sharp plate may be due to a "bluntness" effect. The sharp leading edge has a 30-degree wedge angle on the uninstrumented side of the plate. At sweep angles of 70 and 75 degrees, the Mach number in the plane perpendicular to the leading edge is lower than that for shock wave detachment. This produces an effective bluntness even for zero nose radius.

To illustrate the range of variation in turbulent heating rate over the surface of the 75-degree swept flat plates, the heating rates at a number of discrete points on the surface of the plate are presented in figure 9 as a function of the angle of attack. It appears that the results for the sharp leading edge unswept plate define an upper limit for the heating rates on the sharp leading edge 75-degree swept plate. The heating rates approach this limit as the chordwise distance increases. For the 0.50-inch radius leading edge plates, the results for the unswept plate appear to define a lower limit for the heating rates to the plates investigated. The heating rates in this case also approach the unswept sharp leading edge plate, as an upper limit, as the chord length increases.

For both the sharp and blunt leading edge plates, for equal distances along the chord, the results for the outboard chord are lower than those for the inboard chord. All points along the outboard chord lie outside the Mach cone from the apex of the delta planform for angles of attack less than  $9^\circ$ . On the other hand, the inboard chord is within the influence of the apex for all angles of attack.

#### CONCLUDING REMARKS

Measurements of turbulent heating rates on  $5^\circ$  and  $15^\circ$  half-angle cones for angles of attack ranging to 10 degrees showed, as would be expected, an increase in heating on the windward ray and decrease on the leeward ray, relative to the zero angle of attack levels. The dependence of heating rate on surface length is nearly the same, within 20 or 30%, at angle of attack as at zero angle of attack. The meridional distribution of heating is somewhat like that of the cosine function.

A theory using calculated boundary-layer edge conditions can predict the heating to the windward ray of the cone.

Comparison of the results for the cones with those for the flat plates shows that while the increase in turbulent heating rate is linear with angle of attack on the windward ray of the cone, it is nonlinear on the windward surface of the plate.

Leading edge bluntness decreases the turbulent heating rate throughout the angle of attack range for the unswept plate, but for the 75-degree swept plate the decrease is small for angles of attack greater than four degrees.

Increasing sweep angle decreases the turbulent heating rate of the sharp leading edge plate, but increases it for the blunt (0.500 inch radius) leading edge plate. These effects become more pronounced as angle of attack increases.

For large values of the chord length the turbulent heating, to the 70 and 75 degree swept plates with either sharp or blunt leading edges, appears to approach the values for the unswept sharp leading edge plate.

#### REFERENCES

1. Rakich, John V.: Calculation of Hypersonic Flow Over Bodies of Revolution at Small Angles of Attack. AIAA J., vol. 3, no. 3, Mar. 1965, pp. 458-464.
2. Stetson, Kenneth F.; and Rushton, George H.: A Shock Tunnel Investigation of the Effects of Nose Bluntness, Angle of Attack and Boundary Layer Cooling on Boundary Layer Transition at a Mach Number of 5.5. AIAA Paper No. 66-495, June 1966.
3. Hopkins, Edward J.; Rubesin, Morris W.; Inouye, Mamoru; Keener, Earl R.; Mateer, George C.; and Polek, Thomas E.: Summary and Correlation of Skin-Friction and Heat-Transfer Data for a Hypersonic Turbulent Boundary Layer on Simple Shapes. NASA TN D-5089, 1969. (Paper no. 10 in this volume.)



## NOTATION

$l$	model length
$M$	Mach number
$\dot{q}$	heating rate
$R$	Reynolds number
$s$	surface distance from cone apex, inches
$T$	temperature
$x$	chord distance from leading edge, inches
$\alpha$	angle of attack
$\Lambda$	sweepback angle
$\phi$	meridional angle
$\sigma$	cone half-angle

### Subscripts:

$t$	total condition
$w$	wall condition
REF	reference condition

$$M_{\infty} = 7.4$$

$\sigma$ , deg	$z$ , in	NOSE RAD., in	(R/ft) $_{\infty}$	$\frac{T_w}{T_{\infty}}$
5	28	.005	$(4-8) \times 10^6$	.4
15	20	.002	$8 \times 10^6$	
$\Lambda$ , deg		L.E., RAD., in	$4.1 \times 10^6$	.3
0	47	<.002 .500		
75	32.2	<.002 .500 .750		
70	47	<.002 .500		
75	47	<.002 .500		

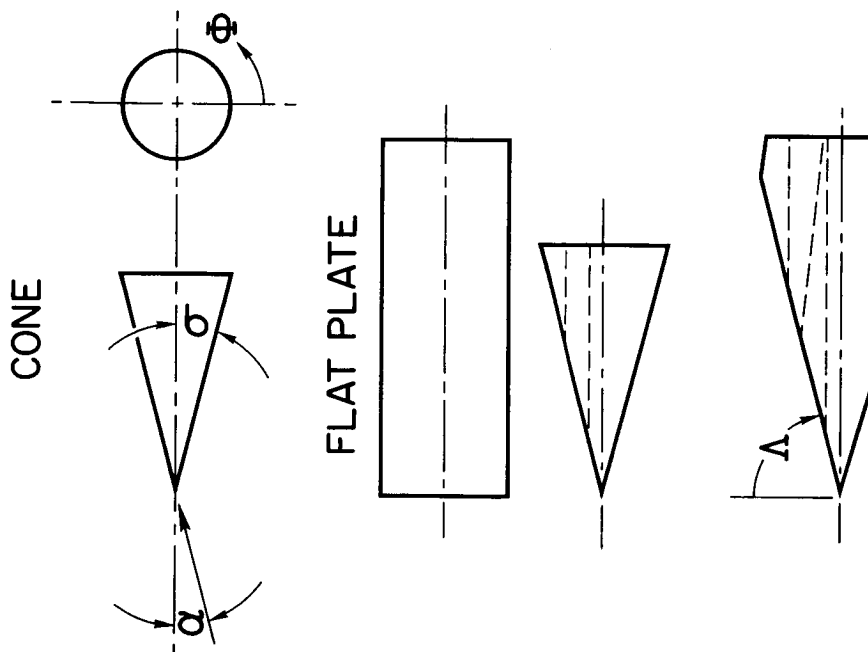


Figure 1.- Models and test conditions.

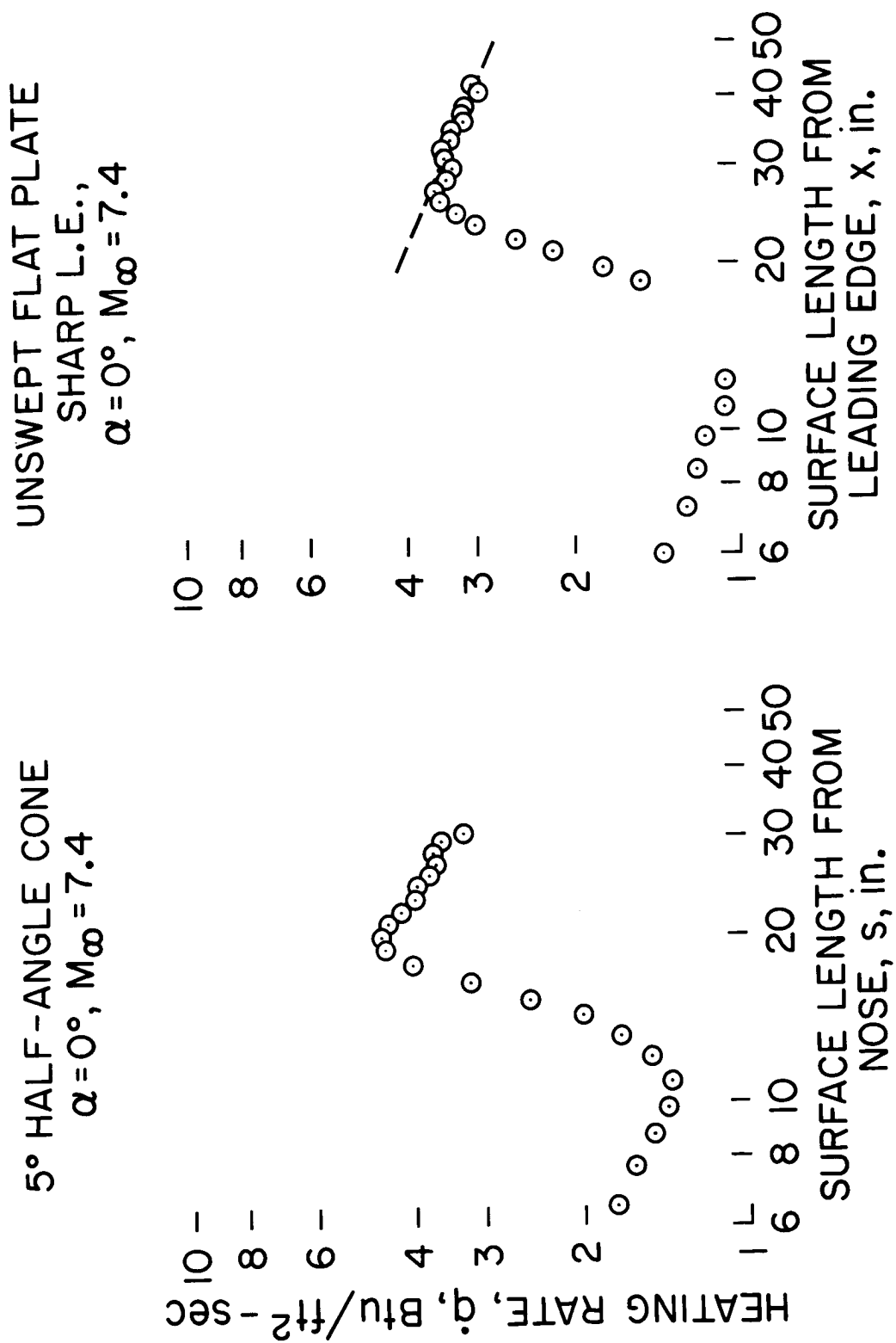


Figure 2.- Typical heating rate distributions.

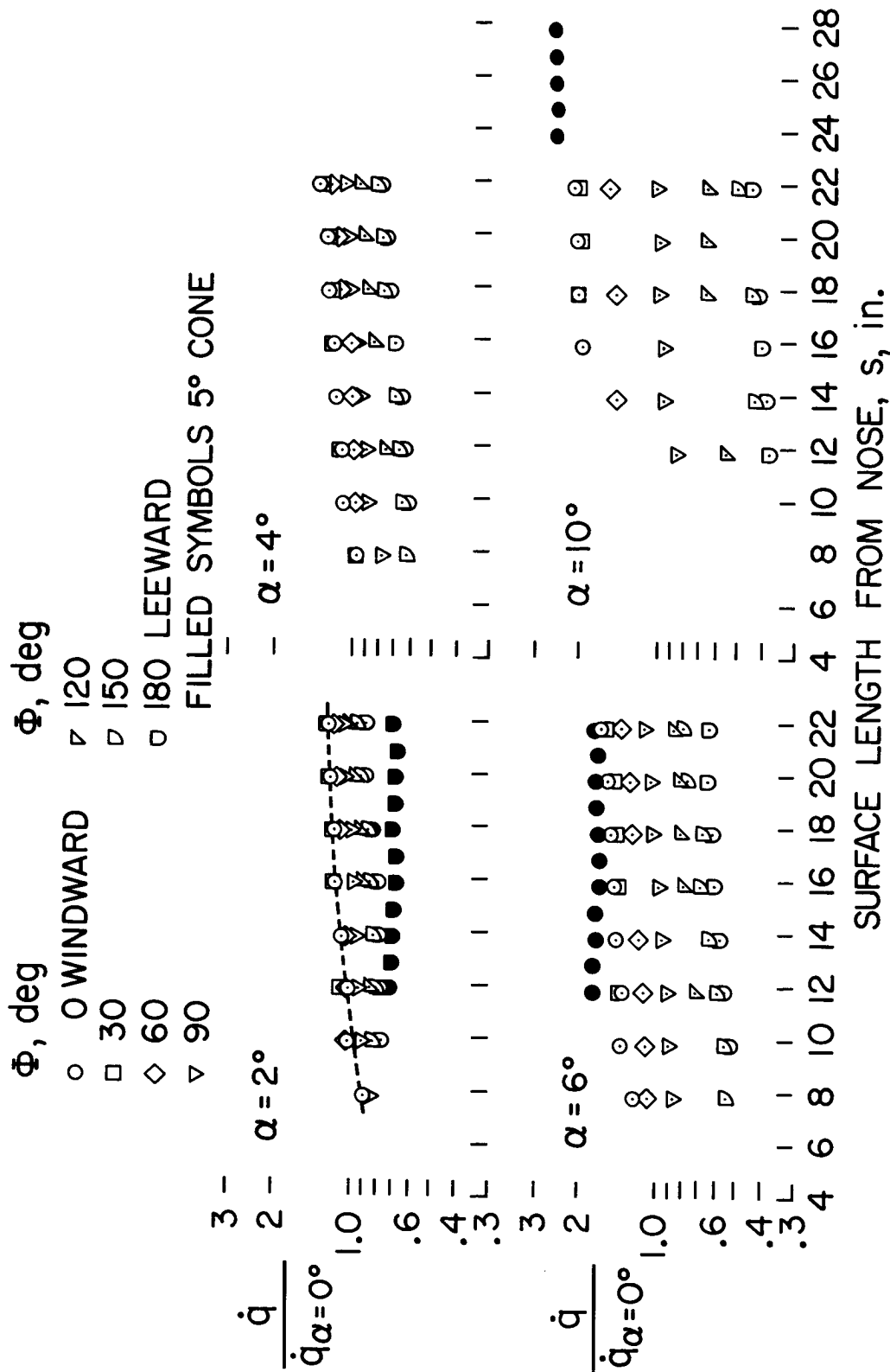
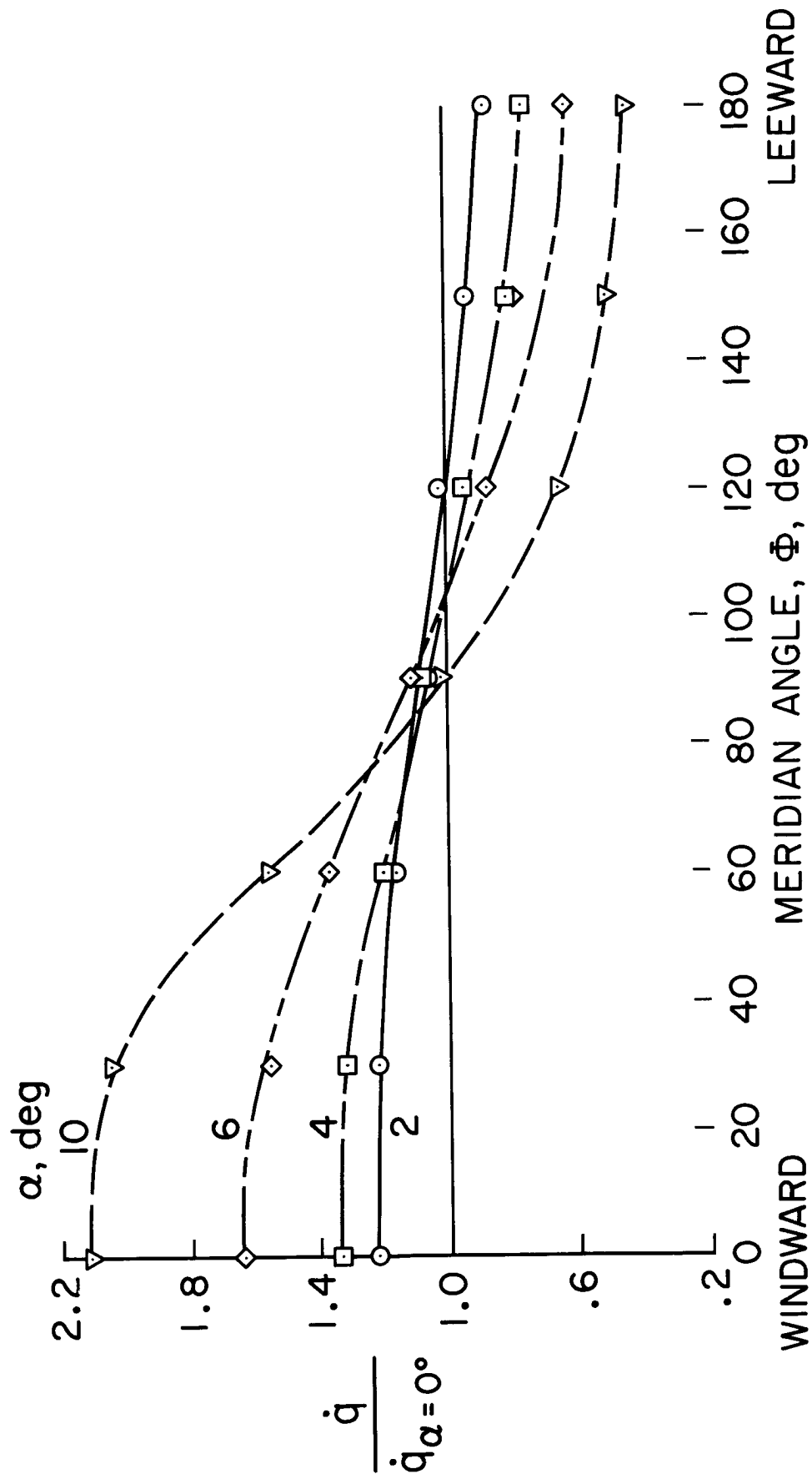


Figure 3.- Effect of angle of attack on heating distributions;  $5^\circ$  and  $15^\circ$  half-angle cones,  $M_\infty = 7.4$ .



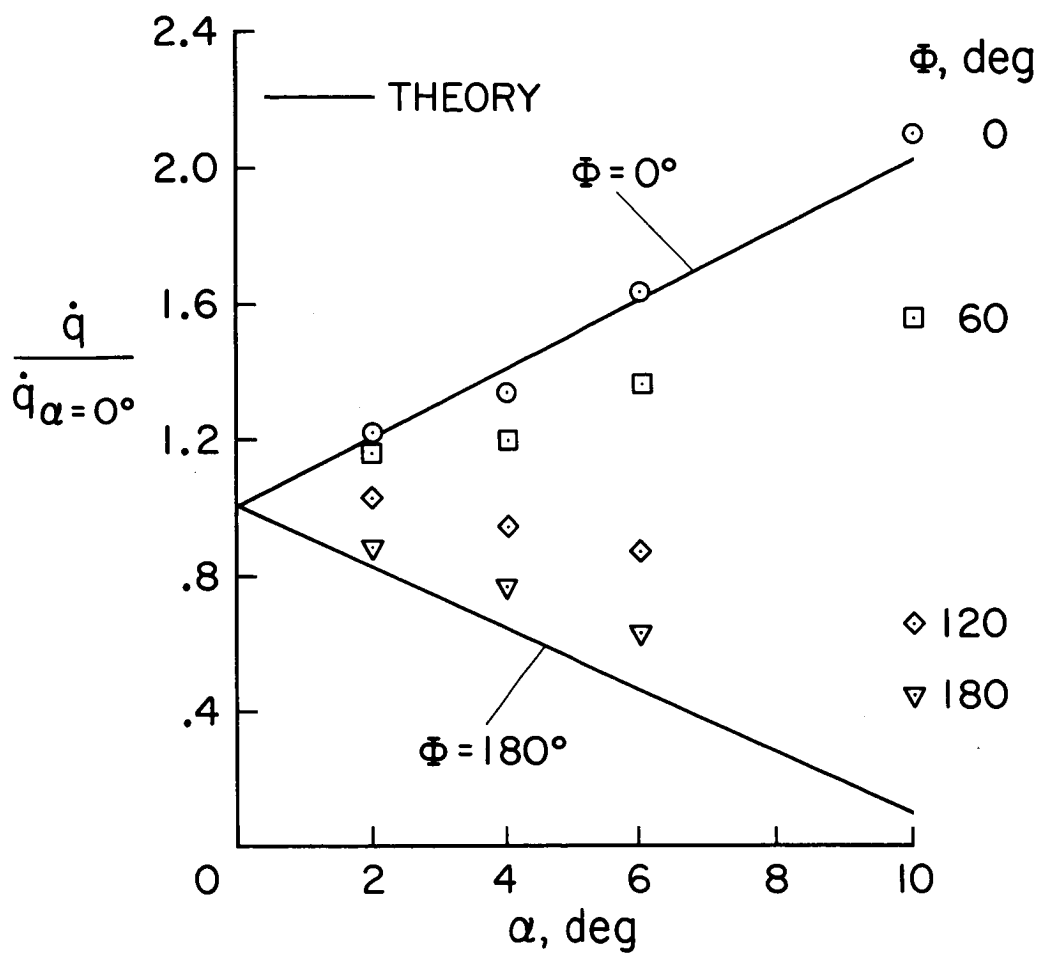


Figure 5.- Effect of angle of attack on heating;  
 $15^\circ$  half-angle cone,  $M_\infty = 7.4$ ,  $s = 21.8$  in.

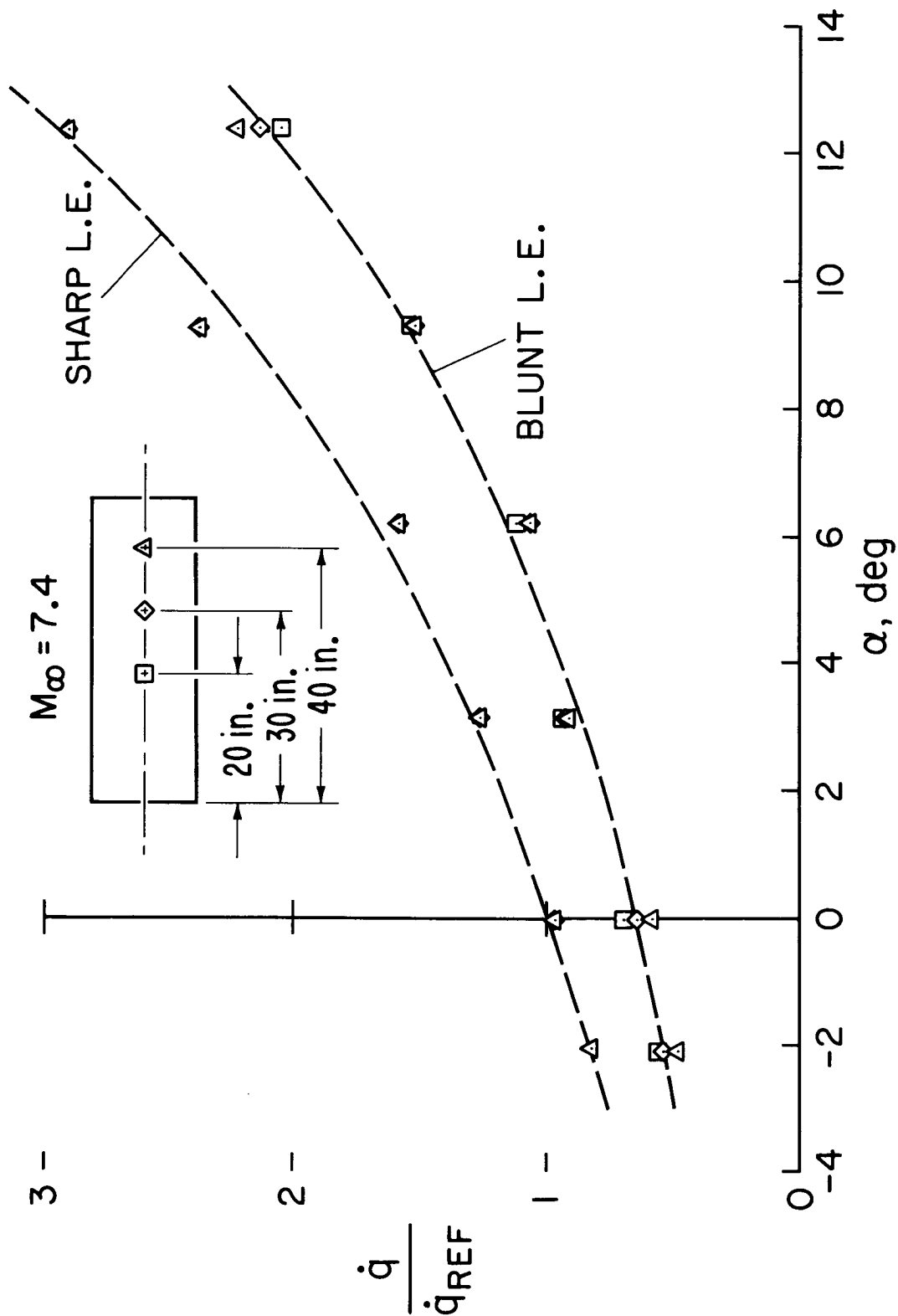


Figure 6.- Effect of angle of attack on heating of unswept, sharp and blunt, flat plates.

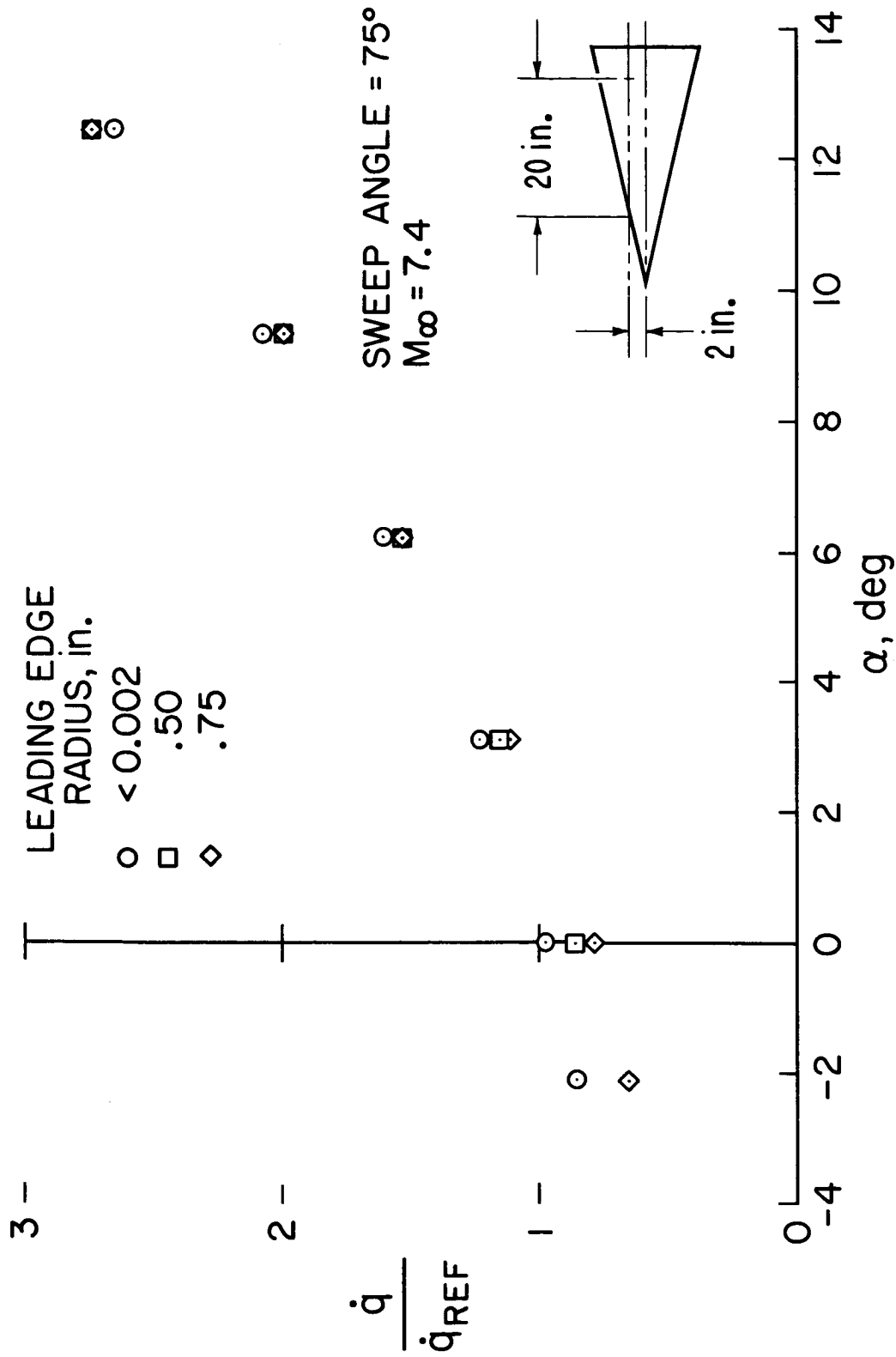


Figure 7.- Effect of angle of attack on heating on sharp and blunt, swept plates.



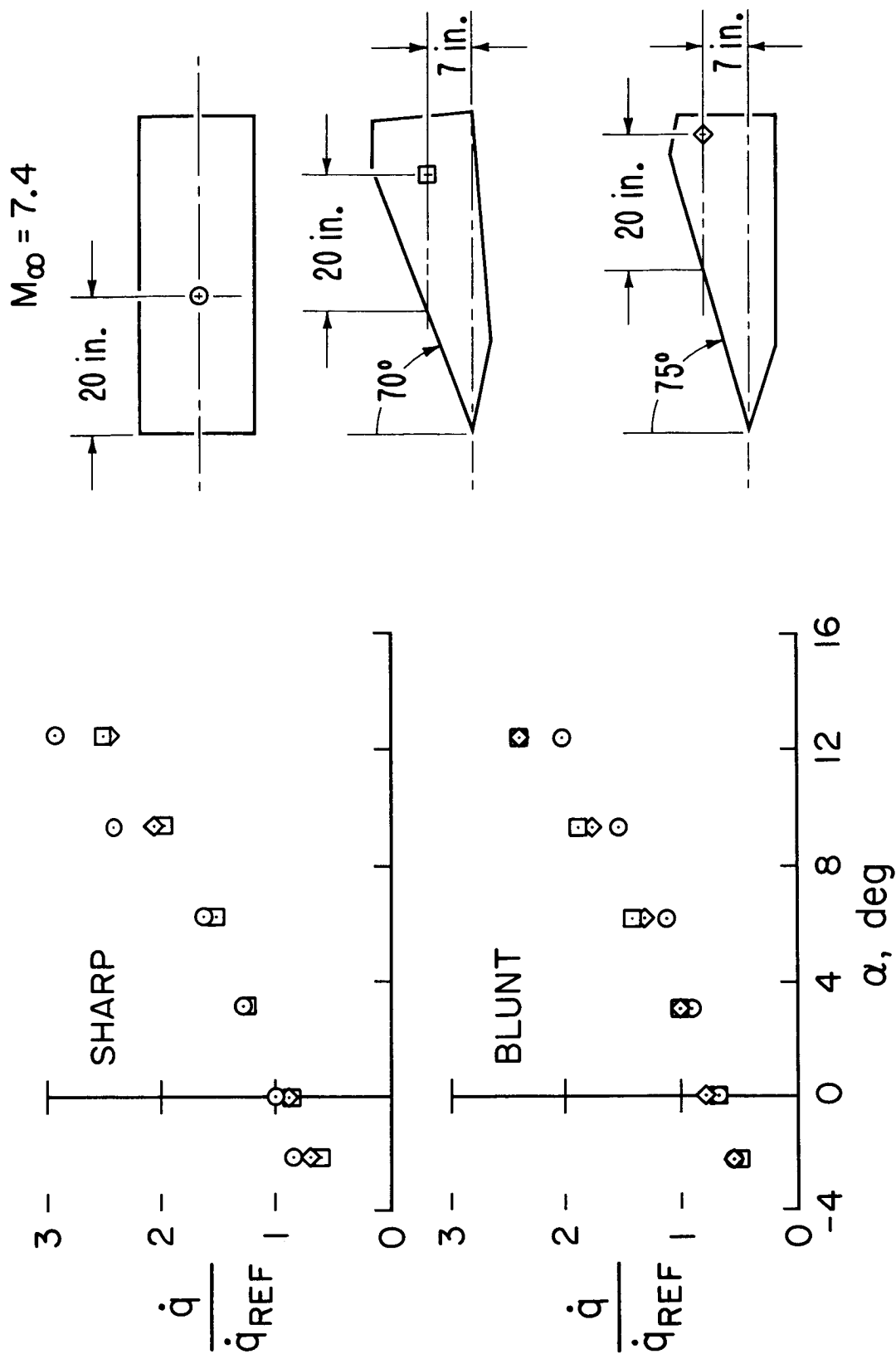


Figure 8.- Effect of sweepback angle on heating of sharp and blunt flat plates at angle of attack.

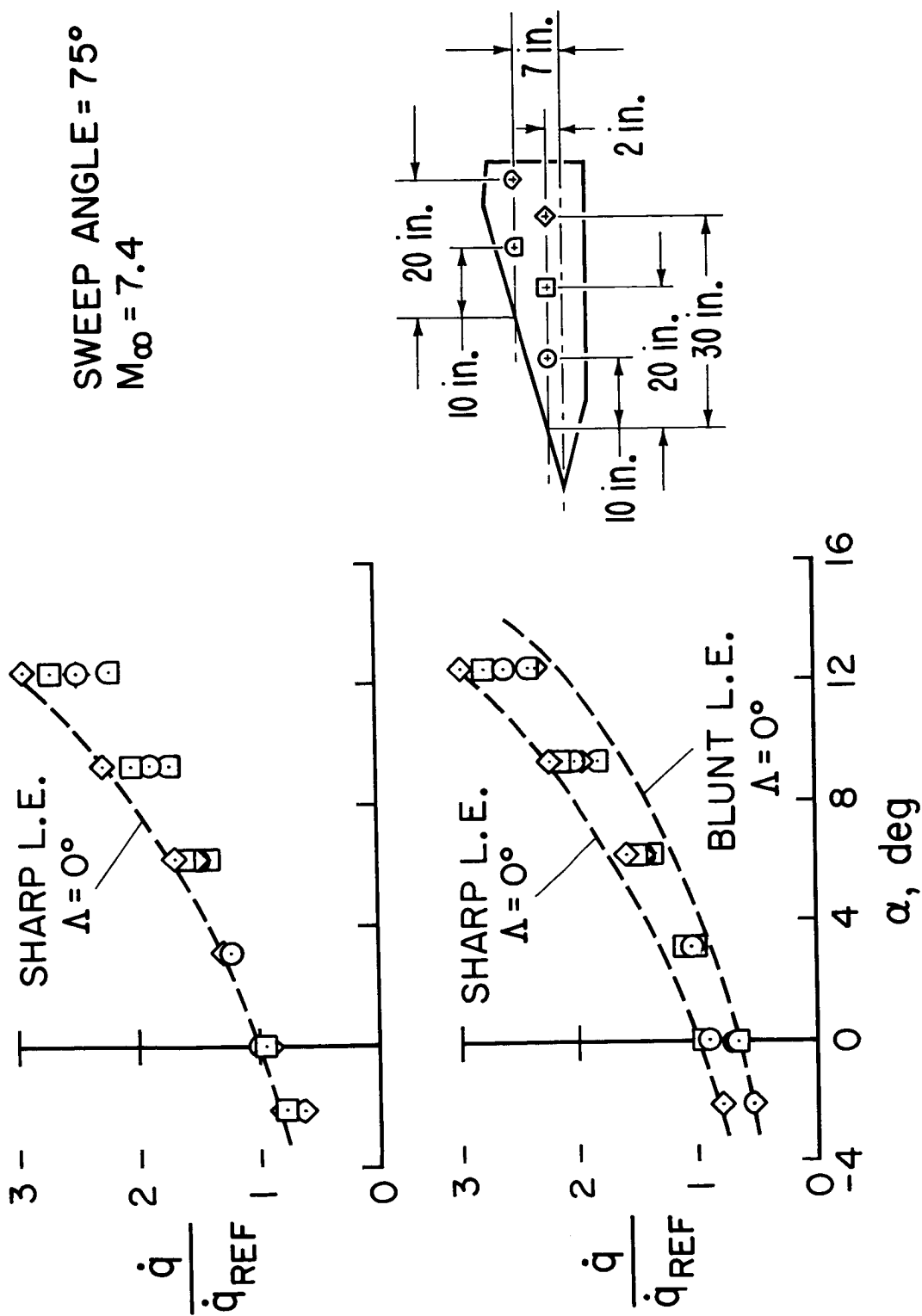


Figure 9.- Combined effects of location and angle of attack on heating on sharp and blunt,  $75^\circ$  swept plates.

A NOTE ON THE EFFECT OF REYNOLDS NUMBER ON THE HEATING  
OVER THE LEE SURFACE OF A DELTA WING AT MACH 6

By Allen H. Whitehead, Jr.

NASA Langley Research Center

SUMMARY

A model for the lee-surface flow field over a highly swept delta wing with a detached shock at a Mach number of 6 and angle of attack of  $5^\circ$  is presented. It is shown that the heating in the center-line region is large because of the presence of vortices on the upper surface. The effect of a variation in free-stream Reynolds number from about  $2 \times 10^6$  to  $20 \times 10^6$ , based on model length, on the lee-surface heating is investigated, and it is found that the maximum values of the Stanton number occur at the center line at the lower unit Reynolds numbers. These values are well above laminar flat-plate predictions and exceed all Stanton number values found at zero angle of attack at a comparable Reynolds number. When the center-line region is fully turbulent, the surface heating across the span can be correlated in conical coordinates. No such correlation exists for the lower Reynolds number data.

INTRODUCTION

In the preceding paper by Polek and Mateer, heat-transfer results on the compression surface of a highly swept delta wing in a hypersonic flow were presented. Preliminary results are given in this note from a study of the lee-surface flow field over the delta wing. This presentation is limited to a brief flow-field description based on surface-flow visualization technique and a discussion of the heat transfer on the lee surface.

SYMBOLS

$L$	model chord length
$M_\infty$	free-stream Mach number
$R_\infty$	free-stream Reynolds number
$N_{St,\infty}$	local Stanton number based on free-stream conditions

x distance down center line from model apex  
 $\alpha$  angle of attack  
 $\theta$  angular displacement from centerline, measured through model apex

Subscripts:

L based on model length  
x based on distance down center line from model apex

## APPARATUS AND TESTS

The delta wing tested in this study has a leading-edge sweep angle of  $75^\circ$  and a sharp leading edge ( $<0.003$  inch) and was constructed of stainless steel with instrumented insert plates. The heat-transfer data were obtained from a thermocouple insert, and center-line surface-pressure data were obtained from an insert with orifices mounted flush with the model surface. The model was sting mounted in a manner to minimize any support-structure effect on lee-surface flow variables. The wedge angle of the leading edge at the base of the model was  $14.6^\circ$  (see fig. 1). Thus, calculations indicate that the leading-edge shock wave is detached for the test conditions herein. The oil-flow technique was used to indicate direction and relative magnitude of the surface shear forces. In this method, a mixture of oil and lampblack is applied to the model surface in random dots prior to the run. The tests were conducted in the Langley 20-inch Mach 6 tunnel.

The entropy level required to provide the recovery temperature and theoretical values of the Stanton number was obtained by assuming a two-dimensional Prandtl-Meyer expansion over the lee surface.

## RESULTS AND DISCUSSION

The lee-surface flow field over the delta wing has not been extensively investigated at hypersonic speeds. Recent studies (refs. 1, 2, and 3) have indicated that pressure and heating levels on this surface are considerably above the two-dimensional values. In general, beyond a certain angle of attack, the flow field on the lee surface is characterized by a separated flow initiating either at the leading edge or at the base of an inboard shock system. A discussion of both types of flow behavior is presented in reference 1. The separated flow subsequently forms a coiled vortex sheet above the lee surface. For the conditions of the present tests, the leading-edge shock is detached and the flow separates at the leading edge as pictured schematically in figure 1.

Previous studies (refs. 1, 3, and 4) have identified a high-heating and high-shear area in the wing center-line region which results in a feather-like oil-flow trace on the model surface. This high-shear region is a result of the downward deflection of the flow by the circulatory motion of the vortices. The existence of this high-shear region was confirmed in the oil-flow studies of the present tests, and the oil-flow "feather" is shown pictorially in the sketch in figure 1. The location of the separation point (be it at, or inboard of, the leading edge) affects the location and strength of the vortex and, hence, the location and magnitude of the maximum heating in the center-line region. Reference 1 has an analysis of the heating on the wing surface for the case not considered here, in which the flow separates inboard of the leading edge on a wing with a sweep angle of  $70^\circ$ .

Previous lee-surface studies have been limited in the extent of the Reynolds number range covered. The effect of a Reynolds number variation from  $2.45 \times 10^6$  to  $18.7 \times 10^6$  on the lee-side center-line heating is examined in the lower portion of figure 1. The data depart initially from laminar theory (ref. 5) and then rise to a peak whose value and location are unit Reynolds number dependent. After the heating decreases beyond this peak to near laminar values and with further increases in  $R_{\infty, x}$ , the data begin an abrupt rise and subsequently enter an apparently turbulent boundary-layer region. The peak Stanton number values obtained on the delta wing in the low Reynolds number range are almost double the values found on the center line with a turbulent boundary layer. Furthermore, these peak values are 10 to 15 percent higher than the largest Stanton number values obtained on the center line at  $\alpha = 0^\circ$  at a comparable free-stream unit Reynolds number.

In figure 1, beyond about  $R_{\infty, x} = 6 \times 10^6$ , a portion of the data at the two highest unit Reynolds numbers correlates with a slope and level predicted by the  $\alpha = 5^\circ$  turbulent strip-theory calculation of Spalding and Chi as modified for heating (ref. 6) wherein the virtual origin is taken as the position of peak heating. Past results have indicated that this simple flat-plate heating calculation can predict the trend of turbulent center-line heating in this high-shear region, but comparison of this prediction with other delta-wing data in reference 1 (not presented) suggests that the present precise agreement of the level of the data is fortuitous. If only a limited amount of this center-line data had been available (i.e., if data had existed only for  $R_{\infty, x} < 10^6$ ), the conclusion might have been reached that transition had occurred. Examining the heating data beyond the peak ( $10^6 < R_{\infty, x} < 4 \times 10^6$ ), however, indicates a departure from known flat-plate boundary-layer characteristics. The center-line pressure distribution exhibits a similar variation with Reynolds number, although the magnitude of the variation is around 15 percent compared to a maximum change of around 400 percent in the surface heating. The variation in the pressure distribution, even though it is small, does indicate the complexity of the flow in the center-line region.

Heating values on the remainder of the lee surface are examined by dividing an off-center-line Stanton number value by the center-line value along a line perpendicular to the leading edge (see sketch in fig. 2). The six chordwise stations nearest the trailing edge were selected; the most

forward station examined was located at about the half-chord station from the apex ( $x/L = 0.48$ ). Heating data in the region where the center-line data are known to be turbulent are shown on the right-hand side of figure 2 ( $R_{\infty,L} = 18.7 \times 10^6$ ). For this condition, the data off the center line correlate as a function of the opening angle from the center line  $\theta$ . This high Reynolds number correlation is characteristic of a conical flow field and has been observed on delta wings at lower Mach numbers (ref. 3). Moving out spanwise from the center line, the Stanton number increases until the exterior boundary of the high-shear region is reached (the feather region determined by the oil-flow technique). Beyond this boundary, the heating falls off to a more constant value.

At the lowest unit Reynolds number ( $R_{\infty,L} = 2.4 \times 10^6$ ) shown on the left in figure 2, no such simple conical correlation was found, though the general trend at a given x-station is the same as that for the higher Reynolds number data, that is, an initial spanwise rise to the boundary of the feather region followed by a sharp drop in the Stanton number farther outboard. However, the initial rise from the center-line heating value increases in magnitude as the distance down the plate increases. Near the trailing edge, the heating just off the center line is 3 times that at the center line. As the data in figure 1 suggest, this lack of correlation is mainly attributable to the decrease in the heating down the center line. The peak heating at the outboard boundary of the high-shear region is nearly constant for the six stations examined in figure 2 at any given unit Reynolds number.

The heating distribution for stations farther upstream shows a departure from the behavior of the data shown in figure 2. At both Reynolds numbers, the heating at these forward stations generally peaks at the center line.

An analogy can be drawn between the flow over the lee surface of a delta wing and the flow over a  $90^\circ$  corner flow model (ref. 7). The flow fields are similar in character, with both geometries exhibiting two or more vortices as a result of interacting flow components. Heating patterns on the model surface in the vicinity of the vortices evidence similar conical flow properties under certain conditions, and the center-line heating for both geometries for a specified Reynolds number range shows a similar departure from predicted laminar results. The interested reader can refer to reference 7 for a direct comparison with the results presented herein for the delta wing.

#### CONCLUDING REMARKS

The results of this investigation of the lee-surface heating when separation and the vortex system initiate at the leading edge indicate that high localized heating occurs in the center-line region which can be attributed to the vortices. A study of the effect of a variation in free-stream Reynolds number from about  $2 \times 10^6$  to  $20 \times 10^6$  based on model length shows that the maximum values of the Stanton number on the lee surface occur on the center line at low unit Reynolds numbers. These values are well above laminar flat-plate predictions and exceed all Stanton number values found at zero angle of attack at a comparable free-stream Reynolds number. This localized high

heating on the lee surface should be considered in the design of hypersonic vehicles, especially for the cruise-type vehicle which operates at low angles of attack. When the center-line region is turbulent, the surface heating across the span can be correlated in conical coordinates. No such correlation exists for the lower Reynolds number data.

## REFERENCES

1. Whitehead, Allen H., Jr.; and Keyes, J. Wayne: Flow Phenomena and Separation Over Delta Wings With Trailing-Edge Flaps at Mach 6. AIAA J., vol. 6, no. 12, Dec. 1968, pp. 2380-2387.
2. Cross, E. J., Jr.; and Hankey, W. L.: Investigation of the Leeward Side of a Delta Wing at Hypersonic Speeds. AIAA Paper No. 68-675, June 1968.
3. Bertram, Mitchel H.; Cary, Aubrey M., Jr.; and Whitehead, Allen H., Jr.: Experiments With Hypersonic Turbulent Boundary Layers on Flat Plates and Delta Wings. AGARD CP No. 30, May 1968, pp. 1-1 - 1-21.
4. Murray, William M., Jr.; and Stallings, Robert L., Jr.: Heat-Transfer and Pressure Distributions on 60° and 70° Swept Delta Wings Having Turbulent Boundary Layers. NASA TN D-3644, 1966.
5. Bertram, Mitchel H.; and Feller, William V.: A Simple Method for Determining Heat Transfer, Skin Friction, and Boundary-Layer Thickness for Hypersonic Laminar Boundary-Layer Flows in a Pressure Gradient. NASA MEMO 5-24-59L, 1959.
6. Neal, Luther, Jr.; and Bertram, Mitchel H.: Turbulent-Skin-Friction and Heat-Transfer Charts Adapted From the Spalding and Chi Method. NASA TN D-3969, 1967.
7. Stainback, P. Calvin; and Weinstein, Leonard M.: Aerodynamic Heating in the Vicinity of Corners at Hypersonic Speeds. NASA TN D-4130, 1967.



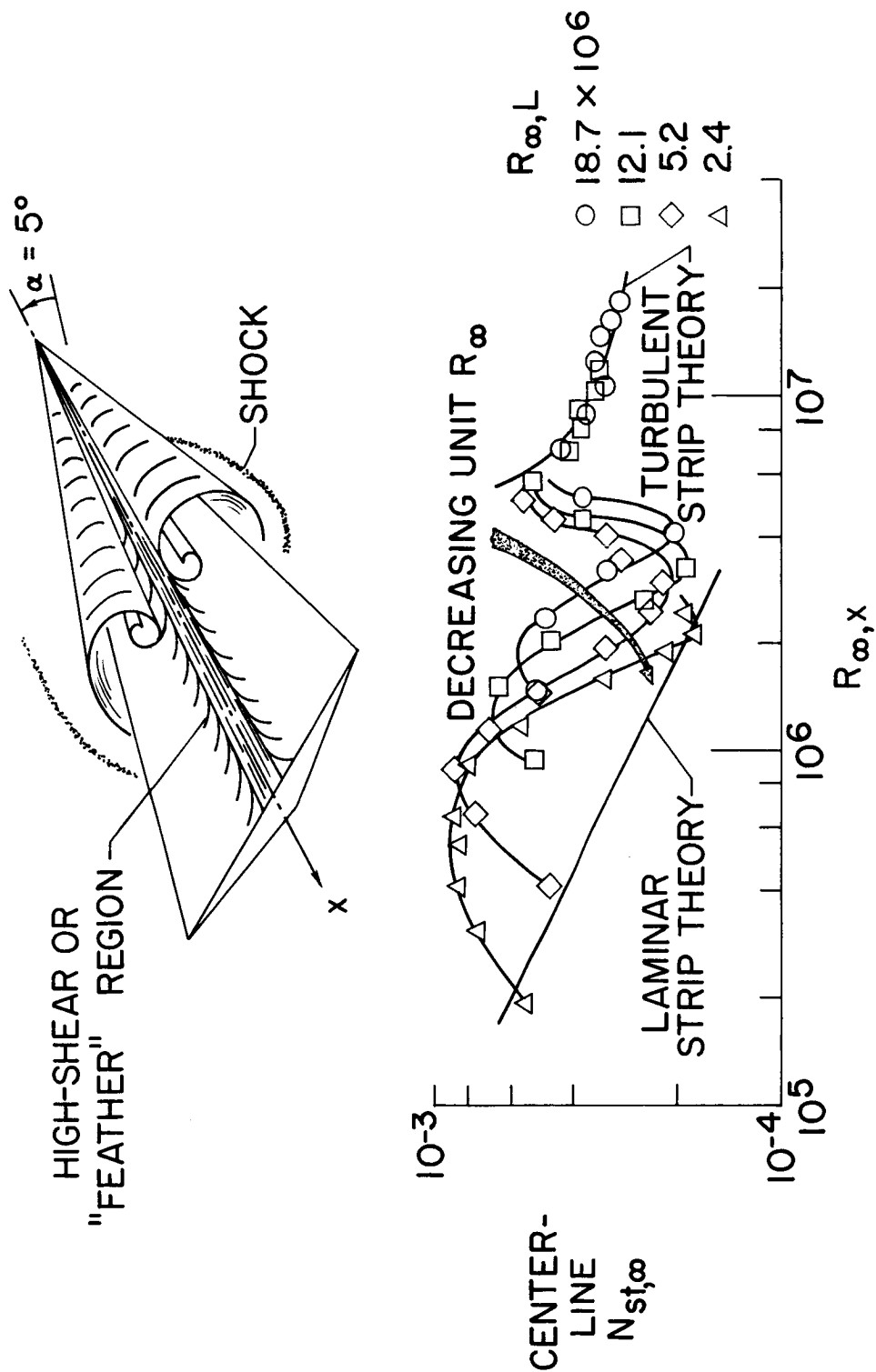


Figure 1.- Flow field and center-line heating on lee surface of 75° swept wing.  $\alpha = 5^\circ$ ;  $M_\infty = 6$ .

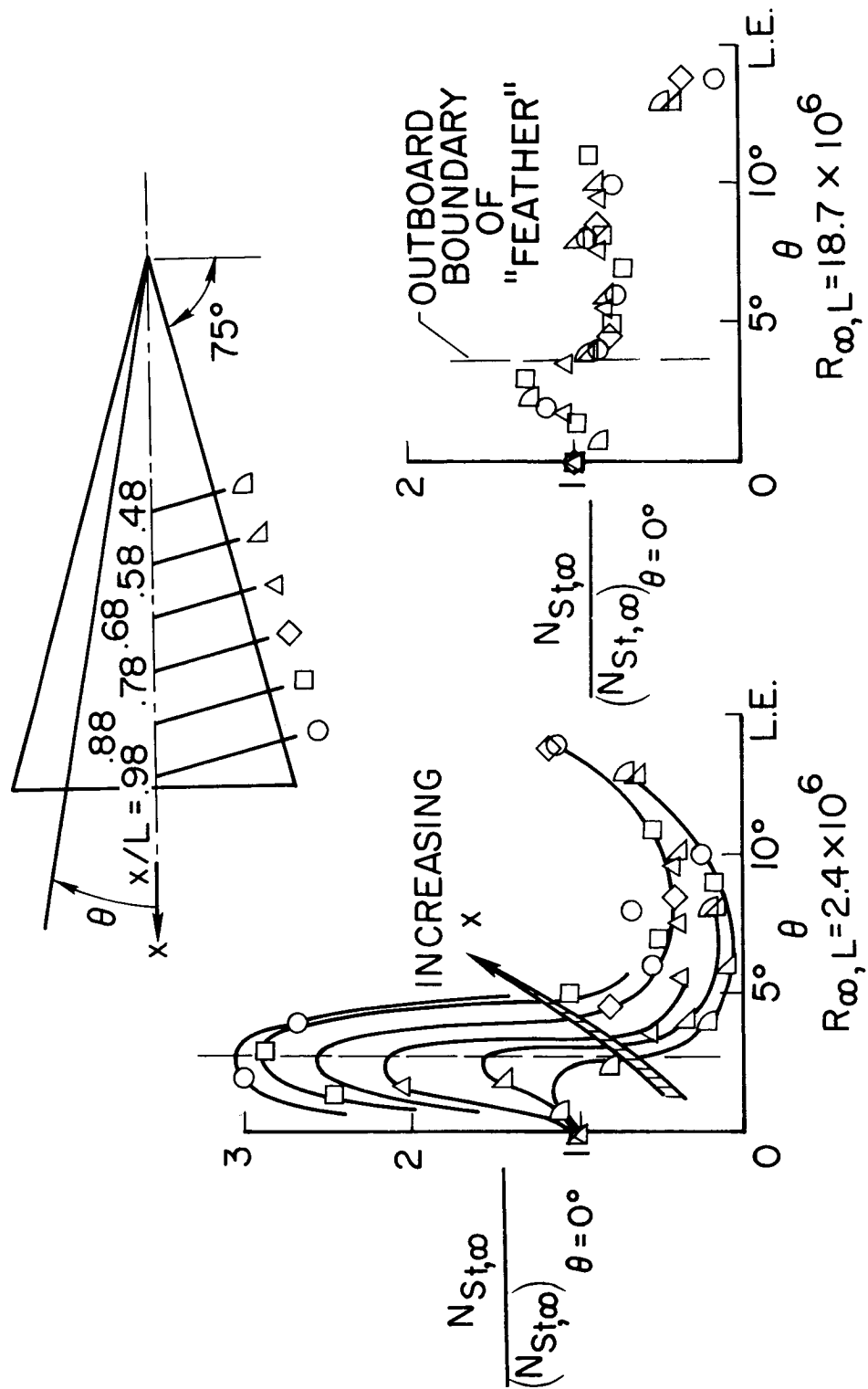


Figure 2.- Heating off the center line on lee surface of delta wing.  
 $M_\infty = 6$ ;  $\alpha = 5^\circ$ ;  $L = 26.1$  inches.

# BOUNDARY LAYER AND STARTING PROBLEMS ON A SHORT

## AXISYMMETRIC SCRAMJET INLET

By J. R. Henry, E. H. Andrews, Jr.,  
S. Z. Pinckney, and C. R. McClinton

NASA Langley Research Center

### SUMMARY

Practical boundary layer problems which were encountered in the experimental development of the inlet for the NASA Hypersonic Research Engine (HRE) Project are discussed. Early experimental investigations conducted at Mach 4 under the Project revealed an inlet starting problem. A subsequent investigation indicated that wall cooling had a favorable effect on starting. The results of in-house analytical and experimental investigations of the starting phenomena are summarized, and a summary of extensive starting investigations conducted under the Project on a revised inlet design is given.

The results of the in-house investigations show that the boundary layer development along the inlet centerbody is predicted within engineering accuracy by an integral boundary layer prediction method developed in-house; however, the method should be extended to include non-equilibrium effects on the velocity distribution. The accuracy of prediction methods is still hampered by the inability to predict the location of transition, to compute accurately through the transition region, and to account correctly for trip losses. A method for predicting inlet starting characteristics is needed which adequately accounts for the complex flow situation which exists at the cowl leading edge station during the starting process.

### INTRODUCTION

The paper will discuss some practical boundary layer problems which were encountered in the experimental development of the inlet for the NASA Hypersonic Research Engine (HRE) Project. The conceptual and preliminary design phase of the project was initiated in 1965 and the development phase in 1967. The HRE is an axisymmetric scramjet engine designed to operate at freestream Mach numbers ranging from 4.0 to 8.0 with a minimum internal thrust performance schedule

specified. Subsonic combustion of hydrogen fuel is employed up to approximately Mach 6 and supersonic combustion above Mach 6. Flight research investigations of the engine mounted beneath the X-15 airplane were planned initially; however, this phase of the project has been dropped.

Early experimental investigations of the inlet at Mach 4 at the Langley Research Center revealed a starting problem which apparently resulted from a shock - boundary - layer interaction in the region of the cowl leading edge station. Subsequent investigations at the Ordnance Aero-Physics Laboratory in Dangerfield, Texas, suggested that wall cooling had a favorable effect on the starting process. Since this problem is of general interest to hypersonic inlet technology, an in-house analytical and experimental investigation was initiated to investigate starting phenomena, with particular emphasis on the effects of wall cooling on the boundary layer development and starting capability. The major portion of the paper will be concerned with the results of the in-house investigations; however, a summary of the results of extensive starting investigations conducted under the Project in Tunnel A at the AEDC in Tullahoma, Tennessee, also will be presented. The latter data cover a freestream Mach number range from 4.0 to 5.5 and were taken on a 2/3-scale model of the "T" design inlet, which is a revised design and which has somewhat different contours than the 1/3-scale model investigated in-house. The material presented in the paper is focused on the capability of current technology relative to the prediction of the boundary layer development on the centerbody, on the details of the flow at the cowl lip station when the inlet is in the unstarted condition, and on the relation of the boundary layer to the inlet starting characteristics.

#### SYMBOLS

C. R.	internal contraction ratio; ratio of geometric flow area at the cowl lip station to that at the throat station
d	diameter, in.
h	gap height at cowl lip as defined in table II
L. E.	cowl leading edge
M	Mach or Mach number
$M_l$	local (boundary layer edge) Mach number at cowl lip station

$p$	static pressure, lb./sq. in.
$p_l$	local static pressure in flow field, lb./sq. in.
$p_t$	total pressure, lb./sq. in.
$r$	radius, in.
$R$	cowl capture radius, in., as defined in table II
$T_t$	total temperature, °R
$T_w$	wall temperature, °R
$u$	velocity, ft./sec.
$x$	longitudinal axial distance from centerbody sharp vertex, in.
$x_{CL}$	x-distance to cowl leading edge as defined in table II
$y$	vertical distance from centerbody surface; perpendicular to surface, in.
$z$	vertical distance from centerbody surface; perpendicular to model center line, in.
$\delta$	boundary layer thickness, in.
$\delta^*$	boundary layer displacement thickness, in.
$\theta$	boundary layer momentum thickness, in.

Subscripts:

EXP.	experimental
THEO.	theory
$\infty$	freestream

## INHOUSE INVESTIGATIONS

### Model and Instrumentation

A sketch of the in-house model is given in figure 1 and table I presents coordinates. The leading edges of the centerbody and cowl were blunted for heat protection purposes. The blunted tip of the centerbody is followed by a conical section with a  $10.25^\circ$  half angle. The conical section precedes an isentropic compression region containing  $11.15^\circ$  of compression which starts at station 8.5 and ends at station 12.60. The isentropic region is followed by a short conical section and an expansion shoulder of the centerbody. The major portion of the internal flow surfaces has a  $5^\circ$  wall slope. The centerbody surface was cooled by an internal liquid nitrogen cooling system; the cowl was uncooled and measured 6.04 inches in diameter at the leading edge. Boundary layer trips were installed at an x-station of 1.756 inches, as noted on figure 1. The cowl (figure 1) was provided with small slots through which pitot survey tubes were inserted in order to conduct surveys at the cowl leading edge and throat stations. The slots were sealed and faired for runs which did not include surveys. The downstream portion of the cowl contained bypass slots to prevent choking downstream of the throat. The longitudinal position of the cowl was set between runs. A single row of static pressure orifices and thermocouples was installed in the centerbody skin extending from an x-location of 4.00 inches to 14.34 inches at incremental lengths varying from 4 inches to 0.25 inches. At station 13.00, four equally spaced static pressure orifices were located, and at stations 13.50 and 14.34, two orifices were spaced  $30^\circ$  apart. The pitot pressure survey tube had a 0.005 by 0.024 inch opening at the tip, which was positioned parallel to the centerbody surface.

### Design Philosophy

One aspect of the philosophy which was used to produce the specific HRE inlet design is illustrated in figure 2. The HRE inlet has a relatively large amount of external compression which permits the throat of the inlet to be located close to the cowl leading edge. A more conventional inlet, such as the one shown at the top of figure 2, has only a small amount of external isentropic compression and significantly more internal compression. These characteristics tend to locate the throat further downstream on the centerbody, producing a longer configuration. The more conventional design has approximately twice the opening height between the centerbody and cowl leading edge when the cowl is in the starting position.

Assuming that the height of the opening relative to the boundary layer thickness is a parameter significant to the starting capability, the HRE inlet design reflects a choice of a shorter configuration with a possible starting problem in preference to a longer configuration with less probability of a starting problem.

#### Flow Field and Boundary Layer Studies Without Cowl

Inviscid flow. - One of the purposes of the in-house investigation was to measure the development of the boundary layer along the centerbody and to assess the capability of state-of-the-art turbulent boundary layer methods to predict this boundary layer development. The conditions at the edge of the boundary layer, or the inviscid flow field, must be known in order to make a boundary layer prediction. Therefore, a comparison of experimental observations of the inviscid flow field with analytical predictions is of interest. Such a comparison is given in figure 3 which presents theoretical and experimental locations for the shock generated by the centerbody tip at a freestream Mach number of 4. The theoretical flow field was determined using blunt body and characteristics theories (references 1 to 3). The centerbody contour was corrected by approximate values for the boundary layer displacement thickness. Figure 3 also indicates that a weak shock was imbedded in the isentropic compression region as a result of small imperfections in the model contour. The agreement between theory and experiment is considered to be satisfactory. For reference purposes, the figure includes the contour of the cowl (dashed lines) and the location of the cowl leading edge station where pitot pressure surveys were made.

The static pressure distribution along the centerbody surface also is required for input to a boundary layer analysis; comparisons of experimental and theoretical values of this parameter are given in figure 4. Experimental data are presented for three wall temperatures; however, a theoretical curve for only the adiabatic case is given because changes in wall temperature produced only small changes in the predicted static pressure. On the lower portion of the figure, the centerbody contour is superimposed. In the region where the wall slope changed rapidly from the end of the isentropic region to the upstream part of the centerbody shoulder ( $x/R$  of 4.0 to 4.4), there are some data excursions and discrepancies between data and theory. At all other locations, including the cowl leading edge station, the agreement is satisfactory. The major portion of the discrepancies between data and theory was caused by insufficient accuracy in the contour coordinates used in the analysis.

Boundary layer studies. - The pitot pressure survey station ( $x_{CL}/R = 4.5$ ) was located on the expansion shoulder of the centerbody which of course set up a longitudinal gradient as well as a normal pressure gradient. The normal pressure gradient caused a problem in processing the pitot data. The model was too small to make static pressure measurements so that a method had to be devised for processing the data. Figure 5 outlines the method that was used. Three static pressure profiles are presented, each for a different wall temperature ratio. The computed total pressure recovery through the shock generated by the tip of the centerbody and the imbedded shock is 97%, a value which can be determined with high accuracy. By combining this total pressure recovery with the pitot readings, the static pressure profiles (circle symbols) in the inviscid flow field were obtained. Wall static pressures were also measured; therefore, a static pressure profile in the boundary layer has to be some faired curve between the wall value and the circle point curve. The shape of this curve was determined by using the inviscid flow field calculations as a guide; an example of these calculations is given by the square symbols for the adiabatic wall case. After the data had been processed in this manner, integrations across the boundary layer were performed to obtain the usual boundary layer integrated parameters. The integrated parameters then were compared with analytical values obtained using a boundary layer prediction method.

Before making these comparisons, the main features of the prediction method will be outlined. This method was developed by one of the co-authors, S. Z. Pinckney. An integral method which included the usual forms of the integral momentum and energy equations was used. Spalding-Chi friction coefficient and heat transfer relations (ref. 4) were employed. Equilibrium velocity profiles corresponding to the law of the wall (ref. 5) and Coles' wake function (ref. 6) also were assumed. A temperature-velocity profile method was used which is similar to a modified Crocco profile and which also was developed by Pinckney (ref. 7). The outstanding feature of this method is that an iterative calculation is performed such that an integration across the boundary layer produces a total energy deficiency for the boundary layer that is consistent with the total amount of heat transfer through the wall of the body up to the station under consideration. The boundary layer calculation was initiated using the laminar theory of reference 8 up to the transition point, which was assumed to occur at an  $x$ -value of approximately 5.0 inches. This transition location was based on limited experimental observations made prior to the main experimental program; transition was assumed to be initiated and completed at this station.



Predictions obtained using the theory and experimental values of momentum thickness,  $\theta$ , are given in figure 6(a) as a function of the wall temperature ratio for Mach numbers 4 and 6. Comparisons of the theory with the corresponding data points indicate that the agreement is within engineering accuracy with the biggest discrepancy occurring at Mach 6 at the lowest wall temperature ratio; this discrepancy amounts to about 18%. Similar comparisons are presented in figure 6(b) for the displacement thickness,  $\delta^*$ . Satisfactory engineering accuracy again is evident. Figure 7 presents a comparison between experimental and theoretical velocity distributions for three different wall temperature ratios. The experimental profiles clearly are considerably flatter than the theoretical predictions. This is a reasonable result because the survey station is located on the expansion shoulder of the centerbody which sets up a favorable longitudinal pressure gradient. With this type of pressure gradient, the profiles would be expected to be flatter than for the equilibrium profiles which were assumed for the theoretical predictions. It would be desirable to be able to predict the details of the velocity distribution more accurately; therefore, it is concluded from figure 7 that the prediction method should be extended to include non-equilibrium effects on the velocity distribution.

#### Boundary Layer Studies With Cowl Installed

Pitot pressure surveys were made at the cowl leading edge station with the cowl in position and with the inlet in the unstarted condition. These measurements were exploratory in nature and were for the purpose of identifying the general type of flow which the inlet would have to ingest in order to start. These data were analyzed in conjunction with the surveys in the inlet throat and also the surveys at the cowl lip station without the cowl installed. From these analyses a simplified flow model was constructed which would be amenable to evaluation using the limited amount of data available. Some preliminary results from these analyses are presented in figures 8(a) and 8(b).

The simplified flow model for the Mach 4 adiabatic wall case is diagrammed in figure 8(a). The cowl lip station survey without the cowl installed provided the conditions in the undisturbed flow upstream of the shock system, as described in a previous section. The survey across the geometric throat station was in a region where the Mach numbers were slightly below sonic indicating that the aerodynamic throat was somewhat further downstream. The flow distribution across the throat station was relatively uniform, and integrations were performed to obtain accurate values of the mass flow ingested

by the inlet. Having established the mass flow, the capture streamtube location was fixed accordingly, as indicated in figure 8(a). The experimentally determined edge of the boundary layer is shown on the sketch and, by comparison with the edge of the capture streamtube, one concludes that the inlet ingested only the lower half of the boundary layer.

The pitot data from the survey at the lip station with the cowl installed indicated that compressions had to exist upstream of the normal shock assumed to be positioned in front of the inlet opening. These compressions were assumed to consist of an oblique shock of appropriate strength, as indicated.

The preceding considerations resulted in the determination that a simple flow configuration consisting of an oblique shock followed by a normal shock was consistent with the data. It is obvious that variations of the adopted flow configuration also would satisfy the data and that, in the case of the real flow, the quasi-plane waves might penetrate only a short distance into the boundary layer before breaking down into more complex configurations. Nevertheless, the results of the limited analysis presented in figure 8(a) clearly suggest that the general type of real flow situation is a complex shock-boundary-layer interaction with an associated separation shock and a separated flow and re-circulation region adjacent to the centerbody surface. Similar flow configurations have been identified experimentally using more extensive measurements on a larger model by Mitchell and Cubbison (ref. 9).

A similar flow configuration to that of figure 8(a) is presented in figure 8(b) for a cooled wall case at Mach 4.0. Comparisons of the two figures indicate that the most significant effect of wall cooling was to increase the mass capture ratio from 81% for the adiabatic wall case to 89% for the case with a value of wall temperature ratio,  $T_w/T_{t,\infty}$ , of 0.2. Mass capture is defined as the ratio of actual mass flow ingested by the inlet to the estimated mass flow required to start the inlet. These results indicate that wall cooling had a favorable effect on the inlet starting characteristics but not favorable enough to start the inlet in this case.

The usual method used for predicting the starting characteristics of inlets is to perform a one-dimensional calculation using the Kantrowitz criterium. The calculation simply determines whether the required amount of mass flow will pass through the inlet throat with a one-dimensional normal shock located upstream of the inlet opening. This type of calculation is not valid for the present application where a significant portion of the ingested flow is boundary layer.

As shown in figures 8(a) and 8(b), the presence of the boundary layer causes a complex two-dimensional flow configuration which invalidates the one-dimensional assumption. The main overall conclusion of this study is that in order to predict successfully the starting characteristics of this inlet type a new method will have to be developed which adequately accounts for the complex flow configurations which exist in the vicinity of the cowl leading edge station during the starting process.

## HRE PROJECT INLET STARTING INVESTIGATIONS

### Model and Experimental Procedure

The overall starting characteristics of the HRE inlet were not determined in-house because the in-house model was not adequate for performing this type of experiment since the position of the centerbody could not be controlled remotely. However, as a part of the inlet development work conducted under the Project, extensive starting investigations were made over the Mach number range from 4.0 to 5.5 for appropriate ranges of Reynolds number, wall temperature, and trip configurations. Some aspects of these data will be discussed in the following paragraphs. The investigations were conducted in the AEDC Tunnel A on a 2/3-scale model of the latest design of the HRE inlet, which has been designated as the "T" design. This design differed somewhat from the in-house model in that the contours were modified to improve the starting characteristics.

The test procedure can be described using the sketch of internal contraction ratio schedule of figure 9. The tunnel conditions were set with the centerbody in the closed position, which is indicated by the dashed line on figure 9. The centerbody then was translated from the closed position following the contraction ratio curve through the minimum value and then to higher values up to the point at which the inlet started. As noted in figure 9, the data show that the inlet had an unusual starting characteristic: it either started in a band of low contraction ratios or the start was delayed until a high contraction ratio was obtained. Starting points were obtained in both high and low contraction ratio bands for duplicate test conditions with no detectable reason for the inlet's selection of one point in preference to the other at a given time.

## Starting Data Correlations

The internal contraction ratios at which the inlet started are depicted in figure 10 as a function of the computed Mach number at the edge of the centerbody boundary layer at the cowl lip station. The inviscid flow field and the boundary layer development on the centerbody were computed for each data point using the same prediction methods previously described. In the case of figure 10, the edge Mach number was determined from these computations, and a subsequent figure contains values of a boundary layer parameter at the cowl lip station which also was obtained from the calculations. The transition points in the boundary layer calculations were assumed to be located just downstream of the trips; or, if no trips were used, transition was assumed to occur near the end of the isentropic compression region, a location which is in agreement with limited survey data taken during the experiments.

Each data point of figure 10 is labeled with its particular values of wall temperature ratio and freestream stagnation pressure, parameters which affect the boundary layer growth and therefore the starting contraction ratio. The general arrangement of the data clearly shows the band of low contraction ratios (square symbols) and the band of high contraction ratios (circle symbols). The split of the data into the families of curves is emphasized further by the dashed lines, which show the data trends. All the low contraction ratio data and the high contraction ratio data with trips show a trend of increasing contraction ratio with increasing boundary layer thickness; increases in boundary layer thickness result from either increases in wall temperature or decreases in stagnation pressure. The variation of the high contraction ratio data without trips relative to changes in wall temperature or stagnation pressure is irregular because of the data scatter; for instance the two circle data points on the extreme left hand side of the figure are for the same test conditions but the contraction ratios differ significantly. This result may be a consequence of some flow instability for this category of starting contraction ratio.

The relation of the data of figure 10 to the boundary layer properties at the cowl leading edge station suggests that a correlation of the inlet starting characteristics using some measure of the boundary layer thickness should be possible. A correlation of this type is presented in figure 11 in which the height of the opening,  $h$ , at the cowl leading edge station is referenced to the computed boundary layer momentum thickness,  $\theta$ . The opening height, which is defined in table II, is the minimum value required to obtain an inlet start and is a unique function of contraction ratio

for a given inlet design. Under these circumstances the use of  $\theta$  as a correlating parameter would be expected to collapse the data relative to changes in wall temperature ratio and stagnation pressure; the curves of figure 11 show that the correlations are successful except for the high contraction ratio case with no trips. In this case the data scatter prevents a significant correlation.

The correlation curves reveal several other points of interest. All the cases with trips correspond to the high end of the free-stream Mach number range. It was not possible to start the inlet at Mach 4 with a trip installation, apparently because the trips increased the boundary layer thickness to the extent that the inlet would not start. The correlation curves in all cases have a discontinuity between the trip and no trip branches which is believed to reflect the inability to accurately predict the location of transition, to accurately compute through the transition region, and to account satisfactorily for trip losses. If these items could have been accomplished, it is believed that the curves would have been continuous. One data point is shown on figure 11 which corresponds to a sharpened leading edge on the cowl; this modification considerably improved the starting characteristic by reducing the required opening,  $h$ .

#### CONCLUDING REMARKS

Some practical boundary layer problems which were encountered in the experimental development of the axisymmetric inlet for the NASA Hypersonic Research Engine (HRE) Project have been reviewed. The inlet type under consideration is characterized by the fact that the flow ingested by the inlet during the starting process contains a significant amount of boundary layer. Experimental evaluations of the inlet starting characteristics obtained in in-house as well as HRE Project investigations have been presented, and an assessment has been made of the capability of current state-of-the-art boundary layer methods relative to predicting these characteristics. The following statements summarize the principal results:

1. The turbulent boundary layer integral method used for predicting boundary layer growth along the inlet centerbody, which included regions of both adverse and favorable pressure gradients, agreed within engineering accuracy with experimental values of displacement and momentum thicknesses. However, significant discrepancies between

experimental and predicted boundary layer velocity profiles were noted indicating that the theory should be modified to include non-equilibrium effects on the velocity profile.

2. The accuracy of theoretical prediction methods still is hampered by the inability to predict the location of transition, to compute through the transition region accurately, and to account adequately for trip losses.
3. Relative to the inlet starting problem itself, the development of a sophisticated method for predicting inlet starting characteristics is needed which adequately accounts for the complex flow situations which exist in the vicinity of the cowl leading edge station during the starting process.

#### REFERENCES

1. Lomax, Harvard; and Inouye, Mamoru: Numerical Analysis of Flow Properties About Blunt Bodies Moving at Supersonic Speed in an Equilibrium Gas. NASA TR R-204, July 1964.
2. Inouye, Mamoru: Blunt Body Solutions for Spheres and Ellipsoids in Equilibrium Gas Mixtures. NASA TN D-2780, May 1965.
3. Inouye, Mamoru; Rakich, John V.; and Lomax, Harvard: A Description of Numerical Methods and Computer Programs for Two-Dimensional and Axisymmetric Supersonic Flow Over Blunt-Nosed and Flared Bodies. NASA TN D-2970, August 1965.
4. Neal, Luther, Jr., and Bertram, Mitchel H.: Turbulent-Skin-Friction and Heat-Transfer Charts Adapted from the Spalding and Chi Method. NASA TN D-3969 May 1967.
5. Van Driest, E. R.: Turbulent Boundary Layer in Compressible Fluids. J. Aeron. Sci., vol. 18, no. 3, Mar. 1951, pp. 145-160, 216.
6. Coles, Donald: The Law of the Wake in the Turbulent Boundary Layer. J. Fluid Mech., vol. 1, pt. 2, July 1956, pp. 191-226.

7. Pinckney, S. Z.: Static-Temperature Distribution in a Flat-Plate Compressible Turbulent Boundary Layer with Heat Transfer. NASA TN D-4611, June 1968.
8. Maslowe, S. A.; and Benson, John L.: Computer Program for the Design and Analysis of Hypersonic Inlets. Rep. No. 18079, Lockheed-California Co. Aug. 31, 1964.
9. Mitchell, Glenn A.; and Cubbison, Robert W.: An Experimental Investigation of the Restart Area Ratio of a Mach 3.0 Axisymmetric Mixed Compression Inlet. NASA TM X-1547, April 1968.

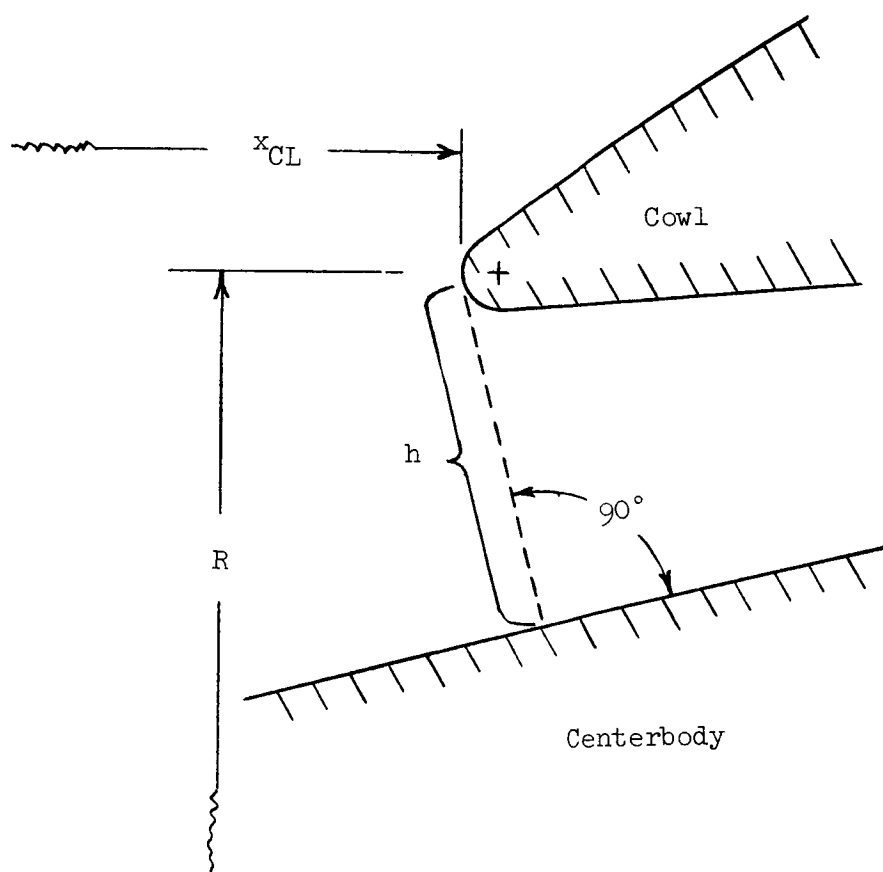
TABLE I. - COORDINATES OF IN-HOUSE  
INLET MODEL

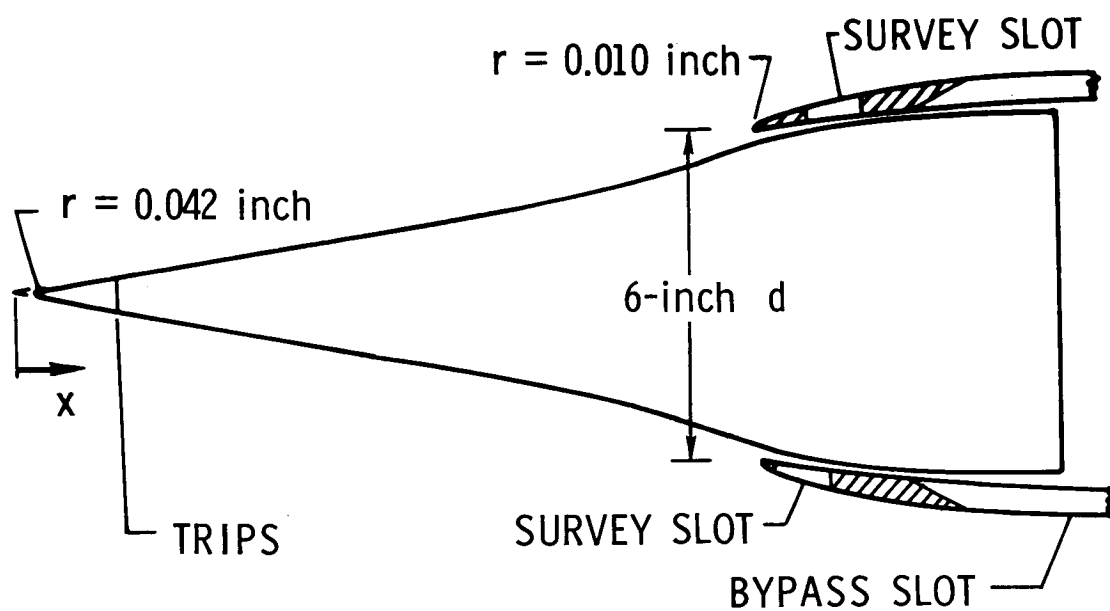
R = 3.020 in.

Centerbody			Cowl $x_{CL}/R = 4.5$		
x/R	y/R		x/R	y/R	
0.0611	0.0000	.04166 in. nose radius	4.4934	1.0000	.01 in. lip radius
0.0749	0.0136	} 10.25° Compression ↓	4.4974	0.9966	
2.8146	0.5086		4.5265	1.0003	
3.1457	0.5702		4.5596	1.0059	
3.3113	0.6034		4.5927	1.0123	
3.4768	0.6389		4.6258	1.0193	
3.6424	0.6789	} 21.4° Expansion ↓	4.6589	1.0254	
3.8079	0.7238		4.6921	1.0297	
3.9735	0.7777		4.7252	1.0335	
4.1722	0.8517		4.7583	1.0371	
4.3377	0.9165		4.7914	1.0406	
4.4702	0.9613	} 5° 0°	4.8245	1.0440	
4.6358	0.9982		4.8907	1.0501	
4.8013	1.0191		4.9238	1.0530	} 5°
4.9669	1.0355		5.3212	1.0877	
5.1325	1.0505				
5.2980	1.0653				
5.4636	1.0797				
5.6291	1.0827				
5.9603	1.0827				



TABLE II. - DEFINITION OF PARAMETERS





$M_\infty = 4$ , 0.018 in. d @ 3 d SPACE

$M_\infty = 6$ , 0.047 in. d @ 3 d SPACE

Figure 1.- In-house model.

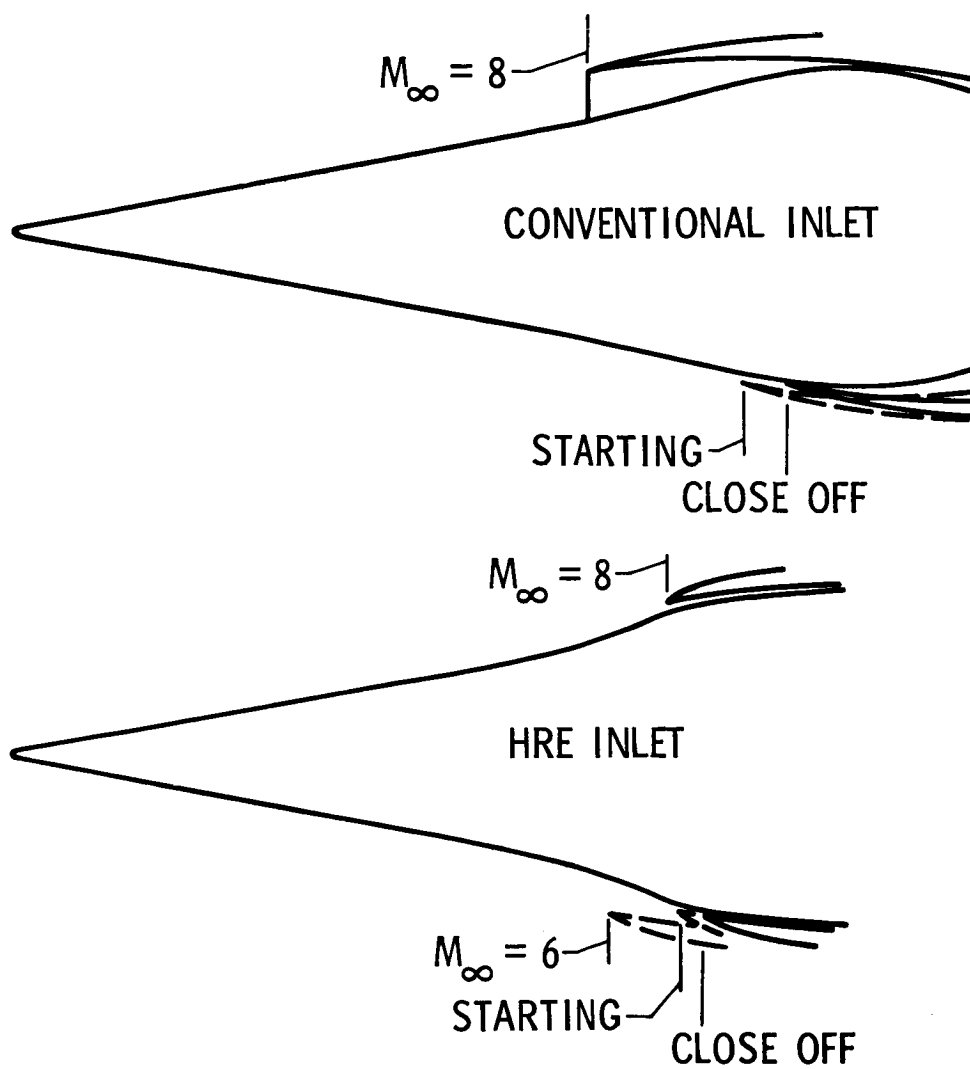


Figure 2.- Inlet designs.

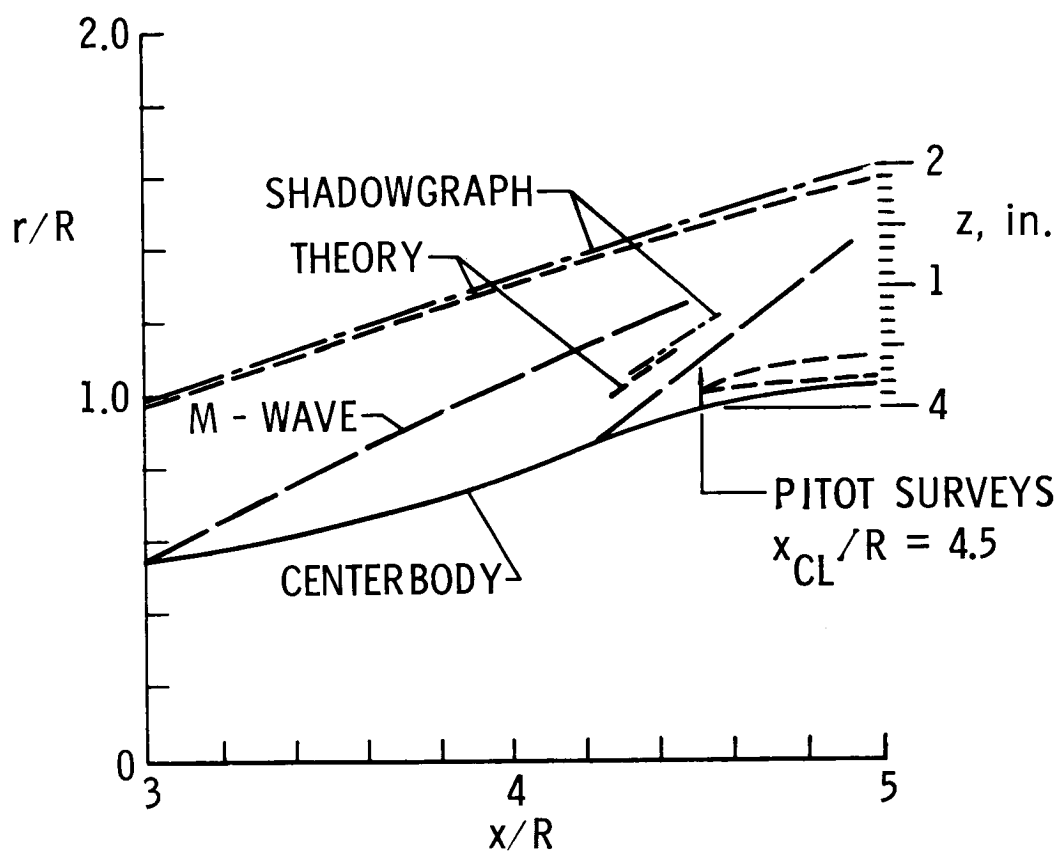


Figure 3. - Flow field of centerbody without cowl.

$$M_{\infty} = 4; p_{t,\infty} = 48 \text{ psia}; T_{t,\infty} = 635^{\circ}\text{R}.$$

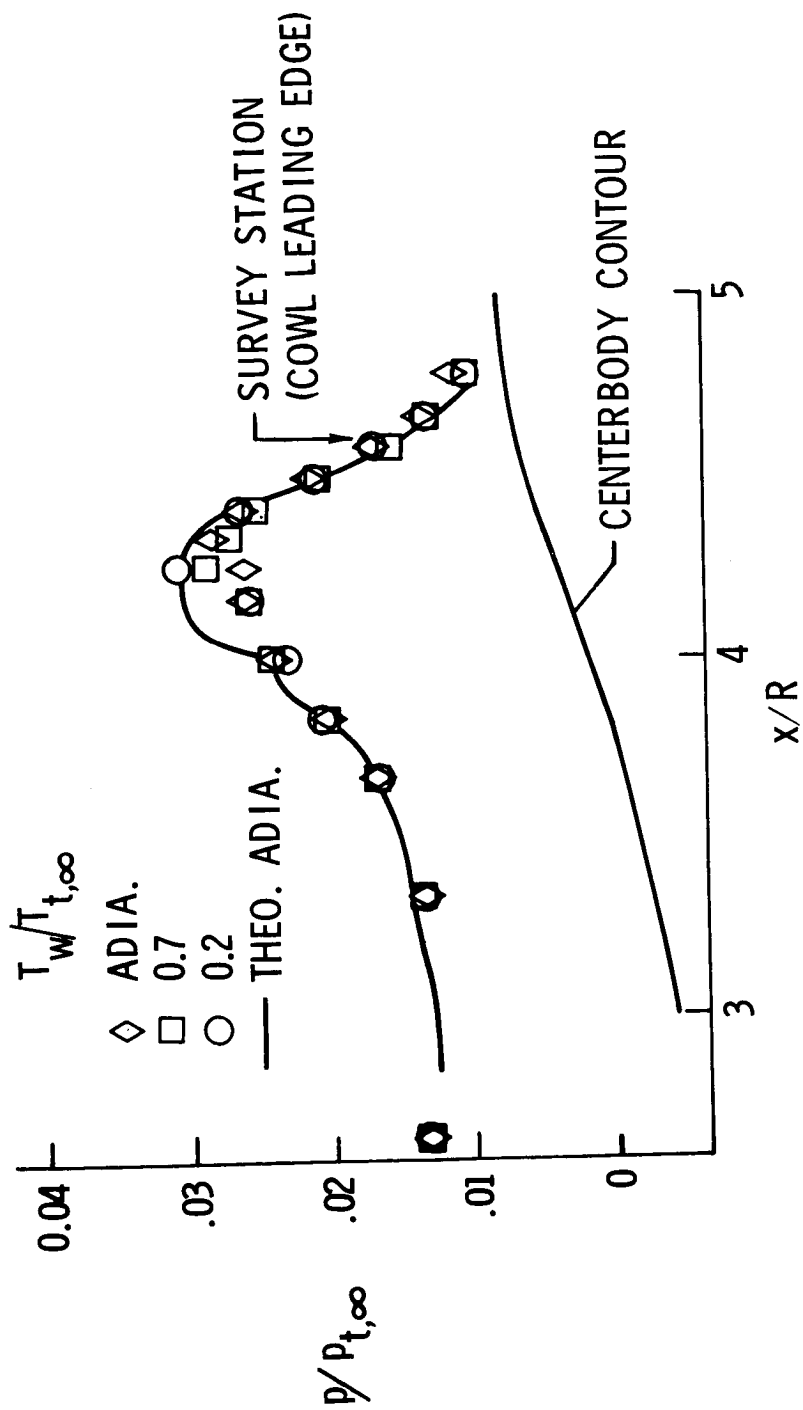


Figure 4.—Centerbody static pressure distributions without cowl.  $R = 3.02$  in.;  $M_\infty = 4$ ;  $p_{t,\infty} = 53.82$  psia;  $T_{t,\infty} = 700^\circ R$ .

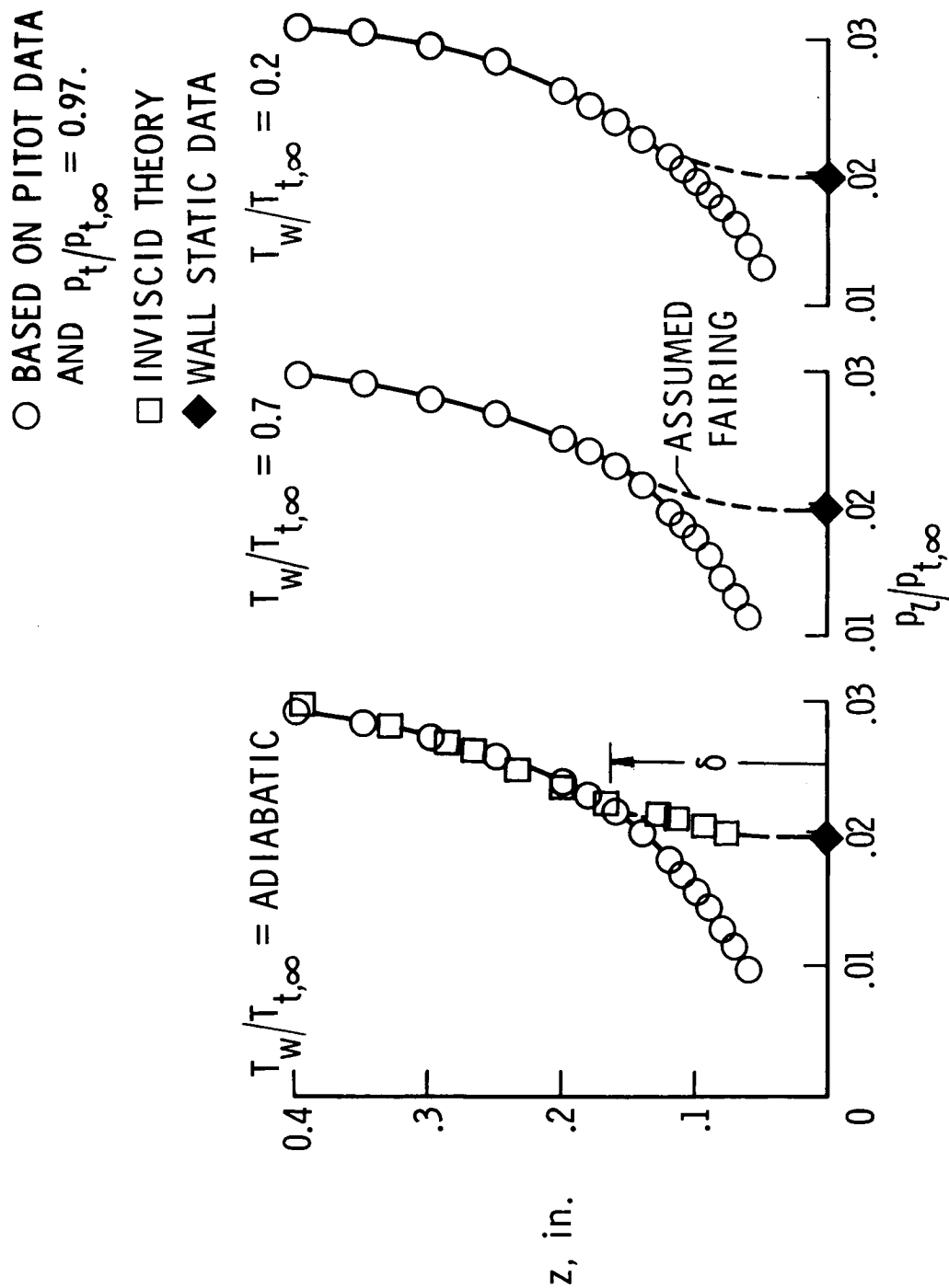
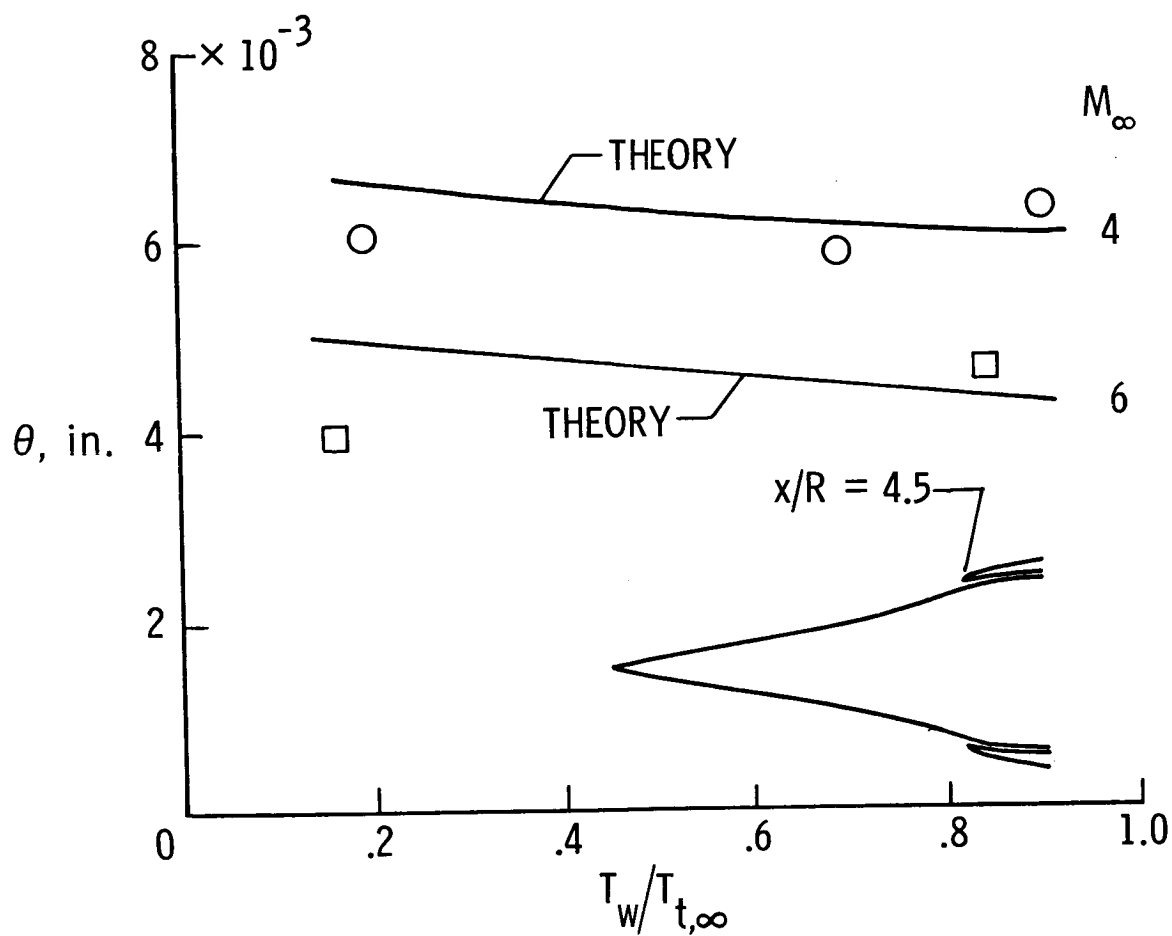
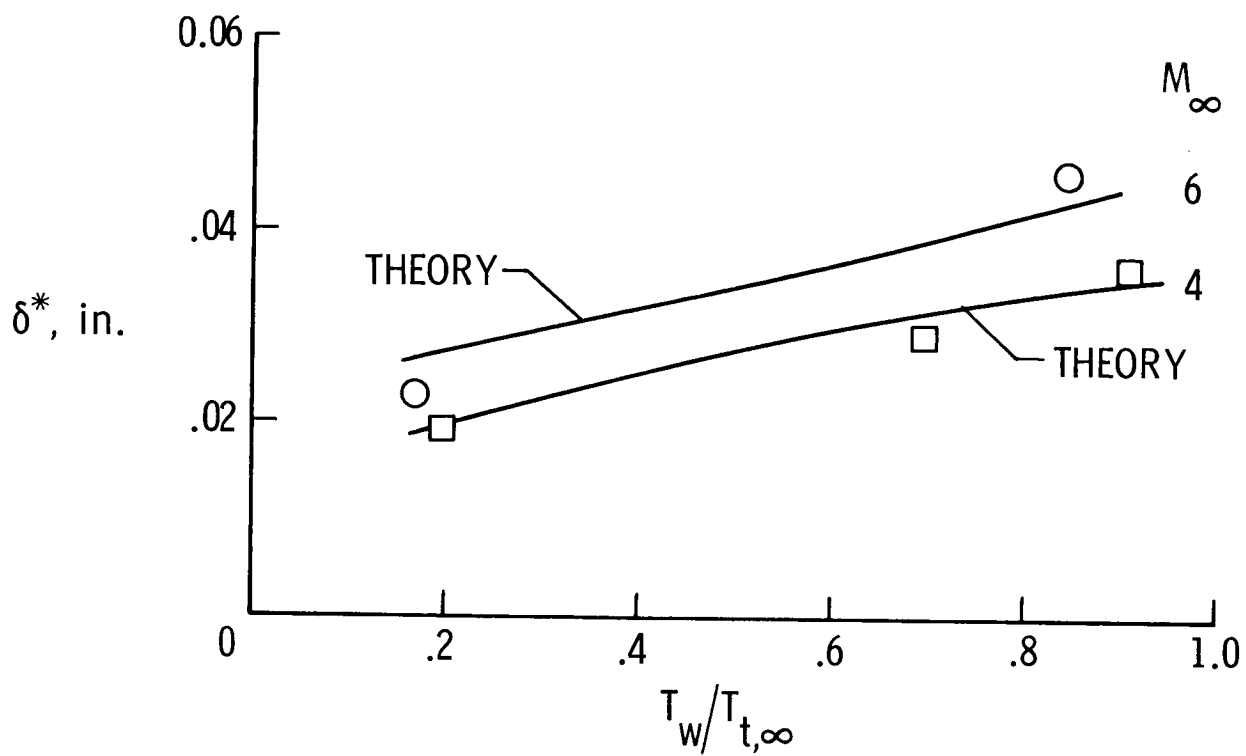


Figure 5. - Static pressure profiles without cowl.  
 $x/R = 4.5$ ;  $M_\infty = 4$ ;  $p_{t,\infty} = 53.82 \text{ psia}$ ;  $T_{t,\infty} = 700^\circ \text{R}$ .



(a) Momentum thickness.

Figure 6. - Boundary layer parameters of centerbody without cowl.  $x/R = 4.5$ .



(b) Displacement thickness.

Figure 6. - Concluded.



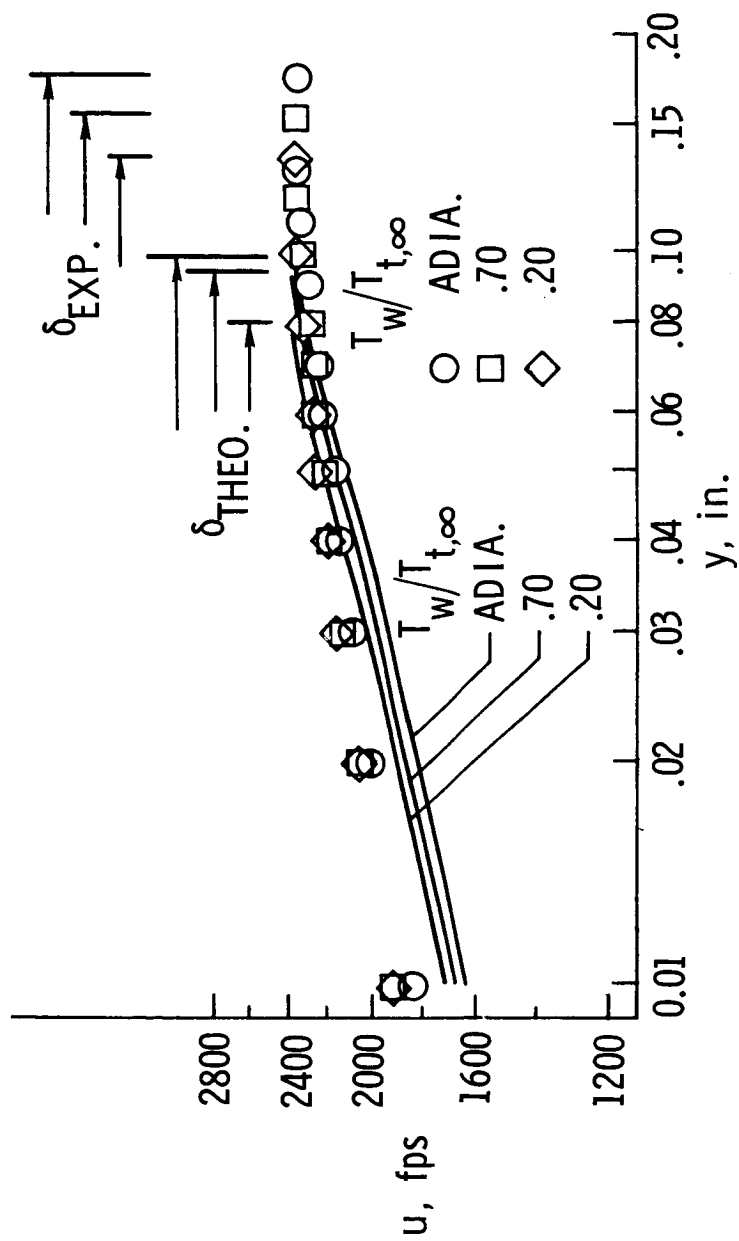
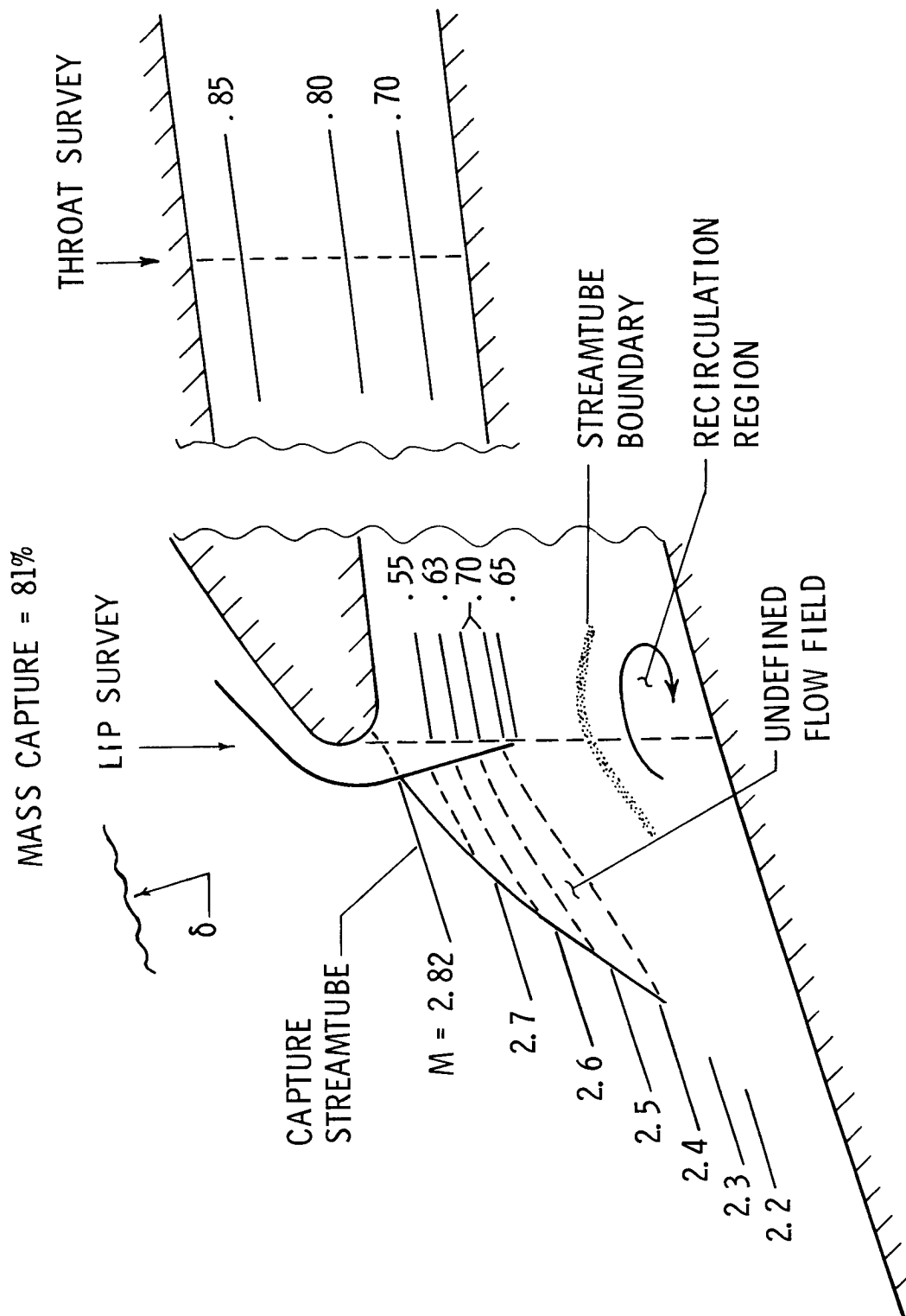


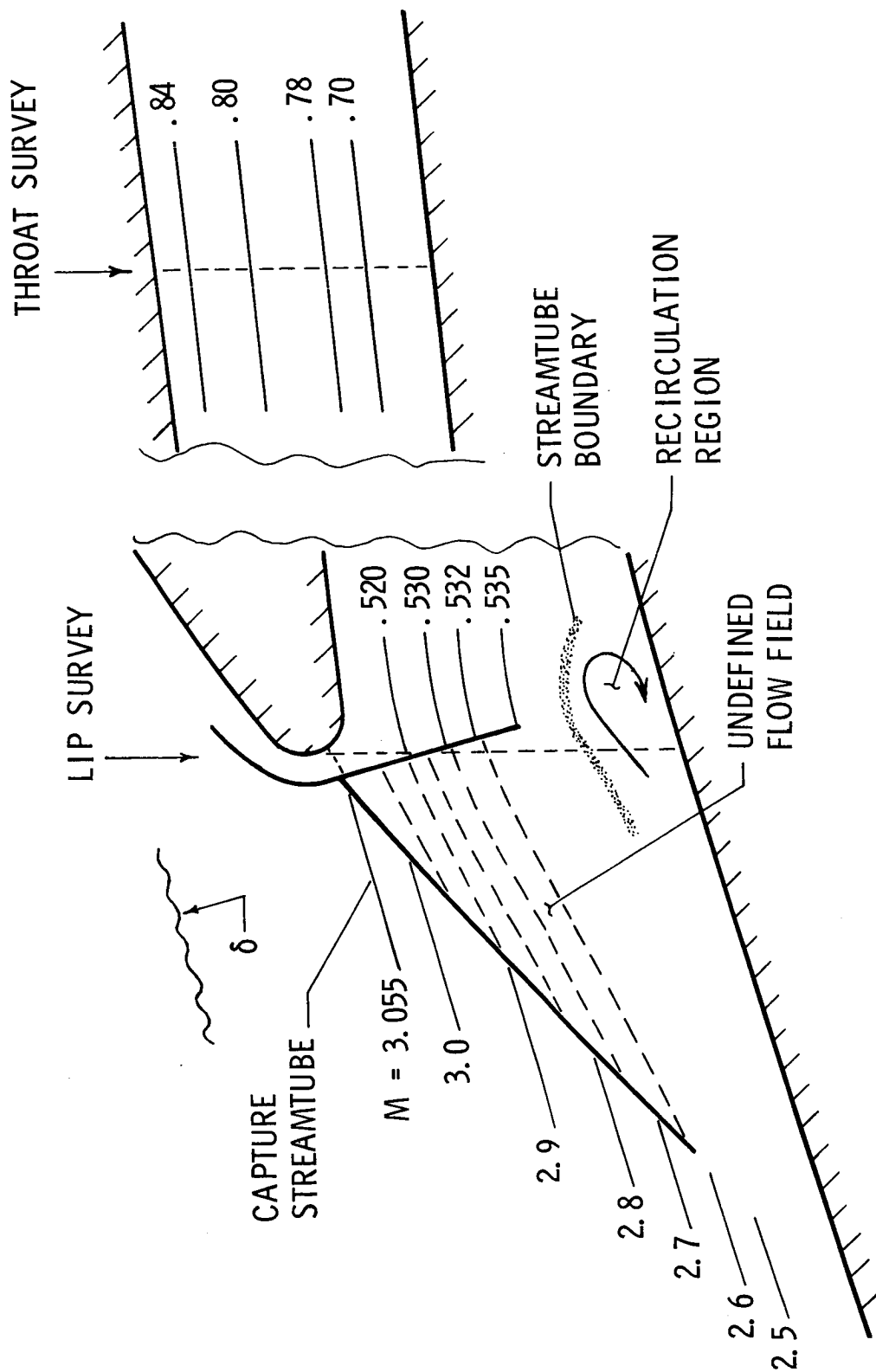
Figure 7. - Boundary layer velocity profiles for centerbody without cowl.  
 $x/R = 4.5$ ;  $M_\infty = 4$ ;  $p_{t,\infty} = 53.82$  psia;  $T_{t,\infty} = 700^\circ R$ .



(a)  $T_w/T_{t,\infty}$  = adiabatic.

Figure 8. - Simplified flow model based on pitot measurements.  $x_{CL}/R = 4.5$ ;  $M_\infty = 4$ ;  $p_{t,\infty} = 53.82$  psia;  $T_{t,\infty} = 700$  °R.

MASS CAPTURE = 89%



$$(b) \quad T_w / T_{t, \infty} = 0.2.$$

Figure 8. - Concluded.

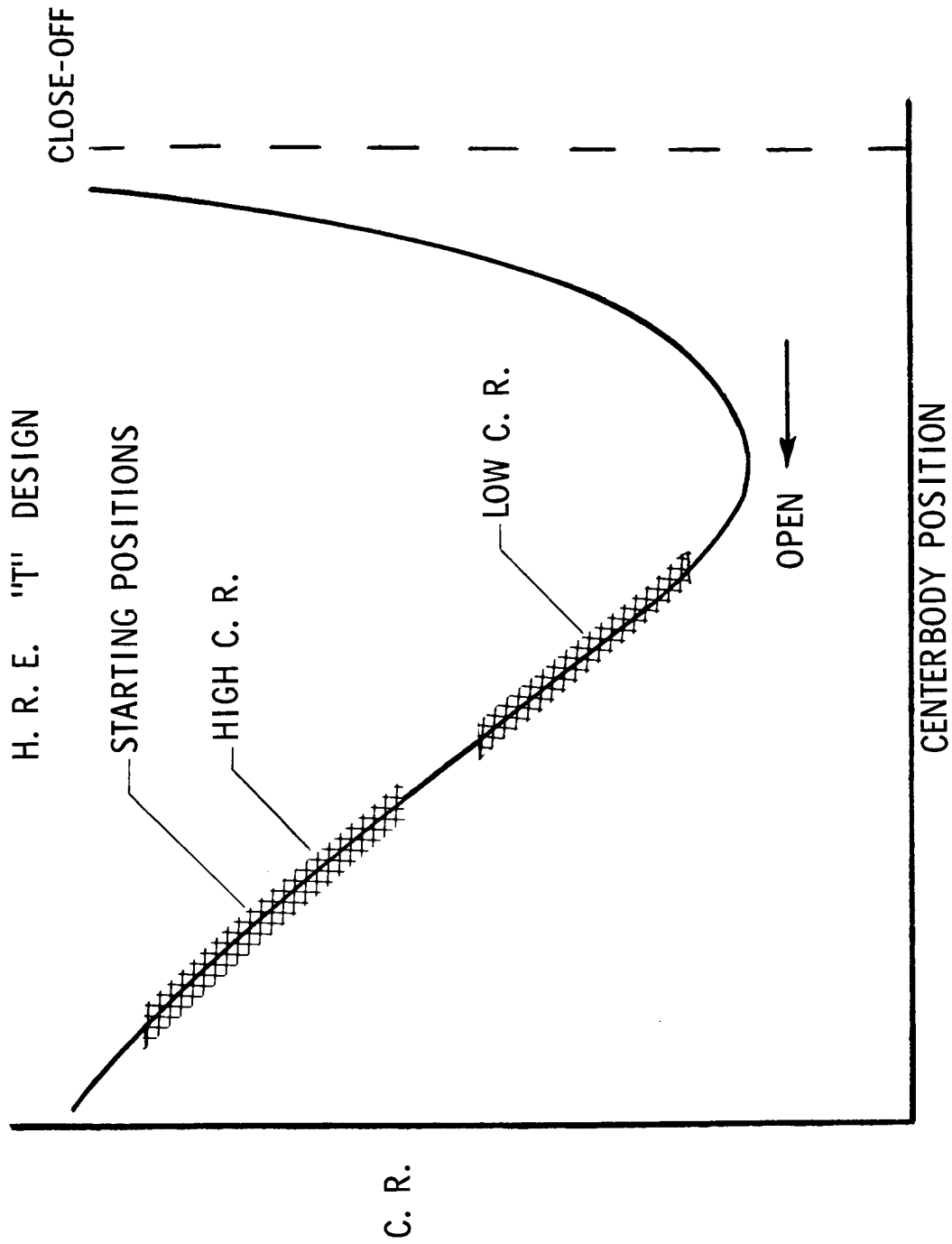


Figure 9. - Internal contraction ratio.

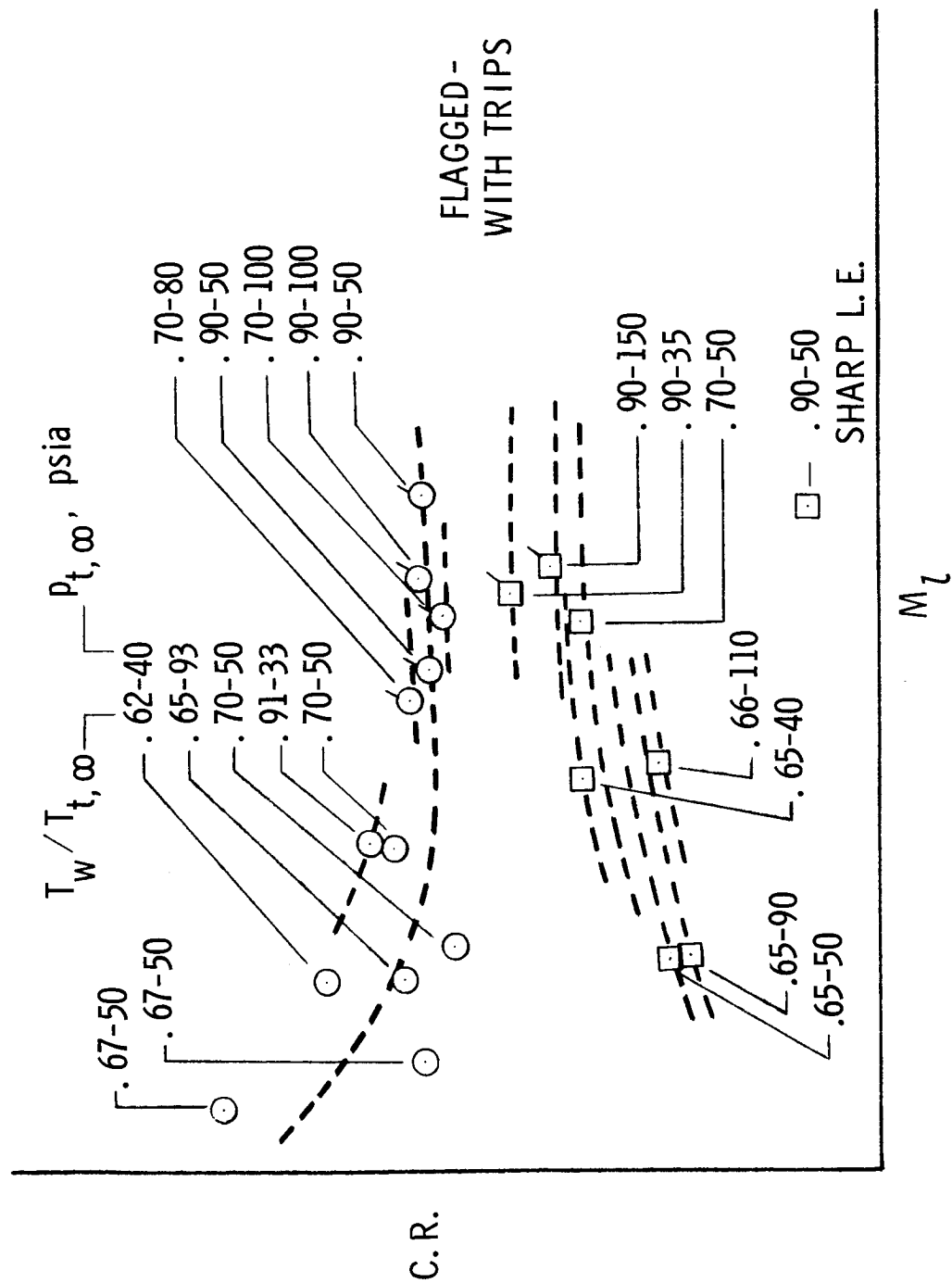


Figure 10.— Inlet starting contraction ratio.

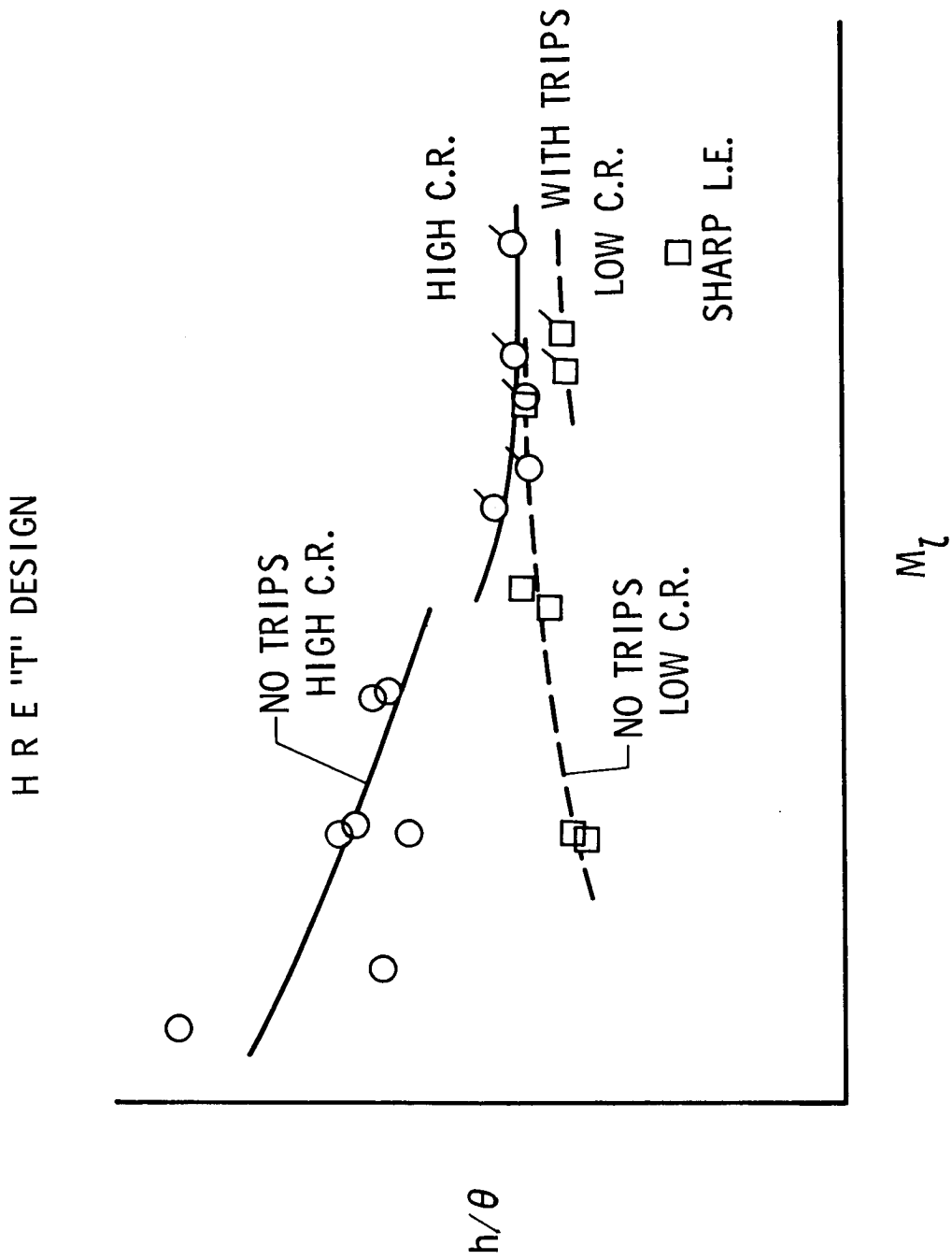


Figure 11.— Inlet starting characteristics.

STUDIES OF THE INTERACTION OF A TURBULENT BOUNDARY  
LAYER AND A SHOCK WAVE AT MACH NUMBERS BETWEEN 2 AND 10

By Earl C. Watson, William C. Rose, Shelby J. Morris, Jr.,  
and William F. Gallo

NASA Ames Research Center

SUMMARY

Interactions between a turbulent boundary layer and a shock wave in two-dimensional flow on a compression surface having nonadiabatic wall conditions have been studied at Mach numbers of 7 and 10 in tests conducted at Ames Research Center. Similar interactions in axisymmetric flow at Mach numbers of about 3 and 4 with adiabatic wall conditions have been studied by the University of Washington under a NASA grant. Results obtained from these investigations are presented in terms of the boundary-layer properties (momentum, displacement and velocity thicknesses), surface-pressure distributions, shock-wave structure, and incipient-separation criteria. Results of the two-dimensional studies include the effects of leading-edge bluntness on the boundary-layer properties and the shock structure for wall cooling with a ratio of wall-to-free-stream total temperature of about 0.3. The results obtained in the axisymmetric study include the effect of boundary-layer bleed in the region of the interaction.

INTRODUCTION

The need for sophisticated analytical techniques to properly account for the flow phenomena which occur in hypersonic inlets has been noted in previous works (ref. 1-3). The boundary layer, for example, begins as a laminar layer but develops downstream under conditions which generally are different than those assumed in most boundary-layer theories. Those conditions may arise from the effects of leading-edge bluntness, boundary-layer transition, or pressure gradients normal to the surface caused by surface curvature, or the interaction with an incident shock. As the boundary layer develops through an inlet it generally interacts with an impinging shock wave. The interaction, especially when the boundary layer is turbulent, is one of the most complicated flow phenomena in an inlet system. It is the general purpose of this paper to consider the flow-field and boundary-layer development with emphasis on the shock-wave boundary-layer interaction.

Most of the past studies of turbulent boundary-layer shock-wave interactions have considered the interaction for two-dimensional flow over a flat plate. (See refs. 4 through 11, for example.) Several methods for analyzing

these interactions have been developed as a result of these studies. The control-volume concept was initially proposed by Reshotko and Tucker (ref. 12) for flow with adiabatic-wall conditions. In references 13 and 14, this concept is extended to include flow with nonadiabatic-wall conditions, and in reference 15 the analysis is developed to include two-dimensional and axisymmetric flows with solid walls and with boundary-layer removal through normal holes, slots or scoops. The control-volume concept does not provide detailed boundary-layer profile information throughout the interaction region, and the method has not been verified by extensive comparisons with data. Other analytical models have been proposed in references 9 and 16. In reference 9 a semi-empirical approach is employed and the various boundary-layer correlation parameters used in the method have been determined for a wide range of Mach numbers, but only for adiabatic-wall conditions. In reference 16 the approach considers that the predominant forces in the vicinity of the interaction are inertial rather than viscous, and therefore the flow is considered as inviscid. This latter analytical model provides both boundary layer profiles and shock structure in the interaction region, but not the skin-friction or heat-transfer characteristics since the viscous sublayer is not included in the analysis.

The present paper considers two investigations of the interaction between a turbulent boundary layer and an impinging shock wave. In one, the interaction occurred in two-dimensional flow over a compression surface with nonadiabatic-wall conditions ( $T_{\text{wall}}/T_{\infty} \approx .3$ ) and various leading-edge bluntnesses. In the other investigation, the interactions occurred in axisymmetric flow on a conical nozzle wall which provided adiabatic-wall conditions, and a specific region in the wall for boundary-layer removal. Different nozzles provided a range of free-stream Mach numbers from 2 to 4. These interactions are the type which correspond with those that occur inside the cowl of an axisymmetric inlet. This study was conducted at the University of Washington under a NASA grant monitored by Ames Research Center. The results obtained in each of these studies are presented separately, and then the data from both are included in a discussion of incipient separation.

For the two-dimensional study the specific objectives are: (1) to present the effects of leading-edge bluntness on the boundary-layer development over the inlet-type compression surface, (2) to show the effects of leading-edge bluntness on the surface-pressure distribution in the region of a shock-wave boundary-layer interaction, and (3) to demonstrate the analytical capability for predicting the boundary-layer and flow-field development, accounting for the presence of an interaction.

For the axisymmetric study the objectives are: (1) to present preliminary results obtained with and without boundary-layer removal for an interaction of sufficient strength to cause separation without boundary-layer removal, and (2) to make an assessment, based on the experimental results of the flow-removal requirements to eliminate separation.



# SYMBOLS

$C_f$	skin-friction coefficient
$\overline{C}_f$	transformed skin-friction coefficient
$C_p$	pressure coefficient, $\frac{P_{\text{final}} - P_1}{q_1}$
$L$	reference length of two-dimensional model, 48 in.
$\dot{m}$	mass flow
$\dot{m}_{\text{bleed}}$	mass flow removed through the bleed system
$\dot{m}_{\text{b.l.}}$	mass flow in boundary layer entering an interaction
$M$	Mach number
$P$	local pressure
$q$	dynamic pressure
$R$	radius of leading edge of ramp of two-dimensional model
$Re$	Reynolds number
$T$	temperature
$u$	velocity
$X$	abscissa of model coordinates for two-dimensional model, Table I, or, longitudinal distance from an arbitrary origin for axisym- metric model, fig. 2
$Y$	ordinate of model coordinates for two-dimensional model, Table I, or distance normal to surface
$\alpha_G$	shock-generator angle, Table I. (Values of $\alpha_G$ used in the report are nominal, actual angle of inner surface = $\alpha_G - 0.97^\circ$ )
$\delta$	boundary-layer thickness
$\delta^*$	boundary-layer displacement thickness, $\delta \int_0^1 (1 - \frac{\rho u}{\rho_\delta u_\delta}) d\frac{Y}{\delta}$

$\theta$  boundary-layer momentum thickness,

$$\delta \int_0^1 \frac{\rho u}{\rho_\delta u_\delta} \left(1 - \frac{u}{u_\delta}\right) d \frac{y}{\delta}$$

$\rho$  density

$\nu$  kinematic viscosity

Subscripts:

aw adiabatic wall

final downstream of interaction

i intercept of linear extension of incident shock and the wall  
(shock-at-the-wall point)

INC incipient

t total

w wall

$X_{eff}$  length of run, turbulent flow

$\delta$  boundary-layer edge

$\theta$  momentum thickness

$\infty$  free-stream

1 local conditions entering a turbulent interaction

## APPARATUS

### Two-Dimensional Compression Surface Model

The two-dimensional compression surface model, shown schematically in figure 1, was tested at Ames Research Center in the 3.5-foot hypersonic wind tunnel (ref. 17). Nominal test conditions for  $M_\infty = 10.5$  were  $P_{t_\infty} = 1800$  psia and  $T_{t_\infty} = 1900^\circ\text{R}$ , and for  $M_\infty = 7.4$ ,  $P_{t_\infty} = 600$  psia for a range of  $T_{t_\infty}$  from  $1300^\circ\text{R}$  to  $1900^\circ\text{R}$ . The model consisted of a curved isentropic compression surface (ramp) 14 inches wide by 48 inches long, and a smaller surface (shock generator) used to generate the incident shock for the interaction studies. The ramp was aligned at  $3^\circ$  with respect to the free stream as indicated in

the lower sketch of figure 1. A schematic diagram of the model and the coordinates for both surfaces are presented in Table I. A small part of each surface near the leading edge was water cooled; this, plus the mass of the model prevented any significant wall temperature change during a run. For a free-stream Mach number of 10.4 the ratio of wall-to-stagnation temperature was 0.28, and for Mach number 7.3 it varied from 0.32 to 0.41, depending on the stagnation temperatures noted above. Surface pressures and temperatures were measured on the compression surface. In addition, small probes were employed to obtain pressure and temperature measurements in the boundary layer. The shock generator could be rotated about a hinge point to vary the strength of the incident shock. Side plates were not employed to restrict the spanwise flow.

### Axisymmetric Model

Tests of the axisymmetric model were conducted at the University of Washington using the continuous flow test facility sketched in figure 2. Nozzles of circular cross section were used to provide Mach numbers over the range from about 2 to 4. The total temperature was 540°R, and the nozzles provided adiabatic-wall conditions. The total pressures were as follows: For  $M_\infty = 2.82$ ,  $P_{t_\infty} = 34.3$  psia; and for  $M_\infty = 3.78$ ,  $P_{t_\infty} = 59.1$  psia. Small cones aligned with the flow on the nozzle centerline were used to generate a shock wave which interacted with the turbulent boundary layer on the nozzle wall. The cone could be positioned longitudinally to locate the interaction in the region of the surface pressure instrumentation on the nozzle wall. Cones having half angles between 8 and 16° were used to generate interactions of various strength. Provision was made for boundary-layer removal in the interaction region by incorporating a removable section in the nozzle (in this paper boundary-layer removal is referred to as bleed). This section was manifolded to a vacuum system for removing boundary-layer air. Although the removable solid section could be replaced by sections with scoops, slots, or normal holes, only the latter have been used in the tests. The normal holes were 0.064 inch in diameter. When more than one row of holes were used the holes in alternate rows were placed so that they were aligned midway between the holes in the upstream row, and the rows were spaced 0.07 inch apart.

The instrumentation consisted of surface orifices in the nozzle wall and a small remotely operated traversing pitot probe which could be positioned at any longitudinal station throughout the interaction region.

## RESULTS AND DISCUSSION

### Boundary-Layer Development on Compression Surface

The boundary-layer thickness on the compression surface at a free-stream Mach number of 7.4 is shown in figure 3. Results are shown for leading-edge

radii of 0.0025 in. without trips, and for 0.0625, and 0.188 in. with trips. The height and the X/L location of the trips are given by a "T" mark.

The thickness was determined on the basis of profile measurements at specific model stations and from schlieren photographs when the boundary-layer edge could be observed. A dotted band faired through the data is used to indicate the uncertainty in the thickness; a symbol indicates the thickness which was obtained from the experimental data, and which was employed in determining the integral properties of the boundary layer. The integral parameters and some boundary-layer-edge properties are shown in figure 4 for a free-stream Mach number of 7.4. These data were used to obtain the local flow conditions at the start of the interactions discussed herein for the compression surface. Similar data were prepared for a free-stream Mach number of 10.5 but are not presented here.

Several observations can be made from the boundary-layer thickness data (fig. 3). With the smallest radius, natural transition occurred and turbulent flow was obtained over the aft portion of the surface. With the larger radii, transition was delayed, and, therefore, trips were required to obtain a turbulent boundary layer for the interaction studies. The trip used with the 0.188 in. radius was effective in initiating turbulent flow near the trip and an abrupt change from the laminar to turbulent growth is indicated in figure 3. With the radius of .0625 in., the growth rate is noticeably different than that for the other radii. In this case, the boundary layer and the entropy layer associated with the leading-edge bluntness merge, and the rate of growth is greatly increased over the midportion of the surface. This flow phenomena is termed "entropy swallowing" and has been described in references 18 and 19.

To predict the turbulent boundary-layer growth an initial, or starting point is required where the thickness and edge conditions are known. For the theoretical results shown in figure 3 the starting point was at  $X/L = .54$ , for the leading edge radii of .0025 inch. A computer program based on the turbulent boundary-layer theory reported in reference 20 was used to obtain the theoretical thickness; results have not yet been obtained with the program for the case with the .188 in. radius. The theory does not account for the boundary-layer development in the presence of entropy swallowing, therefore, no theoretical results are presented for the case with the radius of .0625 inch. It can be seen that the theoretical results for a leading edge of .0025 in. radius agree reasonably well with experiment except near the end of the compression surface where the data indicate a greater rate of thinning, or compression. It is evident from the above results that to attain the desired boundary-layer characteristics in model tests at hypersonic speeds, considerable attention must be given to the choice of trips and to the possibility of the occurrence of entropy swallowing.

#### Interactions on the Compression Surface

Surface-Pressure Distribution: The surface-pressure distribution in the region of an interaction is generally used to obtain significant pressure and

length parameters which describe some of the details of an interaction. Pressure distributions obtained in the tests at  $M_\infty = 7.4$  with the compression-surface model are shown in figures 5 and 6 for leading-edge radii of 0.0625 and 0.188 in., respectively. (The complete pressure distributions for these sets of data are presented in ref. 19.) Similar pressure distributions for a leading-edge radius of 0.0025 in. were presented in reference 3. The pressure distributions have been translated to align the points where the linear extension of the impinging shock intercepts the wall. By examining these figures it can be seen that large separated regions occurred with the blunter leading edge (fig. 6), and for this bluntness the plateau pressure is well defined. In turbulent interactions with flow separation, and with uniform flow in the region outside the boundary layer the plateau is generally not as well defined. It is believed that this present result shows an effect of the entropy layer produced by the leading-edge bluntness. In this case with the largest bluntness, entropy swallowing did not occur prior to the interaction, and the vorticity of the entropy layer might play some part in producing these results. Note also, that for the same overall pressure rise the total interaction length is greater with a leading edge radius of 0.188 inch. With this radius, separation is evident for a generator angle of  $6^\circ$  which provided a pressure rise of 6.7 across the interaction. With the 0.0625 in. radius, separation is evident for a generator angle of  $15^\circ$ , which provided a pressure rise of 8.7. The fact that separation occurred for a lower pressure rise with a leading-edge radius of 0.188 in. than with .0625 in. is primarily attributable to the reduced Mach number at the boundary-layer edge. Data such as these were used to determine the pressure ratio for incipient separation, which will be considered further following the discussion of the axisymmetric test results.

**Flow Field Analysis:** An inlet flow field, in the general sense, includes: (1) flows about blunt leading edges, (2) viscous flow (laminar, transitional or turbulent boundary layers), (3) the inviscid flow field which includes the entropy layer introduced by leading-edge bluntness, and (4) various interactions among these flows. The hypersonic inlet computer program described in reference 21 includes (1), (2), (3), and some of the interactions concerned with (4). It has been employed in the analysis of the data obtained in the present two-dimensional tests and several features should be noted. The equations for both viscid and inviscid flow are combined in the program. An integral form of the turbulent boundary-layer equations which incorporates the skin-friction relation described by Sivells and Payne (ref. 22) is used. A control volume model for shock-wave boundary-layer interactions and a feature for testing interactions for separation are also included. The separation test is based on criteria given by Erdos and Pallone (ref. 23). (If separation occurs the computations continue as if there were no separation.)

Theoretical results obtained with the above computer program have been compared with experimental results obtained with the two-dimensional model for cases with and without separation. The results for separated flow (fig. 7) were obtained at a free-stream Mach number of 7.4, with the model having a leading-edge radius of 0.188 in. and a shock-generator angle of  $6^\circ$ . This composite figure includes a schlieren photograph of the interaction region and the associated surface-pressure distribution, each to the same scale and

and correctly aligned with respect to each other. Examination of this figure shows that the entering boundary-layer thickness and overall pressure rise were predicted well. Prediction of the surface-pressure distribution and the induced shock wave should not be expected since the method does not account for flow separation or an induced shock. (The theory predicted separation for this interaction.) Examination of the schlieren photograph insert shows that the locations of the incident and reflected shocks are predicted reasonably well, being displaced from the observed locations only by about 0.10 in. to 0.20 in., respectively.

Results obtained with no separation are presented in figure 8 for a free-stream Mach number of 7.4, and with a model having a leading-edge radius of 0.0625 in. and a shock-generator angle of  $4^\circ$ . The program did not indicate the occurrence of separation and there is no evidence of separation in the data. Both the shock structure and surface-pressure distribution are predicted well, but the predicted entering boundary-layer thickness is much smaller than that obtained experimentally. The process of entropy swallowing occurred in this case, and, the theory in the program does not account for the boundary-layer edge conditions imposed by this phenomena.

The above comparisons have shown examples where the analytical method yields good results. However, not all the observed phenomena were predicted. Further comparisons between theoretical and experimental results are needed to increase the confidence in the results, and to determine where improvements can be made in the analytical methods.

### Interactions in Axisymmetric Flow

Studies of shock-wave boundary-layer interactions in an axisymmetric flow are important because a large number of inlets are axisymmetric and few data exist. In cases where the inlet diameter is large compared to the boundary-layer thickness, the axisymmetric flow near the cowl leading edge is generally considered to be locally two-dimensional. Experimental results obtained for interactions occurring in such a region should be comparable with those occurring in two-dimensional flows.

The purpose of the axisymmetric tests was to study an interaction between a shock wave and a turbulent boundary layer that is representative of that on the cowl of an inlet, and to determine the effects of boundary-layer bleed in the vicinity of the interaction. A diagram showing a typical interaction on the nozzle wall is shown in figure 9. With this model the shock generator is a cone, and provisions are made for boundary-layer removal as indicated in the diagram. The control-volume analytical model which is to be used in the analysis of the data is indicated in the lower part of the figure. A momentum balance is taken on the control volume with the assumption of no mass addition between the end planes. The length of the interaction and properties of the boundary layer downstream of the interaction are obtained from the analysis.

Specific data have been selected from the tests to consider the details of a separated interaction with no bleed, and with bleed sufficient to eliminate separation. In addition, data for the pressure rise for incipient separation with no bleed were obtained and these will be discussed later.

Experimental results obtained at  $M_1 = 3.78$ , with and without bleed, are presented in figure 10. These results are for a separated flow in the case of no bleed and unseparated flow with bleed. Shock wave locations, surface pressure distributions, and boundary-layer thickness are shown. The data for the location of the incident, induced, and reflected shocks were obtained from pitot traverses made at many closely spaced stations throughout the interaction region. Boundary-layer thickness was obtained from the Mach number profile which was computed using the pitot pressure and the assumption that the static pressure in the boundary layer was constant at the local wall value. A bleed mass-flow ratio of 0.031 was obtained through a single row of holes which were located approximately 0.15 in. upstream of the shock-at-the-wall point,  $X_1$  (see fig. 10). The bleed mass-flow ratio is defined as the ratio of the mass removed through the bleed system to the mass contained in the entering boundary layer. The following results are obtained from examination of these data:

- (1) The bleed was totally effective in preventing the separation that existed without bleed. This is evidenced by the disappearance of the induced shock, and the pressure distribution is typical of that for an unseparated interaction.
- (2) The upstream length and hence the total length of the shock-wave boundary-layer interaction (as measured from the onset of the pressure rise to the peak pressure) is significantly reduced. It should be noted that the pressure decrease in the downstream region is due to the expansion fan emanating from the base corner of the cone. It is believed that this decrease in pressure does not significantly influence the overall features in the initial interaction region.
- (3) The boundary-layer thickness immediately downstream of the interaction is less than that of the entering flow in both cases, and the thickness, upstream or downstream, is not significantly affected by bleed.

Results obtained with the region of bleed extending over a larger area (4 rows of holes) are presented in figure 11. (The no bleed results have been included for comparison purposes.) In this case, 13.1 percent of the entering boundary layer was removed through the area indicated. The following results are evident from examination of the data:

- (1) An additional shock wave is introduced.
- (2) The length of the interaction is not significantly less than the length with 3.1 percent bleed.

- (3) The boundary layer downstream of the interaction is thinner with the increased quantity of bleed.

Examination of the bleed location shows that the area of bleed extended downstream of the shock-at-the-wall point,  $X_1$ , and into the region of high surface pressure. These preliminary results do not permit an evaluation of the relative effect of bleed location, but they do demonstrate that separation can be eliminated by a small amount of bleed over a small area within the interaction region. The results show that with excess bleed over an extended area, extraneous shocks may be formed.

A problem that may arise in an inlet design is to determine the quantity of bleed that may be required to eliminate separation under specific conditions. In addressing this problem it would be desirable to relate the quantity of bleed flow needed to eliminate separation with some significant theoretical value of mass flow. One approach to this problem is illustrated by the use of the sketch and data presented in figure 12. The sketch shows a typical turbulent interaction with Mach number profiles indicated upstream and downstream. Two theoretical mass-flow ratios and one experimental one are shown in the lower figure. Both the theoretical and experimental points are based on the results obtained in the axisymmetric tests at  $M_1 = 3.78$  and with a  $15^\circ$  half-angle cone. The circle indicates the mass-flow ratio contained in the subsonic portion of the entering boundary layer (about 1% for these test conditions). Theoretically, if this quantity of flow were removed there could be no upstream influence from the interaction. The triangle indicates the mass-flow ratio contained in the subsonic portion of the flow downstream of the reflected shock. If this quantity of flow were removed (i.e., about 5% of the entering flow) the boundary layer would be supersonic throughout the interaction, and the analytical method of reference 16 would be applicable. The square symbol shows the experimental result wherein a bleed mass flow of 3.1%, in the area indicated, was effective in eliminating separation. These results lead to the possible design criteria that the minimum quantity of bleed flow should be large enough to remove an amount of flow equal to that in the subsonic portion of the boundary layer downstream of the interaction.

It should be recognized that the axisymmetric tests were set up to study an isolated interaction. Thus, the bleed quantity required to eliminate separation obtained from this study might be expected to differ from the bleed quantity required in an inlet. However, the results obtained for an isolated interaction should represent a lower bleed limit that may be useful for inlet design purposes. A comparison between the bleed removed on the cowl of high-performance axisymmetric inlets and the bleed found necessary to eliminate separation in these isolated interactions is presented in figure 13. It can be seen that the bleed quantity varied considerably, from 33 percent to 54 percent for inlets designed for Mach numbers 3.0 and 3.5, respectively. For reference purposes the two theoretical bleed quantities discussed in figure 12 are also shown for the entering boundary layer in each inlet. The bleed ratios for the inlets are much higher than those required to eliminate separation for the isolated interaction.



On the basis of the above results it is concluded that it may be possible to reduce the amount of bleed presently employed in inlet systems by considering the details of the location of the bleed relative to the interaction and to the quantity of bleed removed. Obviously the bleed actually required in an inlet may depend on many factors not considered here, but the concept for eliminating separation by relating the bleed requirements to the theoretical subsonic-flow quantity in the interaction region should be investigated further.

### Incipient Separation

The determination of whether or not a shock wave will separate a turbulent boundary layer is a problem of general importance in the design of aircraft components, and hypersonic inlets, in particular. With hypersonic vehicles boundary-layer removal may not be used to control or prevent separation since the removal of high temperature air may impose structural difficulties and excessive weight penalties. Further, in order to prevent high local heating rates, undesirable flow distortion, and aerodynamic blockage which may be associated with flow separation, it is essential to be able to predict the pressure rise which can be sustained across an incident-reflected shock system without causing separation.

The incipient separation problem has been re-examined in this study in view of the results obtained from recent investigations which have shown that present parameters for incipient separation do not adequately correlate all of the data. For example, a body of data obtained from several studies have been reduced to obtain the incipient separation parameter

$(C_{P_{INC}} Re_{X_{eff}}^{0.1})$  proposed by Popinski in reference 7. The parameter employs the Reynolds number based on the effective length of run for turbulent flow. However, this effective length is seldom known from experiments; instead, the Reynolds number based on boundary layer thickness is usually given. Popinski used the incompressible relationship,  $Re_{X_{eff}} = 3.47 Re_{\delta_1}^{1.25}$ .

In the present study, this relationship has been modified to account for compressibility, through the use of Eckert reference temperature. The resulting equation is:

$$Re_{X_{eff}}^{.1} = 1.132 Re_{\delta_1}^{.125} \left( \frac{v_{\delta}}{\bar{v}} \right)^{0.025}$$

where the barred quantity is evaluated at the Eckert reference temperature. The results are presented in figure 14. It is evident that the data are not correlated by the parameters.

In view of the above results a dimensional analysis (see Appendix) was made to determine the parameters which should be involved in the separation of a turbulent layer. On the basis of this analysis a function which should

correlate the data is:

$$\frac{C_{P_{INC}} \cdot Re_{\delta_1}^a}{C_{f_1}^b} = f(M_1), \quad (1)$$

where  $a$  and  $b$  are constants. For the data being examined, all of the quantities required in the above relation are readily obtained except the skin-friction coefficient. An expedient method employing the velocity profile was used to obtain the skin friction from the profile data. Use was made of the Eckert reference temperature to obtain a transformed incompressible velocity profile. This transformed profile was then fit to the "law of the wall" in a manner similar to that proposed by Clauser (ref. 24) for constant property flows. An inherent difficulty in the transformation is that the "law of the wall" region of a transformed profile has a range of values of transformed skin-friction coefficient,  $\bar{C}_f$  (see ref. 25 for a discussion of the deduction of skin friction from velocity profiles). In this study the mean value of skin-friction coefficient,  $\bar{C}_f$ , was used to obtain the actual skin-friction coefficient for all of the data with the exception of the Bogdonoff data. For this data, which was obtained on a two-dimensional nozzle wall, no velocity profiles are available and the skin-friction coefficient was taken to be that given by the Spalding-Chi (ref. 26) theory based on the  $Re_{x_{eff}}$ .

Results obtained using the above method are presented in figure 15. The value of  $b$  in equation (1) was set equal to 0.5, following the approach of Chapman, Kuehn, and Larson (ref. 5). The value of  $a$  was determined from the slope of the line through the data in figure 15. No explicit Mach number dependence is evident. The resulting equation which correlates the two-dimensional data is presented in the figure. Examination of the data indicates that all of the data are correlated by the new parameter except the data obtained in the tests with axisymmetric flow. The pressure rise for incipient separation for the axisymmetric conditions was taken to be the local two-dimensional pressure rise across the incident-reflected-shock system (correlation, also, did not occur using the actual pressure rise attained in the test). Since all of the data shown for the two-dimensional flow conditions correlate, it is concluded that the pressure rise for incipient separation may be less for axisymmetric flow conditions. Also, it should be noted that for the axisymmetric tests, in which the ratio of boundary-layer thickness to nozzle-diameter ratio is about 0.07, the flow conditions may not be two-dimensional in the region of the interaction. Further investigation of this matter is obviously needed. In addition, investigations of interactions in axisymmetric flow which represent those that occur on an inlet centerbody, are needed. Such investigations should also include interactions which occur in regions of streamwise pressure gradients.

With respect to the correlating parameter, it is important to note that both the skin-friction coefficient and the Reynolds number must be specified

independently. This demonstrates that in order to properly represent the local flow phenomena in an interaction region both the local skin friction (shear stress profile) and Reynolds number must be properly simulated. This is an important consideration with respect to wind-tunnel models which must employ trips to obtain a turbulent boundary layer.

#### CONCLUDING REMARKS

Data for boundary layer and flow field development, including the interaction of the turbulent boundary layer with an incident shock wave, on a two-dimensional model with three leading-edge bluntnesses are presented. The results show that both the boundary-layer and flow-field development are strongly dependent on the leading-edge bluntness.

Theoretical results obtained from a computer program for hypersonic inlet flow are compared with the experimental results. Whereas some of the observed phenomena are predicted well, others are not. This occurs because the program does not contain provisions to account for all the flow phenomena that may be encountered in hypersonic inlets. Therefore, the program needs further refinement before it can be used for general inlet design purposes.

Preliminary results of a study of the interaction between a turbulent boundary layer and a shock wave which occurred in an axisymmetric environment are presented. The effect of boundary-layer removal in the interaction region is discussed for an interaction where separated flow occurred without bleed, and where a small amount of bleed eliminated separation. With respect to the problem of eliminating boundary-layer separation by boundary-layer removal, it is proposed that the criteria governing the bleed requirements should be related to the mass contained in the subsonic flow downstream of the reflected shock wave.

Results obtained from the present and other studies are presented and discussed in relation to problems of the prediction of incipient separation. In particular, a new parameter has been proposed for correlating incipient separation data. The parameter correlates data obtained in two-dimensional flows for a wide range of Mach numbers, and wall-to-free-stream temperature ratios. Data obtained in axisymmetric flow do not correlate. It is concluded that the pressure rise for incipient separation in axisymmetric flow may be less than that in two-dimensional flow.

## APPENDIX

### Outline of Dimensional Analysis Used to Obtain Incipient Separation Correlation Parameter

Presented herein is a brief outline of the derivation, based on a dimensional analysis, of a parameter which has the capability to correlate incipient-separation pressure data.

The pertinent variables which enter the analysis were based on the following considerations: The boundary layer will tend toward separation when the momentum addition to the fluid near the wall becomes less than that removed by the imposed pressure gradient and the wall shear; further, it is assumed that the contribution of the wall shear is negligible in comparison to that of the imposed pressure gradient. Thus, a correlation parameter is sought to represent the momentum flux entering the interaction and that removed by the action of the imposed pressure gradient.

With respect to the entering momentum, the important quantities which influence the shape of the profile are: The momentum at the boundary layer edge,  $\rho_\delta u_\delta^2$ , the gradient of momentum near the wall,  $\frac{\partial \rho u^2}{\partial Y}$ , and the boundary-layer thickness,  $\delta_1$ . Note that the specification of the conditions at the two boundary points (i.e., the wall and boundary-layer edge) of the momentum profile in no way uniquely defines the entire profile. Of course, the value of the momentum at the wall is zero; but the gradient of momentum near the wall is important in how the momentum changes from zero to the edge value. Therefore, the term for the momentum gradient near the wall is included in the present analysis. The important terms in this gradient are:  $\frac{\partial u}{\partial Y}$ ,  $\frac{\partial \rho}{\partial Y}$ , and  $\rho$ , all evaluated at the wall. The term  $\frac{\partial u}{\partial Y}$  at the wall can be expressed in terms of the initial wall shear stress,  $\tau_{w1}$ , and the viscosity,  $\mu_w$ . The density gradient, for a constant pressure layer, is related simply to the static temperature gradient,  $\frac{\partial T}{\partial Y}$ . Through the Reynolds analogy, the temperature gradient may be given explicitly in terms of the velocity gradient and, therefore, may be omitted from further consideration. The edge velocity, wall-to-edge temperature ratio, and edge Mach number may be used to express the wall density as:

$$\rho_w = f \left( \frac{\mu_w}{\mu_\delta}, M_\delta, u_\delta \right),$$

where a viscosity-temperature relation is employed in addition to the local isentropic relations.

A measure of the pressure gradient,  $\frac{dP}{dX}$ , throughout the interaction is given by the pressure rise across the interaction at incipient separation,  $(P_{\text{final}} - P_1)_{\text{INC}}$ , and the total length of the interaction,  $\ell_T$ .

$$\left(\frac{dP}{dX}\right)_{\text{INC}} \approx \frac{(P_{\text{final}} - P_1)_{\text{INC}}}{\ell_T}.$$

The parameters obtained from the above discussion (i.e.,  $(P_{\text{final}} - P_1)_{\text{INC}}$ ,  $\ell_T$ ,  $\delta_1$ ,  $\rho_\delta$ ,  $u_\delta$ ,  $\tau_{w1}$ ,  $\mu_w$ ,  $\frac{\mu_w}{\mu_\delta}$ , and  $M_\delta$ ) are used to represent the interaction phenomenon. Grouping these terms through a dimensional analysis yields the following functional relationship:

$$\frac{C_{P_{\text{INC}}} \text{Re}_{\delta_1}^a}{C_{f1}^b} \left(\frac{\mu_\delta}{\mu_w}\right)^a \left(\frac{\mu_w}{\mu_\delta}\right)^c \left(\frac{\ell_T}{\delta_1}\right)^d = f(M_\delta). \quad (\text{A-1})$$

In the present analysis two important assumptions are used to reduce the complexity of equation (A-1). First, the term  $\frac{\ell_T}{\delta_1}$  is assumed to be a

function of  $M_\delta$ ,  $\text{Re}_{\delta_1}$ , and viscosity ratio. Thus,  $\frac{\ell_T}{\delta_1}$  need not be explicitly

included in the correlation parameter. It should be noted that this is not the assumption of the existence of a "universal" relation between interaction length and entering boundary-layer thickness employed in reference 23. Secondly, it is assumed that the numerical value of the constant, (c), in equation (A-1) is equal to that of the constant, (a). With these assumptions, equation (A-1) is reduced to the following relationship employed in the present study:

$$\frac{C_{P_{\text{INC}}} \text{Re}_{\delta_1}^a}{C_{f1}^b} = f(M_\delta).$$

## REFERENCES

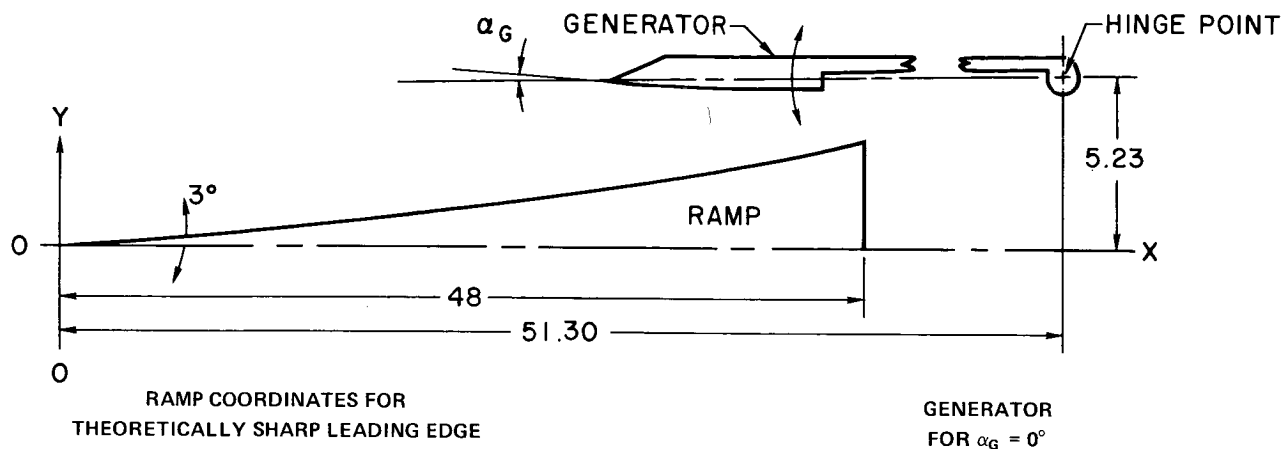
1. Sorensen, Norman E., Morris, Shelby Jr., and Pfyl, Frank A.: A Study of Hypersonic Inlet Technology. Conference on Hypersonic Aircraft Technology, NAS SP-148, 1967, Paper No. 20.
2. Gnos, A. Vernon, Gallo, William F., and Latham, Eldon A.: Two-Dimensional Boundary Layers and Flow Fields of Hypersonic Inlets. Conference on Hypersonic Aircraft Technology, NAS SP-148, 1967, Paper No. 21.
3. Watson, Earl C., Murphy, John D., and Rose, William C.: Shock-Wave Boundary-Layer Interactions in Hypersonic Inlets. Conference on Hypersonic Aircraft Technology. NAS SP-148, 1967, Paper No. 22.
4. Kuehn, Donald M.: Experimental Investigation of the Pressure Rise Required for the Incipient Separation of Turbulent Boundary Layers in Two-Dimensional Supersonic Flow. NASA Memo 1-21-59A, 1959.
5. Chapman, Dean R., Kuehn, Donald M., Larson, Howard K.: Investigation of Separated Flows in Supersonic and Subsonic Streams with Emphasis on the Effect of Transition. NACA Rept. 1356, 1958.
6. Erdos, John and Pallone, Adrian: Shock Boundary Layer Interaction and Flow Separation. Proceedings of the 1962 Heat Transfer and Fluid Mechanics Institute, F.E. Ehlers, J.J. Kauzlarich, C.A. Sleicher, Jr., R.E. Street, eds. Stanford Univ. Press, 1962, pp 239-254.
7. Popinski, Z.: Shock-Wave Boundary-Layer Interaction. Rep LR 18307, Lockheed California Co., 29 June 1965.
8. Popinski, Z., and Ehrlich, C. F.: Development Design Methods for Predicting Hypersonic Aerodynamic Control Characteristics. (AFFDL TR-66-85), Lockheed California Co., September 1966.
9. Pinckney, S. Z.: Semiempirical Method for Predicting Effects of Incident Reflecting Shocks on the Turbulent Boundary Layer. NASA TN D 3029, 1965.
10. Paynter, G. C., and Ross, P. A.: Calculation of Turbulent Boundary Layer Characteristics Across an Oblique Shock Reflection Including the Effects of Mass Bleed. Boeing Document No. D6-2-365, April 1968.
11. Gulbran, C. E., Redeker, E., Miller, D. S., and Strack, S. L.: Heating in Regions of Interfering Flow Fields, Part III: Two-Dimensional Interaction Caused by Plane Shocks Impinging on Flat Plate Boundary Layers. (AFFDL-TR-65-49, Part III), March 1967.
12. Reshotko, E. and Tucker, M.: Effect of a Discontinuity on Turbulent Boundary-Layer-Thickness Parameters with Application to Shock-Induced Separation. NACA TN 3454, May 1955.

13. Kutschenreuter, Paul H., Jr., Brown, David L., and Hoelmer, Werner: Investigation of Hypersonic Inlet Shock-Wave Boundary Layer Interaction, Part II. Continuous Flow Tests and Analyses. Rep. AFFDL TR-65-36 (Contract AF 33(657)-11747) General Electric Co., Evandale, Ohio.
14. Benson, J. L. and Maslowe, S. A.: Bluntness and Boundary-Layer Displacement Effects on Hypersonic Inlet Flow Fields. Journal of Spacecraft and Rockets, vol. 3, No. 9, Sept. 1966.
15. Seebaugh, W. R., Paynter, G. C., and Childs, M. E.: Shock-Wave Reflection From a Turbulent Boundary Layer with Mass Bleed. AIAA Paper 68-110, AIAA 6th Aerospace Sciences Meeting, New York, June 22-24, 1968.
16. Rose, W. C., Murphy, John D., and Watson, Earl C.: Application of an Inviscid Model to the Interaction of a Shock Wave with a Turbulent Boundary Layer. AIAA Journal, vol. 6, No. 9, Sept. 1968, pp 1792-3.
17. Holdaway, George H., Polek, Thomas E., Kemp, Joseph H., Jr.: Aerodynamic Characteristics of a Blunt Half-Cone Entry Configuration at Mach Numbers of 5.2, 7.4, and 10.4. NASA TMX-782, 1963.
18. Cousin, Sheldon B.: Leading Edge Bluntness Effects and Their Importance in Hypersonic Inlet Design. AIAA Paper 67-451. AIAA Third Propulsion Joint Specialist Conference, Wash. D. C., July 17-21, 1967.
19. Sanator, Robert J., Boccio, John L., and Shanshims, Dan: Effect of Bluntness on Hypersonic Two-Dimensional Inlet Type Flows. NASA CR 1145, Oct. 1968.
20. Lynes, Larry L., Nielsen, Jack N., and Kuhn, Gary D.: Calculation of Compressible Turbulent Boundary Layers with Pressure Gradients and Heat Transfer. Nielsen Engineering and Research, Inc., Report NEAR TR 6, August 1968.
21. Maslowe, S. A., and Benson, J. L.: Computer Program for the Design and Analysis of Hypersonic Inlets. Final Report. Lockheed California Company Report No. 18079, Aug. 31, 1964.
22. Sivells, J. C., and Payne, R. G.: A Method of Calculating Turbulent Boundary Layer Growth at Hypersonic Mach Numbers. AEDC TR 59-3, 1959.
23. Erdos, John and Pallone, Adrian: Shock Boundary Layer Interaction and Flow Separation. AVCO Report RAD-TR-61-23, Aug. 1961.
24. Clauser, F. H.: Turbulent Boundary Layers in Adverse Pressure Gradients. J. Aeronautical Sci., vol. 21, No. 91, Feb. 1954.
25. Allen, J. M.: Use of Baronti-Libby Transformation and Preston-Tube Calibrations to Determine Skin Friction from Turbulent Velocity Profiles. NASA TN D-4853, Nov. 1968.

26. Spalding, D. B. and Chi, S. W.: The Drag of a Compressible Turbulent Boundary Layer on a Smooth Flat Plate With and Without Heat Transfer. J. Fluid Mech., vol. 18, pt 1, Jan. 1964, pp 117-143.
27. Pinckney, S. Z.: Data on Effects of Incident-Reflecting Shocks on the Turbulent Boundary Layer. NASA TM X-1221, March 1966.



TABLE I  
2-DIMENSIONAL MODEL COORDINATES



X	Y	X	Y	X	Y
0	0	29	1.926	21.928	3.049
10	0.524	30	2.038	26.927	3.134
11	0.578	31	2.156	27.927	3.153
12	0.634	32	2.280	28.927	3.176
13	0.692	33	2.408	29.927	3.205
14	0.752	34	2.540	30.926	3.242
15	0.813	35	2.676	31.926	3.291
16	0.874	36	2.816	32.926	3.356
17	0.936	37	2.960	33.925	3.439
18	1.000	38	3.108	34.924	3.538
19	1.066	39	3.260	35.924	3.649
20	1.136	40	3.414	36.923	3.768
21	1.210	41	3.572		
22	1.286	42	3.734		
23	1.366	43	3.900		
24	1.450	44	4.070		
25	1.536	45	4.244		
26	1.626	46	4.422		
27	1.720	47	4.604		
28	1.820	48	4.790		

NOTES:

1. ADD 0.002 TO ALL Y DIMENSIONS FOR  $R = 0.0025$
2. ADD 0.059 TO ALL Y DIMENSIONS FOR  $R = 0.062$
3. ADD 0.178 TO ALL Y DIMENSIONS FOR  $R = 0.188$
4. ALL LINEAR DIMENSIONS IN INCHES

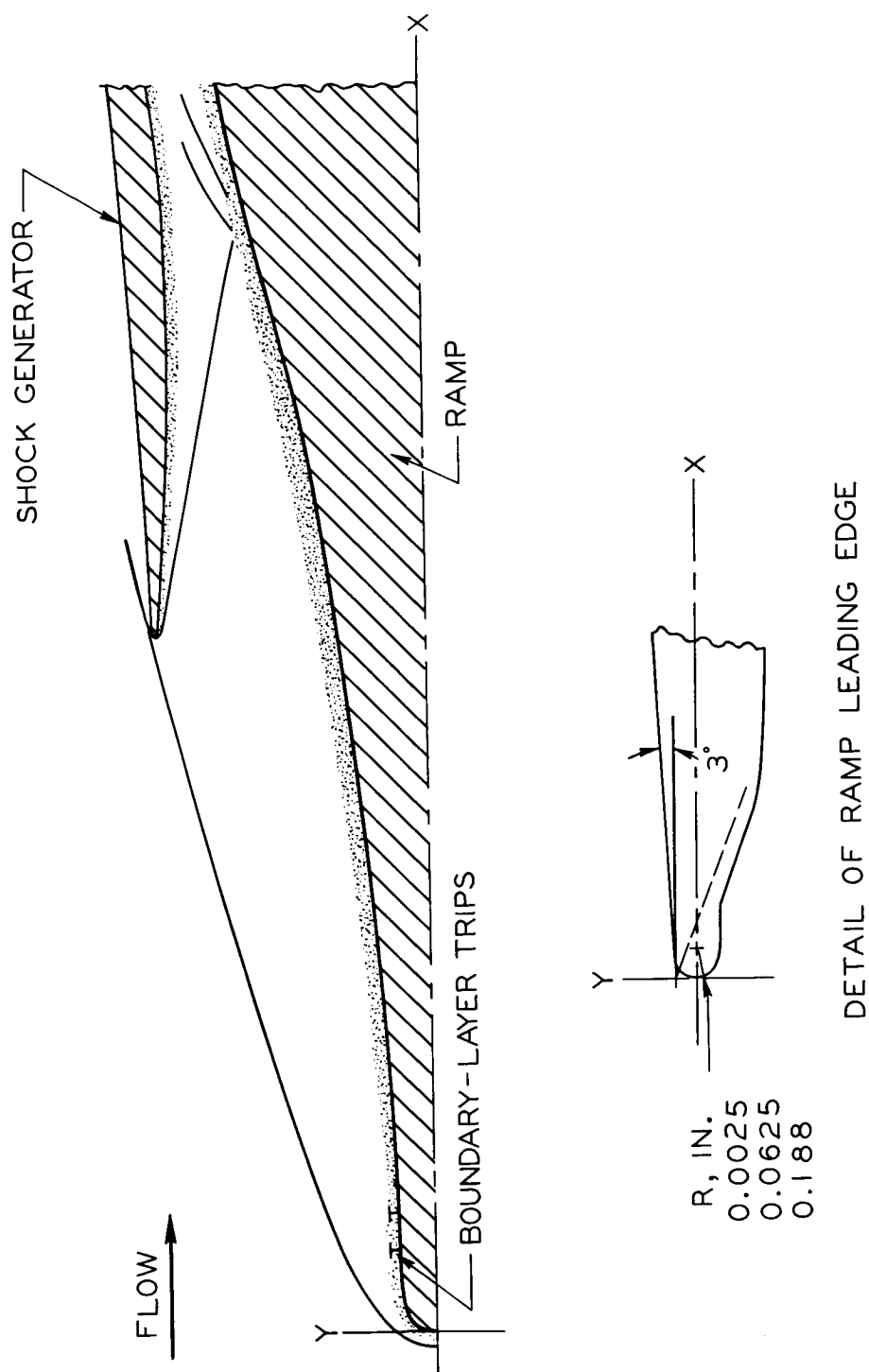


Figure 1.- Compression surface model (2-dimensional flow).

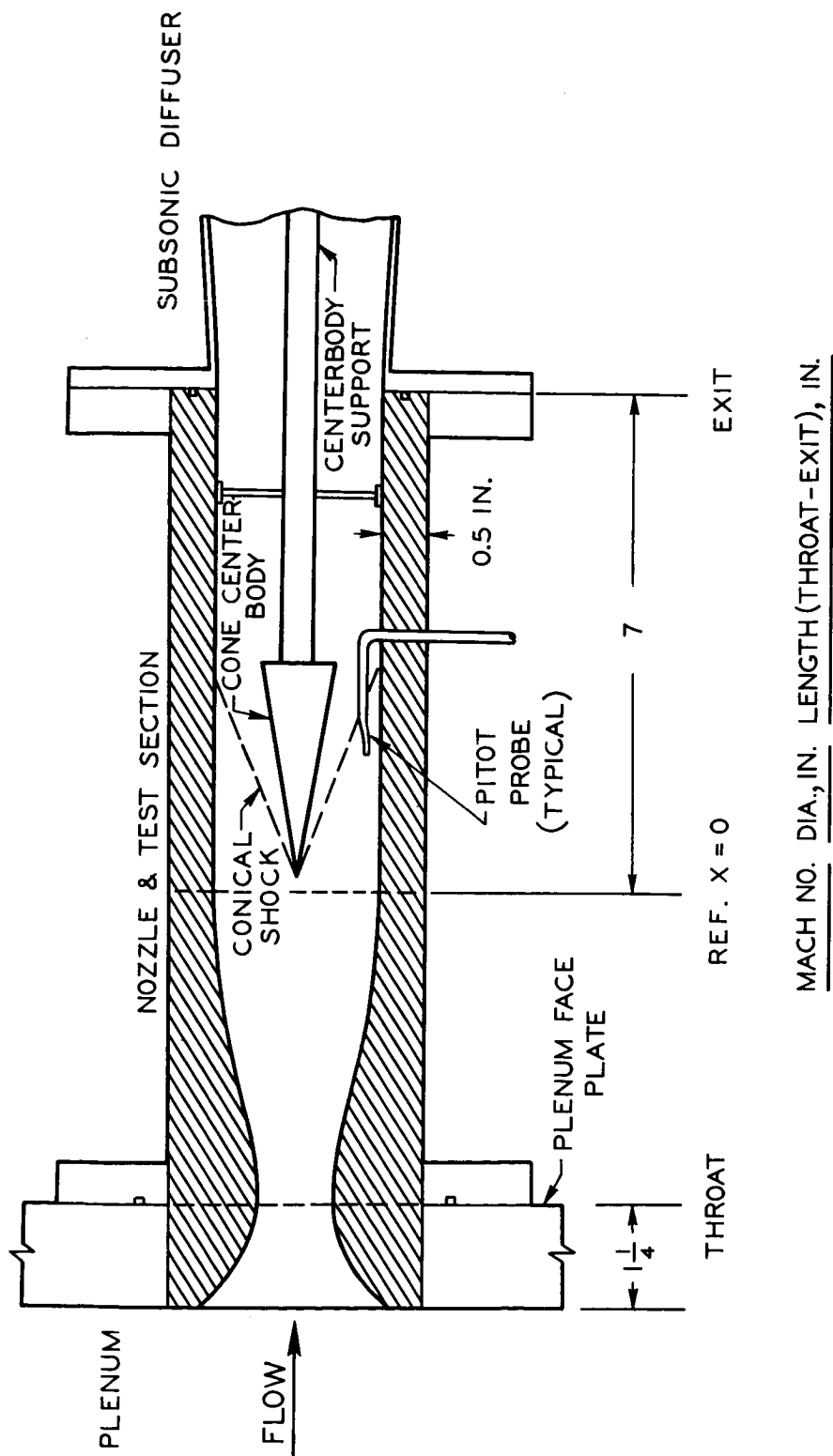


Figure 2.- Axisymmetric model (all dimensions are in inches).

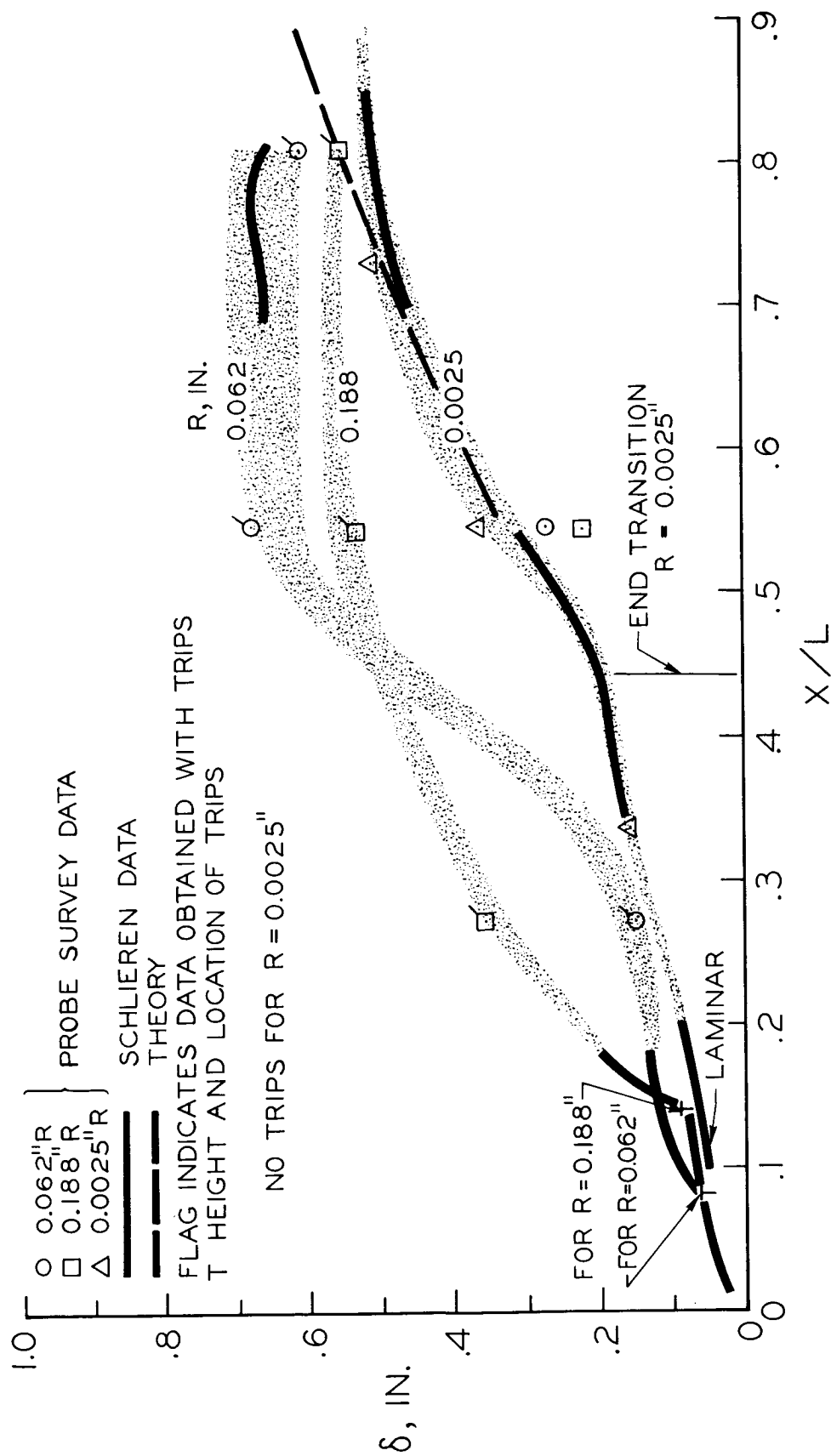
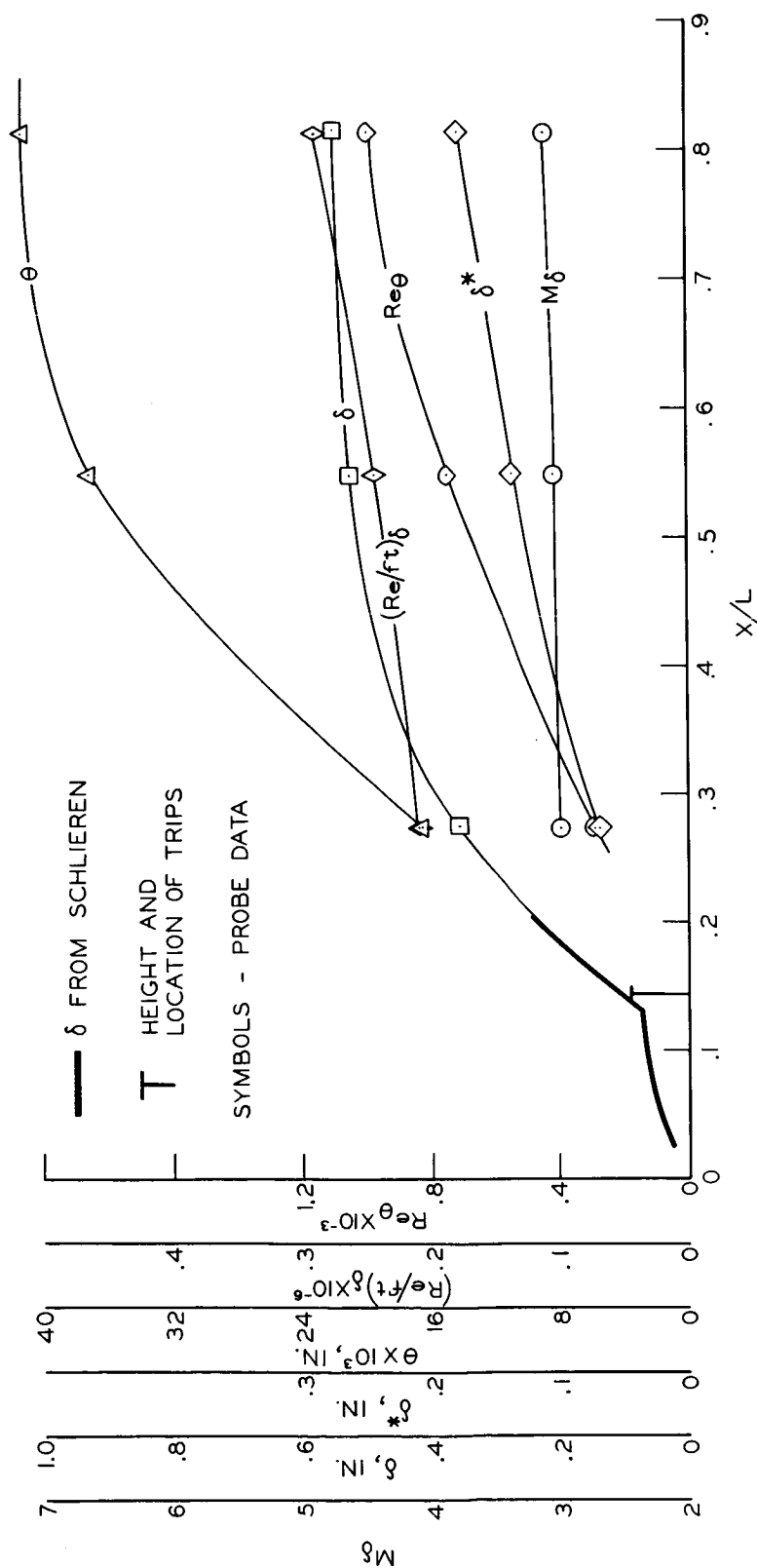
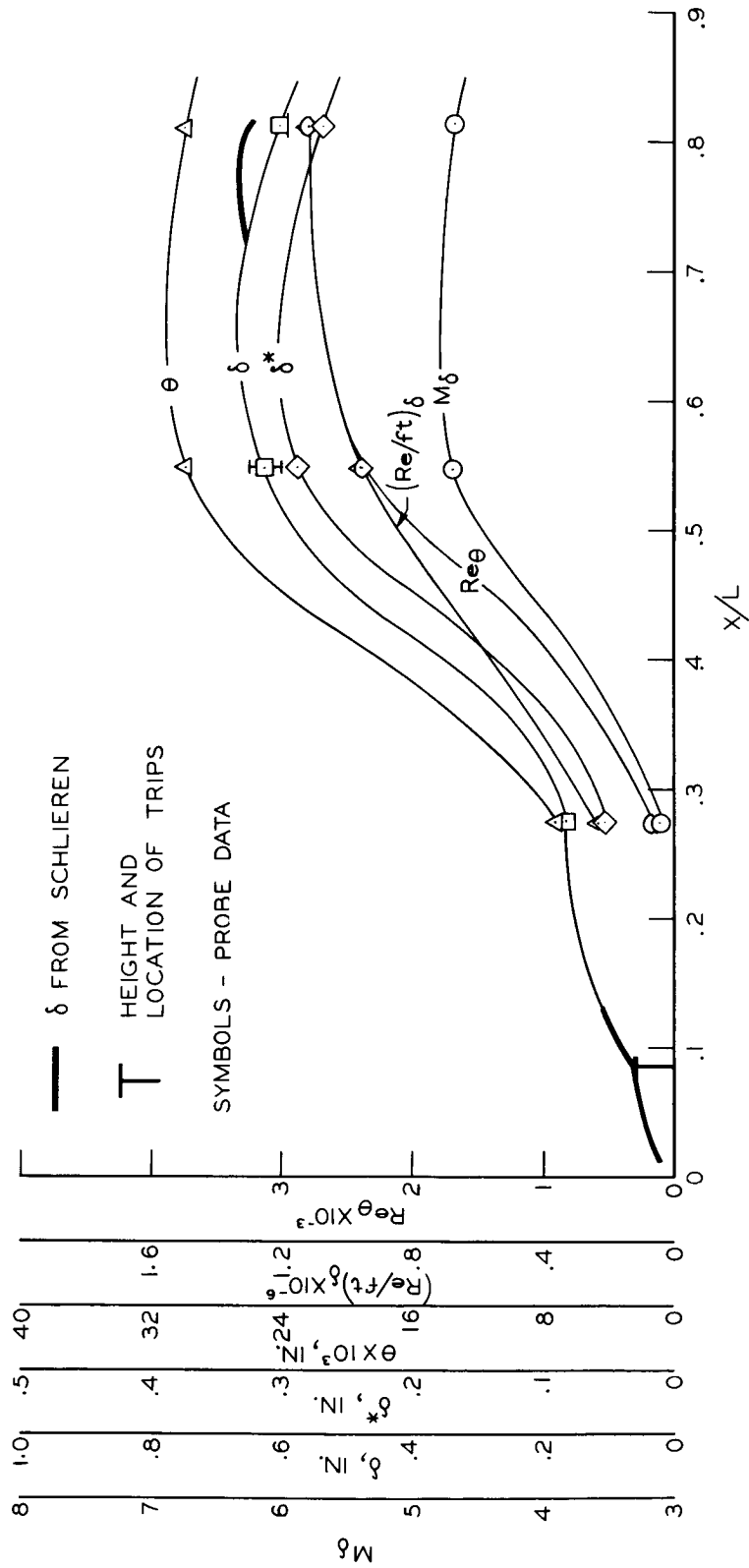


Figure 3.- Boundary-layer growth on compression surface;  $M_\infty = 7.4$ ,  $(Re/ft)_\infty = 1.6 \times 10^6$ .



(a)  $M_\infty = 7.4$ ,  $(Re/ft)_\infty = 1.6 \times 10^6$ ,  $R = 0.188$  in.

Figure 4.- Boundary-layer properties on compression surface.



(b)  $M_\infty = 7.4$ ,  $(Re/ft)_\infty = 1.6 \times 10^6$ ,  $R = 0.0625$  in.

Figure 4.- Concluded.

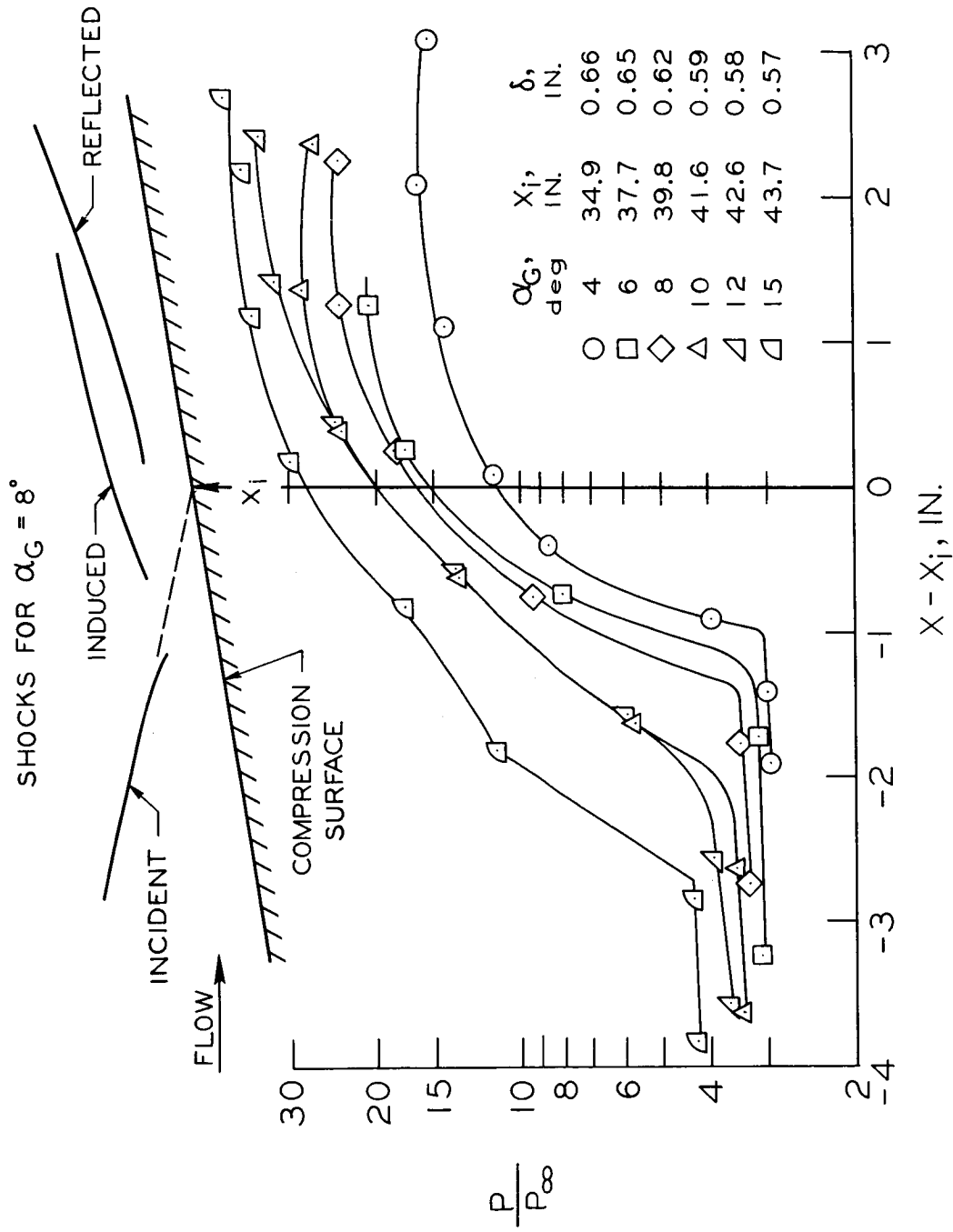


Figure 5.- Turbulent boundary-layer shock-wave interaction.  $R = 0.0625$  in.,  $M_\infty = 7.4$ .

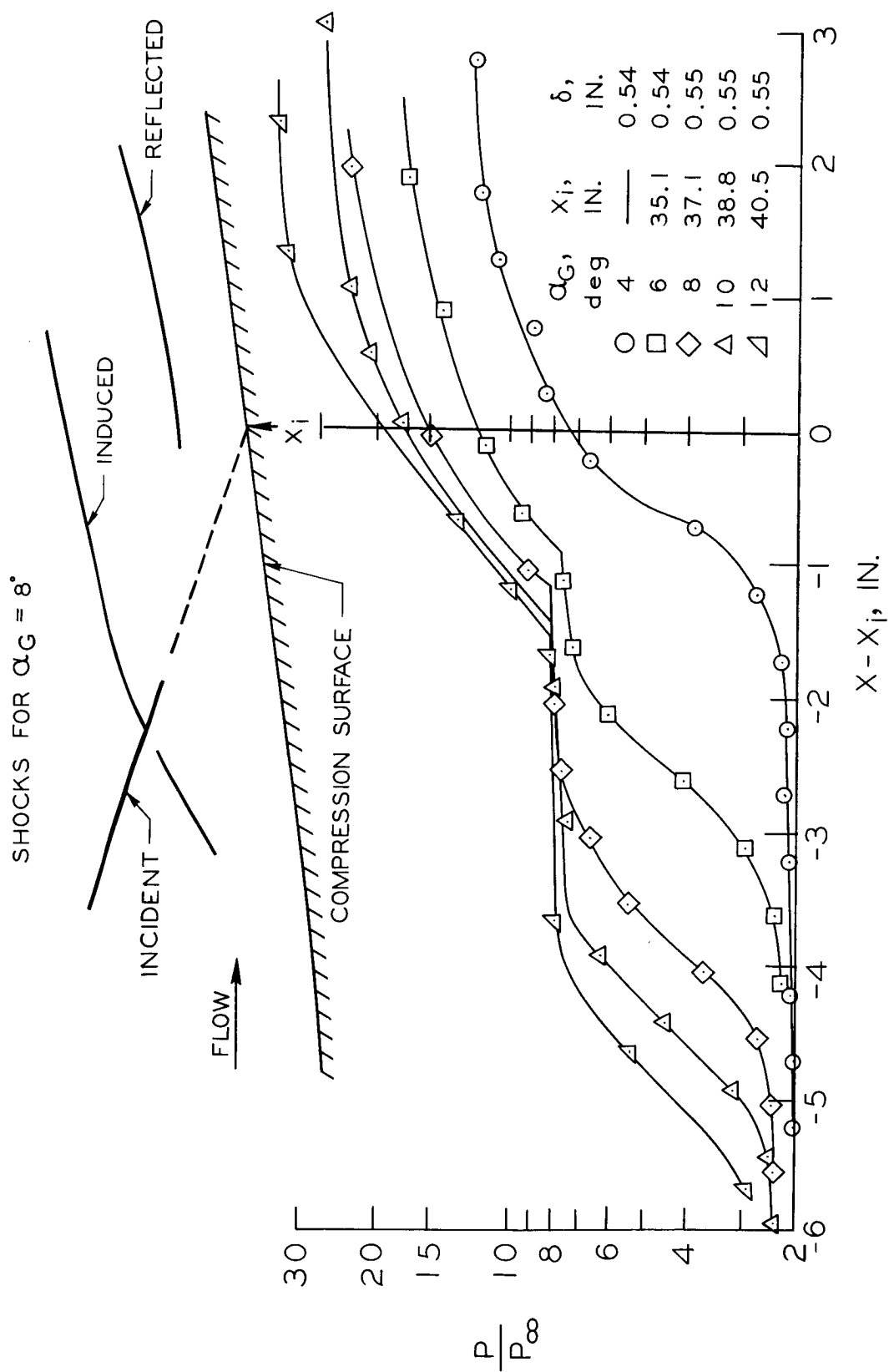


Figure 6.— Turbulent boundary-layer shock-wave interaction.  $R = 0.188 \text{ in.}$ ,  $M_\infty = 7.4$ .



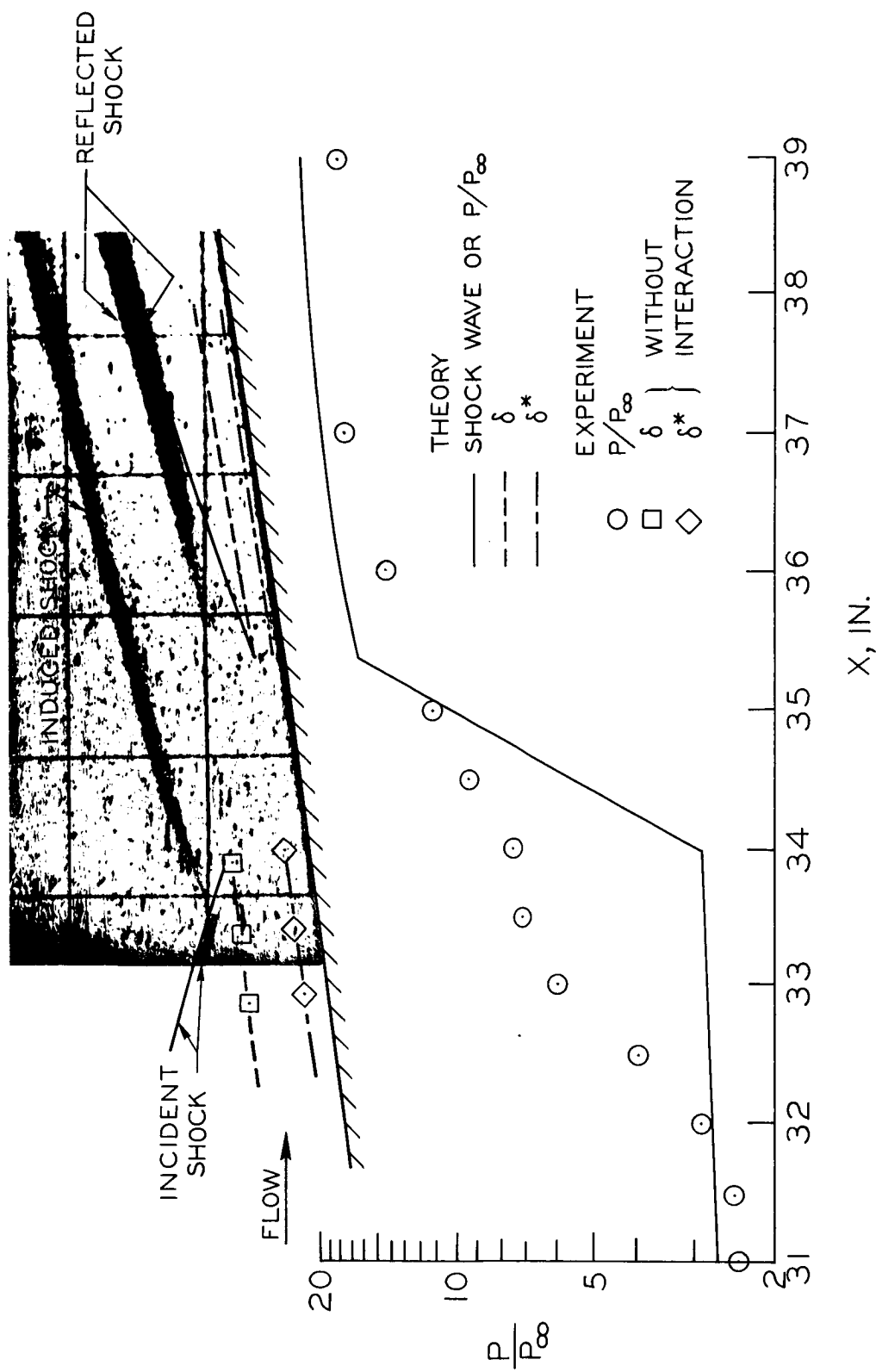


Figure 7.- Turbulent boundary-layer shock-wave interaction combined inviscid and viscous theories. Separated flow;  $M_\infty = 7.4$ ,  $R = 0.188$  in.,  $\alpha_g = 6^\circ$ .

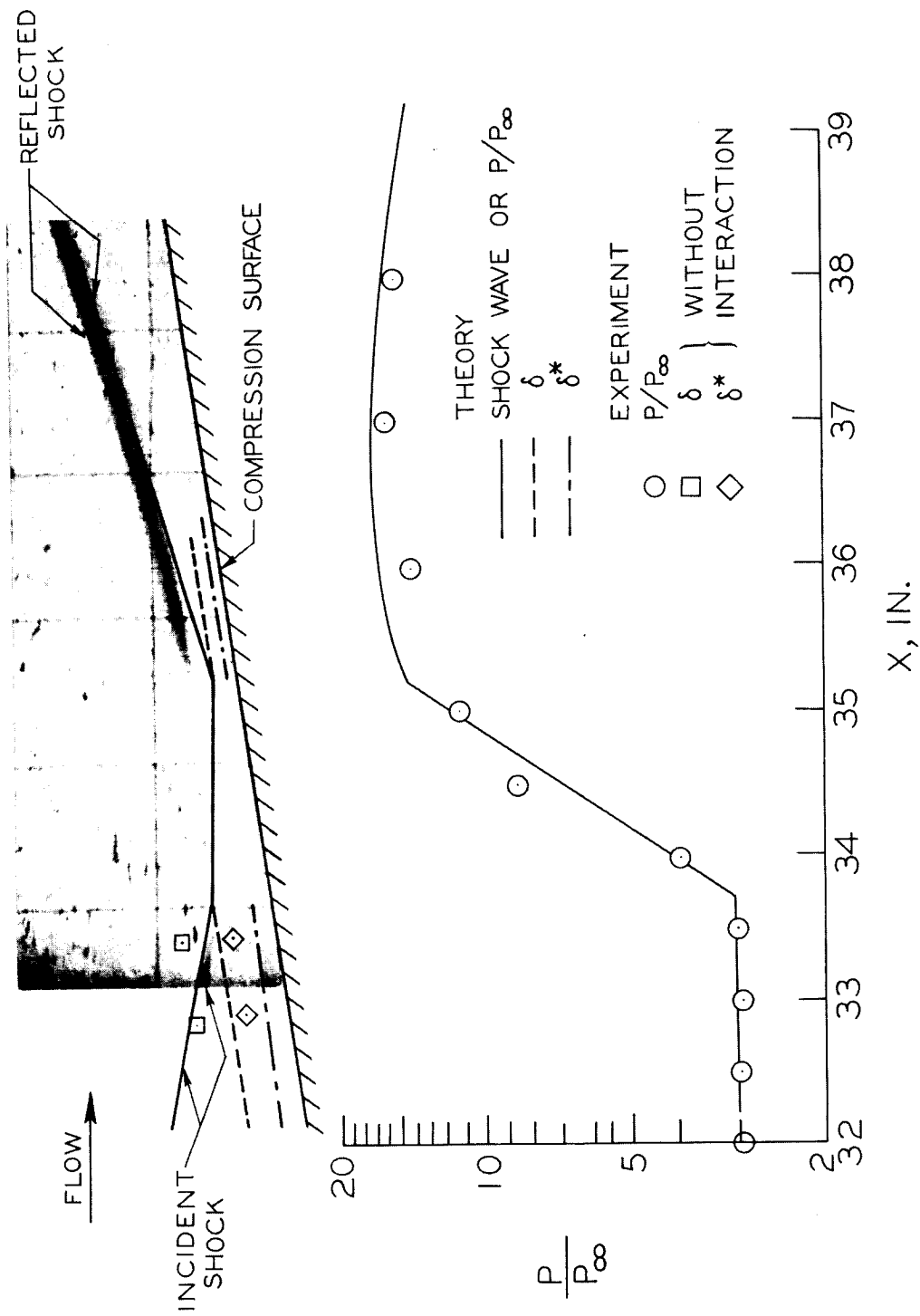


Figure 8.- Turbulent boundary-layer shock-wave interaction combined inviscid and viscous theories.  
No separation;  $M_\infty = 7.4$ ,  $R = 0.0625$  in.,  $\alpha_G = 4^\circ$ .

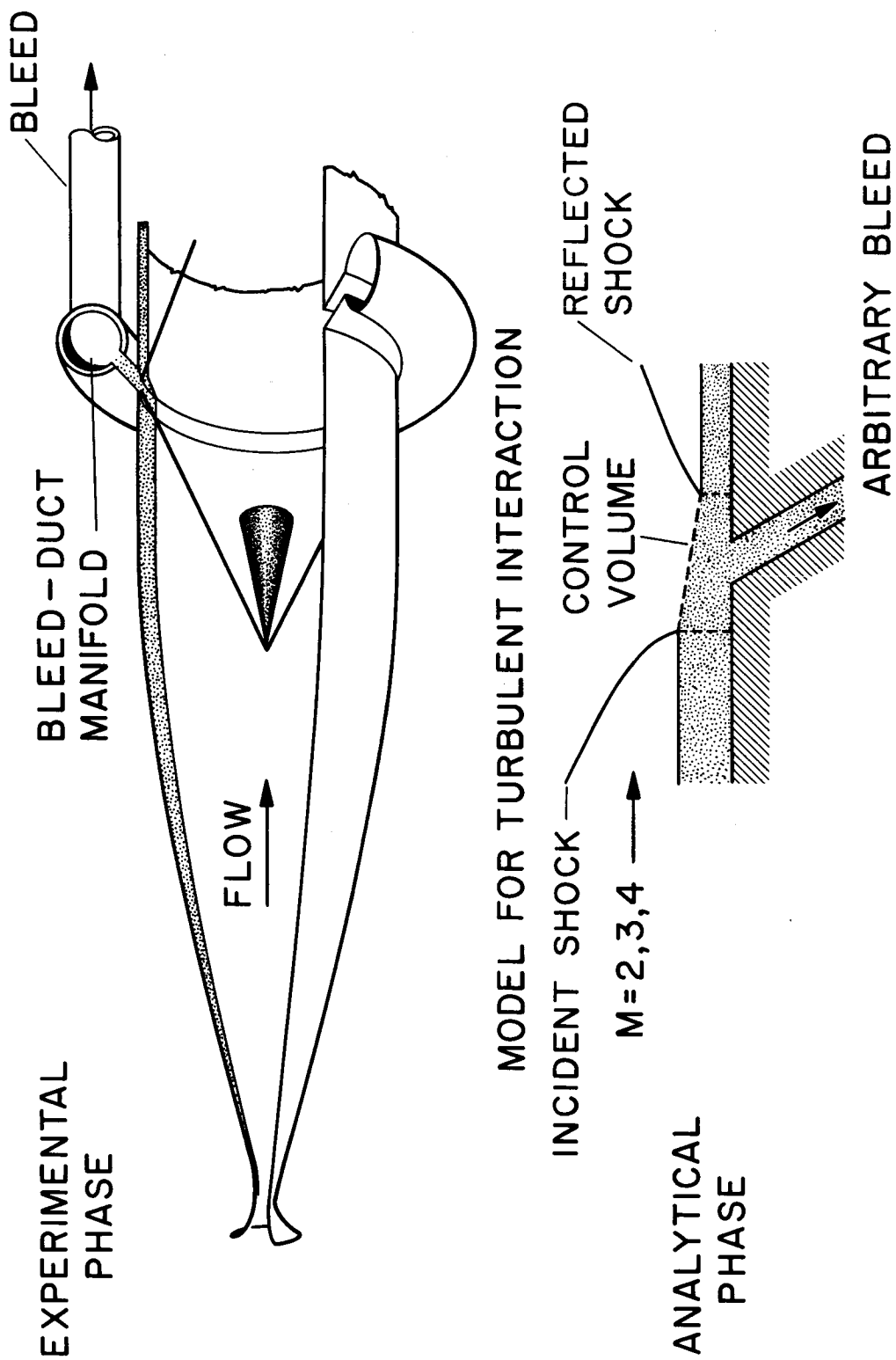


Figure 9.- Interaction of a conical shock with an axisymmetric turbulent boundary layer;  
University of Washington.

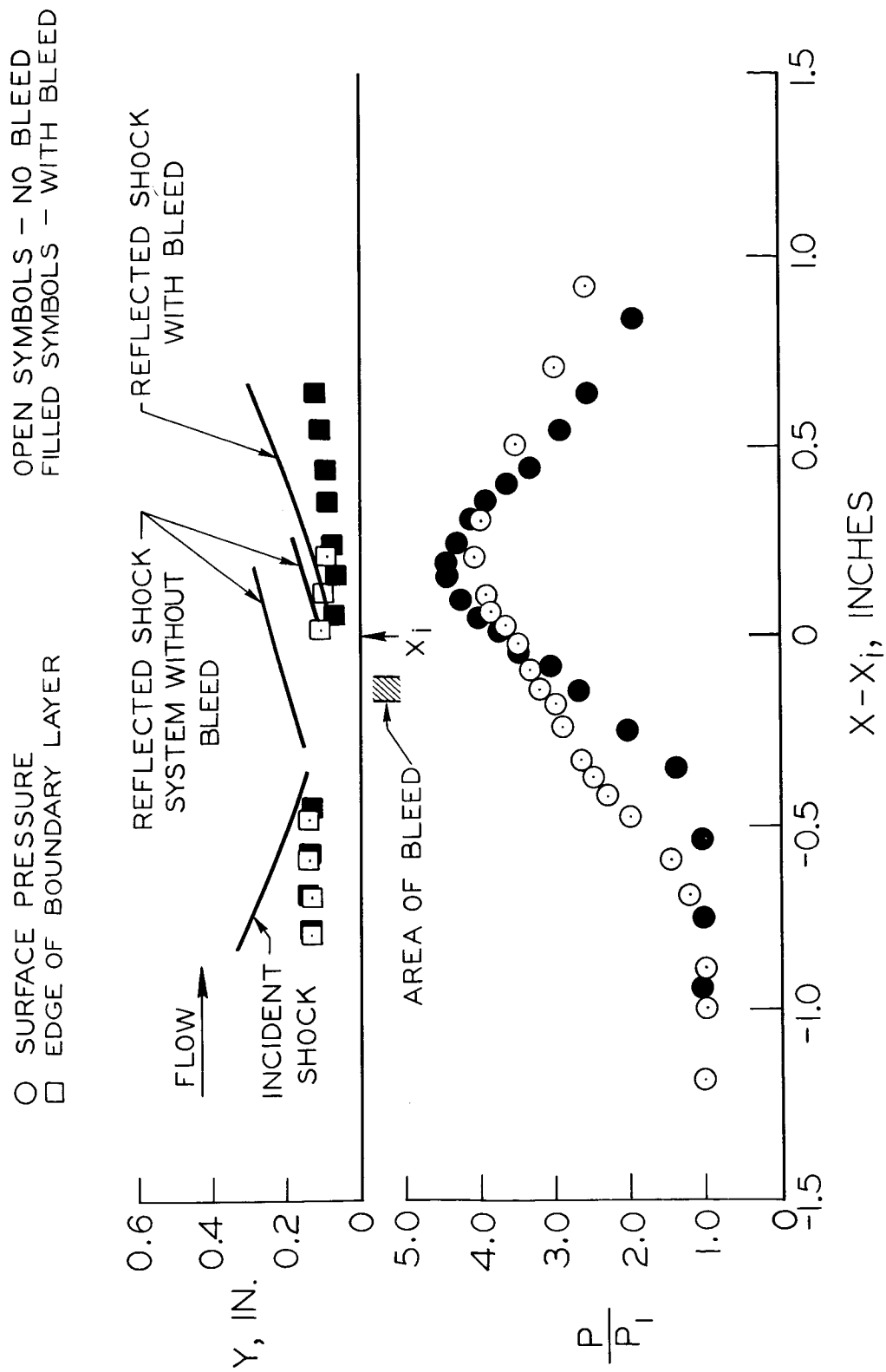


Figure 10.- Effect of boundary-layer bleed on axisymmetric turbulent interaction;  $M_1 = 3.78$ ,  $15^\circ$  half-angle cone,  $\dot{m}_{\text{bled}}/\dot{m}_{b.1.} = 0.031$ .

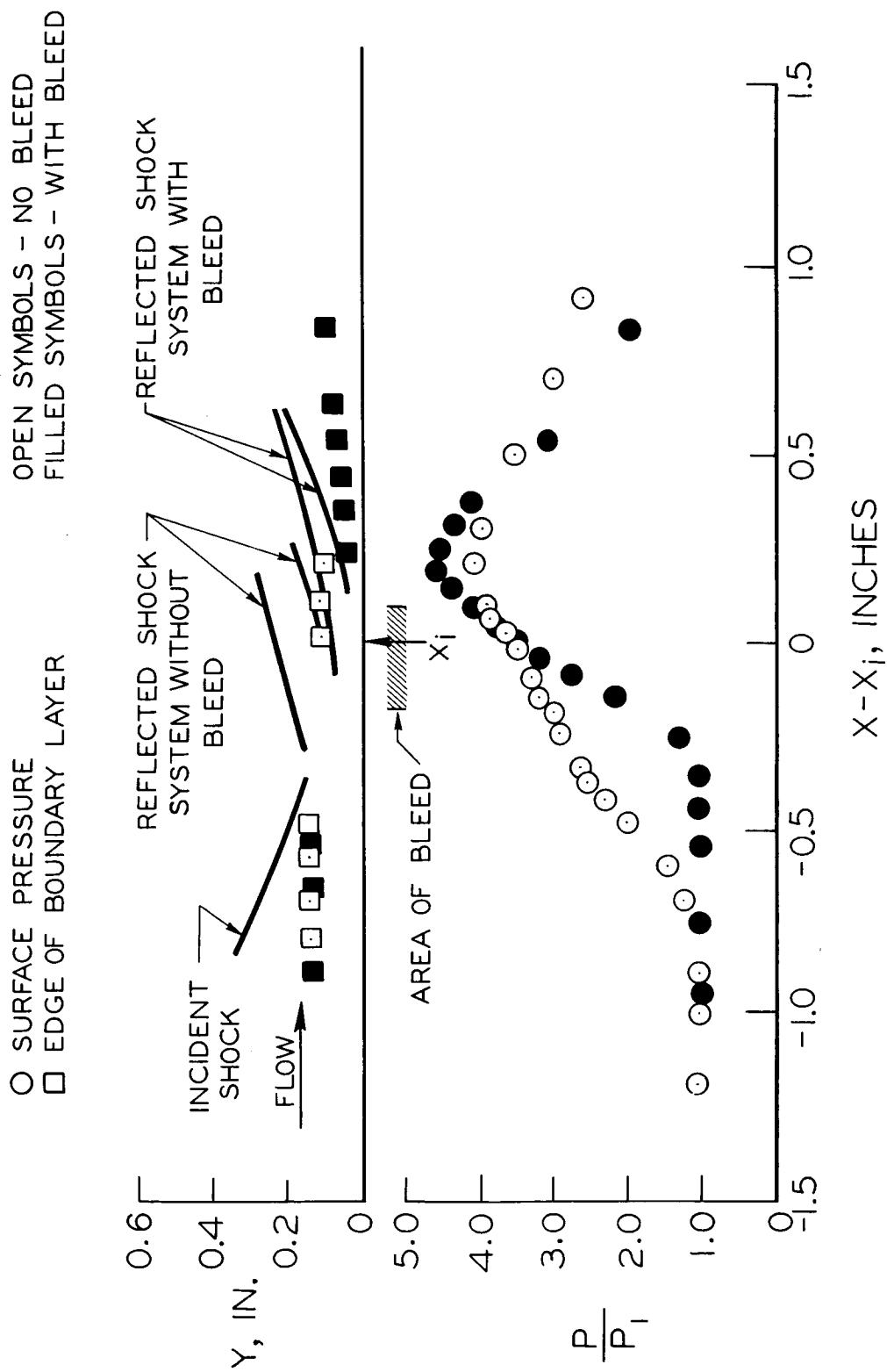


Figure 11.- Effect of boundary-layer bleed on axisymmetric turbulent interaction;  $M_1 = 3.78$ ,  $15^\circ$  half-angle cone,  $\dot{m}_{\text{bleed}}/\dot{m}_{\text{b.l.}} = 0.131$ .

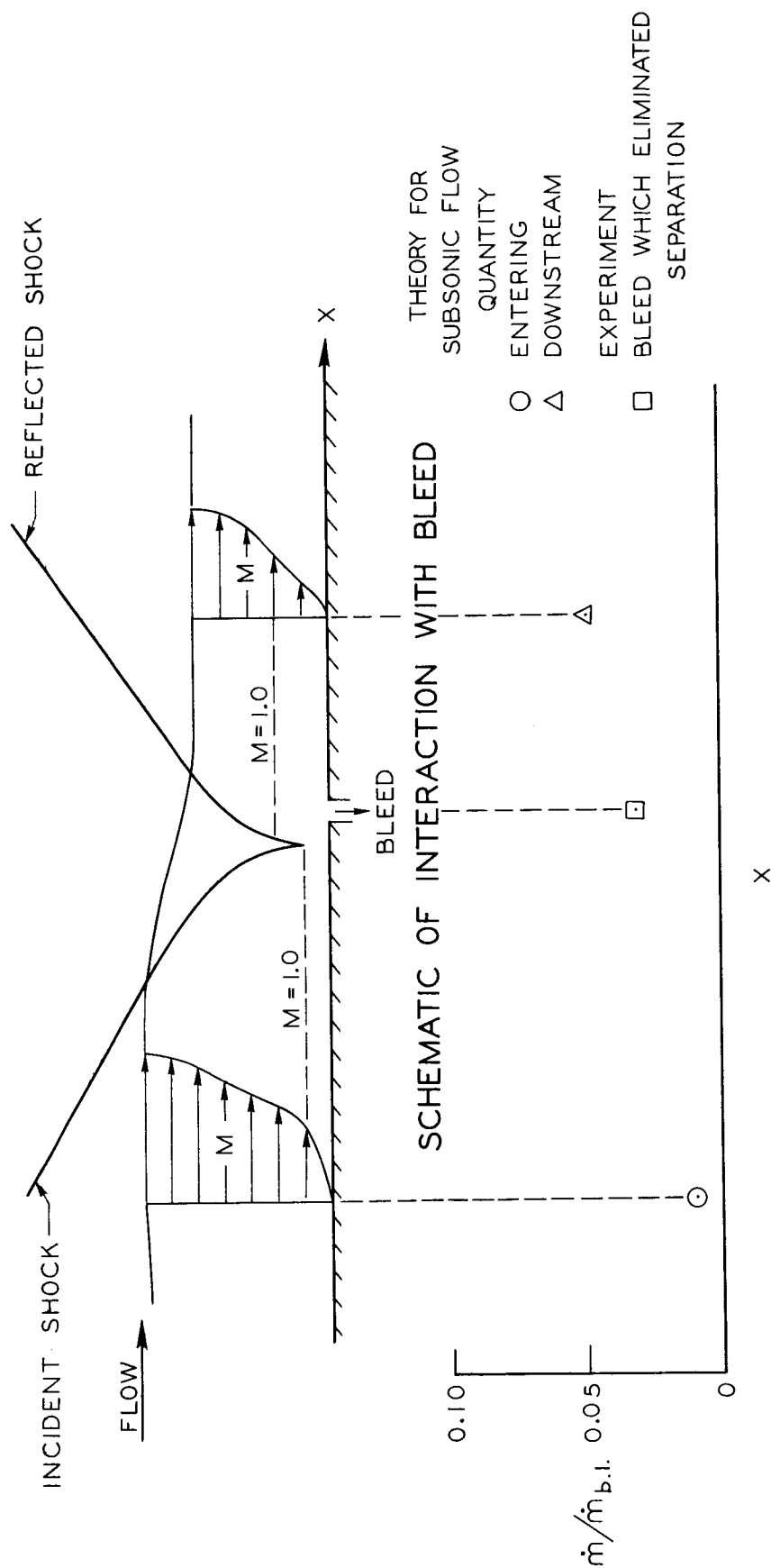


Figure 12.- Bleed required to eliminate separation in an interaction in axisymmetric flow;  
 $M_1 = 3.78$ ,  $15^\circ$  half-angle cone.

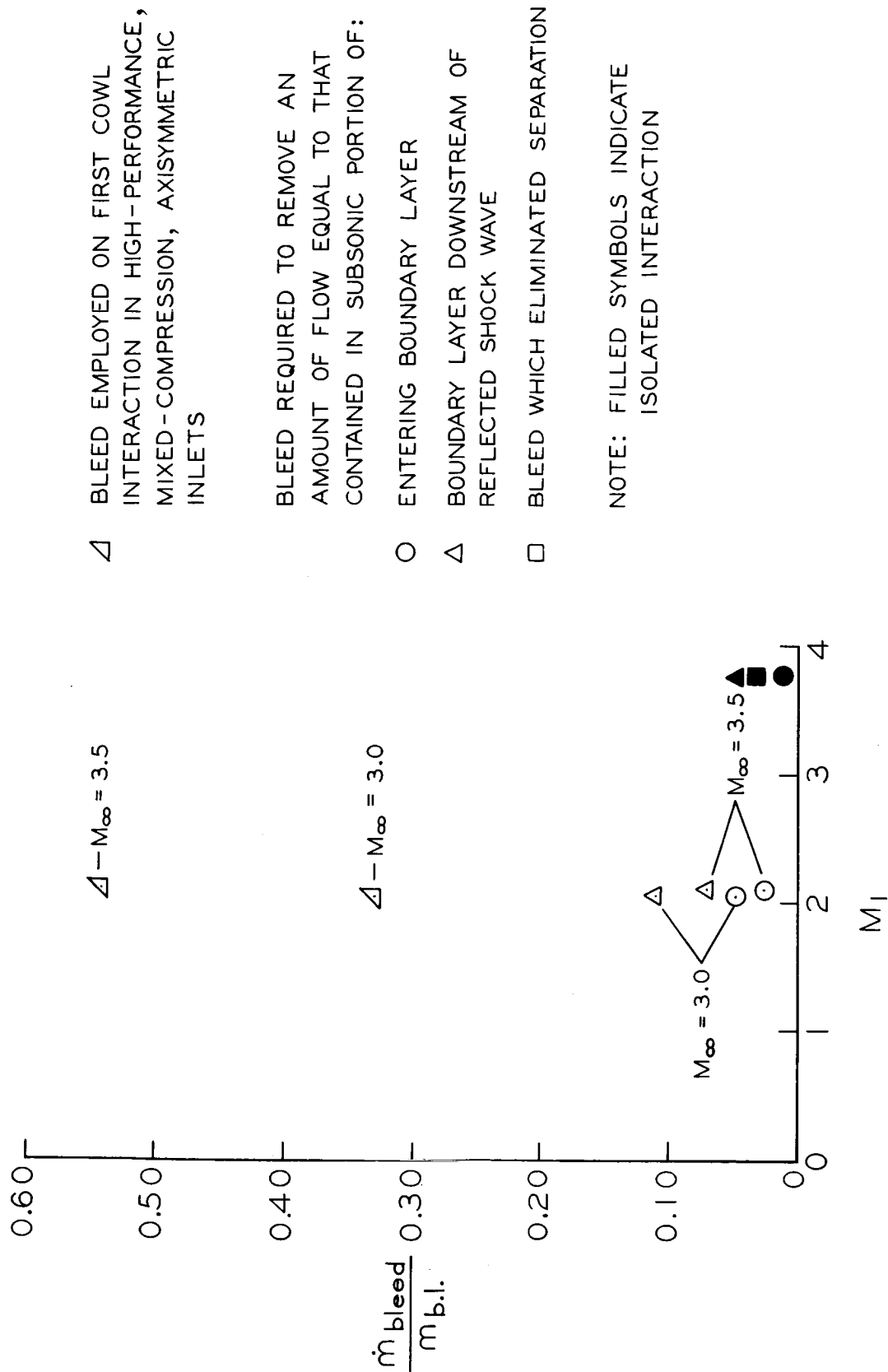


Figure 13.- Comparison of bleed requirements.

SYMBOL	$M_1$	$T_w/T_{t\infty}$	MODEL	SOURCE
○	2.93 & 3.85	$\approx 1$	SHARP FLAT PLATE	KUEHN
□	2.93 & 3.85	$\approx 1$	2-D NOZZLE WALL	BOGDONOFF (GIVEN BY KUEHN)
□	2.0 TO 4.27	$\approx 1$	SHARP FLAT PLATE	CP INC OBTAINED FROM PINCKNEY DATA
◁	2.82 & 3.78	$\approx 1$	AXISYMMETRIC NOZZLE WALL	UNIV. OF WASHINGTON (UNPUBLISHED)
◇	6.47	$\approx 0.40$	0.0025 IN. R FLAT PLATE	WATSON, MURPHY, ROSE
△	5.84	$\approx 0.35$	0.0025 IN. R COMPRESSION SURFACE	WATSON, MURPHY, ROSE
◇	3.05 & 3.60	$\approx 0.30$	0.188 IN. R COMPRESSION SURFACE	PRESENT STUDY
△	4.68	$\approx 0.35$	0.062 IN. R COMPRESSION SURFACE	PRESENT STUDY

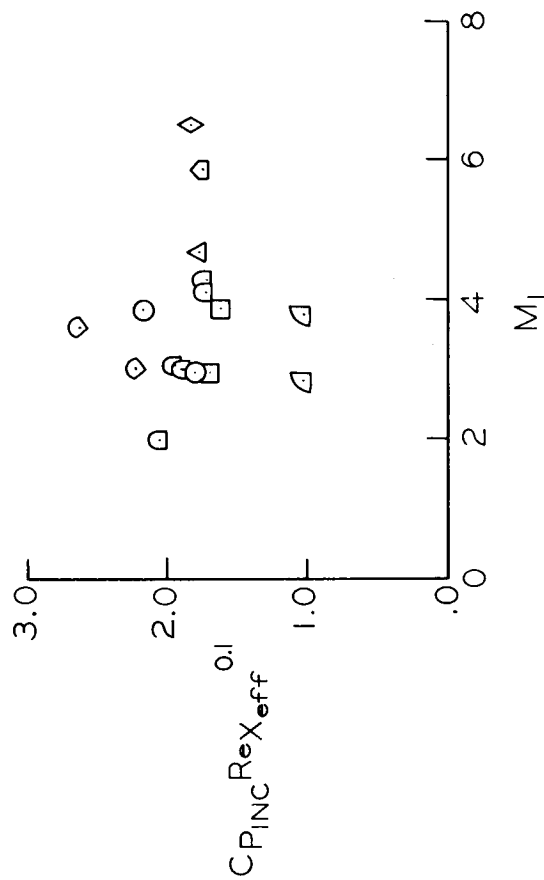


Figure 14.- Correlation of incipient separation data parameter of Popinski (ref. 7).



SYMBOL	$M_1$	$T_w/T_{t\infty}$	MODEL	SOURCE
○	2.93 & 3.85	$\approx 1$	SHARP FLAT PLATE	KUEHN
□	2.93 & 3.85	$\approx 1$	2-D NOZZLE WALL	BOGDONOFF (GIVEN BY KUEHN)
□	2.0 TO 4.27	$\approx 1$	SHARP FLAT PLATE	$C_{PINC}$ OBTAINED FROM PINCKNEY DATA
◁	2.82 & 3.78	$\approx 1$	AXISYMMETRIC NOZZLE WALL	UNIV. OF WASHINGTON (UNPUBLISHED)
◇	6.47	$\approx 0.40$	0.0025 IN. R FLAT PLATE	WATSON, MURPHY, ROSE
△	5.84	$\approx 0.35$	0.0025 IN. R COMPRESSION SURFACE	WATSON, MURPHY, ROSE
◇	3.05 & 3.60	$\approx 0.30$	0.188 IN. R COMPRESSION SURFACE	PRESENT STUDY
△	4.68	$\approx 0.35$	0.062 IN. R COMPRESSION SURFACE	PRESENT STUDY

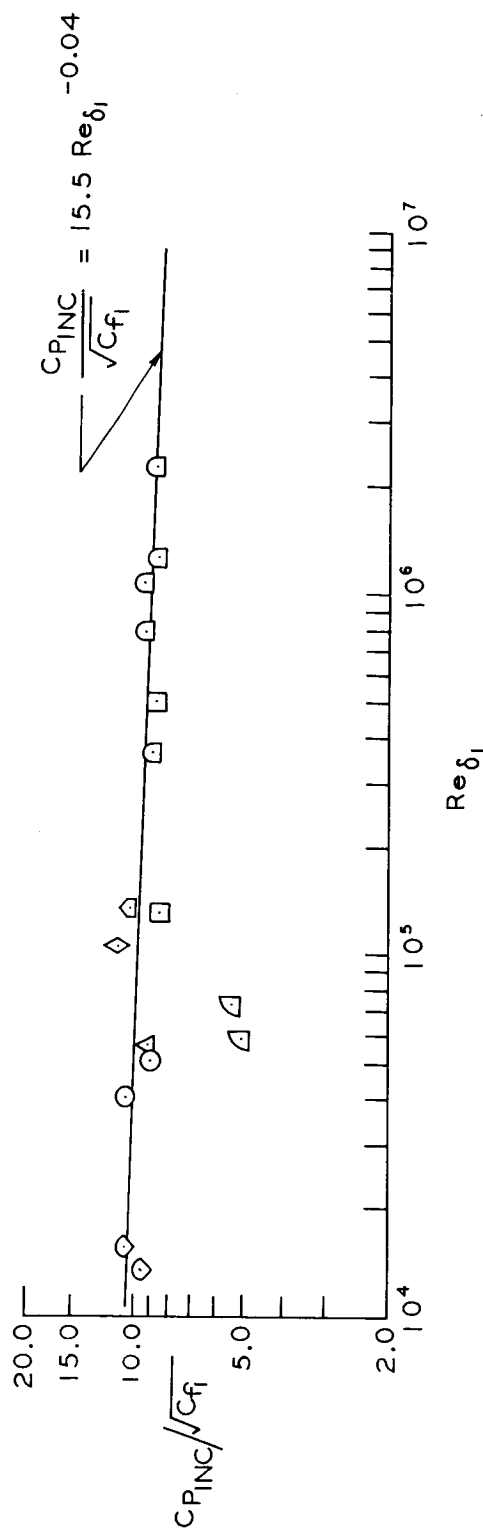


Figure 15.- Correlation of pressure rise for incipient separation of turbulent boundary layers.

## PANEL AND GENERAL DISCUSSION

Moderator - Mitchel H. Bertram, NASA Langley Research Center

The Panel and General Discussion was transcribed from a tape recording of the session. This transcription was edited by the moderator to remove redundancies and assure reasonable grammar and continuity. However, this editing was not done to change an essentially oral exchange into written language. To make this discussion more useful, footnotes have been added in the editing process, most of which give the source of various research works referred to by the speakers. A debt is owed Ivan E. Beckwith for his invaluable assistance in this process.

MHB

## PANEL AND GENERAL DISCUSSION

Moderator - Mitchel H. Bertram, Langley Research Center, NASA

### PANEL MEMBERS:

Professor Mark V. Morkovin, Illinois Institute of Technology  
Professor John Laufer, University of Southern California  
A. M. O. Smith, McDonnell-Douglas Corporation  
Henry McDonald, United Aircraft Research Laboratory

Mitchel H. Bertram: I have asked the panel members to devote 10 minutes to their initial presentation with a chance for further remarks later and interaction with the audience. The audience participation is important to this discussion and you must remember that you were invited not merely as spectators but so as to become involved and contribute as straightforwardly as possible to the problem at hand. We will start the discussion with Professor Morkovin.

Mark V. Morkovin (Illinois Institute of Technology): The 1968 Stanford meeting confirmed that the flows especially challenging for both the theoretician and the experimentalist are the nonequilibrium (nonsimilarity) flows. At the present symposium, I was impressed by the evidence that additional nonsimilarity brought about by the thermal field, i.e., the stagnation enthalpy variation,  $H_t(x,y)$ , may be even more challenging. At incompressible speeds most dynamic unbalances in the turbulent boundary layer tend to approach equilibrium conditions near the wall rather rapidly since this slow, inertial region responds readily - across streamlines - to changes in free-stream velocity and pressure gradient. Thermal changes imposed on the outer regions of the compressible boundary layer, however, will propagate only slowly towards the wall, probably leading to different lag times in heat transfer.

This spells CAUTION for generalizations of experimental techniques and theory as we depart from the comfortable similarity conditions, especially the adiabatic wall conditions (on which my own limited observations were based). The most palpable evidence of the effect was presented to us in the shifts in  $x$  and  $y$  of the stagnation-temperature dependence on the mean longitudinal velocity  $\bar{u}$ . This aspect will probably put a limit on the possibility of the compressible-incompressible mappings we have heard about. The effect is almost surely present downstream of boundary-layer trips at high Mach numbers (which reshuffle the thermal field throughout the boundary layer) and makes their usage even more suspect for simulation than was indicated by the revealing paper presented by Morrisette in this symposium.<sup>1</sup> We have heard of two more cases where the relaxation effects of primarily the thermal field make analysis difficult: the cases of entropy layer stratifications and the nonuniform distribution of stagnation temperature in settling chambers of high-speed wind tunnels.<sup>2</sup> In the latter case, the experimentalists are concerned not only about

---

<sup>1</sup>Paper no. 16 of this volume.

<sup>2</sup>R. Jones discussion after paper no. 11 (paper no. 12).

the induced effect on the measured mean skin friction and heat transfer, but also on the corresponding fluctuation quantities.<sup>3</sup>

My second group of observations deals with the role of theoretical methods. What we really need is a graduated hierarchy of methods starting with "fasties" for prediction of gross wall characteristics and ending with procedures incorporating information on boundary-layer structure beyond that of mean theorems. Despite the overbelief of chief engineers and contracting officers in data from complex computer programs, only reasonable upper and lower bounds are required for most design purposes. The special merit of extra detailed theories (e.g., papers 3, 6, and 11) is that they can provide basic understanding on one hand and can build up confidence in the intermediate and fast predictive methods. An excellent example of a "fasty" improvement on previous "fasties" is the correlation presented here by Ed Hopkins and the Ames group in paper 10. In fact, no current extra detailed method can apparently match this "fasty" correlation on the effect of wall-to-stagnation temperature ratio. A good example of the application of a detailed method has been demonstrated by Bushnell and Company in paper 11 which threw at least partial light on the aforementioned variation of stagnation enthalpy with  $\bar{u}(x,y)$ .

Even more than for low-speed turbulent layers, however, we need careful experimental standards: (a) for guidance of the predictive theories and (b) for understanding of detailed turbulent-layer structure, especially above  $M$  of 10 when substantial differences from phenomena observed by Kline et al.,<sup>4</sup> Kovasznay and Kibbens,<sup>5</sup> Kaplan and Laufer,<sup>6</sup> etc., must be expected since the various low-speed feedback loops can hardly be maintained. In category (a) we need good experiments, preferably with redundant instrumentation (for extra accuracy) for the development of a layer through a long run of (1) a compressible field such as the ramp of J. Henry and Co., of paper 19, (2) of an expansive field, and (3) of a constant pressure field with  $x$ -varying wall temperature and/or boundary-layer edge temperature. Good consistent experimentation worthy of setting standards requires extra time, extra patience, extra "knowhow," extra good instrumentation, good and flexible facility, FUNDING, and confidence and support of supervisors. Had Harry McDonald had such data for his comparisons in paper 6, his conclusion could be more definite including his partial loss of respect for the difference technique.

As to category (b), J. Wallace gave us only a tantalizing taste of the potential of the electron beam for measurements of hypersonic density fluctuations in

---

<sup>3</sup>However, since the characteristic times imposed by low-speed settling chamber processes tend to be long in comparison with the characteristic times of the supersonic boundary layer, no important dynamic coupling should be expected. See also M. V. Morkovin, Trans. ASME, Ser. E: J. Appl. Mech., Sept. 1959, p. 319; see especially discussion, *ibid.*, June 1960, p. 362.

<sup>4</sup>Kline, S. J.; Reynolds, W. C.; Schraub, F. A.; and Rundstadler, P. W.: J. Fluid Mech., vol. 30, pt. 4, 1967, p. 741.

<sup>5</sup>Kovasznay, L. S. G.; and Kibbens, V.: Proc. 12th Int. Cong. of Appl. Mech., Stanford, 1968, Springer Publ. 1969.

<sup>6</sup>Kaplan, R. E.; and Laufer, J.: Proc. 12th Int. Cong. of Appl. Mech., Stanford, 1968, Springer Publ. 1969.

paper 8. I am only too well acquainted with the limitations of the hot wire for fluctuation measurements. Here, the Langley group are correctly concentrating on measurements in helium where some of the heating and support problems disappear and success comparable to that at lower supersonic speeds may be hoped for. Wallace's unsteady-stagnation-pressure measuring device (paper 8) appears to suffer from lack of high-frequency response to compare to the other two devices. All three devices need further development and clarification of true limitations.

My last group of comments is strictly miscellaneous. First, once a boundary layer is turbulent, its random behavior in the small is well averaged out and controlled by the nonlinear processes so that the overall processes are essentially deterministic and predictable. This is not the case for the transition phenomenon where large uncertainties always remain because the disturbance input and local stability characteristic are never known accurately enough. In view of this substantial uncertainty in the "origin" of the turbulent layer, to what accuracy are we justified in pushing the careful computations? For hypersonic vehicles flying at  $M$  of 12 or higher we are likely to run into low enough Reynolds numbers not to have fully developed layers (Coles<sup>7</sup>). In fact, many wind-tunnel experiments suffer from the same problem, leading to scatter and even contradictions.

Returning to the question of mapping of compressible fields into companion incompressible fields.<sup>8</sup> Economos in paper 5 provided extra mathematical freedom by allowing the pressure gradient and wall mass flux of the incompressible "image field" to be arbitrary. However, questions remain as to the physical significance of the corresponding compressible fields. Conceivably, such questions could be elucidated with the difference techniques such as that of Herring-Mellor (paper 3) and Bradshaw<sup>9</sup> (if the difference between these were less than any discrepancies in the mapping).

Finally, one could say that the very existence of a true mapping for  $M > 6$  in the presence of an arbitrary heat transfer  $Nu(x)$  and mass transfer  $\dot{m}(x)$  at the wall is in doubt. Any hypersonic problems with mass ablation are important.

John Laufer (University of Southern California): I think it happens very seldom that major questions are answered in meetings of this kind and I don't think that that happened at this meeting either. On the other hand, listening to the papers of yesterday and today, I did come up with two strong impressions. One,

<sup>7</sup>Coles, Donald: Parts I, II, and III, Rept. Nos. 20-69, 20-70, and 20-71, Jet Propulsion Lab., California Inst. Technol., June 1, 1953.

<sup>8</sup>In a discussion of paper 15 after the symposium, K. G. Winter reiterated that his mapping of the compressible adiabatic field parameters up to  $M \approx 4.4$  into the incompressible correlations gives definitely different results than, say, the Coles mapping. Since in the latter point-by-point mapping the wall invariance  $(C_f R_\theta)_{inc} = (C_f R_\theta)_{com} (\rho_\infty \mu_\infty / \rho_w \mu_w)$  is mandatory, it was concluded that

the R.A.E. correlation must be an empirical one between wall parameters without actual field mapping.

<sup>9</sup>Bradshaw, P.; Ferriss, D. H.; and Atwell, N. P.: J. Fluid Mech., vol. 28, pt. 3, May 26, 1967, pp. 593-616.

a positive one, could be stated in the following way: Apparently there is more and more evidence from widely different sources that, as far as the dynamics of turbulence is concerned, there is no significant difference between a supersonic environment and a low-speed environment. This observation, I believe, was first made by Mark Morkovin, back in 1961, as I indicated yesterday. Since then we have some more indirect evidence such as Mr. Winter's results that he presented in paper 15. It would appear that some of the length ratios determined in terms of kinematic quantities are independent of the Mach number. Furthermore, the fact that George Mellor's calculations express the exchange coefficient in terms of kinematic quantities only also points in that direction. Finally, the success of a Coles type of transformation also seems to indicate that density effects can be accounted for by simple coordinate stretching. Thus, much evidence seems to indicate, at least in the high supersonic or lower hypersonic Mach number ranges, that the general concept of a turbulent mechanism unaffected by the supersonic nature of the mean stream is an acceptable one.

Now the second impression is a negative one. When one looks through the papers of this meeting one finds that there is a ratio of 3 to 1 of analytical-type papers as against experimental. As a matter of fact, when one examines closely the experimental papers that deal with detailed measurements rather than just skin-friction or heat-transfer measurements, the ratio is even higher than that. I think this actually reflects the whole research activity on the problem under consideration in this country. Very much less experimental research is going on than theoretical research. In the particular area of turbulent hypersonic flow this is not a sound situation. I say this because in laminar cases when we do even quite complex calculations we can always compare those calculations to some exact solutions, but we don't have any exact solutions here and we need some acceptable, carefully done experiments - but this is exactly the point that Mark made minutes ago. It seems to me that above Mach number 5 we don't have, even for the simplest case, acceptable detailed measurements of the flow field. Not only measurements of the mean velocity but also of some of the other quantities need to be carried out. The sort of technique that we heard of yesterday from Wallace<sup>10</sup> would be very useful and needs to be further developed. Wallace's paper pointed out the potentialities of such a method, but the technique certainly cannot as yet be considered at the stage to give accurate density distributions that can be compared to calculations. His own measurements are, and I am sure he agrees, only preliminary.

Considering now the fluctuating rather than the mean field, there again a lot of work could be done. I am not necessarily referring to studying the turbulent mechanism per se as we do in the incompressible case because we have problems enough in the low-speed case. But there are certain points that we expect to be different, especially at Mach numbers higher than 5. Let us look at the pressure fluctuations, for instance Kistler's measurements of the pressure fluctuation on the wall.<sup>11</sup> One will find that they are rather high: the rms  $p'$  is something like a factor of 5 greater than the wall shear stress, if I remember, and this factor increases like Mach number square. So at  $M = 20$  apparently one might expect wall pressure fluctuations of the order of the static

---

<sup>10</sup>Wallace, J. E.: CAL No. AN-2112-Y-1, Cornell Aeronaut. Lab., Inc., Aug. 1968 (Paper 8 in this symposium).

<sup>11</sup>Kistler, Alan L.: Phys. Fluids, vol. 2, no. 3, May-June 1959, pp. 290-296.

pressure itself, and a not much less intense radiated pressure field. Two measurements here at Langley indicate that, in terms of the mean static pressure, fluctuations are anywhere from 2 to 6 percent.<sup>12</sup> This is in the free stream. In the turbulent boundary layer we can expect pressure fluctuations of 10, 20, 30 percent or so. It is interesting that apparently at least up to Mach number 5, there is not much interaction between these pressure fluctuations and the vorticity fluctuations (at least as far as we can tell). But they are present, so that when one makes total-pressure fluctuation measurements, it is unwise to say that those measurements are essentially  $u'$  fluctuations. At these Mach numbers the static-pressure fluctuations might make a significant contribution to the total-pressure fluctuations.

A. M. O. Smith (McDonnell-Douglas Corp.): When Mitchel [Bertram] said that he wanted us to be prepared to talk for 10 minutes, I wasn't sure what would happen here so I prepared a few slides to give a quick run-down on the status of the work that we are doing in the calculation area. I'll show them first and will take the remainder of the time for some general comments. It has occurred to me that there are roughly three main points I want to make which I will get into later. One, after listening to Jack Nielsen this morning,<sup>13</sup> I am not sure I want to stick to it but I'll say it anyway to start an argument, "No fooling around with compromise mathematics," and second is the need for more careful test data which Mark Morkovin mentioned. Finally, a few comments about the eddy-viscosity concept versus the idea of Bradshaw<sup>14</sup> and Donaldson.<sup>15</sup>

In the first figure are shown the equations that we are currently trying to solve. I like them myself, they are in rather a clean form and I just want to point out a few things about them. The  $t$  quantity is a transverse curvature measure and the equations are all transformed with a Levy-Lees and Probstein-Elliott type of transformation. The  $\epsilon^+$  is an  $\epsilon/\nu$  ratio and is the turbulent eddy-viscosity measure. If this term is zero then you have laminar flow, if  $t$  is zero you don't have a transverse curvature effect, and the rest of the expressions are the ordinary laminar equations. The second equation is the energy equation and heat transfer shows up in the  $Pr_T$  quantity, a turbulent Prandtl number. I like to characterize these equations as following the principle of good management. The equations are all exact at least to first order except for  $\epsilon$  and the turbulent Prandtl number. So if they don't work at least you know where to pin down the responsibility. The remaining equations give the various definitions plus our form for the inner eddy viscosity ( $\epsilon_i$ ), which has the Van Driest correction, and the outer eddy viscosity, which is essentially

---

<sup>12</sup>Measurements by R. D. Wagner in the Langley 22-inch helium tunnel at  $M = 20$ . (See AIAA Paper No. 69-704 by R. D. Wagner, Jr., D. V. Maddalon, L. M. Weinstein, and A. Henderson, Jr., June 16-18, 1969.

<sup>13</sup>Paper 14.

<sup>14</sup>Bradshaw, P.; Ferriss, D. H.; and Atwell, N. P.: NPL Aero Rept. 1182, Jan. 1966.

<sup>15</sup>Paper 7.

constant with an approximation for the error-function intermittency fade-out. These then are the basic formulas, and now I'll show just a few examples of their application.

# TRANSFORMED EQUATIONS

$$\begin{aligned} & \left[ (1+t)^{2k} c (1+\epsilon^*) f'' \right]' + f f'' + \beta \left[ \frac{\rho_e}{\rho} - (f')^2 \right] = 2 \xi \left[ f' \frac{\partial f'}{\partial \xi} - f'' \frac{\partial f}{\partial \xi} \right] \\ & \left[ (1+t)^{2k} c \left[ (1+\epsilon^*) \frac{g'}{Pr} + \frac{u_e^2}{H_e} \left( 1 - \frac{1}{Pr} \right) f' f'' \right] \right]' + f g' = 2 \xi \left[ f' \frac{\partial g}{\partial \xi} - g' \frac{\partial f}{\partial \xi} \right] \\ & \beta = \frac{2\xi}{u_e} \frac{du_e}{d\xi} \quad f' = \frac{u}{u_e} \quad g = \frac{H}{H_e} \quad c = \frac{\rho \mu}{\rho_e \mu_e} \quad d\xi = \rho_e \mu_e u_e \left( \frac{L}{L_0} \right)^{2k} dx \\ & t = -1 + \left[ 1 + \frac{2L \cos \alpha}{t_0^2} \left( \frac{2\xi}{\rho_e u_e} \int_0^n \frac{\rho_e}{\rho} d\eta \right)^{1/2} \right]^2 \quad d\eta = \frac{\rho u_e}{(2\xi)^{1/2}} \left( \frac{L}{L_0} \right)^{1/2} dy \\ & \epsilon_i = k_i y^2 \left[ 1 - \exp \left[ -\frac{y}{2\delta^*} \left( \frac{\gamma_w}{\rho} + \frac{dp}{dx} \frac{y}{\rho} \right)^{1/2} \right] \right]^2 \quad \left| \frac{\partial u}{\partial y} \right| \quad \epsilon_0 = \frac{0.0168 u_e \delta^*}{1 + 55 \left( \frac{y}{\delta} \right)^6} \end{aligned}$$

Figure 1

# REYNOLDS' HEAT TRANSFER EXPERIMENTS

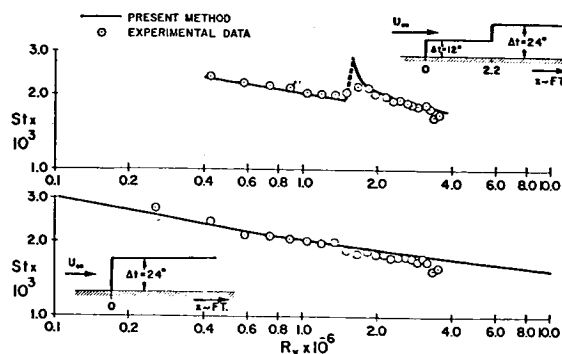


Figure 2

On the next figure [fig. 2] are shown two cases of flat-plate flows. The temperature is  $24^\circ$  above the free stream. The analytic results are compared with Reynolds' experimental data from Stanford.<sup>16</sup> Agreement of theory and experiment is good at the bottom of the figure, though the slope is slightly different. The other example at the top of the figure has a step in the wall temperature, and experiment and theory agree rather well in this case also. I might say that one problem that we wonder about in connection with going on to very high Mach numbers is that of high wall temperature, so it would be very interesting to repeat some kind of experiment like this with appropriate temperatures. As I see it, it wouldn't necessarily have to be at extremely high Mach numbers. It would just have to be a high wall temperature where viscosity gets high and a sort of Reynolds number for the bottom of the boundary layer is real low.

On the next figure [fig. 3] are shown some French data<sup>17</sup> where we compare our method with momentum thickness data on the left and with profile data on the right. Some more heat-transfer data are shown on the next figure [fig. 4]. These are old Ames data taken at Mach number 1.69.<sup>18</sup>

When we get to around Mach 4 we are starting to have some trouble, and I see a lot of work ahead. We are making the modifications of Mellor's right now into the kinematic  $\delta^*$ . (Note added in proof, Aug. 1, 1969: Mellor's introduction of kinematic  $\delta^*$  has worked wonders. See results in AIAA Preprint 69-687 by Cebeci, Smith, and Mosinskis.)

<sup>16</sup>Reynolds, W. C.; Kays, W. M.; and Kline, S. J.: NASA MEMOS 12-1-58W and 12-2-58W, 1958.

<sup>17</sup>Michel: ONERA TM 22, Figs. 5 and 12.

<sup>18</sup>Pappas, C. C.: NACA TN 3222, 1954, Figs. 6(a) and 8(a).



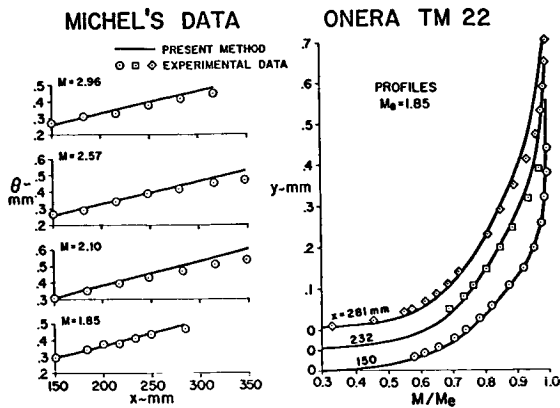


Figure 3

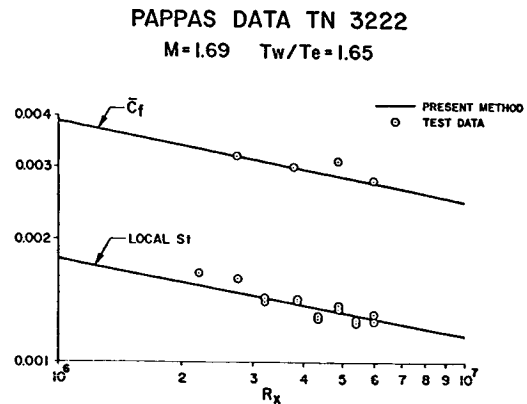


Figure 4

Results with transverse curvature are rather interesting, as shown next [fig. 5]. These are Yasuhara's tests in Japan<sup>19</sup> on a tube about a meter long. There is laminar flow at first, and at transition we switch in the eddy viscosity. The second profile from the left, which was taken in the transition region, does not actually agree well with experiment. But finally you go right through transition and settle down to agree well with the profiles taken in turbulent flow.

It is encouraging to have one method that will go through both laminar and turbulent flow and handle everything.

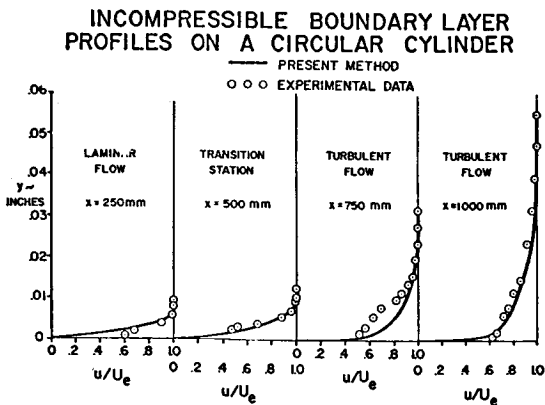


Figure 5

Now as far as my general comments go, it seems to me that there are three types of methods here. Agreeing with Mark Morkovin, there is what I'm inclined to call a big gun method, which is used with some kind of a billion dollar project where we really should go all out. Then there is a very simple method and the in-between ones. I think this last is essentially what Jack Nielsen is doing. Actually, when I say don't fool around with compromise math, I am not entirely following that line myself, but one of the points was that the computers nowadays are sufficiently powerful that you

can solve the problem as exactly formulated as you know how. It takes us about two to three seconds per station, amounting to about one minute for an entire incompressible problem and something like double that on the set of equations that I showed you in figure 1, to solve a compressible problem on a 360-65 computer.

There is a certain amount of tradition in methods of analysis. The computer is a tremendous new tool that should cause vast changes in analysis methods, but

<sup>19</sup>Yasuhara: Trans. Japan Soc. Aero. Space Sci., vol. 2, no. 3, 1959, pp. 72-76.

often the changes are slow to follow. There is need for more test data, as has already been mentioned. One thing is dismaying when you are developing computing methods. If you have empiricism in the turbulent boundary-layer equations, the only way to know whether you have an adequate method is to examine about all the available experimental data, or at least a very good sample of the whole population of experiments, and this means a tremendous amount of work. However, I don't know what to do about it. The laminar case, of course, is different; we accept the equations and the problem resolves to one of just solving them. Spalding checked 419 data points<sup>20</sup> and there are more coming in all the time; in fact, there is an abundant supply of new information which unfortunately is not nearly as detailed as needed. Finally, there is this rather fun controversy between Mellor,<sup>21</sup> Spalding,<sup>22</sup> us, Henry McDonald, Bushnell, Bradshaw, Cole Donaldson, and maybe others, about eddy viscosity, mixing length, and turbulent kinetic energy. We, meaning several of us, have introduced a new technique in being able to solve these partial differential equations in a numerically exact sense. Now the question is: Exactly what do we do in feeding in the necessary empirical information? I can't see right now, from what I know and hear, just what is going to turn out best. I think that several ideas need to be pushed for some time. The fact that somebody like Bradshaw has more logic on his side, I will concede. I think that maybe he is confused on a higher plane than us, to use that old expression. Finally, the problem settles down to numbers. The best method will be the one that gives the best answers regardless of the sophistication of the necessary empiricism.

One point of interest is flow visualization of the turbulent process, which Kline has studied.<sup>23</sup> For the flow on a wall he can see eddies in motion - in addition, he has their trajectories. Despite their interest, these pictures don't tell me anything about whether to favor a simple eddy-viscosity concept or a turbulent kinetic-energy concept. Another point, to add to the confusion, is this business of additives. In water, additives have a tremendous effect upon turbulence - in fact, they decrease the skin friction from the turbulent value to about 80 percent of the way down to the laminar value. Now if we had some basic understanding here, I think this could be explained. There is plenty of information that just leaves you in a high state of confusion, and I think that we are still working blind. A test of calculations against experiments is finally what is going to count.

---

<sup>20</sup>Spalding, D. B.; and Chi, S. W.: J. Fluid Mech., vol. 18, pt. 1, Jan. 1964, pp. 117-143.

<sup>21</sup>J. Fluid Mech., vol. 24, 1966, pp. 225-253 and 255-274; AIAA J., vol. 5, 1967, pp. 1570-1579; also, NASA CR-1144, 1968 (paper no. 3 of this volume).

<sup>22</sup>Patankar and Spalding: Int. J. Heat and Mass Trans., vol. 10, no. 10, Oct. 1967, pp. 1389-1411.

<sup>23</sup>Kim, H. T.; Kline, S. J.; and Reynolds, W. C.: Stanford Univ. Rept. MD-20, Jan. 1968; also see J. Fluid Mech., vol. 30, Dec. 22, 1967.

Mark Morkovin: There is information with respect to the additives at the drag symposium meeting,<sup>24</sup> that you drop the skin friction at the wall something more than 50 percent, but the turbulence level at the center line of the pipe went up by a factor of two.

Henry McDonald (United Aircraft Research Laboratory): I'd like to take a perhaps more pragmatic view of what has been occurring recently. I will split my talk up into three sections: past, present, and future. My mother-in-law is a doll; she gave me some good advice when I came to this country; she said that when you are in a land of foreigners and they don't understand English, when you speak to them and they don't comprehend, say it again louder - so, if you have heard these remarks before, you will excuse me. When I look to the past the most obvious thing which catches my attention is the Stanford Conference that Mark Morkovin talked about yesterday.<sup>25</sup> Here we had 28 predictors all gobbled together to solve a fairly academic problem at a conservative cost of something like a half-million dollars. It seems to me that when we have so many other real problems, to solve that one so many times over - to say it so often, so loud - was more than a bit superfluous. Further work on thin incompressible two-dimensional turbulent unseparated boundary layers is obviously not justified by industry; it can only be carried out by the universities from now on. I think that if you are going to work on the boundary-layer problem, you have got to develop new wrinkles, you have got to start considering suction, blowing, separation, higher order terms, time dependence, etc. Since industry can no longer justify work on the simple problem, universities are going to have to do it.

It seems to me, viewing the universities from outside, that many of the advisors feel a sense of responsibility towards the student to ensure that the student gets his Ph.D. Therefore, they pick a subject that they know will get a Ph.D., and this may be why 28 people solved the boundary-layer problem all at once. I think it might be well to try and solve more difficult problems. In addition, we seem to have a negative attitude towards basic turbulence. Whatever happened to Malkus' theory?<sup>26</sup> Whatever happened to Burgers' equations?<sup>27</sup> They seem to be existing in limbo and people whisper about them in revered tones and do nothing about them. Where are the Ph.D. students working on these aspects of turbulence, developing new models, improving their understanding? I think the negative attitude is promulgated by people like Schlichting who wrote in the textbooks that the turbulence problem will never be solved. It will never be solved if no one ever works on it, and that's for sure.

That is the past. For the present, I don't think I heard anything at this conference which makes me change my optimistic viewpoint. I am sure the nonhyper-sonic compressible turbulent boundary layer will shortly be solved 28 times. It is evident to me that, just at the present conference, there are something

---

<sup>24</sup>Symposium on Viscous Drag Reduction. Sept. 24-25, 1968, Dallas, Texas, sponsored by Office of Naval Res. and NASA-OART.

<sup>25</sup>Paper 2 of this volume.

<sup>26</sup>Malkus, W. V. R.: J. Fluid Mech., Nov. 1956.

<sup>27</sup>Burgers, J. M.: 1939 Proc. Koninkl. Ned. Akad. Wetenschap, vol. 17, no. 2.

approaching that number of people who are all going to have a go at doing it. With about two new ideas - well, two ideas between the lot of them: those who say a simple gradient transport equation or eddy viscosity is adequate and the people who say it is not adequate. You can perhaps superimpose on those two schools the people who say that you ought to solve the partial differential equations of motion and the people who say you ought to go the integral route, and that's four sets of concepts, and if you double up, well, that should allow good going for eight people, and just to be on the safe side, let us double up again, and that is 16 - that is still only about half the amount of people that are going to try and solve the nonhypersonic compressible turbulent boundary-layer problem.

The future - George Mellor remarked in rather colorful language the other evening, "hypersonic turbulence is a can of worms." We obviously need some good measurements; we need to know what the structure is doing. It may well be that we can bootleg the simple structural hypothesis that we have now into the hypersonic region.

I have confidence in what has come to be known in certain circles as "Morkovin's hypothesis," which Professor Laufer was referring to a few minutes ago. I think Morkovin's hypothesis is providing an adequate means of treating the compressible turbulent boundary layer, and the real experimental thrust might well be towards developing structural information on hypersonic-type boundary layers. If any of the 30 people are looking around for simple wrinkles to develop rather than all of us solving the problems again, they might examine simple time-dependent boundary layers. If the frequencies involved are low, one would imagine a quasi-steady approach to the boundary layer might be adequate. Some of us are already looking at three-dimensional boundary layers - people like J. Nash - so we don't all want to promptly abandon the two-dimensional case and go to the already beginning to get crowded three-dimensional case, although there is obviously a lot more room there at the moment. In addition, we can, however, begin to look at boundary conditions which we haven't looked too much at. The finite-difference methods are an excellent vehicle for this type of study. For instance, wall suction - wall blowing - how well are we doing? What we must do is to treat the problem a lot better, but first of all, find out if we really need to do it any better. No one talks about boundary-layer transition too loudly. We don't talk about boundary layer developing into wake. There are so many problems, and I don't think we all need to solve the same problems twice.

Mitchel Bertram: Before turning the discussion loose to the audience, perhaps the panel members would like to make a few short comments about each other's presentations.

A. M. O. Smith: I would like to make one comment in respect to Henry's [McDonald] remarks about this type of work going into the universities. I am not sure I see it quite the same way he does. I'm with the aircraft industry, and Mach number 1 is getting pretty fast for us, so I'm a little out of my field here. As a result of the Stanford contest, we all were pretty well assessed as to the validity of our boundary-layer calculations, but not entirely, because there was still not enough variety of problems. In several cases it looked as

With regard to the use of the "compromise mathematics," whatever that term may mean, I would like to make several points. In the first place, the integral technique we are using is basically a procedure which converges as closely as desired to known "exact" solutions for laminar flows by using enough terms to represent the velocity profile. Now, in turbulent boundary-layer problems, the question of exact solutions to the boundary-layer equations is clouded by the fact that existing eddy-viscosity models are compromises - definite compromises with physical reality. Therefore, I don't think it is generally wise to put too much effort into getting high accuracy in solving the turbulent boundary-layer equations when with less time or effort you can get accuracy which is compatible with the approximation of the eddy-viscosity model. However, some effort is warranted in solving the turbulent boundary-layer equations to a high degree of numerical accuracy for the purpose of checking the approximate numerical methods using the same eddy viscosity. With regard to integral methods versus finite-difference method, I think you will find that integral methods are used by many engineers throughout the industry, whereas few engineers use finite difference as an engineering tool. I believe that the solutions we get using the Dorodnitsyn technique are close enough for most engineering predictive purposes. Anybody who thinks he can get "exact" solutions to the turbulent boundary-layer problem using present "compromise" eddy-viscosity models is in my view mistaken, for such models are still empirical and metaphysical.

Integral methods appear to have an advantage over finite-difference methods in connection with separated flows. The finite-difference schemes are basically unstable when applied to separated boundary layers. They can be patched up by adding stabilizing terms to the boundary-layer equations, but it is necessary to show that the added term has a negligible effect on the solution. Finally, the real turbulent boundary-layer problems of engineering involve many complications such as jets penetrating into the boundary layer, normal pressure gradients, nonisentropic edge effects, etc. If we try to solve such problems precisely using finite-difference techniques or by any other means, we will not make rapid progress. There is a continuing need for approximate techniques which can provide reasonable solutions to a variety of difficult problems in a reasonable amount of time and with a reasonable amount of effort.

Robert Kendall (Aerotherm Corp.): I would like to support A. M. O. Smith. I have a technique which has been called differential and integral and a few other things, but it is basically a procedure which does converge exactly and I think AMO would consider me in his family of exact-solutions procedures. Also, our times are like his or perhaps a shade faster. To answer Jack Nielsen's question - on a problem with chemical reaction of 30 to 40 species, four elements around a body, there is a total time of the order of five seconds per station with big steps between stations on an 1108 computer at \$600 an hour, to be exact. Also, in my experience with integral methods, typically they involve more algebra by the user than the finite-difference methods do - particularly the Dorodnitsyn approach that he espouses. As a consequence, it is often easier to take the finite-difference approach and feed in these other effects which he mentioned. The entropy layer effect becomes a trivial modification of a boundary condition and so forth; therefore, I would stand with AMO and the statement of "let's not go for compromise mathematics."

if people had a method that they could count on at last. I've been needled through the years while doing boundary-layer work by my old boss, the chief engineer, who used to say to me, "Still working on boundary layers, I see, and never any answers." At last we have some numerical methods that we can rather well count on and Douglas applications are just pyramiding.

They are now getting correct answers inside of DC-8 and -10 inlets and things like that by just turning a crank, so to speak. For one wild example, they have gotten interested in rotating cylinder flaps (airfoil with a spinning cylinder flap on back) and with some hedging we say that is no problem at all. We just put in a slip boundary condition and go to it. Only trouble is we are stuck right now in making that particular change because our program will go through the machine if we have a detailed print-out and it won't go through if we just ask for the regular print-out. These are the reasons why jobs take time. People in airfoil design are pushing things to the limit. That's why you are asked to guarantee a separation location to 99.8 percent chord with an accuracy of  $\pm 0.1$  percent, or something like that. That is an example of the kind of pressure you receive. Very high accuracy on location of separation seems to be forced upon you. Where questions about body shaping and drag come up, the answers fall out in routine fashion due to developing a basic method of analysis. The money readily comes for further development when you are getting some real use out of these methods.

Mark Morkovin: I think what Henry McDonald and others are really talking about in terms of good experiments is really a function of funding. Actually, only 11 of the people at the Stanford competition were university people and all of them, I believe, had DOD funding. So that it is a question of a national problem if we have too much proliferation. I think the Stanford conference showed that we had more than enough duplication of new ideas, and that is what Henry was talking about. It is up to the funding people to avoid backing duplicative studies and perhaps shove that money into extra experimental facilities. We must realize that many things enter into good high-speed experiments. It takes a tremendous amount of patience and development of instruments. You really have to develop the instrument or close to it; you have to have practically a new facility. Accessibility is a tremendous problem at high speeds; what the experimentalist can do is strongly a function of funding. I hope I have not offended any of my friends at NASA talking about experiments as if they had not done any. They have done excellent high-speed turbulent experiments within the limitations of facilities, time, and funding. I think we are, in part, talking to the funding people too, who with the help of conferences like this can get a better perspective and provide for a set of more expensive high-speed experiments that could truly be definitive for checking the theories.

Mitchel H. Bertram: At this time I would like to throw the discussion open to the audience.

Jack N. Nielsen (Nielsen Engineering & Research, Inc.): I would like to make a few remarks with regard to quoted computation time in connection with finite-difference schemes. Some numbers were given, but they raise more questions than they answer. First, the machine on which the times were obtained was not mentioned, nor was the cost per hour mentioned. Secondly, the kinds of cases that were calculated were not described.

Mitchel Bertram: One thing I would like to say here is that this is all very interesting, but let's not get bogged down in arguing the various espousals of methods, one against the other. I think we ought to direct ourselves as generally as possible to the problems under consideration. I know that we all have our favorite approaches and will argue to the death for them.

George L. Mellor (Princeton University): I was just about to say the same thing. In a couple of years anybody will have a choice of several computational methods; then it will be like buying a hi-fi set - which one you choose. I'd like to turn our attention somewhat to the empirical content of these predictive methods first, and then to experiments. I think what I tried to say along with the compressible business on the first day was that a lot of methods have more or less the same eddy-viscosity stipulation (mean velocity field closure) which can be transformed into each other. I hope to write a little review paper soon that demonstrates just that. Now, round two is starting where consideration of the mean turbulence field is included in the prediction, and at the Stanford meeting we sort of made the bridge<sup>28</sup> to round two. This really started with Prandtl.<sup>29</sup> But not much has happened since Prandtl suggested the essential hierarchy of equations that was amplified in an important way by Rotta.<sup>30</sup> Glushko<sup>31</sup> also picked up these questions and looked at transition and did very interesting work. (What ever happened to Glushko? He did his work a few years back with computers and seemed not to have carried it further - that's a strange thing.) We have gotten into this business now of trying to get close to the turbulence and bring the calculations closer to the experimentalist, really, because here for years they have been producing turbulence data and the only thing we used previously is the mean-profile pitot-tube data. I think round two is going to be more interesting, in a way, because we are going to have the use of all this turbulence information to discriminate between one person's wild conjecture of term number three and another person's wild conjecture. I think it is going to be fun because now Co Donaldson is going to have his ideas and I'm going to have my ideas and in a year or so we are going to have some good fun debating these things. In the future we are going to have to debate on the basis of turbulence measurements - hot-wire measurements. So I think round two is going to be a fun thing and we have to credit the computer with allowing us to get into this.

Mark Morkovin: I think it is more like round  $1\frac{1}{2}$  as far as the compressible stuff is concerned, with all the heat transfer and the nonsimilarity solutions present. What we are talking about right now is supposed to be for compressible boundary layers and yet we are trying to look toward hypersonic boundary layers. I disagree that the so-called "Morkovin hypothesis" can take care of anything beyond Mach number 5; I think we need an entirely different look for the high

---

<sup>28</sup>Where we compared the results of using mean velocity field closure with turbulent field closure. See Mellor and Herring, Stanford Symposium on Turbulent Boundary Layer Prediction, 1968.

<sup>29</sup>Original paper 1945, available as publication No. 13, JPL-CIT, Aug. 1952, translated by D. Coles.

<sup>30</sup>Rotta, J.: Z. Physik, vol. 129, 1951, pp. 547-572.

<sup>31</sup>Glushko, G. S.: NASA TT F-10080, 1966 (translated from the Russian).

Mach numbers and I think it would be wrong if the panel did not say that as far as high Mach numbers are concerned. As far as the more or less low Mach number is concerned, you are right of course.

Anthony Fiore (Wright Field-ARL): Being primarily an experimentalist I want to come back to this thing about getting very good data in this particular field. I agree with this wholeheartedly, but I also think that the average person does not realize the kind of sweat and blood that goes into getting good data. You people speak of taking data in turbulent boundary layers at high speeds, for example. Does anybody know how to design a static probe to measure the static pressure across the boundary layer in the presence of an adverse pressure gradient? What is the recovery factor of a total-temperature probe throughout the boundary layer? It will take you three years just to get a good calibration out of one. And then on top of this we have to go to sophisticated systems, electron beams, and laser systems for Doppler shift to get velocities. These things are not very simple. They take time to develop, and it takes a Ph.D. in optical physics to do it. Now please give the experimentalist a little hand here; the guy works his tailbone off and then somebody says, "Well, that point is 10 percent off." So let's get the instrumentation and then one can do the job.

Arthur Henderson, Jr. (Langley Research Center): I would just like to address some questions to the theoreticians. Some of us here are experimentalists and as Dr. Fiore said we could spend 10 years on various aspects of the experimental work that we could do. I would like to ask some of the primarily theoreticians here, specifically what experimental work would you like to see done? You know you could always make surface measurements, but I don't think this is what you particularly had in mind. We are working now on hot-wire anemometry at hypersonic speeds, but there are an infinite number of types of measurements you can make there too. How about being specific - what do you suggest we do?

John Laufer: I think perhaps we should pose the question a little differently, because as an experimental man I don't want to and don't like to go to the theoretician and ask him what I should do, because he doesn't know some of the problems that -

Arthur Henderson: That doesn't mean we'll do what he says - I just want to hear what he says.

John Laufer: All right, then, I'll let somebody else answer your question. Let me just finish what I had in mind. I think the experimentalist knows what type of method - what type of equipment is available to him - what sort of measurements he can develop. Yes, it might take one year, it might take three years, but I think the fact that the measurements are difficult should not be used as an excuse for not doing it. The problem of course is, as Mark mentioned, funding and patience. I think the people who give the money for these sorts of things must realize that developing new techniques must take time, but it absolutely has to be done - there is just no question about it. The sort of thing that one can do, for instance, which possibly might not take as much development time (and it just came into my mind because this was one question that was discussed quite a bit yesterday) is the question of the energy integral in the turbulent



boundary layer. How does the velocity vary with the temperature? Does it go as a square, or linearly, or what have you? I think there are one or two fairly simple experiments that one can do with reasonably simple methods to test that out. It will take time, but I think it can be done.

Howard K. Larson (Ames Research Center): I would just like to make a comment on the fact that what is done, and to what accuracy, depends on the final application. Most of the discussion here has been concerned, I believe, with a non-ablating aircraft-type of application where a few percent are important. I would like to point out that there is another field - that once one gets, say, about  $M = 10$  in flight and also for the ICBM work, ablation is going to be pretty important, but in that case, which is a mass-addition case, usually 10-percent-like accuracies are acceptable; so we have to establish whether we are looking at aerodynamics or whether we are looking at the ablation problem.

Richard Johnson (General Electric Co.): I would like to present an opinion from a pragmatist's point of view. I must explain first that I came to the conference primarily to become exposed to the theoreticians and experimentalists involved in boundary-layer research, so I could have a better appreciation of the state of the art and where we are going. I think that one of the things that we have been doing recently that may be of interest and is, I feel, a challenge to both the experimentalists and theoreticians is to understand the causes of the problems that we are concerned with, which are drag, heat transfer, and pressure distribution, and how the boundary layer is affecting them, and these are I think the fundamental questions to be answered by most of the work we are doing. One of the things that possibly may be of some help here is the use of acoustic devices. Professor Laufer's comments in regard to the very high oscillating pressure levels that one discovers in the hypersonic boundary layer is of real interest to the engineering designer who is concerned with, say high-performance reentry vehicles in high-dynamic-pressure regions at very high Mach numbers. These vibratory loads imposed by the high levels of the oscillating pressure can be disastrous to his structures if they were designed for just the static loads. There seems to be a practically virgin field here in the area of acoustics research associated with boundary layers. We have had some very interesting preliminary results from the work that we have done personally at Tullahoma that, for example, are interesting in comparison with some of the work that we saw on the effects of boundary-layer trips on turbulent flow. [See paper 16 of this volume]

It is very preliminary at the present time, but it appears that with sensors of a limited frequency capability we have measured sound levels in tripped turbulent flow that were equal to the sound pressure level for nontripped laminar flow, thus indicating that while there was some mechanism causing the heat-transfer rate to rise, the same mechanism was not causing a comparable rise in the oscillating pressure levels. It may be that by spectral analysis of this type of data, and looking at such things as the change in the frequency spectra as we go from laminar to turbulent, we are beginning to understand more about these basic mechanisms in the boundary layers.

Irwin Alber (Dynamic Sciences): I just want to turn around the question addressed by one of the experimental people to the theoreticians about what

kind of experiments they would like to see designed. I would like to put the question to the people from the industry and government agencies that was being kicked around last night by Henry McDonald, George Mellor, and myself, among others, about the relevance of turbulent boundary-layer calculations to practical industrial design problems. We tend to go off on a tangent looking at all the details of how we would go about calculating turbulent boundary layers, and there are some very important analytical problems, but I would like to hear from somebody from industry as to why they would like us to calculate a turbulent boundary layer accurately for them and what are their design problems that really need these kinds of sophisticated solutions.

Mitchel Bertram: Actually, I think one answer to that is in one of the last papers you heard, John Henry's paper [paper 19], that was intended to expose a very practical problem that was found in the development of the hypersonic ram-jet engine and one which could not be predicted.

A. M. O. Smith: John Henry's paper was a good example of how things like this often happen. I think he had a change of something less than an eighth-inch radius which made that diffuser not work - couldn't swallow the shock - and the one with the smaller radius did. Some of these effects are tremendous. That demands extremely high precision in understanding and analysis.

Fritz Krause (Marshall Space Flight Center): I would like to call your attention to one particular problem that is bothering us. This is the spreading of the exhaust products at high altitudes and parking orbits. You know hypersonic flow expanding into a vacuum can actually expand forward in the flight direction. We have had quite some trouble in contamination of our Pegasus satellite - contamination of surfaces catching solar energy and contamination of telescopes. There is quite some concern about corrosion contamination effects during rendezvous maneuvers, and vehicles landing on the moon. There is a very extensive research program started, entirely experimental for the time being, because theoretical attempts to predict what happens to a jet expanding in a vacuum at the system have almost completely failed. This is the dynamics and thermodynamics of systems which are very far removed from thermodynamic equilibrium. Project High Water [Saturn I, 1962], which is two or three years old, just dumped a couple hundred thousand pounds of water in the stratosphere and the spreading of that water behaved in a completely unpredictable manner, so unpredictable nobody has ever dared to publish a report. It is an area, I think, of compressible and hypersonic flow, and the borderline between potential core and boundary layer is rather hazy, which I consider of great importance. Also, there will be a lot of exhaust products released into the stratosphere by supersonic transports and the upper stratosphere by future rocket flight, and these may change somewhat the absorption of the solar rays. I understand that some meteorologists get concerned about this. It is not just what happens to this vehicle which spreads this stuff. It is what happens to the stratosphere - how far does it spread and where does it go?

Coleman Donaldson (Aeronautical Research Associates of Princeton): I have been sitting here trying to think of an experiment to answer the question, and I'm kind of high on experiments that don't have exactly the same geometry as everything we have looked at in the past. One that is close to it, and somebody on

the panel brought up the problem of time-dependent turbulent boundary layers, and an interesting question that I would kind of like to see something on is a flat plate which is oscillated at an amplitude large enough to cause transition and then survey what the details of turbulent structure above that plate are. I think this might be a very useful exercise; it goes about getting all the terms that exist in the equations in a little bit different way than we are used to thinking of them, and this might be a very important measurement to make.

John Laufer: I believe there exists a set of experiments very similar to this problem, except in this experiment in place of the plate oscillating in the direction of the flow a wavy wall was used with variable wave speed. Jim Kendall at JPL was doing that, but I understand that because of funding problems he had to discontinue that experiment.

Coleman Donaldson: Yes, that is a good experiment. The one I thought of with the plate moving back and forth just in a plane is a very simple one. The particular method that I am touting these days should be applicable to that case; it would be very nice to see whether it worked.

Mark Morkovin: You know the Karlsson experiment at Hopkins? There is a Ph.D. thesis and a JFM paper by Stu Karlsson<sup>32</sup> about 1958 where he had a variable free stream of plus or minus 30 percent over a turbulent boundary layer. The evidence was that the turbulent structure was essentially unaffected by this plus or minus 30 percent sloshing of the free-stream velocity back and forth. However, there always was a minimum mean velocity forward.

William G. Rose (University of Virginia): That paper by Obransky on transition - this is what Cole [Donaldson] was asking.

Mark Morkovin: Well no, I think you wanted the turbulent part - don't you?

Coleman Donaldson: Yes, where the stress completely reverses itself.

Mark Morkovin: Which Karlsson's does not.

William Rose: I would like to, as an experimentalist, direct a remark to other experimentalists. With the advent of new techniques such as the possibilities of scattered laser radiation (say in hypersonic or supersonic turbulent flow, where a lot of development work is being done with lasers and their application to measurement of unsteady flow), I think the choices of test cases that people have made to demonstrate the validity of their techniques and their instruments have been very poor. They have, in case of steady-flow measurements, used fully developed Poiseuille flow, an excellent test case, but I would like to emphasize that there is a good turbulent test case which was done by John Laufer at Reynolds numbers of 50,000 to 500,000 in a pipe.<sup>33</sup> These make excellent test cases for measuring turbulent flow and I would like to see more laser instrumentation tested in this kind of a flow field.

---

<sup>32</sup>Karlsson, S. K. F.: J. Fluid Mech., vol. 5, pt. 4, May 1959, pp. 622-636.

<sup>33</sup>NACA Rept. 1174, 1954.

S. Zane Pinckney (Langley Research Center): There was a mention a few minutes ago about the linear temperature distribution versus the nonlinear temperature distribution. The particular case which was brought forth to us in a paper yesterday<sup>34</sup> was at the end of a nozzle in which the particular profile was in a nonequilibrium condition. Well, your Crocco temperature expression which gives you your linear distribution is a complete equilibrium-type derivation which assumes constant boundary-layer edge conditions, constant wall conditions, constant everything flowing.<sup>35</sup> Well, if we have more heat transfer forward than would correspond to this particular type of condition, this would have a tendency to drive your temperature down across the boundary layer. In other words, it would have the curve coming down below the linear expression. If you progress on down from the exit of the nozzle with a constant wall temperature, this nonequilibrium-type total-energy deficiency would have to be distributed over more and more of a thicker and thicker boundary layer. As a result this would have a tendency to drive the temperature toward the equilibrium condition as you go further and further downstream. Now you could do the reverse where you have a different type of pressure gradient than we had experienced in this nozzle, and you could get the sort of result in which the temperatures would be above a linear distribution. I think this is something a lot of people are ignoring. They are ignoring the upstream history of these boundary layers and how this affects the temperature profile relationship.

Robert Kendall: We have made the point that the effects of high Mach number are more due to variable properties than they are due to supersonic or compressible effects per se or Mach number effects. If this be the case, why are we not doing more experiments at low Mach numbers, where our experimental techniques are well established, involving highly variable properties? Why are we not doing more helium injection, more high temperature ratio, where we can get a hold on the correlation for parameters and check out the transformation that we are trying to use. This seems to me a very fruitful area for the universities to be working in.

Mark Morkovin: I made the suggestion about learning from low-speed variable-properties layers, namely, heated boundary layers, in 1961 in Marseille.<sup>36</sup> A. M. O. Smith made the same point. But when it comes to helium, do you know anybody who has a reliable instrument that will measure fluctuations of helium concentration? A hot wire is not doing it very well. I suspect there are some techniques available, but for your objectives we are talking about accuracies on the order of one percent. If you know of any such accurate technique we should encourage such variable-property low Mach number research.

Mitchel Bertram: Thank you for an informative and stimulating discussion, which, though not solving our problems, has pointed out not only our advances but also our deficiencies in the structure and transformation of compressible turbulent boundary layers.

---

<sup>34</sup>Paper 11 of this volume.

<sup>35</sup>With Prandtl number unity.

<sup>36</sup>Mechanics of Turbulence. Gordon and Breach Sci. Publ., 1964, pp. 367-392.

# LIST OF ATTENDEES

Alber, Dr. I. E.	Dynamic Sciences, Monrovia, Calif.
Andrews, E. H., Jr.	NASA Langley Research Center
Banner, Richard D.	NASA Flight Research Center
Becker, John V.	NASA Langley Research Center
Beckwith, Ivan E.	NASA Langley Research Center
Bertin, Prof. J. J.	University of Texas
Bertram, Mitchel H.	NASA Langley Research Center
Blackwell, James A., Jr.	NASA Langley Research Center
Blottner, Dr. Fred G.	Sandia Corp., New Mexico
Boatright, W. B.	NASA Langley Research Center
Bobbitt, Percy J.	NASA Langley Research Center
Bogdonoff, Dr. S. M.	Princeton University
Bradley, R. G.	General Dynamics Corp., Texas
Bushnell, Dennis M.	NASA Langley Research Center
Carter, Howard S.	NASA Langley Research Center
Cary, Aubrey M., Jr.	NASA Langley Research Center
Czarnecki, Kazimierz R.	NASA Langley Research Center
Danberg, Dr. James E.	University of Delaware
Deissler, Robert G.	NASA Lewis Research Center
Der, Joe, Jr.	Northrop Corp., California
Donaldson, Dr. Coleman DuP.	Aeronautical Res. Assoc. of Princeton
Dowling, W. J.	NASA Langley Research Center
Dunavant, James C.	NASA Langley Research Center
Economos, Dr. Constantino	General Applied Science Laboratories
Erickson, Dr. Wayne D.	NASA Langley Research Center
Feller, William V.	NASA Langley Research Center
Fernandez, Dr. Frank L.	Aerospace Corp., San Bernardino, Calif.
Fiore, Dr. Anthony W.	Wright Patterson AFB, Ohio
Fischer, Michael C.	NASA Langley Research Center
Fridman, Dr. Jonathan	Raytheon Co., Sudbury, Mass.
Garrick, I. Edward	NASA Langley Research Center
Gessow, Alfred	NASA Headquarters, Washington, D.C.
Harvey, William D.	NASA Langley Research Center
Hastings, E. C., Jr.	NASA Langley Research Center
Hastings, R. C.	British Embassy, Washington, D.C.
Henderson, Arthur, Jr.	NASA Langley Research Center
Henry, John R.	NASA Langley Research Center
Herring, Dr. H. J.	Princeton University
Hochrein, G. J.	Sandia Corp., Albuquerque, New Mexico
Hopkins, Edward J.	NASA Ames Research Center
Howe, John T.	NASA Headquarters, Washington, D.C.

Inger, Dr. George R.  
Inouye, Mamoru

Johnson, Charles B.  
Johnson, R. I.  
Jones, Robert A.

Kaufman, Dr. Louis II  
Kendall, Dr. R. M.  
Kistler, Dr. Alan L.  
Klebanoff, Philip S.  
Klunker, E. Bernard  
Korkegi, R. H.  
Krause, Fritz R.  
Kubota, Toshi  
Kurzweg, Hermann H.

Larson, Howard K.  
Laufer, Prof. John  
Lee, Roland  
Lewis, C. H.  
Lewis, Dr. J. E.  
Libby, Prof. P. A.  
Lobb, Dr. R. Kenneth  
Loftin, Laurence K., Jr.  
Long, Joseph E.  
Loving, Donald L.

Maddalon, Dal V.  
Masek, R. V.  
Mayes, William H.  
McClinton, C. R.  
McDonald, Henry  
Mellor, Prof. G. L.  
Miller, L. D.  
Mirels, Dr. Harold  
Moore, Dr. D. R.  
Morkovin, Prof. Mark V.  
Morrisette, E. Leon

Nagamatsu, Dr. Henry  
Nash, J. F.  
Neumann, R. D.  
Nielsen, Dr. Jack N.

Peterson, J. B.  
Pierce, Harold B.  
Pickney, Shimer Z.  
Polek, T. E.

Quinn, Robert D.

McDonnell Douglas Corp., Santa Monica  
NASA Ames Research Center

NASA Langley Research Center  
General Electric, Philadelphia  
NASA Langley Research Center

Grumman Aircraft Co., Bethpage, N.Y.  
Aerotherm Corp., Mountain View, Calif.  
Jet Propulsion Lab.  
National Bureau of Standards  
NASA Langley Research Center  
Wright Patterson AFB, Ohio  
NASA Marshall Space Flight Center  
California Institute of Technology  
NASA Headquarters, Washington, D.C.

NASA Ames Research Center  
University of Southern California  
U.S. Naval Ordnance Lab.  
Virginia Polytechnic Institute  
TRW Systems  
University of California  
U.S. Naval Ordnance Lab.  
NASA Langley Research Center  
NASA Headquarters, Washington, D.C.  
NASA Langley Research Center

NASA Langley Research Center  
McDonnell Douglas Corp., St. Louis  
NASA Langley Research Center  
NASA Langley Research Center  
United Aircraft Research Lab.  
Princeton University  
Lockheed Aircraft Corp., Calif.  
Aerospace Corp., El Segundo, Calif.  
LTV Aerospace Corp.  
Illinois Institute of Technology  
NASA Langley Research Center

General Electric Company, Schenectady  
Lockheed Aircraft Corp., Marietta, Ga.  
Wright Patterson AFB, Ohio  
Nielsen Eng. and Res., Inc.

NASA Langley Research Center  
NASA Langley Research Center  
NASA Langley Research Center  
NASA Ames Research Center

NASA Flight Research Center

Rae, Dr. W. J.  
Raper, J. L.  
Reeves, Dr. Barry L.  
Rose, Dr. W. G.  
Rosenbaum, H.  
Rumsey, Charles B.  
Runyan, Harry L., Jr.

Schadt, Gail H.  
Schueler, C. J.  
Schwartz, Ira R.  
Smith, A. M. O.  
Softley, E. J.  
Spangenberg, W. G.  
Stainback, Calvin P.  
Stallings, Robert L., Jr.  
Sternberg, Dr. Joseph  
Sterrett, James R.  
Stone, David R.  
Sullivan, Edward M.  
Sutton, G. W.

Tauber, Michael E.  
Trimpi, Robert L.  
Tuovila, Weimer, J.

Wagner, Richard D., Jr.  
Wallace, J. E.  
Watson, Earl C.  
Watson, Ralph D.  
Whitehead, Allen H., Jr.  
Whitesides, Dr. John  
Whitfield, J. D.  
Wilson, R. E.  
Winter, K. G.  
Wright, Robert L.

Yoshihara, Dr. H.  
Young, Capt. J. D.

Zakkay, Prof. Victor  
Zoby, Ernest V.

Cornell Aeronautical Lab.  
NASA Langley Research Center  
AVCO Corp., Wilmington, Mass.  
University of Virginia  
Aeronautical Res. Assoc. of Princeton  
NASA Langley Research Center  
NASA Langley Research Center

General Dynamics Corp., San Diego  
ARO Inc., Arnold Air Force Station  
NASA Headquarters, Washington, D.C.  
McDonnell Douglas Corp., Long Beach  
General Electric Co., King of Prussia  
National Bureau of Standards  
NASA Langley Research Center  
NASA Langley Research Center  
Martin Marietta Corp., Baltimore, Md.  
NASA Langley Research Center  
NASA Langley Research Center  
NASA Langley Research Center  
AVCO Corp., Everett, Massachusetts

NASA Ames Research Center  
NASA Langley Research Center  
NASA Langley Research Center

NASA Langley Research Center  
Cornell Aeronautical Lab., Buffalo  
NASA Ames Research Center  
NASA Langley Research Center  
NASA Langley Research Center  
George Washington University  
ARO, Inc., Arnold Air Force Station  
U.S. Naval Ordnance Lab.  
Royal Aircraft Establishment, U. K.  
NASA Langley Research Center

General Dynamics Corp., San Diego  
WLDE, Kirtland AFB, New Mexico

New York University  
NASA Langley Research Center